STRUCTURE-PROPERTY RELATIONS IN 10Mn-3C-7Cr WHITE IRONS ALLOYED WITH 1.5-5.0 COPPER

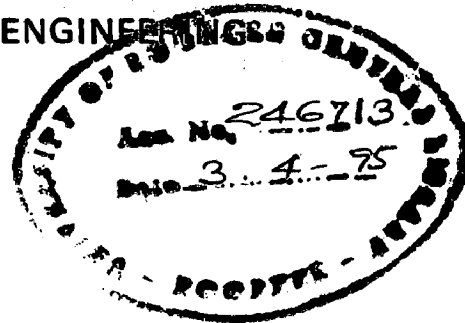**A THESIS**

submitted in fulfilment of the
requirements for the award of the degree
of
DOCTOR OF PHILOSOPHY
in
METALLURGICAL ENGINEERING

by

P. N. V. R. S. S. V. PRASADA RAO

DEPARTMENT OF METALLURGICAL ENGINEERING
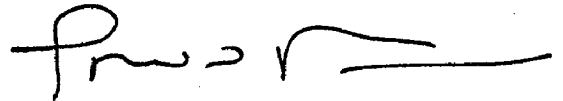UNIVERSITY OF ROORKEE
ROORKEE-247667 (INDIA)

JUNE, 1993

DE

CANDIDATE'S DECLARATION

I hereby certify that the work which is being presented in the thesis entitled 'Structure-property relations in 10Mn-3C-7Cr white irons alloyed with 1.5-5.0 copper in fulfilment of the requirement for the award of the Degree of Doctor of Philosophy and submitted in the Department of Metallurgical Engineering is an authentic record of my own work carried out during a period from June 1988 to April 1992 and August 1992 to June 1993 under the supervision of Dr.A.K.Patwardhan.

The matter presented in this thesis has not been submitted by me for the award of any other degree of this or any other university.

(P.N.V.R.S.S.V. PRASADA RAO)

This is to certify that the above statement made by the candidate is correct to the best of my knowledge.
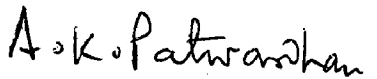
Date: June 25, 1993

(Dr. A.K.PATWARDHAN)
Professor
Department of Metallurgical Engineering
University of Roorkee
Roorkee-247 667 (INDIA)
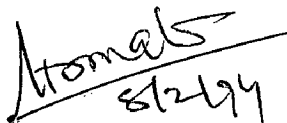
The Ph.D. viva-voce examination of Mr.P.N.V.R.S.S.V. Prasada Rao, Research Scholar has been held on . Feb. 8, 1994

Signature of
Supervisor

Signature of Head of
the Department

Signature of
External Examiner

DEDICATED TO

MY

GRAND PARENTS

LATE SRI P. VENKATA NARASIMHAM

AND

LATE MRS. P. SOVAMMA

Iron seemth a simple metal
but
in its nature are many mysteries

-Joseph Glanville

ACKNOWLEDGEMENT

ii

Sharma(MIE Dept.) is greatly acknowledged. It gives me fabulous delectation to thank Mr.Madhu Kumar Singh, Mr.Rajender Singh Sharma and Mr.V.K.Tyagi for their valuable help in T & K laboratory. I highly appreciate Mr.S.S.Gupta for the high quality xeroxing of my thesis. I am also thankful to Mr.Prem Singh, Security Guard for accompanying me in the department during late working hours.

It gives me fabulous delectation to thank Sri Baleswar Dutt Sharma and his family members who provided their house to me at the critical stage of my Ph.D. work and extended the hospitality and support to my family.

I am dearth of proper words to put my feelings for my respected parents who, apart from providing me the best available education, always have encouraged me in all my endeavors while poignantly bearing the burden of my long absence. I owe much of my academic success to them. I would like to emphasize the support, forbearance and inspiration from my in-laws.

Last but not the least I wish to record most affectionately and with great indebtedness, the patience and excellent understanding shown by my wife Radha and daughter Siva Jyothi, to bear the gross negligence, during the entire period of my research work. I am thankful to all the family members of Dr.A.K. Patwardhan for their kind support and help.

Date: June 25 , 1993   (P.N.V.R.S.S.V.PRASADA RAO)

ABBREVIATIONS

A	Austenite
AC	Air cooled
AVE,Ave,ave	Average
B	Bainite
BCC	Body centered cubic
BHN	Brinell hardness number
C	Carbon
Cb	Carbide
C.C	Correlation coefficient
CE	Carbon equivalent
CI	Coarsening Index
COND	Condition
CONF	Confidence
COP	Cross over point
CR	Corrosion rate
CS	Compressive strength, MN/m^2
DC	Dispersed carbide
DCs	Dispersed carbides
DF	Distribution factor
DIFF	Diffraction angle
DSPs	Dispersed second phase particles
DTA	Differential Thermal Analysis
EPMA	Electron probe micro analysis
exp,Exp	Experimentally determined
FCC	Face centered cubic
GB	Grain boundary

Gms, gms	Grams
H	Hardness
H_M	Heterogeneity of the structure based on volume fraction of massive carbides
$H_M(dist)$	Distributional heterogeneity related with precipitated second phase
HRS,h,hr,hrs,Hrs	Hours; austenizing period; test duration
HT, H/T, h/t	Heat treatment
HV_{30}	Vickers hardness at 30 kg load
INT	Intensity
IPY, ipy	Inch penetration per year
M	Martensite
mA	Milliampere
mV	Millivolt
Max,max	Maximum
Max.Dev	Maximum deviation
MC	Massive carbide
MCs	Massive carbides
M3	M3C (orthorhombic)
M5	M5C2 (monoclinic)
M7	M7C3 (hexagonal)
M23	M23C6 (cubic)
MDD, mdd	Milligram per decimeter^2/ day
Meas,MEAS	Measured
MN/M^2, MN/m^2	Mega newton per square meter
MPa	Mega Pascal
mpy	mils per year
Min	Minimum

NOP	Number of particles
NP	New phase
OQ	Oil quenched
P	Pearlite
P1,P2,P3	Alloy designation
per	permissible
pre, Pre	Predicted from model/equation
RA	Retained austenite
R.T	Room temperature
SD, S.D.	Standard deviation
S.N, S.No.	Serial number
SP	Soaking period/austenitizing period
ST	Soaking temperature
SA, S. AREA	Surface area
Sq.cm	Square centimeter
SD	Standard deviation
SG	Spheroidal graphite
SCC	Stress corrosion cracking
S.S.	Stainless steel
SFE	Stacking fault energy
TD	Test duration
T, Temp	Heat treating temperature
TG	Thermogravimetric
TR	Trigonal
TSI, tsi	Tons per square inch
Sq.	Square
t	Time
μ	Micron

μA	Micron-ampere
UTS	Ultimate tensile strength
VF, Vf, vf	Volume fraction
VPN	Vickers pyramid number
Wt.%	Weight percent
α	Ferrite
α'	Martensite/shear transformation product
σ	Variance
τ	Austenite
τ'	Austenite (low stability)

Note : (i) All spellings conformed to (a) Chamber's dictionary and (b) a word-processing software SOFTWORD's dictionary (commonly employed in U.S.).

Tables, figures, sections and equations start with capital letters wherever table, figure, section and equation numbers are mentioned.

ABSTRACT

[A] Background

Of the three varieties of corrosion resistant alloy cast irons in use, the **high Si** irons have useful applications only in strongly **oxidizing** conditions. They however, **suffer from poor mechanical strength and shock resistance.** The **high nickel irons,** although extensively used in a number of aqueous environments, have a **low** strength, suffer from **graphitic corrosion & pitting** and are **unsuitable** at operating temperatures $\geq 800°C$. The high chromium irons exhibit relatively higher strength and can be employed upto higher service temperatures. Their shock resistance is improved by lowering carbon content.

A critical analysis revealed that **little information is** available on the **structure-property interrelations in alloy cast irons** in general. Furthermore, there is a lack of systematic information on the **electro-chemical** and on the **deformation behaviour** of microstructures commonly encountered in alloy white irons namely, 'martensite + carbide'(M + C), 'austenite + carbide'(A + C), and their allied counterparts.

Detailed **information** on these **aspects** was likely to prove useful in ascertaining whether microstructures exhibiting **good** resistance to aqueous corrosion and useful mechanical properties could be attained through the 'white iron' route. A **major advantage** foreseen was that the **limitations** encountered in **alloyed gray irons** would stand **eliminated.** Equally pertinent would be to investigate whether these microstructures could be generated by utilizing low cost alloying elements(Mn, Cu etc.) in

preference to the conventionally employed costlier alloying elements Ni and Mo.

Work carried out at the University of Roorkee by Jain and Kumar under the supervision of Professor A.K.Patwardhan has demonstrated that new meaningful compositions with very good corrosion resistance and deformation behaviour could be designed/developed based on the Fe-Mn-Cr-Cu system. The data thus obtained; while affirming freedom from the drawbacks encountered in the existing grey irons currently in use, laid down guidelines for developing future alloy compositions with considerably improved properties with the eventual interest in developing a new generation of corrosion resistant cast irons. The inferences arrived at mainly stressed upon the stability and volume fraction of austenite, volume fraction, morphology, and compatibility of the massive carbides(MCs) and size, volume fraction, and distribution of dispersed second phase(DCs)-an unintended constituent in attaining desired 'end properties'. These guidelines were used in conceiving and designing new alloys which were investigated in detail in the present study.

[B] Present Investigation

The present study, essentially comprised a detailed investigation of certain newly designed Fe-Mn-Cr-Cu white iron compositions, namely, Fe-3C-10Mn-7Cr alloys containing 1.5, 3.0, and 5.0%Cu in the air cooled condition. It centered around assessing their heat treatment response aimed at establishing an interrelation between structure and properties. A study of this kind required a detailed insight into the transformation characteristics of the alloys. This aspect accordingly received

maximum attention in the present study.

The alloys which were air induction melted and sand cast (18mm round and 120x22x8mm rectangular strips), were investigated for arriving at their transformation behaviour, by employing hardness measurements, optical and scanning metallography, quantitative metallography, X-ray diffractometry, electron probe micro analysis and differential thermal analysis. The electro-chemical characterization of the alloys was carried out by employing the weight loss/potentiostatic methods. Compression testing was also carried out to assess the deformation behaviour of the experimental alloys. Computational techniques were extensively employed for data analysis using IBM compatible PC-XT and PC-486 systems. Necessary software packages were also developed in FORTRAN IV as and when required.

[C] Major findings and development of models

The experimental work involved subjecting round specimens of the three alloys P1, P2, and P3 to heat treatments comprising holding for 2, 4, 6, 8, and 10 hours at 800, 850, 900, 950, 1000 and 1050°C followed by air cooling. This treatment was preferred over oil quenching because it can be directly utilized for industrial applications. Optical metallography was extensively used to assess how the Cu content and heat treating schedule influenced the microstructure which comprised :

(i)   Austenite (A) + some martensite (M)(?) + MC   in the as-cast
      state,

(ii) A + MC + dispersed second phase (DSPs) on heat treating

P1: 7Cr-10Mn-1.5Cu;   P2: 7Cr-10Mn-3.0Cu;   P3: 7Cr-10Mn-5.0Cu

xi

from up to 950°C,

(iii) A + MC (mostly rounded/hexagonal) on heat treating from

upto 1000°C, and

(iv) A + large agglomerated MCs + some dispersed carbides (DCs)

on heat treating from upto 1050°C

The volume fraction of massive carbides(MC) decreased with temperature or with soaking period at a given heat-treating temperature, the effect being marked at temperatures ≥950°C. Simultaneously, massive carbides were rendered discontinuous from the 'early' stages of heat treating. The 'rounding-off' tendency set in even at 900°C.

Dispersed second phase (DSPs) formed on heat treating at 800°C directly from austenite and comprised to begin with mostly needle/plate shaped precipitates and some DCs. With an increase in temperature/time the needles and the DCs coarsened, needle ends spherodized & slowly, the coarsened needle assumed the shape of a hexagonal/rounded massive carbide (MC). The extent of coarsening which was marked at 900°C and 950°C, has been represented by a newly evolved parameter the 'coarsening index'(CI). The dispersed carbides dissolved on heat treating from 1000°C but reappeared on heat treating at 1050°C.

Hardness measurements provided a quick yet reliable indication of the mechanical properties. A model was developed interrelating heat treating temperature and time on hardness and is of the form

$$H = C1 \, e^{C2/T} + (C3 + C4.T).t$$

where, H = hardness, VHN$_{30}$

T = temperature, °K

t = time in seconds

C1, C2, C3 and C4 are constants and are different for different alloys.

Through intensive calculations it has been possible to demonstrate that the **first term** of this model represents the **matrix related transformations** and the **second term** represents the 'carbide' transformations. The model is thus **physically consistent.** The predicted hardness values are within ±5% of the experimentally determined values.

3D plots interrelating the **hardness-heat treating temperature & time** were also constructed to study the overall transformation behaviour at a glance. The plots revealed that the above said relationship can be represented by a **surface** with opposite slopes on the two sides of the temperature axis.

The aforesaid model(hardness-temperature-time) was based on a total of 30 experiments. Through 'modelling' it has been demonstrated that the transformation behaviour can be **simulated** with **equivalent accuracy** based on merely **4 or 6 experiments.** This is an important inference needing further exploration since the **new idea** put forth could greatly help in **minimizing arduous experimentation** in arriving at the transformation behaviour.

The variation in volume fraction of MCs and DCs for a given heat treatment has been utilized to evolve a **new concept** called the **homogeneity/heterogeneity index.** It is felt that this concept needs to be further enlarged upon to arrive at its fuller implications.

X-ray diffractometry proved extremely helpful in identifying the different micro-constituents observed in the experimental alloys (both in the as-cast and in the heat-treated conditions). It proved helpful in identifying the matrix microstructure in 'marginal' cases e.g. in confirming the presence of martensite(M) in the as-cast condition even when the matrix was by and large austenitic. It also established that amongst the likely carbides to be present namely M_3C, $M_{23}C_6$, M_5C_2 and M_7C_3, only M_3C & M_7C_3 were attained in the as-cast condition as well as formed in differently identified temperature regimes used in the present study. Additionally, presence of Cu in the elemental form and of Fe-Si-carbide(Fe_8Si_2C) was also established. Even after such a detailed analysis, carried out with the help of developed software packages, certain reflections remained unidentified whose indexing was possible on the likely formation of $CrMn_3$ and Cu_2S. This aspect needs further investigation.

EPMA studies carried out on as-cast as well as heat treated specimens besides confirming the deductions arrived at on the basis of X-ray diffractometry and optical metallography, helped in establishing the partitioning behaviour of the different alloying elements e.g. Mn, Cr and Cu into the matrix and carbide phases. Chemical composition of the MCs and the DSPs was also determined and this alone helped in establishing the true identity of the different types of MCs & the DSPs, 'haloed' regions forming around MCs, and the dark etching regions in between adjacent MCs. EPMA also confirmed the (i) existence of Cu enriched regions both in the as-cast and heat treated conditions

and (ii) presence of M_7C_3 and M_3C from amongst the different carbides likely to be present.

Differential thermal analysis(DTA) of the experimental alloys in the as-cast condition revealed that all the alloys underwent transformations at 540-560°C(matrix related transformation) and ≈940-990°C(carbide transformation). Additionally, the alloy P1 underwent a third transformation at 1020°C representing perhaps another carbide transformation.

The same study also proved useful in predicting the suitability of the experimental alloys for high temperature applications based on an analysis of thermogravimetric(weight gain) data. The as-cast microstructures were found to be suitable up to a service temperature of 800°C. This beneficially reflected upon attaining a microstructure, normally observed at high temperatures, down to room temperature for improving the high temperature performance of the alloys. On heat treating from 1000°C, the temperature limit had been raised to ≈950°C.

A mathematical model, developed to interrelate the weight gain with temperature, is of the form

$$\% \text{ TG} = A1 + A2.e^{(-A3/T)}$$

where, % TG = percent weight gain

T = temperature

A1, A2, and A3 are constants.

Weight loss studies, carried out in 5% NaCl solution, were helpful in characterizing the alloys/selected microstructures for their response to corrosion. Corrosion data of two Ni-resist compositions were also considered for the purpose of a comparison. The study clearly brought out the effect of the

second phase(MC + DC) namely the morphology and volume fraction of the MC and the size, shape and distribution of the DC in controlling corrosion e.g. plate like morphology and a large volume fraction of the MC had an adverse effect in spite of the austenite matrix being favourably disposed in improving corrosion resistance. Similarly a favourable morphology of MCs (1000°C, 10 hrs and 1050°C, 10hrs treatments) reduces the adverse effect. Heat treating between 900-950°C adversely affected corrosion resistance due to the presence of needle shaped DSPs and also due to diverse nature of the DSPs present(needle and spherical particles) and matrix heterogeneity. Interestingly, all the three alloys on heat treating from 1050°C(10 hours heat treatment) attained corrosion rates comparable to those attained in standard SG/Flake graphite Ni-Resist compositions. This analysis has enabled laying down of guide lines for developing improved corrosion resistant microstructures.

In the study involving modelling of the corrosion behaviour (interrelating corrosion rate with the microstructure), the models developed in recent studies were critically examined.

(i)   The first model interrelating corrosion rate with the total volume fraction of MC+DC and the number of particles (NOP) was of the form :

CR = [C1 + C2 (VCb) + C3 (VCb)^2] (NOP)^{C4}

where, VCb = volume of carbides (MC+DC)

CR = corrosion rate in mdd

C1, C2, C3 and C4 are constants which were different for different alloys.

(ii)   The second one is:

$$CR = [C1' + C2' (VMC) + C3' (VMC)^2] (NOP)^{C4'}$$

Where, VMC = volume fraction of MCs only

(iii) and the third one is:

$$CR = [C1'' + C2'' (VMC) + C3'' (VMC)^2] (DF)^{C4''}$$

Where, DF = newly evolved term distribution factor(DF) defining DCs

In the present study, the final models arrived at were similar to those type (ii) and (iii) mentioned above. However a greater emphasis was laid on reexamining the various constants and particularly the character of the term $(DF)^{C4}$ duly ensuring that the magnitude of the constants was assessed after normalization.

On comparing the predictions based on the various models, it appeared that inconsistencies, if any, were not of much consequence. This became further evident on constructing 3D-plots between CR, VMC & NOP and CR, VMC & DF. The problem, if any, arose because it was difficult to keep VMC a constant and vary NOP/DF or vice-a-versa. None the less, the 3D-plots proved extremely useful in arriving at the optimal values of VMC/DF or VMC/NOP to obtain the best in terms of corrosion resistance in each of the experimental alloys. The data thus generated formed the basis of optimizing the microstructure and proved extremely helpful in developing a unified model(a single model) describing the corrosion behaviour of all the experimental alloys.

From the point of view of mechanical properties even the as-cast microstructure responded favourably. The austenite bearing

microstructures containing needle type DSPs were somewhat brittle and were characterized by lower compressive strength(CS) and %strain. The austenite based microstructures generated on heat treating from higher temperatures attained high values of compressive strength and %strain. The key parameter in influencing the deformation behaviour was the amount and stability of austenite. The effect of massive carbides on the deformation behaviour was a function of the compatibility, volume fraction and morphology while the effect of DC was governed by their size, shape and distribution.

Mathematical models were developed interrelating (i) CS with hardness and (ii) %strain with hardness. The model thus obtained is similar to the one obtained in an earlier study on similar alloys but in the oil quenched condition.

The relation which comprised a second order polynomial is :

$$R = A1 + A2 \ (H) + A3 \ (H)^2$$

where R = CS/H or %strain/H

H = hardness

A1, A2 and A3 are constants.

This correlation proved useful in characterizing some of the microstructures in the present study whose mechanical properties were not assessed.

PREFACE

The thesis comprises a total of seven chapters. The first chapter deals with a critique on wear, corrosion and high temperature resistant alloyed & unalloyed cast irons. While summarizing this information, the possibilities of evolving a 'unified approach' to develop cast irons exhibiting wear/corrosion/high temperature resistance was mooted. Major deductions resulting from an appraisal of the aforesaid information pointed to the possible utilization of Fe-Mn-Cr-Cu system for achieving the aforesaid objective. Accordingly, the chapter II is devoted to a discussion on the Fe-Mn-Cr-Cu white irons culminating in the formulation of the problem, the design of experimental alloys & planning of experiments.

Chapter III deals with the experimental techniques and procedures employed with major emphasis on the X-ray diffracto-metry, EPMA, DTA, corrosion testing, compression testing, and quantitative optical metallography.

Results and discussion have been divided into three chapters. Chapter IV includes the effect of heat treating parameters on the hardness and microstructure characterized qualitatively as well as quantitatively. This has led to the development of a number of models and some new ideas encompassing 'quantitative characterization of 2nd phase particles' and 'homogeneity/heterogeneity' of the alloy(s)/system.

Chapter V deals with the (i) structural investigations by X-ray diffractometry and EPM analysis to carry out a detailed phase

analysis and for assessing the partitioning behaviour of Mn, Cr, Si, and Cu into the matrix, massive carbide, dispersed second phase(spherical & plate like) and the hitherto unobserved grey etching phase(formed on heat treating from 1000°C and (ii) study of the transformation behaviour of the alloys by DTA primarily to assess the suitability of selected microstructures for high temperature applications.

Chapter VI is devoted to an assessment of the deformation behaviour of selected microstructures in the as-cast and in the heat treated conditions by compression testing, electro-chemical characterization of selected microstructures by potentiostatic and weight loss methods, and a study of the corroded specimens by scanning electron microscopy.

A salient feature of the present study has been the development of a number of mathematical models interrelating the

(i) heat treating parameters with the hardness,

(ii) microstructure (especially the effect of second phase corresponding MC & DC) with the corrosion rate,

(iii) temperature with the oxidation behaviour (characterized by weight gain) in air,

(iv) hardness with the compression strength,

(v) hardness with the %strain,

(vi) compressive strength with the corrosion behaviour,

(vii) %strain with the corrosion behaviour.

(viii) distribution of the massive & dispersed second phase with homogeneity/heterogeneity

(ix) size distribution of the dispersed second phase with coarsening

Based on the above findings, conclusions have been drawn with regard to the transformation behaviour of the alloys under various heat treating conditions and the suitability of different microstructures from the point of view of corrosion resistance, mechanical properties and high temperature oxidation behaviour finally leading to the optimization of microstructure for obtaining the aforesaid properties. They(conclusions) are enumerated in the chapter VII.

The key features of the present investigation are (i) the development of corrosion resistant cast iron having corrosion resistance comparable to that obtained in the conventional Ni-Resist cast irons with an additional advantage of improved mechanical properties, (ii) defining a new parameter to represent the homogeneity/heterogeneity of the structure, (iii) development of several 'models' very useful for optimizing microstructure & for quantifying structure-property relations, and (iv) extensive use of computational techniques and the development of application software, of immense use for materials development/ characterization, for the IBM compatible PC-AT & PC-486 systems.

CONTENTS

LIST OF TABLES

LIST OF FIGURES

CHAPTER I

LITERATURE REVIEW

WEAR, CORROSION, AND HIGH TEMPERATURE RESISTANT CAST IRONS

1.1 INTRODUCTION

Cast irons are Fe-C-Si alloys that contain minor(<0.1%) and often alloying(>0.1%) elements and are used in the as-cast/heat treated condition(s)(1). They contain between 2 and 6.67% carbon and commonly within the range of 2.5 to 4% since higher levels induce brittleness(2).

Cast irons are most extensively used casting alloys due to their ability to produce complex shapes at relatively low cost and to attain a wide range of properties through careful control of chemical composition, solidification process and heat treatment. This makes them an ideal choice for a number of applications.

1.2 ELEMENTS IN CAST IRONS(2-3)

The presence of carbon in the combined form(as carbide) or in the free form(as graphite) has a major influence on the physical and mechanical properties. The term total carbon represents the sum of the free and combined carbon(including carbon in solution). For the Fe-C alloys, the eutectic occurs at 4.3% carbon. Alloys above this carbon level are termed hyper-eutectics and those below it as hypo-eutectics. The hyper-eutectic compositions may develop coarse open-grained structure and comparatively large flakes of "kish" graphite when cooled slowly. Hypo-eutectic alloys, on the other hand, attain relative-

ly fine graphite and denser and tighter structures. The aforesaid tendencies become more marked as the carbon content of the hyper-eutectics is raised and that of the hypo-eutectics lowered.

Presence of unintentionally added elements affects the solubility of carbon. Both silicon and phosphorus(essentially the impurity elements) reduce the eutectic carbon by 0.3% for each 1 weight percent addition through a lowering of the solidification temperature. The "carbon equivalent" concept incorporates and serves as a basis to define and characterize cast irons. Carbon equivalent(CE) is given by the expression,

$$CE= \%C + (\%Si + \%P)/3$$

For alloyed irons, the expression would also include effect(s) from other elements.

Addition of silicon shifts the eutectic composition to the left and lowers the eutectic temperature. Silicon is a graphitizer, and if not counterbalanced by carbide- former(s), favors solidification according to the stable iron-graphite system wherein carbon is precipitated as primary flake graphite. Once this has happened, its shape can not be altered by any method. It is these weak graphite flakes that break up the continuity of the matrix and the notch effect at the end of these flakes accounts for the low strength and low ductility of grey irons.

The main function of manganese in cast irons is to counteract the undesirable effect of sulphur by forming manganese sulphide inclusions. Manganese sulphide is lighter than iron sulphide and tends to float out of the molten iron as slag. Iron sulphide is retained in the melt and deposited around the grain boundaries inducing 'hot shortness' and enhanced tendency to

2

cracking. Manganese in excess of that required to combine with the sulphur stabilizes carbide. This leads to an increase in the chilling tendency and therefore the hardness. As will be made evident, manganese can play an effective role in developing alloyed irons.

Sulphur has a marked hardening influence. It increases stability of the iron carbide and also the chilling tendency. Aside from its carbide forming tendency, sulphur tends to react with iron to form iron sulphide(FeS). This low-melting compound, present as thin interdendritic layers, increases the possibility of cracking at elevated temperatures(red-short). High sulphur tends to reduce fluidity and often is responsible for the presence of blow wholes(trapped air) in castings.

Fortunately, manganese has a greater affinity for sulphur than iron, forming manganese sulphide(MnS). The manganese sulphide particles appear as small, widely dispersed inclusions which do not impair the properties of castings. It is common commercial practice to use a manganese content two to three times the sulphur content.

Phosphorus has limited solubility in austenite and segregates positively during solidification. This can result in phosphide formation in the last areas to solidify. Phosphides are similar to carbides. They cause machining problems but are not eliminated by heat treatment. The eutectic has a relatively low melting point(960°C) and consequently phosphorous bearing irons have better fluidity. High P content has been associated with the segregation of Mo, Cr, V and W. This leaves areas of the matrix

3

depleted in these elements and reduces strength. 'Phosphide eutectic liquid' at cell boundaries creates a mushy state that is difficult to feed. This condition creates high eutectic solidification forces within the outer solidifying shell, causing mould wall movement and a requirement for feed metal in the final stages of solidification. This can lead to shrinkage porosity. Phosphorus increases fluidity and extends the range of eutectic freezing, thus increasing primary graphitization when the silicon content is high and phosphorus content is low. It is therefore useful in very thin castings where a less fluid iron may not take a perfect impression of the mould.

Phosphoric cast irons exhibit **improved wear resistance** and **good** resistance to severe corrosive attack, notably from hydrochloric, sulphuric and acetic acids.

The three elements discussed so far, although considered as **subsidiary elements**, none the less have a **major influence** on the soundness of castings. Once they are taken care of, it becomes relatively simpler to add the 'main' alloying elements for the specific effects(s) they impart. Extensive information is available on the effect of Ni, Cr, Mo, V, W, Mn, Mg, Ce, Si, and Al additions on the properties of different grades of cast irons. As such these effects are not being separately discussed and would be considered as a part of the discussion on different grades of cast irons.

1.3 CLASSIFICATION

Depending upon whether carbon is present in 'free form'(as graphite) or 'combined form'(as carbide), there are two broad categorizations namely 'grey' and 'white' irons. Extensive lite-

rature is available on cast irons, but since the present work falls in the area of 'white irons', the discussion below is mostly confined to 'white irons'.

1.4 WHITE CAST IRONS

White cast irons, so named because of their characteristically white fractured surfaces, are free from graphite and carbon is present in the form of massive carbides(4). White irons are hard and brittle. They have high compressive strength and good retention of strength and hardness at elevated temperatures, but are most often used for their excellent resistance to wear and abrasion.

White irons can be classified as (i) plain carbon and (ii) alloyed white irons and are discussed in detail below.

1.4.1 Plain carbon white irons

Plain carbon or unalloyed white irons, have a microstructure of continuous massive ledeburitic carbide(Fe_3C) in a pearlitic matrix. A large tonnage of unalloyed white irons is used as a starting material for the manufacture of malleable irons.

Unalloyed white irons are also extensively used in certain applications requiring abrasion resistance. However, the main restriction to their use is their extreme brittleness. This can be improved somewhat by maintaining phosphorous to low levels (below 0.1% is needed for significant improvement) and also by keeping carbon content to ≤ 3%. A further improvement in toughness is also brought about by the addition of up to 0.5% chromium. This enables a graphite- free structure to be achieved in thicker sections. The main advantages of unalloyed white irons

5

are their relatively low price and, to a lesser extent, the fact that they can be melted in cupola(5).

Reverting to their industrial relevance, the **high hardness** (410-470 HV) associated with unalloyed white irons makes 'abrasion resistance' as their **main area of application**(3,6,7). In these materials, hardness increases with an increase in the carbon content. Even then hypoeutectic white irons are most extensively used since hypereutectic compositions contain 'undesirable' free Fe_3C plates. Their microstructure comprises pearlite + carbide, the microhardness of the constituents being 200-300 HV and 800-1000 HV respectively. Hardness can be controlled by controlling the proportion of these constituents through a control of carbon content/carbon equivalent(3,6,7). For most applications, a carbon content 3% is considered as an optimum.

Factors which determine whether a given composition **casts 'white'** are the **C/Si** balance, the **solidification** process and the **cooling rate.** The combined effect of these parameters is summarized into a single diagram called the 'Maurer **diagram'** [Figure-1.1](8). It in fact serves as the basis for designing plain carbon white iron compositions. The favourable effect of a high C/Si ratio in ensuring the formation of a white iron structure can be further accentuated by employing **chilling.** However, there are practical **limitations** to doing so. Representative compositions, properties, and applications of plain carbon white irons are summarized in Table-1.1(6,9-10).

Due to a limitation on the **maximum attainable hardness,** unalloyed irons are used in less **rigorous abrasive** conditions eg. as liners for cement mixers, ball mills, certain types of drawing

dies, and extrusion nozzles.

1.4.2 Alloyed white irons

Development of alloyed white irons dates back to 50 years. They are iron-carbon-silicon alloys that contain one or more of the alloying elements intentionally added to attain specific properties such as resistance to corrosion, heat or wear and to improve upon mechanical properties in general(2).

1.4.2.1 Chromium white irons

The practical limitations in ensuring that a given plain carbon white iron composition is cast 'white' over a range of section sizes have been overcome by developing chromium white irons(3,6,9-11). Controlled additions of chromium can most effectively and economically ensure that a composition is cast white(independent of cooling rate and section size). This is attributed to its carbide forming/stabilizing tendency(12,13). Chromium forms complex carbides which are harder than cementite and thus improves wear resistance. Chromium carbides tend to be more compact and do not form the 'cellular eutectic' structure attained in unalloyed white irons.

1.4.2.1.1. High chromium/Straight chromium irons

The first recorded patent of a white iron alloyed with chromium was granted in 1919. Chromium by virtue of being a carbide former markedly influences the behaviour of cast irons and when present in large amounts imparts outstanding wear, corrosion and heat resistance.

There are two principal reasons for the success of high chromium irons. Firstly, the modification of the iron-carbon

7

solidification process at approximately 12% chromium leading to the formation of chromium carbides(Cr_7C_3) in place of the iron carbides(Fe_3C). Not only are chromium carbides harder, and thus more wear resistant than iron carbide, but their morphology is 'favourable', resulting in a significant improvement in toughness. Chromium carbides are more compact and do not form the 'cellular eutectic' as in unalloyed white irons. Secondly, the matrix structure of high chromium irons can be varied to suit individual application requirements, starting from a completely austenitic work hardenable matrix, to a fully heat treated martensitic matrix(4).

Depending upon the chromium content, the high Cr- irons may be divided for practical purposes into three groups(14):

(i) 15-17% Cr for heat and wear resistance applications

(ii) 26-28% Cr for abrasion resistance applications

(iii) 30-35% Cr for heat and corrosion resistance applications

The remainder of the composition of the iron is adjusted to suit a particular area of application.

Typical compositions and properties of some representative (abrasion & wear resistant) chromium cast irons are shown in Table-1.2(6,10). Table-1.3(6,9-10) summarizes information on alloys used for corrosion resistant applications.

[A] Carbide morphology in high chromium cast irons and their effect on properties

As a class of alloyed irons, high chromium irons are characterized by the presence of a hard and a relatively discontinuous M_7C_3 primary or eutectic carbide, or both, as against the softer, relatively continuous M_3C carbides present in low chro-

mium alloyed irons and the continuous M_3C eutectic in unalloyed white irons(15). The carbides present in the Fe-Cr-C system as indicated in Figure-1.2 are of M_3C, M_7C_3 and $M_{23}C_6$ types(16,17).

M_3C is a continuous ledeburitic type carbide and forms when the Cr content is below about 6%. It assumes a less continuous form when Cr is 8-9%. More recent work suggests(18) that at these Cr levels, the eutectic carbide is a duplex carbide comprising an inner core of M_7C_3 and an outer shell of M_3C which is formed during the solid state cooling in the mould. It may be that the $(Cr,Fe)_7C_3$ carbide forms first by the same eutectic reaction as that in high chromium white irons and it controls the subsequent growth of the $(Fe,Cr)_3C$ carbide from the melt either by a peritectic or by an eutectic transformation(18).

Three dimensional studies carried out on M_7C_3 carbides by Powell(19) suggest that the true carbide morphology is fibrous, the fibers being hexagonal in cross section with adjacent fibers frequently attached together to form blades. The high hardness (1600 HV) of this carbide and its relatively 'enhanced discontinuity' within the eutectic colony result in an optimum resistance against wear and impact.

When chromium content of the cast irons is greater than about 10%, eutectic carbides of the M_7C_3 type are formed in preference to the M_3C. More significantly, the higher chromium content alters the solidification pattern so as to yield a microstructure in which the M_7C_3 carbides are surrounded by a matrix of austenite or its transformation products. Because of the changed solidification characteristics, hypoeutectic irons containing M_7C_3 carbides are normally stronger and tougher than

irons containing M₃C carbides(20).

The high Cr-irons(21) are most frequently used in the heat treated condition, in which the austenitic as-cast matrix is rendered less stable by the precipitation of secondary carbides at high temperatures so as to enable its transformation to martensite on cooling. However, some alloys, namely the 27% Cr white irons, are frequently used in the austenitic condition to utilize the amenability of the matrix to work hardening(as in Hadfield steels) even though the service conditions may not entail severe impact loading.

Referring to the liquidus surface of the Fe-Cr-C metastable system(16,17,22) shown in Figure-1.2, the compositions used in high-Cr irons are so chosen that the C and Cr contents are within the austenite(τ) or M₇C₃ 'liquidus field boundaries' so that the binary eutectic solidification comprising τ + M₃C or τ + α is avoided. Compositions meeting these requirements are indicated by the shaded area in Figure-1.2 and essentially constitute ASTM A 532-75 specifications for abrasion-resistant cast irons. As indicated by Figure-1.2, solidification in hypereutectic high-Cr irons(i.e. those with compositions within the 'M₇C₃ carbide liquidus field boundaries') occurs by crystallization of primary M₇C₃ carbides followed by freezing of the eutectic comprising τ + M₇C₃. In hypoeutectic high-Cr-irons(i.e. those with compositions within 'the austenite liquidus field boundaries') solidification occurs by crystallization of austenite dendrites followed by freezing of the eutectic comprising τ + M₇C₃.

Austenite is stable at high temperatures(refer the isother-

mal sections(22,23) in Figure-1.3) but upon cooling under equili-
brium conditions will transform to ferrite plus carbide at some
temperature above 700°C. However, on continuous cooling, auste-
nite formed during solidification becomes supersaturated in C and
Cr. This factor, along with the presence of other alloying
elements such as Mo, Mn, Ni and Cu which affect the transfor-
mation kinetics of austenite would decide whether austenite is
retained to room temperature, or partially/ completely decomposed
into α/carbide, or transforms to martensite.

For example, in 50 mm Y-block castings, an iron containing
normally 2.7%C-27% Cr will have predominantly austenitic matrix
microstructure in the as-cast condition while irons containing
2.7% C and either 15 or 20% Cr will have pearlitic matrix stru-
ctures(22).

High chromium cast irons have been well-known for their
abrasive wear resistance. Typical applications are materials such
as balls, liners, rollers, rings for pulverizer mills, impeller
blades for shotblast equipment and impact crushers, dredge pump
parts and wearing parts for steel making plants(24).

In high chromium irons, the type and the amount of (a)
carbide, and (b) solid solution precipitating as primary phases
or as eutectics, vary widely with chromium and carbon contents
(24). From the Fe-Cr-C diagram(Figure-1.2) the carbide crystalli-
zing from the molten irons containing 9% Cr is M_3C. Above this
level M_3C gives way to $M_{23}C_6$ through an intermediate carbide M_7C_3
and the extent to which this change occurs depends upon the
chromium content. Each carbide has its own hardness(Tables 1.4a &
4b)(25-27) and morphology. Generally, abrasion resistance

increases with an increase in **material hardness**, which in turn is influenced by microstructural features such as the volume fraction of carbide, its morphology and the structure of the matrix.

On the other hand, as the **toughness of cast irons is also** affected by the microstructure, **high chromium** cast irons, which contain discontinuous eutectic carbides of the type M_7C_3 in a matrix, have a higher toughness than low alloyed white irons attaining continuous M_3C carbides. Therefore, it is expected that control of the shape, size and distribution of eutectic carbides should not only improve their toughness but their abrasion resistance.

The **carbides** in the microstructure, depending upon their type morphology and volume fraction, provide the **hardness** required for **crushing materials** without degradation. The supporting matrix microstructure, which controls the abrasion and crack propagation characteristics, can be controlled by alloy content and/or heat treatment to develop pearlitic, austenitic or martensitic structures to provide the most cost effective balance between abrasive wear resistance and toughness(28). Composition and properties of some representative chromium white irons are listed in Table-1.3(6,10).

The **complex dependence** of **wear** on **microstructure** is illustrated in a recent study on the grinding abrasion resistance of Cr irons in the as-cast and heat treated conditions(29). A martensitic matrix displayed higher abrasion resistance than austenitic or pearlitic matrix structures. The 10-15% Cr irons were more resistant than 25-30% Cr irons due to the low C

martensite produced on reducing the stability of the higher Cr irons. The 5% Cr irons exhibited a good wear resistance than the 10-15% Cr irons. This was because cracking in the carbide phase did not lead to its immediate removal from the structure due to the 'continuous' structure of the carbide as in the 5% Cr irons. On the other hand the fractured carbide rods in the 'disconti- nuous' eutectic in the 15% irons became detached readily during wear.

These findings differed when impact loading accompanied wear. Under these conditions, structures with continuous carbides showed insufficient toughness and suffered gross fracture. However, a microstructure with a discontinuous eutectic withstood impact loading effectively and gross failure was avoided at the expense of greater wear, particularly if the carbide is not adequately supported by a hard matrix.

The straight high Cr irons must have a high C content and a martensitic matrix for good wear resistance. Although these irons are cheaper than Ni-Hards, their limited hardenability restricts their use to moderate to thin section castings such as pump volutes and slurry pump impellers. The matrix structure is predominantly pearlite in heavy sections and austenite in lighter sections. The lower the Cr to C ratio, the greater is the tendency for pearlite formation and if pearlite is to be avoided eg. in a 25 mm section, the C content must be restricted to 2.8%. The limitation of this class of irons can be overcome by further alloying(28).

[B] Corrosion Resistance of High Chromium Irons

The excellent corrosion resistance of the high chromium

irons is attributed to the chromium oxide film on the casting surface, and their behaviour in a corrosive media depends on whether the film is formed or repaired more rapidly than it is broken down. Oxidizing agents e.g. nitric acid, maintain the oxide film, while reducing conditions give rise to rapid attack(14).

To ensure maximum corrosion resistance the overall chromium content should exceed the amount required to form carbides by at least 10%, approximately 10% of chromium being required for each 1% of carbon(14).

An improvement in the corrosion resistance is attained through Si and Mo additions by refining the carbides(30,31). This leads to the development of a more continuous oxide film over the metal surface. Molybdenum may alternatively enhance corrosion resistance by displacing some of the Cr by combining with the carbon, thereby increasing the Cr content of ferrite(30). Typical compositions and mechanical properties of corrosion resistant Cr irons are listed in Table-1.3(6,9,10,27)

High chromium irons containing from 20 to 35% chromium give good service in oxidizing acids, particularly nitric, but are not resistant to reducing acids. These irons are also reliable for use in weak acids under oxidizing conditions, in numerous salt solutions, in organic acid solutions and in marine or industrial atmospheres.

High chromium cast irons exhibit excellent resistance to corrosion in nitric acid in all concentrations up to 95% at room temperature. Its corrosion rate is less than 0.15 mm(0.005 in.)

per year at all temperatures up to the boiling point for concentrations up to 70%. In handling nitric acid, the chromium irons are complementary to high-silicon irons- the former exhibit excellent corrosion resistance at all concentrations and temperatures, except in boiling concentrated acids, whereas the latter give better results in stronger acids. The low-carbon, high-chromium irons are satisfactory for annealing pots; lead, zinc and aluminium melting pots, conveyor links, and other parts exposed to corrosion at high temperature. Because the corrosion resistance is imparted by chromium present in solid solution in the ferrite matrix, this element must be present in sufficient quantity to combine with carbon as chromium carbide and still remain in the 'desired' amount in the ferrite so as to affect passivity. Chromium contents of 30 to 33% are common in irons for use under conditions of severe acid corrosion(32).

Aqua-regia corrodes the alloys, although Kuttner(31) has reported that an increase in the Cr content according to the formula %Cr = (%C X 5) + 36 may prove effective in inducing resistance to aqua-regia.

High chromium irons are resistant to all concentrations of sulfurous acid up to 80°C, to sulfite liquors used in the paper making industry, to hypochlorite bleaching liquors at room temperatures, to cold aluminium sulfate in concentrations up to 5%, and to some salts that hydrolyze to give acid solutions. They resist all concentrations of phosphoric acid up to 60% at temperatures up to the boiling point and 85% concentrations up to 80°C. They also have good resistance to aerated seawater and most mine waters, including acidic types(32).

Increasing use is being made of high chromium cast irons (33-34) for applications at high temperatures as well as moderate to high temperatures where their high resistance to abrasion, wear, and corrosion is well known. Besides their excellent corrosion resistance, these irons can be centrifugally cast as tubes and are inexpensive compared to wrought high alloy steels despite their high chromium content.

[C] Heat resistance of high Cr irons

The excellent heat resistance of high chromium irons(14) is due to the formation of an adherent oxide scale which reduces further progressive oxidation to a minimum, and the rigidity and stability of iron chromium carbides which do not break down on exposure to high temperatures. For an iron containing 3%C, 2.25%Si, the chromium contents to give adequate scaling are 12% which is satisfactory up to 840-850°C, 15-17% Cr which is satisfactory up to 900°C, 25% Cr up to 980°C and a 33% Cr iron up to 1050°C.

High Cr white irons offer excellent resistance to growth and oxidation at elevated temperatures and are cost effective alternatives to stainless steels in applications that are not subjected to severe impact loading(28).

For developing resistance to the softening effect of heat, and for protection against oxidation, chromium is the most effective element. It stabilizes iron carbide and therefore prevents breakdown of carbides at elevated temperatures. 1% chromium gives adequate protection against oxidation up to about 750°C in many applications. For temperatures above 750°C, the chromium content

should be greater than 15% for long-term protection. This percentage of chromium suppresses the formation of graphite and makes the alloy solidify as white cast iron(35).

Chromium cast irons have better mechanical properties than those of high silicon irons and respond better to heat(32).

Mechanical properties

The high chromium irons are hard but machinable unlike high silicon irons. Lowering the carbon content to 1.2%C improves their shock resistance(36).

1.4.2.1.2 Chromium-Molybdenum White Cast Irons

Large tonnages of high chromium molybdenum(Cr-Mo) irons are currently being produced(22) for castings which require a combination of abrasive wear resistance and toughness not obtainable in other alloyed white irons or steels. These castings are being used in equipment for the mining industry, coal and mineral processing, the cement industry and in other large castings such as rolling mill rolls. High-Cr-Mo irons are giving reliable performance in large impact hammers, mill liners and pulverizer rolls, applications where other alloyed white irons have proven too brittle. They have also replaced considerable tonnages of steel castings which had good toughness but lacked adequate abrasion resistance.

Experience has shown that high-Cr-Mo irons exhibit the best combination of abrasion resistance and toughness, particularly resistance to spalling and fracture under conditions of severe repeated impact, when they are heat treated at high temperatures 950-1060°C and cooled(or quenched) to obtain a martensitic matrix. However, cast irons with either austenitic or austenitic-

17

martensitic matrix microstructures have been used successfully for castings which do not encounter severe impact in service. The most obvious advantage of using high-Cr-Mo irons in the as-cast condition is the cost savings and energy conservation that results from eliminating the high-temperature heat treatment. In addition, less complex production techniques can be used for producing large, intricate castings which ordinarily show a tendency to cracking during conventional high-temperature heat treatment(22).

High-Cr-Mo irons are used for abrasion-resistant castings ranging in size from very small- 12 mm(0.5 in.) diameter grinding balls up to massive- 335 mm(14 in.) thick table segments for roller pulverizers but in recent years more attention has been focussed on the production of thick-section castings.

The high chromium-molybdenum white cast irons(37) have substantially improved toughness over that of the unalloyed white irons, high chromium irons, and high nickel martensitic irons mostly due to improved carbide morphology and distribution. These alloys have stood to benefit from the superior abrasion resistance provided by the M_7C_3 chromium carbides in applications such as grinding balls and ball mill liner plates where high impact loading is observed.

An expression for the volume fraction of M_7C_3 carbides formed during solidification is given by Maratray(38),

Volume % Carbides = 12.33(%C) + 0.55(%Cr) - 15.2

The volume % carbides given by this expression includes both primary and eutectic M_7C_3 carbides. The fraction of primary vs.

18

eutectic carbides depends upon whether the alloy is hypoeutectic or hypereutectic relative to the liquid-M_7C_3- austenite three phase field in the Fe-Cr-C system as illustrated in Figure-1.4 (37,39). The liquidus surface in the Fe-Cr-C ternary system is given in Figure-1.5(37-38). This diagram illustrates the influence of chromium and carbon contents on the nature of the carbide and matrix phases.

The addition of molybdenum to high chromium white irons suppresses the decomposition of the austenitic matrix to form pearlite. Figure-1.6(37-38), illustrates the influence of the Cr/C ratio and the molybdenum content on the as-cast matrix microstructure of 25-mm diameter round bars. The addition of molybdenum enables the retention of an austenitic matrix at lower Cr/C ratios. Maratray and Usseglio-Nanot(40) concluded that one-half of the molybdenum in the alloy forms the carbide(Mo_2C), one-fourth dissolves in the M_7C_3 carbide, and the remaining one fourth remains in the matrix.

The chromium-molybdenum white irons may be heat treated to produce a martensitic matrix by soaking for 4 hours at a temperature of 982°C, followed by an air cool. The high temperature soak allows the precipitation of M_7C_3 carbides to relieve the supersaturation of carbon and chromium, and — the matrix to transform to martensite on cooling, Dodd, et al, have shown that the martensite transformation is not complete and up to 40% austenite may remain in the microstructure(15,17,37).

Taking an overall view, Cr-Mo cast irons further improve upon the salient features of the high Cr irons namely, superior abrasion resistance, better toughness as well as corrosion and

oxidation resistance with the added flexibility to attain the non-equilibrium matrix microstructure with much greater ease.

Compositions and properties of some prominent Cr-Mo cast irons are summarized in Tables 1.5a,1.5b,1.6a & 1.6b(4,6,10,28).

1.4.2.2 Ni-Cr White Irons

These alloys were developed by the International Nickel Co. (INCO) and are available in four different grades - the lower alloy versions designated as Ni-Hard 1,2,3 and the highest alloyed version as Ni-Hard 4. Their composition and properties are listed in Table-1.7(10,41).

Ni-Hard cast irons are essentially Ni-Cr alloys possessing outstanding resistance to wear. Their use in the mining, power, cement, ceramic, paint, dredging, coal, coke, steel and foundry industry is now well established as an outcome of the experience gained over nearly fifty years.

When added to low-chromium white iron(35) in amounts up to about 2.5%, nickel produces a harder and finer pearlite in the structure, which improves its abrasion resistance. Nickel in somewhat larger amounts- up to about 4.5% - is needed to completely suppress pearlite formation, thereby ensuring that a martensitic iron results when the castings cool in their molds. This latter practice forms the basis for production of the Ni-Hard cast irons(which are usually identified in standard specifications as nickel-chromium martensitic irons). With small castings such as grinding balls, which can be shaken out of the molds while still hot, air cooling from the shake out temperature will produce the desired martensitic structure even when the nickel

20

content is as low as 2.7%. On the other hand, an excessively high nickel content(more than about 6.5%) will so stabilize the austenite that little martensite, if any, can be formed in castings of any size. Appreciable amounts of retained austenite in Ni-Hard cast irons can be transformed to martensite by refrigerating the castings at -55 to -75°C, or by the use of special tempering treatments(35).

Ni-Hard cast irons possess a matrix microstructure akin to heat treated steel. In addition, they contain a multitude of refined carbides which make an important contribution to their wear resistance(41).

Ni-Hard types 1 and 2 which contain relatively lower amounts of Ni and Cr were primarily developed as higher hardness wear resisting materials, their fundamental property being high hardness. Microstructurally they comprise bainite/tempered martensite + carbide(41-42). An important observation concerning Ni-Hard 1 & 2 is that their shock resistance in general is low. However, the shock resistance of Ni-Hard irons particularly of the low carbon and heat treated varieties is substantially better than unalloyed white cast irons.

A modified version of Ni-Hard 1 & 2 containing higher proportions of Ni and Cr and designated as Ni-Hard 4 was developed by INCO around the mid-fifties(41-42). The main objective in doing so was to improve the resistance to fracture under repeated impact. In view of a higher alloy content, the Ni-Hard type 4 variety is harder and has a greater resistance to corrosion.

Dawson(43) studied a series of 16%Cr-3%C white irons with varying nickel contents(0 to 16%Ni) in terms of their response to

annealing and hardening treatments. Full annealing(at 925°C for 3 hours) of 1½% Ni alloy resulted in a machinable pearlitic structure(Rc 36); air cooling an 8% Ni alloy resulted in an austenitic structure of the same hardness which was difficult to machine. Air hardening experiments showed that 1½% Ni irons could be hardened to 60 Rc in 75-mm section sizes and abrasion tests confirmed that iron was comparable to the best commercial alloys listed in ASTM-A 532.

[A] Carbide morphology in Ni-Hard irons

The morphology of eutectic carbides are identical in type I, type II, and type III Ni-Hard irons. It reveals massive and continuous M_3C type of carbides. But the type I alloy is inferior to the rest in respect of shock resistance on account of its maximum carbon content.

Ni-Hard type 4 possesses the highest strength and greatest resistance to impact of all the Ni-Hard varieties. The better resistance to fracture in Ni-Hard 4 as compared with Ni-Hard 1 and 2 is due to the presence of carbides in a discontinuous and less massive form(41). The dispersed finer carbide has primarily been achieved by modifying the composition, principally in relation to Cr so that the carbide is in the form of a discontinuous trigonal carbide $(Cr,Fe)_7C_3$. As per a more recent appraisal, the attainment of a discontinuous and hard $(Cr,Fe)_7C_3$ carbide results from a high Cr content and the eutectic composition of the type 4. This together with the advantage of a lower carbon content and a somewhat tough high nickel matrix makes Ni-Hard type 4 a very useful abrasion resistant material(41).

According to Powell(19), the reason for the similarity of the carbide morphology in Ni-Hard IV alloy(8%Cr) with that in high chromium(17% and 27%) irons is not clear. It may be that in Ni-Hard type IV alloy, $(Cr,Fe)_7C_3$ carbides form first by the same eutectic reaction as that in high Cr irons, and this $(Cr,Fe)_7C_3$ carbide controls the subsequent growth of $(Cr,Fe)_7C_3$ carbides on it, either by the eutectic or peritectic transformation.

The difference in the eutectic structure in type I and IV alloys may be explained by the pseudo-binary phase diagrams (Figure-1.7)(44). From these diagrams the carbide contents in type I and IV have been estimated to be 50% and 31% respectively. By a special etching technique, it is observed that when both the phases are present in equal amounts in an eutectic phase, they are continuous in three dimensions. While on the other hand, if they are not in equal amount, the minor phase will be discontinuous and embedded in the major phase. So in Ni-Hard type IV alloy, the minor phase i.e. carbide (31%) will be discontinuous and embedded in the major phase i.e. austenite, just after solidification.

The chemical composition and properties of Ni-Hard type 4 are summarized in Table-1.7. Important changes brought about in the composition of the type 4 namely Ni=5 to 7% in place of 5.5-6.5%, Cr=7-11% as against 7-9% and Mn=1.3% maximum in place of 0.4-0.7% as per the recent literature published by INCO are noteworthy.

Besides the standard compositions described as Ni-Hard a number of other Ni-Cr white iron compositions are in use. Their representative compositions, properties and applications are

summarized in Table-1.8(6,10).

[B] Ni-Hard for elevated temperature service

Ni-Hard castings have demonstrated outstanding ability to resist abrasion at temperatures up to red heat(41). Tests have shown that sand cast Ni-Hard, which possesses a hardness level of 600 Brinell at room temperature, will maintain a hardness of approximately 475 Brinell at 480°C, thus accounting for its ability to resist abrasive and metal-to-metal wear at elevated temperatures. Ni-Hards can be considered for service at temperatures up to 815°C as long as operating conditions do not involve severely rapid or localized heating or cooling. Ni-Hard liner plates and flight segments can successfully resist the abrasion of cement clinker at temperatures up to 815°C(41).

1.4.2.3 Chromium-Manganese White Cast Irons

With a view to replace the costly alloying element nickel in Ni-Hard cast irons, a comparatively low priced element manganese has been recently tried in chromium cast irons(45). Manganese can be used successfully to suppress the pearlitic transformation in cast irons. In the as-cast condition the matrix of Cr-Mn cast irons can be either a mixture of pearlite, austenite and martensite or fully austenitic depending on the manganese content of the alloy. The corresponding carbide morphology is similar to that of high chromium cast irons i.e. of discontinuous M_7C_3 type. Manganese is a weak carbide former and partially joins the M_7C_3 carbides. Most of the reported Cr-Mn cast irons are with high chromium contents i.e. more than about 12% Cr except a few(46-47) with lower chromium contents(about 7%). In these reports(46-47)

beside the effect of manganese, the effect of copper has also been studied. The retained austenite content in the as-cast microstructure can be minimized by various heat treatments. Depending upon the service conditions, the austenitic alloys may in certain situations exhibit very good performance viz. in impact-abrasive wear applications. In this case, the austenitic matrix gets strained due to impact and subsequently gets transformed probably into strain induced martensite(48).

The microstructure(49) of the 15%Cr-0.0%Mn cast iron consists of pearlite and carbides of the $(Cr,Fe)_7C_3$ type. As the Mn content of the alloy increases, the pearlite/austenite ratio decreases, the matrix of 15%Cr-5.0% Mn iron being mainly austenitic. The eutectic carbides contain lamellar carbides radially starting from centers in the interdendritic spaces. The increase in Mn content influences carbide morphology e.g. a large proportion of lamellar carbides are also observed in a 15Cr-4.5Mn cast irons at room temperature. With differential etching, two different types of carbides are observed: some with dark-grey colour and the others with light-grey color. The dark carbides, revealed by Murakami etchant, are of the $(Cr,Fe)_7C_3$ type. They grew during eutectic solidification. The light-grey carbides also appear during eutectic crystallization, but later on, grow on the darker carbides. The light-grey carbides are not present in the structure at lower Mn contents. From the micro-probe examination, it was found that both carbides are chromium carbides. It was concluded that the difference in colour is due to different Cr contents, Mn partitioning being uniform enough(49).

1.5 GREY CAST IRONS

This group(2) comprises one of the most widely used alloys amongst cast irons. In the manufacture of grey irons, the tendency of cementite to separate into graphite and austenite or ferrite is favoured by controlling alloy composition and cooling rates. Most grey irons are hypoeutectic alloys containing between 2.5 and 4% carbon.

The strength of grey irons depends almost entirely on the matrix in which graphite is embedded. The constitution of the matrix may be varied from pearlite, through mixtures of pearlite and ferrite in different proportions, down to practically pure ferrite. The **graphite-ferrite** mixture provides the softest and **weakest** grey iron; the strength and hardness increase with the increase in combined carbon, reaching a maximum in the pearlitic grey irons. **Large graphite flakes** provide discontinuity to the pearlitic matrix, thereby reducing the strength and ductility. **Small graphite flakes are less damaging** and therefore generally preferred. For a given matrix morphology the key point in controlling the mechanical properties is the **graphite-flake morphology**, size, and distribution. This concept forms the basis of the graphite flake classification chart(28,50). Typical compositions, properties, and applications of high strength grey irons and the basis for developing them have been excluded as this information is already available and has been summarized in certain reports and recent publications(51-55).

Stress relieving is probably the most frequently applied heat treatment to grey irons. Annealing is carried out at 700-760°C to improve machinability. Grey irons, like steels can be

26

hardened when cooled rapidly or quenched from a suitable elevated temperature. Grey irons are usually quenched and tempered to increase the resistance to wear and abrasion by increasing the hardness. A structure consisting of graphite embedded in a hard martensitic matrix is produced by heat treatment. The combination of high matrix hardness and graphite as a lubricant results in a surface with good wear resistance for applications such as farm implement gears, sprockets, diesel cylinder liners, and automotive camshafts. Thus, **heat treatment extends the field of application** of grey irons as an engineering material.

Because grey iron casting are **least expensive**, it should always be **considered as a first option** when a cast metal is being **selected**. Another metal/alloy should be chosen only when the mechanical and physical properties of grey irons are inadequate. Examples of applications requiring a bare minimum of properties and lowest possible cost are counterweights for elevators and industrial furnace doors. These irons are widely used as guards and frames around hazardous machinery. Many types of gear housings, enclosures for electrical equipment, pump housings, and steam turbine housings are cast in grey irons because of their low cost. They are also used for motor frames, fire hydrants, and sewer covers.

Unalloyed grey cast irons(56) have from time immemorial been used for **heat-resisting applications**, typical instances being fire-grates, firebacks and gratebars. While the performance of these has been improved by the addition of small quantities of Ni and Cr, their life has not been sufficient to permit their wide-

spread use for the more critical engineering applications. The introduction of spheroidal graphite(SG) irons overcomes this limitation to some degree whilst further improvement was achieved through the additions of Si and Mo to these irons.

Typical compositions, properties and applications of **heat resisting grey** irons(unalloyed) are summarized in Table-1.9(28).

1.5.1 Alloyed grey irons

Some of the prominent commercial alloys used for **high temperature** and **aqueous** corrosion resistance applications have been considered. Their composition and mechanical properties are summarised in Tables 1.10a & 1.10b(27).

1.5.1.1 Silal(14)

Silal(14) or silicon-containing heat-resisting iron(s) were developed in the laboratories of The British Cast Iron Research Association in 1930. Although the silicon content can be varied over a wide range, it is recognized that **optimum properties are** obtained when it lies between **5 and 7%**. The general micro-structure of Silal comprises **graphite** in a completely **ferritic matrix**.

Size and distribution of **graphite flakes** largely determine the **extent of oxidation** occurring at elevated temperature; it is, thus, important to avoid the formation of hyper-eutectic 'kish' graphite in Silal. The carbon content at which such graphite forms decreases with an increase in silicon content.

For the production of a 5% silicon iron the **total carbon** content should be **less than 2.7%** and lower values will reduce the amount of graphite present and thereby improve mechanical properties.

28

The size of the graphite flakes produced has an important effect on heat resistance and in this respect **fine undercooled graphite** has been found to give the **best results.**

The amount of silicon to be added is dependent on the severity of the service conditions of the material, 5-6% being sufficient for normal use **up to 850°C.** Silicon increases oxidation resistance up to 6%, by forming a **passive oxide film** and then a **silicate film** which provides **resistance** to the transport of **oxygen atoms** into the metal and to the diffusion of metal atoms towards the surface. Silicon also **raises** the **critical temperature** at which ferrite transforms to austenite thereby expanding the useful temperature range of application with regard to **resistance** to growth. In amounts exceeding 5%, silicon reduces toughness and increases the brittle-ductile transition to above room temperature. So, **minimum** quantity of silicon should be used to prevent/resist growth. For **optimum** in terms of properties, the Si content should be **4.5-6.5%.** Such a composition is very well suited from room temperature to service temperatures up to 900°C. Increasing silicon content up to 4.5-5.5% is beneficial in (a) producing a completely ferritic matrix, thereby avoiding growth associated with the decomposition of pearlite; (b) a degree of surface passivation which, probably breaks down at higher service temperatures and (c) raising the critical transformation temperature(s), and thus avoiding the stress and growth associated with the ferrite —> austenite change.

For use at high temperatures the silicon content must be increased up to about 11%. The disadvantage of high silicon content is that the iron is weaker and more brittle at room temperature than a 5% silicon iron.

Although the applications of Silal are restricted due to its brittleness at room temperature, its useful heat-resisting properties and a relatively lower cost(compared with other heat-resisting cast irons) suggest that it could be put to better use. This is further facilitated because toughness is substantially improved with temperature, and above 280°C, their resistance to impact is better than ordinary iron.

1.5.1.2 Nicrosilal(14)

Nicrosilal was developed by the BCIRA in 1930 to provide a high silicon cast iron which was not brittle and with a heat resistance equivalent to or better than that of Silal. This was achieved by adding nickel and chromium to produce an austenitic matrix. The general microstructure of Nicrosilal comprises fine or undercooled graphite in a predominantly austenitic matrix. Areas of acicular chromium-rich carbides are also visible. Morphology of the carbides varies with the graphite structure, being acicular with the undercooled graphite, and relatively coarse and massive when random graphite flakes are produced.

Nicrosilal is a cast iron containing about 5% silicon having a low total carbon content of about 2%. The addition of nickel to this material has the effect that an initial hardening up to about 10% nickel is followed by a gradual softening of the material until a fully austenitic matrix is obtained. When silicon is present, the stability of austenite is reduced as

silicon lowers the solubility of carbon in austenite. To offset this it is usual to maintain the nickel at a minimum of 18% with a chromium content of at least 1.8%.

An excessively high silicon content or too low a nickel content can lead to the instability of austenite and also to the formation of silico-ferrite. To obtain optimum properties, the silicon level should be between 4.5 and 5.0%. The chromium content is usually about 2%, although it may be increased up to 4%, if extra heat or wear resistance is required. A small amount of the chromium enters into solution in the austenite, but the majority forms carbides which helps in strengthening the matrix.

The heat resistance of Nicrosilal is dependent on its high silicon content coupled with the presence of a stable austenite matrix. The amount of scaling at temperatures up to 800°C is, however, greater than in Silal and unless ductility is necessary there appears to be little point in the use of Nicrosilal at these temperatures. A further point to be considered is the instability of the austenite in the temperature range 400-700°C. Where the castings are held in this temperature range, there is a risk of martensite formation on subsequent cooling to room temperature; this will produce dimensional changes and embrittle castings. This tendency can be overcome by maintaining the silicon content at 4.5%, and increasing the nickel content to 22%.

Nicrosilal may be used at temperatures up to about 1000°C, although at this temperature its load-carrying capacity is very low. The scaling characteristics are superior to those obtained with Ni-Resist but are inferior to those of the 30% chromium irons.

1.5.1.3 High Silicon Irons

The matrix microstructure of the high silicon irons containing less than 15.2% Si consists of a silico-ferrite containing a distribution of fine graphite flakes(57). In irons containing more than 15.2% Si some n-phase is also present(30). The high hardness and brittleness of the silicon irons is due to the nature of the silico-ferrite. An attempt has been made to produce high Si irons with a nodular graphite structure for improving the mechanical properties(58). However, since the low strength is due to the brittle matrix rather than the graphite form, the nodular graphite silicon irons have not proved very popular. Compositions and properties of Si- irons are given in the Tables 1.10a & 1.10b(59).

Mechanical properties

These irons are characterized by a high hardness and low resistant to impact(Table-1.10b); machining is therefore, limited to grinding. Fabrication by welding is very difficult, although simple shapes like pipes can be welded if proper precautions are taken(6,30). Mechanical strength and shock resistance can be improved by lowering Si to 12%. This however, reduces resistance to corrosion.

[A] General Corrosion Behaviour

The excellent corrosion resistance of high silicon irons is due to an inert SiO_2 surface film which forms during exposure to the environment. The maximum advantage of protective film is achieved at Si contents >14.25%(30,60). These irons are extremely resistant to H_2SO_4, HNO_3 and organic acids, and least resistant

to hydrofluoric and sulphurous acids. High Si irons offer excellent resistance to attack by all concentrations of nitric-sulphuric acid mixtures. The addition of 3-3.5% Mo to an Fe-14.5% Si alloy results in the formation of extremely stable complex carbides with the consequent elimination of graphite(57). This is perhaps responsible for an improved corrosion resistance (57). Chromium also gives a similar beneficial effect. Good corrosion-erosion resistance is primarily due to its high inherent hardness.

High Si irons are inferior to the unalloyed grey irons when exposed to alkalies e.g. even to a weak base such as ammonium hydroxide, at liquid temperatures >20°C(30).

[B] Applications

These alloys are commonly employed as castings for pumps, valves and other process equipments. They have also found extensive use as anode for impressed current protection. They are used for fittings for concentrated sulphuric and nitric acids. They are used for making mixing nozzles, tanks, outlets and steam jets and for handling severe corrodents like chromic acid, sulphuric acid slurries, bleach solutions and acid chlorides slurries which are frequently encountered in plants that manufacture paper pigments, dyestuffs or those using electro-plating solutions(60).

1.5.1.4 High Nickel Irons or Ni-Resist Irons

These irons contain Ni ranging from 13.5 to 36%, Cr from 1.6 to 6% and Mo up to 1%. Occasionally Cu may also be present(Table-1.11a)(60-61). The microstructures consist of graphite flakes in a matrix of austenite and some carbide if Cr and/or Mo are present.

(i) Mechanical Properties

These. irons do not exhibit high strength and machinability is satisfactory due to the presence of graphite. Toughness/shock resistance is the best amongst all the alloyed cast irons due to austenitic matrix. **Strength and toughness** can be improved upon by converting **flakes into nodules.** Representative mechanical properties are given in the Table-1.11b(61).

(ii) General corrosion Behaviour

Ni-Resist irons can withstand a **wide range of corrosive** media and give highly economical service in marine environment (Table-1.12)(61). They can resist sulphuric acid at room temperature, HCl and H_3PO_4 even at elevated temperatures. Their resistance to nitric acid is similar to that of the unalloyed irons. Ni-Resist irons are resistant to **organic acids** such as acetic, oleic, and stearic. Ni-Resist irons are also immune to **strong** and **weak** alkalies, although they are subjected to **stress corrosion** cracking(SCC) at a stress over 70 MPa in boiling alkali solutions (60).

The excellent corrosion resistance is mainly due to the austenitic matrix(60-61). Unlike the high Si and high Cr alloys, the excellent corrosion resistance exhibited by **Ni-Resist irons** is not due to the **formation of a passive film.** However, potentiodynamic studies have revealed that these alloys exhibit active behaviour only in marine conditions(62).

Ni-Resist irons **do not remain rust free** when exposed to the atmosphere although their corrosion resistance is considerably greater than that of the unalloyed and low alloy cast irons and

34

steels. The rust film which develops over the first few years restricts further corrosion with the result that the corrosion rate becomes low(61,63).

The difference in the electrochemical potential between the graphite and the matrix in Ni-Resist irons is less than in the ordinary grey irons. Therefore, in environment in which graphitic corrosion is a problem, Ni-Resist irons will perform much better than the ordinary or low alloyed cast irons(61).

(iii) Heat Resistance

The adherent character of the scale formed on Ni-Resist castings(61) at elevated temperatures is important for applications such as gas turbines, exhaust manifolds and turbocharger components. Ni-Resist, especially the lower expansion Type-3, offers long and excellent oxidation and heat-resistant service without the difficulty of free scale getting into equipment.

At 700-815°C, the Ni-Resist alloys show up to 10 times better scaling resistance and up to 12 times better growth resistance than plain carbon cast iron. Ni-Resist castings have been found useful up to temperatures 700°C only. Above this temperature, the higher chromium or the ductile grades should be considered. In service where there is 1% or more sulphur in the atmosphere, the ceiling temperature is about 540°C. Type 4(Table-1.11a) will stand both high temperatures and the presence of sulphur in the products of combustion.

Over a temperature range from ambient to 400°C and above, Ni-Resists perform well for pumps and compressors handling materials such as sour gases and crudes, gasolines, caustics and other corrosives.

A grade of Ni-Resist cast iron, designed Type D-5S(56), is now available for service at temperatures exceeding 800°C. It exhibits oxidation resistance similar to that of a 25Cr-20Ni heat resisting cast steel, has good mechanical properties at elevated temperature and high resistance to thermal shock. For optimum properties, the composition should be:

C	Si	Mn	Ni	Cr	Mg
1.7-2.0%	4.9-5.4%	0.4-0.7%	34-36%	1.8-2.0%	0.05-0.07%

and be free from tramp elements and impurities such as molybdenum, lead, cerium, strontium, arsenic and zirconium. Typical applications include turbocharger castings, manifolds, hot forming dies and jet engine components.

(iv) Wear Resistance

Because Ni-Resist(61), just as gray iron, has graphite particles distributed throughout its structure, it is highly resistant to galling and to metal-to-metal-wear. In the hardness range of 130-175 Brinell, the alloys have optimum metal-to-metal-wear properties and exhibit a fine carbide structure. For moving parts operating up to 815°C, Ni-Resist may be used to combat rubbing wear, galling and heat oxidation.

1.5.1.5 Spheroidal Graphite Ni-Resist Irons

These are commonly produced by adding Mg to liquid iron in sufficient quantity to enable graphite to separate as spheroids rather than as flakes.

To distinguish the spheroidal graphite irons from the flake ones, the prefix 'D' has been used. The composition ranges are given in Table-1.13a(61).

(a) Mechanical properties of SG Ni-Resist

Mechanical properties of these irons are better than flake graphite irons. These are given in Table-1.13b(61).

(b) Corrosion Behaviour

It is well established that the corrosion resistance of any S.G. grade is similar to that of the corresponding flake graphite irons.

Applications

They have been successfully used in all environments and also at elevated temperatures(700-800°C). They are mostly used in marine conditions, and also where cyclically varying loads are experienced(60-61).

(c) Heat and Oxidation Resistance

The chromium containing ductile Ni-Resists(61) provide resistance to oxidation and maintain satisfactory mechanical properties to about 760°C. As such, they can be specified for applications including furnace parts, turbocharger and gas turbine parts, engine exhaust liners and valve guides. Should service temperatures in excess of 700°C be contemplated, Type D-2B, D-3 and D-4 would be prime the candidates.

Type D-4 has a high order of oxidation resistance, and if high toughness is not required, it will be found economically useful at least up to 815°C. In service where appreciable sulphur is present, the maximum service temperature is about 540°C

A more recent development D-5S has provided a material with exceptional dimensional stability and oxidation resistance. When two characteristics are particularly desired at temperature up to

37

870°C, D-55 is recommended. The improved properties are achieved by raising the silicon content to about 5.5%(56).

(d) Wear Resistance

The presence of dispersed graphite, as well as the work hardening character of ductile Ni-Resist castings(61), provide a high level of resistance to frictional wear and galling. Types D-2, D-2C, D-3A and D-4 offer good wear properties with a wide variety of other metals and at temperatures from sub-zero to 815°C. Types D-2B and D-3 are not recommended for maximum frictional wear resistance because their microstructure exhibits fairly massive carbides that are likely to abrade the object metal.

Resistance to wear at lower temperatures is attributed to the presence of uniformly distributed spheroidal graphite, and at high temperatures to the nickel oxide film(61).

1.6 SUMMARY

A review has been made of the different grades of unalloyed and alloyed cast irons that are in use.

A critical analysis reveals that alloyed white irons are extensively employed in areas where resistance to (i) abrasive wear, (ii) aqueous corrosion, and (iii) high temperature oxidation are essential requirements. The alloyed grey irons similarly find extensive useful applications when resistance to high temperature and corrosion are the main requirements.

Amongst the alloyed white irons in use, there appears to be a basic similarity in the transformation behaviour of the Cr-Mo and Ni-Hard cast irons. Apparently, the Ni-hards are superior to the Cr-Mo cast irons as they exhibit discontinuous eutectic

carbides(hence better toughness) and their microstructure compri-
ses dispersed carbides which make an important contribution to
their wear resistance. Claims to the contrary also exist.

Although not much information is provided on Cr-Mn cast
irons, at least their matrix transformation behaviour may be
similar to the Cr-Mo/Ni-Hard cast irons.

Looking to the methodologies that have been employed in
developing the aforesaid 'high-tech' casting materials, it
emerges that there is perhaps a strong need for evolving a
unified approach to developing wear, corrosion, and high tempera-
ture resistant cast irons so that the drawbacks present in grey/
white irons are eliminated and their usefulness appropriately
combined. Such a philosophy has been outlined in the next chapter
and forms the basis for developing low cost corrosion resistant
cast irons with substantially improved properties.

CHAPTER II

DESIGN & DEVELOPMENT OF IMPROVED PERFORMANCE ALLOYS
BASED ON THE Fe-Mn-Cr-Cu SYSTEM: FORMULATION OF THE PROBLEM

2.1 INTRODUCTION

A critical analysis of the literature review contained in Chapter-I revealed that amongst the alloy cast irons the Ni-hard (Ni-Cr) and the high Cr cast irons(with or without Mo) are being extensively used for a wide range of applications. Whereas the former are employed as wear resistant cast components/castings in mining, coal and ash handling, paper and pulp, cement, and the power sectors, the Cr-based alloys are being projected as improved alternatives to the Ni-Hard cast irons. It is a matter of opinion whether Ni-Hard cast irons are better than Cr-Mo cast irons or vive-versa. They(Cr - white irons) are also known to exhibit excellent heat and corrosion resistance. Interestingly, the Ni-Hard cast irons have also been shown to resist 'moderately' high temperatures(up to 800°C) and exhibit reasonably good corrosion resistance.

In the Indian context, a major technological impediment to the commercial exploitation of Ni-Hard irons is their dependence on the use of scarcely available high cost alloying elements Ni & Mo. This led to an interest in the development of low cost substitutes for the aforesaid compositions involving substitution of Ni & Mo, either partly or fully, by low cost indigenously available alloying elements(eg. Mn). However, it soon emerged that initiation of such programmes had major technological

implications because of the high prices of metals in the inter-
national market thereby necessitating the development of lower
cost value added products even in the developed countries.

Fundamentally, Ni can be replaced by Mn(both are complete
austenite- stabilizers). The latter is also a mild carbide former
(carbide forming tendency similar to Cr)(13). Therefore, Mn can
be usefully employed to (i) refine pearlite for which Ni is often
used in smaller amounts in cast irons, and (ii) attain a desired
matrix microstructure(bainite/martensite/austenite) in the as-
cast condition. In fact, by all accounts, the amount of Mn
required to obtain a desired transformation product was expected
to be lower than the corresponding amount of Ni(64-66). Further-
more, the morphology of the carbides in the Mn containing Cr
irons was found to be similar to the one in high Cr irons(e.g.
M_7C_3 type) because Mn and Cr have a similar carbide forming
tendency(49,67). In a nut shell Mn could effectively perform the
function of both Ni and Cr.

Cu is a partial austenite- stabilizer due to its low solu-
bility in ferrite(13). For its functional effectiveness to be
utilized, it would be necessary to retain it in solution. For
this the presence of another austenite- stabilizer is essential.
The choice would be between Mn and Ni.

Realizing the immense commercial fallout of such efforts,
developmental efforts were initiated by Patwardhan in the early
seventies(68) with a view to develop low cost substitutes for Ni-
Hard and Cr-Mo cast irons. These efforts were based on the
utilization of low cost indigenously available alloying elements.
Initial results, based on the work of Srinivasan, Patwardhan and

Mehta revealed that the Fe-Mn-Cr-Cu alloys can attain microstructures similar to those observed in Ni-Hard cast irons (47,69). The carbides were essentially massive and could be rendered discontinuous only on heat treating from high tempera-tures(>800°C).

Work on optimizing Cu and Mn was carried out by Sudan(52) and Sharma(51). Sudan, Patwardhan, and Mehta(47), while studying the effect of 0.5,1,2 & 3% Cu on the microstructure and hardness of a 7%Cr, 1.5%Si and 3.1%C cast irons reported that attainment of high hardness(>650 VPN) was possible only on quenching. Cu was however very useful in rendering the carbide net work discontinuous. The optimum Cu appeared to be 1%.

Patwardhan, Mehta, and Sharma(70) while reporting on the possible effects of 2,4 and 6% Mn on the transformation behaviour of a 7Cr-1.5Si-3.1C base iron, observed that while high hardness (>650 VPN) could be attained without quenching, the carbide net work could not be rendered discontinuous. The optimum Mn content, under the experimental conditions, appeared to be 4%.

Based on the above data, it was conceived by Patwardhan that an alloy Fe-4Mn-1Cu-7Cr-1.5Si could prove to be a useful alternative to Ni-Hard-4 composition. This was duly demonstrated through limited experiments carried out by Jha et.al.(71). It was however concluded that the evidence thus provided could be considered as 'decisive' only after extensive experimentation.

At this juncture two lines of approaches were evolved by Patwardhan(68). The first essentially comprised developing low cost wear resistant compositions and was pursued by Singh(72) who arrived at optimum alloy compositions based on the Fe-Mn-Cr-Cu

system which could serve as effective low cost substitutes to Ni-Hard/Cr-Mo cast irons. Considerable information in this regard is awaiting publication(68).

The second line of approach comprised developing corrosion resistant microstructures by following the 'white iron' route. The reasons for following this line of approach, the advantages that were likely to accrue and the key results obtained have been highlighted in the next section. The analysis put forth formed the basis of formulating the present problem.

2.2 SALIENT FEATURES OF THE APPROACH: Philosophy behind developing alternative & improved corrosion resistant materials

The present investigation is primarily aimed at developing low cost corrosion resistant 'white irons'. It was felt appropriate to undertake such a study since microstructurally the domain of corrosion resistant alloy cast irons(austenite based structures) is a logical extension of the domain of wear resistant cast irons(martensite based structures)(68). It was reasonable to expect that this could be effectively achieved by utilizing the Fe-Mn-Cr-Cu system but with the altered compositional limits so that the entire gamut of microstructures expected to be attained in corrosion resistant white irons could also be developed in the Fe-Mn-Cr-Cu alloys. This necessitated a comprehensive review of the state of the art on corrosion resistant alloy cast irons.

This revealed that of the three types of irons currently in use, the high(up to 15%) Si irons(ferritic) are most usefully utilized under oxidizing conditions(30, 73-75). However, their poor mechanical strength and shock resistance precluded their

43

general engineering applications(30). The high Nickel(14-36%) Ni-resist cast irons(austenitic), although useful in a variety of aqueous environments, have a low mechanical strength, suffer from graphitic corrosion, and pitting and are unsuitable at service temperatures $\geq 800°C(62,74-76)$. The high Cr irons, which in principle can develop all matrices(ranging from ferritic to austenitic) and are more known for their high wear/abrasion resistance, can in principle be employed up to higher 'service' temperatures owing to the presence of a large Cr content. Their shock resistance is improved by lowering 'C' content(36). Dodd(15) has demonstrated that irons containing 0.5-2%C and 20-28%Cr can offer a useful compromise between resistance to corrosion and abrasion. Presence of Mo may prove additionally advantageous. Unavailability of published literature led to a possible inference that not much effort has gone into studying the electro-chemical and deformation behaviour of microstructures encountered in high Cr irons. Furthermore, it appeared that the high Ni irons are the most popular ones amongst corrosion resistant alloy cast irons. If the major drawbacks exhibited by them could be eliminated then such an effort would prove both technologically and commercially promising.

Since the major drawbacks associated with high Ni- irons could be attributed to the presence of graphite, Patwardhan (68,77) propounded the idea that development of corrosion resistant cast irons was not only feasible but held promise if the 'white iron' route were to be adopted. He was further encouraged in his belief by the realization that the difference in the electrochemical potential between austenite and carbide

(white irons) was lower than that between austenite and graphite (grey irons). Such a study was expected to become additionally meaningful if it were possible to develop alloys at a minimum of cost i.e. by employing low cost alloying elements. Patwardhan(68,76) further opined that Fe-Mn-Cr-Cu alloys could be successfully developed to resist corrosion, wear and corrosive wear as the system provides complete flexibility in attaining different matrices(pearlite, bainite, martensite and austenite) through a minimum of alloying. The work done by Singh(72), Basak et.al.(67), and experiences gained earlier(51-55,69) provided useful inputs into strengthening this belief.

This prompted Patwardhan(78) to initiate an alloy development programme for developing low cost alternatives to the existing high Ni- irons. The idea propounded was investigated by Jain(63) in a study involving the characterization of 5Cr-1.5Cu and 5Cr-3.0Cu alloys containing two different Mn contents namely 6% and 7.5%, for their transformation, electrochemical and deformation behaviour. Major conclusions of design interest emerged from this study(Table 2.2)(62,79-85), one of the major highlights being the quantization of different relations. On the basis of these relations, Patwardhan & Jain(79-82) were able to propose models between (i) hardness, heat treating temperature and time, (ii) microstructure with the corrosion behaviour and deformation behaviour and (iii) coarsening behaviour of the alloy as influenced by heat treating temperature and time. The data thus obtained proved useful in optimizing the microstructure and in designing future alloy compositions.

2.3 AIM OF THE PRESENT STUDY

The present investigation is a logical extension of the work done earlier and essentially comprised designing new compositions with a view to attain the different microstructures(of interest) through a minimum of alloying either in the as-cast condition or at best through simple heat treatment(s). It was decided to attain microstructures comprising varying proportions of austenite and carbide(both massive and dispersed) since austenite based microstructures were found to be most effective in resisting corrosion and at the same time in attaining useful mechanical properties. It was decided to concentrate on optimizing the microstructure vis-a-vis the morphology and distribution of the 2nd phase(both massive and dispersed carbides). Priority was accorded to the possible elimination of dispersed carbides as they do not constitute a part of the 'intended' microstructure.

2.3.1 DESIGN OF ALLOYS

The Fe-Mn-Cr-Cu system was chosen for the present study. Its choice can be justified in view of the following(62,76,77,83):

(i) Mn enhances hardenability significantly at a low cost, helps in retaining austenite at room temperature, stabilizes carbide and does not adversely affect fluidity.

(ii) Cu is a useful graphitizer/renders carbides discontinuous on heat treating, solution hardens, improves corrosion resistance in the presence of dilute acids(acetic, sulfuric, hydrochloric) and acid mine waters.

(iii) Cr stabilizes carbide, is helpful in attaining a uniform microstructure(i.e. with a minimum of segregation) and may

prove useful in attaining martensite/austenite even if present singly in large proportions.

Since the aim was to attain an austenitic matrix with a minimum of carbides, the carbon content was restricted to 3%. A parallel study with alloys containing a higher carbon content (3.7%) was also planned(86). Carbon besides increasing the fluidity, stabilizes austenite and increases the solubility of Cu in cast irons. Si was adjusted to 1.5-2%, -a range in which it is normally present in white irons. Cr was restricted to 7% to ensure that a composition is cast white. The amount was based on the data of Singh(72) who showed that raising the Cr from 6 to 9% did not significantly alter the behaviour of various Fe-Mn-Cr alloys. Mn was fixed at 10% to ensure attainment of a completely or near complete austenitic matrix even in the as-cast state. The data on Mn partitioning into austenite and carbide phases and the experiences gained from earlier studies were duly considered while arriving at this figure(62,72). Mn like Ni & C is also expected to raise the solubility limit of Cu in cast irons(87).

A great stress was laid on the stability of the austenitic matrix as a prerequisite to attaining good corrosion resistance. Its importance can be assessed on the basis of the findings in a recent study by Rao and Patwardhan(84-85) wherein it was shown that stress relieving adversely affected the corrosion behaviour of a 8Mn-5Cr-1.5Cu cast iron. This was attributed to the decomposition of austenite, on stress relieving at 600°C, into dispersed alloy carbides and martensite(formed on cooling after stress relieving) thereby implying that the matrix was not stable enough.

Cu was added in 3 different amounts, 1.5, 3.0, 5.0%. Besides enhancing austenite stability, its presence in solution would improve corrosion resistance. Thus in all 3 alloys were designed with the same base composition 3%C, 7%Cr, 10%Mn and 1.5-2.0%Si, but with different Cu contents namely, P1 = 1.5%Cu, P2 = 3.0%Cu and P3 = 5.0%Cu.

2.4 PLANNING OF EXPERIMENTS

The experiments were planned as follows:

Phase I

Study of the structure-property relations by subjecting specimens of alloys to different heat treatments, assessing their hardness and conducting structural investigations by optical metallography.

Phase II

Electrochemical characterization of the alloys by weight loss method and further detailed structural examination by x-ray diffractometry and by quantitative optical metallography to enable work to be carried out on the optimization of micro-structure for different end applications.

Phase III

Deformation behaviour through compression testing, structural investigation by EPMA and Electrochemical characterization by Potentiostatic method.

The experimental techniques employed in the present investigation have been highlighted in the next chapter.

CHAPTER III

EXPERIMENTAL TECHNIQUES AND PROCEDURE

3.1 Alloy preparation

Raw materials used for preparing alloys were pig iron, low carbon ferro-alloys (ferro-chrome, ferro-manganese and ferro-silicon), graphite powder, electrolytic copper and mild steel scrap. Composition of the pig iron and the ferro-alloys are reported in the Table-3.1.

The charge comprised the aforesaid raw materials in the requisite proportion so as to ensure that the desired compositions are attained. Due consideration was given to the metal content of the ferro-alloys and to the melt losses while making charge calculations. Alloys were air melted in a graphite crucibles in a medium frequency induction furnace.

Initially a base alloy, weighing 65 Kgs. and containing 3%C, 6-7% Cr and 10% Mn was prepared by first melting requisite proportions of pig iron, mild steel scrap and graphite to a super-heat followed by deslagging and subsequent addition of ferro-chromium, ferro-silicon and ferro-manganese. After ensuring complete dissolution of alloy additions, small samples were taken out of the melt for estimation of carbon by LECO analyzer. In the intervening period the melt temperature was lowered to reduce losses. After ensuring that the carbon content had reached the desired level, the liquid metal temperature was raised to about 1400°C and slag removed. Molten alloy was then cast into three cylindrical blocks of approximately equal weight. Thus in all three castings were poured.

Finally, the Cu content was adjusted to the desired level (i.e. 1.5, 3.0 & 5.0%) by adding requisite amount of electrolytic copper to each of the three base alloy castings in the molten condition. Carbon content was rechecked even at this stage to ensure that it was maintained at the desired level. After deslagging, temperature of the molten metal was measured with an optical pyrometer. The alloys were then poured at about 1425°C into 18 mm. diameter x 250 mm. long cylindrical molds and 8x22x120 mm rectangular strips in resin bonded self setting sand molds.

Alloys were analyzed for C,S,P,Si,Mn,Cr on x-ray fluorescence spectrometer. Detailed chemical analysis is reported in Table-3.2.

3.2 Specimen preparation

Alloys were very hard and could not be cut either with power saw or with high speed steel tools. Round samples(height 14-18mm.) were sliced off from the cylindrical ingots on a cut-off wheel. Heating of the specimens during slitting was kept to a minimum through water cooling. Specimens thus obtained were ground to have parallel faces and paper polished in the usual manner.

For corrosion studies by weight loss method, specimens of the size 15x10x5 mm. were employed. They were cut from rectangular strips by a procedure outlined above. As before they were ground to have parallel faces and paper polished to the 4/0 stage to obtain mirror finish.

246713.

3.3 Heat treatment

Heat treatments primarily comprised soaking at 800, 850, 900, 950, 1000 & 1050°C for 2,4,6,8 and 10 hours followed by air cooling. They were carried out in muffle furnaces whose temperatures were measured with a Pt-Pt/Rh(13%) thermocouple and controlled to an accuracy of ±3°C.

3.4 Hardness measurement

3.4.1 Macro-hardness

Hardness testing was extensively employed because it provides a quick yet reliable indication of the effect of heat treatment on properties.

Heat treated specimens were initially ground to a uniform depth of about 1 mm to remove any decarburized layer. Thereafter, they were paper polished up to the 3/0 stage in the usual manner. Hardness measurements were carried out on both the faces of a specimen on a Vicker's hardness testing machine employing a 30 Kg. load. A minimum of 20 impressions were taken on each specimen. The permissible scatter in the hardness value was ±17 VPN(88). In the event of variation exceeding this limit, hardness has been represented as a band denoting both the maximum and the minimum values.

As the alloy system under investigation is heterogeneous in character, the representative hardness readings as well as the average values have been reported.

3.4.2 Micro-hardness

Micro-hardness measurements were carried out on polished and etched specimens using a TUKON MICRO-HARDNESS TESTER(MODEL 300) at 50 grams load and an objective magnification of X 20.

Micro-hardness measurements were made at different locations within a region as also in a number of carbide and matrix regions.

3.5 Compression testing

Deformation behaviour of the different microstructures was assessed by carrying out compression tests. They were carried out on cylindrical specimens(size 10 mm diameter x 10 mm height) on a 60 ton capacity microprocessor based Instron compression testing machine, at a cross head speed of 1.0 mm/minute. Compression strength and percent deformation(height strain) were calculated from the stress-strain curves in the usual manner.

3.6 Metallography

3.6.1. Optical Microscopy

This has been extensively employed to study how heat treatment influenced microstructure. Specimens were paper polished in the usual manner(section 3.2). The final(wheel) polishing was carried out using 1 and 0.1 micron alumina as the abrasives. After proper cleaning, specimen surfaces were etched in freshly prepared alkaline picrate and 2% nital solutions. Metallographic examination was carried out on REICHERT-JUNG MeF-3 microscope.

3.6.2. Quantitative metallography

This was carried out on a LEITZ image analyzer(Auto-scan) at a magnification of 3000 X. Specimen size was the same as that employed during optical metallography. Twenty different fields of view were examined on each specimen. Quantitative estimations including plotting of hystograms were carried out with the help of computational techniques.

3.6.3. Scanning electron microscopy

Scanning electron microscopy was also extensively employed on specimens, which had been subjected to corrosion studies in a 5% NaCl solution, to ascertain the nature of the attack.

To ensure good electrical contact, specimens were glued to the specimen holder using a silver paint. They were then allowed to dry before being examined on a Phillips 501 scanning electron microscope at an operating voltage of 15 KV.

3.7 Electron probe micro-analysis

This study was carried out for assessing the partitioning behaviour of different alloying elements, particularly Mn, Cr, Cu, C and Si, as influenced by heat treatment. This was carried out on CAMEBAX EPMA/SEM at 15 KV and 60µA beam current using the crystals LiF(for Fe, Cr, Ni and Cu), TAP(for Mn and Si) and ODPb (for carbon) using the fixed probe technique.

Specimens for electron probe micro-analysis were the same as used for optical metallography. The samples were hot mounted (mount size: 25 mm x 10 mm height) and, after polishing, were etched just enough to reveal the microstructure. This way it was ensured that the composition of different phases/micro constituents was practically unaltered.

3.8 X- ray diffractometry

As-cast and heat treated specimens of the alloys were subjected to structural investigations on a PHILLIPS diffractometer PW 1140/90, employing an iron target and a manganese filter, at a voltage of 35 KV and a current of 12 mA.

Specimens, which were polished and lightly etched, were scanned from 40 to 150°. Time constant and scanning speeds were

kept at 2 seconds and 1° per minute respectively. Diffractograms were indexed/analyzed by adopting the following procedure.

Indexing of x- ray diffractograms

Indexing of the diffractograms and a detailed analysis of the probable microconstituents present were done with the help of a computer package'XRAY'(89) as follows:

- Based on the chemical composition of the alloy and the heat-treatment employed, a list of 196 probable micro-constituents was prepared. This included all constituents that were likely to form as a consequence of possible interactions amongst the alloying elements present eg. carbides, sulphides, oxides, silicides etc. including the possible presence of metals(eg. Cu) in elemental form.

- Standard 'd'- values, relative intensities, their miller indices of planes, and lattice parameter(s) for the above said constituents were noted down from the ASTM powder diffraction data cards(90-92). This data served as input data for carrying out the analysis.

- The experimental error limit for 2θ- matching was taken as ±0.2°(the minimum value of 2θ- which can be measured accurately at a chart speed of 1° per cm). The experimental error limit for d- matching was calculated on the basis of this assumption.

- The computer software performs the following functions:

   a. Experimental error determination for d- matching.

   b. Calculation of d- values from 2θ- values and vice versa.

   c. Matching of the calculated d- values or the 2θ- values

with the standard values.

d. Prediction of the confidence limit of peak angle/d- value matching as well as the confidence limit of the possible presence of a phase.

e. Reporting of the result of matching in the form of a 2 dimensional matrix and/or in the descending order of confidence limits of the possible phase(s)/microconstituents that may be present.

f. Reporting of the miller indices of Planes(arising out of the above said exercise) of the possible phases present.

g. Calculation of the possible peak-angles corresponding to the K_β- radiation.

3.9 DTA studies

DTA was extensively employed to investigate the phase transformation characteristics and for assessing the high temperature response of the different microstructures.

This was carried out on NETZSCH Simultaneous Thermal Analyzer STA 409 using KEOLINE as reference material. The powder sample of the alloy weighing nearly 45 mg. was taken in a alumina crucible and heated at a rate of 10°C per minute in air. The experimental data were analyzed and integrated plots of DTA(mV), TG(mg.), and DDTA were obtained plotted by NETZSCH DATA ACQUI-SITION SYSTEM.

3.10 Corrosion studies

Corrosion studies were carried out by weight loss method and the potentiostatic methods.

3.10.1 Weight loss method

These tests were carried out in accordance with the relevant ASTM standards(93). Specimens were prepared by adopting the procedure outlined in the section 3.2 and cleaned as per the standard procedure laid down(94). A specimen was tied to glass rod by a nylon thread /cord. It was then suspended in a 100 ml. capacity beaker containing 5% NaCl solution up to a preset level. Each specimen was weighed and its surface area calculated prior to being subjected to test. Tests wee conducted for 7 days. After completion of a test, the specimen was cleaned by scrubbing followed by washing in double distilled water, degreasing in acetone and finally air drying (94). It was then weighed again and the loss in weight calculated. Corrosion rates were calculated by using the formula(94):

$$\text{Corrosion rate} = \frac{K.W.}{A.T.D.}$$

A = area in cm^2 to the nearest 0.01 cm^2

W = weight loss in gms. nearest 1 mg.

D = density in g/cm^3

T = exposure time in hours to the nearest 0.01 hour

K = constant (3.45 x 10^3) for ipy

K = constant (2.40 x 10^6 x D) for mdd

(Density is not needed to calculate the corrosion rate in mdd units. The density in the constant K cancels out the density in the corrosion rate equation)

Corrosion rates have been reported in inches per year(ipy) and in mdd(milligrams per square decimeter per day). The latter unit is more reliable since density does not figure in the final calculations.

3.10.2 Potentiostatic studies

This technique is useful in determining whether the alloy under investigation exhibits the active-passive transition(in the present study they were confined to assessing corrosion rates).

The experimental set-up consisted of a corrosion cell which was connected to a computer based potentiostat(EG & G PRINCETON APPLIED RESEARCH potentiostat/Galvanostat Model 273).

The corrosion cell consisted of a flask which was modified by the addition of various necks to introduce the test and the counter electrodes, and a reference electrode. This cell and its components have been described in detail by Greene(95).

The test electrode, also known as the working electrode, was made of the test material of approximately 1.0 cm² cross-sectional area. It was hot mounted in a manner that it was leak proof. The surface of the test electrode was prepared just before the experimental measurements in accordance with the recommended practice(93).

The reference electrode was a saturated calomel electrode (SCE) and was throughout dipped in solution. The potential of the reference electrode was checked frequently to ensure the stability.

Tests were carried out in a potential range of -250 to +250 mV to obtain tafel plots. The scan rate was kept constant at 0.2 mV/sec. Tafel plots were automatically plotted through computer.

3.11 Data analysis

Analysis of the data obtained was carried out with the help of computational techniques using PC-AT/486.

CHAPTER IV

EFFECT OF HEAT TREATMENT ON HARDNESS AND MICROSTRUCTURE

The present investigation was primarily aimed at assessing the heat treatment response of the three alloys namely P1, P2, P3 with the help of hardness measurements, optical metallography, and quantitative metallography.

The results thus obtained have been summarized in the following sections.

4.1 Results

4.1.1 Effect of heat treatment on hardness

Transformation behaviour of the alloys was investigated in the first instance (i) to ascertain the different microstructures that can be generated, (ii) to determine how the heat treating schedule influenced the as-cast hardness, (iii) to assess the effect of composition and heat treatment on hardness and (iv) to characterise the microstructures initially on the basis of hardness. This was achieved by heat treating round specimens (18-20 mm diameter x 14-18 mm height) of the three alloys by air cooling from 800, 850, 900, 950, 1000, and 1050°C after holding for periods ranging from 2 to 10 hours.

Effect of time and temperature on the hardness is summarized in the Tables 4.1-4.34(Table 4.34 summarizes data contained in the Tables 4.1-4.33) and in the Figures 4.1-4.3(the base curves). The data contained in the figures represents the experimentally determined values whereas the actual plots conform to the best fit data. A perusal of the tables and the figures revealed that :

similarity in their transformation characteristics (Figure 4.5).

6. On air cooling from 900 and 950°C, the alloys P1 and P3 responded similarly as revealed by an equivalent rate of decrease in their hardness with time. However, the response of P2 differed showing a constancy in hardness (Figures 4.6-4.7).

7. On air cooling from 1000°C, the differences in the hardness levels of the three alloys evened out and their overall behaviour was similar as is evidenced by a decrease in hardness with time with approximately similar slopes(Figure 4.8).

8. On heat treating from 1050°C, the transformation behaviour would have been the same but for a 'hardness arrest' at 8 hours soaking period which is marked in alloy P1 and the least in P3(Figure 4.9).

9.(a) The hardness vs temperature plots as influenced by time(Figures 4.10-4.12) represented how effectively each alloy sustained its hardness on heat treating.

  (b) These curves had an inverted parabolic shape.

  (c) The slope of the curve altered around a threshold temperature called the 'cross over point'(COP). The overall slope varied with the Cu content, its effect being marked at 5%Cu(in alloy P3).

10. The (qualitative) profile of the hardness vs temperature plots(Figures 4.10-4.12) for the three alloys is nearly the same. It was further evident that with an increase in the Cu content, the hardness vs temperature plots are

acquiring a somewhat linear profile, the effect being marked in the alloy P3 with the highest Cu content.

11. A clear cut COP of the alloys could not be obtained from the plots. However it was observed to be in the range 850-900°C.

12. A comparison of the hardness vs temperature plots as influenced by time(Figures 4.13-4.17), further revealed that:

(i) At 2 and 4 hours soaking period, P2 and P3 responded similarly as is evident from the similarity in the slope of the hardness vs temperature plots. However, P1 sustained a higher level of hardness.

(ii) At 6 hours soaking period, the aforesaid dissimilarity considerably reduced. Moreover, at 1000°C, all the three alloys attained identical hardness. On raising the temperature to 1050°C, the overall level of hardness in P1 and P3 got interchanged whereas the response of P2 was on expected lines i.e. the decrease in hardness in P1 and P3 is not directly related with the Cu content.

(iii) The nature of hardness vs temperature plots at 8 hours and 10 hours soaking period is nearly similar for all the three alloys. The overall hardness level is inversely related to the Cu content; the larger the Cu content, the lower the hardness.

(13) The bar diagrams summarized in Figures 4.18-4.21 clearly bring out the individual and comparative behaviour of

62

the three alloys at a glance besides reinforcing the different deductions arrived at earlier.

4.1.2 Microstructure

Effect of heat treatment on the hardness was substantiated by carrying out microstructural examination. Initially the experiments were confined to assessing qualitative changes in the microstructure and these are summarized as photomicrographs in the Figures 4.22-4.42. Subsequently, quantitative estimations involving massive and dispersed carbides were also carried out. This data have been dealt with separately.

(a) Considering the microstructure of the alloy P1 to start with:

1. The as-cast microstructure essentially comprised austenite + carbide(Figure 4.22). Austenite was present as dendrites and carbides were located in the interdendritic spaces(Figure-4.22a). The carbide had different morphologies namely, (i) flower or eutectic type, (ii) massive/platy type, and (iii) mesh type(resembling phosphide eutectics). The eutectic carbides were apparently inter-linked with platy carbides (Figures 4.22a-b). In addition to the above, certain dark etching features with 'leaf like' morphology were also observed(Figure 4.22c).

2. On heat treating from 800°C for 2 hours, the austenite regions showed needle like precipitation(Figures 4.23a-b) whose morphology became evident at a higher magnification(Figure 4.23a). Its volume fraction was not uniform. The needles had an obtuse plate like appearance although occasionally straight needles/plates growing/protruding into austenite were also observed(Figure 4.23c).

1. The overall transformation behaviour of the alloys could be classified as follows :

   (a) Hardness increasing marginally with soaking period on air cooling from 800°C(valid for P1 and P2); however for P3, hardness was independent of the soaking period.

   (b) Hardness remaining independent of the soaking period on air cooling from 850°C(valid for all the alloys).

   (c) Hardness decreasing marginally with the soaking period on heat treating from 900°C(valid for all alloys); the decrease being more pronounced in P3.

   (d) A slight decrease in hardness with soaking period on heat treating from 950°C(valid for all the alloys); the decrease being a maximum in P1.

   (e) Hardness decreasing with soaking period on heat treating from 1000 and 1050°C(valid for all the alloys).

   (f) The hardness, in general, decreasing with the soaking temperature in the order

   $H_{1050} < H_{1000} < H_{950} < H_{900} < H_{850} < H_{800}$

2. Heat treating from 800°C had little effect on the as-cast hardness. The apparent increase/decrease falls within the permissible experimental scatter(Figures 4.1 -4.3).

3. However, on heat treating from temperatures between 850 to 1050°C hardness in general was lower than that in as-cast state(Figures 4.1-4.3).

59

The aforesaid data(Figures 4.1-4.3) although providing useful information fell short of revealing a comprehensive understanding of the transformation behaviour. The additional information required was obtained by replotting the data contained in the Tables 4.1-4.33 in the following manner:

(i) Effect of time on the hardness as influenced by the heat treating temperature(Figures 4.4-4.9).

(ii) Effect of temperature on the hardness as influenced by the holding period for each alloy(Figures 4.10-4.12)

(iii) Effect of temperature on the hardness at each of the five soaking periods for all the alloys(Figures 4.13-4.17).

(iv) Effect of alloy composition on the hardness as influenced by the heat treating parameters [for each alloy](Figures 4.18-4.21 which are in the form of bar diagrams)

The following deductions would reveal the usefulness of the Figures 4.4-4.21 when considered along with the Figures 4.1-4.3, in providing further useful information on the (a) individual and (b) comparative behaviour of the alloy(s).

4. The comparative hardness vs time plots, as influenced by temperature, further confirmed the similarity between P1 and P2 upon heat treating from 800°C; alloy P3 responded differently as is evidenced by hardness remaining unchanged(Figure 4.4).

5. On air cooling from 850°C, hardness was independent of time for all the alloys, thereby revealing a basic

similarity in their transformation characteristics (Figure 4.5).

6. On air cooling from 900 and 950°C, the alloys P1 and P3 responded similarly as revealed by an equivalent rate of decrease in their hardness with time. However, the response of P2 differed showing a constancy in hardness (Figures 4.6-4.7).

7. On air cooling from 1000°C, the differences in the hardness levels of the three alloys evened out and their overall behaviour was similar as is evidenced by a decrease in hardness with time with approximately similar slopes(Figure 4.8).

8. On heat treating from 1050°C, the transformation behaviour would have been the same but for a 'hardness arrest' at 8 hours soaking period which is marked in alloy P1 and the least in P3(Figure 4.9).

9.(a) The hardness vs temperature plots as influenced by time(Figures 4.10-4.12) represented how effectively each alloy sustained its hardness on heat treating.

   (b) These curves had an inverted parabolic shape.

   (c) The slope of the curve altered around a threshold temperature called the 'cross over point'(COP). The overall slope varied with the Cu content, its effect being marked at 5%Cu(in alloy P3).

10. The (qualitative) profile of the hardness vs temperature plots(Figures 4.10-4.12) for the three alloys is nearly the same. It was further evident that with an increase in the Cu content, the hardness vs temperature plots are

61

acquiring a somewhat linear profile, the effect being marked in the alloy P3 with the highest Cu content.

11. A clear cut COP of the alloys could not be obtained from the plots. However it was observed to be in the range 850-900°C.

12. A comparison of the hardness vs temperature plots as influenced by time(Figures 4.13-4.17), further revealed that:

(i) At 2 and 4 hours soaking period, P2 and P3 responded similarly as is evident from the similarity in the slope of the hardness vs temperature plots. However, P1 sustained a higher level of hardness.

(ii) At 6 hours soaking period, the aforesaid dissimilarity considerably reduced. Moreover, at 1000°C, all the three alloys attained identical hardness. On raising the temperature to 1050°C, the overall level of hardness in P1 and P3 got interchanged whereas the response of P2 was on expected lines i.e. the decrease in hardness in P1 and P3 is not directly related with the Cu content.

(iii) The nature of hardness vs temperature plots at 8 hours and 10 hours soaking period is nearly similar for all the three alloys. The overall hardness level is inversely related to the Cu content; the larger the Cu content, the lower the hardness.

(13) The bar diagrams summarized in Figures 4.18-4.21 clearly bring out the individual and comparative behaviour of

the three alloys at a glance besides reinforcing the different deductions arrived at earlier.

4.1.2 Microstructure

Effect of heat treatment on the hardness was substantiated by carrying out microstructural examination. Initially the experiments were confined to assessing qualitative changes in the microstructure and these are summarized as photomicrographs in the Figures 4.22-4.42. Subsequently, quantitative estimations involving massive and dispersed carbides were also carried out. This data have been dealt with separately.

(a) Considering the microstructure of the alloy P1 to start with:

1. The as-cast microstructure essentially comprised austenite + carbide(Figure 4.22). Austenite was present as dendrites and carbides were located in the interdendritic spaces(Figure-4.22a). The carbide had different morphologies namely, (i) flower or eutectic type, (ii) massive/platy type, and (iii) mesh type(resembling phosphide eutectics). The eutectic carbides were apparently inter-linked with platy carbides (Figures 4.22a-b). In addition to the above, certain dark etching features with 'leaf like' morphology were also observed(Figure 4.22c).

2. On heat treating from 800°C for 2 hours, the austenite regions showed needle like precipitation(Figures 4.23a-b) whose morphology became evident at a higher magnification(Figure 4.23a). Its volume fraction was not uniform. The needles had an obtuse plate like appearance although occasionally straight needles/plates growing/protruding into austenite were also observed(Figure 4.23c).

On raising the soaking period through 6 to 10 hours, the precipitation of needle type second phase was more pronounced (Figures 4.23e-f). Each needle appeared to comprise a 'jagged region' surrounding it which has been described as 'feathering'(Figure 4.23c). The tendency towards 'feathering' was pronounced at 10 hours soaking period(Figure 4.23d). Dispersed spherical carbides were also observed at 6 hours and more so at 10 hours(Figures 4.22c,d & f).

3. On heat treating at 850°C for 2 hours, there was a general coarsening of the needles as well as the dispersed carbides (DCs). DCs appeared to have increased in amount and 'feathering' was prevalent and appeared to be a part of the needle morphology(Figures 4.24a-c).

On raising the soaking period to 6 hours, features similar to the above were observed. Apparently, the extent of coarsening was more(Figure 4.24d).

On raising the soaking period to 10 hours, the extent of feathering greatly diminished(Figure 4.24e). There was a general coarsening of the 'obtuse needles'/plates as well as the dispersed spherical carbides(Figure 4.24e). Disintegration/delinking of massive carbides(MCs) was also observed without any graphite forming(Figures 4.24e-g). An interesting feature was that the dispersed particles acquired a tendency to align themselves along specific directions(Figure 4.24f).

4. On heat treating at 900°c for 2 hours, the needles were elongated as well as coarsened(Figures 4.25a-b)(sidewise and edgewise growth). Simultaneously, the formation of 'aligned'

DCs was on the increase(Figures 4.25b-d). The disintegration of MCs continued as observed earlier, and the extent of feathering had diminished although it was still observed up to 6 hours soaking period(Figures 4.25e-f).

At 6 hours soaking period, the above said features were somewhat coarsened(Figures 4.25e-f).

On raising the soaking period to 10 hours, there was general coarsening of the needles as well as DCs(Figures 4.25g-i). It looked as though at least some of the needles had acquired a plate like morphology as a result of coarsening(Figure 4.25i). An interesting feature is that the MCs tended to align themselves. Simultaneously, 'rounding off' at their edges was observed(Figures 4.25g-i).

5. On heat treating from 950°C, the matrix in general exhibited an 'evened out' texture*(Figure 4.26a-c) at 2 hours soaking period. The amount of needles, which had substantially coarsened, greatly reduced. No feathering around them was observed. The second phase now mostly comprised DCs which were undergoing coarsening and at the same time aligning themselves along specific directions. An equally important aspect was that the MCs were seen to be linking themselves/approaching one another to link up. A similar tendency was also observed amongst DCs(Figures 4.26a&c).

On raising the soaking period through 6 to 10 hours, the basic features were similar to those mentioned above. However, the morphology of MCs was either near spherical or with 'rounded edges'(Figures 4.26d-f). Occasionally hexagonal shap-

---

* used to convey matrix character

ed carbides were visible(Figure 4.26f). The austenitic matrix etched somewhat differently around some massive/dispersed carbide regions(Figure-4.26f).

6. On heat treating from 1000°C for 2 hours, there were some marked but interesting structural changes. First of all no needles were present(Figure 4.27a-b). Secondly, linking of DCs, which had by now acquired a favourable morphology, continued even along certain boundaries resulting in their merging together or interdiffusing(Figure 4.27b). Similarly, the aligned MCs also appeared to link-up with one another (Figure 4.27b). The disintegration and rounding off amongst MCs continued and was more prevalent at 6 hours soaking period(Figures 4.27c-e).

On raising the soaking period through 6 to 10 hours, the microstructure now comprised massive carbide regions with favourable morphologies in a matrix of austenite(Figures 4.27f-i). The various tendencies especially the one involving 'alignment' and 'rounding off' in MCs was in evidence. Dark grey etching regions appeared to develop both around massive as well as around dispersed carbides. The austenite matrix was very 'evenly'/uniformly 'textured'(Figures 4.27f-i).

7. On raising the temperature to 1050°C and at 2 hours soaking period, the 'rounding off' and coalescing tendencies among the MCs were greatly enhanced(Figures 4.28a-c) giving rise to the formation of large 'agglomerates' at higher soaking periods (Figures 4.28d-j). Very often these agglomerates had either a massive or sometimes a 'plate like' morphology. Occasionally

regions having either massive or 'plate like' morphologies but with 'rounded edges' were also observed. It appeared as though some of the original DCs have become MCs with rounded or hexagonal morphologies as observed on heat treating for 6 and 10 hours(Figures 4.28f & i-j). The 'rounding off' tendency was clearly dominant but equally dominant was also the tendency of 'aligned linking' amongst MCs. In certain areas, 'dark etching' regions appeared to form essentially around MCs or at the interface between two or more massive carbide regions which were joining one another(Figure 4.28h). In certain regions peculiar 'chain like' structures interlinking MCs were seen to form(Figure 4.28i). In some instances, stray DCs were also seen to form(Figures 4.27c,d & g). All in all, a large number of interrelated changes appeared to be occurring thereby disturbing the 'evenness' of the matrix.

(b) Alloys P2 and P3

The structural changes in P2 & P3 are on similar lines as those in P1 barring some areas of difference centering around:

(i)   type of carbides present in the as-cast state,

(ii) the type of the needle morphology, the main precipitating second phase at 'lower temperatures'

(iii) the stages(temperature/time) at which feathering appeared/ disappeared

(iv) stage(s) at which disintegration/rounding off within massive carbide sets in,

(v)   possible interaction between coarsening/growing needles and dispersed carbides(DCs),

(vi) general state of MCs at high temperature, and

(vii) the extent of the formation of dark/grey etching regions at
the highest heat treating temperature, namely, at 1000°C &
1050°C.

Alloy P2

(a) As-cast : — same basic features as in Alloy P1
(Figures 4.29a-c)

— dark areas(martensite ?)(Figures 4.29a-c)

— leaf like areas are present as in P1
(Figure 4.29c)

— carbides are compact, discontinuous, and
less platy compared to P1(Figure-4.29b)

(b) 800°C, 2 hours — needles & DCs are present in austenite;
their amount lesser than in P1
(Figures 4.30a-c)

6 hours, — needles are straight(less of obtuse variety
& more of straight edged showing alignment
similar to a layered structure)
(Figure 4.30e)

— feathering is present(Figure 4.30d)

10 hours — basic structure as in 6 hours
(Figures 4.30f-h)

— structure more uniform

— some coarsening of needles seen
(Figures 4.30f-g)

— feathering not apparent

— DCs are more in amount and coarsened
(Figure 4.30g)

(c) 850°C,2 hours   —general coarsening of DCs(Figure 4.31c)

—feathering seen(Figure 4.31a)

—DCs are more

—discontinuity in MCs(Figure 4.31b)

6 hours   —aligned needles(Figures 4.31d-e)

—general coarsening

—coarsening of needles at tips forming

globular shape(Figure 4.31e)

10 hours   —general coarsening of needles   —

(Figures 4.31f-g)

—'needle' volume fraction less

—coarsening of needles, needles acquiring

'rod like' configuration(Figure 4.31h)

—alignment of DCs

—needles approaching/joining DCs

(Figures 4.31g-h)

(d) 900°C,2 hours   —'uneven' matrix etching(Figures 4.32a-c)

—needles & DCs coarsened(Figure 4.32c)

—needles & DCs less than in P1(at this stage)

—no feathering

—dark etching spots around MCs(Figure 4.32c)

6 hours   —discontinuous MCs

—dark etching spots around MCs

—less DCs & needles

10 hours   —as above(Figures 4.32d-f)

—DCs appear more in some regions(some of

them may be disintegrated MCs)(Figure 4.32f)

—needles approaching DCs(Figure 4.32e)

-'haloed' regions around MCs(Figure 4.32f)

-rounding of MCs at edges(general)

(e) 950°C,2 hours   -rounding of MCs(Figures 4.33a-c)

-dissolved MCs or interlinking of MCs & DCs

  observed(Figure 4.33a)

-joining/approaching of MCs(Figure 4.33c)

-both needles & DCs present

6 hours   -pronounced general disintegration and

  'rounding off' of MCs(Figures 4.33d-e)

-needles & DCs are present

-'haloed' regions(Figure 4.33e)

-linking tendency among needles & DCs

  (Figures 4.33d-e)

10 hours   -same as above(Figures 4.33f-g)

-DCs coarsened(Figure 4.33g)

(f) 1000°C, 2 hours -matrix plain(Figures 4.34a-b)

-needles almost nonexistent

-DCs are a part of disintegrated MCs

  (Figure 4.34b)

-linking as before among MCs(Figure 4.34b)

-aligned MCs & DCs

-hexagonal or rounded 'carbides' are present

  (Figure 4.34b)

6 hours   -as above(Figure 4.34c)

10 hours   -rounded MCs(Figures 4.34d-g)

-dark grey/light grey regions adjoining MCs

  (Figures 4.34e-g)

-'haloed' regions around MCs(Figure 4.34g)

-Hexagonal, rounded & some elongated MCs
  (Figure 4.34g)

-interdiffusion of DCs & MCs seen
  (Figures 4.34f-g)

(g) 1050°C, 2 hours -rounded, hexagonal, and rectangular carbides
  observed(Figures 4.35a-c)

-favourable carbide morphology
  (Figures 4.35d-f)

6 hours =grey/dark regions around MCs
  (Figures 4.35e-f)

10 hours -joining of large MCs(Figures 4.35g-i)

-perforated MCs(Figures 4.35i-k)

-general 'morphology' of MCs useful

Alloy P3

(a) As-Cast -similar to P1 including nature and amount of
  carbide(Figures 4.36a-b)

(b) 800°C, 2 hours -minute platelets/DCs(Figures 4.37a-b)

-straight platelets/needles-curving type
  (Figures 4.37b-c)

-obtuse needles/plates also present
  (Figure 4.37c)

6 hours -as above(Figures 4.37d-e)

-'feathering' prominent as in P1
  (Figures 4.37d-e)

-DCs marked/prominent(Figure 4.37e)

10 hours -MCs discontinuous(Figures 4.37f-h)

-coarsening of needles(Figures 4.37f&h)

71

-DCs are present and somewhat coarsened
(Figure 4.37h)

(c) 850°C, 2 hours
-feathering continues(Figures 4.38a&c)

-discontinuous MCs with hexagonal shape
(Figure 4.38a)

-discontinuous MCs with massive morphology
also observed(Figures 4.38b-c)

-'rounding off' at edges already initiated
(Figure 4.38a)

6 hours
-as above(Figures 4.38d-e)

-DCs apparent(Figure 4.38e)

-agglomerating & linking tendency amongst DCs
(Figure 4.38e)

10 hours
-matrix 'even textured' than at 2 & 6 hours
(Figure 4.38f-h)

-coarsening of needles & DCs(Figure 4.38h)

-interlinking of MCs(Figure 4.38f)

-edges of needles are rounding(Figure 4.38h)

(d) 900°C, 2 hours
-'rounding off' at edges of MCs
(Figures 4.39a-b)

-general coarsening

-MCs linking(Figure 4.39b)

-feathering absent(Figure 4.39b)

-formation of dark/grey regions seen(showing
concentration difference)(Figure 4.39b)

6 hours
-same as above(Figures 4.39c-d)

-DCs coarsening(Figures 4.39c-d)

	-needles 'rounding off' at edges
	(Figure 4.39d)
10 hours	-rounding off as before(Figures 4.39e-g)
	-disintegration of MCs(Figures 4.39f-g)
	-aligned DCs and agglomerating tendency
	(Figure 4.39g)
(e) 950°C, 2 hours	-as above(Figures 4.40a-c)
	-MCs linking and alignment observed
	(Figures 4.40a-c)
6 hours	-hexagonal carbides(Figures 4.40d-e)
	-rest as before
	-existence of dark/grey patches continues
	(Figures 4.40d-e)
	-formation of 'haloed regions' around MCs
	(Figure 4.40e)
10 hours	-same as above(Figures 4.40f-h)
	-directional growth amongst MCs and DCs
	(Figures 4.40f-h)
	-general coarsening(both needles and DCs)
	(Figure 4.40f)
(f) 1000°C, 2 hours	-clean matrix(Figures 4.41a-c)
	-rounding of MCs
	-no needles
	-interlinking amongst MCs(Figures 4.41b-c)
	-some 'haloeing' around MCs(Figure 4.41c)
6 hours	-same as above(Figures 4.41d-e)
	-interlinking marked(Figure 4.41e)
	-rounded MCs(both at the edges and overall)

10 hours   -MCs coarsening(Figures 4.41f-h)

                     -aligned MCs/DCs(Figure 4.41h)

(g) 1050°C, 2 hours -general rounding(Figures 4.42a-c)

                     -formation of grey/dark regions around MCs

                      (Figures 4.42b-c)

                     -light grey regions also seen(Figure 4.42a)

6 hours   -basic features as before(Figures 4.42d-g)

                     -interlinking of MCs

10 hours   -general features as before(Figures 4.42h-k)

                     -etching streaks in MCs & light grey regions

                      (Figure 4.42k)

                     -perforated carbides are also seen

                      (Figures 4.42h-j)

                     -apparently no DCs

On comparing the three alloys(i.e. on increasing the Cu content), the following observations emerged:

(i)   DCs formed at an early stage and were more in number,

(ii) no trend was observed with regard to the amount of needles,

(iii) needle morphology tended to become straighter,

(iv) feathering disappeared earlier(lower temperatures & smaller periods),

(v)   matrix microstructure was cleaner and comprised lesser grey/dark regions(at 1000 and 1050°C); carbide morphology and distribution was better,

(vi) better morphology of carbides even on heat treating at high temperature.

4.1.3 Quantitative Metallography

4.1.3.1 Massive Carbides

Effect of heat treatment on the volume fraction of massive carbides was investigated with the help of a LEITZ image analyzer. The data thus obtained have been summarized in Tables 4.35-4.38(Table 4.38 summarizes data contained in the Tables 4.35-4.37).

A perusal of these tables revealed that :

1. Volume fraction of the massive carbides in the as-cast condition ranged from 16-25%, it being the highest in P1 and the least in P3.

2. An increase in the temperature/time, in general, led to a decrease in the amount of massive carbides except in P2 in some of the instances wherein the heat treating at 800°C time had little effect on the volume fraction.

3. Up to 950°C, the decrease in volume fraction was gradual/minimal.

4. Raising the temperature from 950°C to 1000°C led to a marked decrease in the amount of MCs except in P3 which contained the least amount of MCs even in the as-cast condition. On heat treating from 1050°C, a general marked decrease in the volume fraction of massive carbides with time was observed.

5. An interesting observation to emerge from the quantitative data is that with an increase in the copper content, there is a general decrease in the volume fraction of massive carbides with temperature/time even on heat treating from temperatures < 950°C. However at

higher temperatures, trend was reversed on increasing the time.

6. Increasing the copper content also made the micro-structure(s) more uniform with regard to the variation in and the average volume fraction of massive carbides.

7. To understand the nature of variation at (5) and (6) above, the volume fraction of MCs̄ was plotted as a function of temperature as influenced by soaking period (Figures 4.43-4.45).

(i) such a perusal revealed that the variations conform to a second order polynomial, i.e.

% MCs = C1 + C2.T + C3.T^2 (at t in hours).

(ii) On increasing the Cu content, the overall volume fraction of MCs in the as-cast state decreased, and

(iii) the decrease in the volume fraction of MCs with temperature was a function of time, it being slow at lower soaking periods and gaining in momentum with time.

4.1.3.2 Dispersed second phase(DSPs)

Dispersed second phase(both needles and dispersed carbides) were characterized on the basis of the following parameters :

(i) Total number of DSPs

(ii) their 'size based' distribution

(iii) Volume fraction of the DSPs

(iv) their average particle size and

(vi) Percent number and percent area occupied by the DSPs in different size ranges

In the present study also(62) the particles have been classified on the basis of different size ranges with a mean of 0.58µ; a total of four classes existed.

The data thus generated are summarized in the Tables 4.39-4.43, Figures 4.46-4.47, and in Appendix A-1 to A-3. Figures 4.46-4.47 depicts representative hystograms showing a variation in the amount of DSPs at five different locations as influenced by heat treating. The aforesaid data were analyzed in two ways, (a) by assessing whether any general trend existed and (b) by laying down a detailed account of how the heat treating variables affected the parameters employed to characterize the dispersed second phase.

Considering to start with the former, the following general trends were observed for all the alloys:

(i)   Dispersed carbides predominantly belonged to class I(0-0.58µ) and II i.e. size 0.58-1.16 microns(Tables 4.39-4.40 and Appendix A-1 to A-3).

(ii)   The number of particles was a maximum for heat treatments carried out at 800°C & 850°C barring in P1(Table 4.41).

(iii)   On increasing the heat treating temperature up to 950°C, the behaviour of alloys P1 and P2 was similar whereas that of alloy P3 differed, e.g.

Taking the 10 hours treatment to be a representative one to begin with, in P1 and P2, the average particle diameter remained unchanged up to 900°C and then abruptly increased at 950°C followed by a decrease on raising the temperature to 1000°C(Table 4.43). However in P3, the average diameter appeared to remain virtually unchanged up to

77

850°C and decreased thereafter(Table 4.43).

A more detailed analysis revealed that in the alloys P1 and P2, at temperature up to 900°C, a general slight increase in the average particle size was observed or else there was no change with time. At 950°C, there was an abrupt increase in average diameter at 10 hours soaking period whereas at 1000°C there was a reasonable amount of constancy or a slight increase in particle size with time. However at 1000°C, there was a decrease in the average particle size at 10 hours soaking period(Table 4.43).

In P3, the situation up to 850°C was similar to that in P1 and P2. However, hereafter there was a marked coarsening with temperature & time at a fixed temperature (marked up to 8 hours soaking period at 900°C and 6 hours soaking period at 950°C). However, the abrupt decrease in particle(size observed in P1 & P2 at 1000°C at 10 hours soaking period) was initiated(in P3) on heat treating at 900°C at 10 hours soaking period.

(iv) The effect of heat treating parameters on the number of particles and their volume fraction did not conform to a definite trend(Tables 4.41-4.42). Hence this aspect is not being commented upon.

(v) In a general way, it can be stated that for a given time, the number of particles in classes I & II decreased or remained unaltered with an increase in temperature. A similar trend was observed on increasing the heat treating time at a given heat treating temperature(Tables 4.39-4.40).

(vi) The changes described in (v) above were simultaneously supplemented by an increase in the number of particles in class III(Tables 4.39-4.40)

(vii) Representative histograms summarized in Figures 4.46-4.47 proved extremely helpful in appreciating as to how the distribution of the particles varied with temperature and time at different fields of view/specimen cross section.

4.2 Discussion

The main aim of the present investigation was to establish the transformation behaviour of the alloys. This was achieved by heat treating the alloys from different temperatures after holding for different lengths of time followed by assessing the microstructural changes by hardness measurements. Subsequently, the microstructures were quantitatively characterized by studying the variation in (i) the volume fraction of massive carbide and (ii) the size and distribution of dispersed second phase as influenced by heat treating parameters. The data thus generated proved helpful in modelling (i) the transformation behaviour, (ii) the coarsening behaviour of dispersed carbides, and (iii) the heterogeneity based on the distribution of massive carbides and dispersed carbides as influenced by heat treating parameters.

4.2.1 Structural changes during heating

Before embarking upon this analysis, it would be useful to mention once again that the alloys investigated in the present study were designed to ensure that the matrix comprised austenite with higher stability. This has been achieved by maintaining the Mn content at 10%. The Cr content of the alloys was maintained at

7% on the basis of data generated by Singh(72) who studied the abrasion resistance of 6% and 9% Cr cast irons alloyed with 1% Cu and varying amounts of Mn. The 7% limit ensured that there was no danger of graphitization occurring even if Cu was employed in larger amounts(as has been presently done). Thus the present set of alloys contained Cr higher than the one investigated by Jain & Kumar(62,83). Similarly, the copper levels presently used(up to 5%) are higher than the ones employed earlier(62,83). Further, whereas the earlier alloys contained up to 7.5% Mn, the alloys presently investigated contain 10% Mn.

It has been established that (a) nearly 45% of the Mn added partitions to austenite and the balance to the carbide phase, (b) bulk of the chromium partitions to the carbide phase, and (c) bulk of the Cu partitions to austenite(72). This enables an understanding of the ensuing structural changes that will occur which comprise (i) a reduction in the volume fraction of the massive carbides due to the presence of Si and Cu(attributed to their graphitizing tendency), (ii) an increase in the stability of austenite arising out of the dissolution of the additional alloying elements made available as a consequence of (i), and (iii) a possible 'rounding off' of the massive carbides and their being rendered discontinuous due to (i), (iv) occurrence of a carbide transformation which would be governed by the nature of the phase diagrams, and (v) the possible precipitation of carbides from austenite on prolonged soaking as represented by the reaction

austenite --> austenite + DC   ...(4.1)

The likely structural changes therefore, can be summarized with

the help of the following equations :

austenite --> austenite(lesser alloy content) + DC ...(4.2)

MC --> MC(discontinuous with reduced VF)

+ interstitial and substitutional solutes   ...(4.3)

MC --> other types of carbides   ...(4.4)

Interstitial + substitutional solutes + austenite ->

austenite(with increased stability)   ...(4.5)

austenite(with higher stability) increase in SP/ST-->

austenite(relatively lower stability) + DC   ...(4.6)

$$\text{DC} \quad \text{increase in} \quad \frac{\text{ST at given SP}}{\text{SP at given ST}} \rightarrow \text{DC(coarse)} \quad ...(4.7)$$
or possible dissolution
at higher temperature(s)

4.2.2 Changes during cooling to room temperature

They will be governed by the cooling rate and the alloy content and would primarily be confined to austenite. Some changes may also occur in the massive carbides and the DCs that have formed. The possible changes in austenite would depend upon the temperature and time as they govern the relative stability of austenite in accordance with the Equations (4.2), (4.5), and (4.6). If air cooling is done, austenite may reject excess solute in the form of dispersed carbides and would subsequently transform to either B/M and or remain untransformed. Since the minimum Mn content in the alloys is appreciably higher(10%) to ensure that no martensite can form on air cooling from 800 and 850°C, it is evident that the transformation product in the present alloys on air cooling would essentially be austenite independent of the temperature from which they are cooled. This tendency is further aided by the amount of Cr that would

81

partition to τ in spite of its being a carbide former. Similarly, Cu would essentially partition to τ only. Any martensite if at all present, may at best be observed on air cooling from 800 and/or confined to the as-cast state.

Carbide precipitation during cooling mainly occurs because of a decrease in the solid solubility of carbon with temperature in the austenite. If austenite is supersaturated after heat treatment, it would reject out excess solute as carbides and these would be inherited by the transformation product of austenite on cooling which in the present situation is most likely to be austenite only and therefore the chances of excess carbon precipitating as carbides are greatly reduced since part of Cr partitioning to it also has large solubility in austenite. If however the austenite is not supersaturated and is in a state wherein the solute is fully or 'near completely' dissolved (requiring a higher heat treating temperature), it will be retained as such on cooling.

Taking an overall view, the possible structural changes on cooling can be summarized with the help of the following equations :

Slow cooling(as during casting)

austenite --> austenite(τ) + some martensite(M) ?   ...(4.8)

(relative proportion of the τ & M depending upon the Cu content)

Carbide --> unchanged or otherwise, depending upon

carbide transformation   ...(4.9)
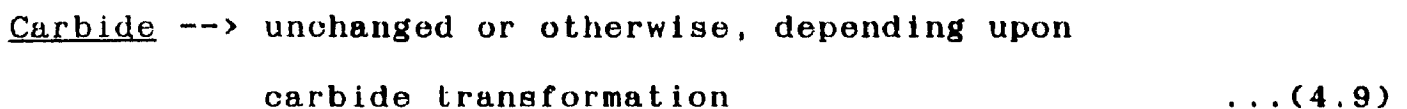
Final likely structure : τ + M(?) + MCs

Heat treated condition

(a) Lower temperatures 800 and 850°C

    austenite --> austenite* + DC   ....(4.10)

    austenite* --> τ mostly + M(?)   or exclusively τ   ...(4.11)

(extent of M, if any, depends upon soaking period i.e. less at lower soaking period and likely to be negligible at higher soaking period)

Massive carbide --> M'C' + M"C" etc.   ...(4.12)

DC --> DC(coarse)   ...(4.7)

Final likely structure : τ + M(?) + MC + DC

(b) Temperatures 900 & 950°C

austenite* --> austenite   ...(4.13)

DC --> DC(coarse)   ...(4.7)

MC --> M'C' + M"C" + --- (volume fraction reduced)   ...(4.12)

Likely final structure : austenite + DC + MC

(c) 1000 and 1050°C

austenite* --> austenite(matrix completely austenitic)   ...(4.14)

DC --> DC(coarse) and possible dissolution at higher

        soaking period(s) and temperature(s)   ...(4.7)

MC --> M'C' + M"C" + --- (volume fraction low, possible rounding

               off may be observed)   ...(4.12)

Final likely structure : austenite + MC + some DC(?)

            or austenite + MC

4.2.3 Strengthening response of different transformations

    Before analyzing the structure-property relations it would be appropriate to consider the strengthening associated with different transformations.

The austenite to martensite transformation leads to hardening and to simultaneous embrittlement. It is of little significance in so far as the present study is concerned. The attainment of austenitic matrices would lead to an improvement in the ease of deformation. In such instances, the stacking fault energy(SFE) of the matrix would determine the strength-ductility interrelation as it(SFE) controls the extent of work hardening. It is relevant to record here that Mn-austenites have a low SFE and hence exhibit a high rate of work hardening(96).

Massive carbides have a higher hardness and the strengthening response would be directly related to their volume fraction. Its morphology and compatibility with the matrix are also equally important. The latter is governed by the crystal structure. The effect of dispersed carbides would be governed by the volume fraction, compatibility with the matrix, size, shape and distribution(82).

4.2.4 Interrelation between microstructure and hardness

The general microstructural changes that may occur in the experimental alloys, highlighted in the earlier sections, facilitate interpretation of the structural changes that would occur in P1, P2, and P3. As hardness is governed by the microstructure, the two have been discussed together.

4.2.4.1 As-cast state

The microstructure of the alloys in the as cast condition namely, τ + MCs + dark areas(M ?) appearing as 'leaves'(Figures 4.22c, 4.29c & 4.36b), is consistent with the analysis outlined in the sections 4.2.1-4.2.3(Equation-4.8). At 10% Mn the matrix is expected to be austenitic as has been observed. The precise

84

identity of dark areas is difficult to surmise, i.e whether they in fact represent martensitic regions. None the less these features are common to all the alloys.

Apparently the three alloys do differ in some respects especially with regard to the morphology of the massive carbides. While describing the microstructure, three types of massive carbides have been identified, namely, (a) flower type or eutectic, (b) massive/platy type, and (c) mesh type. The amount of type (a) & (b) carbides will be governed by the carbon equivalent of the composition and its(compositions's) disposition with respect to the modified eutectic composition. The (c) type carbide is governed by the phosphorous content which is approximately the same in all the three alloys. Considering the carbon equivalent of the compositions being investigated on the basis of the data reported by Merchant(97), the modified eutectic composition is 4.5%. Thus effectively the compositions being investigated are hypoeutectic in nature. Based on this analysis the reasons for the compactness of the massive carbides(Figure 4.29b) in alloy P2 are not clear. The microstructure of alloy P1 does in fact conform to its being hypoeutectic in character by exhibiting a fair proportion of platy carbides(which incidentally are 'discontinuous')(Figures 4.22a-c). The same is true for the composition P3(Figures 4.36a-b). The presence of primary(proeutectic) carbide(Figure 4.36a) may be due to localized solute enrichment and the formation of platy and discontinuous carbides (Figures 4.22,4,29 & 4.36) is as per expectations. Thus the microstructures in the as-cast condition are appropriately

explained. In alloys with an austenitic matrix, the strengthening is essentially governed by the amount of MCs which would be directly related to the amount of copper present(the levels of Mn and Si being nearly the same in the three alloys). Accordingly the maximum hardness in the as-cast condition should be attained in P1 and the minimum in P3 as has been observed(Figures 4.1-4.3).

4.2.4.2 Heat treated condition

The structural changes in the heat treated condition have been outlined with the help of equations in the sections 4.2.2.1-4.2.2.3. The prominent changes would be the precipitation of carbides from the austenite during soaking and a reduction in the amount of MCs and their eventual 'rounding off'.

For the sake of simplicity, transformations in P1 will be initially discussed and subsequently the similarities/ differences between P1 and the transformations observed in P2 and P3.

4.2.4.3 Alloy P1:

(a) 800°C: The interesting aspect is the formation of 'a needle like' precipitated second phase(Figure 4.23). At 2 hours soaking period the needles formed although having different morphologies, (Figures 4.23a-b) appear to have etching characteristics similar to the dispersed carbides, more clearly seen at higher soaking periods(Figures 4.23c-d). This leads to an inference that they could either be carbides which is most likely and/or some intermetallics. It is not possible to identify them through optical metallography except on the basis of microhardness measurements. As this proved difficult, the identification aspect has been separately dealt with and would be discussed in the next

chapter. The obtuse morphology of some of the needles, more prominent at higher heat treating temperatures/periods(Figures 4.23c&f), may lead to a mistaken inference that the precipitated phase is martensite. However based on 'alloy design' considerations, such a possibility is rather remote. Moreover, the 'obtuse plate' feature is observed even on heat treating from higher soaking temperatures. This establishes beyond doubt that the obtuse plates do not represent martensite because the alloys are so designed so as to exclude its formation and to ensure the retention of austenite over a wide range of temperatures.

An important observation is the occurrence of feathering around needles/obtuse plates(Figures 4.23c,d & f). Its presence gives an impression as though a new phase is forming. However careful etching through a succession of reagents, such as Murakami, nital and permanganate solution, reveals to the contrary. It is postulated that 'feathering' basically represents 'regions' around needles/plates whose alloy concentration differs from the rest of the matrix. It is apparently a precursor to the initiation of coarsening which predominantly occurs at 'higher' heat treating temperatures and holding periods. The observation that lends credence to this analysis is that 'feathering' is not observed beyond a certain heat treating temperature/time after the needles with 'planar' or 'obtuse' morphologies had attained a certain level of coarsening.

The observance of large volume fraction of DCs at 10 hours soaking period(Figure 4.23f) is logical because the tendency to precipitate/coarsen would naturally be dominant at higher soaking

periods at a given temperature as a larger activation is available for the intended changes.

850°C: On heat treating at 850°C for 2 hours, the major expected changes are a general coarsening and the formation of a larger volume fraction of DCs and DSPs(needle/plate)(Figure 4.24) because the temperature is higher. The coarsening tendencies would be marked at higher soaking periods. This is what has been observed(Figures 4.24d-f). The absence of 'feathering' beyond 6 hours(Figure 4.24f) is perhaps an indication that the 'prerequisite' state to initiate coarsening had been apparently reached and hereafter it would gain momentum as is demonstrated by the microstructures attained on heat treating for 10 hours(Figures 4.24f-g).

The formation of differentially etching regions within the austenitic matrix(Figures 4.24e-f) is an indication of 'heterogeneity' which is being sustained/accentuated due to the possible disintegration of MCs(Equation-4.12). As the heat treating temperature is low, the concentration gradients thus formed persist. It is expected to be evened out as the temperature increases. The disintegration of MCs is occurring because of the combined graphitizing action of Cu and Si(as already discussed) whose intensity will increase with temperature. This leads to a reduction in the volume fraction of MCS(which is minimal at this temperature) and in their being rendered discontinuous to begin with(Figures 4.24a,c,d & f).

The most interesting feature i.e. the formation of aligned DCs(Figure 4.24f) suggests the 'precipitating tendency' to be directional which appears reasonable as the precipitating phase

will pick out directions of closest packing. This could also be interpreted differently by stating that the 'aligned' carbides are in fact the 'globularized segments' of the precipitating needle morphology being so rendered due the combined graphitizing tendency of Cu and Si. Otherwise no specific reasons exist as to why the carbides should be 'aligned'.

900°C: The structural changes at 900°C as influenced by an increase in the soaking period are essentially on similar lines as those observed on heat treating at 850°C(Figure 4.25). Evidently the temperature being higher, the extent of coarsening of DCs and needles and disintegration of MCs will be more marked(Figures 4.25b-d,f,g,i). The same could also be stated for 'feathering' which is still observed up to 6 hours soaking period(Figure 4.25f). The etching characteristics of the matrix are more or less uniform(Figures 4.25b&g) because the non-uniformity of the matrix vis-a-vis the solute concentration is evened out at a higher temperature(as the present one). The coarsening of needles is occurring both along the length as well as along the width(Figures 4.25b,e & i) akin to the 'edgewise' and 'side wise' growth patterns observed in the coarsening of 'layered morphologies'(such as pearlite). However, the special features namely the 'needle ends'(now plate ends) acquiring rounded shapes and 'aligned' precipitation of carbides(both dispersed and massive) are strikingly distinctive in character representing 'preferred directional growth' and needing a more careful analysis(Figures 4.25g&i). Rounding off amongst MCs is occurring to enable them to acquire lower energy configuration(s)

at higher heat treating temperatures(section 4.2.1).

950°C: The microstructures observed at this temperature as influenced by soaking period(Figure 4.26a) are consistent with the reasoning put forward to explain similar changes earlier. The main difference is that 'feathering' has disappeared which is what is expected at higher temperatures. Presence of needles is mostly limited up to 6 hours which is logical since around this temperature or higher a near spherical morphology is more preferred, more so at a higher soaking periods. Rounding off of MCs will be more, the extent of coarsening will be larger and the remaining portions of MCs will acquire lower energy configuration (spherical/hexagonal) particularly so at higher soaking periods since this temperature is the same as that employed for malleablizing(98). All of these features can be attributed to enhanced diffusion rates at 950°C. Only hereafter would pronounced changes occur in the massive carbide morphology and a marked reduction in their volume fraction(Figures 4.26).

Massive carbide regions are seen approaching one another in an effort to reduce their volume fraction and also perhaps to acquire low energy configurations(Figures 4.26a,d & f). This is a unique feature observed, which although similar to 'diffusion bonding', has neither been hither to reported nor observed so distinctly in alloyed white irons or in other materials where large sized carbides are present in the microstructure. Although Ostwald- ripening does come close enough to this situation but its occurrence has been mostly observed/confined to dispersed second phase. What is bringing about a similar situation amongst MCs is perhaps the tendency of the alloy to pronounced

directional precipitation/growth and a desire to minimize the volume fraction of the second phase with a view to reduce energy.

At some locations 'haloed' regions(representing a different etching character within the matrix) are observed especially around MCs/coarsening DCS(Figures 4.26c&f). They may represent regions with a different alloy concentration(indicative of a different strain field compared to the matrix) during the process of carbide growth/coalescence.

1000°C: On heat treating at 1000°C for 2 hours, the changes described at 950°C especially at 10 hours heat treating period are further accelerated. Linking of MCs along boundaries(Figures 4.27a-b) may represent the disintegration of the earlier existing larger MCs thereby leaving behind regions such as those presently observed. However if this is not the case, then the reasons for such a link up existing at least at 2 hours soaking period are not easy to understand. Similarly the nature of these boundaries is not clearly understood. In fact, going by the observations of the Jain and Kumar(62,83), these boundaries may in fact represent regions contributing to the formation of a new(carbide) phase. This appears to be a more reasonable/plausible assessment of the nature of the boundaries.

The observation that the austenitic matrix is relatively clean is an indication that compositional heterogeneities are minimized and simultaneously the number of transformations occurring within the matrix are at a minimum. This is to be expected in view of the temperature being high which would contribute to the structure attaining as high a stability as

possible. None the less the formation of some small sized dispersed second phase is still in evidence(Figures 4.27b-d).

The absence of needles, as on prolonged soaking at 950°C, is a welcome feature and signifies the process of growth to be equiaxial rather than directional as would be expected at high temperatures. For similar reasons, the MCs would acquire morphologies such as 'near spherical' or 'hexagonal'(Figures 4.27c,e & i) and their volume fraction would reduce. The latter is aided by the observed 'linking up' amongst massive carbides.

The formation of localized dark grey etching regions around massive and dispersed carbides(Figures 4.27g & i) needs commenting upon. Such regions are apparently forming as a prelude to either the DCs or the MCs linking up/agglomerating. There are also instances where isolated MCs are developing dark etching regions around themselves which may be due to the initiation of the formation of a new phase(Figures 4.27g-i). All the aforesaid tendencies will be marked at higher heat treating temperatures/ soaking periods.

1050°C: The prominent features observed on heat treating at 1050°C are essentially an extension of changes occurring on heat treating at 1000°C(Figures 4.28), namely, (a) general 'rounding off' of MCs, (b) their linking/agglomerating along specific directions, (c) formation of dark grey/dark etching regions around MCs and in the regions separating adjoining MCs, and (c) formation of linkages and eventual 'spherodization'* and/or formation of hexagonal MCs. The only difference is that all of the aforesaid tendencies are marked due to the temperature being

* Refers to small sized MCs as distinct from the usual MCs or DCs

higher. The driving force for marked 'agglomeration' amongst MCs is the tendency of the microstructure to reduce its energy. Further, the 'dark grey' and 'dark etching' regions are definitely austenitic depicting solute concentration different from the austenitic matrix— so essential to facilitating the agglomerating/linking up processes(Figures 4.28).

It is of significance that a greater unevenness within the austenitic matrix and the formation of small sized DCs have been observed. In fact the former and the latter add up to suggest that the unevenness is because of initiation of certain precipitation based transformation(s) afresh. The reason for the formation of 'linkups'(Figures 4.28d&i) appears to be that they are acting as initiators for the formation of a new(carbide) phase.

Occasionally the existence of 'differently etching-carbide free' regions(Figures 4.28d&g) reveals the possibility of producing fully austenitic matrix locally. Its creation while minimizing the energy of the microstructure creates heterogeneity within the microstructure.

When these alloys are compared with those investigated by Jain and Kumar(82,83), it then becomes evident that the microstructures in the 6-8% Mn and 5% Cr and 1.5-3.0% Cu white irons examined by them were less complex than the ones being presently observed with regard to (i) the initiation of transformation(s) afresh at a number of points within the matrix even on heat treating at 1050°C and (ii) the formation of varied dispersed second phases. In fact the earlier alloys although free from these changes, none the less suffered from problems resulting

from the formation of an 'eutectic type' of platy carbide at lower soaking periods on heat treating at 1050°C. The presently investigated alloys are free from this problem.

4.2.4.4 Alloys P2 and P3

Structural changes observed in P2(Figures 4.29-4.35) and P3(Figures 4.36-4.42) are on similar lines as those described in the alloy P1(Figures 4.22-4.28). Therefore no specific comment is being made so as to avoid repetition.

Taking an overall view, the difference on proceeding from P1 to P3 can be attributed to copper increasing from 1.5% to 5%.

The differences between P1 and the alloys P2 & P3, namely-

(a) the 'straight' needle morphology being prevalent than the 'obtuse plate' morphology,

(b) dispersed carbides forming at relatively lower temperatures/ soaking period(s),

(c) disappearance of plates at relatively lower temperature(s) and soaking period(s),

(d) disintegration amongst MCs being faster-initiated at lower heat treating temperature(s)/soaking periods,

(e) unevenness of the matrix being lesser except on heat treating at 1050°C,

(f) overall distribution of MCs being better;

(g) the elimination of 'feathering' around needles setting in at lower heat treating temperatures and soaking periods, and

(h) the overall distribution of MCs at higher temperature being better,

confirm the above reasoning to be correct as the aforesaid changes are duly related with an increase in the carbide destabi-

lizing tendency and austenite stabilizing tendencies thereby enabling structural changes to be initiated/occur at lower temperature(s) and/or lower period(s).

A similar reasoning explains why dark grey/dark etching regions at higher heat treating temperatures are the least in the alloy P3.

This in essence would conclude the discussion on the nature of the structural changes. The aforesaid similarities and differences are clearly reflected in the hardness data and the next section would therefore be devoted to this aspect. Being a useful indicator of the likely properties, the hardness-microstructure interrelations assume major significance as a precursor to an understanding of the microstructure-property correlations.

4.2.4.5 Hardness-microstructure interrelation

The aforesaid analysis provides a basis for explaining the hardness changes as influenced by the temperature and time.

(a) Alloy P1

Considering the alloy P1(Figure 4.1), on heat treating at 800°C for 2 hours, the hardness is lower than the as-cast hardness which indirectly suggests that no martensite is forming on heat treating. A very general gradual increase in hardness with time is due to an increase in the amount of precipitated second phase(needles and/or DCs). The hardness at 10 hours soaking period is still lower than in the as-cast state because the volume fraction of the marginally reduced MCs is lower than in the as-cast state(Table 4.35) and the increase in hardness due to DSPs is insufficient to offset the overall balance.

On raising the temperature to 850°C, there is little change in the hardness levels up to 6 hours soaking period over that observed at 800°C as there is little change in the micro-structure. The small decrease in hardness on increasing the period further is an indication that coarsening of the DCs has perhaps set in and at the same time the reduction in the amount of MCs is marginally higher than at 800°C. Unlike the situation at 800°C, the overall hardness is independent of the soaking time since the factors promoting increase and decrease in hardness approximately balance one another.

On heat treating at 900°C, the coarsening of precipitated second phase and a larger reduction in the amount of MCs(an indirect increase in the amount of austenite) has resulted in the hardness decreasing with soaking period. Evidently, the overall hardness at 900°C is lower than that at 850°C for reasons already stated. A similar analysis would also explain the reasons for a decrease in hardness with time on heat treating at 950°C and also its overall level being lower than the one attained on heat treating at 900°C. It is noteworthy that the decrease in the amount of MCs would be marked hereafter for reasons already discussed(section-4.2.4.3).

On comparing the hardness levels at 850°C, 900°C, and 950°C at higher soaking periods, the decrease in hardness is getting marked with an increase in temperature. This is due to (i) the coarsening of dispersed second phase up to 900°C, (ii) its more or less complete disappearance at 950°C, and (iii) more impor-tantly because of an enhanced tendency at reducing the volume fraction of MCs. All these add up to an increase in the amount of

austenite and its stability(Equation-4.5).

On raising the temperature to 1000°C, the matrix is practically free from DCs and the reduction in hardness with time is basically due to a reduction in the volume fraction of MCs. A similar situation also exists at 1050°C except that changes occurring are more marked than at 1000°C. The maximum reduction in hardness is occurring at 10 hours soaking period on transiting from 1000 to 1050°C due to (i) a marked decrease in volume fraction of MCs(as a result of enhanced graphitizing/carbide destabilizing tendency) and (ii) an enhanced interdiffusing/ agglomerating tendencies amongst MCs..

(b) Hardness changes in alloys P2 and P3

The hardness changes in P2 and P3(Figures 4.2-4.3) can be interpreted on similar lines. The only difference is that on heat treating at 800°C, the overall hardness is slightly higher than in the as-cast state contrary to what is observed in P1 and on heat treating from temperatures > 800°C, the decrease in hardness is more marked as compared to that observed in P1(Figures 4.1-4.3).

The initial difference on heat treating at 800°C i.e. (a) the observance of a marginal increase in hardness with time(only in P2) and (b) the overall level of hardness being marginally higher than in the as-cast state is because the amount of precipitating second phase is more in P2 and P3. Both P2 and P3 attain volume fraction of MCs lower than in P1(P3 attains the least) and accordingly heat treating would have little effect on the volume fraction of MCs in the heat treated condition to begin

with(Tables 5.35-4.37), i.e. hardness change is being controlled by the volume fraction of DSPs.

Apart from the above, the other major difference between P1 and, P2 & P3 is that whereas in P1 the hardness begins to decrease with time on heat treating at 900°C, it is remaining unaltered or independent of time up to 900°C in P2 and up to 850°C in P3. The overall decrease/the rate of decrease is maximum in P3 and a minimum in P1 with P2 falling in between. All the aforesaid differences are essentially related to the carbide destabilizing/DSPs forming tendencies and therefore can be attributed to the higher copper content in P2 and highest in P3. This results in the overall hardness being less and the decrease in hardness being steeper and setting in early in P3.

On comparing P2 and P3, the commonality exists only upon heat treating from 800 and 850°C that to with a proviso that the hardness on heat treating P3 at 850°C is marginally lower than that attained on heat treating P2 at the same temperature. Hereafter the differences between the overall hardness levels between P2 and P3 get marked especially at higher holding periods. The aforesaid observations, namely, the decreasing trend in hardness setting early in P3 and the overall hardness being lower at higher soaking periods can once again be attributed to a larger copper content in P3 and hence to a larger carbide destabilizing and austenite stabilizing effects. Accordingly the least hardness is observed in alloy P3 on soaking for 10 hours at 1050°C.

4.2.4.6 Comparative changes in hardness in P1, P2, and P3 as influenced by heat treating parameters

The discussion up till now centered around explaining the base curves(Figures 4.1-4.3). It would now be appropriate to compare the relative behaviour of the three alloys as influenced by time(Figures 4.4-4.9).

The general behaviour of the alloys P1 and P2 is similar on heat treating at 800°C because, overall, the precipitating second phase is playing a major role in controlling it. P3 however responded differently(Figure 4.4) more due to a lower initial volume fraction of massive carbides(Table 4.38). This is further borne out by the observation that the hardness values in P2 and P3 in the as-cast condition are marginally lower than in the heat treated condition(temperature 800°C)(Tables 4.7 & 4.13). This reaffirms the relevance of the precipitating second phase overall and a greater emphasis they command in the higher Cu containing alloys P2 and P3(Figure 4.4).

The similarity amongst the three alloys on heat treating at 850°C(hardness being independent of time)(Figure 4.5) is a pointer that the overall contributions of an increasing second phase and decreasing MCs approximately balanced out, the lower initial volume fraction of MCs not withstanding(Tables 4.8 & 4.14).

The similarity in P1 and P3 on heat treating at 900 and 950°C(denoting a decrease in hardness with time) is due to (i) the dominant role of decreasing MCs in P3 and (ii) a reducing volume fraction of precipitated second phase in P1; both the changes contributing to indirectly a similar end result(Figures

4.6-4.7). The structural changes in P2 constitute a via media between the changes in P1 & P3 resulting in the hardness remaining more or less unaltered with time(Tables 4.9-4.10 & 4.15-4.16).

On heat treating at 1000°C, the precipitating second phase is practically absent and the differentiating factor is the rate at which volume fraction of MCs is decreasing with time; this being equivalent, leads to the similarity in the overall behaviour of the experimental alloys(Figure 4.8, Tables 4.11 and 4.17).

On heat treating at 1050°C, the changes are on similar lines as those indicated at 1000°C, the difference essentially arising only because of a 'hardness arrest' at 8 hours soaking period (Figure 4.9, Tables 4.12 and 4.18) and an enhanced carbide destabilizing tendency. Reasons for the former are not clearly understood whilst that for the latter are explained.

Thus overall, the Figures 4.4-4.9 reiterate the commonality and differences amongst the three alloys discussed individually on the basis of the Figures 4.1-4.3.

4.2.5 Hardness and time interrelation

The data contained in the Tables 4.1-4.18 and Figures 4.1-4.9 were analyzed with the help of a computer programme to arrive at the aforesaid interrelation. Constants for the first, second and third order variations were calculated using the least square technique(99,100) and are also reported at the bottom of each of the Tables 4.1-4.18. Although the variance decreased as the order of equations increased, plotting of the data revealed that the hardness-time interrelation and its interpretation(already discussed) can be best explained on the

basis of a first order equation. The calculated values of hardness on this basis(also indicated in the Tables) are in excellent agreement with the experimental values. Thus, hardness H can be expressed by an equation :

$$H = C1 + C2.t \text{ (at a constant temperature)} \qquad ...(4.15)$$

The values of the constants C1 and C2 for each of the alloys at different heat treating temperatures are indicated in the Tables 4.1-4.18.

4.2.6 Hardness-temperature interrelations

4.2.6.1 Nature of variation

In order to arrive at the aforesaid correlation, the hardness vs temperature data for each of the alloys(summarized in the Tables 4.19-4.33) were analyzed and the constants for the first to fourth order variations calculated(Tables 4.19-4.33). It is not reasonable to assume that hardness varies linearly with temperature especially so when changes in the microstructure are being brought about by at least two major transformations. On a similar ground a third or a fourth order variation is also ruled out. Of the available options a second order variation represents the microstructural changes most appropriately which comprise an initial gradual/minimal decrease in hardness which is followed by a marked decrease in hardness at T ≥ 950°C. Hence the variation in hardness with temperature at each of the soaking periods can be most appropriately represented by a second order polynomial :

$$H = C1 + C2.T + C3.T^2 \qquad ...(4.16)$$

The values of the constants C1, C2, and C3 have been

indicated in the Tables 4.19-4.33. This analysis forms the basis of arriving at the hardness vs temperature plots(Figures 4.10-4.17) which are in the form of an inverted parabola.

4.2.6.2 Effect of temperature on hardness and microstructure

The aforesaid data summarised in the Figures 4.10-4.12 can be interpreted on a basis similar to the one employed for interpreting the data contained in the Figures 4.1-4.3. However, it is the shape of the hardness vs temperature plots that needs analyzing. As already stated(section 4.2.6.1), the hardness vs temperature plots should have an inverted parabolic configuration i.e. the hardness decreasing somewhat slowly to begin with and gaining momentum after a threshold temperature is exceeded. Since the base microstructure is nearly identical in all the three alloys(austenitic matrix), the hardness changes would be governed by the overall outcome of the two transformations namely, (i) formation of precipitated second phase and (ii) decrease in MCs. As already noted the former increases the hardness whereas the latter decreases it. Evidently, the overall change in hardness with temperature will be very slow to begin with especially at lower soaking periods and in alloy(s) exhibiting the least austenite stabilizing/carbide destabilizing tendencies(i.e. alloy P1) and would gain momentum as more activation is provided by increasing time(Figure 4.10). The extent of activation provided increases with temperature & time at a given temperature and would be more at higher temperatures. This analysis satisfactorily explains the general features of the hardness vs temperature plots(Figures 4.10a-e).

102

The higher Cu alloys P2 and P3 exhibit a near linear behaviour to begin with since the austenite stabilizing/carbide destabilizing tendency in them is larger and directly related with the copper content. Thus the transformation products conducive to sustaining a higher level of hardness are not as effective(due to their reduced V_f) and therefore the decrease in hardness with temperature and time sets in early although a more steeper decrease in hardness is observed only at temperatures ≥ 950°C as in P1(Figure 4.10). This explains the data summarized in Figures 4.11-4.12.

The aforesaid analysis would also explain why the COP (signifying a change in the slope of the hardness vs temperature plots) would occur at higher temperature in P1 and to some extent in P2 and at lower temperature in P3(Figures 4.10-4.12). The maximum decrease in the hardness(hardness band) in the alloys has occurred at 1050°C firstly because this is the highest heat treating temperature employed and secondly because at this temperature the different structural changes leading to a decrease in hardness occur the fastest and to the maximum extent. At 1050°C, the higher the soaking period, the smaller would be the volume fraction of massive carbide and larger the volume fraction of austenite and therefore, the lower would be the hardness(Figures 4.10-4.12).

4.2.6.3 Comparative hardness vs temperature data

The comparative hardness vs temperature plots(Figures 4.13-4.17), essentially derived from the data summarized in the Figures 4.10-4.12, indicate the effect of soaking period in influencing H vs T relation and can essentially be interpreted on

a similar basis as the one employed for interpreting the Figures 4.10-4.12. The usefulness of the Figures 4.13-4.17 is that they reveal the comparative data at a glance and this is further summarized in the form of bar diagrams depicted in Figures 4.18-4.21.

4.2.7 Effect of temperature and time on the morphology and volume fraction of massive carbides

Although the effect of massive carbides in controlling the overall hardness has been discussed at length in sections 4.2.4.5 & 4.2.6.2, it would be appropriate to comment upon the effect of heat treating parameters on their morphology and volume fraction. Massive carbides present in the as-cast structure(Figures 4.22, 4.29, and 4.36) are partly discontinuous and have been so rendered due to the graphitizing action of Cu and Si(sections 4.2.1-4.2.3). This tendency, which increases with Cu content, temperature and time, also reduces the volume fraction of massive carbides on heat treating.

Based on physical metallurgical considerations associated with malleablizing in so far as carbide destabilization/disintegration is concerned(98), it is expected that the tendency towards attaining (a) a discontinuous morphology and (b) a reduced volume fraction would become marked at temperature $\geq$ 950°C. Another reason why volume fraction of massive carbides may not significantly decrease until 950°C is that other transformation(s) involving the formation of precipitated second phase as needles and DCs(highlighted earlier) take precedence over the carbide transformation. This is because they require lesser activation in terms of temperature.

However, unlike in malleable irons, the carbide phase in the experimental alloys has been rendered stable by Cr additions (section 2.2). Additionally a fair proportion of Mn also partitions to it, thereby enhancing its stability(72). Therefore, as the heat treating temperature and time are increased the massive carbides instead of decomposing into graphite, will acquire a low energy near rounded or hexagonal morphologies. The precise nature would be governed by the crystal structure of the massive carbides as influenced by heat treating temperature and time. This analysis explains why (i) carbides are rendered discontinuous, (ii) their volume fraction reduced with temperature and time, and (iii) the 'rounding off' tendency is observed on heat treating from higher temperatures/periods (Figures 4.22-4.42).

Considering the decrease in the Vf of massive carbides, the Cr containing carbides, as already stated, are further rendered stable because Mn(55-60% of the added amount) partitions to them(72). Therefore, normally the decrease in the volume fraction of massive carbides will be faster only at temperatures around 950°C or higher(i.e. 1000°C) because this is the temperature at which carbide is destabilized during malleablizing. This is duly supported by the observations discussed earlier(Figures 4.43-4.45). This process(involving a reduction in the volume fraction of massive carbides) will be further aided by the presence of a fully austenitic matrix and this occurs in the experimental alloys even in the as-cast state. This may account for a reasonable reduction in the Vf of MCs even at temperatures lower than 950°C.

Although copper is a mild graphitizer, the carbide destabilizing tendency is directly proportional to the copper + silicon content. An important effect of raising Cu content will be that the volume fraction of MCs in the as-cast state will reduce and the reduction in the Vf of MCs will set in at lower temperatures/soaking periods. Thus the data summarized in Table 4.38 and in Figures 4.43-4.45 thus stand appropriately explained. The least volume fraction of massive carbides will be observed at the highest soaking temperature and time(Table 4.38).

An analysis of the manner in which MCs decreased revealed that an increase in the soaking period had only a marginal effect at least to begin with and gathers momentum with time more markedly at higher temperatures. It was therefore felt appropriate to quantify the decrease as a function of temperature at different soaking periods(Figures 4.43-4.45). On doing so it emerged that the plots should logically follow a second order variation, namely, the same as the one observed when the variation in hardness with temperature as influenced by soaking period was considered(Figures 4.10-4.12). Evidently the data in Figures 4.43-4.45 would be interpreted similarly as the one in Figures 4.10-4.12.

4.2.8 Effect of time and temperature on the distribution of dispersed second phase

Sections 4.2.1-4.2.2 highlight the mechanism of formation of dispersed second phase from austenite. The results summarized in the Tables 4.39-4.43, Figures 4.46-4.47, and in Appendix A-1 to A-3 prove helpful in characterizing them comprehensively. Particles constituting the dispersed carbides have a size up to

1.16µ because they exclusively fall into classes I and II at the formation stage. This is valid for all the alloys. On heat treating, their distribution is altered in a manner consistent with the attributes of nucleation and growth type of transformations. Simultaneously, coarsening would also set in. This would lead to a reduction in the number of particles in the first two classes and a simultaneous increase in their number in the class III or higher. Additionally, the mean diameter would also increase. This is what has been observed in a majority of the instances at least in alloys P1 and P2 and partly in P3. The main deviation is that a 'general coarsening' is followed by a phenomenon in reverse. This is because, after a certain stage of heat treating the matrix begins to dissolve the DSPs leading to a decrease their mean diameter as well as in their numbers(which is also reflected in the Vf getting reduced(Tables 4.39-4.43). The extent and the stage at which this sets in would be governed by the τ- stabilizing tendency of the matrix and the carbide destabilizing tendency. This in the present instance is being controlled by the Cu content and accordingly the extent of coarsening is lesser in P3 and the 'carbide' dissolution tendency sets in early(at lower heat treating temperature/time) in P3. In fact, for similar reasons P3 does not exhibit a marked tendency towards coarsening. Such a thinking could also form a useful basis for analyzing the data related with DSPs in a general sense.

The comparative data given in the Tables 4.39-4.43 reveal that it would not be easy to arrive at a broad based correlation

between composition and heat treating parameters with coarsening. Arriving at such an understanding is of interest as the coarsening behaviour & heterogeneity of distribution would govern the overall properties of the alloys. Till date Ostwald's equation(101) given below is the most authentic formulation for studying the coarsening behaviour of second phase particles, i.e.

$$r_1^3 - r_0^3 = k(t_1 - t_0) \qquad \qquad ...(4.17)$$

where r_1 = particle radius at time t_1, and

r_0 = particle radius at time t_0

A major limitation of this equation is that a large number of data points are required to ascertain its validity/to ensure its application under a given set of experimental conditions. Moreover the equation merely correlates the arithmetical mean of particle radius with time but in no way reflects upon how the particle distribution is influenced by heat treating parameters. Further, finding out the arithmetical average of particle radius does not represent the true picture since the particle size distribution is statistical in nature. In the present investigation the data related with the second phase are available for all soaking periods at a given temperature. Generally, this should have sufficed for any further analysis of the data but not so with the above equation especially when it is intended to represent distribution. The difficulties arising thus were resolved by evolving a new parameter called the 'coarsening index'(CI)(62).

In order to calculate coarsening index, it is necessary to first evolve a parameter which can represent particle size distribution for a given heat treating schedule. Development of

such a parameter was greatly facilitated by the manner in which the quantitative metallographic data was generated, namely, the (a) categorization of particles into different classes, (b) assessment of the number of particles in different classes, (c) calculation of percent number and area occupied by particles in different classes, and (d) measurement of the average particle diameter. The new parameter termed the 'distribution factor'(DF) which incorporated the variables (a) to (d) is defined as(62,81)

$$DF = \frac{\sum_{i=1}^{n} X_i . N_i}{\sum_{i=1}^{n} N_i} \qquad \qquad ...(4.18)$$

where, n = the number of classes,

N_i = the number of particles in i^{th} class,

X_i = volume fraction in the ith class /VDC,

and, VDC = total volume fraction of dispersed carbides.

Distribution factors, calculated on the basis of the aforesaid formula, are summarized in the Table 4.44.

Having defined this parameter(DF), the coarsening index can now be calculated with respect to a specified reference base - a concept also implicitly in-built into the Ostwald's formula. In the present instance, this reference base was taken to be the heat treating schedule at which the dispersed carbide particles/ DSPs just about formed namely the heat treating schedule corresponding to which dispersed carbides/DSPs were present in classes I and II only.

109

The coarsening index(CI) is thus defined as

$$CI = \frac{\text{DF for a given heat treatment}}{\text{DF for the h/t with particles in classes I \& II}} \qquad ...(4.19)$$

Based on the above formulation, the coarsening index for the different alloys was calculated and is summarized in the Table 4.45.

As already discussed above, the aforesaid table proved extremely useful in assessing the relative coarsening tendency of the different alloys.

The data on the relative coarsening behaviour of the alloys is relevant to an understanding of their deformation and the corrosion behaviour as would be evident from an analysis put forth in Chapter VI.

Although the aforesaid analysis does explain the data obtained in a majority of instances in the alloys P1 and P2 and to some extent in P3(for heat treatments up to 850°C), a number of data points did not follow a specific trend(Table 4.45). A possible reason could be that the system under investigation is intrinsically 'heterogeneous'. This is evident from the representative hystograms summarized in Figures 4.46-4.47 and from the data given in Appendix A-1 to A-3. This reporting not withstanding, it became prudent to analyze/interpret the entire data more comprehensively/methodically. A possible methodology is to assess the percent number and percent area occupied by particles of different classes as influenced by heat treating parameters(62,83). This may lead to incomplete/erroneous assessments as is evident from the data summarized in the Tables 4.46-4.48. To overcome this problem, instead, DF was calculated

110

for each heat treatment(Tables 4.49-4.51). Subsequently for each heat treating temperature, the DF was plotted as a function of time for the experimental alloys(Figures 4.48-4.50). Their perusal revealed that-

Temp. °C	Alloy P1	Alloy P2	Alloy P3
800	Predominantly class I + some class II; classes I and II coarsening with time	Predominantly class I & II + some class III; extent of coarsening with time less than in P1, changes are less pronounced	Predominant class I & II + some class III(similar to P2). With time, initially some precipitation; mainly is class II; coarsening less than P1 but more than P2
850	Dominantly class II + some more precipitation of second class up to 8 hours followed by coarsening. Similar changes in class I and III but at different times.	same as P1. Extent of coarsening is more. Reprecipitation tendency is less	same as in P2
900	Dominantly class II; changes similar to 850°C treatment except reprecipitation trend shifts towards lower periods and coarsening more. Class I 'particle behaviour' same as at 850°C; behaviour of class III particles is similar to class I and II i.e. an increase in amount followed by coarsening	mainly class II; lesser variation than P1(some coarsening); class I particle behaviour similar to that P1, but lesser formation of class III than in P1 but more pronounced than at 850°C.	steep coarsening of class II particles; re-emergence of class I and their coarsening; class III following same pattern as in P1-DF peak at lesser time than P1 and extent of formation less than in P1

950	Mostly coarsening dominant; behaviour of class I, II, and III nearly similar	class I particles behaviour similar to P1; some reprecipitation of class II and then coarsening. Class III particles precipitation more than at 900°C and more than in P1 and hence the difference	same as at 900°C; class III particles effect less pronounced
1000	Dominantly class II; rapid coarsening of class II except at 8 hours; definite contribution from first class particles but coarsening fast; effect of class III dominant at lower soaking periods	class II particles behaviour same; some increase in class II at 6 hours; class I particles reprecipitating & coarsening; class III particles exhibit marked effect at higher periods	class II showing coarsening but class I reprecipitation tendency at higher soaking periods; class III absent, this feature not observed in any other alloy.

On comparing the above description/analysis with that put forward to explain the microstructural changes(sections 4.1.2, 4.1.3.2, and 4.2.4.3), it emerges that the qualitative descriptions of the nature and extent of precipitated second phase as employed in section 4.1.3.2 is not adequate and complete. Thus quantitative estimates as the ones presently mooted(Figures 4.48-4.50) are a more realistic and authentic basis of differentiating between the microstructures of the experimental alloys vis-a-vis DSPs.

The aforesaid analysis in a nutshell can be summed up thus:

(i) particles predominantly precipitate in class II(size 0.58-0.16μ)

(ii) with an initial increase in temperature(800/850°C), further precipitation in the same ranges occurs; this is followed by coarsening

(iii) with an increase in temperature or time at a given temperature, the coarsening tendency predominates.

(iv) the changes in class I sized particles are mostly prefunctory except on heat treating at 1000°C.

(v) the relevance of Class III type particles increases with temperature, reaching a maximum at 900°C in P1 and becoming inconsequential. A similar situation arises in P2 till 950°C and in P3 900°C-950°C.

(vi) P3 is prone to forming class I particles through precipitation. This is initiated at 900°C and increases/persists over large periods at 950°C and 1000°C.

Except (vi) all the other quantitative formulations summarized above reflect that (a) coarsening occurs in general, (b) a higher Cu content favors the formation of class II (relatively coarser particles), (c) the occurrence of events as in (a) and (b) on heat treating till/at 900°C, is favoured by the presence of a higher copper content, and (d) the processes becoming complex thereafter as manifested by accelerated coarsening(bringing in particles of class III into reckoning) and some reprecipitation of class I particles initiated at 900°C, gaining in prominence with heat treating temperature and marked in P3. All these can be attributed to enhanced τ stabilizing and carbide destabilizing tendencies which increase with Cu content.

The aforesaid analysis is quantitatively re-substantiated through the data summarized in the Table 4.52 which reveal the percent contribution of DF in each class as influenced by heat treatment. An important objective of doing so is to arrive at homogeneity/heterogeneity based on the size and distribution of

113

the DSPs. This aspect has been separately dealt with in a later section 4.2.11.

4.2.9 Mathematical modelling of the transformation behaviour

Figures 4.1-4.3 reveal how time and temperature control the transformation behaviour and therefore, the hardness of the experimental alloys. It was concluded that hardness, H varies linearly with time, t and can be represented by

$$H = C1 + C2t \qquad\qquad ... (4.15)$$

The values of C1 and C2 were found to be different for different temperatures(T) and therefore can be expressed as a function of temperature in the form of equations

$$C1 = f(T) \qquad\qquad ...(4.20)$$

$$C2 = f(T) \qquad\qquad ...(4.21)$$

The plots of C1 vs T and C2 vs T revealed that the C2 vs T is linear and gives a relationship C2 = A3 + A4T. However, the lnC1 vs 1/T plots indicated a linear behaviour and hence, the relation between C1 and T can be expressed as :

$$\ln C1 = \ln A1 + A2.(1/T) \qquad\qquad ...(4.22)$$

or $$\qquad C1 = A1.e^{A2/T} \qquad\qquad ...(4.23)$$

Substituting for C1 and C2 in the equation 4.15, the final relationship is

$$H = A1.e^{A2/T} + (A3+A4T)t \qquad\qquad\qquad ...(4.24)$$

The constants A1, A2, A3, A4 were calculated for different alloys using the multi-variable nonlinear constraint optimization technique (99,100). The final equations along with the overall standard deviations are reported below :

P1 : $H = 263.376\ e^{607.01/T} + (0.009839 - 0.86 \times 10^{-5}T)t$

$$\text{Overall SD} = 11.39 \qquad ...(4.25)$$

114

P2 : H = 262.689 $e^{604.37/T}$ + (0.008998-0.786x10^{-5}T)t

Overall SD = 7.88   ...(4.26)

P3 : H = 273.39 $e^{552.705/T}$ + (0.0101-0.9068x10^{-5}T)t

Overall SD = 7.33   ...(4.27)

Where T = temperature in °K

t = time in seconds

H = hardness, HV$_{30}$

The theoretical hardness values calculated from the above equations were plotted against the corresponding experimental values and are shown in Figure 4.51. It reveals that barring a few instances, the calculated values are well within ±5%.

It is observed that the constants A1, A2, and A3 are positive for all the alloys. Hence their effect would be similar and additive. The constant A4 is negative and therefore, its effect needs to be analyzed. This calls for assessing the contribution of second factor of the Equation 4.24. Its values, as influenced by the heat treating temperature and time are given below. As will be evident, the contribution of the factor becomes negative at temperatures ≥900°C for P1 & P2 and 850°C for P3.

Contribution of the second factor

Heat-treatment	Contribution of the second factor		
	P1	P2	P3
800 2 AC	4	4	2
800 4 AC	9	8	4
800 6 AC	13	12	6
800 8 AC	18	16	8
800 10 AC	22	20	10
850 2 AC	1	1	-1
850 4 AC	3	2	-2
850 6 AC	4	3	-3
850 8 AC	5	5	-5
850 10 AC	6	6	-6

900	2	AC	−1	−1	−4
900	4	AC	−3	−3	−9
900	6	AC	−5	−5	−13
900	8	AC	−7	−6	−18
900	10	AC	−9	−8	−22
950	2	AC	−4	−4	−7
950	4	AC	−9	−9	−15
950	6	AC	−14	−13	−23
950	8	AC	−19	−18	−31
950	10	AC	−24	−22	−39
1000	2	AC	−8	−7	−11
1000	4	AC	−16	−14	−22
1000	8	AC	−24	−22	−33
1000	8	AC	−32	−29	−44
1000	10	AC	−40	−36	−55
1050	2	AC	−11	−10	−14
1050	4	AC	−22	−20	−28
1050	6	AC	−33	−30	−43
1050	8	AC	−44	−40	−57
1050	10	AC	−55	−50	−71

It will be seen that the contribution of this factor to the overall hardness varies linearly with time for a given h/t temperature.

The above discussion reveals that the term (A3 + A4.T)t has a significant impact on the overall hardness especially when the alloys are being heat treated from 'higher' temperatures.

Because of a difference in the nature of the contribution of the second factor, as influenced by temperature, further calculations were made to find out the temperature at which the contribution of the aforesaid factor became negative. The change over occurred at 871, 871, and 840°C in P1, P2, and P3 respectively, which are in fact, the temperatures representing the cross-over point(section 4.2.6.2). This deduction is valid for all the alloys, duly remembering that the value of the COP would differ from alloy to alloy.

When the values of COP(obtained from the Figures 4.10-4.12),
namely, 850-900°C are compared with those observed on the basis
of the model, the apparent difference can be explained by stating
that whereas the equations represent transformations without
reflecting upon their complexities, the actual situation is to
the contrary due to heterogeneity of the system and also because
a large number of phases with greatly different 'inherent' chara-
cteristics are participating in the transformations. The lag
between the 'ideal' and 'actual' situations is what is contribu-
ting to the difference and evidently can not be computed
mathematically.

4.2.9.1 Physical consistency of the proposed model

The data summarized in the Tables 4.53-4.55 , when viewed in
the context of the structural changes already discussed, leads to
certain important inferences. Firstly, the hardness is essen-
tially controlled by the parameter $A1.e^{A2/T}$. This is independent
of the matrix microstructure, i.e, independent of whether the
matrix is martensitic/austenitic, or simply austenite as in the
present case. Recalling the basis on which the alloys are
designed, it is easy to visualise why the matrix is austenitic
irrespective of the heat treating temperature employed. Its
hardness values vary inversely with temperature, with time at
best playing a secondary role, as has been observed (Tables 4.53-
4.55).

The contribution from the second factor, although less
significant to begin with, assumes prominence at higher tempera-
tures and soaking periods. The parameter $(A3 + A4.T)t$ can there-

fore, be said to represent the carbide transformation. At lower temperatures(800°C), its contribution is positive and increases with time because the precipitated second phase(DSPs/ DCs) is in a condition to harden/strengthen in view of its size and distribution. The correctness of this analysis is proved by the data obtained on heat treating from 850°C, wherein the contribution has decreased due to some coarsening of the DSPs. The contribution, on heat treating from 900°C is either negligible or marginally negative(from 850°C in P3) thereby signifying that the precipitated second phase ~~seizes~~ ceases to be effective.

The negative contribution is seen to have a sizable effect only on heat treating from upwards of 950°C, a temperature at which hardness begins to decrease with time markedly. It is thus noteworthy that the negative contribution is assuming reasonable proportions just when the Vf of MC is beginning to decrease. As the DSPs have already been shown to be ineffective, the second factor is representing 'massive carbide' related transformations at T > 850-900°C. Therefore its(second factor) magnitude will increase steeply (i) as the temperature is raised beyond 950°C and (ii) at higher soaking periods at a given temperature. The reasons for the negative contribution of this parameter, with an increase in temperature, have already been analyzed in the section 4.2.7. Therefore, the two parameters constituting the model are physically consistent with the attendant microstructural changes; the first term representing the matrix transformations and the second term the carbide transformations.

4.2.9.2 'Simulation' of the transformation behaviour through modelling

As is known, the overall transformation behaviour of the alloys has been arrived at on the basis of a total of 30 experiments per alloy. This is a time consuming exercise. If it were possible to arrive at/or simulate the transformation behaviour of the alloys on the basis of a minimum yet optimal number of experiments with an accuracy equivalent or there abouts to that of the models developed, then it would greatly help in cutting down on arduous experimentation and would also lead to a saving on energy and the overall costs.

Recent studies by Patwardhan, Mukundan, Rao, Sharma, and Kumar(102) have shown that the transformation behaviour of Fe-5Cr-1.5Cu cast irons containing 7.5% Mn and 6% Mn with austenitic and martensitic matrices studied on the basis of 30 arduous experiments and mathematically modelled(79), could be 'simulated' on the basis of either 4 or at the maximum 6 data points. They comprise hardness values at two extremes of heat treating temperature & time, namely, 800°C(2 hours & 10 hours) and 1050°C (2 hours & 10 hours) and at an intermediate temperature namely 850°C/900°C(2 hours and 10 hours). The logic of selecting the intermediate is that the hardness should be independent of time i.e. $dH/dt = 0$. This also made the choice of the heat treatments, selected for the purpose of simulation, more representative/broad based.

It was felt appropriate to apply the concept thus developed to assess whether the transformation behaviour of the alloys P1, P2, and P3 could be similarly 'simulated'.

On following the procedure outlined by Patwardhan et.al.(102), the following emerges-

The 'models' representing the transformation behaviour of the experimental alloys(section 4.2.9) are-

P1 : H = 263.376 $e^{607.01/T}$ + (0.009839-0.86x10^{-5}T)t

$$\text{Overall SD} = 11.39 \qquad ...(4.25)$$

P2 : H = 262.689 $e^{604.37/T}$ + (0.008998-0.786x10^{-5}T)t

$$\text{Overall SD} = 7.88 \qquad ...(4.26)$$

P3 : H = 273.39 $e^{552.705/T}$ + (0.0101-0.9068x10^{-5}T)t

$$\text{Overall SD} = 7.33 \qquad ...(4.27)$$

The hardness values predicted on the basis of the above models are summarized in the Tables 4.56-4.58.

On selecting the hardness values at the two extremities of heat treating temperature & time, namely, 800°C(2 hours & 10 hours) and 1050°C (2 hours & 10 hours), the 'simulated' models are-

P1 : H = 242.8 $e^{661.1/T}$ + (0.01013-0.88x10^{-5}T)t

$$\text{Overall SD} = 19.11 \qquad ...(4.28)$$

P2 : H = 260.0 $e^{618.4/T}$ + (0.0094-0.847x10^{-5}T)t

$$\text{Overall SD} = 11.07 \qquad ...(4.29)$$

P3 : H = 225.5 $e^{782.9/T}$ + (0.0942-0.875x10^{-5}T)t

$$\text{Overall SD} = 11.42 \qquad ...(4.30)$$

On the basis of the above models, hardness values at different temperatures and periods were computed and are summarized in the Tables 4.56-4.58. The correlation coefficients which increase with Cu content auger well for the approach developed.

On selecting the hardness values at two extremities of heat treating periods(2 hours & 10 hours) at 800 & 1050°C and at an additionally selected heat treating temperature(900°C), the simulated models are-

P1 : $H = 262.27 \; e^{605.24/T} + (0.0108 - 0.964 \times 10^{-5}T)t$

$$\text{Overall SD} = 15.88 \quad \ldots(4.31)$$

P2 : $H = 264.01 \; e^{597.84/T} + (0.00991 - 0.8806 \times 10^{-5}T)t$

$$\text{Overall SD} = 9.88 \quad \ldots(4.32)$$

P3 : $H = 224.68 \; e^{786.83/T} + (0.0094 - 0.875 \times 10^{-5}T)t$

$$\text{Overall SD} = 11.65 \quad \ldots(4.33)$$

On the basis of the above models, hardness values at different temperatures and times were computed and are summarized in the Tables 4.56-4.58. The correlation coefficients are slightly better than the ones obtained on the basis of similar models outlined in Equations 4.28-4.30. Higher correlation coefficients (revealing improved relations between the actual & the simulated behaviour) have been obtained because the selection of hardness values at two extremities of periods at the three heat treating temperatures has made the exercise more representative vis-a-vis transformation behaviour.

Thus the transformation behaviour can be simulated with reasonably high accuracy(correlation coefficient ranging between 0.942 to 0.975) on the basis of either four or six data points. The correlation coefficients increase with copper content and are a maximum in alloy P3 because a higher Cu content may be said to reduce the level of heterogeneity through exercising better control over the 'carbide related' transformations. For example, at higher copper contents the starting volume fraction of massive

carbides is low and accordingly its decrease on heat treating is not as marked as that observed in P1 or to some extent P2 which contain 25% and 20% volume percent of MCs in the as-cast state. Thus the attendant heterogeneity brought about due to a (i) variable massive carbide content and (b) variations in the amount of DSPs would be a maximum in P1, lesser in P2 and the least in P3. This is what has been apparently observed.

4.2.10 Mathematical modelling of the distribution factor

A critical analysis reveals that the DF can be mathematically represented with the help of the following equations :

P1: $0.00135 \, e^{6336.5/T} - (7000 - 5.761T) \times 10^{-8} . t$ ...(4.34)

P2: $0.00227 \, e^{5736/T} - (5733 - 4.784T) \times 10^{-8} . t$ ...(4.35)

P3: $0.01765 \, e^{3472.9/T} - (5697 - 4.795T) \times 10^{-8} . t$ ...(4.36)

The basis of arriving at these equations is the same as the one on which the mathematical modelling of the transformation behaviour of the alloys was carried out(section 4.2.9).

4.2.11 Homogeneity/heterogeneity of the alloys

A careful perusal of the data summarized in the Tables 4.35-4.37 and especially the one pertaining to the volume fraction of massive carbides as influenced by heat treating parameters reveals that for a given heat treatment, the amount of massive carbides varied over a considerable range. Higher values are obtained close to the core of the specimens and lower values were obtained towards the periphery. This is primarily due to the inhomogeneities which are intrinsic to alloys/system. The usual statistical methods available to analyze such a data did not

prove useful since if mean and the ±3σ limit(indicative of 95% reliability) are applied to find out the permissible range over which the parameter being assessed could vary, then all the experimental values fall within the ambit of 'permissible' data. The aforesaid observation and the resulting implications are being analyzed separately.

It was however opined by Patwardhan(78) that variations in the data indicate a lack of homogeneity and therefore this could become a basis for calculating the homogeneity/heterogeneity of the alloy(s)/alloy system under investigation.

In a broad sense homogeneity of the experimental alloys can be adjudged on the basis of:

(i) a variation in the alloy concentration within the austenitic matrix- chemical homogeneity/heterogeneity,

(ii) uneven distribution of MCs, leading to a highly variable volume fraction of MCs and thereby to a variable homogeneity which may be termed as distributional heterogeneity; additionally carbide transformations and carbide destabilizing tendency will also contribute to this situation.

(iii) uneven distribution of precipitated second phase(variation in size, distribution, and volume fraction discounting the morphology to begin with).

Assessing homogeneity/heterogeneity at (i) would require an accurate assessment of the (a) alloy concentration and (b) the concentration gradients, if any. Such an information could be generated through extensive electron-probe micro analysis which although used in the present study may not prove sufficient to arrive at the desired assessments. Thus the main emphasis would

be on assessing the homogeneity/heterogeneity at (ii) and (iii). To begin with the one at (ii) would be addressed to.

In order to fully appreciate the nature of variation, curves were plotted for the experimental alloys depicting all 20 observations(Vf of MCs) as influenced by heat treating parameters. Representative data thus obtained is summarized in the (figures) Appendix A-4 to A-9. Interestingly the data points do not reveal the existence of 'median points'(or similar data points) which otherwise could have enabled 'assessment' of the 'average'/reasonably relevant value. It was therefore decided to consider all the data points and to arrive at the 'mean' in the usual manner. Having done so, the overall homogeneity/heterogeneity of the alloy as influenced by heat treating has been defined as

$$H_M = \frac{\text{The net variation in Vf of MCs around the mean}}{\text{Permissible variation around a mean}} \quad ..(4.37)$$

$$= \frac{V_{fexp} \times \text{overall standard deviation(exp)} / [Vf_{max,exp} - Vf_{min,exp}]}{\text{permitted standard deviation around the mean} \times Vf_{exp} / [Vf_{max,per} - Vf_{min,per}]} \quad ..(4.38)$$

$$= \frac{Vf \times SD_{exp}}{[Vf_{max,exp} - Vf_{min,exp}]} \times \frac{[Vf_{max,per} - Vf_{min,per}]}{Vf \times SD_{per}} \quad ..(4.39)$$

$$= \frac{SD_{exp}}{SD_{per}} \times \frac{[Vf_{max,per} - Vf_{min,per}]}{[Vf_{max,exp} - Vf_{min,exp}]} \quad ..(4.40)$$

To calculate SD_{per}, we recall that a given parameter being measured can have values $Vf_{ave} \pm 3\sigma$. This concept can be extended further by stating that under the existing constraints(i.e. for a permitted variation of 15%),

$$\frac{3\sigma_{per}}{\sqrt{n}} = 15\% \times Vf_{ave} \qquad \ldots(4.41)$$

where n = number of readings

σ_{per} = permissible variance

Hence $\sigma_{per} = SD_{per} = 15\% \times \dfrac{\sqrt{n} \times Vf_{ave}}{3}$

$$SD_{per} = 0.15 \times \frac{\sqrt{n} \times Vf_{ave}}{3} \qquad \ldots(4.42)$$

and for a 15% permissible variation in the Vf of MCs

$$Vf_{max,per} = Vf_{ave} + 0.15 \times Vf_{ave} \qquad \ldots(4.43)$$

$$Vf_{min,per} = Vf_{ave} - 0.15 \times Vf_{ave} \qquad \ldots(4.44)$$

H_M could be expressed as a fraction or percent. Under ideal condition H_M = 1. $Vf_{max,per}$, $Vf_{min,per}$, and SD_{per} could be computed on the basis of the error limit permissible e.g. $\pm$ 15% or higher as the case may be except in a situation where H_M exceeds 1.

This homogeneity can be described as 'intrinsic' or compositional homogeneity. However, if it were possible to predict 'theoretically' the Vf of MCs an alloy should attain for a given heat treatment, then another parameter 'theoretical homogeneity' can be defined which would be given by the expression-

Homogeneity (theoretical/optimal),

$$H_M(Th/opt) = \frac{Vf_{exp} \times SD_{exp} \times [Vf_{max,per} - Vf_{min,per}]}{SD_{per} \times Vf_{theo} \times [Vf_{max,exp} - Vf_{min,exp}]} \quad ..(4.45)$$

This would additionally require estimating Vf_{theo}. To do so a possible basis would be to theoretically compute the Vf from the Vf vs t(at a given T) and also from Vf vs T(for a given t) model and to arrive at a mean of the two values. Thereafter the permissible variation($\pm20\%$ or $\pm15\%$) will have to be considered to arrive SD_{per} as before. The ratio of the compositional to the optimum/ theoretical homogeneity could then reflect upon the deviation exhibited by the alloy/alloy system to heat treating.

To begin with H_M was calculated on the basis of the equation 4.40 for a variation of $\pm15\%$. The data thus computed is summarized in the Table 4.59. The implications of this data are being analyzed and this aspect does not form a part of this thesis.

The other form of heterogeneity namely, distributional heterogeneity could result from the unevenness of size/distribution of the precipitated dispersed second phase whose nature has already been commented upon. Variation in it could then be utilized for expressing 'distributional heterogeneity and as per the concept developed(78) could be defined on the basis of the following consideration.

Distributional heterogeneity, $H_M(dist)$ (related with precipitated second phase) could then be expressed as

$$= \frac{\text{Deviation in distribution function/factor with respect to the majority size fraction}}{\text{Overall distribution function/factor}} \quad .... (4.46)$$

or more precisely

$$H_M(dist) = \frac{\text{underspill ratio X spillover ratio}}{\text{overall distribution factor}} \quad \dots (4.47)$$

expressed as a ratio or as percentage.

The data summarized in the Table 4.60 puts forth such an information and this proves additionally useful in understanding the structural changes already quantitatively and qualitatively discussed. It would be interesting to analyze the impact of such a variation on properties- a theme which has been left out of the ambit of the present investigation.

The concept of determining the homogeneity/heterogeneity based on the data generated through quantitative metallography has not been hitherto pursued/evolved and the following additional steps are suggested to explore this idea/concept further:

(i) a systematic and detailed reporting of the quantitative data on the lines outlined in the present investigation and some of the earlier investigations(62,83).

(ii) a more detailed and comprehensive analysis of the data to assess the nature of 'events' it represents and the implications there off.

It is however certain that the earlier assessments regarding the possible effect of heat treating parameters and copper on the extent of homogeneity/heterogeneity are perhaps over simplistic as would be evident from a perusal of the Figures A-4 to A-9 and the data summarized in Tables 4.59-4.60.

4.2.12.1 3D plots representing interrelation between temperature, time and hardness

Till now the effect of heat treatment on the hardness has been analyzed on the basis of varying one of the parameters while keeping the other a constant. This has been represented in Figures 4.1-4.21. Although, these plots provided useful and necessary explanations of the transformation behaviour, they failed to provide the overall effect of heat treatment at a glance.

This difficulty was resolved by constructing 3-dimensional plots(Figures 4.52-4.54) using the Equations 4.25-4.27, at rotation angles 45° and 225° around the Z-axis and at a tilt angle of 30°. For each of the alloy ^{S} Figure (a) represents a gradual change in the slope of the hardness vs time plots as influenced by temperature which are represented over a surface.

The Figure (b) clearly reveals that the so called COP is not a sharply delineated temperature but that the change over is occurring over a narrow dark region represented by a surface. It may be of interest to record that the surface observed in P1 comprises two triangular inter-penetrating segments which have different orientations in space. On transiting from alloy P1 to P3 i.e., with an increase in copper content, the extent of inter-penetration, the relative spread and the difference in orientation(in space) are reduced so much that in P3 the earlier two segments have merged into a single triangular segment with a gradually enlarging base. This most likely reflects a gradual change over in properties(hardness) as a result 'smoother' phase transitions unlike in the other two alloys.

A comparison of the Figures (a) for the experimental alloys further brings out that the slope of the hardness vs temperature/ time plot is generating a surface which has been depicted in Figures (b). The 3-D plots reaffirm the relative differences in the transformation behaviour of the three alloys.

4.2.12.2 Iso-hardness plots

Iso-hardness plots were made by plotting out hardness(as influenced by temperature and time) as contours(Figures 4.55-4.57). Evidently, the hardness is a constant along a contour and as such it would be possible to determine the different temperature and time combinations(from the plot) to get a desired hardness. The existence of approximately equally spaced contours with a gradual change over of the slope/orientation in alloy P1 is because it sustains hardness over a longer range of heat treating temperature(s) and period(s). A nearly similar situation exists in P2 which additionally exhibits a greater flexibility in attaining hardness levels lower than what could be attained in P1.

In the alloy P3, after an initial gradual change over in the slope of the contours, there is a sudden change in the 'contour profile' and contours with 'reduced spacing' are seen to exist i.e. a large number of contours exist in the temperature range 950°C to 1050°C up to covering different levels of hardness lower than those attained in P2 & P3. Thus, although a greater flexibility in terms of temperature and time exists in attaining a given level of hardness towards lower heat treating temperatures, this is not so towards 'lower hardness regimes'(higher heat treating temperatures) i.e. a more careful control over temperature and time is required to attain a given hardness in P3 especially at

higher heat treating temperatures compared to that in either P1 or P2.

The aforesaid observations while reinforcing the earlier deductions vis-a-vis the transformation behaviour of the alloys do bring about additional useful information. The data thus obtained could be related to enhanced austenite stabilizing/ carbide destabilizing tendencies resulting from an increase in the copper content.

4.3 Conclusion

This chapter has dealt at length with the transformation behaviour of the experimental alloys characterized on the basis of hardness measurements and the attendant microstructural changes. A detailed analysis of the latter proved extremely helpful in arriving at a qualitative understanding of the interrelation between microstructure and properties(indicated by hardness). The behaviour of the dispersed second phase as influenced by heat treating schedule has been mathematically represented by evolving a parameter called the 'distribution factor'. This enabled calculation of the coarsening behaviour of the second phase on the basis of a parameter called as the 'coarsening index'. The evolution of these parameters has proved extremely helpful in overcoming the limitations of the Ostwald's ripening formula which is regarded as the sole basis for characterizing the distribution of the second phase particles. The development of these models has proved useful in establishing models interrelating properties with the microstructure. This has been discussed in Chapter VI. An equally interesting aspect has

been to quantify/define 'heterogeneity'/'homogeneity' on the basis of the distribution of massive second and dispersed second phase as influenced by heat treating parameters. Such an analysis has not perhaps been put forth earlier.

Finally mathematical models have been developed inter-relating hardness with the heat treating temperature and time (microstructures). It has been established that the model is physically consistent i.e. it truly represents the structural changes occurring on heat treating. With the help of empirical modelling, it has been possible to establish that the transformation behaviour of the alloys could be 'simulated', with nearly equivalent accuracy as the modelled ones, on the basis of 4 to 6 experiments as against the original thirty. This is an important contribution which is of major technological significance.

Although much has been said about the characterization of different phases, the absence of martensite could not be unequivocally established in marginal cases. Similarly, the nature and types of carbides needed identifying. Therefore, a detailed study comprising X-ray diffractometry and EPMA was carried out. The data thus obtained have been discussed in the next chapter.

CHAPTER V

PHASE ANALYSIS AND PHASE IDENTIFICATION

5.1 Structural analysis by X-ray diffractometry

Specimens of the alloys in the as-cast, as well as in the heat treated conditions were extensively examined by X-ray diffractometry to identify/confirm (i) the nature of matrix microstructure, and (ii) the nature of different carbides that formed during heat treatment. The data emerging from an analysis of the x-ray diffractograms has been summarized in the Tables 5.1-5.42. Summary tables(Tables 5.43-5.45) have also been prepared to make the discussion more concise. With the help of diffraction data, it was possible to interpret the micro-structures more or less fully as would be evident from the ensuing analysis.

5.1.1 Results

5.1.1.1 As-cast condition

The microconstituents attained in the experimental alloys comprise a matrix of austenite with some martensite and carbides namely M_3C (isomorphous with Fe_3C) + M_7C_3 (isomorphous with Cr_7C_3) and M_5C_2. Additionally, Fe_8Si_2C, $CrMn_3$ and elemental copper were also indexed. Lower angle peaks corresponding to α/M were observed in all the alloys. However, the higher angle peaks characterizing martensite were found to be absent in all the three alloys.

5.1.1.2 Heat treated condition

On heat treating, the 2θ values of the matrix differed from the standard 2θ-values as obtained from the diffraction data

cards(Tables 5.2-5.42). Further the nature of carbides formed and the presence/absence of other constituents observed in the as-cast state also differed. This along with the effect of heat treating temperature and time on the possible transformations occurring within the matrix and the carbides, and any additional features that were observed, have been discussed below.

5.1.1.2.1 Effect of heat treatment on the matrix microstructure

On heat treating(temperatures $\geq 800^\circ C$), the following changes were observed in the matrix microstructures :

(i) The matrix essentially comprised austenite independent of the heat treating temperature and time.

(ii) It was free of martensite.

(iii) An important observation is that the 2θ-values for austenite decreased with respect to the standard 2θ-values on increasing the heat treating temperature and time. Temperature had a more marked effect. Further the shift in the 2θ values was significant at temperatures $\geq 900^\circ C$. The extent of decrease was nearly similar in the experimental alloys.

5.1.1.2.2 Effect of heat treatment on the nature of carbides

On heat treating, a clear cut carbide transformation sequence was observed. However, the main difference was with regard to the carbide stability as influenced by heat treating parameters and the alloy (copper) content.

(i) M$_3$C:

(a) This is a commonly occurring carbide in the as-cast condition. It was clearly indexed in P1 and P3 but not in P2. Further, it was indexed with greater certainty in P1.

(b) On heat treating, it was indexed in P1 up to $900^\circ C$, 10 hours

heat treatment and in traces up to 1000°C, 2 hours heat treatment. Hereafter it was again indexed upon heat treating from 1050°C(2 hours & 6 hours only).

(c) In P2, it was indexed at best in traces on heat treating from 950°C and in some measure on heat treating from 1050°C.

(d) In P3, the M_3C carbide formed with greater regularity i.e. up to 1000°C, 2 hours heat treatment and also upon heat treating from 1050°C(6 hours and 10 hours soaking period)

(ii) M_7C_3:

This carbide formed in all the alloys both in the as-cast as well as in the heat treated conditions. Heat treating parameters seemed to have little effect on its formation/indexing.

(iii) M_5C_2:

Its occurrence in the experimental alloys was also on similar lines as the M_7C_3 carbide.

5.1.1.2.3 Other features

(a) Elemental copper :

Copper was indexed in the as-cast condition as well as in the heat treated condition in all the alloys. Overall its presence appeared to be less marked in P2 whereas it was indexed with equivalent certainty in P1 and P3.

(b) Fe_8Si_2C:

It was invariably indexed at all the heat treatments.

(c) $CrMn_3$:

It was present in the as-cast and in the heat treated conditions. Overall the alloy P2 appeared less susceptible to its formation. The needle like constituent observed through optical

metallography may represent this constituent since inter-metallics are known to have a needle like appearance.

5.1.2 Discussion

5.1.2.1 Matrix microstructure

A summary of the findings relating to the matrix microstructure has been presented in the Section 5.1. The alloys presently investigated were primarily designed to attain an austenitic matrix on air cooling from all temperatures. That this has been achieved is duly corroborated by the optical metallographic studies on the as-cast and the heat treated specimens(Section 4.1.2). The x-ray observations while duly supporting and confirming the findings in a majority of instances have proved helpful in resolving, by and large, the identity of the 'leaf like' features in the as-cast condition. Since the x-ray data revealed that at least some martensite was present in the as-cast condition, the 'leaf-like' regions apparently represent martensite. This being so, the matrix microstructure in the heat treated condition is expected to be only austenitic (refer alloy design) as is duly confirmed through the diffracto-metric analysis.

As the heat treating temperature is raised or time at a given temperature is raised, the volume fraction of MCs decreased (Equation-4.3). The solute atoms thus made available will dissolve into austenite increasing its stability/the lattice parameter. This tendency would be marked at or above a threshold temperature at which the tendency to dissolve the MCs/DCs is also marked. An. increase in the lattice parameter will mean that the diffracted beam will shift towards lower 2θ values for austenite.

Its magnitude is not easy to assess. To overcome this problem, the maximum intensity peak in each diffractogram has been attributed to austenite.

5.1.2.2 Carbide transformation

Based on an analysis of the data contained in Section-5.1.1.2(Tables 5.2-5.41 and summary(Tables 5.43-5.45), it is evident that the general carbide transformation sequence in the experimental alloys is as follows:

Carbide(s)	Temperature regime
$M_3C + M_5C_2 + M_7C_3$	As-cast state except in P2 where M_3C apparently not present
↓	
$M_3C + M_5C_2 + M_7C_3$	up to 900°C (M_3C present in traces in P2)
↓	
M_3C (trace/some) $+ M_5C_2 + M_7C_3$	up to 950°C (in traces in P2)
↓	
$M_5C_2 + M_7C_3$	up to 1000°C
↓	
$M_5C_2 + M_7C_3 + M_3C$ (reforming)	up to 1050°C, lower SP
↓	
$M_3C + M_5C_2 + M_7C_3$ (some amount)	up to 1050°C; higher SP
↓	

Predominant carbides at high temperature are $M_7C_3 + M_5C_2$

A study of the Fe-Mn-C and Fe-Cr-C ternary diagrams revealed that M_7C_3, M_5C_2 and $M_{23}C_6$ are essentially high

136

temperature carbides and the last mentioned one has a relatively lower dissolution temperature/thermal stability as compared to the other two(66). Further, the predominant carbide at lower temperatures is M_3C. Accordingly, the carbide expected to be present in the as-cast state should be M_3C as this is the stable form at room temperature. The possible presence of higher temperature forms of carbides can be explained by stating that because of the complexity of the alloy system under study, the different high temperature carbides have not fully transformed successively to their lower temperature variants due to the reactions being sluggish. This can also be looked at differently as would be evident from the discussion below.

The attainment of M_5C_2 and M_7C_3 carbides in the as-cast/heat treated condition with the M_3C carbides playing at best a secondary role affirms that what was outlined in 'design of alloys'(attainment of high temperature microstructure/carbides with a minimum of processing) has in fact been achieved. Equally satisfying is the absence of 'boundary carbide' $M_{23}C_6$. The apparent 'absence' of M_3C in P2 even in the as-cast condition may also mean an absence of 'platy' & 'continuous boundary' carbides as has been already demonstrated through optical metallography(Figures 4.29). Thus x-ray diffractometry has re-affirmed this important inference although the reasons for the same are not understood.

Looking to the general trend of the data summarized in the Tables 5.43-5.45, it is evident that the carbide transformation occurring in the alloys could be visualized as follows:

(i) retention of the 'high temperature carbides' M_5C_2 & M_7C_3,

137

attained in the as-cast condition, even on heat treating

(ii) gradual phasing out of M_3C(room temperature/lower temperature form) upon heat treating which is governed by the 'temperature regime' of stability.

This is what has been observed. The only additional feature is that M_3C is reforming on heat treating from 1050°C. This observation/inference reveals the identity of the small sized DCs formed upon heat treating from 1050°C(Figures 4.28,4.35 & 4.42).

5.1.2.2.1 The M_3C

This carbide (in massive/platy form) was present up to 950°C and reformed on heat treating from 1050°C. It was found to be isomorphous with Fe_3C, although small amounts of Mn and Cr were also present in it as confirmed through EPMA(Tables 5.46-5.48). This in fact made the Fe_3C little more stable(103) otherwise it might have dissolved/transformed even at relatively lower temperature(s) and soaking period(s). On the other hand the presence of Cu in the alloys(although not partitioning to Fe_3C) has an opposite effect and therefore, the dissolution of this carbide is enhanced. This could also be gauged from the subtle differences in its temperature range of stability of M_3C in the alloys P1(1.5% Cu) and P3(5%Cu)(Tables 5.43 & 5.45) although P2 totally differed from P1 and P3 in this regard(Table 5.44). Further, it appears that the phasing out of M_3C is in some way linked with the formation of higher volume fraction/larger proportions of M_6C_2 and M_7C_3 carbides. Whether M_3C could directly transform to M_7C_3 or via an intermediate carbide M_6C_2 carbide needs to be looked at carefully.

5.1.2.2.2 The M_7C_3

This carbide was present in the as-cast condition and upon heat treating from practically all temperatures. It may be Cr based (Cr_7C_3), Fe based (Fe_7C_3), or Mn based (Mn_7C_3), but Cr_7C_3 is the only carbide to form singly. Others namely Fe_7C_3 or Mn_7C_3 are always present in combination as $(Cr,Fe)_7C_3$, $(Fe,Mn)_7C_3$, or $(Cr_7C_3+Mn_7C_3)$(103). In the present study the carbide formed was a mixed carbide of Fe, Cr & Mn(Table 5.47) with a preponderance of Fe & Cr atoms(Table 5.47).

The formation of M_7C_3 has been the subject matter of a number of studies and its mechanism of formation from M_3C has been described as (i) in-situ(104-110), (ii) combination of in-situ and separate nucleation(111,112) and (iii) also as separate nucleation(113). In the presently investigated alloys, a part of the MCs comprise M_7C_3. Its appearance was not similar to the one described in earlier studies(62,83) nor could it have formed 'in situ' as suggested earlier. The additionally forming M_7C_3, coinciding with the phasing out of M_3C, is most likely to be 'nucleated' at the M_3C-matrix interface. In the absence of any $M_{23}C_6$ forming, the earlier hypothesis that it is the dissolution of $M_{23}C_6$ carbide which may initiate the formation of M_7C_3(84,85) would not hold good under the existing conditions. Thus one could visualize a transformation sequence

$$M_3C \longrightarrow \text{metal atoms} \longrightarrow \text{nucleation/ formation of } M_7C_3 \qquad \ldots(5.1)$$
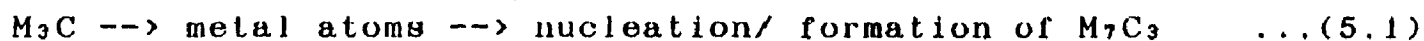
5.1.2.2.3 The M_5C_2

As has already been stated, the M_5C_2 carbide is present even in the as-cast condition; reasons for its presence have already been stated. Its persistence even upon heat treating(even when

the dis-persed second phase is absent) could be attributed to the successful implementation of alloy design strategy which aims at attaining the high temperature carbides even in the as-cast state. Inertness and sluggishness of M_6C_2 to transform to the 'other carbide' forms have also contributed to its retention in the microstructure. Evidently, M_6C_2 carbide constitutes a part of the MCs. Additionally, a part of the DSPs comprise M_6C_2 in addition to M_3C. This observation is consistent with the carbide transformation sequence as observed in the Fe-Cr-C and Fe-Mn-C ternary systems(114). A further perusal of Table 4.42 revealed that either the decrease in the volume fraction of dispersed carbides with time at 950°C is too small/negligible or alternatively, the volume fraction of DCs initially decreases with soaking period up to 6 hours and thereafter increases on raising the soaking period to 10 hours(Table 4.42). Both these observations in a nut shell reveal that some new carbide is definitely forming and it would not be incorrect to deduce that this is in fact M_6C_2. Further, a carbide such as the one presently under consideration i.e. forming through a precipitation process by ageing of austenite at 950°C, is more likely to be of a dispersed type. Hence at least a part of the dispersed carbides comprise M_6C_2. This can be established unequivocally only through selective etching techniques and or by EPMA.

5.1.2.2.4 Fe_8Si_2C

Even after considering various possibilities of indexing diffractograms, some peaks still remained unidentified. One of the possible options considered was the presence of the aforesaid

140

phase. From the Tables 5.2-5.42, it can be observed that this phase is indexed in all the alloys at least up to 1000°C and even on heat treating at 1050°C either in traces or in small amounts. Other than this no further comment is being made as to its mechanism of formation and/or the morphology it assumes.

5.1.2.2.5 Presence of elemental Cu and other phases

The possible presence of Cu in the as-cast condition and its being indexed even on heat treating in spite of the matrix being austenitic is additionally an unexpected result. Quite clearly it's difficult to fathom its presence on the basis of physical metallurgical principles. None the less a detailed EPM analysis is imperative to confirm whether Cu is present.

After considering all possibilities, some reflections still remained unindexed. It was observed that this problem could be partly resolved by considering the formation of $CrMn_3$ and Cu_2S phases. The possibility of the formation of inter-metallics such as $CrMn_3$ is more on heat treating from higher temperatures. The formation of Cu_2S is feasible in all the alloys perhaps more so in the higher Cu containing alloys. It is suggested that a more detailed investigation is required to confirm the presence of phases such as $CrMn_3$ and Cu_2S etc. in future studies.

Before concluding, a comment regarding the possible indexing of $Mn_{15}C_4$ would be in order. Evidently this carbide is not forming in the experimental alloys. Its inclusion in the Tables 5.43-5.45 meant to convey that the mixed carbides to form come close enough to a composition not much different from $Mn_{15}C_4$.

5.1.2.3 Concluding remarks

The above said analysis can be concised to pin point the deductions/tentative conclusions arrived on the basis of x-ray diffractometry:

(i) matrix of the experimental alloys is austenitic

(ii) some martensite is present in the as-cast state; thus the 'leaf like' regions in the as-cast state may represent martensite.

(iii) bulk of the MCs comprise M_5C_2 and M_7C_3

(iv) M_3C is present on heat treating up to 950°C and may partly constitute the MCs

(v) DSPs(needle & globular morphology) mostly comprise M_3C and M_5C_2; the plate/needle morphologies etch similarly as the MCs and therefore there are reasons to believe that they are carbides rather than being inter-metallics of the type $CrMn_3$; this needs to be verified through EPMA

(vi) the fine reprecipitated particles on heat treating from 1050°C[class I particles(Figures 4.48-4.50 & Table 4.52)] are most likely M_3C carbides.

(vii) indications of the possible presence of Cu and other phases such as Fe_8Si_2C, $CrMn_3$ etc. make it incumbent to carry out detailed EPM analysis

(viii) the above said line of approach would also help in identifying the 'haloed' regions around MCs(light grey & dark grey) as well as dark etching regions often present between two bridging massive carbide regions on heat treating from 1000/1050°C.

5.2 Electron probe micro analysis results

This was carried out on the experimental alloys to ascertain (i) the distribution of major alloying elements into the matrix and the carbide phase, (ii) the manner in which the distribution was affected by heat treating/alloying(copper content), (iii) the type of carbides constituting the MCs, DCs and DSPs(needle/plate type), (iv) whether Cu was present, and (v) the identity of the 'haloed' regions around MCs and new regions/ phases such as dark etching areas abridging agglomerating MCs. The relevant data is summarized in the Figures 5.1 and Tables 5.46-5.52.

The analysis of the data will be specific to the points that have been mentioned above.

5.2.1 Elemental distribution

5.2.1.1 As-Cast condition

The distribution of alloying elements into the matrix and carbide phases is illustrated in the Tables 5.46-5.48. The relevant electron density images are shown in the Figures 5.1a & d. It can be observed that:

(i) A larger amount of Mn partitioned to the carbide than to the matrix phase. The ratio of Mn in the carbide to Mn in the matrix was approximately 1.7 and this was uniformly so for all the three alloys except in P2 wherein it was still higher(Table 5.53).

(ii) Majority of the Cr partitioned to the carbide phase as is evident from the high ratio of Cr in the carbide to that in the matrix(Table 5.53).

(iii) Bulk of the Cu and Si were present in the matrix.

(iv) Carbon distribution into the carbide and matrix phases is on the expected lines.

143

5.2.1.2 Effect of heat treatment on element distribution

The above said observations concerning element distribution are also valid in the heat treated condition. However there are certain additional observations meriting consideration(Tables 5.46-5.53), namely:

(i) The amount of Mn partitioning into the matrix slightly increased when the heat treating temperature was $\geq 950°C$(valid for all the three alloys)

(ii) The concentration of 'C' within the matrix similarly increased on heat treating from $1050°C$ (valid for P1 & P2). However in P3, the variation in 'C' concentration as influenced by heat treating parameters did not conform to a specific trend.

(iii) Cr distribution either remained unchanged or at best slightly increased(as in P1) on heat treating from $1000/1050°C$.

(iv) As stated earlier, Cu & Si mainly partitioned to the matrix, and heat treating had negligible effect on their partitioning.

(v) An important observation is that heat treating did not have a tangible effect on the amount of Mn & Cr present in the MCs except on heat treating at $1050°C$ for 10 hours wherein a slight increase in the Cr concentration was observed (this is valid for all the three alloys).

5.2.1.3 Nature of MCs

While discussing the microstructural changes, three types of carbide had been mentioned, (a) massive/platy and (b) flower type and (c) perforated. All of them etched bright during optical metallography. However, on observing under an electron micro-probe analyzer, the flower type and massive carbides appeared differently as grey and dark etching areas respectively.

On heat treating the distinction in the etching characteristics between two types of carbides persisted(Figures 5.1). A perusal of Tables 5.47 & 5.48 indicated that the compositions of the two carbides also differed.

5.2.1.4 Identity of the different carbides

Based on the element distribution data, it can be inferred that-

(i) In P1, the MCs are mostly M_7C_3 & M_3C type

(ii) In P2 & P3, the MCs are mostly M_7C_3 type

(iii) Reprecipitation of M_3C on heat treating from high temperatures is in accordance with the indications available from x-ray diffractometric data

5.2.1.5 Identity of DSP's

Identifying the 'needle' like phase and dispersed carbides proved extremely difficult because of their size and the difficulty in focussing(Figure 5.1e). The limited information available(Table 5.51) suggested these to be carbides. Careful perusal revealed that the needles and carbides have nearly similar composition(Tables 5.51 & 5.52).

5.2.1.6 Identity of haloed regions & dark etching areas adjoining MCs

Representative electron density images of the aforesaid regions are shown in Figures 5.1a,b,e,f,g,i,k, & 1. Considering the former(haloed regions) to begin with, it is clearly seen that these represent a carbide whose composition is similar to that of the MCs except for the Cr content which is less by 10%(Tables 5.47 & 5.48). Similarly the 'C' content of these regions was also somewhat lower than normally associated with carbides.

The dark etching regions adjoining the agglomerating carbides(Figure 5.1j) contained approximately the same amounts of Mn, Cr and C as the massive carbides but additionally also contained Cu & Si(Table 5.50). This indicate that these regions represent areas having an alloy concentration different from the rest of the matrix.

5.2.1.7 Identification of Cu

Copper was observed in the as-cast as well as in the heat treated conditions. This has been duly supported by EPMA as is evident through the micrographs summarized in Figures 5.1m(white spots in the figure).

5.2.2 DISCUSSION

The EPMA data which has been critically represented in the above sections needs to be carefully analyzed to arrive at useful inferences regarding the partitioning behaviour and its consequent impact on alloy design. Equally important would be to resolve the unanswered queries arising out of x-ray diffractometry and optical metallographic analyses such as the identity of the MCs and DSPs and the identity of the differently etching matrix regions(haloed and dark etching) obtained on heat treating from high temperatures. Although a more extensive EPM analysis would have proved substantially more beneficial, the experience gained thus far could serve as a basis of arriving at useful conclusions.

The primary interest in such studies centers around the basic partitioning data and as Mn is being given primacy, the initial interest would centre around its partitioning.

Subsequently partitioning behaviour of Cr has also been commented upon. Overall, the partitioning ratio Mn$_{carbide}$/Mn$_{matrix}$ in the present study has varied from 1.4 to 2.0. This appears to be in fair agreement with an earlier study conducted by Singh(72) in which this partition ratio was found to be 1.5. and by Kumar(83) where the partition ratio was found to be 1.5-1.8. The difference, however, is that in the former the heat treating temperatures did not exceed 850°C, whereas in the latter temperatures have been relatively higher as is also the case in the present study. This difference in itself can account for the slightly larger partition ratios presently obtained.

Looking to the heterogeneous nature of the microstructure certain generalizations can be arrived at regarding the partitioning data which have also been appropriately explained

(i)   Mn$_{carbide}$/Mn$_{matrix}$ ratio in the as-cast state is relatively unaffected by heat treatment except on heat treating from high temperature when the ratio reduced(valid for all the three alloys). This could have resulted from two possible sources, firstly that the nature of the carbide(s) formed at higher temperature(s) require(s) a higher concentration of alloying elements and carbon content (i.e. high concentration of metal atoms such as Mn & Cr) and/or secondly that Mn is preferentially partitioning to the matrix phase(austenite) due to its intrinsic tendency to stabilize austenite or perhaps a combination of the two(Table 5.53). Thirdly, a considerably reduced Vf of MCs on heat treating from high temperatures should not be overlooked.

147

(ii) The said ratio increased marginally with Cu content (least in P1, more in P2 and still higher in P3). The possible reasons are that (a) a carbide with a higher metal concentration is forming and/or (b) an increase in the Cu content(τ- stabilizer) is allowing a larger concentration of Mn to partition to the carbide since Cu is now additionally playing the role of a τ-stabilizer(Table 5.53).

(iii) In the heat treating temperature range of 900-950°C, there appeared to be a slight increase in the $Mn_{carbide}/Mn_{matrix}$ ratio. This was also accompanied by an increase in the $Cr_{carbide}/Cr_{matrix}$ ratio(Table 5.53). Interestingly the level of carbon partitioning to the carbide phase also appeared to increase. This may be attributed to the formation of DSPs comprising higher forms of carbide and/or a combination of two types of carbides.

Having discussed the Mn partitioning it would be pertinent to comment upon the partitioning of Cr. The partition ratio $Cr_{carbide}/Cr_{matrix}$ in the as-cast state is 6:1, somewhat lower than the expected partitioning ratio(12,115) thereby indicating that the carbides formed incorporates lesser Cr content than normal. This is perhaps due to a part of Cr being replaced by Mn. On heat treating, the ratio initially increased with temperature/ time for reasons already discussed while considering Mn partitioning. This is followed by a decrease thereby implying a larger partitioning of Cr into the matrix. This is because the volume fraction of carbide (both MCs & DSPs) is substantially

decreasing. The least ratio would naturally be obtained on heat treating from the highest temperature of soaking for the largest length of time (i.e. 10 hours) as has been observed. On heat treating from 1050°C for 10 hours, the $Cr_{carbide}/Cr_{matrix}$ is larger than what was observed in the as-cast condition thereby implying that the carbide to form is richer in Cr(Table 5.53) and lower in Mn content as has already been discussed and commented upon. The inference is that the preferred carbides to form would be of the type M_7C_3 and/or M_5C_2. X-ray diffractometric analysis has suggested this to be so and this is duly corroborated by EPM analysis as discussed in the ensuing sections

The important implications of these observations are that although Mn is considered to be an austenite stabilizer(implying a large partitioning into austenite), its known carbide forming tendency is enabling a larger proportion of it to partition into the carbide phase. This is further made apparent when the partition ratio of a conventional austenite stabilizer like Ni is considered(based on data reported by Sandoz(115). Therefore, in order to ensure that the requisite amount of Mn is available in austenite a substantially larger amount of Mn would have to be added.

If the partition ratio of Mn is considered after correcting for volume fraction of different phases then at the lower heat treating temperature the effective partition ratio ($Mn_{carbide}/Mn_{matrix}$) is 1:1 which reduces to 0.11-0.12 : 1 on raising the temperature to 1050°C. The former suggests a general evening out of Mn distribution into the carbide and matrix phases when lower temperature heat treatments are being utilized. This data in no

149

way contradicts the earlier inference suggesting a much larger partitioning of Mn into the carbide phase. As such the earlier inferences necessitating addition of a larger Mn content, to obtain the desired structural changes hold true. The marked decrease in Mn concentration in the carbide on heat treating at high temperatures can be explained by stating that the preferred carbide to form has a greater affinity for Cr thereby implying a larger presence of Mn in the (austenitic) matrix. The same can also be looked at differently by stating that the volume fraction of carbide is greatly reduced at higher temperature(s) thereby reducing the presence of Mn into the carbide phase.

Talking about Cu partitioning it is seen that bulk of the Cu partitions into the matrix. This is to be expected in view of its (i) inherent tendency to stabilize austenite and (ii) negligible carbide stabilizing tendency. On raising the heat treating temperature, the amount of Cu in the carbide is negligible. This is again as per expectations and consistent with the behaviour of other graphitizing elements Ni and Si, which are essentially found in the matrix(12,115). It may, however, be remembered that the graphitizing tendency of Cu is not as marked as that of either Ni or Si and that it is effective only at higher temperatures and when added in larger amounts.

Having thus discussed the general partitioning pattern, it would now be appropriate to comment upon the nature of the carbides formed in the as-cast condition and the effect of heat treatment on their nature. The observation that both Mn and Cr partition to the carbide phase makes it evident that the carbides

formed are mixed Fe, Mn, Cr type. Based on the element distribution, the MCs forming in P1 are mostly M_7C_3 and/or M_3C. Thus the possible indexing of the M_5C_2 carbide, as revealed through the analysis in the sections 5.1.1.1 & 5.1.1.2(Tables 5.43-5.45) would have to be revised. This is further confirmed by the observation that the carbides formed contain Fe, Mn, and Cr whereas only Fe and Mn are known to form M_5C_2 type carbide(116).

Similarly the presence of M_7C_3 type carbide in P2 and P3 is on the expected lines since an increase in Cu content(compositions of P2 & P3) enables a larger partitioning of Cr into the carbide phase thereby enhancing the tendency to form Cr enriched M_7C_3 type carbide. The possible reoccurrence of M_3C carbide, although unexpected, corroborates the x-ray diffractometric analysis data.

In the light of the above, it can be concluded that the DSPs are mostly M_7C_3 and/or M_3C type. Thus once again the conclusions arrived at on the basis of x-ray diffractometric analysis regarding the possible attainment of M_5C_2 have to be modified by excluding its presence. This conclusion is also in agreement with the deductions arrived at in a study involving the transformation behaviour of Cr-Ni in the heat treated condition wherein the formation 'needle shaped' DSPs of the type M_3C has been reported (117-118). This further confirms the analysis put forth while analyzing the structures that the needle type DSPs based on their etching characteristics and growth behaviour are in fact carbides and not intermetallics. The observation that part of the DSPs are needle like & partly dispersed may also be differently interpreted to mean that the DSPs are essentially in the form of needles

151

and the DCs observed may in fact represent the 'end view' of the needles that are oriented perpendicular to the plane of observation. This may be considered as an appropriate justification for treating the DSPs and DCs as one entity while carrying out quantitative metallographic studies.

The identity of the 'haloed regions' has been confirmed as a carbide although with a Cr content about 10% less than in the MCs. The formation of such massive carbides has been reported in the literature(49). Irrespective of the reasons for their formation, such an occurrence reflects upon the heterogeneity of the alloys.

As already appropriately reasoned(section 4.2.4.2), the dark etching areas(Figures 4.28,4.35,4.42, & 5.1j) represent those regions within the matrix whose composition differs from the rest of the matrix(Table 5.50). Their composition approximates to M_7C_3 type carbide except for the high concentrations of Cu and Si. In fact with time these regions would have developed into well formed carbide(s) thereby abridging the two agglomerating carbide regions into a whole mass.

Finally it becomes incumbent to comment upon the influence of one element on the partitioning of the others into different phases.

Considering now the effect of Cu on the partitioning of Mn, it is seen that the effect on Mn partitioning is marked only at higher temperatures(Table 5.53). More or less unchanged Mn levels both within the matrix and in the carbides at lower heat treating temperature(Tables 5.46-5.47) is an indication that Cu is either

having little effect or is perhaps promoting Mn to perform its customary function(of being a τ-stabilizer/carbide former). A somewhat similar effect is observed on Cr partitioning. In fact, as expected, the amount of Cr in the matrix appears reduced(Table 5.46) thereby further confirming that Cu is promoting Cr to perform its usual function of forming/stabilizing carbide(s).

The formation of copper in the as-cast condition(Table 5.43-5.45), although not expected, may be explained by stating that in the as-cast condition, the alloys contain some martensitic regions and elemental copper could have been present in those regions. However its formation even in the heat treated condition in the form of Cu enriched regions(Figure 5.1m) is a surprising result since the matrix in the heat treated condition is fully austenitic and Cu has a large solubility in austenite. None the less the result is important one and its implications could be examined only after a more detailed EPM analysis.

5.2.3 Concluding remarks

Based on the above critique, it can be concluded that-

(i) MCs are mostly of the type M_7C_3 and/or M_3C

(ii) DSPs mostly comprise M_7C_3/M_3C

(iii) Cu is present both in the as-cast/heat treated condition

(iv) the haloed regions represent massive carbides whose Cr content is less by 10% compared with Cr content of MCs

(v) the dark etching regions observed on heat treating from high temperature(s) represent regions with an 'alloy concentration' different from that of the matrix. They represent a composition close to an M_7C_3 type carbide but containing large amounts of Cu and Si.

(vi) Mn partitioned more to the carbide phase and less to the matrix. This situation was not altered even on heat treating from high temperature(s)

(vii) the distribution of Cr, Si, and Cu was on the expected lines.

A more conclusive and detailed investigation is required to unequivocally suggest the absence of M_sC_2 type of carbides. For this reason their indexing has not been deleted while analyzing the x-ray diffractometric data(Tables 5.43-5.45).

5.3 Thermal analysis

Differential thermal analysis comprised (i) assessment of the critical/transformation temperatures, and (ii) compilation of the thermogravimetric (TG) data, and (iii) modelling of the TG data, carried out to a limited extent. The data thus obtained have been summarized in the Tables 5.54-5.57 and in the Figures 5.2-5.4. Results have been discussed in the following sections.

5.3.1 Results

5.3.1.1 Critical/transformation temperatures

(i) First transformation occurred 540-560°C(Table 5.54).

(ii) The second transformation similarly occurred in the temperature range of 940-990°C(Table 5.54).

(iii) In P1, a third transformation was seen to occur at 1020°C(Table 5.54).

5.3.1.2 DTA

(i) For the first transformation, DTA values were negative and were in the range of 0.25-0.5mV(Table 5.55).

(ii) For the second transformation, DTA values were positive

and ranged from <2.0mV for P1 to about 2.1-2.3 for P2 and P3(Table 5.55).

(iii) For the third transformation, occurring only in P1, the DTA value was positive and 1.5mV(Table 5.55).

5.3.1.3 Thermogravimetric studies

This data, summarized in the form of plots between %TG as a function of temperature, are shown in the Figures 5.2-5.5 and Tables 5.56-5.57(Figure 5.5 summarizing the overall information).

From the figures, the following inferences were drawn:

(i) %TG increased very slowly with an increase in temperature. This was followed by an exponential increase on raising the temperature further.

(ii) The nature of these plots was a function of the microstructure.

(iii) In the as-cast state, the weight gain was nearly a constant up to approximately 800°C. %TG corresponding to this condition was a minimum for P1 followed by P2 & P3. A steep increase in the %TG was observed on moving from 900°C to 1000°C. In fact up to 900°C, the increase in %TG with temperature was gradual(Figure-5.5).

(iv) In the 1000°C, 10 hours heat treated condition, the weight gain was nearly a constant up to approximately 900°C. %TG corresponding to this condition was a minimum for P3 followed by P1 and P2(Table 5.58).

(v) Taking an overall view, an increase in the Cu content accounted for an increase in %TG at least in the as-cast condition i.e. a higher Cu content was not conducive to

improving high temperature oxidation resistance. However for samples heat treated at 1000°C for 10 hours, presence of 5% Cu(highest value employed in the present study) resulted in the least gain in weight till the stage up to which the experiment was conducted.

5.3.2 Discussion

The DTA studies proved useful in substantiating the structural observations reported earlier(section 4.1.2). Such a study was expected to prove helpful in resolving some of the existing inconsistencies and in providing additional information on the possibility of employing the experimental alloys for high temperature applications. The least that was expected from the study was by way of information on the transformation/critical temperatures.

5.3.2.1 Critical/transformation temperature(s)

The first set of transformation temperature(s) occurring at 540-560°C evidently represent the $\alpha \to \tau$ transformation in the experimental alloys 'Evidently, those regions which were α/α' would transform. A near similarity in the DTA values suggests that the three alloys have roughly similar τ forming tendency thereby suggesting that an increase in the copper content has little effect on the τ stabilizing tendency. This deduction belies the normally held view since Cu is known to be a τ-stabilizer and should prove effective in doing so since another austenite stabilizer is already present. Moreover, the $\alpha \longrightarrow \tau$ transformation temperature has been considerably reduced due to the presence of 10% Mn(common to all the alloys). A more

plausible explanation is that this temperature represents the formation of FeO through a process of internal oxidation. In the presence of Mn,Si,P, & Si, the formation of FeO is mildly exothermic as has been observed in the present study for alloys both in the as-cast and heat treated conditions. As the first set of transformation occurs at 550-570°C in these experimental alloys irrespective of the condition in which the TG data is obtained, it is evident that the aforesaid analysis is a more plausible explanation of the events representing the data in Tables 5.54-5.55.

The next set of transformation temperatures(940-990°C) evidently represents a carbide transformation which is duly suggested by optical metallographic studies(Figures 4.22-4.42) and confirmed through x-ray diffractometric analysis(Tables 5.43-5.45). The possible transformation in the temperature range 940-990°C will comprise the (a) precipitation/growth of carbides constituting the DSPs(M_3C and/or M_7C_3) and (b) conversion of M_3C/M_5C_2(?) into the higher temperature carbide forms. While saying so it should also be remembered that the magnitude of the peak in the DTA plot does suggest that more than one transformation is occurring perhaps involving a change of state otherwise it would be difficult to account for the pronounced peak(Figures 5.2-5.4)(119). At the same time it is equally true that optical metallography does not in any way suggest a change of state(formation of a liquid phase). A close scrutiny of the data summarized in the Tables 5.43-5.45 and the aforesaid discussion supplementing these observations reveal that the DTA data is in fact representing a carbide transformation involving a

change over from M_3C to M_7C_3 via the formation of a transition carbide of the type M_5C_2.

Although an attempt has been made to arrive at definitive deductions on the basis of DTA results, perhaps a more rigorous experimentation would have enabled doing so with greater certainty. Such an experimentation would comprise (i) employing different heating rates starting from the lowest value e.g. of the order of $0.1°C/min.$, (ii) plotting out of the initial and peak transformation temperatures, (iii) extrapolating the initial and peak transformation temperatures to a heating rate equivalent to zero to obtain the equilibrium transformation temperatures, and (iv) calculation of heat of reaction based on the peak area finally culminating in the calculation of heat capacities of the reactants and that of the products(121-122). It is suggested that the DTA studies be more rigorously carried out in order to arrive at precise information on the transformation behaviour of the experimental alloys.

5.3.2.2 Thermogravimetric studies

Thermogravimetric studies proved helpful in drawing inferences regarding the usefulness of the experimental alloys for high temperature applications. Since, the basic aim of the study was to optimize the microstructure for obtaining the best in terms of corrosion and heat/oxidation resistance and deformation behaviour, even the as-cast microstructure was expected to respond favourably when exposed to high temperature. Therefore to begin with, its high temperature behaviour was

investigated to arrive at some initial data especially with regard to the effect of copper content. It was reasonable to do so since 'alloy design' had been aimed at stabilizing the high temperature microstructure to room temperature in as large a measure as possible.

From a perusal of the thermogravimetric data(Figure 5.5 & Tables 5.56-5.57), it emerges that the TG data for as-cast microstructure has two distinct regions, (i) up to 800°C and (ii) beyond 800°C and extending up to 1050°C. The first of these is characterized by a very small and more or less uniform increase in %TG suggesting the usefulness of as-cast structure up to 800°C. An equally important aspect is that whereas till a temperature of 700°C the behaviour of the alloy P2 was superior to the other two, at T > 700°C the behaviour varied linearly with the copper i.e. the higher the copper content the larger the weight gain. This difference in the high temperature behaviour can be explained by stating that below 700°C, P2's superiority over the other two alloys is because it predominantly attains M_7C_3 type carbide whereas both P1 and P2 attain M_3C in addition to M_7C_3. Presence of M_3C is disadvantageous from the point of view of high temperature oxidation resistance because (i) to begin with it has a high coarsening tendency and (ii) its transition to a higher temperature form. A temperature of 800°C could be considered as representing the transition stage. At temperature ≳ 900°C, the high temperature behaviour is being governed by the volume fraction of the MCs(the nature of carbide being mostly M_7C_3; this in the as-cast state is the highest in P1 and least in P3) which is controlled by the Cu content. The

larger the Cu content the lesser is the Vf of MCs and inferior would be the high temperature response.

The TG data for 1000°C, 10 hours heat treatment differs from the one reported for the as-cast samples in that the weight gain is negligibly small. This reflects favourably upon the philosophy of stabilizing the high temperature microstructure, to room temperature in improving high temperature behaviour.

To understand the interrelation, if any, between the TG data and the DTA results, the data summarized in the Tables 5.56-5.57 and Figure 5.5 were reexamined. From this comparison, it also emerges that the sharp increase in %TG may also be directly related with the susceptibility to carbide transformation; the more marked the susceptibility the less useful the alloy. This can be explained by stating that an alloy susceptible to carbide transformation essentially exhibits proneness to configurational changes at the atomistic level. And this would lead to enhanced oxidation. Thus the key aspect would be to employ heat treatments to exclude such transformations.

Before proceeding on to modelling, it would be useful to compare the TG data obtained in the present study with that obtained in an earlier study dealing with similar investigations in 6-8%Mn, 5% Cr, 1.5-3.0% Cu alloys. The alloys investigated by Kumar(83) had revealed their usefulness in the as-cast condition to be restricted to 600°C & that in 1050°C, 10 hours heat treated condition to be up to 800°C. It was suggested(83) that the high temperature response could be improved by increasing the stability of τ-matrix and by inducing the high temperature

carbides M_7C_3 and/or M_5C_2. Both these conditions have been usefully met in the experimental alloys which together have raised the 'temperature' limit of usefulness of the 'as-cast' structure itself to 800°C. This is also reflected in the greatly improved response of the heat treated microstructures (1000, 10 hrs, AC) of the alloys P1, P2, and P3 as the %TG was now unaltered up to 900°C and its overall magnitude was greatly reduced.

Thus summing up, the basic parameters controlling the high temperature performance are (i) the stability and volume fraction of austenite, (ii) volume fraction of the 'high temperature' carbide forms $M_7C_3/M_{23}C_6/M_6C_2$, and (iii) presence/absence of 'low temperature' carbide forms. Based on the quantitative metallographic data, the most useful microstructures in the as-cast condition will comprise about 15-20% carbide and balance austenite. This situation changes when heat treated microstructures are considered as the volume fraction of carbides reduces. This will certainly not be useful from the point of view of high temperature properties in the sense that the strength will reduce but the absence of susceptibility to 'carbide transformation' is advantageous. Thus if we could attain all the merits of the 'high temperature heat treated' microstructure and yet retain a larger volume fraction of the MCs, that would be ideal. The existence of lower temperature carbides is not desirable since their effectiveness is greatly reduced at (high) temperatures at which they could coarsen and/or may undergo transformation, either of which is undesirable.

Finally, the occurrence of a phase transformation during heating at or below the temperature at which the alloy is

intended to be used would adversely affect high temperature performance as the base/expected microstructure is prone to a change in its configuration at the atomistic level i.e. it is susceptible to enhanced rate of migration of atoms/material flow.

5.3.3 Modelling of the TG data

The discussion contained in the Section 5.3.2.1 essentially dealt with the high temperature response of some selected microstructures and of the possible impact of various transformations, occurring during heating/treating, in affecting the overall high temperature performance. Having done so, it would now be appropriate to look into modelling aspect of the TG data. In order to do so, it would be necessary to examine the processes involving high temperature oxidation per se and arrive at the possible rate laws relevant to the present study, which would eventually form the basis for modelling.

Oxidation of metals can be expressed by a simple chemical reaction as

$$aMe + \frac{b}{2} O_2 \longrightarrow Me_aO_b \qquad \qquad ...(5.2)$$

However, the reaction path and the oxidation behaviour of a metal may depend on a variety of factors, and reaction mechanism(s) may as a result prove complex.

The initial step in the metal-oxygen reaction involves the adsorption of gas on the metal surface. As the reaction proceeds, oxygen may dissolve in the metal forming an oxide on the surface either as a film or as a separate oxide nuclei. Adsorption and the initial oxide formation are both functions of surface

162

orientation and condition, concentration of crystal defects at the surface, and impurities in both the metal and the gas(122).

The surface oxide separates the metal from the gas. This oxide may either be in the form of thin tenacious film or as a porous oxide scale.

For a particular metal, the reaction mechanism is a function of the pre-treatment and surface condition, temperature, gas composition and pressure, and elapsed time of reaction. Looking to the possibility of a large variation in the properties of different metals and alloys and their oxides, a number of theories are needed to describe the oxidation behaviour of metals(123-125).

A detailed understanding of this phenomenon requires knowledge of reaction rates and kinetics, the temperature and oxygen pressure dependence of the reaction, the composition, structure, and growth mechanism of the reaction products.

Rate equations describing oxidation may be classified as logarithmic, parabolic, and linear. These are discussed in detail elsewhere(123-129) and are not relevant to the present study because temperature dependence of oxidation behaviour alone has been studied.

Numerous oxidation reactions have shown empirically that the temperature dependence of oxidation rate constants at a constant ambient oxygen pressure obeys an Arrhenius-type equation

$$k = k_o exp(-Q/RT) \qquad \qquad ...(5.3)$$

where Q is the activation energy commonly given in cal/mole, R is the gas constant(1.986 cal/°K mole), and the T the absolute temperature. The pre-exponential factor, k_o, is within

experimental accuracy, usually found to be independent of temperature. Using Equation 5.3, the activation energy Q is determined by plotting $\log_{10}k$ as a function of $1/T$, in which case the slope of the curve is given by $Q/2.303R$. The rate constant at different temperatures is commonly determined from isothermal measurements, but may also be determined from a single run under conditions of linearly increasing temperature(130).

Nucleation and growth phenomena may give rise to unusual oxygen pressure-dependence of the process of oxidation(131-133). Considering oxidation of Fe as an example, Fe_3O_4 is initially formed on the surface (FeO is unstable below 570°C), and Fe_2O_3 is subsequently nucleated in the Fe_3O_4 surface. When Fe_2O_3 has grown to form a continuous layer, the oxidation rate is substantially reduced.

A scrutiny of the Figure 5.5 reveals that although the %TG varies exponentially with temperature, the plot has two distinct parts, the nature of variation in one being opposite to that of the other. The first part (from ambient temperature to 200°C) can be represented by an asymptotic curve as

$$\%TG = A1'(exp^{-T/A2'}-1) \qquad \qquad ...(5.4)$$

and the second part can be represented as

$$\%TG = A1 + A2(exp^{-A3/T}) \qquad \qquad ...(5.5)$$

where, A1', A2', A1, A2, and A3 are constants, and T is temperature in °K.

The %TG increase in the first part is very small(2%) compared to the overall increase of up to (18-24%) attained at highest heating temperature. It was therefore, felt appropriate

to neglect the former in arriving at the proposed model. As before multi-variable nonlinear constraint optimization technique(99-100) was employed to do so. The correlations thus obtained are summarized as follows:

Alloy P1   %TG = 0.9914 + 5821.89 exp(-7999.99/T)   ...(5.6)

Alloy P2   %TG = 0.5559 + 7592.84 exp(-7999.99/T)   ...(5.7)

Alloy P3   %TG = 1.4996 + 7922.62 exp(-7999.99/T)   ...(5.8)

The %TG was calculated from the aforesaid correlations and a plot of predicted %TG as a function of temperature obtained(Figures 5.6). The predicted %TG values lie very close to the experimentally determined values thereby indicating the validity of the models developed.

CHAPTER VI

DEFORMATION & CORROSION BEHÁVIOUR

6.1 Introduction

Having established the transformation characteristics of the alloys and carried out the phase analysis and phase identification with a reasonable accuracy and certainty, it becomes essential to carry out an in depth analysis of the deformation and corrosion behaviour as this alone would decide as to how far the objectives outlined in the introduction/alloy design have been achieved. While the deformation behaviour was assessed through compression testing, the corrosion characterization has been carried out with the help of weight loss and potentiostatic studies.

6.2 Effect of heat treatment on the deformation behaviour

As already stated, the deformation behaviour was assessed through compression testing and the data have been reported in the form of (i) plots between stress vs height strain (representative ones summarized in the Figures 6.1-6.3) and (ii) nominal compressive strength and % strain to fracture, and summarized in Tables 6.1-6.3.

Apparently, the data thus summarized did not conform to a specific trend. However a careful scrutiny revealed that this was perhaps due to some anomalous data points because some of the specimens marked * fractured prematurely due to the existence of pipe not visible outwardly. This problem was resolved through a normalization process carried out in the following manner-

(i) by modelling the hardness-strength interrelation on a basis

adopted by Kumar(83)

(ii) by computing the predicted value(s) of CS based on the above model, and

(iii) by indirectly computing the likely experimental values on the basis of their differing from the predicted values by ±15%.

6.2.1 Modelling of the deformation behaviour

Hardness is a very useful measure of the mechanical properties(deformation behaviour) of materials. Therefore, it is regarded as a quick yet a reliable measure of strength. Normally higher the hardness the larger is the UTS/CS and smaller the % elongation value. In ferrous materials(steels) hardness and tensile strength are related empirically through a conversion factor

$$5 \text{ VHN}_{30} \equiv 1 \text{ tsi UTS} \equiv 15.5 \text{ MPa}$$

A similar empirical law is not expected to be obeyed in cast irons in general and white irons in particular because, as engineering materials, they are a class apart from steels due to their brittleness and due to a generally complex microstructure. An attempt was, therefore, made to examine the possibility of establishing a quantitative relation between hardness and deformation behaviour in the experimental alloys. The information thus generated was expected to provide a back up to the mathematical modelling work being actively pursued.

6.2.1.1 Interrelation between compressive strength and hardness

To begin with CS was plotted as a function of hardness. As no definite relationship emerged, it was decided to plot CS/H as a function of hardness. On doing so a second order polynomial

functional relationship between emerged and therefore hardness can be represented as

$$R = A1 + A2 (H) + A3 (H)^2 \qquad \qquad ...(6.1)$$

where R = CS/H,

H = hardness, HV_{30},

A1, A2 and A3 are constants.

The constants A1, A2, and A3 were computed as before and the correlations thus obtained are :

Alloy P1 : $R = 50.11 - 0.1985H + (0.2186E-03)H^2$ ...(6.2)

Alloy P2 : $R = 83.55 - 0.3507H + (0.3903E-03)H^2$ ...(6.3)

Alloy P3 : $R = 12.09 - 0.02746H + (0.2511E-04)H^2$ ...(6.4)

CS values for the experimental alloys were computed on the basis of above models. On comparing them with the experimentally determined values, it emerged that the difference in most cases does not exceed $\pm10\%$(Table-6.4). In some instances the experimental and the predicted values differed by a larger margin due to casting defects present in the test specimens.

6.2.1.2 Interrelation between %strain and hardness

Similar steps as above were initiated to arrive at models interrelating %strain with hardness. The quantitative relationships arrived at are :

Alloy P1 : $R = 0.53 - 0.1726E-02H + 0.1501E-05H^2$ ...(6.5)

Alloy P2 : $R = 0.7936 - 0.2955E-02H + 0.2901E-05H^2$ ...(6.6)

Alloy P3 : $R = -0.2117 + 0.183E-02H - 0.2774E-05H^2$ ...(6.7)

where R = %strain/H,

H = hardness, HV_{30}

%Strain calculated on the basis of the above models were compared with the experimentally determined values of %strain. It was found that the difference was well within ±10% except in one or two instances reflecting favourably on the validity of the models developed(Table-6.5).

6.2.2 Effect of heat treating temperature/time

Having thus completed the first two steps outlined in section 6.2, it became necessary to analyze the experimental and predicted variation in CS as a function of temperature, as influenced by soaking period, for the three experimental alloys. While doing so, the 'approximated'-experimentally determined values were duly considered. It emerged that—

(i) For the alloy P1(2 hours soaking period), CS initially decreased and subsequently increased with temperature(Figure 6.4a). The predicted values also followed a similar pattern although the decrease/increase was negligible and for all practical purposes the variation could be considered as being linear.

(ii) On increasing the soaking period to 10 hours(Figure 6.4b), both the experimental and the predicted values were unchanged to begin with and thereafter marginally increased.

(iii) On increasing the Cu content to 3%(i.e. in P2), CS increased and then decreased (somewhat) on increasing the temperature, at 2 hours soaking period(Figure 6.5a). The predicted values followed a trend similar to that observed in P1.

(iv) At 10 hours soaking period(Figure 6.5b), CS either remained unaffected or increased slightly with heat treating temperature to begin with, followed by a steep rise in it, i.e. the trend was

similar to the one observed in P1 at 10 hours soaking period but more marked. The predicted values also showed a similar trend.

(v) On increasing the Cu content further to 5%(as in P3), the initial increase in CS with temperature was less pronounced than in P2(Figure 6.6a). This was followed by a small decrease in CS with an increase in temperature. The predicted values however exhibited a different trend.

(vi) However on raising the soaking period to 10 hours(Figure 6.6b), CS to begin with was high, it decreased with temperature and then became a constant. The predicted values followed a similar trend.

6.2.3 Discussion

The aforesaid data can be suitably interpreted on the basis of the effect of temperature/time in influencing the formation & morphology of DSPs and their effect in decreasing the volume fraction of MCs. That this contention is true can be judged by recalling that the property changes are being controlled through structural changes which are already discussed.

DSPs by and large are expected to strengthen and also embrittle the material somewhat especially in view of their morphology being needle like/platy. This is true especially at the lower soaking periods. With an increase in time their embrittling response is expected to reduce because their volume fraction reduces as a result of coarsening and also because the DSPs then predominantly comprise DCs. However on raising the temperature at either of the soaking periods, embrittlement reduces because the Vf of DSPs and MCs is reducing and the

morphology of latter is assuming favourable configurations. With an increase in temperature the DSPs/DCs are less relevant and therefore the overall properties would be governed by the volume fraction, distribution and morphology of MCs as the matrix in combination with the MCs/DCs is constituting a composite comprising MCs & DSPs up to 950°C and mostly MCs at T > 950°C. Based on this analysis, the data summarized in the Figures 6.4-6.6 can be reasonably well understood; only the trends would be analyzed in the following sections.

In P1, at 2 hours soaking period, a CS higher than in the as-cast state is due to the formation of DSPs. A higher % strain corroborates the presence of a larger volume fraction of the τ-matrix and absence of martensite. With an increase in temperature to 900°C, the volume fraction of DSPs increases, and therefore embrittling effect is larger. This has stalled the increase in CS and hence both the CS and % strain decrease. Some improvement in CS and % strain is expected at 950°C which is not explicitly manifested based on % strain. With a further increase in temperature to 1000°C a marked improvement in CS and % strain, over that obtained in the 950°C heat treated condition, is expected to materialize as the amount of DSPs(mostly DCs) is negligibly small, the amount of MCs is reduced & their morphology is favourable. On heat treating from 1050°C, the CS is nearly restored to the level attained on heat treating at 850°C but with substantially improved % strain even though DSPs are absent and Vf of MCs substantially reduced, due to an improved compatibility between the second phase(MCs) and the matrix and enhanced work hardening associated with low SFE(Mn bearing) austenites.

At 10 hours soaking period, CS was higher than the one obtained on soaking for 2 hours due to additional strengthening produced by a larger volume fraction of DSPs; this reduces %strain due to their larger volume fraction and adverse morphology. The gradual improvement in CS with heat treating temperature could be explained on a similar basis as the one outlined in explaining the data at 2 hours soaking period while duly remembering that for each of the 10 hours heat treatment the volume fraction of DSPs & MCs would be lower. This would enable the τ-matrix to contribute more to strengthening thereby marginally improving %strain.

In P2, a near constancy in strength followed by a decrease is what is expected at 2 hours soaking period because the volume fraction of MCs even in the as-cast condition is lower and would reduce markedly with temperature due to a higher Cu content. That this trend is not manifested/indicated is due to the anomalous data points for the 850°C, 1000°C, and 1050°C heat treatments (Figure 6.5a). Because of this the trend followed by the predicted CS values was opposite to what was expected.

On soaking for 10 hours, the trend followed by the experimentally determined and predicted values was similar to that observed in P1 except that the changes are more marked. This can be explained on the basis of an enhanced tendency of the DSPs/DCs to dissolve & to a larger decrease in the amount of MCs as is also confirmed through optical metallography. This not only reduced embrittlement but enhanced both CS & % strain.

In P3, at 2 hours soaking period, the plot would correspond to a trend observed in P2 except that the extent of embrittlement is more because the deformation behaviour is initially being governed by the DSPs which have an adverse morphology. This is due to a relatively lower volume fraction of MCs in the as-cast. The said effect persists till about 900°C. On increasing the temperature further the reasons for a decrease in CS are not clearly understood. It is likely that a larger variation(non uniform distribution) in the MCs(whose volume fraction is low) has in someway contributed to this observation. The other possible reason could be the presence of stray DC particles.

That this reasoning is correct is further borne out by the data obtained on soaking for 10 hours wherein to begin with CS is high due to favourable microstructural features already described. The decrease in CS with time & its eventual 'tapering off' can be explained on the basis of a similar reasoning as put forward in the preceding paragraph.

6.3 Corrosion studies

The results reported thus far dealt with the transformation behaviour of the experimental alloys arrived at on the basis of hardness measurements, optical metallography, X-ray diffraction, EPMA, and compression testing. Having achieved this target, it was appropriate to characterize the alloys for their corrosion behaviour. Potentiostatic and weight loss studies were used for this purpose. The data thus obtained have been summarized and discussed in the following sections.

6.3.1 Electro-chemical characterization

Studies were carried out on selected samples of the experimental alloys in the potential range -250 mV to +250 mV by constructing polarization curves within the Tafel region(Figures 6.7-6.9). Corrosion potentials and the currents obtained from the plots were noted down and I_{corr}, E_{corr} and corrosion rates were calculated. These are reported in the summary Table 6.6.

A scrutiny of the Figures 6.7-6.9 and the Table 6.6 revealed that:

(i) E_{corr} values for the experimental alloys ranged from -510 mV in P1 through -584 mV in P2 to -632 mV in P3.

(ii) Barring few exceptions, E_{corr} in the heat treated condition was lower than in the as-cast condition(microstructures become noble), the effect being marked on heat treating from high temperature(1000-1050°C)

(iii) The I_{corr} values similarly decreased on increasing the heat treating temperature and time

(iv) The least corrosion rate was obtained on heat treating from the highest temperature(1050°C). However the precise role of the soaking period at this temperature in influencing corrosion rate differed. Whereas in P1 a shorter duration was more useful, in P3 duration did not seem to matter.

(v) In summary, the overall E_{corr} and I_{corr} values were the least in P1, higher in P2 and still more higher in P3.

6.3.1.1 Discussion

A careful study of the basics of electro-chemical characterization reveals that one method of conducting accelerated aqueous corrosion testing is by determining the

potentiostatic behaviour of a material. Rather than plotting the entire polarization curve, it may suffice to confine the studies to the Tafel region. The critical parameters of interest are E_{corr} and I_{corr}; the latter is determined by drawing a tangent at the linear portion of the cathodic and anodic regions of the plot(designated as E_{corr} cathodic & E_{corr} anodic) and noting down current corresponding to the point of intersection of the tangent with the horizontal(representing E_{corr}).In the present instance, however, the various values summarized in the Table 6.6 have been directly indicated by the instrument.

A microstructure would resist corrosion if it has an E_{corr} which is less negative i.e. more closer to the H_2 electrode potential. Any heat treatment that alters the microstructure so that the E_{corr} becomes more noble would be adjudged to be a beneficial heat treatment. It is equally important that a given microstructure should additionally exhibit a low I_{corr} value. Thus, if two microstructures attain a nearly similar E_{corr}, the one exhibiting a lower I_{corr} value will be more preferred. Similarly, a low value of I_{corr} is desirable irrespective of whether or not a material shows 'active-passive' behaviour. This is because I_{corr} is synonymous with H_2 liberation/formation and a large value would signify a large H_2 adsorption/absorption and hence embrittlement. The above said analysis is useful in explaining the data obtained.

Corrosion resistance in general improved upon heat treating from high temperature(s) in comparison to that obtained on heat treating from lower temperature(s) since the alloys investigated

in the present study are conducive to attaining an austenite based microstructure with greater stability. On heat treating, a general improvement in corrosion resistance is due to (i) a reduction in the Vf of MC and DSPs, (ii) exclusion of DSPs and rounding off and or formation of hexagonal MCs especially on heat treating from 1000°C and 1050°C, and (iii) the formation of a successively increasing amount of austenite whose stability increases with temperature as more and more amount of MCs and DSPs dissolve in it. Needless to add that in the absence of a second phase(both MC and DC) the corrosion resistance would have been better than what has been obtained.

After having made the aforesaid observations, it would be appropriate to proceed into the data analysis.

The data summarized in the Table 6.6 can be interpreted in two ways, (i) by analyzing the general trends & (ii) by analyzing the specifics. Doing the latter has been made somewhat difficult due to the paucity of the corrosion data for P2 and P3 vis-a-vis P1. All the same, an effort would be made to interpret the data as much as possible. To facilitate this process, it was felt appropriate to supplement the polarization data with corrosion data obtained on the basis of weight loss studies.

The principle impediment to analyzing the limited potentiostatic data is that the main condition of only one of the surfaces being exclusively exposed to the corroding media is not strictly satisfied. This is because the specimens used were mounted in bakelite & in spite of taking all the precautions the solution did 'seep' into the crevices between the mount & the specimen. This process continued right through the test in effect

producing more severe corroding condition than should have otherwise existed. In view of the difficulties in machining the alloys, this problem is likely to persist unless castings of the requisite shape and size are made so as to facilitate preparation of test specimens for potentiostatic studies. Another problem with this kind of material is the excessive work hardening of the surface due to the low SFE of the Mn containing austenites. Possible remedy is to carry out a low temperature stress relief prior to corrosion testing.

In spite of the above mentioned problems contributing to enhanced corrosion, certain rationalized assessments could be arrived at e.g. in alloy P1 for the 2 hours soaking period, the corrosion rate steeply decreased on shifting from 950°C to 1000°C due to more or less complete elimination of DSPs, a reasonably favourable carbide morphology and to the attainment of a larger volume fraction of stable τ. The corrosion rate further decreased, although not as markedly as before, on raising the heat treating temperature to 1050°C. due to a reduction in the volume fraction of MCs & to a further improvement in their morphology. As against this, for a 10 hours soaking period, increase in the heat treating temperature from 900 to 1000°C through 950°C decreased corrosion rate first due to a gradual decrease in the Vf of DSPs up to 950°C, its complete absence at 1000°C & also because of a reduction in the volume fraction of MCs. However the reasons for a sudden increase in corrosion rate on increasing the heat treating temperature to 1050°C can not be fathomed. If, however the data is indeed a true representation of

the state of affairs then it may be due to the formation of dark etching regions surrounding MCs and also due to the 'tranquility' of the matrix being disturbed due to the formation of small sized particles. Perhaps distributional heterogeneity associated with MCs(Table 4.59) may have also contributed to such an occurrence.

As against this, the alloy P2 seems rather disadvantageously placed as is evident from the corrosion rate data corresponding to the 1050°C, 2 hours heat treatment. However, for the 1050°C, 10 hours heat treatment, the corrosion rates are lower than the ones attained in P1 due to a reduced heterogeneity of the microstructures(Figures 4.28 & 4.35 and Tables 4.59 & 4.60).

In P3, the improvement in corrosion resistance on increasing the heat treating temperature from 900°C to 1050°C for the 10 hours soaking period is rather small. Reasons for this could be a lower overall corrosion rate(initially) due to a much lower Vf of MCs even in the as-cast state & relatively faster 'elimination'/ dissolution of DSPs. None the less on comparing with P1, the reasons as to why heat treatment did not have a marked influence on the corrosion behaviour of P3 is difficult to fathom.

6.3.2 Analysis of the electro chemical data based on 'weight loss studies'

6.3.2.1 Weight loss data :

Weight loss studies, carried out on as-cast/heat treated specimens of the experimental alloys as per the relevant ASTM specifications, revealed a different state of affairs. The data presented in the Tables 6.7-6.8 revealed that-

(a) The corrosion rate even in the as-cast state was reasonably good, it being the maximum in P1 and comparable in P2 & P3.

(b) On heat treating from 'lower temperatures, the corrosion rate increased over that in the as-cast state up to a particular heat treating temperature/time and began decreasing there after.

(c) The adverse effect persisted up to 900°C, 4 hours heat treatment in P1, whereas in P2 and P3 it persisted till 950°C, 2 hours heat treatment.

(d) Although the beneficial effect of increasing the heat treating temperature in improving corrosion resistance was in evidence as early as at 950°C, 10 hours heat treatment(marked in P1 & marginal in P2 and P3), a tangible effect set in only on heat treating from 1000°C. The magnitude of improvement was proportional to the amount of copper present(minimum in P1 and a maximum in P3) and soaking period.

(e) This is duly reflected in the alloy P3 attaining the least corrosion rate & marginally better than either P1 or P2 which attained nearly identical corrosion rates.

The data contained in the Tables 6.7-6.8 could be looked at differently on the basis of the plots summarized in Figures 6.10-6.12. The plots besides revealing a second order variation between corrosion rate and temperature, revealed the relative usefulness of microstructures generated in the experimental alloys, in resisting corrosion e.g. in P1 the microstructure attained on heat treating at 900°C(2 hours) had an adverse effect & it(adverse effect) decreased gradually by increasing the heat treating temperature/time; this adverse effect is observed in P2 in a limited sense for the 950°C, 2 hours heat treatment and very markedly in P3 for the same heat treatment. The adverse effect of this microstructure persisted to a limited extent even at the 10

hour soaking period. The plots further revealed the usefulness of the following structures in resisting corrosion:

P1   --   microstructures at 10 hours soaking period,

P2   --   microstructures at 2 hours soaking period, and 10 hours soaking period at the highest heat treating temperature

P3   --   microstructures at 10 hours soaking period

6.3.2.2. Nature of corroded surfaces

The corroded surfaces on being examined under a scanning microscope revealed absence of pitting and or graphitic corrosion(Figures 6.13-6.15). The attack was uniform and even after the completion of the test, the specimen surfaces retained a fair amount of polish revealing negligible surface attack. The corrosion product was non-adherent.

6.3.2.3. Discussion

The weight loss data give a more substantial and authentic information on the corrosion behaviour of different micro-structures not provided for by the potentiostatic data . In a general sense it reveals reasonably good corrosion resistance in the as-cast condition, its marginal deterioration at best on heat treating up to a certain temperature(900/950°C)/time for each alloy, the maximum deterioration occurring at a specified heat treatment to be followed by a substantial improvement in corrosion resistance on heat treating from high temperatures (1000/1050°C) preferably on soaking for larger periods. This is indeed a welcome trend because in the temperature range of 800-950°C needle or plate shaped DSPs have formed in all the three alloys(Figures 4.23-25, 4.30-32, and 4.37-4.39). That the corro-sion rate on heat treating from temperatures within 'this range'

is not much different from that in the corresponding as-cast state reveals that the adverse morphology/distribution of the DSPs & the alignment of DCs and MCs(Figures 4.23-25, 4.30-32, and 4.37-4.39) has a minimal adverse effect on corrosion behaviour thereby reflecting favourably upon the τ/DSP & τ/MC couple in resisting aqueous corrosion in 5% NaCl solution. In fact the data summarized in the Table 6.8 and Figures 6.10-6.12 further indirectly indicate that the DSPs are of a similar character as the MCs i.e. the DSPs & DCs should in fact be either M_7C_3 and or M_3C type carbides. It is surmised that the possible formation of M_5C_2 may have adversely affected the corrosion behaviour more than what is reflected by the data summarized in Table 6.8 due to its monoclinic structure inducing enhanced incompatibility between second phase and the τ-matrix.

Having said so it would be pertinent to examine the microstructures/heat treatments which have given rise to a substantial increase in corrosion rate. A clue to this emerges on perusing Table 6.8.

Alloy	Heat treatment	Microstructures	Features
P1	900°C, 2 hours	τ-matrix, Aligned DCs, Plate type DSPs	Matrix uneven, Feathering, Aligned DCs
	950°C, 2 hours	τ-matrix unevenness negligible, Vf of DSPs/DCs low, Bunching of DCs harmful	At 800°C, 10 hours matrix is uneven, at 900°C, 6 hours matrix is uneven but less than at 2 hours, feathering is there
P2	900°C, 10 hours	τ-matrix, aligned MCs, aligned DCs	Matrix uneven (starting at 900°C, 2 hours), aligned DCs, chain formation at

			grain boundary(obser- ved at 950°C, 2 hrs), bunched DCs(prominent at 950°C,2 hours
P3	950°C, 2 hours	τ-matrix, aligned DCs, bunching DCs	τ-matrix uneven, aligned DCs bunched, needles/DCs bunched, chain like structures, non uniform matrix & bunching even at 900°C 10 hours and 950°C 6 hours.

Thus summarizing, in P1(900°C,2hours)*, the main adverse feature appears to be the unevenness of the τ-matrix which was marked even on heat treating at 850°C(10 hours heat treatment). Whether or not the MCs were 'chained' could not be specifically ascertained. In P2(900°C,10 hours)*, the adverse features are uneven matrix(marked even at 900°C, 2 hours), aligned/bunched DCs (prominent at 950°C, 2 hours), chain formation, and coarse needles(?). In P3(950°C,2 hours)*, once again the main deficiencies are a large unevenness of the matrix, chained structures and aligned DCs. These features are initiated corresponding to the 900°C, 10 hours heat treatment and persisted to a lesser/reduced extent even on heat treating at 950°C(2 hours) heat treatment.

Thus taking an overall view, the features common to the three alloys which affected corrosion resistance adversely are (i) unevenness of the matrix(matrix heterogeneity), (ii) bunching & alignment of carbides, and (iii) the formation of 'chained' structure(whose precise identity/reasons for its formation are not fully understood). Interestingly none of the other parameters used to define distributional heterogeneity(Tables 4.59-4.60)

---

* most deleterious heat treatments

apparently show the aforesaid microstructures in a poorer light thereby suggesting that chemical heterogeneity(associated with the matrix) appears to be the dominant factor in adversely affecting the corrosion resistance. This analysis also suggests that the presence of DSPs with unfavourable morphology appeared to have minimal adverse effect whereas the matrix unevenness (heterogeneity) appeared to have a marked effect in adversely affecting corrosion resistance. On the other hand unfavourable morphology of the DSPs has a definite adverse impact on the deformation behaviour of the alloys as already discussed in section-6.2.3. This explains the corrosion data on heat treating from temperatures up to 950°C.

On heat treating from 1000°C, the three alloys showed a marked improvement in corrosion resistance due to the elimination of DSPs, the MCs attaining spherical/hexagonal morphologies (favourable), 'rounding off' at the edges of MCs, and due to a reduction in the Vf of MCs. Alloy P3 with the highest Cu content(at 2 hours soaking period) attained a marginally lower corrosion rate than either P1 or P2 due to its lowest Vf of MCs, a more stable τ, and a better morphology of MCs. These beneficial effects are further accentuated at 10 hours soaking period leading to considerable improvement in corrosion resistance in P2 & P3(Table 6.8, Figures 6.11b & 6.12b). That the corrosion rate in P1 did not improve could be attributed to the formation of haloed carbide regions not observed in P2 & P3(Table 6.8). However the aforesaid beneficial changes are attained, in general, on heat treating from 1050°C leading to the attainment

183

of minimum corrosion rates in the experimental alloys(Table 6.8, Figure 6.10-6.12). It is of significance to note that in spite of a heterogeneity arising out of the formation of 'degenerate' dark regions around MCs and a general unevenness of the matrix due to reprecipitation of DCs(attributed to enhanced graphitizing action resulting from an increase in the Cu content from 1.5% in P1 to 5% in P3), the alloys are attaining very low corrosion rates and yet not exhibiting any kind of localized attack(Figures 6.13-6.15). It is evident that in the absence of the above mentioned heterogeneities, the alloys would have exhibited still lower corrosion rates. The discussion would imply that to reduce heterogeneity the process(es) responsible for accelerating different transformations(already discussed) have to be contained. There is thus a need to optimize the Cu content keeping in mind the seemingly contradictory effects it is producing namely (i) the transformation 'accelerating effect' promoting a reduction in the amount of second phase(partly beneficial & partly retrograde), (ii) increasing the Cu content of the matrix thereby improving corrosion resistance(beneficial), and (iii) microstructural degeneracy/heterogeneity that is being created due to an enhancement in the transformation kinetics (retrograde).

It would not be out of place to mention here that a more detailed SEM examination of the corroded surface would have yielded more detailed information especially with regard to the formation of chain structure(Figures 4.26-4.28 & 4.33-4.34), haloed regions(Figures 4.26,4.32-4.34, & 4.40), and triple point regions observed on corrosion testing samples heat treated from

1050°C, 10 hours(Figures 6.13-6.15). None the less the information provided by SEM is very encouraging, reaffirms the findings of Jain(62), Kumar(83), and Rao, Patwardhan & Jain(119) regarding the absence of pitting, graphitic corrosion, and the nature of attack being 'uniform dissolution'. The retention of mirror finish on the specimen surfaces even in the corroded condition is a clear indication that some kind of passive layer is perhaps forming. This is concluded from the observation that the corrosion product is non-adherent and 'falls off' merely on shaking the specimen in the aqueous media.

The corrosion rates attained in the experimental alloys are substantially better than the ones reported by Jain(62) in the Fe-Mn-Cr-Cu alloys containing 7.5% Mn & up to 3% Cu. The deformation behaviour of the presently investigated alloys has already been adjudged to be promising(section 6.2.3). On the strength of these observations the key elements of the alloy design, outlined in the Chapter II, stand vindicated.

Corrosion rates attained on heat treating from higher temperatures are comparable or better than the ones attained in standard Ni-Resist(both flake & S.G. type) compositions(Table .12) being very extensively used under marine conditions. incidentally the strength of the Ni-Resist compositions is approximately half of that obtained in the experimental alloys. These observations may be regarded as the highlights of the present study with major technological fall out. This aspect has been considered in the next chapter, in detail, in the section dealing with general discussion.

6.4 Modelling of the corrosion behaviour

An analysis of the corrosion data in the previous section reveals how the different microconstituents influenced corrosion behaviour. Excluding the matrix to begin with, their effect depends upon their nature and size, shape and distribution. When the matrix is also considered, its characteristics (crystal structure and stability) and difference in the electro-chemical potentials between the matrix and the constituents also assume significance. Interestingly, most of the correlations have been qualitative in character. Any effort aimed at modelling the corrosion behaviour will have to incorporate the above said aspects.

6.4.1 Back ground information

The first effort in this regard was made by Jain(62,80-81) who attempted to correlate corrosion rate with the microstructural features comprising austenitic matrix, massive carbides and dispersed carbides. He selected heat treatments carried out at 900 & 950°C primarily because the different alloys constituting the study attained nearly constant hardness values at these temperatures. Whereas the hardness was more or less independent of the soaking period, the volume fraction of MCs & DCs varied. It was felt appropriate to examine the methodology adopted by him before enlarging upon the ideas conceived in his work reported recently by Patwardhan & Jain(80-81).

It was conceived that the CR could be expressed as a function of different parameters namely,

$$CR \approx f(\text{austenite } Vf/ \text{ stability})$$

$$CR \approx f(Vf \text{ of } MC)$$

$$CR \approx f(\text{Vf of DC})$$

$$CR \approx f(\text{distribution of the DC})$$

or $CR \approx F [(\text{Vf/stability of } \tau).(\text{Vf of MC}).(\text{Vf of DC}).(\text{distribution of DC})]$

....(6.8)

To begin with, the last term was excluded and the volume fraction of MCs & DCs was combined into a single term to develop the initial stage model. This was justified on the assumption that since the second phase in general would enhance CR, their overall effect can be cumulated into a single factor.

From the experimental data it was concluded that the functional relationship interrelating corrosion rate with the total volume fraction of carbides(VCb) can be represented by a second order polynomial :

$$CR = A1 + A2(VCb) + A3(VCb)^2 \qquad ...(6.9)$$

where VCb = total volume fraction of MC + DC

The contribution of the second phase, i.e. the role of dispersed carbides, was included in the above expression by incorporating a factor based on the number of particles, NOP. This led to the following expression :

$$CR = [A1' + A2'(VCb) + A3'(VCb)^2](NOP)^{A4'} \qquad ...(6.10)$$

The constants A1', A2', A3', and A4' were calculated by using multi-variable constraint optimization technique(99-100) and the final equations are:

Alloy P1:

$$CR = (40.635-2.971(VCb)+0.08417(VCb)^2)(NOP)^{0.0000112} \qquad ..(6.11)$$

Alloy P2:

$$CR = (9.190-0.000922(VCb)+0.00722(VCb)^2)(NOP)^{0.1687} \qquad ..(6.12)$$

Alloy P3:

$$CR = (6.198 - 0.000441(VCb) + 0.01925(VCb)^2)(NOP)^{0.160496} \quad ..(6.13)$$

The above constants were determined within a limiting condition of ±8000. When this restriction was set aside and a larger number of iterations were taken to obtain better optimum values, then the above equations assumed a more reasonable form:

Alloy P1:

$$CR = (54.01 - 3.865(VCb) + 0.1127(VCb)^2)(NOP)^{-0.1451} \quad ..(6.14)$$

Alloy P2:

$$CR = (6.746 + 0.261(VCb) + 0.000218(VCb)^2)(NOP)^{0.1717} \quad ..(6.15)$$

Alloy P3:

$$CR = (-17.2878 + 2.961(VCb) - 0.06741(VCb^2)(NOP)^{0.11376} \quad ..(6.16)$$

Through a suitable analysis involving the effect of two factors in contributing to corrosion, it can be shown that the model is neither physically consistent nor theoretically justifiable since NOP do not truly represent the DC and that the constants were calculated without adequately understanding the physical implications of the their effect on the corrosion rate. Further the effect of DCs was getting considered twice as it figured as a part of VCb and again as NOP. This was also observed by Jain(62,80,81). Therefore further stress was laid on developing models interrelating the corrosion behaviour with massive second phase and dispersed second phase. Thus the two models developed were CR vs VMC/NOP and CR vs VMC/DF.

Kumar's(83) work reiterated that the VMC-NOP and VMC-DF models were a satisfactory representation of the corrosion behaviour of the alloys developed. Of the two models, the former emerged as a more effective representation of the corrosion

behaviour, some what surprisingly, although his and Jain's(62) studies had convincingly demonstrated that DF was a far better representation of the DCs than the NOP. Through 3-D plotting the idea of 'microstructural optimization' was mooted which proved useful in assessing what best to expect in terms of properties from a given composition. The method to arrive at the optimal minimal values of MC, DF/NOP to obtain the best in terms of performance was also indicated. This enabled optimization of the heat treating parameters to be carried out. Finally the idea of developing a 'unified model', wherein a single model could predict the corrosion behaviour of all the experimental alloys, was also mooted(83).

It was decided to expand upon the ideas initially proposed by Jain and Kumar and to arrive at a rationalized assessment of the modelling of the corrosion behaviour of the alloys being presently investigated. It was also proposed to compare the data presently obtained with that reported by Kumar(83) so that a considered appraisal of the state of the art(of this new area) was made possible.

6.4.2 Modelling of the corrosion behaviour of the experimental alloys

6.4.2.1 The VMC-NOP model

The basis for this model is the qualitative formulation represented by equation (6.8)

CR ≈ F [(Vf/stability of τ).(Vf of MC).(Vf of DC).(distribution
of DC)]   ....(6.8)

As proposed by Jain and Kumar(62,83), the effect of the parameter Vf/stability of τ was considered as constant to begin

with so that the equation could be rewritten as

$$CR \; \alpha \; F \; [.(Vf \; of \; MC).(Vf \; of \; DC).(distribution \; of \; DC)] \; ...(6.17)$$

From the experimental data, it was considered that relationship between CR & Vf of MCs could be represented by a second order polynomial

$$CR = A1 + A2.VMC + A3.(VMC)^2 \qquad\qquad ...(6.18)$$

The role of dispersed second phase in influencing corrosion was considered by incorporating the total number of particles (NOP) into the equation 6.18, which now assumes the form

$$CR = (A1 + A2.VMC + A3.(VMC)^2)(NOP)^{A4} \qquad ...(6.19)$$

The constants A1,A2,A3, and A4 were calculated by the nonlinear optimization technique permitting the constants to vary over a large unlimited range. The models arrived at are

Alloy P1:

$$CR = (19.484-0.3468(VMC)+0.03409(VMC)^2)(NOP)^{-0.120223} \qquad ..(6.20)$$

Alloy P2:

$$CR = (10.834-0.1088(VMC)+0.02763(VMC)^2)(NOP)^{0.04558} \qquad ..(6.21)$$

Alloy P3:

$$CR = (-6.1151+1.6559(VMC)-0.03476(VMC)^2)(NOP)^{0.20056} \qquad ..(6.22)$$

The values of the two factors constituting the models were computed and the data are summarized in the Table 6.9.

A scrutiny of the data summarized in the Table 6.9 revelaed that the corrosion rates predicted on the basis of the models agree well with the experimentally determined values. Secondly, the contribution of factor I to the corrosion rate follows a systematic pattern, namely, with an increase in temperature/time of the heat treating its contribution reduces in all the three

alloys and so also does the corrosion rate. Moreover its contribution to corrosion is inversely proportional to the Cu content(or the τ-stabilizing/carbide destabilizing tendency). This result is consistent with the analysis put forth in the earlier sections(sections 6.3-6.4) to explain the corrosion behaviour of the experimental alloys. However the contribution of the factor II did not appear to be consistent either in itself or with the corresponding variation in the NOP as influenced by temperature & time in the three experiential alloys(Table 6.9). A possible reason could be that the constants A1,A2,A3, and A4 have been calculated without exercising any constraint on the range over which they can vary. Alternatively, it was likely that the NOP is not a relevant representation of the effect of the dispersed second phase.

On putting constraints on the range over which the constants A1 to A4 could vary, namely, A4 is less than 1.0 & negative and other constants could assume value up to 20, the models take the form:

Alloy P1:

$$CR = (19.4863-0.3474(VMC)+0.03411(VMC)^2)(NOP)^{-0.10217} \quad ..(6.23)$$

Alloy P2:

$$CR = (13.1915-0.3553(VMC)+0.04393(VMC)^2)(NOP)^{-0.020004} \quad ..(6.24)$$

Alloy P3:

$$CR = (8.9278-0.000197(VMC)+0.03553(VMC)^2)(NOP)^{-0.001} \quad ..(6.25)$$

A comparison between the predicted and experimentally determined corrosion rates revelaed that the agreement between the two sets had considerably improved(Table 6.10). A reappraisal of the effective contribution of the two factors in influencing

corrosion(emerging from an analysis of the data summarized in Table 6.10), revealed that the models represented by equations 6.23-6.25 are in fact a true representation of the corrosion behaviour of the experimental alloys justifiable on the basis of a similarity in the nature of the constants A1 to A4. They are also theoretically justifiable since the contribution from the factor II to the occurrence of corrosion is consistent with the characteristics of the 2nd phase as represented by the NOP(Table 4.39).

A single model(called the unified model) was also developed which could predict the corrosion behaviour of the three experimental alloys and is of the from:

$$CR = (9.1472+0.25096(VMC)-0.01051(VMC)^2)(NOP)^{0.04848} \quad ..(6.26)$$

The predicted values of corrosion rate estimated on the basis of this model, although in good agreement with the experimentally determined values in alloys P1 and P2, none the less showed some deviation in alloy P3(Table 6.11). However looking into the differences in the transformation behaviour of the experimental alloys elaborately discussed in Chapter-V, the overall agreement between the predicted values of CR based on the 'unified model' and the experimentally determined values should be regarded as excellent.

3-D plots between CR,VMC, and NOP as summarized in Figures 6.16a-c. reveal very interesting information. For alloy P1, the corrosion rate decreased with VMC along(more or less) a smooth gradual surface except for some deviation towards the right hand side edge(Figure 6.16a). Corrosion rate appeared to be independen-

dent of the NOP except when the 'end' representing reduced number of particles is approached i.e. when the number of particles tend to be low. The slight adverse effect may be due to a 'smaller particle size of DCs' formed on 'heat treating' from 'higher temperature(s)'. Thus taking an overall view the key factor in controlling corrosion appeared to be the VMC, with NOP making a small yet a more or less 'uniform' contribution to corrosion which for all practical purposes is independent of the number of particles. Thus VMC has to be maintained at a low level to obtain lower corrosion rates.

The aforesaid effects are more marked in P2(Figure 6.16b) in which the changes are along a smooth surface without any deviations. As before NOP do make a small contribution towards influencing corrosion which appeared to marginally decrease if the NOP are low perhaps because the particle size is not conducive to enhancing corrosion(compare with P1 where the situation is to the contrary). Thus as in P1, corrosion control is through controlling VMC.

The resulting surface in P3 is similar to that observed in P1 and P2. The overall surface profile is tending to be planar with the NOP apparently having no effect in controlling corrosion except offering a contribution which is independent of NOP. This analysis further implies that the alloy P3 is attaining a particle density(i.e. NOP/unit area) and a size distribution which apparently do not have an adverse effect on corrosion. Thus as in P1 and P3, corrosion control is through controlling VMC.

3D- plots corresponding to the unified model(Figure 6.17) is generating a surface in the form of an inverted parabola.

193

However, its operative profile over the admissible levels of VMC & NOP and the likely admissible levels of corrosion rates would be similar to that observed earlier. Although an impression is generated that lower corrosion rates could be attained, but practically this is not the situation since negative corrosion rates can't be attained.

The contour plots summarized in the Figures 6.18a-c & 6.19 very usefully represent an interplay between NOP and VMC in controlling corrosion and the information summarized in them can be explained on a similar basis as the data contained in the Figures 6.16a-c & 6.17 respectively. An additional advantage of these figures is that it would be possible to predict corrosion rates for those heat treatments/conditions at which experimental data is not available.

6.4.2.2 The VMC-DF model

Models(based on DF) Evaluated without constraints

Alloy P1:

$$CR = (16.4983-0.6345(VMC)+0.03558(VMC)^2)(DF)^{-0.0752} \quad ..(6.27)$$

$$CR = (-1.2423+0.9559(VMC)-0.02236(VMC)^2)(DF)^{-0.5765} \quad ..(6.28)$$

$$CR = (-36.346+7.0937(VMC)-0.1768(VMC)^2)(DF)^{0.575816} \quad ..(6.29)$$

Models(based on DF) Evaluated with constraints

Alloy P1:

$$CR = (10.000+0.09488(VMC)+0.01235(VMC)^2)(DF)^{-0.130245} \quad ..(6.30)$$

Alloy P2:

$$CR = (7.1009+0.28262(VMC)+0.01339(VMC)^2)(DF)^{-0.132449} \quad ..(6.31)$$

Alloy P3:

$$CR = (1.3361+1.01899(VMC)+0.00161(VMC)^2)(DF)^{-0.003181} \quad ..(6.32)$$

Unified Model

$$CR = (7.7095+0.46516(VMC)+0.00504(VMC)^2)(DF)^{-0.067201} \qquad ..(6.33)$$

The data pertaining to the modelling of the corrosion behaviour based on the VMC-DF combination, as summarized in Tables 6.12-6.14 & Figures 6.20-6.23 can be explained on similar lines as the data pertaining to the VMC-NOP model. The differences, if any, center around the figures depicting the data emerging from the unified model.

The profile of the resulting surface emerging from the unified model based on VMC-DF combination(Figure 6.23), although in itself planar, is essentially similar to the surface profile observed in the VMC-NOP unified model(Figure 6.17). It may be further mentioned that the overall data depicted in Figure 6.23 (in terms of attainable corrosion rates) is realistic in the sense that no negative corrosion rate values are envisaged. Thus, taking an overall view, the VMC-DF unified model provides a more realistic representation of the actual state of affairs when compared with the projections emerging from the VMC-NOP unified model.

Thus summing up, it is a happy augury that the explanation put forward to explain the corrosion behaviour of the alloys based on the VMC-NOP model is duly reflected in its behaviour based on the VMC-DF model namely the range over which DF varies having no effect in controlling the corrosion behaviour although the DF in itself does make a small yet uniform contribution. Further the role of the matrix and of a low Vf of MCs in controlling corrosion is more specifically highlighted. Thirdly,

of the two 'unified models', the VMC-DF & VMC-NOP the former combination appears to yield a more balanced picture of the relative effects of factors I and II in controlling corrosion as already discussed above. This appears reasonable since 'size distribution' as represented by DF is a more precise representation of an assembly of particles rather than their actual number more so as the former also takes into consideration the number of particles.

6.4.3 Interrelation between corrosion and deformation behaviour

A perusal of the data on the corrosion and the deformation behaviour indicated that an 'improvement' in the deformation behaviour in general 'improved' corrosion resistance. It was therefore felt appropriate to establish such an interrelation. Mathematically it meant that

$$CS = A1 + A2 (X) \qquad\qquad ....(6.34)$$

where X could represent either CS or %strain. On calculating the constants as before, the models are

Alloy P1	$CS = 3417 - 78.54 (CR)$	...(6.35)
Alloy P2	$CS = 3402 - 64.15 (CR)$	...(6.36)
Alloy P3	$CS = 1711 + 16.07 (CR)$	...(6.37)
Alloy P1	$\% Strain = 58.63 - 1.792 (CR)$	...(6.38)
Alloy P2	$\% Strain = 54.36 - 1.522 (CR)$	...(6.39)
Alloy P3	$\% Strain = 39.63 - 0.6924 (CR)$	...(6.40)

CS and % strain calculated on the basis of the above formulations are summarized in the Tables 6.15-6.16. Barring a few instances (wherein there was an error in estimating CS_{exp} due to defects in specimens), there is an excellent agreement between the predicted and experimentally determined values of CS and % strain.

The above said formulations also reveal the possibility of estimating CR from CS and % strain values and if this is done, the agreement between the experimentally determined and predicted CR is very good.

6.5 Concluding remarks

The data analyzed in sections 6.1-6.4 touches upon a number of· new ideas, namely, assessment/modelling of the deformation behaviour, an analyses of the corrosion behaviour based on the potentiostatic and weight loss studies to arrive at an overall 'performance' appraisal. The final sections deal with the modelling of the corrosion behaviour, efforts aimed at micro-structural optimization with a view to assess the key parameter involved in corrosion control, checking on the 'physical consistency' of the models developed, plotting contour maps of CR vs VMC/NOP and CR vs VMC/DF not only to have a birds eye view but also with a view to finding out the corrosion behaviour under those conditions at which it has not been experimentally determined e.g. for 800°C and 850°C heat treatments. Towards the concluding stages of this analyses a correlation has been sought to be established between the corrosion and the deformation via the agency of microstructure. Such an interrelation not only helps in predicting corrosion data based on CS and % strain but also establishes a link between the microstructure and the deformation behaviour. It emerges that CS is less strongly dependent upon the microstructure(VMC & DF) than % strain. This is to be expected since MCs and DSPs/DCs would influence the ease of deformation of the matrix markedly and hence the percent strain.

CHAPTER VII

GENERAL DISCUSSION, CONCLUSIONS, AND SUGGESTIONS FOR FUTURE WORK

7.1 General Discussion

The present investigation has succeeded in assessing the transformation behaviour of the experimental alloys in a fair detail. The alloys intended to resist corrosion, were designed to include low cost indigenously available alloying elements Mn,Cr and Cu. Possible clues to their transformation behaviour were provided by their compositions and from previous work of Jain and Kumar(62,83).

The alloys were so designed that austenite is retained in the as-cast condition itself thereby implying it to be the matrix. Optical metallography and x-ray diffractometry duly confirm this to be so. This is further confirmed through micro-hardness measurement which indicates the matrix hardness to be 320-330 VPN. The 'leaf like' black areas, identified as martensite, appropriately have a micro-hardness of 620 VPN. On heat treating from 800°C, the matrix is essentially austenitic and has microhardness 370 VPN. The stability and volume fraction of austenite increased with an increase in the heat treating temperature/time/copper content (i.e. while moving from alloy P1 to P3) accompanied by a simultaneous decrease in the volume fraction of massive carbides. This was corroborated through the EPMA, macro-hardness and micro-hardness measurements; e.g. the micro-hardness of the matrix increased from 370 VPN as above to

420 VPN through 400 VPN obtained on heat treating at 1000°C, thereby confirming increased stability of the matrix due to increased solute enrichment. X-ray diffractometric studies confirmed this through a decrease in the diffraction angle. The above changes, brought about by increasing the heat treating temperature/soaking period/Cu content, were conducive to improving the corrosion resistance and the deformation behaviour. Thermogravimetric data on samples heat treated at 1000°C, 10 hours also indirectly indicated the usefulness of increased stability/Vf of austenitic matrix.

The second phase in the as-cast microstructure is massive carbide only. Three types of massive carbides were observed, namely, massive/platy type, flower type, and mesh type. Massive carbides have a hardness of 680-700 VPN and flower type carbides 1000-1100 VPN. On heat treating, the following changes have been observed:

1. Mesh type carbide disappeared(dissolved) and dispersed second phase precipitated from the austenitic matrix.

2. There was a considerable variation in the chemical composition of the carbides as ascertained through EPMA and corroborated by micro-hardness measurements. As already discussed, the Vf of MCs decreased with an increase in the heat treating temperature/time and the 'rounding off' tendency was observed at 900/950°C heat treatments. On heat treating from higher temperatures massive carbides assumed different morphologies such as rounded, hexagonal etc. So also it appeared that there was an increase in the Vf of discontinuous free carbides, some of which appeared to form though agglomeration of DCs.

199

Massive/platy carbides have a micro-hardness of 850 VPN at 800°C, 1000 VPN at 1000°C, and 1080 VPN at 1050°C whereas the free carbides have micro-hardness of 1100 VPN at 800°C, 1450-1550 VPN at 1000°C, and 1600-1800 VPN at 1050°C heat treatments.

At 1000°C, 10 hours heat treatment, a 'peculiar' feature involving 'agglomeration' of massive carbides was observed. These carbides have micro-hardness of 1800 VPN and the dark phase in between the agglomerating carbides has a micro-hardness of 800 VPN. EPMA studies revealed that the dark grey regions in between the agglomerating MCs would become MCs except for their Cu and Si content.

3. Optical metallography and EPMA studies have revealed two types of massive carbides on heat treating at 900/950°C differing in their Cr content by about 10%. The inherent nature of the white cast irons to form heterogeneous structures may have lead to such an occurrence. This could be one of the reasons for deterioration in the corrosion resistance and deformation behaviour on heat treating from these temperatures.

As already discussed, dispersed second phase(DSP) precipitated from the austenitic matrix on heat treating from 800°C. They essentially comprised needles(plates) + DCs up to 900°C, 10 hours heat treatments, only DCs up to 950°C, 6 hours heat treatments, and reprecipitated particles of Class I size upon heat treating up to 1050°C, 4 hours. DCs finally dissolved on raising the temperature/time. The dispersed second phase adversely influences corrosion behaviour due to an unfavorable

morphology and enhanced galvanic action. However, it is the heterogeneity of the matrix which appears to have a more dominant effect on the corrosion behaviour than the dispersed second phase. The DSPs and MCs have more pronounced effect on the deformation behaviour especially on % strain to fracture. Deformation behaviour was assessed on the basis of compression testing. In some of the instances the experimentally determined values have been low due to defects in specimen present in the form of a pipe running right through the casting.

Optical metallography revealed a similarity between the needle type DSPs and DCs. X-ray diffractometric studies have shown them to be M_5C_2/M_3C whereas EPMA indicated them to be M_3C/M_7C_3 type carbide. Not much is known as to whether M_5C_2 could form in the experimental alloys. The possibility that these needles are partly M_3C and/or partly M_7C_3/M_5C_2 type carbides can not be ruled out.

EPMA studies also revealed the possibility of the formation of extraneous phases besides providing the useful data on the partitioning behaviour of Mn, Cr and also Cu.

Extensive 'modelling work' has provided a wealth of the information on the transformation behaviour, 'second phase' characteristics, and the 'overall performance' which has major 'fundamental and applied implications'.

Before concluding, it may be appropriate to compare the performance of the experimental alloys with that of some proprietary Ni-Resist compositions. Such a comparison revealed that the expected benefits of adopting the 'line of approach' as highlighted in the design of alloys/formulation of the problem,

are positively accruing and are promising.

Comparison of performance of experimental alloys with Ni-Resist irons

	Composition	condition	compressive strength, MPa	% strain to fracture	corrosion rate, mdd
1.	21-24% Ni SG Ni-Resist type D-2C	as-cast	——	20-40* (400-448)	14,3
2.	18-22% Ni flake graphite Ni-Resist type-2	as-cast	689-826	——	10,7
3.	18-22% Ni SG Ni-Resist type D-2	as-cast	1240-1378	8-20* (400-413)	10,1
4.	Experimental Alloys				
	P1	1050°C, 10 hours, AC	2657.58	39.39	11.33***
	P2	,,	3130.19	40.95	11.99***
	P3	,,	1852.01**	28.61**	10.99***

* % strain (tensile) in 2 inches,

** low values due to defects in the specimens,

*** best values attained in the present investigation, and

Bracketed values represent the ultimate tensile strength (MPa)

7.2 Conclusions

Under the experimental conditions, the following conclusions are arrived at:

1. Corrosion resistant cast irons can be developed through 'white iron' route employing low cost indigenously available alloying elements Mn,Cr, and Cu. The microstructures that were characterized for their deformation and corrosion behaviour(in 5% NaCl solution) are A + MC + DSPs, A + MC + DC, A + MC, A + and MC(agglomerated). All these microstructures were generated through heat treatments. The temperature ranges over which the different microstructures exist are given below:

   As-cast   : A + M (?) + MC

   up to 900°C   : A + MC + DSPs

   up to 1000°C   : A + MC + DC

   1050°C   : A + MC

2. The volume fraction of MC decreased with temperature or with soaking period at a given heat treating temperature. The decrease was marked at temperatures ≥ 950°C. MCs were rendered discontinuous from the early stages of heat treatment. The 'rounding off' tendency(in MCs) set in at 950°C; and an increase in Cu content accelerated this process. Agglomeration amongst MCs was observed at 1050°C. This has perhaps stalled the expected marked decrease in the Vf of MCs at 1050°C, 10 hours heat treatment.

3. Dispersed second phase formed on heat treating at ≥ 800°C comprised (a) needles + dispersed carbides up to 900°C, 10 heat treatment, only dispersed carbides upto 1000°C, 2 hours heat treatment, (b) then dissolved into matrix, and (c) again

reappeared at 1050°C, 2 hours heat treatment as class-I particles. The DSP forms by a mechanism involving precipitation from austenite and also during air cooling. Particles constituting them belonged to Classes I and II(size up to 1.16 microns). As the heat treating temperature/soaking duration is raised the overall spread of the particles is increased to Class IV(size up to 3.32 microns).

4. Dispersed carbides underwent coarsening which was characterized by the 'spill over' of the particles into classes III and IV. Coarsening was marked at 900 and 950°C and was assessed with the help of coarsening index.

5. DCs get dissolved at 1000°C heat treatment and reappeared on heat treating at 1050°C, 2 hours as Class I size particles and again dissolved at 1050°C 6 hours heat treatment.

6. The carbides to form in the experimental alloys are M_3C, M_7C_3, and M_5C_2. The massive carbides are mostly of the type M_3C/M_7C_3. The haloed regions observed at 850 and 900°C are essentially massive carbides but with 10% less Cr. The dark grey regions between 'agglomerating massive carbides' approximately exhibit the same composition as the agglomerating MCs except for their Cu and Si content. The dispersed carbides and needles are M_3C/M_5C_2 type. The carbide transformation sequence is:

Carbide	Stability range

M_3C + M_5C_2(?) + M_7C_3 As-cast state except in P2 where M_3C apparently not present

↓

M_3C + M_5C_2(?) + M_7C_3 up to 900°C (M_3C present in traces in P2)

↓

M_3C (trace/some) + M_5C_2(?) + M_7C_3 up to 950°C (in traces in P2)

↓

M_5C_2(?) + M_7C_3 up to 1000°C

↓

M_5C_2(?) + M_7C_3 + M_3C (reforming)   up to 1050°C, lower SP

↓

M_3C + M_5C_2(?) + M_7C_3 (some amount)   up to 1050°C; higher SP

↓

Predominant carbides at high temperature are M_7C_3 & M_5C_2(?)

7. Hardness in general decreased with an increase in the heat treating temperature in the order

H_{1050} < H_{1000} < H_{950} < H_{900} < H_{850} < H_{800}

8. For a given heat treating temperature, hardness varied linearly with the soaking period. In P1 and P2, hardness increased with an increase in soaking period on heat treating from 800 & 850°C, remained practically unaltered on heat treating from 900°C, and decreased thereafter on heat treating from 1000 & 1050°C. However in P3, hardness increased with an increase in soaking period on heat treating from 800°C, remained practically unaltered on heat treating from 850 and

900°C, and decreased thereafter on heat treating from 950, 1000 & 1050°C.

9. For a given heat treating period, the variation in hardness with temperature was in the form of inverted parabola and this assumed near linear behavior while moving from alloy P1 to P3(i.e. with an increase in Cu content)/or at higher heat treating temperatures(i.e. 1000 and 1050°C)

10. Transformation behaviour of the alloys, over the entire range of temperature and soaking period, on being modelled is of the form:

P1 : $H = 263.376 \, e^{607.01/T} + (0.009839 - 0.86 \times 10^{-5}T)t$

Overall SD = 11.39

P2 : $H = 262.689 \, e^{604.37/T} + (0.008998 - 0.786 \times 10^{-5}T)t$

Overall SD = 7.88

P3 : $H = 273.39 \, e^{552.705/T} + (0.0101 - 0.9068 \times 10^{-5}T)t$

Overall SD = 7.33

Where T = temperature in °K

t = time in seconds

H = hardness, HV_{30}

The first parameter models the matrix transformation and the second parameter the carbide transformation

11. The aforesaid transformation behaviour of the experimental alloys can be 'simulated' through mathematical modelling based on selecting the hardness values at two extremities of heat treating periods(2 hours & 10 hours) at 800 & 1050°C and at an additionally selected heat treating temperature(900°C). The simulated models are-

P1 : $H = 262.27\ e^{605.24/T} + (0.0108 - 0.964 \times 10^{-5}T)t$

Overall SD = 15.88

P2 : $H = 264.01\ e^{597.84/T} + (0.00991 - 0.8806 \times 10^{-5}T)t$

Overall SD = 9.88

P3 : $H = 224.68\ e^{786.83/T} + (0.0094 - 0.875 \times 10^{-5}T)t$

Overall SD = 11.65

Thus the transformation behaviour can be simulated with reasonably high accuracy on the basis of only six data points as against the original thirty.

12. 3-D plots interrelating temperature and time with hardness revealed that the 'change over' at which the second factor in the above model becomes negative can be represented by a surface. Iso-hardness plots for the experimental alloys revelaed the range over which hardness varied and the different temperature and time combinations to arrive at a desired hardness.

13. A new parameter 'distributional homogeneity/heterogeneity' of the micro-structure has been defined.

(i) The overall homogeneity/heterogeneity(based on Vf of MCs) of an alloy as influenced by heat treating parameters has been defined as

$$H_M = \frac{\text{The net variation in Vf of MCs around a mean}}{\text{Permissible variation around a mean}}$$

or

$$= \frac{SD_{exp}}{SD_{per}} \times \frac{[Vf_{max,per} - Vf_{min,per}]}{[Vf_{max,exp} - Vf_{min,exp}]}$$

This could be expressed as a fraction or percent. Under ideal condition $H_M = 1$. Homogeneity can be assessed depending

upon the permissible variation in the parameter(s) being measured.

Heterogeneity = 1 - Homogeneity

(ii) Distributional heterogeneity, H_M(dist) (related with precipitated second phase) has been expressed as

$$= \frac{\text{Deviation in distribution function/factor with respect to the majority size fraction}}{\text{Overall distribution function/factor}}$$

or more precisely

$$H_M(\text{dist}) = \frac{\text{underspill ratio X spillover ratio}}{\text{overall distribution factor}}$$

expressed as a ratio or as percentage.

14. The dispersed second phase has been represented by a parameter called the 'distribution factor' which is given by the expression

$$DF = \frac{\sum_{i=1}^{n} X_i . N_i}{\sum_{i=1}^{n} N_i}$$

where, n = the number of classes,

N_i = the number of particles in i^{th} class,

X_i = volume fraction in the ith class /VDC,

and, VDC = total volume fraction of dispersed carbides.

15. X-ray diffractometric studies proved helpful in establishing the presence of 'martensite islands' in the as-cast structure and in deciding upon the likely identity of the MCs and the DSPs.

16. EPMA confirmed that the carbides to form mostly comprised M_3C and M_7C_3, the needle like DSPs are in fact carbides, that on heat treating at 900/950°C two types of carbides differing in their Cr content by about 10% formed and that the dark etching regions abridging agglomerating carbides in fact have a composition close to M_7C_3 except for their Cu and Si content. In addition to the above, useful partitioning data on the distribution of Mn and Cr into the matrix and carbide phases has been generated.

17. DTA data showed that whereas the alloys P1, P2, and P3 undergo the (i) martensite —> austenite as well as internal oxidation reaction at 540-560°C and (ii) carbide transformation(s) involving a transition of M_3C to M_7C_3 via M_5C_2 transition carbide at 940-990°C, an additional transformation occurred in P1 at 1020°C.

18. TG data showed that the as-cast microstructure was suitable up to 800°C. However, on heat treating from 1000°C, the temperature up to which the alloys could be usefully employed was increased to at least 900°C.

19. Mathematical modelling of the TG data showed that %TG is related to the temperature by the equation

    Alloy P1   %TG = 0.9914 + 5821.89 exp(-7999.99/T)

    Alloy P2   %TG = 0.5559 + 7592.84 exp(-7999.99/T)

    Alloy P3   %TG = 1.4996 + 7922.62 exp(-7999.99/T)

20. The deformation studies carried out on the experimental alloys have established that compressive strength and ductility improved on heat treating. CS and % strain are not linearly interrelated with hardness as is found in the case

of steels. It is because of the heterogeneous nature of the microstructure generally found in cast irons. It was established that the CS and %Strain can be related with hardness through a second order polynomial (i) CS vs Hardness

Alloy P1 : $R = 50.11 - 0.1985H + (0.2186E-03)H^2$

Alloy P2 : $R = 83.55 - 0.3507H + (0.3903E-03)H^2$

Alloy P3 : $R = 12.09 - 0.02746H + (0.2511E-04)H^2$

where R = CS/H,

H = hardness, HV_{30},

(ii) % Strain vs Hardness

Alloy P1 : $R = 0.53 - 0.1726E-02H + 0.1501E-05H^2$

Alloy P2 : $R = 0.7936 - 0.2955E-02H + 0.2901E-05H^2$

Alloy P3 : $R = -0.2117 + 0.183E-02H - 0.2774E-05H^2$

where R = %strain/H,

H = hardness, HV_{30}

21. From the point of view of mechanical properties, austenite based microstructure with little dispersed second phase and containing 'appropriate' volume fraction of 'massive second phase' with near 'rounded' morphology are the most suitable. Accordingly high CS and % Strain are obtained on heat treating from high temperatures(i.e 1000 & 1050°C), The effect of DCs on the deformation behaviour depends upon their size, shape, and distribution. Similarly the effect of MC is governed by their volume fraction, morphology, and compatibility with the matrix.

22. Corrosion rate in the as-cast condition is consistent with its microstructure. It, in general, decreased with an

increase in the heat treating temperature/soaking duration and also with an increase in Cu content(i.e. while moving from alloy P1 to P3) due to enhanced stability and a larger volume fraction of austenite and simultaneous decrease in the Vf of MCs; the exceptions are those heat treatments which produced adverse microstructural feature namely matrix heterogeneity, aligned DCs, and 'chain' like structures.

23. The effect of dispersed second phase on corrosion resistance depends on their size, shape and distribution. In the present study dispersed particles affected the corrosion resistance adversely to some extent as is seen on heat treating from 900 and 950°C. Heat treatment 1050°C, 10 hour, AC provided the best corrosion resistance and most useful deformation behaviour.

24. Corrosion rate is interrelated with the volume fraction of VCb (MC + DC) and NOP through the following equations

Alloy P1: $CR = (40.635 - 2.971(VCb) + 0.08417(VCb)^2)(NOP)^{0.0000112}$

Alloy P2: $CR = (9.190 - 0.000922(VCb) + 0.00722(VCb)^2)(NOP)^{0.1667}$

Alloy P3: $CR = (6.198 - 0.000441(VCb) + 0.01925(VCb)^2)(NOP)^{0.160496}$

where CR = corrosion rate in mdd

VCb = total volume fraction of MCs + DCs

NOP = number of particles(DSPs)

This model when modified as

$CR = (C1 + C2(VMC) + C3(VMC)^2)(NOP)^{C4}$

gave a more representative idea of the true physical happenings

Alloy P1:

$CR = (19.484 - 0.3468(VMC) + 0.03409(VMC)^2)(NOP)^{-0.120223}$

211

Alloy P2:

$$CR = (10.834-0.1088(VMC)+0.02763(VMC)^2)(NOP)^{0.04558}$$

Alloy P3:

$$CR = (-6.1151+1.6559(VMC)-0.03476(VMC)^2)(NOP)^{0.20056}$$

when constraints are imposed on the constants(of the equations) while optimizing, the equations assumed the form:

Alloy P1:

$$CR = (19.4863-0.3474(VMC)+0.03411(VMC)^2)(NOP)^{-0.10217}$$

Alloy P2:

$$CR = (13.1915-0.3553(VMC)+0.04393(VMC)^2)(NOP)^{-0.020004}$$

Alloy P3:

$$CR = (8.9278-0.000197(VMC)+0.03553(VMC)^2)(NOP)^{-0.001}$$

This clearly indicates a systematic change over with regard to the role of constants/microstructure and the contribution of the two factors in influencing performance while moving from alloy P1 to alloy P3(i.e. with an increase in Cu content)

25. On incorporating the effect of DC on the basis of the distributional factor(DF), the above equations are modified as:

Alloy P1: $CR = (16.4983-0.6345(VMC)+0.03558(VMC)^2)(DF)^{-0.0752}$

Alloy P2: $CR = (-1.2423+0.9559(VMC)-0.02236(VMC)^2)(DF)^{-0.5765}$

Alloy P3: $CR = (-36.346+7.0937(VMC)-0.1768(VMC)^2)(DF)^{0.575816}$

and again when constraints are imposed on the constants of the equation while optimizing, the equations so obtained are-

Alloy P1:

$$CR = (10.000+0.09488(VMC)+0.01235(VMC)^2)(DF)^{-0.130245}$$

Alloy P2:

$$CR = (7.1009+0.28262(VMC)+0.01339(VMC)^2)(DF)^{-0.132449}$$

Alloy P3:

$$CR = (1.3361+1.01899(VMC)+0.00161(VMC)^2)(DF)^{-0.003181}$$

and 'truly' represented the effect of second phase on the corrosion resistance.

26. A 'unified model' describing the corrosion behaviour of all the experimental alloys has been obtained and is of the form

    (i) CR vs VMC & NOP

    $$CR = (9.1472+0.25096(VMC)-0.01051(VMC)^2)(NOP)^{0.04848}$$

    (ii) CR vs VMC & DF

    $$CR = (7.7095+0.46516(VMC)+0.00504(VMC)^2)(DF)^{-0.067201}$$

    The aforesaid models especially the latter predict the corrosion behaviour of the alloys with excellent accuracy.

27. On the basis of specially constructed contour plots, it is possible to predict the corrosion behaviour for those heat treatments at which experimental assessment of the corrosion rates has not been carried out. An equally important aspect is that from the 3-D and contour plots it is possible to determine the 'performance controlling features' for the experimental alloys, e.g. in the present study corrosion essentially centers around reducing the volume fraction of MCs and matrix heterogeneity seemed to have a larger adverse effect than the adverse effect associated with unfavorable morphology of the DSPs. For controlling the deformation behaviour especially % strain, a careful control over the distribution of massive and second phase particles is more specifically required.

28. From the 'overall performance' point of view alloy P2 has been found to be better followed by P3 and P1. Hence it is recommended that the future modifications in the alloy chemistry should incorporate the beneficial features of the compositions P2 and P3 which have many positive features. Further, the alloying elements should be so adjusted that the microstructures of interest(formed in the present investigation at 1000 and 1050°C) should form in the as-cast condition or at almost at 800°C heat treatment.

29. On making a comparison between the performance of experimental alloys and that of the standard Ni-Resist compositions, it emerges that the experimental alloys attain a level of strength at least twice as much as the standard alloys. From the point of view of corrosion behaviour, the experimental and proprietary compositions can be considered as comparable.

30. The above said discussion reveals that a detailed study of the phase transformations and of the resulting microstructures has major technological fallout and major implications in the design of future alloy compositions to obtain the best corrosion resistance and deformation behaviour.

7.3 Suggestions for future work

The future work should be carried out on the following lines:

1. Detailed study of the nature and formation of needles at lower heat treating temperature and dark grey phase at high temperature heat treatments.

2. Further work on the defining the 'homogeneity/heterogeneity' index of the microstructure

3. Extensive electro-chemical characterization of different microstructures by potentiostatic methods.

4. Crystal structure determination of carbides by x-ray diffractometry.

5. Detailed study of the high temperature behaviour of the alloys in the heat treated condition.

6. Studying the founding characteristics of the alloys

7. Detailed investigations of the performance of the experimental alloy P3.

REFERENCES

1. Elliott, R., 'Cast iron Technology', Butterworths, 1988. p.1

2. Avner, S.H., 'Introduction to Physical Metallurgy', McGraw-Hill, 1984, P.423-460

3. Rollason, E.C., 'Metallurgy for Engineers', Edward Arnold, London, 1973, pp.270-285.

4. Metals Hand Book, vol.1, 9th edition, ASM, Metals Park, Ohio, 'Properties and Selection of Irons and Steels', 1978, p.75.

5. Durman, R.W., 'The applications of alloyed white cast irons in crushing, grinding, and materials handling processes', conference paper, reprinted from 'Modern Castings' journal

6. Angus, H.T., 'Cast Iron- Physical and Engineering Proper-ties', Butterworths, London, 1976, pp.161-253 and 286-354

7. Heine, R.W., Loper, C.R., and Rosenthal, P.C., 'Principles of Metal Casting'; Mcgraw-Hill, New York, 1967, p.504

8. Rollason, E.C., 'Metallurgy for Engineers', Edward Arnold, London, 1973, p. 272.

9. Metals Hand Book, 8th edition, ASM, Metals Park, Ohio, 1961, pp.394-406

10. Patwardhan, A.K., Singh, S.S., and Jain, N.C., Tool & Alloy Steels, October, 1987, pp.369-377.

11. 'The Metallurgy of Cast Irons', Proc. of 2nd Int. Symp., Geneva, Switzerland, May 29-31, 1974, Ed. B. Lux Battelle, Minkoff, I, and Mollard, F.

12. Sandoz, G., 'The Partitioning of alloying elements in malleable irons' NRL report 5268, U.S. Naval Research Laboratory, Washington. D.C., February, 1959, pp.1-25.

13. Bain, E.C., and Paxton, H.W., 'Alloying Elements in Steels' ASM, Metals Park, Ohio, 1962, pp.59-87

14. Barton, R., 'Special Cast Irons', Report No.576, BCIRA Journal, November, 1960, vol.8, No.6, November, pp.857-882

15. Dodd, J and Parks, J.L., Metals Forum, vol.3, No.1,1980, pp.4

16. Jackson, R.S., Journal of Iron & Steel Institute, 1970, vol.208, pp.163-167

17. Dodd, J., and Parks, J.L., AFS International Cast Metal Journal, September, 1980, p.48.

18. Torpe, W.R., Chicco, B., Material Science and Engineering, 51, 1981, p11-p19

19. Powell, G.L.F., Metals Forum, vol.3, No.1, 1980, pp.37-46.

20. Metals Hand Book, vol.1, 9th edition, ASM, Metals Park, Ohio, 'Properties and Selection of Irons and Steels', 1978, p.78.

21. Sare, I.R., Metals Technology, November, 1979, pp.412-419.

22. Parks, J.L., AFS Transactions, vol.86, 1978, pp.93-102

23. Benz, R., Elliott, J.F., and Chipman, J., Metallurgical Transactions, vol.5, pp.2235-40 (1974).

24. Matsuraba, Y., Ogi, K., and Matsuda, K., AFS Transactions, vol.89, 1981, pp.183-196.

25. Ohide, T., and Ohira, G., British Foundryman, vol.76, part 1, January, 1983, p.9

26. Goldschmidt, H.J., 'Interstitial Alloys' Butterworths, London, 1967, pp.94-95

27. Metals Hand Book, 9th edition, ASM, Metals Park, Ohio, 1978, pp.76-92.

28. Roy Elliott, 'Cast Iron Technology', Butterworths, 1988, pp.24-36.

217

29. Pearce, J.T.H., British Foundryman, vol.78, part-1, 1985, pp.13-23

30. 'Corrosion' edited by L.L.shreir, Newnes-Butterworths, London, vol.1, 1976, p.3:77 to 3:126.

31. Kutner, C., Tech. Mitt. Krup., No.1, March, 17, 1933.

32. Metals Hand Book, vol.1, 9th edition, ASM, Metals Park, Ohio, 'Properties and Selection of Irons and Steels', 1978, p.89-90.

33. Boyes, J.W., Iron and Steel, March, 1966, pp.2-9.

34. Corti, C.W., Boyes, J.W., and King, C.W., Iron and Steel, October, 1969, pp.337-342.

35. Metals Hand Book, vol.1, 9th edition, ASM, Metals Park, Ohio, 'Properties and Selection of Irons and Steels', 1978, p.79

36. Metals Hand Book, vol.1, 8th edition (1964), p.403

37. Frost, R.H., Majewski, T., and Krauss, G., AFS Transactions, vol.94, 1986, pp.297-332.

38. Maratray, F., AFS Transactions, vol.79, 1971, pp.121-124.

39. Durman, R.W., Foundry Trade journal, vol.134, 1973, pp.645-651.

40. Maratray, F., Ussenglio-Nanot, R., Climax-Molybdenum company, S.A., 1971, pp.1-31.

41. 'Engineering Properties and applications of Ni-Hard Cast irons'; International Nickel Co., INC, New York, 1978,pp.2-15

42. Boyes, J.W., Iron and Steel, 42 (1), February, 1968, pp.57-63

43. Dawson, R.J., and Craig, G.B., AFS Transactions, vol.91, 1983, pp.235-242.

44. Chakraborthy, I., Ph.d. Thesis, I.I.T, Kharagpur, India, 1988

45. Tsypin, T.I. et.al., Materials science and Heat treatment,12, 1970, p.612.

46. Srinivasan, T., Patwardhan, A.K., and Mehta, M.L., AFS International Cast Metal Journal, March, 1977, pp.57-60

47. Sudan, A.S., Mehta, M.L., and Patwardhan, A.K., AFS International Cast Metal Journal, March, 1980, p.42-46

48. Rozhkove, E.V. et.al., Materials Science and Heat treatment, 23, 1, 1981, p.59.

49. Stefanescu, D.M., Mitea, D., and Cracium, S., AFS International Cast Metal Journal, June, 1976, vol.1. No.2, pp.19-

50. Walton, C.F., and Opar, T.J., 'Iron Castings Hand Book', Iron Castings Society, Des Plaines, IL, 1981, p.145

51. Sharma, C.P., M.E. Dissertation, University of Roorkee, Roorkee, 1976

52. Sudan, A.S., M.E. Dissertation, University of Roorkee, Roorkee, 1976

53. Viswanadham, Ch., M.E. Dissertation, University of Roorkee, Roorkee, 1981

54. Viswanadham, Ch., Patwardhan, A.K. & Mehta, M.L., 'Gisserei' (FGR), 73(4), 1986, p.238

55. Patwardhan, A.K., Mehta, M.L., and Viswanadham, Ch., AFS Transactions, 1988, pp.919-924.

56. Rickard, J., The British Foundryman, vol.77, part 6, July 1984, pp.313-317

57. Hurst, J.E., and Piley, R.V., JISI, vol.155, February, 1947, pp.172-178

58. Dumitsescu, T., Medeleanu, V., Nicolaid, M., and Dinu, I., Rev. Metall. (Roummania), vol.3, No.2, 1958, p.19

59. Metals Hand Book, Desk Edition, Ed. by Boyer, H.E., and Gall, T.L., ASM, Metals Park, Ohio, 1984, p.5-16 and 5-19

60. Metals Hand Book, vol.1, 9th edition, ASM, Metals Park, Ohio, 'Properties and Selection of Irons and Steels', 1978, p.88-91

61. 'Engineering Properties of Ni-Resists and Ductile Ni-Resists': International Nickel Co. In Corp., 1976, pp.1-40

62. Jain, N.C., Ph.D. Thesis, University of Roorkee, Roorkee, India, 1986.

63. 'Ni-Resist irons for fluid handling in the Chemical Industry': International Nickel Co. In Corp., Publication No. 2773, pp.2-8

64. Magee, C.L., and Davis, R.G., 'Low Alloy Steels'; Iron and Steel Instt, London, Special Report No.111, 1968

65. Roberts, M.J., and Owen, W.S., Trans. ASM Quart., vol. 60, 1967, p.679

66. Owen, W.S., and Wilson, E.A., 'Physical properties of Martensite and Bainite', Iron and Steel Instt., London, Special Report No. 93, 1965, p.103

67. Basak, A., Penning, J., and Dilewijns, AFS International Cast Metal Journal, vol.6, No.3, September 1981, pp.12-17.

68. A.K.Patwardhan, Personal communication

69. Srinivasan, T., M.E.Dissertation, University of Roorkee, Roorkee, 1975

70. Patwardhan, A.K., Mehta, M.L., and Sharma, C.P., AFS International Cast Metal Journal, March, 1981, pp.3-9.

71. Jha, B.K., Sharma, P.K., B.E. Project Report, University of Roorkee, Roorkee, May, 1978.

72. Singh, S.S., Ph.D. Thesis, University of Roorkee, Roorkee, 1982

73. Kumar. V., Rao, P.N.V.R.S.S.V.P., and Patwardhan, A.K., Proceedings of the International Conference on 'Corrosion and Corrosion control for Offshore and Marine Construction' held on September 6-9, 1988, Xiamen, China; Pergamon Press, Incorp, New York (USA), pp.623-628.

74. Jain, N.C., Patwardhan, A.K., and Kumar, V., Tool & Alloy Steels, Vol.22, No.7 & 8, July & August 1988, pp.215-227

75. Jain, N.C., Patwardhan, A.K., and Kumar, V., Tool & Alloy Steels, September, 1988, Vol.22, No.9, pp.271-278

76. Kumar, V., Rao, P.N.V.R.S.S.V.P., and Patwardhan, A.K., Materials Performance, Vol.30, No.8, August, 1991, pp.72-74

77. Kumar, V., Rao, P.N.V.R.S.S.V.P., and Patwardhan, A.K., Tool & Alloy Steels, Vol.25, No.6, June, 1991, pp.221-225

78. A.K.Patwardhan, Personal communication

79. Patwardhan, A.K., and Jain, N.C., AFS Transactions, Vol.96, 1988, pp.329-338

80. Patwardhan, A.K., and Jain, N.C., AFS Transactions, Vol.97, 1989, pp.201-206

81. Patwardhan, A.K., and Jain, N.C., Metallurgical Transactions, Vol.22A, October, 1991, pp.2319-2325

82. Jain, N.C., and Patwardhan, A.K., Metallurgical Transactions, Vol.23A, March, 1992, pp.891-901

83. Kumar, V., Ph.D. Thesis, University of Roorkee, Roorkee, 1990

84. Rao, P.N.V.R.S.S.V.P., M.E. Dissertation, University of Roorkee, Roorkee, 1988.

85. Rao, P.N.V.R.S.S.V.P., and Patwardhan, A.K., Materials Forum, vol.16, 1992, pp.51-67

86. Sharma, C.P., Ph.D. Thesis(in progress), University of Roorkee, Roorkee

87. Pearce, J.G., and Bromage, K., 'Copper in Cast Iron', C.D.A. publication No.65, Copper Development Association, London, 1964, pp.41-43

88. Angus, H.T., 'Cast Iron- Physical and Engineering Properties', Butterworths, London, 1976, p.53.

89. Kumar,V., and Mohanty,B., 'Indexing of x-ray diffractograms', software section, Scripta Metallurgica, Vol.20, 1986.

90. 'Selected powder diffraction data' Metals and alloys data book, JCPOS, vol. I, 1978

91. 'Selected powder diffraction data' Metals and alloys data book, JCPOS, vol. II, 1978

92. 'Selected powder diffraction data' Metals and alloys data book, JCPOS, Inorganic, sets 1-22, 1967.

93. G-1-72, 'Standard recommended practice for preparation, cleaning, and evaluating corrosion test specimens', Annual book of ASTM standards, part 10, Philadelphia, 1978.

94. G-31-72, 'Standard recommended practice for laboratory immersion corrosion testing of materials', Annual book of ASTM standards, part 10, Philadelphia, 1978.

95. Greene, N.D., 'Experimental electrode kinetios' Ressenlaer Polytechnic Institute, Troy, New York, 1965.

96. Patwardhan, A.K., Ph.D.Thesis, University of Roorkee, Roorkee, 1979.

97. Merchant, H.D.(Editor), 'Recent Research on Cast Irons', G.B. Science Publications, New York, 1968, p.7

98. Heine, R.W., Loper, C.R., and Rosenthal, P.C., 'Principles of Metal Casting'; Mcgraw-Hill, New York, 1967, p.504

99. Himmelblau, D.M., 'Applied Non-linear Programming', McGraw-Hill book company, 1975

100. Non-linear programming-2, Edited by Mangasarain, O.L., Meyer, R.R., and Robinson, S.M., Academic Press, Inc., New York, San Francisco, London, 1975.

101. Haasen, Peter, 'Physical Metallurgy', Cambridge University press, 1986, pp.214-216

102. Patwardhan, A.K., Mukundan, R., Rao, P.N.V.R.S.S.V., Sharma, C.P., and Kumar, S., 'Simulation of the Transformation behaviour of 7.5% and 6% manganese C-Cr-1.5Cu corrosion resistant white irons through mathematical modelling', accepted for publication in Metallurgical Transactions-A.

103. Goldschmidt, H.J., 'Interstitial Alloys', 1967

104. Wever, F., and Koch, W., Stehl Eisen, 1954, 74, p.989

105. Smith, E., and Nutting, J., JISI, 1957, 187, pp.314-329

106. Pickering, F.B., 4th Int. Cof. on Electronmicroscopy, 1958, Berlin, 668.

107. Nutting, J., JISI, vol.207, June 1969, pp.872-893.

108. Woodhead, J.H., and Quarrell, A.G., JISI, 605, 1965, p.203.

109. Mills, K.C., Argent, B.B., and Quarrell, A.G., JISI, Jan, 1961, pp.9-21

110. Kuo, K., JISI, 1953,173,pp.363-374.

111. Honeycombe, R.W.K., and Seal, A.K.,JISI,188,1958,p.9

112. Bilby, B.A., and Pickering, F.B., ISI Sp. Report-64, 313.

113. Balluffi, R.W., et.al., Trans. ASM, 1951,43,p.493.

114. Metals Hand Book, 8th Editon, Metals Park, Ohio, 1961,

115. Sandoz, G., 'Recent research in Cast Iron' Ed. Merchant, H., Gordon and Beach, New York, 1968, p.50

116. Kuo, K., and Persson, L.E., JISI, Sept.1954, pp.39-44.

117. Laird-II, G., Nielsen, R.L., and MacMillan, N.H., Vol.22A, August, 1991, pp.1709-1720

118. Laird-II, G., Brown, R.R., and Neilson, R.L., Material Science and Technology, July, 1991, vol.7, pp.631-642.

119. Rao, P.N.V.R.S.S.V.P., Patwardhan, A.K., and Jain, N.C., Metallurgical Transactions, February, 1993, pp.445-457.

120. Schutze, D., 'Differential Thermal Analysis', Weinhim Verlag, Cherie, 1969.

121. Mackenzie, R.C., Differential Thermal Analysis', vol.1., Academic Press, London, 1970,p.32.

122. Kofstad, P., 'High temperature oxidation of Metals', John Wiley & Sons Inc., New York, 1966.

123. Kubaschewski, O., and Hopkins, B.E., Oxidation of Metals and Alloys', Butterworths, London, 1962.

124. Hauffi,K., 'Oxydation Von Metallen Und Metallefierungen Springer' Berlin, 1957.

125. Benard, J., 'Oxydation des Metaux', Gauthier Villars etc., Paris, 1962.

126. Evans, U.R., 'The corrosion and oxidation of Metals', Edward Arnold Ltd., London, 1960.

127. Loviers, J., Compt. rend., 229(1949), p.547.

128. Webb, W.W., Norton, J.J., and Wagner, C., J. electrochem. Soc., 103,1956,p.107.

129. Haycock, E.W., J.Electrochem. Soc.,106,1959,p.771.

130. Kofstad,P., Acta Chem. Scand. 12,1959,p.501

131. Sewell, P.B., and Cohen, M, J.Electrochem. Soc., 111, 1964, p.501.

132. Sewell, P.B., and Cohen, M, J.Electrochem. Soc., 111, 1984, p.508.

133. Rahmel, a., Z.Elekrochem., 66, 1962, 363, p.284.

TABLE-1.1

COMPOSITION AND PROPERTIES OF SOME REPRESENTATIVE PLAIN CARBON WHITE IRONS(6,9,10)

Sl. No.	Type/Class Designation	TC	Si	Mn	S	P	Hardness BHN	Micro-structure	Wear Rate (relative)	Application
1.	Pearlitic Iron	2.80	0.3	0.4	0.15	0.1-0.12	415-477	C+P	179.0	Grinding Balls
2.	Unalloyed, low hardness Iron	3.0	0.75	0.25	0.4	0.12	320-440	C+P	—	Iron Rolls
3.	Unalloyed high hardness Iron	3.5	0.5	0.25	0.4	0.12	440-520	C+P	—	Iron Rolls
4.	Unalloyed chill Cast Iron	2.78	0.53	0.42	—	—	444 as-cast	Carbide in C.P.	174.0	—
5.	Unalloyed Iron (Sand Cast)	3.05	0.4	0.5	—	—	444	C+P	122.0	Grinding Balls
6.	Chill Cast unalloyed Iron	3.59	0.7	0.8	—	0.1	495	C+P	100.0	Grinding Balls
7.	Pearlitic Iron	2.9	0.5	0.5	0.12	0.3	415-460	C+P	—	—
8.	Cupola White Iron	3.3-3.6	0.4-1.0	0.5-0.7	0.15 max.	max.	400	C+P	—	—
9.	Unalloyed high hardness alloys	3.2-3.8	0.4-0.8	0.3-0.7	0.1	0.2	380-600	C+P	—	—
		3.0-3.4	0.9-1.3	0.6-1.0	0.1	0.2	380-520	C+P	—	—

*Wear rates are relative to an assigned rate of 100 for Chill Cast Unalloyed Iron

PHYSICAL AND MECHANICAL PROPERTIES

1. Hardness (DPN).
   410 520 (sand Cast)
   435-550 (Chill Cast) (abrasion resistant)
   400 (L.C., 2.5-2.6%C)
   650 (H.C., 3.75-4.0%C)

2. Tensile strength (ton/in²)
   15-30 (sand Cast)
   18-30 (Chill Cast)
   16-18 (H.C., 3.0—3.5%C) (Pearlitic, Hard)
   18-30 (L.C., 2.75—2.9%C) (Pearlitic, Tough)

3. Modulus of elasticity (lb/in² x10⁶)
   30 (Sand Cast, Chill Cast)

4. Transverse rupture stress 1.2 bar, 12 in span (ton/in²)
   24-40 (Sand Cast)
   33-47 (Chill Cast)

5. Transverse deflection
   0.05-0.1 (H.C., 3.0—3.5%C)
   0.07-0.11 (L.C., 2.75—2.9%C)

6. Specific gravity
   7.6—7.8

7. Electrical resistivity (microhm/cm³ at 78°F)
   53—72

8. Impact strength (0.798 in dia machined from 0.875 in as-cast dia.) (ft. lb.)
   6-11 (impact strength of white cast iron is about one third that of gray iron)

9. Thermal conductivity (Cat/cm³/s/°C)
   0.035—0.076

10. Thermal expansion coefficient 0-276°C 276-684°C
    $10\text{-}11 \times 10^{-8}$
    $15.9\text{-}16.4 \times 10^{-8}$

11. Yield strength
    Usually not determined because of low ductity of white irons. The yield strength is considered to be close to the tensile strength.

TABLE-1.2

COMPOSITION AND PROPERTIES OF SOME REPRESENTATIVE CHROMIUM WHITE IRONS(6,10)

Sl. No.	Type|class Designation	T.C.	Si	Mn	Composition Cr	P	S	Hardness BHN
1.	Cupola white iron (1% Cr)	3.30-3.60	0.40-1.0	0.5-0.70	0.80-1.00	0.3 (Max)	0.15 (Max)	444
2.	High Cr white iron	2.25-2.85	0.25-1.0	0.5-1.25	24.00-30.00	0.3 (Max)	0.15 (Max)	500
3.	Pearlitic	3.3	0.5	0.5	1.0	0.20	0.12	444
4.	Sand cast** Pearlitic white iron	3.2-3.5	—	—	1.2	—	—	—
5.	Plain Cr white iron	3.50	0.5	0.5	1.0	0.30	0.12	444-477
6.	Plain Cr white iron	3.20	0.6	0.5	2.0	0.15	0.15	477-555
7.	Low Cr Iron (chill cast)	3.20	1.7	0.4	0.9	—	—	477
8.	Low Cr iron (sand cast)	3.00	0.9	0.6	0.8	—	—	477
9.	Sand cast 5% Cr Iron	3.65	0.6	0.6	5.0	—	—	514
10.	Pearlitic Cr-iron	3.00	0.6	0.5	2.0	0.10	0.15	—
11.	30% Cr	2.5-2.9	0.33-0.65	0.6-08	28.00-33.0	0.10	0.10	340-420

**Transeverse strength (kg) 635-815

Deflection (mm) 2.0-2.3

Toughness (kgm) 1.27-1.87

TABLE-1.3

RANGE OF ALLOY CONTENT AND TYPICAL MECHANICAL PROPERTIES of CORROSION RESISTANT CHROMIUM CAST IRONS(6,9,10,27)

Description	COMPOSITION, (Wt %)									Matrix structure as-cast
	TC(a)	Mn	Si	P	S	Ni	Cr	Mo	Cu	
High chromium iron	1.2-4.0	0.3-1.5	0.5-3.0	0.15	0.15	5.0	12-35	4.0	3.0	M,A

Type of iron	Hardness HB	Tensile strength		Compressive strength		Impact energy		Transverse breaking load(b)		Transverse deflection(b)	
		MPa	Ksi	MPa	Ksi	J	ft.lb	Kg.	lb.	mm	in.
High chromium iron	250-740	205-830	30-120	690	100	27-47(c)	20-35(c)	910-1590	2000-3500	1.5-3.8	0.06-0.15

(a) Total carbon
(b) For as-cast 30.5 mm (1.2 in.) dia. bar broken over a 457 mm (18 in.) span
(c) Unnotched 30.5 mm dia. test bar broken over a 152 mm (6 in.) span in a Charpy testing machine

INFORMATION ON CHROMIUM, MANGANESE, AND IRON BEARING CARBIDES(26)

Base Metal	Carbide	Crystal structure Type	Spacing, A°	Stability Range, °C	Melting Point, °C	Harness
Cr	Cr23C6	Comp. Cubic	10.60	upto 1577	1580	1000 Kg/mm2*
	Cr7C3	Comp. hex.	a= 4.53 c=14.01	upto 1768	1780	1600 Kg/mm2*
	Cr3C2	Ortho.	a= 2.82 b= 5.53 c=11.47	upto 1813	1895	1300 Kg/mm2*
Mn	Mn23C6	Comp. cubic	a=10.586	upto 1025	1010	
	Mn7C2	----	-----	850-1000		
	Mn3C	Ortho.	a=5.0806 b=6.772 c=4.530	950-1050	1520	
	Mn5C2	Mono-	a=5.806 b=4.573 c=11.66 β=92.75°	upto 1050	----	
	Mn7C3	Comp. hex.	a=13.838 c=4.539	upto 1100	1340	840 Brin
Fe	Fe3C	Ortho. rhombic	a=5.088 b=6.744 c=4.524	upto 1227	1650	
	Fe5C2	Mono- clinic	a=11.563 b=4.573 c=5.058 β=	upto 350	----	

* hardness at 50-200 gms. load

TABLE-1.4b

IRON CARBIDE IN Fe-C-Cr ALLOYING SYSTEM(25,26)

Type	Crystalline system	Lattice const.	Specific gravity	
$(Fe,Cr)_3C$	Rhombic	a=4.52 b=5.09 c=6.74	7.67	can contain a maximum of 18% Cr
	Hexagonal	a=6.88 b=4.54 a=4.54		
$(Fe,Cr)_3C_3$	Rhombic	b=6.88 c=11.94	6.92	can contain a maximum of 50% Cr
	Rhombohedral	a=13.98 b= 4.52		
$(Cr,Fe)_{23}C_6$	F.C.C	a=10.64 a=2.82	6.97	Max. 35% Fe
$(Cr,Fe)_3C_2$	Rhombic	b=5.52 c=11.46	6.68	little Fe

Microconstituent(s)	Microhardness
M3C	840-1100 HV
M7C3	1200-1800 HV
M3C(low Cr irons)	1060-1240 HV
M7C3(high Cr irons)	1500-1800 HV
Pearlite	300-960 HV
Pearlite(high carbon)	240-425 HV
Austenite(high Cr)	300-600 HV
Austenite(high Cr)	350-400 HV
Martensite	500-1000 HV
Martensite(high carbon)	770-800 HV

TABLE-1.5a

COMPOSITION OF Cr-Mo TYPE ABRASION RESISTANT ALLOY CAST IRONS(4,6,10,27)

Sl. No.	Type|Class| Designation	Composition								Hardness BHN	Micro-structure
		T.C.	Si	Mn	Cr	Mo	S	P	Other element		
1.	ASTM A-532-750 II Grade 1	3.1-3.6	0.3-0.8	0.4-0.9	14.0-18.0	2.5-4.5	0.06 Max	0.1 Max	0.5 Ni	—	—
2.	II Grade 2	2.4-3.1	0.3-0.8	0.4-0.9	14.0-18.0	2.5-3.5	0.06 Max	0.1 Max	0.5 Ni	—	—
3.	III Grade 2	2.3-3.0	0.2-1.5	1.5 Max	24.0-28.0	0.06 Max	0.06 Max	0.1 Max	0.5 Ni	—	—
4.	Martensitic 15% Cr, H.C.	3.25	0.6	0.7	15.0	3.0	0.03	.06	—	600-750	M.A.
5.	Martensitic 27%Cr	2.75	0.7	0.7	27.0	3.0	0.03	.06	—	653	—
6.	Martensitic 15% Cr, 3% Mo	2.75	0.7	0.7	15.0	10.5	0.03	.06	—	712	—
7.	Sand cast	2.8-3.4	—		12-16	2.4	—	—	—	—	—
8.	Sand cast	3.5-4.1	—	—	12-16	2.5-3.0	—	—	—	—	—
9.	Chill cast martensitic	3.2-3.4	—	—	12-16	1.5-3.0	—	—	—	—	—
10.	Chill cast martensitic	3.5-4.1	—	—	12-16	2.5-3.0	—	—	—	—	—
11.	12-18% Cr. 2-4% Mo	3.0-4.0	0.4-1.0	0.5-0.9	12-18	2-4	0.06	0.1	—	600-950 VPN	—

TABLE-1.5b

PROPERTIES OF Cr-Mo IRONS(4,6,10)
(FROM Sl. no. 5 TO 10 OF TABLE-1.5a)

Sl. No.	Type|Class|Designation	Wear rate relative to pearlitic iron*			
		Crushing plant chute liners	Ball Mill end liners	Akin classifier wear shoes	Flotation impellers
5.	Martensitic 27% Cr	70	49	48	27
6.	Martensitic 15% Cr, 3% Mo	51	44	44	—

		Transverse strength (kg.)	Deflection (mm)	Toughness** kgm.
7.	Sand cast	1015-1370	3.2-3.6	3.25- 4.93
8.	Sand cast	800-1000	2.0-2.8	1.60- 2.8
9.	Chill cast Martensitic	1980-2300	5.1-6.5	10. 1-15.0
10.	Chill cast martensitic	1270-1570	3.6-3.8	4.57- 5.9

*　The pearlitic white iron (3.3%C, 0.5% Mn, 0.5% Si, 1.0% Cr, 0.12% S, 0.2% P) had a noniqually assigned relative wear rate of 100 in each application. The other wear rates are relative to this rate of the pearlitic white iron.

**　Data from as cast 30.5mm dia. test bars broken over a 457 mm span. Relative toughness evaluated as product of transverse strength.

TABLE-1.6a

COMPOSITION OF Cr-X TYPE ABRASION RESISTANT IRONS(4,6,10,28)

Class	Type	Designation	Limit	C%	Mn%	Si%	Ni%	Cr%	Mo%	P%	S%	Cu%
I	A	Ni-Cr-HC	minimum	3.0			3.3	1.4				
			maximum	3.6	1.3	0.8	5.0	4.0	1.0	0.3	0.15	
I	B	Ni-Cr-LC	minimum	2.5			3.3	1.4				
			maximum	3.0	1.3	0.8	5.0	4.0	1.0	0.3	0.15	
I	C	Ni-Cr-GB	minimum	2.9			2.7	1.1				
			maximum	3.7	1.3	0.8	4.0	1.5	1.0	0.3	0.15	
I	D	Ni-HiCr	minimum	2.5		1.0	5.0	7.0				
			maximum	3.6	1.3	2.2	7.0	11.0	1.0	0.10	0.15	
II	A	12% Cr	minimum	2.4	0.5			11.0	0.5			
			maximum	2.8	1.5	1.0	0.5	14.0	1.0	0.10	0.06	1.2
II	B	15% Cr-Mo-LC	minimum	2.4	0.5			14.0	1.0			
			maximum	2.8	1.5	1.0	0.5	18.0	3.0	0.10	0.06	1.2
II	C	15% Cr-Mo-HC	minimum	2.8	0.5			14.0	2.3			
			maximum	3.6	1.5	1.0	0.5	18.0	3.5	0.10	0.06	1.2
II	D	20% Cr-Mo-LC	minimum	2.0	0.5			18.0	1.0			
			maximum	2.6	1.5	1.0	1.5	23.0	1.5	0.10	0.06	1.2
II	E	20% Cr-Mo-HC	minimum	2.6	0.5			18.0	1.0			
			maximum	3.2	1.5	1.0	1.5	23.0	2.0	0.10	0.06	1.2
III	A	25% Cr	minimum	2.3	0.5			23.0				
			maximum	3.0	1.5	1.0	1.5	28.0	1.5	0.10	0.06	1.2

TABLE-1.6b

TYPICAL PROPERTIES OF Cr-X TYPE IRONS(4,6,10,28)

Class	Type	Designation	Brinell hardness				Typical section thickness (mm)
			Sand cast (minimum)	Chill cast (minimum)	Hardened (minimum)	Softened (minimum)	
I	A	Ni-Cr-HC	550	600			200
I	B	Ni-Cr-LC	550	600			200
I	C	Ni-Cr-GB	550	600			75 diameter ball
I	D	Ni-HiCr	550	500			300
II	A	12% Cr	550		600	400	25 diameter ball
II	B	15% Cr-Mo-LC	450		600	400	100
II	C	15% Cr-Mo-HC	550		600	400	75
II	D	20% Cr-Mo-LC	450		600	400	200
II	E	20% Cr-Mo-HC	450		600	400	300
III	A	25% Cr	450		600	400	200

TABLE-1.7

CHEMICAL ANALYSIS AND PROPERTIES OF Ni-HARD(10,41)

	Type 1-Regular (ASTM A 532 1-A)		Type 2-Hi-Stren. (ASTM A 532 1-B)		Type 3 (ASTM A532 1-C)		Type 4 (ASTM A 532 1-D)
Chemical Analysis, %							
Total Carbon	3.0-3.6		2.90 max		2.9-3.7		2.5-3.6
Silicon	0.8 max		0.8 max		0.8 (max		1.0-2.2
Manganese	1.3 max		1.3 max		1.3 max		1.3 max
Sulfur	0.15 max		0.15 max		0.15max		0.15max
Phosphorus	0.30 max		0.30 max		0.30max		0.10max
Nickel	3.3-5.0		3.3-5.0		2.7-4.0		5.0-7.0
Chromium	1.4-4.0		1.4-4.0		1.1-1.5		7.0-11.0

Engineering Properties	Sand Cast	Chill Cast	Sand Cast	Chill Cast	Sand Cast	Chill Cast	Chill Cast
Brinell Hardness, Minimum	550	600	550	600	550	600	550
Trans. Strength, 1.20" DIA. Test Bars, 12" Span, lb.	4000 to 5000	4500 to 6800	4500 to 5500	5500 to 7000	5000 to 6000	5500 to 7000	5500 to 7000
Trans. Defl., 1.20" DIA. Test Bars, 12" Span, in.	0.080 to 0.110	0.080 to 0.120	0.100 to 0.120	0.100 to 0.120	0.08 to 0.11	0.10 to 0.15	0.10 to 0.15
Tensile Strength, 1.20" DIA. Test Bars, psi.	40 to 50,000	50 to 60,000	45 to 55,000	60 to 75,000	75 to 85,000	80 to 110,000	80 to 110,000
Modulus of Elasticity, million psi	24-26	24-26	24-26	24-26	24-26	24-26	24-26
IZOD AB impact, ft-lb	20-30	25-40	25-35	35-55	35-45	35-45	35-45

TABLE-1.8

COMPOSITION, PROPERTIES AND APPLICATIONS OF VARIOUS Cr-Ni-WHITE CAST IRONS(8,10)

Sl. No.	Type|Class Designation	COMPOSITION								Hardness	Microstructure	Application
		T.C.	Si	Mn	Cr	Ni	S	P	Other element			
1	2	3	4	5	6	7	8	9	10	11	12	13
1.	Martensitic Ni-Cr	3.2	0.5	0.6	2.0	4.5	0.12	0.2	—	601 BHN		Wear rate relative to Pearlitic White Iron: Ball mill end liner 55; Akin classifier shoe 80
2.	Martensitic Ni-Cr	3.2	0.5	0.6	2.0	4.5	0.12	0.2	—	550-650 BHN	M A	Application Mill liners
3.	Martensitic Ni-Cr	3.5	0.5	0.6	2.0	3.0	0.12	0.1	1.0 Mo	600-650 BHN	M A	Mill liners
4.	Martensitic Ni-Cr	3.2	0.5	0.3	1.4	3.5	0.15	0.2	—	555-627 BHN		Grinding balls
5.	L.C. White Iron	2.2-2.8	1.0-1.6	0.2-0.6	1.0	1.5	0.15	0.15	0.5 Mo	—	C P (as-cast)	(a) Where a single value is given rather than a range that value is a maximum limit.
6.	H.C.L. Si, White Iron	2.8-3.6	0.3-1.0	0.3-2.0	3.0	2.5	0.15	0.3	1.0 Mo	—	C P (as-cast)	(b) C P — Coarse Pearlites MA — Martensite Austenite
7.	Martensitic Ni-Cr Iron	2.5-3.7	0.8	1.3	1.1-4.0	2.7-5.0	0.15	0.3	1.0 Mo	—	M A	
8.	Alloyed Intermediate	3.4	0.6	0.3	1.25	4.5	0.1	0.35	0.4 Mo	690-830 VPN	Precise hardness obtained will depend on specific composition & section size	
9.	Alloyed Intermediate hardness	3.4	0.8	0.3	0.6	2.5	0.1	0.35	0.4 Mo	610-690 VPN		
10.	Chill Cast Ni-Cr iron	2.85	0.56	0.48	0.98	1.67	—	—	—	600 BHN	Micro-structure Carbides in Fine Pearlite	Wear rate (Relative) 134
11.	Chill Cast Ni-Cr iron	2.83	0.60	0.50	1.33	2.2	—	—	—	627 BHN	Carbides in very fine pearlite	124
12.	Chill Cast Ni-Cr iron	2.87	0.60	0.50	1.55	2.54	—	—	—	600 BHN	Carbides in Martensitic matrix	59

1	2	3	4	5	6	7	8	9	10	11	12	13
13.	Chill Cast Ni-Cr iron		3.79	0.55	0.50	1.49	2.61	—	—	—	744 BHN	Carbides in Martensitic matrix
14.	Martensitic Ni-Cr iron		2.8	0.5	0.3	1.4	2.5	0.15	0.1	—	—	Relative wear rate 106 (Where Martensitic forged steel — (0.8% C, 0.3% Si, 0.7% Mn, 0.2% Cr, 0.2% Mo, 0.3% S, 0.01% P) had a nominally assigned relative wear rate of 100
15.	ASTM I A-532	Grade 1	3.0-3.6	0.3-0.8	0.3-0.8	1.4-2.5	3.3-0.5	0.15	0.3	0.75 Mo	500 SC / 600 CC	
16.	I -750	Grade 2	2.5-3.0	0.3-0.8	0.3-0.8	1.4-2.5	3.3-5.0	0.15	0.3	0.75 Mo	450 SC / 500 CC	MHN
17.	I	Grade 3	2.9-3.7	0.3-0.6	0.2-0.5	1.1-1.5	2.7-4.0	0.15	0.3	0.75 Mo	525 SC / 600 CC	

SC-SAND CAST, CC-CHILL CAST

PHYSICAL AND MECHANICAL PROPERTIES

1. Specific gravity — 7.6-7.8 (Ni-Cr Martensitic white cast iron)

2. Coefficient of thermal expansion (Micro-in per in per °F)
   0-430°C — 8-9x10^{-6} (2.5-4.75% Ni, H.C 3-3.5%C)
   0-95°C — 12.2-14.2 x 10^{-6} (2.5-4.75% Ni, L.C. 2.75-2.9% C)

3. Electrical resistivity microhm|cm^{-3} at 78°F — 80-100

4. Modulus of elasticity lb:in²x10^6 — 24-26 (2.5-4.75% Ni, 2.75-3.5%C); 16-17 (2.5-4.75% Ni, H.C. 3-3.5%C)

5. Tensile strength, ton|in² — 21-36 (2.5-4.75% Ni, L.C 2.75-2.9%C)

6. Hardness (DPN) — 590-800 (2.5-4.75% Ni, H.C. 3-35%C); 550-650 (2.5-4.75% Ni, L.C. 2.75-2.9%C)

7. Transverse rupture stress ton|in² — 31-53 (H.C. 2.5-4.75% Ni); 35-55 (L.C. 2.5-4.75% Ni)

8. Transverse deflection (12 in bar, 12 in span) in. — 0.08-0.11 (H.C. 2.5-4.75% Ni); 0.1-0.12 (L.C. 2.5-4.75% Ni)

TABLE-1.9

UNALLOYED GREY IRONS SUITABLE FOR HEAT RESISTING APPLICATIONS (28)

Type	Typical service conditions	Total C %	Si %	Mn %	S %	P %	Ni %	Cr %	Mo %	Room T.S. N mm⁻²	Temp. Prop. BH	Coefficient of expansion per °C × 10⁶	Stress to rupture in 1000h (N mm⁻²)		
													350°C	500°C	700°C
High Phosphorus grey iron	cheap; moderately scale resistant to 600°C suitable for fire bars.	3.0	2.2	0.4	<0.12	0.9				154	200	13	154	46	2
		3.3	3.0	0.7		1.4				185	240	upto 650°C	232		3
Low alloy grey iron	used 400–700°C. dimensional stability and oxidation resistance better than unalloyed iron	3.0	1.6	0.4	<0.12	0.1	0.5	0.5	≤0.5	293	200–260 Grey	11–12 air temperature			
		3.4	2.8	1.0		0.4	2.0			386	350–450 White	13–14 up to 650°C	232 309	46 62	2 3

TABLE-10a

RANGES OF ALLOY CONTENT FOR THE CORROSION & HEAT RESISTANT ALLOYED GREY CAST IRONS(27)

Description	TC(a)	Mn	P	S	Si	Ni	Cr	Mo	Cu	Matrix structure as-cast(c)
Corrosion-Resistant Irons										
High silicon iron(d)	0.4-1.1	1.5	0.15	0.15	14-17	...	5.0	1.0	0.5	F
Ni-Cr grey iron(e)	3.0	0.5-1.5	0.08	0.12	1.0-2.8	13.5-36	1.5-8.0	1.0	7.0	A
Ni-Cr ductile iron(f)	3.0	0.7-4.5	0.08	0.12	1.0-3.0	18-36	1.5-5.5	1.0	...	A
Heat-Resistant Grey Irons										
Medium silicon iron(g)	1.6-2.5	0.4-0.8	0.30	0.10	4.0-7.0	...	...	...	...	F
High Cr-iron	1.2-4.0	0.3-1.5	0.15	0.15	0.5-3.0	5.0	12-35	4.0	3.0	F,CP
Ni-Cr iron(e)	1.8-3.0	0.4-1.5	0.15	0.15	1.0-2.7	13.5-36	1.8-6.0	1.0	7.0	A
Ni-Cr-Si iron(h)	1.8-2.6	0.4-1.0	0.10	0.10	5.0-6.0	13-43	1.8-5.5	1.0	...	A
Heat-Resistant Ductile Irons										
High Al-iron	1.3-2.0	0.4-1.0	0.15	0.15	1.3-6.0	...	20-25 Al	...	...	F
Medium Si-ductile iron	2.8-3.8	0.2-0.6	0.08	0.12	2.5-6.0	1.5	...	...	...	F
Ni-Cr ductile iron(f)	3.0	0.7-2.4	0.08	0.12	1.75-5.5	18-36	1.75-3.5	1.0	...	A

(a) Where a single value is given rather than a range, that value is a maximum limit
(b) Total Carbon
(c) F, Ferrite; A, austenite; CP, coarse pearlite
(d) such as Duriron, Durichlor 51, Superchlor
(e) Such as Ni-Resist austenitic iron (ASTM A436)
(f) Such as Ni-Resist austenitic ductile iron (ASTM A439)
(g) Such as Silal
(h) Such as Nicrosilal

TABLE-1.10b

TYPICAL MECHANICAL PROPERTIES OF CORROSION RESISTANT CAST IRONS(27)

Type of iron	Hardness, HB	Tensile strength		Compressive strength		Impact energy		Transverse breaking load(b)		Transverse deflection(b)	
		MPa	ksi	MPa	ksi	J	ft·lb	kg	lb	mm	in.
High-silicon iron	480 to 520	90 to 180	13 to 26	690	100	2.7 to 5.4(c)	2 to 4(c)	545 to 1000	1200 to 2200	0.65	0.026
High-chromium iron	250 to 740	205 to 830	30 to 120	690	100	0.1 to 3(d) 27 to 47(c)	0.1 to 2(d) 20 to 35(c)	910 to 1590	2000 to 3500	1.5 to 3.8	0.06 to 0.15
High-nickel gray iron	120 to 250	170 to 310	25 to 45	690 to 1100	100 to 160	80 to 200(c)	60 to 150(c)	820 to 1590	1800 to 3500	5 to 25	0.20 to 1.00
High-nickel ductile iron	130 to 240	380 to 480	55 to 70	1240 to 1380	180 to 200	14 to 40(d)	10 to 30(d)	...	...	...	...

(b) For as-cast 30.5-mm (1.2-in.) diam bar broken over a 457-mm (18-in.) span. (c) Unnotched 30.5-mm diam test bar broken over a 152-mm (6-in.) span in a Charpy testing machine. (d) Standard Charpy.

TYPICAL MECHANICAL PROPERTIES OF HEAT RESISTANT ALLOY CAST IRONS

Type of iron	Hardness, HB	Tensile strength		Compressive strength		Impact energy		Transverse breaking load(b)		Transverse deflection(b)	
		MPa	ksi	MPa	ksi	J	ft·lb	kg	lb	mm	in.
Medium-silicon gray iron	170 to 250	170 to 310	25 to 45	620 to 1040	90 to 150	20 to 31(c)	15 to 23(c)	455 to 1090	1000 to 2400	4.6 to 8.9	0.18 to 0.35
High-chromium gray iron	250 to 500	210 to 620	30 to 90	690	100	27 to 47(c)	20 to 35(c)	910 to 1590	2000 to 3500	1.5 to 3.8	0.06 to 0.15
High-nickel gray iron	130 to 250	170 to 310	25 to 45	690 to 1100	100 to 160	80 to 200(c)	60 to 150(c)	820 to 1360	1800 to 3000	5 to 25	0.2 to 1.0
Ni-Cr-Si gray iron	110 to 210	140 to 310	20 to 45	480 to 690	70 to 100	110 to 200(c)	80 to 150(c)	820 to 1130	1800 to 2500	7 to 35	0.3 to 1.4
High-aluminum gray iron	180 to 350	235 to 620	34 to 90	...	...	...	...	...	...	...	...
Medium-silicon ductile iron	140 to 300	415 to 690	60 to 100(c)	...	...	7 to 155(d)	5 to 115(d)	...	...	...	...
High-nickel ductile iron (20 Ni)	140 to 200	380 to 415	55 to 60(e)	1240 to 1380	180 to 200	16(f)	12(f)	...	...	...	...
High-nickel ductile iron (23 Ni)	130 to 170	400 to 450	58 to 65(g)	...	...	38(f)	28(f)	...	...	...	...

(b) Unnotched 30.5-mm (1.2-in.) diam test bar broken on 152-mm (6-in.) supports in a Charpy testing machine. (c) Yield strength, 310 to 520 MPa (45 to 75 ksi); elongation, 0.2%. (d) Standard Charpy test on 10-mm unnotched specimen. (e) Yield strength, 210 to 240 MPa (30 to 35 ksi; elongation, 8 to 20%. (f) Standard Charpy test on 10-mm notched specimen. (g) Yield strength, 195 to 240 MPa (28 to 35 ksi; elongation, 20 to 40%.

TABLE-11a

CHEMICAL COMPOSITION OF Ni-RESIST IRONS, PERCENT (60,61)

	Type 1[1] Aus 101a	Type 1B Aus 101b	Type 2[2] Aus 102a	Type 2B Aus 102b	Type 3 Aus 105	Type 4	Type 5
C	3.00 max	3.00 max	3.00 max	3.00 max	2.60 max	2.60 max	2.40 max
Si	1.00-2.80	1.00-2.80	1.00-2.80	1.00-2.80	1.00-2.00	5.00-6.00	1.00-2.00
Mn	1.00-1.50	1.00-1.50	0.80-1.50	0.80-1.50	0.40-0.80	0.40-0.80	0.40-0.80
Ni	13.50-17.50	13.50-17.50	18.00-22.00	18.00-22.00	28.00-32.00	29.00-32.00	34.00-36.00
Cu	5.50-7.50	5.50-7.50	0.50 max	0.50 max	0.50 max	0.50 max	0.50 max
Cr	1.75-2.50	2.75-3.50	1.75-2.50	3.00-6.00[3]	2.50-3.50	4.50-5.50	0.10 max[4]

1 Where the presence of copper offers corrosion-resistance advantages. Type 1 is recommended.

2 For handling caustics, food, etc., where copper contamination cannot be tolerated. Type 2 is recommended.

3 Where some machining is required, the 3.0-4.0 chromium level is recommended.

4 Where higher hardness, greater strength and added heat resistance are desired, the chromium may be 2.5-3.0% at the expense of increased expansivity.

T-15

TABLE-11b

MECHANICAL PROPERTIES OF Ni-RESIST IRONS (61)

	Type 1 Aus 101a	Type 1B Aus 101b	Type 2 Aus 102a	Type 2B Aus 102b	Type 3 Aus 105	Type 4	Type 5
Tensile Strength ton/in² (kg/mm²)	11-13.5 (17-21)	11-15.5 (17-24)	11-13.5 (17-21)	11-15.5 (17-24)	11-15.5 (17-24)	11-15.5 (17-24)	9-11 (14-17)
Compressive Strength ton/in² (kg/mm²)	44-53 (69-84)		44-53 (69-84)	58-71 (91-112)	44-50 (69-79)	36 (57)	36-44 (57-69)
Torsional Strength lb/in² x 10⁴ (kg/mm²)	35-40 (25-28)		35-40 (25-28)	45-60 (32-42)	35-45 (25-32)	29 (20)	30-35 (21-25)
Torsional Modulus lb/in² x 10⁶ (kg/mm² x 10³)	4.5 (3.2)		4.5 (3.2)	5.5 (3.9)	5.0 (3.5	4.0 (2.8)	4.5 (3.2)
Modulus of Elasticity lb/in² x 10⁴ (kg/mm² x 10³) (at 25% of Tensile Strength)	12-14 (8.4-9.8)	14-16 (9.8-11.2)	15-16.2 (10.5-11.4)	15-16.5 (10.5-11.6)	15-15.5 (10.5-10.9)	15 (10.5)	10.5 (7.4)
Permanent Set Point lb/in² (kg/mm²)	3,000 (2.1)		3,000 (2.1)				
Transverse Properties (18 in) load — lb x 10³ (kg x 10³) deflection — inch (cm)	2.0-2.2 (0.9-1.0) 0.3-0.6 (0.8-1.5)		2.0-2.2 (0.9-1.0) 0.3-0.6 (0.8-1.5)	2.4-2.8 (1.1-1.3) 0.2-0.4 (0.5-1.0)	2.0-2.4 (0.9-1.1) 0.5-0.6 (1.3-1.5)	1.8 (0.8) 0.3-0.6 (0.8-1.5)	1.8-2.0 (0.8-0.9) 0.5-1.0 (1.3-2.5)
Vibration Damping Capacity	High	Medium	High	Medium	High	Medium	High
Endurance Limit lb/in² (kg/mm²)	12,000 (8.4)		12,000 (8.4)	18,000 (12.6)	13,500 (9.5)	9,000 (6.3)	9,900 (7.0)
Hardness Brinell	130-170	150-210	125-170	170-250	120-160	150-210	100-125
Toughness by Impact (Izod) ft. lbf (kgm)*	100 (14)	80 (11)	100 (14)	60 (8)	150 (21)	30 (11)	150 (21)

*1.2 inch (3cm) diameter bar unnotched — struck 3 inches (7.6 cm) above supports (Grey iron shows 25-35 ft-lbf (3.46-4.48 kgm)

TABLE-12

CORROSION RESISTANCE OF Ni-RESIST EXPRESSED IN IPY (MM PER YEAR)

Corrosive Media	SG Ni-Resist Iron Type D-2C	SG Ni-Resist Iron Type D-2	Flake Graphite Type 2 Ni-Resist Iron
1	2	3	4
Ammonium chloride solution : 10% NH$_4$ Cl$_1$ pH 5.15, 13 days at 30°C 6.25 ft|min (1.9 m|min)	0.0280 (0.711)	0.0168 (0.427)	
Ammonium Sulphate solution : 10% (NH$_4$) 2SO$_4$ pH 5.7, 15 days at 30°C 6.25 ft|min (1.9 m|min)	0.0128 (0.325)	0.0111 (0.282)	0.0095 (0.2413)
Ethylene Vapours & splash : 38% ethylene glycol, 50% dicethylene glycol. 4.5% H$_2$O$_1$ 4% Na$_2$SO$_4$, 2.7% NaCl. 0.8% Na$_2$CO$_3$ + trace NaOH. pH 8 to 9, 85days at 135-150°C	0.0023 (0.057)	0.0019*(0.048)	0.0013 (0.033)
Fertilizer : commercial '5-10-5', damp. 290 days at atmospheric temperature		0.0012 (0.030)	0.0025 (0.064)
Nickel chloride solution.: 15% NiCl$_2$, pH 5.3, 7 days at 30°C 6.25 ft|min (1.9 m|min)	0 0062 (0.157)	0.0040 (0.102)	0.0040 (0.102)
Phosporic acid : 85% aerated at 30°C. Velocity 16 ft|min. (4.9 m|min), 12 days	0.213 (5.410)	0.235 (5.969)	0.087 (2.210)
Raw sodium chloride brine : 300 gpl of chlorides, 2.7 g|l CaO, 0.06 g|l NaOH, traces of NH$_3$ & H$_2$S, pH, 6-6.5, 61 days at 10°C, 0.1 to 0.2.ft|s (30-60 mm|s)	0.0023 (0.058)	0.0020*(0.051)	0.0020 (0.051)
Sea water at 26.6°C : 27°C velocity ft|s (8.2 m|s), 60 days test	0.039 (0.991)	0.018 (0.457)	0.016 (0.406)
Soda & brine : 15% NaCl, 9.0% NaOH, 1.0% Na$_2$SO$_4$, 32 days at 80°C	0.0028 (0.071)	0.0015 (0.038)	0.0025 (0.064)
Sodium bisulphate solution : 10% NaHSO$_4$, pH 1.3, 13 days at 30°C 6.25 ft|min (1.9 m|min)	0.0431 (1.095)	0.0444 (1.128)	0.0612 (1.545)
Sodium chloride solution : 5% NaCl, pH 5.6, 7 days at 30°C 6.25 ft|min (1.9 m|min)	0.0028 (0.071)	0.0019 (0.048)	0.0021 (0.053)
Sodium hydroxide : 50% NaOH + heavy conc. of suspended NaCl, 173 days at 55°C 40 gal|min (181.81 l|min)	0.0002 (0.005)	0.0002 (0.005)	0.00018 (0.0046)
Sodium hydroxide : 50% NaOH saturated with salt, 67 days at 95°C, 40 gal|min (181.81 l|min)	0.0009 (0.023)	0.0006 (0.015)	0.0006 (0.015)
Sodium hydroxide : 50% NaOH, 10 days at 128 C, 4days at 21°C	0.0048 (0.122)	0.0049 (0.124)	0.0046 (0.117)
Sodium hydroxide : 30% NaOH + heavy conc. of suspended NaCl, 82 days at 85°C	0.0004 (0.010)	0.0005 (0.013)	0.0004 (0.010)
Sodium hydroxide : 74% NaOH, 191 days at 128°C	0.005 (0.127)	0.0056 (0.142)	0.006 (0.15)
Solium sulphate solution : 10% Na$_2$ SO$_4$, pH 4.0 7 days at 30°C, 6.25 ft|min (1.9m|min)	0.0136 (0.345)	0.0130 (0.330)	0.0132 (0.235)
Sulphuric Acid : 5% at 30°C aerated, Velocity 14 ft|min 4.3 m|min), 4days	0.120 (3.048)	0.104 (2.642)	0.112 (2.845)
Synthesis of sodium bicarbonate by Solvay process : 44% solid NaHCO, slurry plus 200 g|l NH$_4$Cl, 100g|lNH HCO$_3$, 80 g|l NaCl, 8g|l NaHCO$_3$, 40 g|l CO$_2$, 64 days at 30°C	0.0009 (0.023)	0.0003 (0.008)	0.0006 (0.015)
Tap water : aerated, Velocity 16 ft|min (4.9 m|min), 28 days	0.0015 (0.038)	0.0023 (0.058)	0.0045.(0.114)
Vapoura bove ammonia liquor : 40% NH$_3$, 9% CO$_2$, 51% H$_2$O, 109 days at 85°C, low velocity	0.011 (0.279)	0.025 (0.635)	0.017 (0.432)
Zinc chloride solution : 20% ZnCl$_2$, pH 5.25, 13 days at 30°C, 6.25 ft|min (1.9 m|min) * Contains 1% chromium	0.0125 (0.318)	0.0064 (0.163)	

TABLE-13a

CHEMICAL COMPOSITION OF S.G. Ni-RESIST IRONS, PERCENT (61)

	Type D-2 Aus 202a	Type D-2B Aus 202b	Type D-2C Aus 203	Type D-2M	Type D-3 Aus 205	Type D-3A	Type D-4	Type D-5	Type D5B
C	3.00 max	3.00 max	2.90 max	2.7 max	2.60 max	2.60 max	2.60 max	2.40 max	2.40 max
Si	1.75-3.00	1.75-3.00	2.0-3.0	1.5-2.6	1.50-2.3	1.50-2.80	5.0-6.0	1.50-2.75	1.50-2.75
Mn	0.70-1.0	0.70-1.0	1.80-2.40	3.75-4.50	0.50 max	0.50 max	0.50 max	0.50 max	0.50 max
P	0.08 max	0.08 max	0.08 max	0.08 max	0.08 max	0.08 max	0.08 max	0.08 max	0.08 max
Ni	18.0-22.0	18.0-22.0	21.0-24.0	21.5-24.0	28.0-32.0	28.0-32.0	29.0-32.0	34.0-36.0	34.0-36.0
Cr	1.75-2.50	2.75-4.0	0.50 max	0.2 max	2.50-3.50	1.00-1.50	4.50-5.50	0.10 max	2.0-3.0

TABLE-13B

MECHANICAL PROPERTIES OF S.G. Ni-RESIST IRONS (59,81)

	Type D-2 Aus 202a	Type D-2B Aus 202b	Type D-2C Aus 203	Type D-3 Aus 205	Type D-3A	Type D-4	Type D-5	Type D-5B
Tensile Strength ton/in² (kg/mm²)	24-30 (38-47)	26-31 (41-49)	24-29 (38-46)	24-30 (38-47)	24-29 (38-46)	27-32 (43-50)	24-27 (38-43)	24-29 (38-46)
Yield Strength (2% Offset) ton/in² (kg/mm²)	14-16 (22-25)	14.5-16.5 (23-26)	13.5-15.5 (21-24)	14.5-16.5 (23-26)	14-17 (22-27)	17-20 (27-32)	13.5-16.5 (21-26)	16.5-19 (26-30)
Elongation, % on 2 in (5.1 cm)	8-20	7-15	20-40	7-18	13-18	1.5-4.0	20-40	5-10
Proportional Limit ton/in² (kg/mm)	7.3-8.3 (11.6-13.0)	7.1-8.5 (11.2-13.4)	5.4-7.1 (8.4-11.2)	7.1-8.5 (11.2-13.4)	6.7-8.5 (10.5-13.4)	5.4-7.1 (8.4-11.2)	4.2-4.9 (6.7-7.7)	4.7-5.8 (7.4-9.1)
Modulus of Elasticity lb/in² x 10⁶ (kg/mm² x 10³)	16.5-18.5 (11.6-13.0)	16.5-19 (11.6-13.4)	15 (10.5)	13.5-14.5 (9.5-10.2)	16-18.5 (11.2-13.0)	13 (9.1)	16-20 (11.2-14.1)	16-17.5 (11.2-12.3)
Hardness Brinell	140-200	150-210	130-170	140-200	130-190	170-240	130-180	140-190
Impact ft-lbf (kgm/cm²) Charpy V-notch Room Temperature	12 (2.075)	10 (1.73)	28 (4.84)	7 (1.21)	14 (2.42)		17 (29.4)	6 (1.04)

Table-2.1 Summary of the structure-property relations in some Fe-Mn-Cr-Cu corrosion resistant cast irons(62,83)

(1) Alloys studied	3%C, 5%Cr, 6.8%Mn, 1.5-3.0%Cu cast irons
(2) Heat treatments	Held at 800,850,900,950,1000 and 1050°C for 2,4,6,8, and 10 hours followed by OQ(62) and AC(83).
(3) Microstructures	(a) As-Cast: P/B + M + MC + some RA (b) Upto 900°C: M + τ + MC + DC (c) Upto 1000°C: τ + DC + MC or τ + MC (d) At 1050°C: τ + MC (M_7C_3 in eutectic form)
(4) Effect of cooling	OQ: larger τ, lesser DC AC: more DC, lesser τ, 'M' up to higher heat treating temperatures
(5) various carbides formed	M_3C, M_5C_2, M_7C_3, and $M_{23}C_6$ M_3C: up to 950°C prolonged soaking $M_{23}C_6$: boundary carbide up to 900°C,10 hrs. M_5C_2 & M_7C_3: up to 1050°C

(6) Structure-Property interrelations

(a) Martensite : Resists corrosion, but embrittles

(b) Austenite : Most desirable matrix to resist corrosion & to give good strength and ductility. Increase in the amount and stability enhance properties.

(c) Dispersed Carbides:

-They precipitate as M_3C/M_5C_2 from matrix during heat treatment (represented as no. of particles or by distribution factor).
-Overall adverse effect on properties;attains a maximum at 950°C, 10 hours treatment

(d) Massive carbides:

-Represented as area fraction
-Platy morphology in as-cast/low temperature heat treatments
-Rounding-off at ≥950°C
-Platy morphology detrimental to properties (corrosion & mechanical)
-Near rounded/hexagonal forms preferred

(e) Grain boundary carbide $M_{23}C_6$:

-Adversely affects corrosion resistance and deformation behaviour

(f) M_7C_3 & M_5C_2:

-M_7C_3 present in the from of MC and also as eutectic carbide (eutectic form not preferred)
-M_5C_2 present as MC and part of DC

(7) Structure-property correlations (Models):

(a) Heat treating temperature, time and hardness

(b) Weight gain as a function of temperature

(c) A correlation between corrosion rate and microstructure denoting the effect of MC & DC

(d) Interrelating corrosion & deformation behaviour

Table- 3.1 Chemical analysis of Raw Materials

Raw Material	C	Si	P	S	Mn	Cr	Cu
Pig Iron	3.55	2.15	0.40	0.05	1.12	....	....
Ferro-Chromium (low carbon)	0.10 max.	0.70 max.	0.03 max.	0.01 max.	....	67.0-75.0	....
Ferro-Manganese (low carbon)	0.03 max.	....	0.03 max.	0.008	97.0	....	....
Ferro-silicon (low carbon)	0.03 max.	75.0	....	....	....	....	....
Copper (Electrolytic)	....	....	....	....	....	....	99.99

Table- 3.2 Chemical analysis of alloys (weight percent)

Alloy	C	S	P	Si	Mn	Cr	Cu
P1	3.0	0.04	0.27	1.83	10.4	6.85	1.52
P2	3.0	0.04	0.30	1.79	10.4	6.85	3.06
P3	3.0	0.04	0.28	1.81	10.4	6.85	4.82

ALLOY : P1 ; AS CAST HARDNESS(HV30)= 482
TABLE : 4.1   TEMPERATURE   = 800°C

TIME (HOURS)	HARDNESS (HV30)										SD	AVERAGE (HV30)
2	484	484	475	475	473	467	459	456	456	451		
	451	451	448	446	446	444	444	441	440	440	14.63	456
4	486	484	480	478	464	461	460	460	458	457		
	456	456	456	454	454	450	446	445	445	443	12.89	459
6	490	487	477	477	475	475	475	470	469	467		
	467	467	466	464	464	462	462	458	458	441	10.74	468
8	489	489	489	484	480	480	479	478	478	478		
	478	477	477	477	477	477	477	476	473	462	6.02	478
10	490	490	489	484	484	481	480	479	478	477		
	477	476	473	470	470	467	459	459	445	443	13.41	473

FOR DEGREE OF 1   COEFFICIENTS ARE
     450.90000000   2.65000000
BEST FIT VALUES   456.2   461.5   466.8   472.1   477.4
STANDARD DEVIATION IS   4.5423890
FOR DEGREE OF 2   COEFFICIENTS ARE
     443.40000000   5.86428500   -.26785710
BEST FIT VALUES   454.1   462.6   468.9   473.2   475.3
STANDARD DEVIATION IS   4.7868870
FOR DEGREE OF 3   COEFFICIENTS ARE
     472.80280000   -14.78771000   3.67002400   -.21877120
BEST FIT VALUES   456.2   458.4   468.9   477.4   473.2
STANDARD DEVIATION IS   1.3147480

TABLE : 4.2   TEMPERATURE   = 850°C

TIME (HOURS)	HARDNESS (HV30)										SD	AVERAGE (HV30)
2	478	477	475	465	465	464	462	460	458	458		
	458	456	454	454	453	448	448	446	446	445	10.05	458
4	481	480	475	473	473	470	469	465	465	465		
	462	460	458	457	450	450	449	446	446	445	11.56	461
6	473	472	470	469	469	468	467	466	465	465		
	465	464	464	464	462	461	461	461	461	459	3.94	465
8	472	469	466	465	464	464	461	459	458	458		
	458	458	457	457	455	454	452	452	448	443	7.00	458
10	470	459	457	457	456	452	451	451	450	449		
	449	448	448	448	448	447	445	445	445	444	6.24	450

FOR DEGREE OF 1   COEFFICIENTS ARE
     464.10000000   -.95000000
BEST FIT VALUES   462.2   460.3   458.4   456.5   454.6
STANDARD DEVIATION IS   5.3260440
FOR DEGREE OF 2   COEFFICIENTS ARE
     447.60000000   6.12142900   -.58928570
BEST FIT VALUES   457.5   462.7   463.1   458.9   449.9
STANDARD DEVIATION IS   1.9123750
FOR DEGREE OF 3   COEFFICIENTS ARE
     450.39810000   4.15609600   -.21454000   -.02081921
BEST FIT VALUES   457.7   462.3   463.1   459.3   449.7
STANDARD DEVIATION IS   2.6294990

EFFECT OF SOAKING PERIOD ON HARDNESS IN A.C. CONDITION

ALLOY : P1 ; AS CAST HARDNESS(HV30)= 482
TABLE : 4.3   TEMPERATURE   = 900°C

TIME (HOURS)	HARDNESS (HV30)										SD	AVERAGE (HV30)
2	467 466 466 464 464 462 462 461 460 457											
	457 453 452 450 450 448 449 448 444 444										7.70	456
4	465 450 450 450 449 444 444 444 442 441											
	441 440 440 438 438 436 435 434 434 432										7.73	442
6	472 470 465 465 461 454 454 454 450 450											
	450 450 450 446 444 444 443 438 438 435										10.51	451
8	459 457 451 450 449 445 444 443 443 443											
	443 442 441 438 436 436 434 434 434 433										7.52	442
10	449 444 444 441 441 441 439 436 435 435											
	435 433 433 432 432 432 431 431 426 426										6.07	435

FOR DEGREE OF 1   COEFFICIENTS ARE
    457.80000000   -2.10000000
BEST FIT VALUES   453.6   449.4   445.2   441.0   436.8
STANDARD DEVIATION IS   5.7271340
FOR DEGREE OF 2   COEFFICIENTS ARE
    455.80000000   -1.24285700   -.07142857
BEST FIT VALUES   453.0   449.7   445.8   441.3   436.2
STANDARD DEVIATION IS   6.9734130
FOR DEGREE OF 3   COEFFICIENTS ARE
    485.20290000   -21.89486000   3.86645300   -.21877120
BEST FIT VALUES   455.1   445.5   445.8   445.5   434.1
STANDARD DEVIATION IS   7.2909130

TABLE : 4.4   TEMPERATURE   = 950°C

TIME (HOURS)	HARDNESS (HV30)										SD	AVERAGE (HV30)
2	456 451 449 448 445 440 439 438 436 433											
	433 433 432 431 428 427 427 427 424 422										9.63	435
4	450 445 445 445 443 441 439 439 439 437											
	436 435 435 431 427 427 427 424 422 406										10.30	434
6	443 441 439 438 438 438 435 434 434 434											
	433 433 432 432 431 430 429 428 424 412										6.73	432
8	431 430 427 427 427 426 426 426 426 425											
	425 423 423 423 423 421 420 420 417 412										4.40	423
10	435 432 431 429 425 422 422 422 421 421											
	420 420 420 420 420 419 415 413 413 412										6.27	421

FOR DEGREE OF 1   COEFFICIENTS ARE
    440.70000000   -1.95000000
BEST FIT VALUES   436.8   432.9   429.0   425.1   421.2
STANDARD DEVIATION IS   2.4426790
FOR DEGREE OF 2   COEFFICIENTS ARE
    436.20000000   -.02142859   -.16071430
BEST FIT VALUES   435.5   433.5   430.3   425.7   419.9
STANDARD DEVIATION IS   2.4611160
FOR DEGREE OF 3   COEFFICIENTS ARE
    424.99850000   7.84630600   -1.66091800   .08334464
BEST FIT VALUES   434.7   435.1   430.3   424.1   420.7
STANDARD DEVIATION IS   2.3904610

ALLOY : P1 ; AS CAST HARDNESS(HV30)= 482
TABLE : 4.5   TEMPERATURE   = 1000°C

TIME (HOURS)	HARDNESS (HV30)										SD	AVERAGE (HV30)
2	428	428	424	423	419	419	418	418	417	417		
	417	416	415	415	415	413	412	412	411	408	5.29	417
4	418	418	418	417	415	415	414	414	414	413		
	413	412	412	412	411	411	411	411	411	406	3.01	413
6	409	409	408	408	406	406	404	403	399	399		
	399	398	397	395	393	392	391	386	370	370	11.36	397
8	401	393	386	385	384	383	382	382	382	382		
	381	380	380	380	380	377	377	374	373	373	6.50	381
10	418	415	410	408	408	402	400	399	399	398		
	398	398	396	396	396	393	393	390	388	368	10.69	398

FOR DEGREE OF 1   COEFFICIENTS ARE
    422.20000000   -3.50000000
BEST FIT VALUES   415.2   408.2   401.2   394.2   387.2
STANDARD DEVIATION IS   10.5640900
FOR DEGREE OF 2   COEFFICIENTS ARE
    443.20000000   -12.50000000   .75000000
BEST FIT VALUES   421.2   405.2   395.2   391.2   393.2
STANDARD DEVIATION IS   10.2176300
FOR DEGREE OF 3   COEFFICIENTS ARE
    380.20170000   31.74880000   -7.68727100   .46873730
BEST FIT VALUES   416.7   414.2   395.2   382.2   397.7
STANDARD DEVIATION IS   2.5099800

TABLE : 4.6   TEMPERATURE   = 1050°C

TIME (HOURS)	HARDNESS (HV30)										SD	AVERAGE (HV30)
2	406	401	395	395	393	393	391	391	390	390		
	390	390	390	389	388	386	385	384	382	382	5.85	390
4	398	395	387	381	378	377	377	376	376	375		
	371	370	368	367	366	366	361	360	360	357	11.14	373
6	374	373	370	369	369	368	367	366	366	366	—	
	364	363	360	360	360	359	356	356	356	353	6.03	363
8	395	393	392	391	388	388	388	384	384	383		
	383	383	382	382	382	380	376	374	371	371	6.85	383
10	351	350	349	348	347	347	347	346	345	345		
	344	343	341	341	340	339	339	338	334	331	5.32	343

FOR DEGREE OF 1   COEFFICIENTS ARE
    395.60000000   -4.20000000
BEST FIT VALUES   387.2   378.8   370.4   362.0   353.6
STANDARD DEVIATION IS   14.7150700
FOR DEGREE OF 2   COEFFICIENTS ARE
    387.60000000   -.77142810   -.28571430
BEST FIT VALUES   384.9   379.9   372.7   363.1   351.3
STANDARD DEVIATION IS   17.7667500
FOR DEGREE OF 3   COEFFICIENTS ARE
    481.39560000   -66.65170000   12.27620000   -.69788410
BEST FIT VALUES   391.6   366.5   372.7   376.5   344.6
STANDARD DEVIATION IS   13.5060700

EFFECT OF SOAKING PERIOD ON HARDNESS IN A.C. CONDITION

ALLOY : P2 ; AS CAST HARDNESS(HV30)= 464
TABLE : 4.7   TEMPERATURE   = 800°C

TIME (HOURS)	HARDNESS (HV30)										SD	AVERAGE (HV30)
2	472	470	470	469	469	467	467	468	465	465		
	465	465	464	464	464	462	462	460	460	457	3.80	465
4	475	473	469	468	468	468	468	467	467	466		
	466	464	464	462	461	460	459	458	457	439	7.54	463
6	486	483	483	483	480	479	479	478	477	476		
	476	476	476	475	475	475	472	472	472	458	5.87	476
8	483	483	481	476	475	475	473	473	472	472		
	472	471	470	470	470	469	469	469	467	467	4.78	472
10	492	486	483	483	478	478	476	475	474	474		
	473	473	473	470	469	469	467	465	464	464	7.48	474

FOR DEGREE OF 1   COEFFICIENTS ARE
    461.90000000   1.35000000
BEST FIT VALUES   464.6   467.3   470.0   472.7   475.4
STANDARD DEVIATION IS   4.3627150
FOR DEGREE OF 2   COEFFICIENTS ARE
    457.40000000   3.27857200   -.16071430
BEST FIT VALUES   463.3   467.9   471.3   473.3   474.1
STANDARD DEVIATION IS   5.0652880
FOR DEGREE OF 3   COEFFICIENTS ARE
    489.99600000   -5.56862700   1.52625200   -.09372033
BEST FIT VALUES   464.2   466.1   471.3   475.1   473.2
STANDARD DEVIATION IS   6.5737610

TABLE : 4.8   TEMPERATURE   = 850°C

TIME (HOURS)	HARDNESS (HV30)										SD	AVERAGE (HV30)
2	470	470	469	469	466	464	463	462	462	459		
	459	459	458	456	455	453	453	451	449	443	7.48	459
4	467	462	457	454	454	453	451	450	450	450		
	448	447	447	446	446	446	443	440	436	429	8.43	448
6	470	470	465	463	461	459	458	457	456	456		
	456	456	456	455	453	451	451	448	444	439	7.67	456
8	467	461	454	454	454	452	451	451	451	446		
	445	445	444	443	443	443	443	439	431	429	9.00	447
10	459	459	458	457	456	453	453	453	451	451		
	451	451	451	451	451	450	449	446	446	438	4.94	451

FOR DEGREE OF 1   COEFFICIENTS ARE
    457.30000000   -.85000000
BEST FIT VALUES   455.6   453.9   452.2   450.5   448.8
STANDARD DEVIATION IS   5.0957590
FOR DEGREE OF 2   COEFFICIENTS ARE
    463.80000000   -3.63571400   .23214290
BEST FIT VALUES   457.5   453.0   450.3   449.6   450.7
STANDARD DEVIATION IS   5.7370970
FOR DEGREE OF 3   COEFFICIENTS ARE
    472.20340000   -9.53811500   1.35760100   -.06252543
BEST FIT VALUES   458.1   451.8   450.3   450.8   450.1
STANDARD DEVIATION IS   7.8885240

ALLOY : P2 ; AS CAST HARDNESS(HV30)= 464
TABLE : 4.9   TEMPERATURE   = 900°C

TIME (HOURS)	HARDNESS (HV30)										SD	AVERAGE (HV30)
2	449	445	445	441	441	440	439	438	437	436		
	436	436	436	435	435	435	432	426	425	424	6.44	436
4	444	444	439	438	438	438	438	438	436	436		
	436	435	435	435	434	433	432	430	415	415	7.47	434
6	453	453	451	451	450	444	443	443	442	441		
	441	441	440	438	438	436	436	435	434	418	8.17	441
8	453	451	450	446	446	446	444	442	440	440		
	440	439	439	439	438	438	430	429	428	427	7.48	440
10	444	443	441	440	435	432	431	431	431	431		
	430	430	429	429	429	428	425	420	420	418	7.18	430

FOR DEGREE OF 1   COEFFICIENTS ARE
     438.00000000   -.30000000
BEST FIT VALUES 437.4 436.8 436.2 435.6 435.0
STANDARD DEVIATION IS   5.0727950
FOR DEGREE OF 2   COEFFICIENTS ARE
     426.00000000   4.84285700   -.42857140
BEST FIT VALUES 434.0 438.5 439.6 437.3 431.6
STANDARD DEVIATION IS   4.2460110
FOR DEGREE OF 3   COEFFICIENTS ARE
     451.20110000   -12.85794000   2.94658100   -.18750850
BEST FIT VALUES 435.8 434.9 439.6 440.9 429.8
STANDARD DEVIATION IS   1.9123590

TABLE : 4.10   TEMPERATURE   = 950°C

TIME (HOURS)	HARDNESS (HV30)										SD	AVERAGE (HV30)
2	441	441	441	439	439	436	436	431	430	429		
	429	427	427	427	422	422	422	422	418	415	8.11	429
4	444	434	431	431	429	429	428	427	426	425		
	425	424	424	424	422	419	419	417	415	415	6.90	425
6	439	439	438	432	432	431	430	428	428	428		
	428	428	427	427	426	425	425	419	419	415	6.25	428
8	439	439	439	439	438	438	436	434	433	432		
	431	431	430	429	429	428	428	418	417	417	7.18	431
10	431	429	427	426	425	425	424	424	424	422		
	422	422	421	421	420	420	418	415	415	413	4.62	422

FOR DEGREE OF 1   COEFFICIENTS ARE
     429.40000000   -.40000000
BEST FIT VALUES 428.6 427.8 427.0 426.2 425.4
STANDARD DEVIATION IS   3.8122840
FOR DEGREE OF 2   COEFFICIENTS ARE
     424.40000000   1.74285700   -.17857140
BEST FIT VALUES 427.2 428.5 428.4 426.9 424.0
STANDARD DEVIATION IS   4.2695000
FOR DEGREE OF 3   COEFFICIENTS ARE
     450.99560000   -16.93741000   3.38334400   -.19788420
BEST FIT VALUES 429.1 424.7 428.4 430.7 422.1
STANDARD DEVIATION IS   .5976188

EFFECT OF SOAKING PERIOD ON HARDNESS IN A.C. CONDITION

ALLOY : P2 ; AS CAST HARDNESS(HV30)= 464
TABLE : 4.11   TEMPERATURE   = 1000°C

TIME (HOURS)	HARDNESS (HV30)										SD	AVERAGE (HV30)
2	427	427	424	419	417	417	415	415	415	414		
	413	412	412	409	409	408	408	408	408	402	6.61	413
4	426	425	422	422	421	420	419	417	417	417		
	415	414	413	413	413	410	409	401	401	400	7.60	414
6	422	418	413	408	408	408	406	404	404	404		
	404	403	402	401	401	401	398	398	398	398	6.53	404
8	420	418	408	406	404	403	403	400	399	399		
	399	398	398	396	395	393	390	390	389	389	8.59	399
10	406	404	402	402	400	399	398	398	396	395		
	392	390	389	389	388	388	386	362	362	353	14.65	389

FOR DEGREE OF 1   COEFFICIENTS ARE
      422.70000000   -3.15000000
BEST FIT VALUES   416.4   410.1   403.8   397.5   391.2
STANDARD DEVIATION IS   3.3615560
FOR DEGREE OF 2   COEFFICIENTS ARE
      414.20000000   .49285700   -.30357140
BEST FIT VALUES   414.0   411.3   406.2   398.7   388.8
STANDARD DEVIATION IS   2.5745950
FOR DEGREE OF 3   COEFFICIENTS ARE
      405.79660000   6.39525700   -1.42902900   .06252543
BEST FIT VALUES   413.4   412.5   406.2   397.5   389.4
STANDARD DEVIATION IS   3.1075760

TABLE : 4.12   TEMPERATURE   = 1050°C

TIME (HOURS)	HARDNESS (HV30)										SD	AVERAGE (HV30)
2	414	414	413	410	409	409	408	406	406	404		
	403	403	402	398	396	395	395	390	390	390	8.00	402
4	397	397	396	396	390	390	388	388	385	385		
	384	384	383	379	378	378	378	378	371	371	8.04	384
6	376	375	375	375	369	368	367	367	366	366		
	365	364	364	363	360	360	360	360	359	358	5.77	365
8	387	385	385	379	377	375	375	373	373	373		
	372	372	370	368	368	367	367	361	357	356	8.42	372
10	364	361	358	358	353	352	352	352	351	351		
	350	349	349	348	348	348	345	344	342	329	7.42	350

FOR DEGREE OF 1   COEFFICIENTS ARE
      409.40000000   -5.80000000
BEST FIT VALUES   397.8   386.2   374.6   363.0   351.4
STANDARD DEVIATION IS   8.1158300
FOR DEGREE OF 2   COEFFICIENTS ARE
      418.40000000   -9.65714300   .32142860
BEST FIT VALUES   400.4   384.9   372.0   361.7   354.0
STANDARD DEVIATION IS   9.3396180
FOR DEGREE OF 3   COEFFICIENTS ARE
      457.60080000   -37.19101000   5.57153000   -.29167230
BEST FIT VALUES   403.2   379.3   372.0   367.3   351.2
STANDARD DEVIATION IS   9.8008810

ALLOY : P3 ; AS CAST HARDNESS(HV30)= 457
TABLE : 4.13   TEMPERATURE   = 800°C

TIME (HOURS)	HARDNESS (HV30)										SD	AVERAGE (HV30)
2	475	473	472	470	470	469	469	469	469	469		
	469	468	468	467	467	466	465	464	462	459	3.64	468
4	475	470	470	466	464	464	464	462	462	461		
	461	460	459	459	459	458	453	445	445	443	8.32	460
6	476	472	469	469	464	461	459	458	456	455		
	454	454	452	451	451	449	446	446	431	429	12.05	455
8	481	480	478	477	476	473	467	464	464	464		
	464	463	463	461	459	454	453	453	453	451	9.72	464
10	481	480	478	478	477	477	472	470	470	470	.	
	470	470	469	469	467	466	464	462	449	449	8.74	469

FOR DEGREE OF 1   COEFFICIENTS ARE
    461.40000000   .30000000
BEST FIT VALUES   462.0   462.6   463.2   463.8   464.4
STANDARD DEVIATION IS   6.6131130
FOR DEGREE OF 2   COEFFICIENTS ARE
    481.40000000   -8.27142800   .71428570
BEST FIT VALUES   467.7   459.7   457.5   460.9   470.1
STANDARD DEVIATION IS   2.9081270
FOR DEGREE OF 3   COEFFICIENTS ARE
    491.19790000   -15.15329000   2.02650600   -.07290112
BEST FIT VALUES   468.4   458.3   457.5   462.3   469.4
STANDARD DEVIATION IS   3.4661700

TABLE : 4.14   TEMPERATURE   = 850°C

TIME (HOURS)	HARDNESS (HV30)										SD	AVERAGE (HV30)
2	464	462	458	448	446	446	445	445	445	445		
	445	445	443	443	441	441	441	438	438	438	7.32	445
4	459	456	456	449	446	445	445	443	443	442		
	442	441	441	438	436	436	436	436	433	431	7.68	442
6	461	453	453	446	446	445	444	443	443	443		
	441	441	440	439	438	438	438	438	438	435	6.36	443
8	453	453	453	446	444	443	442	441	441	441		
	441	441	441	440	438	438	436	436	432	427	6.55	441
10	465	465	459	457	454	451	451	450	450	450		
	449	448	448	446	445	443	443	442	433	433	8.50	449

FOR DEGREE OF 1   COEFFICIENTS ARE
    441.90000000   .35000000
BEST FIT VALUES   442.6   443.3   444.0   444.7   445.4
STANDARD DEVIATION IS   3.4205190
FOR DEGREE OF 2   COEFFICIENTS ARE
    451.40000000   -3.72142800   .33928570
BEST FIT VALUES   445.3   441.9   441.3   443.3   448.1
STANDARD DEVIATION IS   2.1580480
FOR DEGREE OF 3   COEFFICIENTS ARE
    442.99660000   2.18097300   -.78617200   .06252543
BEST FIT VALUES   444.7   443.1   441.3   442.1   448.7
STANDARD DEVIATION IS   2.3904570

EFFECT OF SOAKING PERIOD ON HARDNESS IN A.C. CONDITION

ALLOY : P3 ; AS CAST HARDNESS(HV30)= 457
TABLE : 4.15   TEMPERATURE   = 900°C

TIME (HOURS)	HARDNESS (HV30)										SD	AVERAGE (HV30)
2	445	443	443	440	439	436	435	434	433	433		
	431	431	430	430	428	428	428	427	427	426	5.91	433
4	458	453	451	448	445	445	441	441	441	440		
	440	440	440	440	436	434	432	431	428	427	8.06	440
6	456	448	445	443	440	439	439	439	439	438	—	
	438	437	437	436	434	434	429	428	421	419	8.44	436
8	443	443	438	428	425	424	421	420	420	419		
	419	417	415	414	412	412	410	410	405	404	11.17	419
10	427	412	412	412	412	411	411	410	408	408		
	408	408	405	405	404	404	403	403	402	400	5.83	408

FOR DEGREE OF 1   COEFFICIENTS ARE
     448.50000000   -3.55000000
BEST FIT VALUES 441.4   434.3   427.2   420.1   413.0
STANDARD DEVIATION IS   8.3005990
FOR DEGREE OF 2   COEFFICIENTS ARE
     424.00000000   6.95000000   -.87500000
BEST FIT VALUES 434.4   437.8   434.2   423.6   406.0
STANDARD DEVIATION IS   4.1952390
FOR DEGREE OF 3   COEFFICIENTS ARE
     400.20250000   23.66493000   -4.06217000   .17706500
BEST FIT VALUES 432.7   441.2   434.2   420.2   407.7
STANDARD DEVIATION IS   2.5099950

TABLE : 4.16   TEMPERATURE   = 950°C

TIME (HOURS)	HARDNESS (HV30)										SD	AVERAGE (HV30)
2	431	428	425	425	425	424	419	418	418	418		
	417	417	416	415	415	415	415	412	403	397	7.93	417
4	431	429	428	427	426	425	424	424	424	422		
	421	421	420	420	419	418	417	404	403	403	8.20	420
6	435	433	432	429	428	428	427	426	423	422		
	422	420	420	419	417	413	412	410	410	404	8.53	421
8	432	424	424	422	421	421	420	420	417	416		
	415	415	414	413	413	413	413	412	408	398	7.04	416
10	418	415	414	413	412	411	411	409	409	406		
	406	406	405	405	404	404	393	393	391	391	8.08	405

FOR DEGREE OF 1   COEFFICIENTS ARE
     424.20000000   -1.40000000
BEST FIT VALUES 421.4   418.6   415.8   413.0   410.2
STANDARD DEVIATION IS   5.3040900
FOR DEGREE OF 2   COEFFICIENTS ARE
     407.20000000   5.88571400   -.60714290
BEST FIT VALUES 416.5   421.0   420.7   415.4   405.3
STANDARD DEVIATION IS   .9561829
FOR DEGREE OF 3   COEFFICIENTS ARE
     412.79620000   1.95504800   .14234850   -.04163841
BEST FIT VALUES 416.9   420.2   420.7   416.2   404.9
STANDARD DEVIATION IS   .4781032

EFFECT OF SOAKING PERIOD ON HARDNESS IN A.C. CONDITION

ALLOY : P3 ; AS CAST HARDNESS(HV30)= 457
TABLE : 4.17   TEMPERATURE   = 1000°C

TIME (HOURS)	HARDNESS (HV30)										SD	AVERAGE (HV30)
2	415	413	412	410	410	410	410	409	409	405		
	404	403	403	403	403	402	402	402	401	398	4.73	406
4	414	411	410	408	408	406	405	405	404	403		
	402	401	401	400	400	400	400	399	394	390	5.68	403
6	413	404	404	403	403	400	398	397	397	396		
	396	395	394	393	393	393	389	389	386	386	6.74	396
8	402	395	393	386	385	385	383	383	381	380		
	380	380	379	379	378	375	373	371	370	369	8.36	381
10	386	384	379	376	373	373	373	372	372	372		
	371	371	370	369	368	366	360	358	356	355	8.26	370

FOR DEGREE OF 1   COEFFICIENTS ARE
    419.40000000   -4.70000000
BEST FIT VALUES   410.0   400.6   391.2   381.8   372.4
STANDARD DEVIATION IS   4.1311860
FOR DEGREE OF 2   COEFFICIENTS ARE
    407.40000000   .44285730   -.42857140
BEST FIT VALUES   406.6   402.3   394.6   383.5   369.0
STANDARD DEVIATION IS   2.2424450
FOR DEGREE OF 3   COEFFICIENTS ARE
    396.19850000   8.31059300   -1.92877500   .08334464
BEST FIT VALUES   405.8   403.9   394.6   381.9   369.8
STANDARD DEVIATION IS   1.9123620

TABLE : 4.18   TEMPERATURE   = 1050°C

TIME (HOURS)	HARDNESS (HV30)										SD	AVERAGE (HV30)
2	409	408	408	405	401	400	398	394	393	391		
	390	387	387	386	384	384	383	380	378	374	10.56	392
4	402	402	398	393	391	389	389	386	385	385		
	385	385	384	383	382	382	382	376	376	372	7.97	386
6	391	389	389	386	386	380	380	379	377	376		
	376	373	373	372	372	371	371	371	368	359	8.16	376
8	377	365	365	365	361	361	359	357	357	357		
	357	357	357	356	356	356	356	352	348	331	8.61	357
10	360	344	339	337	335	333	331	330	328	328		
	328	326	326	326	325	325	324	322	322	320	9.27	330

FOR DEGREE OF 1   COEFFICIENTS ARE
    414.10000000   -7.65000000
BEST FIT VALUES   398.8   383.5   368.2   352.9   337.6
STANDARD DEVIATION IS   7.9141270
FOR DEGREE OF 2   COEFFICIENTS ARE
    388.60000000   3.27857200   -.91071430
BEST FIT VALUES   391.5   387.1   375.5   356.5   330.3
STANDARD DEVIATION IS   1.0281700
FOR DEGREE OF 3   COEFFICIENTS ARE
    394.19620000   -.65209480   -.16122290   -.04163841
BEST FIT VALUES   391.9   386.3   375.5   357.3   329.9
STANDARD DEVIATION IS   .7171304

EFFECT OF SOAKING TEMPERATURE ON HARDNESS IN A.C. CONDITION

ALLOY : P1 ; AS CAST HARDNESS(HV30)= 482
TABLE : 4.19

TIME = 2 HOURS

TEMP (DEG.C)	HARDNESS (HV30)										SD	AVERAGE (HV30)
800	484	484	475	475	473	467	459	456	456	451		
	451	451	448	446	446	444	444	441	440	440	14.63	456
850	478	477	475	465	465	464	462	460	458	458		
	458	456	454	454	453	448	448	446	446	445	10.05	458
900	467	466	466	464	464	462	462	461	460	457		
	457	453	452	450	450	448	449	448	444	444	7.70	456
950	456	451	449	448	445	440	439	438	436	433		
	433	433	432	431	428	427	427	427	424	422	9.63	435
1000	428	428	424	423	419	419	418	418	417	417		
	417	416	415	415	415	413	412	412	411	408	5.29	417
1050	406	401	395	395	393	393	391	391	390	390		
	390	390	390	389	388	386	385	384	382	382	5.85	390

FOR DEGREE OF 1   COEFFICIENTS ARE
    685.87620000   -.27085720
BEST FIT VALUES   469.2   455.6   442.1   428.6   415.0   401.5
STANDARD DEVIATION IS   11.7225800
FOR DEGREE OF 2   COEFFICIENTS ARE
    -578.16020000   2.48568700   -.00149002
BEST FIT VALUES   456.8   458.1   452.0   438.5   417.5   389.1
STANDARD DEVIATION IS   3.1446540
FOR DEGREE OF 3   COEFFICIENTS ARE
    -578.16020000   2.48568700   -.00149002   .00000000
BEST FIT VALUES   456.8   458.1   452.0   438.5   417.5   389.1
STANDARD DEVIATION IS   3.8513980

TABLE : 4.20

TIME = 4 HOURS

TEMP (DEG.C)	HARDNESS (HV30)										SD	AVERAGE (HV30)
800	486	484	480	478	464	461	460	460	458	457		
	456	456	456	454	454	450	446	445	445	443	12.89	459
850	481	480	475	473	473	470	469	465	465	465		
	462	460	458	457	450	450	449	446	446	445	11.56	461
900	465	450	450	450	449	444	444	444	442	441		
	441	440	440	438	438	436	435	434	434	432	7.73	442
950	450	445	445	445	443	441	439	439	439	437		
	436	435	435	431	427	427	427	424	422	406	10.30	434
1000	418	418	418	417	415	415	414	414	414	413		
	413	412	412	412	411	411	411	411	411	406	3.01	413
1050	398	395	387	381	378	377	377	376	376	375		
	371	370	368	367	366	366	361	360	360	357	11.14	373

FOR DEGREE OF 1   COEFFICIENTS ARE
    737.96190000   -.33257140
BEST FIT VALUES   471.9   455.3   438.6   422.0   405.4   388.8
STANDARD DEVIATION IS   12.8493100
FOR DEGREE OF 2   COEFFICIENTS ARE
    -580.87080000   2.54347000   -.00155462
BEST FIT VALUES   458.9   457.9   449.0   432.4   408.0   375.8
STANDARD DEVIATION IS   5.6171760
FOR DEGREE OF 3   COEFFICIENTS ARE
    309.52060000   -.38209520   .00163353   -.00000115
BEST FIT VALUES   459.3   457.3   448.7   432.8   408.6   375.3
STANDARD DEVIATION IS   6.5305900

EFFECT OF SOAKING TEMPERATURE ON HARDNESS IN A.C. CONDITION

ALLOY : P1 ; AS CAST HARDNESS(HV30)= 482
TABLE : 4.21   TIME =   6 HOURS

TEMP (DEG.C)	HARDNESS (HV30)									SD	AVERAGE (HV30)
800	490	487	477	477	475	475	475	470	469	467		
	467	467	466	464	464	462	462	458	458	441	10.74	468
850	473	472	470	469	469	468	467	466	465	465		
	465	464	464	464	462	461	461	461	461	459	3.94	465
900	472	470	465	465	461	454	454	454	450	450		
	450	450	450	446	444	444	443	438	438	435	10.51	451
950	443	441	439	438	438	438	435	434	434	434		
	433	433	432	432	431	430	429	428	424	412	6.73	432
1000	409	409	408	408	406	406	404	403	399	399		
	399	397	395	394	393	392	391	386	370	370	11.37	396
1050	374	373	370	369	369	368	367	366	366	366		
	364	363	360	360	360	359	356	356	356	353	6.03	363

FOR DEGREE OF 1   COEFFICIENTS ARE
     826.12380000   -.42914290
BEST FIT VALUES   482.8   461.4   439.9   418.4   397.0   375.5
STANDARD DEVIATION IS   13.2067800
FOR DEGREE OF 2   COEFFICIENTS ARE
    -612.51840000   2.70817300   -.00169585
BEST FIT VALUES   468.7   464.2   451.2   429.7   399.8   361.4
STANDARD DEVIATION IS   2.7896800
FOR DEGREE OF 3   COEFFICIENTS ARE
    -443.65120000   2.15332400   -.00109120   -.00000022
BEST FIT VALUES   468.7   464.1   451.1   429.8   399.9   361.3
STANDARD DEVIATION IS   3.5005080

TABLE : 4.22   TIME =   8 HOURS

TEMP (DEG.C)	HARDNESS (HV30)									SD	AVERAGE (HV30)
800	489	489	489	484	480	480	479	478	478	478		
	478	477	477	477	477	477	477	476	473	462	6.02	478
850	472	469	466	465	464	464	461	459	458	458		
	458	458	457	457	455	454	452	452	448	443	7.00	458
900	459	457	451	450	449	445	444	443	443	443		
	443	442	441	438	436	436	434	434	434	433	7.52	442
950	431	430	427	427	427	426	426	426	426	425		
	425	423	423	423	423	421	420	420	417	412	4.40	423
1000	401	393	386	385	384	383	382	382	382	382		
	381	380	380	380	380	377	377	374	373	373	6.50	381
1050	395	393	392	391	388	388	388	384	384	383		
	383	383	382	382	382	380	376	374	371	371	6.85	383

FOR DEGREE OF 1   COEFFICIENTS ARE
     810.71430000   -.41428570
BEST FIT VALUES   479.3   458.6   437.9   417.1   396.4   375.7
STANDARD DEVIATION IS   9.2813230
FOR DEGREE OF 2   COEFFICIENTS ARE
     846.00700000   -.49125020   .00004160
BEST FIT VALUES   479.6   458.5   437.6   416.9   396.4   376.1
STANDARD DEVIATION IS   10.7104900
FOR DEGREE OF 3   COEFFICIENTS ARE
    -489.58060000   3.89709800   -.00474063   .00000173
BEST FIT VALUES   479.1   459.4   438.0   416.3   395.4   376.8
STANDARD DEVIATION IS   12.4681500

EFFECT OF SOAKING TEMPERATURE ON HARDNESS IN A.C. CONDITION

ALLOY : P1 ; AS CAST HARDNESS(HV30)= 482
TABLE : 4.23   TIME =   10 HOURS

TEMP (DEG.C)	HARDNESS (HV30)									SD	AVERAGE (HV30)
800	490	490	489	484	484	481	480	479	478	477		
	477	476	473	470	470	467	459	459	445	443	13.41	473
850	470	459	457	457	456	452	451	451	450	449		
	449	448	448	448	448	447	445	445	445	444	6.24	450
900	449	444	444	441	441	441	439	436	435	435		
	435	433	433	432	432	432	431	431	426	426	6.07	435
950	435	432	431	429	425	422	422	422	421	421		
	420	420	420	420	420	419	415	413	413	412	6.27	421
1000	418	415	410	408	408	402	400	399	399	398		
	398	398	396	396	396	393	393	390	388	368	10.69	398
1050	351	350	349	348	347	347	347	346	345	345		
	344	343	341	341	340	339	339	338	334	331	5.32	343

FOR DEGREE OF 1   COEFFICIENTS ARE

   853.42860000   -.46857140

BEST FIT VALUES   478.6   455.1   431.7   408.3   384.9   361.4

STANDARD DEVIATION IS   13.6224600

FOR DEGREE OF 2   COEFFICIENTS ARE

  -307.98020000   2.06416800   -.00136905

BEST FIT VALUES   467.2   457.4   440.8   417.4   387.1   350.0

STANDARD DEVIATION IS   10.0570000

FOR DEGREE OF 3   COEFFICIENTS ARE

  2010.10800000   -5.55238900   .00693114   -.00000300

BEST FIT VALUES   468.1   455.9   440.1   418.5   388.8   348.7

STANDARD DEVIATION IS   10.2263400

EFFECT OF SOAKING TEMPERATURE ON HARDNESS IN A.C. CONDITION

ALLOY : P2 ; AS CAST HARDNESS(HV30)= 464
TABLE : 4.24   TIME =   2 HOURS

TEMP (DEG.C)	HARDNESS (HV30)										SD	AVERAGE (HV30)
800	472	470	470	469	469	467	467	466	465	465		
	465	465	464	464	464	462	462	460	460	457	3.80	465
850	470	470	469	469	466	464	463	462	462	459		
	459	459	458	456	455	453	453	451	449	443	7.48	459
900	449	445	445	441	441	440	439	438	437	436		
	436	436	436	435	435	435	432	426	425	424	6.44	436
950	441	441	441	439	439	436	436	431	430	429		
	429	427	427	427	422	422	422	422	418	415	8.11	429
1000	427	427	424	419	417	417	415	415	415	415		
	415	414	413	412	409	408	408	404	404	404	6.84	414
1050	414	414	413	410	409	409	408	406	406	404		
	403	403	402	398	396	395	395	390	390	390	8.00	402

FOR DEGREE OF 1   COEFFICIENTS ARE
    675.72380000   -.26114280
BEST FIT VALUES   466.8   453.8   440.7   427.6   414.6   401.5
STANDARD DEVIATION IS   3.7174020
FOR DEGREE OF 2   COEFFICIENTS ARE
    687.79760000   -.28747280   .00001423
BEST FIT VALUES   466.9   453.7   440.6   427.5   414.6   401.6
STANDARD DEVIATION IS   4.2906360
FOR DEGREE OF 3   COEFFICIENTS ARE
    426.82090000   .57002030   -.00092023   .00000034
BEST FIT VALUES   466.8   453.9   440.7   427.4   414.4   401.8
STANDARD DEVIATION IS   5.1926850

TABLE : 4.25   TIME =   4 HOURS

TEMP (DEG.C)	HARDNESS (HV30)										SD	AVERAGE (HV30)
800	475	473	469	468	468	468	468	467	467	466		
	466	464	464	462	461	460	459	458	457	439	7.54	463
850	467	462	457	454	454	453	451	450	450	450		
	448	447	447	446	446	446	443	440	436	429	8.43	448
900	444	444	439	438	438	438	438	438	436	436		
	436	435	435	435	434	433	432	430	415	415	7.47	434
950	444	434	431	431	429	429	428	427	426	425		
	425	424	424	424	422	419	419	417	415	415	6.90	425
1000	426	425	422	422	421	420	419	417	417	417		
	415	414	413	413	413	410	409	401	401	400	7.60	414
1050	397	397	396	396	390	390	388	388	385	385		
	384	384	383	379	378	378	378	378	371	371	8.04	384

FOR DEGREE OF 1   COEFFICIENTS ARE
    695.45720000   -.28914280
BEST FIT VALUES   464.1   449.7   435.2   420.8   406.3   391.9
STANDARD DEVIATION IS   6.0071430
FOR DEGREE OF 2   COEFFICIENTS ARE
    313.73860000   .54328880   -.00044996
BEST FIT VALUES   460.4   450.4   438.2   423.8   407.1   388.1
STANDARD DEVIATION IS   5.6889620
FOR DEGREE OF 3   COEFFICIENTS ARE
    1419.05200000   -3.08844700   .00350774   -.00000143
BEST FIT VALUES   460.8   449.7   437.9   424.3   407.8   387.5
STANDARD DEVIATION IS   6.0512490

EFFECT OF SOAKING TEMPERATURE ON HARDNESS IN A.C. CONDITION

ALLOY : P2 ; AS CAST HARDNESS(HV30)= 464
TABLE : 4.26   TIME =   6 HOURS

TEMP (DEG.C)	HARDNESS (HV30)									SD	AVERAGE (HV30)
800	486 483 483 483 480 479 479 478 477 476										
	476 476 476 475 475 475 472 472 472 458									5.87	476
850	470 470 465 463 461 459 458 457 456 456										
	456 456 456 455 453 451 451 448 444 439									7.67	456
900	453 453 451 451 450 444 443 443 442 441										
	441 441 440 438 438 436 436 435 434 418									8.17	441
950	439 439 438 432 432 431 430 428 428 428										
	428 428 427 427 426 425 425 419 419 415									6.25	428
1000	422 418 413 408 408 408 406 404 404 404										
	404 403 402 401 401 401 398 398 398 398									6.53	404
1050	376 375 375 375 369 368 367 367 366 366										
	365 364 364 363 360 360 360 360 359 358									5.77	365

FOR DEGREE OF 1   COEFFICIENTS ARE
     811.01900000   -.41371430
BEST FIT VALUES   480.0   459.4   438.7   418.0   397.3   376.6
STANDARD DEVIATION IS   8.8473850
FOR DEGREE OF 2   COEFFICIENTS ARE
     17.86172000   1.31596100   -.00093496
BEST FIT VALUES   472.3   460.9   444.9   424.2   398.9   368.8
STANDARD DEVIATION IS   6.0223780
FOR DEGREE OF 3   COEFFICIENTS ARE
     1384.15200000   -3.17326700   .00395720   -.00000177
BEST FIT VALUES   472.8   460.0   444.5   424.9   399.8   368.0
STANDARD DEVIATION IS   6.1298710

TABLE : 4.27   TIME =   8 HOURS

TEMP (DEG.C)	HARDNESS (HV30)									SD	AVERAGE (HV30)
800	483 483 481 476 475 475 473 473 472 472										
	472 471 470 470 470 469 469 469 467 467									4.78	472
850	467 461 454 454 454 452 451 451 451 446										
	445 445 444 443 443 443 443 439 431 429									9.00	447
900	453 451 450 446 446 446 444 442 440 440										
	440 439 439 439 438 438 430 429 428 427									7.48	440
950	439 439 439 439 438 438 436 434 433 432										
	431 431 430 429 429 428 428 418 417 417									7.18	431
1000	420 418 408 406 404 403 403 400 399 399										
	399 398 398 396 395 393 390 390 389 389									8.59	399
1050	387 385 385 379 377 375 375 373 373 373										
	372 372 370 368 368 367 367 361 357 356									8.42	372

FOR DEGREE OF 1   COEFFICIENTS ARE
     771.99050000   -.37314290
BEST FIT VALUES   473.5   454.8   436.2   417.5   398.8   380.2
STANDARD DEVIATION IS   9.0453820
FOR DEGREE OF 2   COEFFICIENTS ARE
     106.07270000   1.07905600   -.00078497
BEST FIT VALUES   466.9   456.1   441.4   422.7   400.2   373.6
STANDARD DEVIATION IS   7.8151290
FOR DEGREE OF 3   COEFFICIENTS ARE
     1349.55000000   -3.00664700   .00366745   -.00000161
BEST FIT VALUES   467.4   455.3   441.0   423.3   401.0   372.9
STANDARD DEVIATION IS   8.8030750

EFFECT OF SOAKING TEMPERATURE ON HARDNESS IN A.C. CONDITION

ALLOY : P2 ; AS CAST HARDNESS(HV30)= 464
TABLE : 4.28

TIME = 10 HOURS

TEMP (DEG.C)	HARDNESS (HV30)										SD	AVERAGE (HV30)
800	492	486	483	483	478	478	476	475	474	474		
	473	473	473	470	469	469	467	465	464	464	7.48	474
850	459	459	458	457	456	453	453	451	451	451		
	451	451	451	450	450	449	446	446	446	443	4.50	451
900	444	443	441	440	435	432	431	431	431	431		
	430	430	429	429	429	428	425	420	420	418	7.18	430
950	431	429	427	426	425	425	424	424	424	422		
	422	422	421	421	420	420	418	415	415	413	4.62	422
1000	406	404	402	402	400	399	398	398	396	395		
	392	390	389	389	388	388	386	362	362	353	14.65	389
1050	364	361	358	358	353	352	352	352	351	351		
	350	349	349	348	348	348	345	344	342	329	7.42	350

FOR DEGREE OF 1   COEFFICIENTS ARE

849.59050000   -.46514280

BEST FIT VALUES   477.5   454.2   431.0   407.7   384.4   361.2

STANDARD DEVIATION IS   9.6653530

FOR DEGREE OF 2   COEFFICIENTS ARE

75.47272000   1.22301200   -.00091252

BEST FIT VALUES   469.9   455.7   437.0   413.8   386.0   353.6

STANDARD DEVIATION IS   7.7164170

FOR DEGREE OF 3   COEFFICIENTS ARE

1656.68500000   -3.97238700   .00474920   -.00000205

BEST FIT VALUES   470.5   454.7   436.5   414.5   387.1   352.7

STANDARD DEVIATION IS   8.2355950

ALLOY : P3 ; AS CAST HARDNESS(HV30)= 457
TABLE : 4.29   TIME =   2 HOURS

TEMP (DEG.C)	HARDNESS (HV30)										SD	AVERAGE (HV30)
800	475	473	472	470	470	469	469	469	469	469		
	469	468	468	467	467	466	465	464	462	459	3.64	468
850	464	462	458	448	446	446	445	445	445	445		
	445	445	443	443	441	441	441	438	438	438	7.32	445
900	445	443	443	440	439	436	435	434	433	433		
	431	431	430	430	428	428	428	427	427	426	5.91	433
950	431	428	425	425	425	424	419	418	418	418		
	417	417	416	415	415	415	415	412	403	397	7.93	417
1000	415	413	412	410	410	410	410	409	409	405		
	404	403	403	403	403	402	402	402	401	398	4.73	406
1050	409	408	408	405	401	400	398	394	393	391		
	390	387	387	386	384	384	383	380	378	374	10.56	392

FOR DEGREE OF 1   COEFFICIENTS ARE
    697.99050000   -.29314290
BEST FIT VALUES   463.5   448.8   434.2   419.5   404.8   390.2
STANDARD DEVIATION IS   3.4378740
FOR DEGREE OF 2   COEFFICIENTS ARE
    994.26350000   -.93923940   .00034924
BEST FIT VALUES   466.4   448.2   431.8   417.2   404.3   393.1
STANDARD DEVIATION IS   2.4961930
FOR DEGREE OF 3   COEFFICIENTS ARE
    1285.94400000   -1.89761400   .00139364   -.00000038
BEST FIT VALUES   466.5   448.0   431.7   417.3   404.5   392.9
STANDARD DEVIATION IS   2.8640530

TABLE : 4.30   TIME =   4 HOURS

TEMP (DEG.C)	HARDNESS (HV30)										SD	AVERAGE (HV30)
800	475	470	470	466	464	464	464	462	462	461		
	461	460	459	459	459	458	453	445	445	443	8.32	460
850	459	456	456	449	446	445	445	443	443	442		
	442	441	441	438	436	436	436	436	433	431	7.68	442
900	458	453	451	448	445	445	441	441	441	440		
	440	440	440	440	436	434	432	431	428	427	8.06	440
950	431	429	428	427	426	425	424	424	424	422		
	421	421	420	420	419	418	417	404	403	403	8.20	420
1000	414	411	410	408	408	406	405	405	404	403		
	402	401	401	400	400	400	400	399	394	390	5.68	403
1050	402	402	398	393	391	389	389	386	385	385		
	385	385	384	383	382	382	382	376	376	372	7.97	386

FOR DEGREE OF 1   COEFFICIENTS ARE
    693.15230000   -.28971430
BEST FIT VALUES   461.4   446.9   432.4   417.9   403.4   389.0
STANDARD DEVIATION IS   4.9169340
FOR DEGREE OF 2   COEFFICIENTS ARE
    360.65790000   .43537220   -.00039194
BEST FIT VALUES   458.1   447.5   435.0   420.5   404.1   385.7
STANDARD DEVIATION IS   4.4978910
FOR DEGREE OF 3   COEFFICIENTS ARE
    606.28310000   -.37168020   .00048755   -.00000032
BEST FIT VALUES   458.2   447.4   434.9   420.6   404.3   385.5
STANDARD DEVIATION IS   5.4765380

EFFECT OF SOAKING TEMPERATURE ON HARDNESS IN A.C. CONDITION

ALLOY : P3 ; AS CAST HARDNESS(HV30)= 457
TABLE : 4.31   TIME = 6 HOURS

TEMP (DEG.C)	HARDNESS (HV30)										SD	AVERAGE (HV30)
800	476	472	469	469	464	461	459	458	456	455		
	454	454	452	451	451	449	446	446	431	429	12.05	455
850	461	453	453	446	446	445	444	443	443	443		
	441	441	440	439	438	438	438	438	438	435	6.36	443
900	456	448	445	443	440	439	439	439	439	438		
	438	437	437	436	434	434	429	428	421	419	8.44	436
950	435	433	432	429	428	428	427	426	423	422		
	422	420	420	419	417	413	412	410	410	404	8.53	421
1000	413	404	404	403	403	400	398	397	397	396		
	396	395	394	393	393	393	389	389	386	386	6.74	396
1050	391	389	389	386	386	380	380	379	377	376		
	376	373	373	372	372	371	371	371	368	359	8.16	376

FOR DEGREE OF 1   COEFFICIENTS ARE
     712.40950000   -.31485720
BEST FIT VALUES   460.5   444.8   429.0   413.3   397.6   381.8
STANDARD DEVIATION IS   6.6647550
FOR DEGREE OF 2   COEFFICIENTS ARE
      35.34668000   1.16164600   -.00079811
BEST FIT VALUES   453.9   446.1   434.4   418.6   398.9   375.2
STANDARD DEVIATION IS   3.0737530
FOR DEGREE OF 3   COEFFICIENTS ARE
     296.32350000   .30415260   .00013635   -.00000034
BEST FIT VALUES   454.0   445.9   434.3   418.7   399.1   375.0
STANDARD DEVIATION IS   3.7519760

TABLE : 4.32   TIME = 8 HOURS

TEMP (DEG.C)	HARDNESS (HV30)										SD	AVERAGE (HV30)
800	481	480	478	477	476	473	467	464	464	464		
	464	463	463	461	459	454	453	453	453	451	9.72	464
850	453	453	453	446	444	443	442	441	441	441		
	441	441	441	440	438	438	436	436	432	427	6.55	441
900	443	443	438	428	425	424	421	420	420	419		
	419	417	415	414	412	412	410	410	405	404	11.17	419
950	432	424	424	422	421	421	420	420	417	416		
	415	415	414	413	413	413	413	412	408	398	7.04	416
1000	402	395	393	386	385	385	383	383	381	380		
	380	380	379	379	378	375	373	371	370	369	8.36	381
1050	377	365	365	365	361	361	359	357	357	357		
	357	357	357	356	356	356	356	352	348	331	8.61	357

FOR DEGREE OF 1   COEFFICIENTS ARE
     792.51430000   -.41028570
BEST FIT VALUES   464.3   443.8   423.3   402.7   382.2   361.7
STANDARD DEVIATION IS   7.5061880
FOR DEGREE OF 2   COEFFICIENTS ARE
     447.94600000   .34113070   -.00040817
BEST FIT VALUES   460.9   444.4   426.0   405.5   382.9   358.3
STANDARD DEVIATION IS   7.8886680
FOR DEGREE OF 3   COEFFICIENTS ARE
    1461.15000000   -2.98796000   .00322173   -.00000131
BEST FIT VALUES   461.3   443.8   425.6   405.9   383.6   357.7
STANDARD DEVIATION IS   9.1705970

EFFECT OF SOAKING TEMPERATURE ON HARDNESS IN A.C. CONDITION

ALLOY : P3 ; AS CAST HARDNESS(HV30)= 457
TABLE : 4.33   TIME =   10 HOURS

TEMP (DEG.C)	HARDNESS (HV30)										SD	AVERAGE (HV30)
800	481	480	478	478	477	477	472	470	470	470		
	470	470	469	469	467	466	464	462	449	449	8.74	469
850	465	465	459	457	454	451	451	450	450	450		
	449	448	448	446	445	443	443	442	433	433	8.50	449
900	427	412	412	412	412	411	411	410	408	408		
	408	408	405	405	404	404	403	403	402	400	5.83	408
950	418	415	414	413	412	411	411	409	409	406		
	406	406	405	405	404	404	393	393	391	391	8.08	405
1000	386	384	379	376	373	373	373	372	372	372		
	371	371	370	369	368	366	360	358	356	355	8.26	370
1050	360	344	339	337	335	333	331	330	328	328	—	
	328	326	326	326	325	325	324	322	322	320	9.27	330

FOR DEGREE OF 1   COEFFICIENTS ARE

   899.38100000   −.53428570

BEST FIT VALUES   472.0   445.2   418.5   391.8   365.1   338.4

STANDARD DEVIATION IS   10.0237800

FOR DEGREE OF 2   COEFFICIENTS ARE

   440.11130000   .46726530   −.00054138

BEST FIT VALUES   467.4   446.1   422.1   395.4   366.0   333.9

STANDARD DEVIATION IS   10.5379200

FOR DEGREE OF 3   COEFFICIENTS ARE

   1714.29200000   −3.71931900   .00402098   −.00000165

BEST FIT VALUES   467.9   445.3   421.7   396.0   366.9   333.1

STANDARD DEVIATION IS   12.3242600

Table- 4.34 Summary table of effect of heat treatment on hardness

	SOAKING DURATION (HOURS)														
	ALLOY P1					ALLOY P2					ALLOY P3				
H/T TEMP. DEG.C	2	4	6	8	10	2	4	6	8	10	2	4	6	8	10
800	456	459	468	478	473	465	463	476	472	474	468	460	455	464	469
850	458	461	465	458	450	459	448	456	447	451	445	442	443	441	449
900	456	442	451	442	435	436	434	441	440	430	433	440	436	419	408
950	435	434	432	423	421	429	425	428	431	422	417	420	421	416	405
1000	417	413	397	381	398	413	414	404	399	389	406	403	396	381	370
1050	390	373	363	383	343	402	384	365	372	350	392	386	376	357	330

Table-4.35 Effect of heat treatment on volume fraction of massive carbide

Temp °C	Time (hours)	Volume fraction of massive carbide (Alloy P1) (%)										Ave (%)	S.D
As-Cast		35.8	34.1	31.5	30.6	30.4	29.9	29.2	27.5	27.3	27.0	25.3	6.4
		26.5	25.8	24.9	24.1	21.5	19.3	18.8	15.3	14.1	12.5		
800	2	33.0	31.4	30.5	29.7	26.9	25.9	25.7	25.3	24.5	23.9	23.1	6.2
		23.5	21.9	21.5	21.3	20.9	20.5	19.4	17.6	11.1	7.0		
	4	38.7	29.7	29.6	29.4	27.8	26.2	25.4	25.2	24.4	23.7	23.8	6.0
		23.5	23.3	23.0	22.7	21.8	21.2	17.6	16.9	16.7	8.9		
	6	36.3	25.0	22.8	22.2	21.7	21.1	20.2	19.7	18.4	17.5	17.6	6.6
		17.2	16.8	15.5	14.8	13.6	13.1	11.9	11.2	7.0	5.8		
	8	34.3	28.7	28.7	28.5	27.3	26.8	26.5	25.1	24.7	24.3	22.7	6.0
		23.5	23.2	22.8	21.3	20.7	16.4	14.1	13.2	12.5	12.3		
	10	32.2	31.1	30.4	26.0	24.1	23.5	22.9	22.8	22.4	22.4	21.3	5.8
		21.3	20.6	20.0	19.1	19.1	16.5	15.6	13.4	12.6	10.1		
850	2	35.9	34.2	33.2	32.7	30.7	28.6	28.1	27.3	26.3	25.4	25.9	5.2
		24.7	22.6	22.6	22.5	22.5	22.0	21.0	20.5	19.5	17.4		
	4	30.8	28.7	25.1	23.7	21.8	21.1	20.9	20.6	20.5	20.4	19.9	4.7
		19.0	18.9	18.9	18.0	17.8	17.0	16.4	14.5	13.7	10.1		
	6	25.9	22.6	22.3	19.8	19.2	17.8	17.8	16.9	16.9	16.3	16.2	4.4
		16.1	15.4	15.4	14.8	14.3	13.2	12.9	11.2	8.9	6.8		
	8	18.0	18.0	17.9	17.1	17.0	17.0	16.9	16.3	14.8	13.7	13.6	3.8
		13.2	13.1	13.1	11.6	11.1	10.8	10.3	10.1	7.6	3.4		
	10	26.2	24.3	23.1	21.9	21.8	19.6	18.5	17.0	15.9	15.6	17.0	4.2
		15.6	15.2	14.6	14.3	13.9	13.5	13.0	12.6	12.3	11.9		
900	2	31.9	26.9	26.7	26.2	26.1	25.5	25.2	23.9	23.0	22.6	22.5	4.2
		22.5	21.6	20.8	20.7	20.2	19.5	18.6	18.5	16.9	12.9		
	4	24.4	19.5	19.3	17.1	15.8	15.6	13.7	13.7	13.5	13.2	12.9	4.8
		12.9	12.0	11.9	11.8	9.3	8.9	8.3	6.8	5.7	4.6		
	6	27.0	26.3	24.4	21.3	20.8	20.7	19.8	19.1	19.0	18.8	18.2	4.4
		18.7	16.5	16.2	15.5	14.6	14.4	14.3	13.8	11.6	10.3		
	8	24.3	23.1	23.1	22.7	21.6	21.2	20.8	19.8	19.5	19.3	18.9	3.5
		19.2	19.1	18.0	17.5	17.3	16.6	15.9	15.0	14.6	9.4		
	10	24.7	24.4	22.6	21.9	21.6	20.2	19.9	18.9	17.9	17.8	18.1	3.5
		17.5	17.4	16.9	16.5	15.4	15.0	15.0	13.4	13.1	12.5		

950	2	24.2	22.8	22.1	20.8	19.9	19.8	19.3	19.2	18.8	17.4	17.5	3.5
		17.1	16.9	16.3	15.9	14.1	13.9	13.7	13.2	12.4	12.1		
	4	28.1	22.9	21.7	19.1	18.8	18.5	17.6	16.2	15.5	14.5	15.2	5.3
		14.4	14.2	12.3	11.8	11.6	11.3	11.1	10.6	8.9	4.5		
	6	19.7	19.5	17.4	17.4	16.1	15.6	15.3	14.5	14.2	14.1	13.0	4.1
		12.7	12.2	11.9	11.5	11.3	10.2	9.4	7.8	5.3	4.6		
	8	29.0	23.7	23.5	19.8	19.3	17.2	17.1	17.0	16.5	16.3	16.2	5.2
		16.1	15.6	15.6	14.9	13.6	12.7	11.4	10.1	8.6	6.3		
	10	20.8	20.6	19.9	18.1	18.1	17.8	17.5	17.4	17.1	16.4	14.5	5.0
		15.6	15.5	15.4	12.5	11.3	10.6	10.3	6.9	4.4	3.3		
1000	2	19.8	16.7	16.3	15.5	15.1	15.0	14.3	13.3	13.3	11.7	11.6	4.1
		11.2	9.8	9.6	9.6	9.3	7.5	7.2	6.7	6.6	3.2		
	4	15.8	12.5	12.4	12.3	11.6	10.4	8.9	8.2	7.9	7.5	7.6	3.7
		6.3	6.1	5.3	5.1	4.0	3.7	3.6	3.6	3.4	2.7		
	6	14.1	12.5	11.1	10.7	10.4	10.2	9.8	9.8	9.2	8.8	8.7	2.4
		8.6	8.2	8.1	8.0	7.3	7.2	6.0	6.0	4.7	4.3		
	8	15.5	11.9	11.0	9.7	9.4	9.4	9.3	9.2	9.0	9.0	8.2	2.7
		8.6	8.5	7.2	7.2	6.0	5.5	5.3	5.1	4.6	3.6		
	10	15.2	14.0	13.7	11.2	10.6	10.4	10.1	10.0	9.8	9.5	9.4	2.7
		9.1	8.7	8.6	8.1	8.1	7.3	7.0	6.6	5.8	4.1		
1050	2	24.0	20.7	14.7	14.3	14.3	13.8	11.8	11.1	9.5	9.1	10.5	5.1
		9.0	8.1	7.2	6.9	6.8	6.2	6.0	5.9	5.7	4.1		
	4	21.1	19.1	17.1	15.1	15.1	14.5	14.2	14.0	13.3	12.2	11.9	4.2
		10.6	9.5	9.5	9.2	8.8	7.8	7.7	6.7	6.6	5.9		
	6	16.0	13.2	8.7	7.8	6.9	6.2	6.2	4.8	4.7	4.7	5.4	3.7
		4.7	4.2	3.5	3.3	3.1	2.6	2.5	2.2	2.2	.6		
	8	18.3	15.5	13.5	12.9	12.6	12.4	12.4	12.1	12.0	10.8	9.3	4.3
		6.9	6.8	6.7	6.3	6.0	5.9	5.1	4.7	3.3	2.3		
	10	17.1	15.3	13.7	11.9	7.3	6.9	6.8	6.8	6.6	6.1	6.3	4.6
		4.6	3.7	3.5	3.2	2.9	2.7	2.6	1.9	1.4	1.0		

Table-4.36 Effect of heat treatment on volume fraction of massive carbide

Temp °C	Time (hours)	Volume fraction of massive carbide (Alloy P2) (%)										Ave (%)	S.D
As-Cast		29.0 27.5 25.6 25.3 24.5 23.6 23.4 22.8 21.7 21.1										20.5	4.6
		20.6 18.7 18.6 17.6 16.7 16.5 15.6 15.5 14.7 11.7											
800	2	31.6 31.4 28.9 25.9 24.8 24.5 23.3 22.3 22.0 21.8										22.0	4.8
		21.7 21.1 20.0 19.5 18.9 18.6 17.3 15.8 15.7 14.2											
	4	35.9 30.7 30.1 28.6 26.3 23.8 19.6 17.9 16.0 15.5										18.7	7.6
		15.4 15.0 14.4 13.9 13.7 13.5 13.0 11.1 10.3 8.7											
	6	21.3 18.6 17.3 17.3 16.4 14.9 14.9 13.9 13.9 13.7										13.5	3.4
		13.4 12.7 12.1 11.4 11.3 10.5 10.0 9.9 8.2 7.9											
	8	27.2 26.5 23.7 22.3 22.3 21.9 21.9 21.4 20.6 20.3										20.3	3.3
		20.0 19.9 19.9 18.8 17.9 17.8 17.3 16.3 16.1 13.1											
	10	25.4 25.2 24.3 23.1 21.9 21.4 20.3 20.2 20.0 19.9										19.7	3.8
		19.5 19.5 19.3 19.1 19.0 18.3 18.0 17.6 11.7 9.2											
850	2	22.1 21.5 20.4 19.2 18.2 18.1 17.7 17.1 15.5 15.3										13.0	6.1
		11.9 9.7 9.6 8.7 8.5 7.8 6.6 4.5 3.8 3.1											
	4	22.7 22.4 22.3 21.7 21.6 17.8 17.8 17.6 17.4 17.0										15.3	5.6
		16.6 16.3 15.3 12.5 11.2 10.4 9.4 7.2 6.0 3.7											
	6	22.9 22.8 22.4 19.5 19.2 19.0 19.0 18.8 18.3 18.0										18.1	2.5
		18.0 17.3 17.1 16.6 16.5 15.7 15.4 15.4 15.3 13.9											
	8	23.5 22.7 22.3 21.6 21.1 19.5 19.3 18.1 17.2 16.7										17.0	4.2
		16.6 16.5 15.6 15.4 15.3 15.3 15.1 11.3 8.7 7.9											
	10	22.9 21.9 21.7 21.3 20.9 20.8 20.5 20.2 20.1 19.8										19.3	2.2
		19.8 19.7 18.7 18.4 18.1 17.9 17.8 16.8 15.3 13.9											
900	2	21.8 21.5 21.5 18.6 18.4 18.1 18.0 17.7 17.4 17.3										16.7	3.0
		17.2 16.5 16.0 15.6 14.4 14.0 13.4 12.9 12.5 10.4											
	4	23.1 22.5 21.6 21.3 18.6 17.8 17.6 17.5 16.3 16.3										15.5	4.6
		14.8 14.1 14.1 13.2 13.1 12.8 12.2 11.2 7.4 5.6											
	6	23.3 18.3 17.9 17.7 17.3 16.8 15.9 15.6 15.3 14.6										14.6	3.3
		13.4 13.3 12.9 12.7 12.6 12.6 11.3 10.3 10.1 9.7											
	8	21.3 18.4 18.3 18.0 18.0 17.8 17.1 17.0 16.5 15.7										15.5	2.8
		15.1 15.1 14.5 14.2 13.7 13.6 13.6 11.0 10.9 10.1											
	10	24.2 23.5 23.3 23.1 22.4 21.0 20.9 20.2 19.8 19.7										18.8	3.4
		19.0 17.8 17.2 16.4 15.2 15.1 14.9 14.9 14.5 13.3											

950	2	22.9	21.0	20.8	20.5	19.3	18.8	18.3	17.9	16.6	16.3	15.3	4.7
		16.2	13.9	13.6	12.8	12.2	11.3	10.4	9.4	7.0	6.2		
	4	20.5	19.7	19.3	18.4	17.8	17.8	17.0	16.9	16.3	16.1	15.7	2.7
		16.0	15.2	14.5	14.1	13.6	12.7	12.5	12.3	12.2	11.3		
	6	20.3	19.4	19.4	19.2	19.1	17.9	17.7	17.1	17.1	17.1	15.8	3.3
		16.4	16.1	15.6	15.2	14.3	12.6	12.5	11.1	9.8	8.7		
	8	31.4	19.2	18.1	17.9	17.0	17.0	16.8	15.8	15.8	14.1	15.2	4.7
		13.7	13.3	13.2	13.2	12.8	12.4	12.2	11.7	10.3	7.6		
	10	19.2	18.4	18.2	18.1	17.7	16.0	15.6	15.5	14.9	14.7	14.9	2.5
		14.6	14.3	13.7	13.5	13.3	13.2	12.9	12.8	11.4	9.4		
1000	2	25.1	24.6	20.9	20.0	19.6	17.4	16.0	15.9	15.6	15.3	15.6	4.5
		15.2	14.1	14.1	13.4	13.3	12.2	11.7	9.8	9.1	8.0		
	4	20.8	20.1	19.8	17.0	16.9	16.4	15.6	15.1	15.0	14.6	14.4	3.5
		14.5	13.7	13.2	12.7	12.6	12.3	12.1	11.7	7.8	6.6		
	6	25.5	24.1	21.8	20.2	19.5	17.8	14.3	13.3	12.8	12.6	13.7	5.8
		12.5	12.1	10.8	10.6	8.8	8.4	8.1	7.6	6.3	6.1		
	8	15.7	15.6	15.4	14.6	14.0	12.5	12.4	12.2	12.2	12.0	11.6	2.5
		11.4	11.2	11.0	10.4	10.3	9.1	8.8	8.3	8.2	6.6		
	10	16.0	15.8	15.1	15.0	11.5	11.5	11.0	10.6	10.0	9.9	10.2	3.1
		9.8	9.6	9.6	8.5	7.4	7.3	7.1	6.9	6.6	5.2		
1050	2	22.1	19.7	19.2	18.1	16.1	15.5	15.0	14.7	14.4	14.0	13.9	3.8
		14.0	13.0	12.6	11.1	10.6	10.6	10.5	9.9	9.1	6.9		
	4	22.6	21.8	15.8	13.5	13.4	11.4	11.3	11.0	10.6	10.1	11.1	4.6
		10.1	10.0	9.9	9.7	7.9	7.7	7.4	7.4	4.9	4.5		
	6	12.2	11.9	11.5	10.4	8.2	8.1	7.1	6.5	6.2	6.1	7.1	2.4
		6.1	6.1	5.9	5.8	5.8	5.7	5.7	5.1	4.2	4.2		
	8	12.0	10.9	10.0	8.2	7.8	6.7	6.1	5.9	4.9	4.6	4.9	3.4
		3.7	3.3	3.2	2.7	1.8	1.6	1.3	1.0	.9	.7		
	10	19.0	13.4	11.0	10.0	8.2	8.0	7.9	6.6	5.9	5.7	6.1	4.5
		5.1	4.5	3.2	3.0	2.9	2.8	2.7	2.1	1.0	.0		

Table-4.37 Effect of heat treatment on volume fraction of massive carbide

Temp °C	Time (hours)	Volume fraction of massive carbide (Alloy P3) (%)										Ave (%)	S.D
As-Cast		33.1 31.5 30.3 26.2 25.8 25.6 19.9 16.0 13.2 12.8 12.5 12.4 12.3 10.9 7.8 7.3 7.3 6.2 4.3 4.1										16.0	9.3
800	2	32.3 30.1 30.0 29.7 28.9 27.0 26.0 24.5 22.5 22.0 21.8 21.6 20.0 19.9 19.0 17.4 15.3 14.6 14.0 10.6										22.4	6.0
	4	29.3 26.5 23.1 22.4 21.3 20.4 20.3 19.9 19.9 18.5 18.0 15.9 15.5 14.2 13.6 11.7 11.2 10.4 9.3 7.3										17.4	5.7
	6	24.5 24.1 22.8 22.7 22.6 22.3 21.8 21.1 20.6 20.5 20.0 19.8 19.6 19.2 19.1 18.4 18.1 17.7 17.0 16.8										20.4	2.2
	8	22.0 19.4 18.7 18.6 18.5 18.4 18.4 18.3 17.9 17.7 17.7 17.5 16.9 16.7 16.4 13.9 10.8 10.5 8.2 4.2										16.0	4.2
	10	21.7 21.5 19.1 18.9 17.4 17.2 16.4 16.1 15.7 15.2 15.1 14.9 14.7 13.9 12.1 10.4 10.2 8.8 8.2 7.9										14.8	4.0
850	2	26.4 19.6 18.7 18.2 17.4 17.3 16.7 16.6 16.5 15.5 14.5 14.2 13.8 13.5 13.5 12.6 12.1 11.4 11.0 10.1										15.5	3.6
	4	27.4 19.2 18.3 13.8 13.4 13.3 12.8 12.7 12.4 12.4 11.6 11.3 11.3 10.9 10.2 9.8 9.7 9.5 8.7 8.2										12.8	4.3
	6	22.9 19.8 19.3 19.2 18.4 18.3 18.3 17.7 17.3 16.9 16.9 16.9 16.8 16.0 15.8 14.3 13.2 12.6 12.0 11.4										16.7	2.8
	8	26.5 25.5 24.8 22.9 21.3 20.9 20.6 20.4 19.4 19.2 19.0 18.0 17.7 16.6 16.5 16.2 15.6 15.3 13.2 11.6										19.1	3.9
	10	26.4 23.8 23.7 22.0 19.0 18.1 17.9 17.8 16.6 16.3 16.1 16.0 15.8 15.6 15.4 15.3 15.2 14.6 14.0 12.9										17.6	3.5
900	2	21.5 21.1 20.7 20.5 20.0 19.9 19.9 19.0 18.1 17.9 17.4 17.1 16.6 16.5 16.1 15.5 15.0 15.0 14.6 13.8										17.8	2.3
	4	28.9 20.7 19.0 18.9 18.1 17.6 16.8 15.9 15.8 15.8 15.8 14.8 14.6 14.5 14.5 14.5 13.5 12.8 12.4 10.1										16.2	3.8
	6	28.6 21.5 20.6 20.5 18.7 18.4 17.9 17.2 16.7 16.6 15.5 15.2 12.8 12.7 12.5 11.6 10.9 10.9 10.1 10.0										15.9	4.6
	8	22.8 22.2 21.8 18.5 18.4 18.2 18.1 18.0 17.9 17.9 17.9 17.8 17.0 16.7 15.9 15.5 14.3 11.1 10.6 9.2										17.0	3.5
	10	22.8 21.7 21.6 19.0 18.9 18.3 17.7 17.6 17.5 17.2 16.0 15.5 15.2 14.5 14.1 13.5 13.3 13.2 10.1 8.5										16.3	3.6

950	2	25.8	22.0	21.9	20.2	19.0	18.9	18.7	18.1	18.0	17.8	17.2	4.1
		17.8	17.5	16.7	16.4	16.3	16.1	13.2	12.9	8.2	8.1		
	4	21.9	21.6	19.2	17.5	17.5	17.4	16.7	15.8	15.7	15.4	15.1	3.6
		15.1	15.0	13.9	13.9	13.7	13.1	11.9	11.8	9.0	6.7		
	6	22.8	21.0	20.3	19.2	17.8	17.0	15.7	15.5	15.1	14.4	14.6	4.1
		14.1	14.0	13.7	12.3	11.8	10.7	10.6	10.2	8.1	7.7		
	8	27.3	22.9	20.3	19.6	18.0	17.8	16.8	16.8	16.5	15.7	16.2	3.9
		15.4	14.7	14.0	13.5	13.4	13.3	12.8	12.6	11.6	10.6		
	10	24.2	19.1	17.5	17.5	17.1	16.5	16.5	16.1	15.9	15.7	14.8	3.7
		15.4	15.3	13.2	12.8	11.7	11.6	11.1	9.8	9.7	8.5		
1000	2	20.7	20.3	20.1	18.8	18.7	18.0	17.7	17.5	17.5	14.8	13.7	5.3
		14.1	12.1	11.3	9.8	9.6	9.3	8.3	7.2	5.1	3.3		
	4	17.5	17.3	17.3	17.2	16.6	16.3	15.4	13.8	13.4	13.1	12.1	4.5
		12.8	12.0	10.8	10.5	10.2	9.7	6.9	4.6	4.1	3.5		
	6	19.8	19.1	17.9	13.9	13.2	12.9	12.8	11.9	11.5	11.1	11.2	4.1
		10.4	9.7	9.1	8.9	8.9	7.8	7.7	7.0	5.7	4.7		
	8	21.4	18.6	18.0	17.6	17.1	16.4	16.1	15.9	12.7	12.6	13.1	4.2
		12.3	11.6	11.6	10.9	10.4	9.1	8.7	8.6	6.9	5.9		
	10	22.5	17.7	16.8	16.4	15.0	14.7	13.4	12.1	11.9	11.9	11.6	4.4
		10.0	10.0	9.2	8.5	8.5	8.3	7.7	7.5	6.4	3.6		
1050	2	21.7	20.4	20.2	19.9	19.6	18.2	17.4	16.8	16.3	16.0	15.6	3.5
		15.9	14.1	13.9	12.4	11.9	11.9	11.8	11.5	11.5	10.4		
	4	26.6	21.7	19.4	19.3	16.8	16.3	14.8	14.6	14.5	14.3	14.3	4.7
		14.1	13.8	13.2	11.6	11.3	10.8	10.3	9.3	7.8	6.7		
	6	20.3	18.6	17.5	17.1	15.6	15.6	15.5	13.9	13.3	13.2	12.6	4.2
		12.5	11.2	10.9	10.2	10.0	10.0	9.8	6.8	5.7	4.4		
	8	18.2	17.9	16.8	16.8	16.6	15.5	14.6	14.6	14.0	13.8	12.9	3.5
		13.1	12.4	11.0	10.8	10.8	10.7	8.7	7.7	7.5	6.9		
	10	18.8	18.6	13.5	12.2	12.0	9.6	9.4	9.0	8.8	8.3	8.9	4.2
		7.9	7.6	6.3	5.9	5.9	5.6	5.4	5.0	4.2	3.3		

Table-4.38 Summary table of effect of heat treatment on volume percent of massive carbide

Alloy	Temp °C	S O A K I N G P E R I O D (hours)				
		2	4	6	8	10
P1	800	23.1	23.8	17.6	22.7	21.3
	850	25.9	19.9	16.2	13.6	17.0
	900	22.5	12.9	18.2	18.9	18.1
	950	17.5	15.2	13.0	16.2	14.5
	1000	11.6	7.6	8.7	8.2	9.4
	1050	10.5	11.9	5.4	9.3	6.3
P2	800	22.0	18.7	13.5	20.3	19.7
	850	13.0	15.3	18.1	17.0	19.3
	900	16.7	15.5	14.6	15.5	18.8
	950	15.3	15.7	15.8	15.2	14.9
	1000	15.6	14.4	13.7	11.6	10.2
	1050	13.9	11.1	7.1	4.9	6.1
P3	800	22.4	17.4	20.4	16.0	14.8
	850	15.5	12.8	16.7	19.1	17.6
	900	17.8	16.2	15.9	17.0	18.3
	950	17.2	15.1	14.6	16.2	14.8
	1000	13.7	12.1	11.2	13.1	11.6
	1050	15.6	14.3	12.6	12.9	8.9

Table-4.39 Effect of h/t on the average no. of dispersed carbides in different classes

Alloy	Temp °C	S O A K I N G P E R I O D (hours)																			
		Class I					Class II					Class III					Class IV				
		2	4	6	8	10	2	4	6	8	10	2	4	6	8	10	2	4	6	8	10
P1	800	10	11	11	7	8	5	5	4	6	4	0	0	1	1	1	0	0	0	0	0
	850	8	7	5	10	7	4	3	4	6	5	1	1	1	0	1	0	0	0	0	0
	900	7	13	9	6	9	4	8	4	3	5	1	1	1	3	2	0	0	0	0	0
	950	9	5	6	8	5	6	4	3	2	4	2	1	1	1	1	0	0	1	1	1
	1000	11	6	5	5	6	4	3	2	3	2	0	1	1	0	0	0	0	0	0	1
P2	800	11	9	10	11	8	12	6	7	7	6	1	0	1	1	1	0	0	0	0	0
	850	10	6	9	7	10	8	5	7	7	5	1	1	2	1	1	0	0	0	0	1
	900	8	5	6	7	8	4	3	4	4	3	1	1	2	2	2	0	0	0	0	0
	950	6	5	5	3	3	2	3	3	2	2	1	2	2	2	2	0	0	0	0	0
	1000	4	6	6	8	3	4	3	3	2	2	1	1	0	0	1	0	0	0	0	0
P3	800	13	10	8	8	8	11	10	6	7	5	1	0	1	1	1	0	0	0	0	0
	850	6	6	7	4	6	5	4	4	4	3	1	1	1	1	1	0	0	0	0	0
	900	7	5	7	5	9	2	4	5	3	4	0	2	3	2	0	0	0	0	1	0
	950	7	6	6	10	12	2	4	6	6	2	0	1	2	1	0	0	0	0	0	0
	1000	6	9	6	10	--	2	2	3	2	-	0	0	0	0	-	0	0	0	0	-

Frame area = 207.81 µm²

Table-4.40 Effect of h/t on percent number of dispersed carbides in different classes

Alloy	Temp °C	Class I					Class II					Class III					Class IV				
		2	4	6	8	10	2	4	6	8	10	2	4	6	8	10	2	4	6	8	10
P1	800	67	69	69	50	57	33	31	25	43	29	0	0	6	7	14	0	0	0	0	0
	850	61	64	50	63	54	31	27	40	37	38	8	9	10	0	8	0	0	0	0	0
	900	58	59	64	50	56	34	36	29	25	31	8	5	7	25	13	0	0	0	0	0
	950	53	50	55	66	46	35	40	27	17	36	12	10	9	8	9	0	0	9	8	9
	1000	73	60	62	62	67	27	30	26	38	22	0	10	12	0	0	0	0	0	0	11
P2	800	46	60	55	58	53	50	40	39	37	40	4	0	6	5	7	0	0	0	0	0
	850	53	50	50	47	59	42	42	39	46	29	5	8	11	7	6	0	0	0	0	6
	900	61	56	50	54	62	31	33	33	30	23	8	11	17	16	15	0	0	0	0	0
	950	67	50	56	43	43	22	30	33	29	28	11	20	11	28	29	0	0	0	0	0
	1000	44	60	67	80	50	44	30	33	20	33	11	10	0	0	17	0	0	0	0	0
P3	800	52	50	53	50	57	44	50	40	44	36	4	0	7	6	7	0	0	0	0	0
	850	50	55	58	44	60	42	36	33	44	30	8	9	8	11	10	0	0	0	0	0
	900	78	46	47	46	69	22	36	33	27	31	0	18	20	18	0	0	0	0	0	0
	950	78	55	43	59	86	22	36	43	35	14	0	9	14	6	0	0	0	9	0	0
	1000	75	82	67	83	--	25	18	33	17	--	0	0	0	0	--	0	0	0	0	-

SOAKING PERIOD (hours)

Frame Area = 207.81 μm²

Table-4.41 Effect of h/t on the avarage no. of dispersed carbides

Temp °C	Alloy	Soaking period (hrs) 2	4	6	8	10	Alloy	Soaking period (hrs) 2	4	6	8	10
800	P1	15	16	16	14	14	P2	24	15	18	19	15
850		13	11	10	16	13		19	12	18	15	17
900		12	22	14	12	16		13	9	12	13	13
950		17	10	11	12	11		9	10	9	7	7
1000		15	10	8	8	9		9	10	9	10	6
800	P2	25	20	15	16	14						
850		12	11	12	9	10						
900		9	11	15	11	13						
950		9	11	14	17	14						
1000		8	11	9	12	--						

Table-4.42 Effect of heat treatment on volume percent of
dispersed carbides

Alloy	Temperature °C	S O A K I N G P E R I O D (Hrs)				
		2	4	6	8	10
P1	800	3.61	3.68	4.73	5.64	6.17
	850	4.53	3.87	4.33	4.20	5.05
	900	4.46	7.22	4.59	7.09	6.83
	950	7.42	4.33	7.02	6.56	7.55
	1000	3.08	3.81	3.15	2.10	4.79
P2	800	9.45	4.13	6.43	6.50	5.71
	850	7.02	4.99	8.01	6.23	8.47
	900	4.53	3.74	6.04	6.10	5.58
	950	3.22	5.38	3.74	4.66	4.66
	1000	4.27	3.81	2.17	1.71	3.02
P3	800	8.99	6.56	5.71	6.30	5.12
	850	4.99	4.40	4.46	4.27	3.81
	900	1.64	5.97	8.33	8.60	2.95
	950	1.64	4.40	7.22	5.84	1.97
	1000	1.58	1.77	2.17	1.84	----

Table-4.43 Effect of h/t on the mean diameter
of dispersed carbides

Alloy	Temp °C	Soaking period (hrs)				
		2	4	6	8	10
P1	800	0.48	0.46	0.50	0.61	0.61
	850	0.55	0.55	0.63	0.50	0.60
	900	0.57	0.55	0.53	0.72	0.61
	950	0.62	0.63	0.70	0.62	0.76
	1000	0.44	0.57	0.57	0.50	0.61
P2	800	0.62	0.52	0.57	0.56	0.59
	850	0.59	0.62	0.64	0.63	0.62
	900	0.55	0.61	0.67	0.64	0.60
	950	0.54	0.69	0.61	0.78	0.78
	1000	0.67	0.57	0.48	0.40	0.67
P3	800	0.58	0.57	0.59	0.61	0.57
	850	0.62	0.60	0.57	0.67	0.57
	900	0.41	0.70	0.71	0.81	0.46
	950	0.41	0.60	0.70	0.56	0.37
	1000	0.43	0.39	0.48	0.38	----

Table-4.44 Effect of heat treatment on
Distribution Factor

Heat treatment	P1	P2	P3
800,2	0.394	0.417	0.375
800,4	0.386	0.429	0.500
800,6	0.252	0.321	0.316
800,8	0.331	0.312	0.345
800,10	0.234	0.316	0.288
850,2	0.260	0.345	0.314
850,4	0.239	0.314	0.278
850,6	0.294	0.283	0.267
850,8	0.414	0.361	0.316
850,10	0.299	0.182	0.245
900,2	0.267	0.260	0.378
900,4	0.318	0.255	0.269
900,6	0.255	0.254	0.262
900,8	0.264	0.242	0.177
900,10	0.244	0.222	0.385
950,2	0.263	0.220	0.378
950,4	0.294	0.251	0.278
950,6	0.162	0.255	0.299
950,8	0.145	0.292	0.297
950,10	0.192	0.292	0.429
1000,2	0.376	0.316	0.375
1000,4	0.245	0.245	0.394
1000,6	0.224	0.394	0.394
1000,8	0.414	0.385	0.405
1000,10	0.184	0.254	-----

Table-4.45 Relative coarsening behaviour
of the alloys

Heat treatment	P1	P2	P3
800,2	1.000	1.000	1.000
800,4	0.979	1.028	1.333
800,6	0.639	0.769	0.842
800,8	0.840	0.748	0.920
800,10	0.593	0.757	0.768
850,2	1.000	1.000	1.000
850,4	0.919	0.910	0.885
850,6	1.130	0.820	0.850
850,8	1.592	1.046	1.006
850,10	1.150	0.527	0.780
900,2	1.000	1.000	1.000
900,4	1.191	0.980	0.711
900,6	0.955	0.976	0.693
900,8	0.988	0.930	0.468
900,10	0.913	0.853	1.018
950,2	1.000	1.000	1.000
950,4	1.117	1.140	0.735
950,6	0.615	1.159	0.791
950,8	0.551	1.327	0.785
950,10	0.730	1.327	1.134
1000,2	1.000	1.000	1.000
1000,4	0.651	0.775	1.050
1000,6	0.595	1.246	1.050
1000,8	1.101	1.218	1.080
1000,10	0.489	0.803	-----

Table-4.46 Effect of heat treatment on size and distribution of dispersed carbides (Alloy P1)

Temp °C	Time (hrs)	Hard-ness HV30	MD μm	CLASS I		CLASS II		CLASS III		CLASS IV	
				%area	%NOP	%area	%NOP	%area	%NOP	%area	%NOP
800	2	456	.482	18	66	81	33	0	0	0	0
	4	459	.470	19	68	80	31	0	0	0	0
	6	468	.416	15	68	50	25	34	6	0	0
	8	478	.516	8	50	62	42	29	7	0	0
	10	473	.413	8	57	38	28	53	14	0	0
850	2	458	.445	11	61	52	30	36	7	0	0
	4	461	.420	11	63	45	27	42	9	0	0
	6	465	.491	7	50	54	40	37	10	0	0
	8	458	.506	15	62	84	37	0	0	0	0
	10	450	.489	9	53	58	38	32	7	0	0
900	2	456	.458	10	58	52	33	36	8	0	0
	4	442	.486	11	59	65	36	22	4	0	0
	6	451	.434	12	64	51	28	35	7	0	0
	8	442	.361	5	50	25	25	69	25	0	0
	10	435	.434	8	56	43	31	48	12	0	0
950	2	435	.459	7	52	47	35	44	11	0	0
	4	434	.491	7	50	54	40	37	10	0	0
	6	432	.394	5	54	25	27	23	9	0	9
	8	423	.337	8	66	17	16	25	8	0	8
	10	421	.447	4	45	31	36	21	9	0	9
1000	2	417	.443	23	73	76	26	0	0	0	0
	4	413	.434	10	60	46	30	43	10	0	0
	6	397	.397	10	62	37	25	52	12	0	0
	8	381	.506	15	62	84	37	0	0	0	0
	10	398	.385	8	66	24	22	0	0	0	11

Table-4.47 Effect of heat treatment on size and distribution of dispersed carbides (Alloy P2)

Temp °C	Time (hrs)	Hard-ness HV30	MD μm	CLASS I		CLASS II		CLASS III		CLASS IV	
				%area	%NOP	%area	%NOP	%area	%NOP	%area	%NOP
800	2	465	.566	7	45	75	50	17	4	0	0
	4	463	.520	14	60	85	40	0	0	0	0
	6	476	.498	10	55	64	38	25	5	0	0
	8	472	.487	11	57	63	36	25	5	0	0
	10	474	.501	9	53	62	40	28	6	0	0
850	2	459	.517	9	52	67	42	23	5	0	0
	4	448	.506	7	50	59	41	32	8	0	0
	6	456	.482	7	50	51	38	40	11	0	0
	8	447	.540	7	46	66	46	26	6	0	0
	10	451	.425	7	58	34	29	19	5	0	5
900	2	436	.445	11	61	52	30	36	7	0	0
	4	434	.450	8	55	47	33	43	11	0	0
	6	441	.434	6	50	39	33	54	16	0	0
	8	440	.422	7	53	38	30	53	15	0	0
	10	430	.378	9	61	31	23	58	15	0	0
950	2	429	.385	12	66	36	22	51	11	0	0
	4	425	.405	6	50	32	30	60	20	0	0
	6	428	.450	8	55	47	33	43	11	0	0
	8	431	.372	4	42	25	28	70	28	0	0
	10	422	.372	4	42	25	28	70	28	0	0
1000	2	413	.514	6	44	55	44	38	11	0	0
	4	414	.434	10	60	46	30	43	10	0	0
	6	404	.482	18	66	81	33	0	0	0	0
	8	399	.405	30	80	69	20	0	0	0	0
	10	389	.434	6	50	39	33	54	16	0	0

Table-4.48 Effect of heat treatment on size and distribution of dispersed carbides (Alloy P3)

Temp °C	Time (hrs)	Hard-ness HV30	MD μm	CLASS I		CLASS II		CLASS III		CLASS IV	
				%area	%NOP	%area	%NOP	%area	%NOP	%area	%NOP
800	2	468	.532	9	52	72	44	18	4	0	0
	4	460	.578	9	50	89	50	0	0	0	0
	6	455	.501	9	53	62	40	28	6	0	0
	8	464	.524	8	50	65	43	26	6	0	0
	10	469	.475	10	57	57	35	32	7	0	0
850	2	445	.506	7	50	59	41	32	8	0	0
	4	442	.473	8	54	53	36	37	9	0	0
	6	443	.458	10	58	52	33	36	8	0	0
	8	441	.514	6	44	55	44	38	11	0	0
	10	449	.434	10	60	46	30	43	10	0	0
900	2	433	.418	27	77	71	22	0	0	0	0
	4	440	.447	5	45	39	36	54	18	0	0
	6	436	.424	5	46	35	33	59	20	0	0
	8	419	.368	3	45	20	27	38	18	0	9
	10	408	.467	20	69	80	30	0	0	0	0
950	2	417	.418	27	77	71	22	0	0	0	0
	4	420	.473	8	54	53	36	37	9	0	0
	6	421	.496	5	42	49	42	45	14	0	0
	8	416	.476	11	58	60	35	28	5	0	0
	10	405	.372	39	85	59	14	0	0	0	0
1000	2	406	.434	25	75	74	25	0	0	0	0
	4	403	.394	33	81	66	18	0	0	0	0
	6	396	.482	18	66	81	33	0	0	0	0
	8	381	.385	35	83	64	16	0	0	0	0

Table-4.49 Effect of h/t on the contribution of Distribution Factor
of different classes (Alloy P1)

Temp °C	Time (hrs)	Hardness HV30	MD μm	Volume fraction of DC	Contribution of from various classes				Total DF
					CLASS I	CLASS II	CLASS III	CLASS IV	
800	2	456	.482	3.609	.121	.273	.000	.000	.394
	4	459	.470	3.675	.135	.251	.000	.000	.386
	6	468	.416	4.725	.105	.125	.022	.000	.252
	8	478	.516	5.644	.041	.269	.021	.000	.331
	10	473	.413	6.169	.049	.109	.076	.000	.234
850	2	458	.445	4.528	.071	.161	.028	.000	.260
	4	461	.420	3.872	.076	.125	.039	.000	.239
	6	465	.491	4.331	.038	.218	.038	.000	.294
	8	458	.506	4.200	.098	.316	.000	.000	.414
	10	450	.489	5.053	.049	.225	.025	.000	.299
900	2	456	.458	4.463	.060	.176	.031	.000	.267
	4	442	.486	7.219	.070	.238	.010	.000	.318
	6	451	.434	4.594	.083	.147	.026	.000	.255
	8	442	.361	7.088	.028	.063	.174	.000	.264
	10	435	.434	6.825	.049	.135	.060	.000	.244
950	2	435	.459	7.416	.042	.169	.052	.000	.263
	4	434	.491	4.331	.038	.218	.038	.000	.294
	6	432	.394	7.022	.031	.069	.021	.042	.162
	8	423	.337	6.563	.053	.030	.021	.041	.145
	10	421	.447	7.547	.020	.114	.020	.039	.192
1000	2	417	.443	3.084	.172	.204	.000	.000	.378
	4	413	.434	3.806	.062	.140	.043	.000	.245
	6	397	.397	3.150	.065	.094	.065	.000	.224
	8	381	.506	2.100	.098	.316	.000	.000	.414
	10	398	.385	4.791	.055	.055	.000	.075	.184

Table-4.50 Effect of h/t on the contribution of Distribution Factor of different classes (Alloy P2)

Temp °C	Time (hrs)	Hardness HV30	MD μm	Volume fraction of DC	Contribution of from various classes				Total DF
					CLASS I	CLASS II	CLASS III	CLASS IV	
800	2	465	.566	9.450	.035	.375	.007	.000	.417
	4	463	.520	4.134	.086	.343	.000	.000	.429
	6	476	.498	6.431	.057	.250	.014	.000	.321
	8	472	.487	6.497	.064	.234	.013	.000	.312
	10	474	.501	5.709	.049 -	.248	.019	.000	.316
850	2	459	.517	7.022	.049	.283	.012	.000	.345
	4	448	.506	4.988	.039	.247	.027	.000	.314
	6	456	.482	8.006	.037	.201	.046	.000	.283
	8	447	.540	6.234	.034	.309	.018	.000	.361
	10	451	.425	8.466	.046	.103	.011	.022	.182
900	2	436	.445	4.528	.071	.161	.028	.000	.260
	4	434	.450	3.741	.049	.158	.049	.000	.255
	6	441	.434	6.038	.033	.130	.091	.000	.254
	8	440	.422	6.103	.041	.119	.083	.000	.242
	10	430	.378	5.578	.058	.073	.090	.000	.222
950	2	429	.385	3.216	.082	.082	.057	.000	.220
	4	425	.405	5.381	.030	.099	.122	.000	.251
	6	428	.450	3.741	.049	.158	.049	.000	.255
	8	431	.372	4.659	.018	.072	.201	.000	.292
	10	422	.372	4.659	.018	.072	.201	.000	.292
1000	2	413	.514	4.266	.027	.246	.043	.000	.316
	4	414	.434	3.806	.062	.140	.043	.000	.245
	6	404	.482	2.166	.121	.273	.000	.000	.394
	8	399	.405	1.706	.246	.138	.000	.000	.385
	10	389	.434	3.019	.033	.130	.091	.000	.254

Table-4.51 Effect of h/t on the contribution of Distribution Factor of different classes (Alloy P3)

Temp °C	Time (hrs)	Hardness HV30	MD μm	Volume fraction of DC	Contribution of from various classes				Total DF
					CLASS I	CLASS II	CLASS III	CLASS IV	
800	2	468	.532	8.991	.049	.318	.007	.000	.375
	4	460	.578	6.563	.050	.450	.000	.000	.500
	6	455	.501	5.709	.049	.248	.019	.000	.316
	8	464	.524	6.300	.042	.287	.016	.000	.345
	10	469	.475	5.119	.059	.206	.023	.000	.288
850	2	445	.506	4.988	.039	.247	.027	.000	.314
	4	442	.473	4.397	.049	.195	.034	.000	.278
	6	443	.458	4.463	.060	.176	.031	.000	.267
	8	441	.514	4.266	.027	.246	.043	.000	.316
	10	449	.434	3.806	.062	.140	.043	.000	.245
900	2	433	.418	1.641	.218	.160	.000	.000	.378
	4	440	.447	5.972	.025	.144	.100	.000	.269
	6	436	.424	8.334	.026	.118	.118	.000	.262
	8	419	.368	8.597	.017	.056	.069	.034	.177
	10	408	.467	2.953	.138	.246	.000	.000	.385
950	2	417	.418	1.641	.218	.160	.000	.000	.378
	4	420	.473	4.397	.049	.195	.034	.000	.278
	6	421	.496	7.219	.023	.210	.065	.000	.299
	8	416	.476	5.841	.066	.214	.017	.000	.297
	10	405	.372	1.969	.343	.086	.000	.000	.429
1000	2	406	.434	1.575	.188	.188	.000	.000	.375
	4	403	.394	1.772	.273	.121	.000	.000	.394
	6	396	.482	2.166	.121	.273	.000	.000	.394
	8	381	.385	1.838	.298	.107	.000	.000	.405

Table-4.52 Effect of heat treatment on the percent distribution factor in different classes

H/T temp. Deg.C	SOAKING TIME																			
	2 hours				4 hours				6 hours				8 hours				10 hours			
	I	II	III	IV	I	II	III	IV	I	II	III	IV	I	II	III	IV	I	II	III	IV
Alloy P1																				
800	30	69	0	0	27	61	10	0	22	66	11	0	16	64	19	0	45	54	0	0
850	34	65	0	0	31	52	16	0	21	74	3	0	12	74	12	0	25	57	17	0
900	41	49	8	0	12	74	12	0	32	57	9	0	18	42	13	25	29	41	29	0
950	12	81	6	0	23	76	0	0	10	23	65	0	36	20	14	28	23	76	0	0
1000	20	46	32	0	16	75	8	0	19	55	24	0	10	59	10	20	29	29	0	40
Alloy P2																				
800	8	89	1	0	14	82	3	0	27	62	10	0	37	37	25	0	8	77	13	0
850	20	79	0	0	12	78	8	0	19	61	19	0	12	39	48	0	25	57	17	0
900	17	77	4	0	13	70	16	0	12	51	35	0	19	61	19	0	30	69	0	0
950	20	75	4	0	9	85	4	0	16	49	34	0	6	24	68	0	63	35	0	0
1000	15	78	6	0	25	56	6	12	26	33	40	0	6	24	68	0	12	51	35	0
Alloy P3																				
800	13	84	1	0	12	78	8	0	57	42	0	0	57	42	0	0	50	49	0	0
850	10	89	0	0	17	70	12	0	9	53	37	0	17	70	12	0	69	30	0	0
900	15	78	6	0	22	66	11	0	9	45	45	0	7	70	21	0	30	69	0	0
950	12	83	4	0	8	77	13	0	9	31	39	19	22	72	5	0	73	26	0	0
1000	20	71	7	0	25	57	17	0	36	63	0	0	80	20	0	0	.	.	.	.

Table-4.53 Relative contribution of the factors constituting
the model

ALLOY: P1

Heat treatment		Overall hardness HV30	First factor		Second factor	
			value	%	value	%
800	2	468	464	99.15	4	0.85
800	4	473	464	98.10	9	1.90
800	6	477	464	97.27	13	2.73
800	8	481	464	96.47	17	3.53
800	10	486	464	95.47	22	4.53
850	2	453	452	99.78	1	0.22
850	4	454	452	99.56	2	0.44
850	6	456	452	99.12	4	0.88
850	8	457	452	98.91	5	1.09
850	10	458	452	98.69	6	1.31
900	2	441	442	99.77	-1	0.23
900	4	439	442	99.32	-3	0.68
900	6	437	442	98.86	-5	1.14
900	8	435	442	98.39	-7	1.61
900	10	433	442	97.92	-9	2.08
950	2	429	433	99.07	-4	0.93
950	4	424	433	97.88	-9	2.12
950	6	419	433	96.66	-14	3.34
950	8	414	433	95.41	-19	4.59
950	10	409	433	94.13	-24	5.87
1000	2	416	424	98.08	-8	1.92
1000	4	408	424	96.08	-16	3.92
1000	6	400	424	94.00	-24	6.00
1000	8	392	424	91.84	-32	8.16
1000	10	384	424	89.58	-40	10.42
1050	2	406	417	97.29	-11	2.71
1050	4	395	417	94.43	-22	5.57
1050	6	384	417	91.41	-33	8.59
1050	8	373	417	88.20	-44	11.80
1050	10	362	417	84.81	-55	15.19

Table-4.54 Relative contribution of the factors constituting the model

ALLOY: P2

Heat treatment		Overall hardness HV30	First factor value	%	Second factor value	%
800	2	465	461	99.14	4	0.86
800	4	469	461	98.29	8	1.71
800	6	473	461	97.46	12	2.54
800	8	477	461	96.65	16	3.35
800	10	481	461	95.84	20	4.16
850	2	451	450	99.78	1	0.22
850	4	452	450	99.56	2	0.44
850	6	454	450	99.12	4	0.88
850	8	455	450	98.90	5	1.10
850	10	456	450	98.68	6	1.32
900	2	439	440	99.77	−1	0.23
900	4	437	440	99.31	−3	0.69
900	6	436	440	99.08	−4	0.92
900	8	434	440	98.62	−6	1.38
900	10	433	440	98.38	−7	1.62
950	2	427	431	99.06	−4	0.94
950	4	423	431	98.11	−8	1.89
950	6	418	431	96.89	−13	3.11
950	8	414	431	95.88	−17	4.11
950	10	409	431	94.62	−22	5.38
1000	2	415	422	98.31	−7	1.69
1000	4	408	422	96.57	−14	3.43
1000	6	401	422	94.76	−21	5.24
1000	8	393	422	92.62	−29	7.38
1000	10	386	422	90.67	−36	9.33
1050	2	405	415	97.53	−10	2.47
1050	4	395	415	94.94	−20	5.06
1050	6	385	415	92.21	−30	7.79
1050	8	375	415	89.33	−40	10.67
1050	10	365	415	86.30	−50	13.70

Table-4.55 Relative contribution of the factors constituting the model

ALLOY: P3

Heat treatment		Overall hardness HV30	First value	factor %	Second value	factor %
800	2	460	458	99.57	2	0.43
800	4	461	458	99.35	3	0.65
800	6	463	458	98.92	5	1.08
800	8	465	458	98.49	7	1.51
800	10	466	458	98.28	8	1.72
850	2	446	447	100.22	−1	0.22
850	4	444	447	100.68	−3	0.68
850	6	443	447	100.90	−4	0.90
850	8	441	447	101.36	−6	1.36
850	10	440	447	101.59	−7	1.59
900	2	434	438	99.08	−4	0.92
900	4	429	438	97.90	−9	2.10
900	6	424	438	96.70	−14	3.30
900	8	419	438	95.47	−19	4.53
900	10	414	438	94.20	−24	5.80
950	2	422	430	98.10	−8	1.90
950	4	414	430	96.14	−16	3.86
950	6	406	430	94.09	−24	5.91
950	8	398	430	91.96	−32	8.04
950	10	390	430	89.74	−40	10.26
1000	2	411	422	97.32	−11	2.68
1000	4	400	422	94.50	−22	5.50
1000	6	388	422	91.24	−34	8.76
1000	8	377	422	88.06	−45	11.94
1000	10	365	422	84.38	−57	15.62
1050	2	401	415	96.51	−14	3.49
1050	4	386	415	92.49	−29	7.51
1050	6	371	415	88.14	−44	11.86
1050	8	357	415	83.75	−58	16.25
1050	10	342	415	78.65	−73	21.35

Table-4.56 Effect of temperature and time on hardness (Alloy P1)

H/T	Experi-mental hardness HV30	Original model equation (4.25)			model according to equation (4.31)			model according to equation (4.28)		
		(a)	(b)	(c)	(a)	(b)	(c)	(a)	(b)	(c)
800,2	456	468	-12	-2.6	464	-8	-1.7	455	1	.2
850,2	458	453	5	1.1	449	9	2.0	440	18	4.1
900,2	456	440	16	3.6	435	21	4.8	426	30	7.0
950,2	435	427	8	1.9	422	13	3.1	413	22	5.3
1000,2	417	416	1	.2	411	6	1.5	401	16	4.0
1050,2	390	405	-15	-3.7	400	-10	-2.5	389	1	.3
800,4	459	472	-13	-2.8	467	-8	-1.7	460	-1	-.2
850,4	461	454	7	1.5	449	12	2.7	441	20	4.5
900,4	442	438	4	.9	431	11	2.6	424	18	4.2
950,4	434	422	12	2.8	415	19	4.6	407	27	6.6
1000,4	413	408	5	1.2	400	13	3.3	392	21	5.4
1050,4	373	394	-21	-5.3	386	-13	-3.4	378	-5	-1.3
800,6	468	476	-8	-1.7	470	-2	-.4	464	4	.9
850,6	465	456	9	2.0	448	17	3.8	442	23	5.2
900,6	451	436	15	3.4	428	23	5.4	422	29	6.9
950,6	432	417	15	3.6	408	24	5.9	402	30	7.5
1000,6	396	400	-4	-1.0	389	7	1.8	384	12	3.1
1050,6	363	383	-20	-5.2	371	-8	-2.2	366	-3	-.8
800,8	478	481	-3	-.6	473	5	1.1	468	10	2.1
850,8	458	457	1	.2	448	10	2.2	443	15	3.4
900,8	442	434	8	1.8	424	18	4.2	419	23	5.5
950,8	423	413	10	2.4	401	22	5.5	397	26	6.5
1000,8	381	392	-11	-2.8	379	2	.5	375	8	1.6
1050,8	383	372	11	3.0	357	26	7.3	354	29	8.2
800,10	473	485	-12	-2.5	477	-4	-.8	473	0	.0
850,10	450	458	-8	-1.7	448	2	.4	444	6	1.4
900,10	435	432	3	.7	420	15	3.6	417	18	4.3
950,10	421	408	13	3.2	394	27	6.9	391	30	7.7
1000,10	398	384	14	3.6	368	30	8.2	367	31	8.4
1050,10	343	361	-18	-5.0	343	0	.0	343	0	.0

		C.C = 0.945			C.C = 0.942			C.C = 0.945		
		S.D = 11.39			S.D = 15.18			S.D = 19.11		
		MAX.DEV.= 21			MAX.DEV.= 30			MAX.DEV.= 31		

(a) represents the calculated hardness value from the model
(b) represents the deviation of the calculated hardness from the experimental hardness
(c) represents the % deviation of the calculated hardness from the observed hardness

Table-4.57 Effect of temperature and time on hardness (Alloy P2)

H/T	Experimental hardness HV30	Original model equation (4.26)			model according to equation (4.32)			model according to equation (4.29)		
		(a)	(b)	(c)	(a)	(b)	(c)	(a)	(b)	(c)
800,2	465	465	0	.0	464	1	.2	464	1	.2
850,2	459	451	8	1.8	449	10	2.2	450	9	2.0
900,2	436	438	-2	-.5	436	0	.0	436	0	.0
950,2	429	426	3	.7	424	5	1.2	424	5	1.2
1000,2	414	415	-1	-.2	412	2	.5	412	2	.5
1050,2	402	404	-2	-.5	402	0	.0	401	1	.2
800,4	463	469	-6	-1.3	467	-4	-.9	467	-4	-.9
850,4	448	452	-4	-.9	449	-1	-.2	449	-1	-.2
900,4	434	436	-2	-.5	433	1	.2	432	2	.5
950,4	425	421	4	1.0	418	7	1.7	417	8	1.9
1000,4	414	407	7	1.7	403	11	2.7	402	12	3.0
1050,4	384	394	-10	-2.5	389	-5	-1.3	388	-4	-1.0
800,6	476	473	3	.6	470	6	1.3	469	7	1.5
850,6	456	453	3	.7	450	6	1.3	448	8	1.8
900,6	441	434	7	1.6	430	11	2.6	428	13	3.0
950,6	428	417	11	2.6	411	17	4.1	410	18	4.4
1000,6	404	400	4	1.0	394	10	2.5	392	12	3.1
1050,6	365	384	-19	-4.9	377	-12	-3.2	375	-10	-2.7
800,8	472	477	-5	-1.0	474	-2	-.4	471	1	.2
850,8	447	454	-7	-1.5	450	-3	-.7	447	0	.0
900,8	440	433	7	1.6	427	13	3.0	425	15	3.5
950,8	431	412	19	4.6	405	26	6.4	403	28	6.9
1000,8	399	393	6	1.5	384	15	3.9	382	17	4.5
1050,8	372	374	-2	-.5	364	8	2.2	362	10	2.8
800,10	474	481	-7	-1.5	477	-3	-.6	473	1	.2
850,10	451	455	-4	-.9	450	1	.2	446	5	1.1
900,10	430	431	-1	-.2	424	6	1.4	421	9	2.1
950,10	422	408	14	3.4	399	23	5.8	396	26	6.6
1000,10	389	385	4	1.0	375	14	3.7	372	17	4.6
1050,10	350	364	-14	-3.8	352	-2	-.6	349	1	.3

		C.C = 0.97			C.C = 0.967			C.C = 0.986		
		S.D = 7.88			S.D = 9.98			S.D = 11.07		
		MAX.DEV.= 19			MAX.DEV.= 26			MAX.DEV.= 28		

(a) represents the calculated hardness value from the model
(b) represents the deviation of the calculated hardness from the experimental hardness
(c) represents the % deviation of the calculated hardness from the observed hardness

Table-4.58 Effect of temperature and time on hardness (Alloy P3)

H/T	Experimental hardness HV30	Original model equation (4.27)			model according to equation (4.33)			model according to equation (4.30)		
		(a)	(b)	(c)	(a)	(b)	(c)	(a)	(b)	(c)
800,2	468	460	8	1.7	467	1	.2	468	0	.0
850,2	445	446	-1	-.2	449	-4	-.9	449	-4	-.9
900,2	433	434	-1	-.2	433	0	.0	433	0	.0
950,2	417	422	-5	-1.2	418	-1	-.2	418	-1	-.2
1000,2	406	411	-5	-1.2	404	2	.5	404	2	.5
1050,2	392	401	-9	-2.2	391	1	.3	392	0	.0
800,4	460	462	-2	-.4	468	-8	-1.7	468	-8	-1.7
850,4	442	445	-3	-.7	446	-4	-.9	447	-5	-1.1
900,4	440	430	10	2.3	427	13	3.0	427	13	3.0
950,4	420	415	5	1.2	409	11	2.7	409	11	2.7
1000,4	403	401	2	.5	392	11	2.8	392	11	2.8
1050,4	386	387	-1	-.3	376	10	2.7	376	10	2.7
800,6	455	465	-10	-2.2	468	-13	-2.8	468	-13	-2.8
850,6	443	445	-2	-.4	443	0	.0	444	-1	-.2
900,6	436	426	10	2.3	421	15	3.6	421	15	3.6
950,6	421	407	14	3.4	399	22	5.5	400	21	5.3
1000,6	396	390	6	1.5	379	17	4.5	380	16	4.2
1050,6	376	373	3	.8	360	16	4.4	361	15	4.2
800,8	464	467	-3	-.6	468	-4	-.9	468	-4	-.9
850,8	441	444	-3	-.7	440	1	.2	441	0	.0
900,8	419	422	-3	-.7	414	5	1.2	415	4	1.0
950,8	416	400	16	4.0	390	26	6.7	390	26	6.7
1000,8	381	380	1	.3	367	14	3.8	367	14	3.8
1050,8	357	360	-3	-.8	345	12	3.5	345	12	3.5
800,10	469	470	-1	-.2	468	1	.2	468	1	.2
850,10	449	443	6	1.4	437	12	2.7	438	11	2.5
900,10	408	418	-10	-2.4	408	0	.0	409	-1	-.2
950,10	405	393	12	3.1	381	24	6.3	381	24	6.3
1000,10	370	369	1	.3	354	16	4.5	355	15	4.2
1050,10	330	346	-16	-4.6	329	1	.3	329	1	.3

C.C = 0.976
S.D = 7.33
MAX.DEV.= 16

C.C = 0.974
S.D = 11.65
MAX.DEV.= 26

C.C = 0.974
S.D = 11.42
MAX.DEV.= 26

(a) represents the calculated hardness value from the model
(b) represents the deviation of the calculated hardness from the experimental hardness
(c) represents the % deviation of the calculated hardness from the observed hardness

Table- 4.59 Massive carbide based Heterogeneity Index of the alloys as influenced by heat treating parameters

SOAKING DURATION (hours)

H/T Temp. °C	Alloy P1					Alloy P2					Alloy P3				
	2	4	6	8	10	2	4	6	8	10	2	4	6	8	10
800	.320	.270	.290	.368	.352	.367	.374	.342	.316	.315	.371	.347	.385	.320	.390
850	.375	.304	.312	.352	.397	.429	.397	.367	.361	.327	.299	.301	.327	.347	.351
900	.294	.326	.355	.312	.388	.354	.350	.325	.336	.418	.407	.270	.333	.343	.338
950	.385	.300	.365	.306	.386	.378	.390	.379	.263	.338	.312	.320	.364	.317	.313
1000	.333	.383	.330	.309	.324	.357	.335	.398	.375	.388	.409	.428	.361	.362	.315
1050	.343	.374	.320	.361	.383	.335	.339	.403	.404	.317	.416	.316	.352	.411	.364
AS-CAST	0.367					0.354					0.429				

Table- 4.60 Dispersed second phase based Heterogeneity Index of the alloys as influenced by heat treating parameters

SOAKING DURATION (hours)

H/T Temp. °C	Alloy P1					Alloy P2					Alloy P3				
	2	4	6	8	10	2	4	6	8	10	2	4	6	8	10
800	.31	.35	.50	.19	.53	.10	.20	.22	.25	.22	.15	.10	.22	.17	.28
850	.38	.48	.26	.24	.25	.18	.21	.29	.14	.43	.21	.30	.34	.22	.43
900	.34	.25	.43	.77	.45	.38	.38	.49	.51	.67	.58	.46	.55	.68	.36
950	.36	.26	.58	.79	.41	.63	.61	.38	.75	.75	.58	.30	.29	.28	.80
1000	.46	.43	.58	.24	.71	.22	.43	.31	.64	.49	.50	.69	.31	.74	--

TABLE-5.1 PHASES UNDER CONSIDERATION

X-RAY WAVE LENGTH(A°)=   1.9373

NO. (S)	ASTM CODE	PHASE(S)	LATTICE TYPE	LATTICE PARAMETER A	B	C
1	06-0696	ALPHA IRON	CUBIC(BCC)	2.8684	.0000	.0000
2	23-298	AUSTENITE	CUBIC(FCC)	3.6000	.0000	.0000
3	-------	MARTENSITE	CUBIC(BCT)	-----	-----	-----
4	14-0407	CR23C6	CUBIC	10.6380	.0000	.0000
5	--------	MN23C6	-------	-----	-----	-----
6	23-1113	FE3C(CEMENTITE)	ORTHORHOMBIC	4.5144	5.0787	6.7297
7	20-509	FE5C2	MONOCLINIC	11.5630	4.5730	5.0580
8	20-508	FE5C2(HAGG)	MONOCLINIC	11.5600	4.5600	5.0300
9	14-176	MN5C2	MONOCLINIC	5.0860	4.5730	11.6600
10	16-0038	MN5C2(PD5B2)	MONOCLINIC	11.6600	4.5730	5.0860
11	17-333	FE7C3(2)	HEXAGONAL	6.8820	.0000	4.5400
12	-------	CR7C3(2)	HEXAGONAL	13.9000	.0000	4.5400
13	11-0550	CR7C3	HEXAGONAL(TR)	13.9800	.0000	4.5230
14	05-0720	(CR,FE)7C3	HEXAGONAL	13.9800	.0000	4.5230
15	03-0975	(CR7C3+MN7C3)	-------	2.2220	.0000	.0000
16	14-519	CR2C	HEXAGONAL	2.7900	.0000	4.4600
17	14-406	CR3C2	ORTHORHOMBIC	11.4600	5.5200	2.8210
18	26-782	FE2C(NETA)	ORTHORHOMBIC	4.7040	4.2180	2.8300
19	20-522	FE0.6MN5.4C2	HEXAGONAL	5.7700	.0000	6.9800
20	23-0064	C(GRAPHITE)	HEXAGONAL	2.4630	.0000	6.7140
21	13-534	FE2O3	RHOMBOHEDRAL	5.0340	.0000	13.7520
22	13-504	CR2O3	HEXAGONAL	4.9540	.0000	13.5840
23	26-1116	CU2S(1)	HEAXGONAL	3.9610	.0000	36.7220
24	06-518	MNS	CUBIC	5.2236	.0000	.0000
25	04-836	COPPER	CUBIC	3.6150	.0000	.0000
26	26-798	FE8SI2C	TRICLINIC	6.3470	6.4140	9.7200
27	05-0708	FE-CR	TETRAGONAL	8.7990	.0000	4.5440
28	06-645	CRMN3	TETRAGONAL	8.8000	.0000	4.5880
29	20-706	MN15C4	HEXAGONAL	7.4920	.0000	12.0700
30	17-897	FE2C	MONOCLINIC	2.7940	2.7940	4.3600

TABLE-5.2   SUMMARY TABLE OF DIFFRACTOGRAM INDEXING

ALLOY: P1:   (AS-CAST)

```
DIFF.                              PHASE(S)                                    INT
ANGLE   1  3  5  7  9 11 13 15 17 19 21 23 25 27 29

47.5   0 0 0 0 0 0 0 0 0 0 0 0 0 0 0 1 0 1 0 0 0 0 1 0 0 0 0 0 1 1    4.0
49.2   0 0 0 0 0 0 0 0 0 0 0 0 0 0 0 0 0 0 1 0 0 0 0 0 0 1 0 1 0 0    4.0
50.2   0 0 0 0 0 0 1 0 1 1 0 0 1 0 0 0 0 0 0 0 1 0 0 0 0 0 0 1 1 0    5.0
51.4   0 0 0 0 0 0 0 0 0 0 0 0 0 0 0 1 0 0 0 0 0 0 0 0 0 0 0 0 0 0    3.0
54.4   0 0 0 0 0 0 1 0 1 1 1 0 1 1 1 0 0 1 0 1 0 0 0 0 0 0 1 0 1 1    6.0
54.9   0 0 0 0 0 1 0 0 0 0 0 1 0 0 0 1 1 0 1 0 1 0 0 0 0 0 0 0 1 1   16.0
56.5   0 0 0 1 1 0 1 0 0 0 0 0 1 1 1 0 0 0 0 0 1 0 0 0 1 0 0 0 0 0    3.0
61.9   0 0 0 1 1 0 0 0 0 0 0 0 0 0 0 0 1 0 0 0 0 0 1 0 0 1 1 1 0 0    3.0
62.6   0 0 0 0 0 1 0 0 0 0 0 0 0 0 1 0 1 0 0 0 0 0 0 0 0 0 0 0 1 0    3.0
64.1   0 0 0 0 0 0 1 0 1 1 1 1 0 0 0 0 0 0 1 0 0 0 0 0 0 1 1 0 0 0   49.0
65.2   0 1 0 1 1 0 0 1 0 0 0 0 0 0 0 0 0 0 1 0 0 0 0 1 0 0 1 0 1 0    4.0
98.0   0 0 0 0 0 0 0 0 0 0 0 0 0 0 0 0 0 0 0 0 0 1 0 0 0 0 0 0 0 0    9.0
113.0  0 0 0 0 0 0 0 1 0 0 0 0 0 1 0 0 1 0 0 1 0 0 1 0 0 0 0 0 0 0    3.0
117.1  0 0 0 0 0 0 0 0 0 0 0 0 0 0 0 0 0 0 0 0 0 0 0 0 0 0 0 0 0 0    3.0
124.4  0 0 0 0 0 0 0 0 0 0 0 0 0 0 0 0 0 0 0 0 0 0 0 0 0 0 0 0 0 0   44.0
126.2  0 0 0 1 0 0 0 0 0 0 0 0 0 0 0 0 0 0 0 1 0 0 0 0 0 0 0 0 0 0    5.0
127.0  0 1 0 0 0 0 0 0 0 0 0 0 0 0 0 0 0 0 0 0 0 0 1 0 0 0 0 0 0 0    4.0

       0 2 0 3 4 2 4 2 3 3 2 2 3 3 3 2 5 2 3 2 2 2 4 0 0 5 3 3 6 3
```

0 = ABSENT   1 = PRESENT   * = PROBABLE DIFF. ANGLE FOR K-BETA RADIATION

DETAILED ANALYSIS OF PHASE(S) ACTUALLY PRESENT

S.N.	PHASE PRESENT	DIFF. ANGLE	PEAK INT	I/IO	D MEAS	D STD	DIFF PLANE	INT STD	CONF LIMIT
(1)	AUSTENITE	65.2	8	100	1.798	1.800	200	80	99.9
		127.0	8	100	1.083	1.083	311	80	99.9
(2)	FE3C(CEMENTITE)	54.9	32	100	2.102	2.100	121	60	99.9
		62.6	6	18	1.865	1.870	113	30	99.8
(3)	FE5C2	50.2	10	10	2.284	2.287	020	20	99.9
		54.4	12	12	2.120	2.112	112	25	99.8
		56.5	6	6	2.047	2.049	510	100	99.9
		64.1	100	100	1.826	1.821	511	20	99.8
(4)	MN5C2	50.2	10	10	2.284	2.277	020	40	99.8
		54.4	12	12	2.120	2.121	211	80	100.0
		64.1	100	100	1.826	1.831	115	60	99.8
(5)	CR7C3	50.2	10	83	2.284	2.280	411	70	99.9
		54.4	12	100	2.120	2.120	202	70	100.0
		56.5	6	50	2.047	2.040	421	100	99.8
(6)	(CR,FE)7C3	54.4	12	100	2.120	2.120	202	60	100.0
		56.5	6	50	2.047	2.040	122	100	99.8
		113.0	6	50	1.162	1.160	750	60	99.7
(7)	(CR7C3+MN7C3)	54.4	12	100	2.120	2.120	555	100	100.0
		56.5	6	50	2.047	2.040	666	100	99.8
		62.6	6	50	1.865	1.860	888	100	99.8
(8)	FE8SI2C	49.2	8	8	2.328	2.320	104	40	99.8
		56.5	6	6	2.047	2.050	121	80	99.9
		61.9	6	6	1.884	1.880	331	60	99.9
		64.1	100	100	1.826	1.820	031	20	99.8
		65.2	8	8	1.798	1.794	312	20	99.8
(9)	CRMN3	49.2	8	80	2.328	2.340	311	40	99.7
		50.2	10	100	2.284	2.272	002	60	99.7
		61.9	6	60	1.884	1.888	777	90	99.9

TABLE-5.3 SUMMARY TABLE OF DIFFRACTOGRAM INDEXING

ALLOY: P1;   H/T TEMPERATURE: 800°C ;   SOAKING DURATION: 6 HOURS

```
DIFF.                          PHASE(S)                                    INT
ANGLE  1  3  5  7  9 11 13 15 17 19 21 23 25 27 29

51.8   0 0 0 0 0 0 0 0 1 1 0 0 1 0 0 1 1 0 1 0 0 0 0 0 0 1 0 0 1 0    4.0
54.7   0 0 0 0 0 1 1 0 0 1 0 1 0 0 0 1 1 0 1 0 0 0 0 0 0 0 0 0 0 1   10.0
55.5   0 1 0 0 0 0 1 0 1 1 0 0 0 0 0 0 0 0 0 0 0 0 0 0 1 1 0 0 0 0   31.0
57.3   1 0 1 0 0 1 0 1 1 1 1 1 1 0 0 0 0 0 1 0 0 0 0 0 1 0 1 0        5.0
58.7   0 0 0 0 0 1 0 1 0 1 0 0 0 0 0 0 0 0 0 0 0 1 0 0 1 0 1 0 0      5.0
63.0   0 0 0 0 0 1 0 0 0 0 0 0 0 0 1 0 1 0 0 0 0 0 1 0 0 0 0 0        3.0
64.2   0 0 0 0 0 0 1 0 1 1 1 1 0 0 0 0 0 1 0 0 1 0 0 0 1 1 0 0        4.0
64.8   0 0 0 0 0 0 1 0 0 0 1 0 1 1 0 0 1 0 0 0 0 0 0 0 1 1 0 0       20.0
66.1   0 0 0 1 0 0 0 0 0 1 0 0 1 0 1 0 1 0 0 0 0 0 0 0 1 0 0 1 0      3.0
98.8   0 0 0 0 0 0 0 0 0 0 0 0 0 0 0 0 0 0 0 0 0 0 0 1 0 0 0 0 0      7.0
125.5  0 0 0 0 0 0 0 1 0 0 0 0 0 0 0 0 0 0 0 0 0 0 0 0 1 0 0 0 0      8.0

       0 0 0 0 0 4 4 3 4 7 3 3 4 0 2 2 5 0 3 0 0 1 0 0 4 6 2 0 3 1
```

0 = ABSENT 1 = PRESENT * = PROBABLE DIFF. ANGLE FOR K-BETA RADIATION

DETAILED ANALYSIS OF PHASE(S) ACTUALLY PRESENT

S.N.	PHASE PRESENT	DIFF. ANGLE	PEAK INT	I/IO	D MEAS	D STD	DIFF PLANE	INT STD	CONF LIMIT
(1)	FE3C(CEMENTITE)	54.7	32	100	2.109	2.100	121	60	99.7
		57.3	16	50	2.021	2.020	022	60	100.0
		58.7	16	50	1.977	1.970	211	55	99.8
		63.0	9	30	1.854	1.850	122	40	99.8
(2)	FE5C2	54.7	32	32	2.109	2.112	112	25	99.9
		55.5	100	100	2.081	2.080	021	70	100.0
		64.2	12	12	1.823	1.821	511	20	99.9
		64.8	64	64	1.808	1.814	312	25	99.8
(3)	MN5C2(PD5B2)	51.8	12	12	2.218	2.212	112	80	99.8
		54.7	32	32	2.109	2.117	112	70	99.8
		55.5	100	100	2.081	2.078	021	100	99.9
		57.3	16	16	2.021	2.016	312	80	99.8
		58.7	16	16	1.977	1.972	600	80	99.8
		64.2	12	12	1.823	1.820	312	70	99.9
		66.1	9	9	1.777	1.779	402	70	99.9
(4)	FE7C3(2)	57.3	16	25	2.021	2.019	121	100	99.9
		64.2	12	20	1.823	1.820	301	10	99.9
		64.8	64	100	1.808	1.807	022	20	99.9
(5)	CR7C3	51.8	12	20	2.218	2.220	102	50	100.0
		57.3	16	25	2.021	2.020	---	50	100.0
		64.8	64	100	1.808	1.810	431	70	99.9
		66.1	9	15	1.777	1.780	521	50	99.9
(6)	COPPER	55.5	100	100	2.081	2.088	111	100	99.8
		64.8	64	64	1.808	1.808	200	46	100.0
		98.8	22	22	1.276	1.278	220	20	99.8
		125.5	25	25	1.090	1.090	311	17	99.9
(7)	FE8SI2C	51.8	12	12	2.218	2.220	014	40	100.0
		55.5	100	100	2.081	2.080	131	80	100.0
		58.7	16	16	1.977	1.970	212	60	99.8
		64.2	12	12	1.823	1.820	031	20	99.9
		64.8	64	64	1.808	1.810	015	20	99.9
		66.1	9	9	1.777	1.780	301	20	99.9
(8)	MN15C4	51.8	12	80	2.218	2.209	204	50	99.8
		57.3	16	100	2.021	2.012	006	50	99.7
		66.1	9	60	1.777	1.772	116	50	99.8

TABLE-5.4   SUMMARY TABLE OF DIFFRACTOGRAM INDEXING

ALLOY: P1;   H/T TEMPERATURE: 850°C ;   SOAKING DURATION: 6 HOURS

```
DIFF.                          PHASE(S)                                       INT
ANGLE  1  3  5  7  9  11 13 15 17 19 21 23 25 27 29
-------------------------------------------------------------------------------
 47.9  0 0 0 0 1 1 0 1 0 0 0 0 0 0 1 1 0 0 0 0 0 0 1 0 0 0 0 0 0 0          8.0
 54.6  0 0 0 0 0 0 1 0 1 1 1 0 1 1 1 1 1 1 1 1 0 0 0 0 0 0 0 0 0 0          7.0
 55.1  0 0 0 0 0 1 0 0 0 0 0 1 0 0 0 0 0 0 0 0 0 0 0 0 1 1 0 0 1 1         25.0
 55.8  0 1 1 0 0 0 1 0 0 1 0 0 0 0 0 0 0 0 0 1 0 0 0 0 0 1 1 1 0 0         12.0
 58.5  0 0 0 0 0 0 0 1 0 1 1 1 0 0 0 0 1 0 0 0 0 0 1 0 0 1 0 0 0 0          4.0
 59.4  0 0 0 0 0 0 1 0 0 0 0 0 1 0 0 0 0 0 0 0 0 0 0 0 1 1 0 0 0 0          8.0
 64.8  0 0 0 0 0 0 1 0 0 0 1 0 1 1 0 0 1 0 0 0 0 0 0 0 1 1 0 0 0 0         12.0
 98.7  0 0 0 0 0 0 0 0 0 0 0 0 0 0 0 0 0 0 0 0 0 0 0 0 1 0 0 0 0 0          8.0
112.3  0 0 0 0 0 0 0 0 0 0 0 0 0 0 0 1 0 0 0 0 0 0 0 1 0 0 0 0 0 1          3.0
117.2  0 0 0 0 0 0 0 0 0 0 0 0 0 0 0 0 0 0 0 0 0 0 0 0 0 0 0 0 0 0          4.0
125.4  0 0 0 0 0 0 0 1 0 0 0 0 0 0 0 0 0 0 0 0 0 0 0 0 1 0 0 0 0 0         13.0
125.8  0 0 0 0 1 0 0 0 0 0 0 0 0 0 0 0 0 0 0 0 0 0 0 0 1 0 0 0 0 1         12.0
-------------------------------------------------------------------------------
       0 0 0 0 2 2 4 3 0 3 3 2 3 2 2 3 3 0 0 0 0 0 2 0 4 5 2 0 0 3
```

0 = ABSENT   1 = PRESENT   * = PROBABLE DIFF. ANGLE FOR K-BETA RADIATION

DETAILED ANALYSIS OF PHASE(S) ACTUALLY PRESENT

S.N.	PHASE PRESENT	DIFF. ANGLE	PEAK INT	I/IO	D MEAS	D STD	DIFF PLANE	INT STD	CONF LIMIT
(1)	FE3C(CEMENTITE)	47.9	32	32	2.387	2.380	112	65	99.9
		55.1	100	100	2.095	2.100	121	60	99.9
(2)	FE5C2	54.6	28	58	2.113	2.112	112	25	100.0
		55.8	48	100	2.071	2.080	021	70	99.7
		59.4	32	66	1.956	1.950	221	45	99.8
		64.8	48	100	1.808	1.814	312	25	99.8
(3)	MN5C2(PD5B2)	54.6	28	58	2.113	2.117	112	70	99.9
		55.8	48	100	2.071	2.078	021	100	99.8
		58.5	16	33	1.983	1.990	511	80	99.8
(4)	FE7C3(2)	54.6	28	58	2.113	2.122	012	40	99.7
		58.5	16	33	1.983	1.989	300	16	99.8
		64.8	48	100	1.808	1.807	022	20	99.9
(5)	CR7C3	54.6	28	58	2.113	2.120	202	70	99.8
		59.4	32	66	1.956	1.960	511	70	99.9
		64.8	48	100	1.808	1.810	431	70	99.9
(6)	(CR,FE)7C3	54.6	28	58	2.113	2.120	202	60	99.8
		64.8	48	100	1.808	1.810	431	60	99.9
(7)	(CR7C3+MN7C3)	47.9	32	100	2.387	2.380	333	80	99.9
		54.6	28	87	2.113	2.120	555	100	99.8
(8)	CU2S(1)	47.9	32	100	2.387	2.401	102	88	99.7
		58.5	16	50	1.983	1.980	110	100	99.9
(9)	COPPER	55.1	100	100	2.095	2.088	111	100	99.8
		64.8	48	48	1.808	1.808	200	46	100.0
		98.7	32	32	1.277	1.278	220	20	99.9
		125.4	52	52	1.090	1.090	311	17	100.0
(10)	FE8SI2C	55.1	100	100	2.095	2.090	130	80	99.9
		55.8	48	48	2.071	2.070	210	80	100.0
		58.5	16	16	1.983	1.980	114	60	99.9
		59.4	32	32	1.956	1.960	224	60	99.9
		64.8	48	48	1.808	1.810	015	20	99.9

TABLE-5.5   SUMMARY TABLE OF DIFFRACTOGRAM INDEXING

ALLOY: P1;   H/T TEMPERATURE: 900°C ;   SOAKING DURATION: 2 HOURS

DIFF. ANGLE	PHASE(S) (1 3 5 7 9 11 13 15 17 19 21 23 25 27 29)	INT
51.5	0 0 0 0 0 0 0 0 0 0 0 1 0 0 1 1 0 0 0 0 0 0 0 0 1 0 0 0 0	4.0
52.5	0 0 0 0 0 1 1 1 0 1 0 0 0 0 0 0 0 0 0 0 1 0 0 0 0 1 0 1 0 1	4.0
54.4	0 0 0 0 0 0 1 0 1 1 1 0 1 1 1 1 1 1 0 1 0 0 0 0 0 0 1 0 1 1	7.0
55.0	0 0 0 0 0 1 0 0 0 0 0 1 0 0 0 0 0 0 1 0 0 0 0 0 1 1 0 0 1 1	5.0
55.6	0 1 0 0 0 0 1 0 1 1 0 0 0 0 0 0 0 0 0 0 1 0 0 0 1 0 1 0 0 0	5.0
56.8	0 0 0 0 0 0 0 1 1 1 0 0 1 1 1 0 0 0 0 1 0 0 0 0 0 0 0 1 1 0	3.0
* 60.5	0 0 0 0 0 0 0 0 1 0 0 0 0 0 0 0 0 0 0 0 0 0 0 0 1 1 1 0 0	5.0
62.7	0 0 0 0 0 1 0 0 0 0 0 0 0 0 1 0 1 0 0 0 0 0 0 0 0 0 0 0 0 0	5.0
64.5	0 0 0 0 0 0 1 0 1 1 1 1 1 1 0 0 1 0 0 0 0 1 0 0 1 0 0 0 0	61.0
65.6	0 0 0 0 0 0 0 0 0 0 0 1 0 0 0 0 0 0 0 0 0 0 0 0 1 0 0 1 0	4.0
69.7	0 0 0 0 0 0 0 0 1 1 0 0 0 0 0 0 1 0 0 0 1 0 0 0 1 0 0 0 0	3.0
98.8	0 0 0 0 0 0 0 0 0 0 0 0 0 0 0 0 0 0 0 0 0 0 0 0 0 0 0 0 0 0	5.0
125.2	0 0 0 0 0 0 0 1 0 0 0 0 0 0 0 0 0 0 0 0 0 0 0 0 1 0 0 0 0 0	25.0
	0 0 0 0 0 4 4 3 6 6 2 3 5 3 3 2 5 0 0 2 3 0 0 0 2 8 3 4 5 3	

0 = ABSENT   1 = PRESENT   * = PROBABLE DIFF. ANGLE FOR K-BETA RADIATION

DETAILED ANALYSIS OF PHASE(S) ACTUALLY PRESENT

S.N.	PHASE PRESENT	DIFF. ANGLE	PEAK INT	I/IO	D MEAS	D STD	DIFF PLANE	INT STD	CONF LIMIT
(1)	FE3C(CEMENTITE)	52.5	6	80	2.191	2.200	120	25	99.8
		55.0	8	100	2.098	2.100	121	60	100.0
		62.7	8	100	1.862	1.870	113	30	99.7
(2)	FE5C2	52.5	6	6	2.191	2.190	202	30	100.0
		54.4	11	11	2.120	2.112	112	25	99.8
		55.6	8	8	2.078	2.080	021	70	99.9
		64.5	100	100	1.816	1.814	312	25	99.9
(3)	MN5C2	54.4	11	11	2.120	2.121	211	80	100.0
		55.6	8	8	2.078	2.084	120	80	99.8
		56.8	4	4	2.037	2.034	204	60	99.9
		60.5	8	8	1.923	1.920	006	60	99.9
		64.5	100	100	1.816	1.818	213	60	99.9
		69.7	4	4	1.696	1.697	215	60	99.9
(4)	FE7C3(2)	54.4	11	11	2.120	2.122	012	40	99.9
		64.5	100	100	1.816	1.820	301	10	99.8
(5)	CR7C3	51.5	6	6	2.230	2.220	102	50	99.7
		54.4	11	11	2.120	2.120	202	70	100.0
		56.8	4	4	2.037	2.040	421	100	99.9
		64.5	100	100	1.816	1.810	431	70	99.8
(6)	(CR7C3+MN7C3)	54.4	11	100	2.120	2.120	555	100	100.0
		56.8	4	42	2.037	2.040	666	100	99.9
		62.7	8	71	1.862	1.860	888	100	99.9
(7)	COPPER	55.0	8	20	2.098	2.088	111	100	99.7
		125.2	40	100	1.091	1.090	311	17	99.8
(8)	CRMN3	52.5	6	80	2.191	2.200	400	40	99.8
		55.6	8	100	2.078	2.069	330	100	99.7
		56.8	4	60	2.037	2.036	202	70	100.0
		60.5	8	100	1.923	1.918	331	90	99.8
(9)	MN15C4	54.4	11	100	2.120	2.129	301	10	99.7
		55.0	8	71	2.098	2.094	213	100	99.9
		56.8	4	42	2.037	2.037	302	100	100.0
		65.6	6	57	1.789	1.789	222	50	100.0

TABLE-5.6 SUMMARY TABLE OF DIFFRACTOGRAM INDEXING

ALLOY: P1;   H/T TEMPERATURE: 900°C ;   SOAKING DURATION: 6 HOURS

```
DIFF.                          PHASE(S)                                         INT
ANGLE   1  3  5  7  9 11 13 15 17 19 21 23 25 27 29

 47.6   0 0 0 0 0 0 1 0 0 0 0 0 0 0 1 0 0 0 0 0 0 1 0 0 0 0 1 1        6.0
 54.0   0 0 0 0 0 0 0 0 0 0 0 0 1 0 0 0 0 0·0 0 1 0 0 0 0 0 0 1 1 1 1  8.0
 54.8   0 0 0 0 0 1 1 0 0 0 0 1 0 0 0 0 1 1 0 1 0 0 0 0 0 0 0 0 1      6.0
 55.3   0 1 0 0 0 0 1 0 1 0 0 0 0 0 0 0 0 0 0 0 0 0 0 1 1 0 0 1 0     43.0
 55.8   0 0 1 0 0 0 0 0 0 1 0 0 0 0 0 0 0 0 0 1 0 0 0 0 1 1 1 0 0      8.0
 56.8   0 0 0 0 0 0 0 1 1 1 0 0 1 1 1 0 0 0 0 1 0 0 0 0 0 0 1 1 0      5.0
 58.5   0 0 0 0 0 0 0 1 0 1 1 1 0 0 0 0 1 0 0 0 0 0 1 0 0 1 0 0 0 0    8.0
 64.6   0 0 0 0 0 0 1 0 1 1 1 1 1 1 0 0 1 0 0 0 0 1 0 0 1 1 0 0 0 0    8.0
 98.6   0 0 0 0 0 0 0 0 0 0 0 0 1 0 0 0 1 0 0 0 0 0 0 0 1 0 0 0 0      8.0
112.7   0 0 0 0 0 0 0 0 0 0 0 0 0 0 0 0 0 0 0 0 0 0 0 0 0 0 0 0 1      4.0
113.2   0 0 0 0 0 0 0 1 0 0 0 1 0 1 0 0 1 0 0 0 1 0 0 0 1 0 0 0 0 0    4.0
125.5   0 0 0 0 0 0 0 1 0 0 0 0 0 0 0 0 0 0 0 0 0 0 0 0 1 0 0 0 0 0   16.0
126.0   0 0 0 0 1 0 0 0 0 0 0 0 0 0 0 0 0 0 0 0 0 0 1 0 0 0 0 0 0 1   10.0

        0 0 0 0 0 0 3 5 3 4 2 4 4 3 0 2 5 0 0 2 2 2 0 4 4 2 3 4 5
```

0 = ABSENT   1 = PRESENT   * = PROBABLE DIFF. ANGLE FOR K-BETA RADIATION

DETAILED ANALYSIS OF PHASE(S) ACTUALLY PRESENT

S.N.	PHASE PRESENT	DIFF. ANGLE	PEAK INT	I/IO	D MEAS	D STD	DIFF PLANE	INT STD	CONF LIMIT
(1)	FE5C2	54.8	13	13	2.106	2.112	112	25	99.8
		55.3	100	100	2.088	2.080	021	70	99.8
		64.6	18	18	1.813	1.814	312	25	100.0
(2)	MN5C2	55.3	100	100	2.088	2.084	120	80	99.9
		56.8	11	11	2.037	2.034	204	60	99.9
		64.6	18	18	1.813	1.818	213	60	99.8
(3)	FE7C3(2)	58.5	18	100	1.983	1.989	300	16	99.8
		64.6	18	100	1.813	1.807	022	20	99.7
(4)	CR7C3(2)	54.8	13	75	2.106	2.100	012	60	99.8
		58.5	18	100	1.983	1.990	300	20	99.8
		64.6	18	100	1.813	1.820	301	30	99.7
		113.2	9	50	1.160	1.159	330	30	99.8
(5)	(CR,FE)7C3	56.8	11	62	2.037	2.040	122	100	99.9
		64.6	18	100	1.813	1.810	431	60	99.9
		113.2	9	50	1.160	1.160	750	60	99.9
(6)	COPPER	55.3	100	100	2.088	2.088	111	100	100.0
		64.6	18	18	1.813	1.808	200	46	99.8
		98.6	18	18	1.278	1.278	220	20	100.0
		125.5	37	37	1.090	1.090	311	17	99.9 ·
(7)	FE8SI2C	55.3	100	100	2.088	2.080	131	80	99.8
		55.8	18	18	2.071	2.070	210	80	100.0
		58.5	18	18	1.983	1.980	114	60	99.9
		64.6	18	18	1.813	1.810	015	20	99.9
(8)	CRMN3	54.0	18	100	2.134	2.132	410	100	99.9
		55.8	18	100	2.071	2.069	330	100	99.9
		56.8	11	62	2.037	2.036	202	70	100.0
(9)	MN15C4	47.6	13	13	2.401	2.404	211	50	99.9
		54.0	18	18	2.134	2.129	301	10	99.9
		55.3	100	100	2.088	2.094	213	100	99.8
		56.8	11	11	2.037	2.037	302	100	100.0

TABLE-5.7   SUMMARY TABLE OF DIFFRACTOGRAM INDEXING

ALLOY: P1;   H/T TEMPERATURE: 900°C ;   SOAKING DURATION: 10 HOURS

DIFF. ANGLE	1	3	5	7	9	11	13	15	17	19	21	23	25	27	29	INT
53.5	0 0	0 0	0 0	0 0	0 0	0 0	0 1	0 0	1 0	0 0	0 0	0 0	0 0	0 1	1 0	6.0
54.4	0 0	0 0	0 0	1 0	1 1	1 0	1 1	1 1	1 1	0 1	0 0	0 0	0 0	1 0	1 1	4.0
55.2	0 0	0 0	0 1	0 0	1 0	0 1	0 0	0 0	0 0	0 0	0 0	0 0	1 1	0 0	1 0	22.0
56.6	0 0	0 1	1 0	1 0	1 1	0 0	1 1	1 0	0 0	0 0	1 0	0 0	1 0	1 1	1 0	4.0
57.2	1 0	1 0	0 1	0 1	1 1	1 1	1 0	0 0	0 0	1 0	0 0	0 0	0 1	0 0	0 0	6.0
64.5	0 0	0 0	0 0	1 0	1 1	1 1	1 1	0 0	1 0	0 0	0 1	0 0	1 0	0 0	0 0	7.0
98.5	0 0	0 0	0 0	0 0	0 0	0 0	1 0	0 0	1 0	0 0	0 0	1 0	1 0	0 0	0 0	5.0
100.4	0 0	0 0	0 0	0 0	0 0	0 0	1 0	1 0	1 0	0 0	0 0	0 0	0 0	0 0	0 0	8.0
119.8	0 0	0 0	0 0	0 0	0 0	0 0	0 0	0 0	0 0	1 0	0 1	0 0	0 0 0 0	0 0	5.0
125.4	0 0	0 0	0 0	0 1	0 0	0 0	0 0	0 0	0 0	0 0	0 0	0 0	1 0	0 0	0 0	14.0
126.2	0 0	0 0	1 0	0 0	0 0	0 0	0 0	0 0	0 0	0 0	0 0	1 0	0 0	0 0	0 0	8.0

```
        0 0 0 0 2 2 3 2 5 4 3 3 6 3 4 0 4 2 0 3 0 3 2 0 3 3 2 2 4 0
```

0 = ABSENT   1 = PRESENT   * = PROBABLE DIFF. ANGLE FOR K-BETA RADIATION

DETAILED ANALYSIS OF PHASE(S) ACTUALLY PRESENT

S.N.	PHASE PRESENT	DIFF. ANGLE	PEAK INT	I/IO	D MEAS	D STD	DIFF PLANE	INT STD	CONF LIMIT
(1)	FE3C(CEMENTITE)	55.2	100	100	2.091	2.100	121	60	99.8
		57.2	27	27	2.024	2.020	022	60	99.9
(2)	FE5C2	54.4	18	57	2.120	2.112	112	25	99.8
		56.6	18	57	2.044	2.049	510	100	99.8
		64.5	31	100	1.816	1.814	312	25	99.9
(3)	MN5C2	54.4	18	18	2.120	2.121	211	80	100.0
		55.2	100	100	2.091	2.084	120	80	99.8
		56.6	18	18	2.044	2.034	204	60	99.7
		57.2	27	27	2.024	2.019	213	100	99.8
		64.5	31	31	1.816	1.818	213	60	99.9
(4)	FE7C3(2)	54.4	18	57	2.120	2.122	012	40	99.9
		57.2	27	85	2.024	2.019	121	100	99.8
		64.5	31	100	1.816	1.820	301	10	99.8
(5)	CR7C3	54.4	18	50	2.120	2.120	202	70	100.0
		56.6	18	50	2.044	2.040	421	100	99.9
		57.2	27	75	2.024	2.020	---	50	99.9
		64.5	31	87	1.816	1.810	431	70	99.8
		98.5	22	62	1.279	1.280	---	60	99.9
		100.4	36	100	1.261	1.260	---	70	99.9
(6)	(CR7C3+MN7C3)	53.5	27	75	2.153	2.150	444	40	99.9
		54.4	18	50	2.120	2.120	555	100	100.0
		56.6	18	50	2.044	2.040	666	100	99.9
		100.4	36	100	1.261	1.260	555	60	99.9
(7)	COPPER	55.2	100	100	2.091	2.088	111	100	99.9
		98.5	22	22	1.279	1.278	220	20	99.9
		125.4	63	63	1.090	1.090	311	17	100.0
(8)	FE8SI2C	55.2	100	100	2.091	2.090	130	80	100.0
		56.6	18	18	2.044	2.050	121	80	99.8
		64.5	31	31	1.816	1.810	015	20	99.8
(9)	CRMN3	53.5	27	100	2.153	2.162	321	40	99.8
		56.6	18	66	2.044	2.036	202	70	99.8
(10)	MN15C4	53.5	27	27	2.153	2.163	300	50	99.7
		54.4	18	18	2.120	2.129	301	10	99.7
		55.2	100	100	2.091	2.094	213	100	99.9
		56.6	18	18	2.044	2.037	302	100	99.8

TABLE-5.8   SUMMARY TABLE OF DIFFRACTOGRAM INDEXING

ALLOY: P1;   H/T TEMPERATURE: 950°C ;   SOAKING DURATION: 2 HOURS

DIFF. ANGLE	1		3		5		7		9		11		13		15		17		19		21		23		25		27		29		INT
47.8	0	0	0	0	1	1	0	1	0	0	0	0	0	0	1	1	0	0	0	0	0	0	1	0	0	0	0	0	1	1	8.0
54.7	0	0	0	0	0	1	1	0	0	1	0	1	0	0	0	1	1	0	1	0	0	0	0	0	0	0	0	0	0	1	5.0
55.3	0	1	0	0	0	0	1	0	1	1	0	0	0	0	0	0	0	0	0	0	0	0	0	0	1	1	0	0	1	0	46.0
57.3	1	0	1	0	0	1	0	1	1	1	1	1	1	0	0	0	0	0	0	1	0	0	0	0	0	0	1	0	1	0	7.0
58.7	0	0	0	0	0	1	0	1	0	1	0	0	0	0	0	0	0	0	0	0	0	0	1	0	0	1	0	1	0	0	5.0
64.4	0	0	0	0	0	0	1	0	1	1	1	1	0	0	0	0	0	1	0	0	1	0	0	0	1	0	0	0	0	0	8.0
70.2	0	0	0	0	1	0	0	0	0	1	0	0	0	0	0	0	0	1	0	0	0	1	0	0	0	0	0	0	0	0	6.0
70.6	0	0	0	0	0	1	0	0	0	0	0	0	0	0	0	0	0	1	0	1	0	1	1	0	0	1	0	0	0	0	6.0
96.2	0	0	0	0	0	0	0	0	0	0	0	0	0	0	0	0	0	1	0	0	0	0	0	0	0	0	0	0	0	0	5.0
97.0	0	0	0	1	0	0	0	0	0	0	0	0	0	0	0	0	0	1	0	0	1	1	0	0	0	0	0	0	0	0	4.0
98.4	0	0	0	0	0	0	0	0	0	0	0	0	1	0	0	1	0	0	0	0	0	1	0	1	0	0	0	0	0	0	8.0
*113.2	0	0	0	0	0	0	0	1	0	0	0	1	0	1	0	0	1	0	0	1	0	0	0	1	0	0	0	0	0	0	6.0
113.7	0	0	0	0	0	0	0	0	0	0	0	0	0	0	0	0	0	0	0	0	1	0	0	0	0	0	0	0	0	1	6.0
114.7	0	0	0	0	0	0	0	0	0	0	0	0	0	0	0	1	1	0	0	0	0	0	0	0	0	0	0	0	0	0	4.0
115.1	0	0	0	0	0	0	0	0	0	0	0	0	0	0	0	0	0	0	0	0	0	1	0	0	0	0	0	0	0	0	6.0
125.4	0	0	0	0	0	0	0	1	0	0	0	0	0	0	0	0	0	0	0	0	0	0	0	1	0	0	0	0	0	0	9.0
125.8	0	0	0	0	1	0	0	0	0	0	0	0	0	0	0	0	0	0	0	0	0	0	1	0	0	0	0	0	0	1	7.0
	0	0	0	0	3	5	3	5	3	6	2	4	2	0	0	2	5	3	3	3	2	5	5	0	3	4	0	0	3	4	

0 = ABSENT   1 = PRESENT   * = PROBABLE DIFF. ANGLE FOR K-BETA RADIATION

DETAILED ANALYSIS OF PHASE(S) ACTUALLY PRESENT

S.N.	PHASE PRESENT	DIFF. ANGLE	PEAK INT	I/I0	D MEAS	D STD	DIFF PLANE	INT STD	CONF LIMIT
(1)	FE3C(CEMENTITE)	47.8	17	100	2.392	2.380	112	65	99.8
		54.7	10	62	2.109	2.100	121	60	99.7
		57.3	15	87	2.021	2.020	022	60	100.0
		58.7	10	62	1.977	1.970	211	55	99.8
		70.6	13	75	1.677	1.680	023	16	99.8
(2)	FE5C2	54.7	10	10	2.109	2.112	112	25	99.9
		55.3	100	100	2.088	2.080	021	70	99.8
		64.4	17	17	1.818	1.814	312	25	99.8
(3)	MN5C2	55.3	100	100	2.088	2.084	120	80	99.9
		57.3	15	15	2.021	2.019	213	100	99.9
		64.4	17	17	1.818	1.818	213	60	100.0
(4)	FE7C3(2)	57.3	15	87	2.021	2.019	121	100	99.9
		64.4	17	100	1.818	1.820	301	10	99.9
(5)	CR7C3(2)	54.7	10	62	2.109	2.100	012	60	99.7
		57.3	15	87	2.021	2.020	121	100	100.0
		64.4	17	100	1.818	1.820	301	30	99.9
		113.2	13	75	1.160	1.159	330	30	99.8
(6)	COPPER	55.3	100	100	2.088	2.088	111	100	100.0
		98.4	17	17	1.280	1.278	220	20	99.8
		125.4	19	19	1.090	1.090	311	17	100.0
(7)	FE8SI2C	55.3	100	100	2.088	2.080	131	80	99.8
		58.7	10	10	1.977	1.970	212	60	99.8
		64.4	17	17	1.818	1.820	031	20	99.9
		70.6	13	13	1.677	1.680	233	20	99.8
(8)	MN15C4	47.8	17	17	2.392	2.404	211	50	99.7
		55.3	100	100	2.088	2.094	213	100	99.8
		57.3	15	15	2.021	2.012	006	50	99.7

TABLE-5.9 SUMMARY TABLE OF DIFFRACTOGRAM INDEXING

ALLOY: P1;   H/T TEMPERATURE: 950°C ;   SOAKING DURATION: 6 HOURS

```
DIFF.                          PHASE(S)                                        INT
ANGLE  1  3  5  7  9  11 13 15 17 19 21 23 25 27 29

 54.8  0 0 0 0 0 1 1 0 0 0 0 1 0 0 0 1 1 0 1 0 0 0 0 0 0 0 0 0 0 1    10.0
 55.3  0 1 0 0 0 0 1 0 1 0 0 0 0 0 0 0 0 0 0 0 0 0 0 0 1 1 0 0 1 0    32.0
 55.8  0 0 1 0 0 0 0 0 0 1 0 0 0 0 0 0 0 0 0 0 1 0 0 0 0 1 1 1 0 0     5.0
 64.1  0 0 0 0 0 0 1 0 1 1 1 1 0 0 0 0 0 1 0 0 0 0 0 0 1 1 0 0 0 0     3.0
 64.8  0 0 0 0 0 0 1 0 0 0 1 0 1 1 0 0 1 0 0 0 0 0 0 0 1 1 0 0 0 0    19.0
 98.6  0 0 0 0 0 0 0 0 0 0 0 0 1 0 0 0 1 0 0 0 0 0 0 0 1 0 0 0 0 0     4.0
125.0  0 0 0 0 0 0 0 0 0 0 0 0 0 0 0 0 0 0 0 0 0 0 0 0 0 0 0 0 0 0     6.0

       0 0 0 0 0 0 4 0 2 2 2 2 2 0 0 0 3 0 2 0 0 0 0 0 3 4 2 0 0 0
```

0 = ABSENT   1 = PRESENT   * = PROBABLE DIFF. ANGLE FOR K-BETA RADIATION

DETAILED ANALYSIS OF PHASE(S) ACTUALLY PRESENT

S.N.	PHASE PRESENT	DIFF. ANGLE	PEAK INT	I/IO	D MEAS	D STD	DIFF PLANE	INT STD	CONF LIMIT
(1)	FE5C2	54.8	31	31	2.106	2.112	112	25	99.8
		55.3	100	100	2.088	2.080	021	70	99.8
		64.1	9	9	1.826	1.821	511	20	99.8
		64.8	59	59	1.808	1.814	312	25	99.8
(2)	MN5C2	55.3	100	100	2.088	2.084	120	80	99.9
		64.1	9	9	1.826	1.831	115	60	99.8
(3)	MN5C2(PD5B2)	55.8	15	100	2.071	2.078	021	100	99.8
		64.1	9	60	1.826	1.820	312	70	99.8
(4)	FE7C3(2)	64.1	9	15	1.826	1.820	301	10	99.8
		64.8	59	100	1.808	1.807	022	20	99.9
(5)	CR7C3(2)	54.8	31	100	2.106	2.100	012	60	99.8
		64.1	9	30	1.826	1.820	301	30	99.8
(6)	CR7C3	64.8	59	100	1.808	1.810	431	70	99.9
		98.6	12	21	1.278	1.280	---	60	99.8
		64.1	9	30	1.826	1.825	211	20	100.0
(7)	COPPER	55.3	100	100	2.088	2.088	111	100	100.0
		64.8	59	59	1.808	1.808	200	46	100.0
		98.6	12	12	1.278	1.278	220	20	100.0
(8)	FE8SI2C	55.3	100	100	2.088	2.080	131	80	99.8
		55.8	15	15	2.071	2.070	210	80	100.0
		64.1	9	9	1.826	1.820	031	20	99.8
		64.8	59	59	1.808	1.810	015	20	99.9

TABLE-5.12   SUMMARY TABLE OF DIFFRACTOGRAM INDEXING

ALLOY: P1:   H/T TEMPERATURE: 1000°C ;   SOAKING DURATION: 6 HOURS

```
DIFF.                          PHASE(S)                                              INT
ANGLE  1  3  5  7  9 11 13 15 17 19 21 23 25 27 29

 55.3  0 1 0 0 0 0 1 0 1 1 0 0 0 0 0 0 0 0 0 0 0 0 0 0 1 1 0 0 1 0      59.0
 56.1  0 0 1 0 1 1 0 1 1 1 0 0 0 0 0 0 1 0 0 1 0 0 0 0 1 1 1 0 0 0       4.3
 64.5  0 0 0 0 0 0 1 0 1 1 1 1 1 1 0 0 1 0 0 0 0 1 0 0 0 1 0 0 0 0       9.0
 65.7  0 0 0 1 0 0 0 0 0 0 0 1 1 0 1 0 1 0 0 0 0 0 0 0 1 0 0 1 0         4.0
 98.4  0 0 0 0 0 0 0 0 0 0 0 0 1 0 0 0 1 0 0 0 0 0 1 0 1 0 0 0 0 0       8.0
 99.0  0 0 0 0 0 0 0 0 0 0 0 0 0 0 0 0 0 0 0 0 0 0 1 0 0 0 0 0 0 0       4.0
110.8  0 0 0 0 0 0 0 0 0 0 0 0 0 1 0 0 0 0 1 0 0 0 0 0 0 0 1 1 0 1       4.0
124.8  0 0 0 0 0 0 0 0 0 0 0 0 0 0 0 0 0 0 0 0 0 0 0 0 0 0 0 0 0 0       5.0
125.4  0 0 0 0 0 0 0 1 0 0 0 0 0 0 0 0 0 0 0 0 0 0 0 0 1 0 0 0 0 0       4.0
129.0  0 0 0 0 0 0 0 0 0 0 0 0 0 0 0 0 0 0 0 0 0 0 0 0 0 0 0 0 0 0       7.0

       0 0 0 0 0 0 2 2 3 3 0 2 3 2 0 0 3 0 0 0 0 0 2 0 3 4 2 2 2 0
```

O = ABSENT   1 = PRESENT   * = PROBABLE DIFF. ANGLE FOR K-BETA RADIATION

DETAILED ANALYSIS OF PHASE(S) ACTUALLY PRESENT

S.N.	PHASE PRESENT	DIFF. ANGLE	PEAK INT	I/IO	D MEAS	D STD	DIFF PLANE	INT STD	CONF LIMIT
(1)	FE5C2	55.3	100	100	2.088	2.080	021	70	99.8
		64.5	15	15	1.816	1.814	312	25	99.9
(2)	MN5C2	55.3	100	100	2.088	2.084	120	80	99.9
		56.1	7	7	2.061	2.060	015	80	100.0
		64.5	15	15	1.816	1.818	213	60	99.9
(3)	CR7C3(2)	64.5	15	100	1.816	1.820	301	30	99.8
		65.7	6	44	1.786	1.790	022	50	99.8
(4)	CR7C3	64.5	15	100	1.816	1.810	431	70	99.8
		65.7	6	44	1.786	1.780	521	50	99.7
		98.4	13	88	1.280	1.280	---	60	100.0
(5)	(CR,FE)7C3	64.5	15	100	1.816	1.810	431	60	99.8
		110.8	6	44	1.177	1.178	642	60	99.9
(6)	CR3C2	64.5	15	100	1.816	1.810	130	30	99.8
		65.7	6	44	1.786	1.780	501	30	99.7
		98.4	13	88	1.280	1.280	531	5	100.0
(7)	CU2S(1)	98.4	13	100	1.280	1.281	114	11	99.8
		99.0	6	50	1.274	1.273	211	4	99.9
(8)	COPPER	55.3	100	100	2.088	2.088	111	100	100.0
		98.4	13	13	1.280	1.278	220	20	99.8
		125.4	6	6	1.090	1.090	311	17	100.0
(9)	FE8SI2C	55.3	100	100	2.088	2.080	131	80	99.8
		56.1	7	7	2.061	2.070	210	80	99.7
		64.5	15	15	1.816	1.810	015	20	99.8
		65.7	6	6	1.786	1.780	301	20	99.7
(10)	CRMN3	56.1	7	100	2.061	2.069	330	100	99.8
		110.8	6	93	1.177	1.179	---	90	99.7
(11)	MN15C4	55.3	100	100	2.088	2.094	213	100	99.8
		65.7	6	6	1.786	1.780	311	50	99.7

TABLE-5.10   SUMMARY TABLE OF DIFFRACTOGRAM INDEXING

ALLOY: P1;   H/T TEMPERATURE: 950°C ;   SOAKING DURATION: 10 HOURS

DIFF. ANGLE	1		3		5		7		9		11		13		15		17		19		21		23		25		27		29		INT
54.4	0	0	0	0	0	0	1	0	1	1	1	0	1	1	1	1	1	1	0	1	0	0	0	0	0	0	1	0	1	1	3.
55.2	0	0	0	0	0	1	0	0	1	0	0	1	0	0	0	0	0	0	0	0	0	0	0	1	1	0	0	1	0		56.
56.0	0	0	1	0	0	1	0	1	1	1	0	0	0	0	0	0	1	0	0	1	0	0	0	0	1	1	1	0	0		4.
56.8	0	0	0	0	0	0	0	1	1	1	0	0	1	1	1	0	0	0	0	1	0	0	0	0	0	0	1	1	0		4.
63.9	0	0	0	0	0	0	0	0	1	1	0	0	0	0	0	0	0	0	1·0		1	0	0	0	0	0	1	1	0	0	5.
64.5	0	0	0	0	0	0	1	0	1	1	1	1	1	1	0	0	1	0	0	0	1	0	0	0	1	0	0	0	0		16.
65.2	0	1	0	1	1	0	0	1	0	0	0	0	0	0	0	0	0	0	1	0	0	0	0	0	1	0	0	1	0		3.
67.8	0	0	0	0	0	0	0	0	0	0	1	0	0	0	1	0	0	0	0	0	0	0	0	0	1	0	0	0	0		7.
98.5	0	0	0	0	0	0	0	0	0	0	0	0	1	0	0	0	1	0	0	0	0	0	1	0	1	0	0	0	0		6.
125.2	0	0	0	0	0	0	0	1	0	0	0	0	0	0	0	0	0	0	0	0	0	0	0	1	0	0	0	0	0		22.
126.6	0	1	0	0	0	0	0	0	0	0	0	0	0	0	0	0	0	0	0	0	0	0	0	0	0	0	0	0	0		3.

| | 0 | 2 | 0 | 0 | 0 | 2 | 2 | 4 | 6 | 6 | 2 | 2 | 4 | 4 | 2 | 0 | 3 | 2 | 0 | 3 | 2 | 0 | 0 | 0 | 3 | 5 | 3 | 3 | 4 | 0 |

O =   ABSENT   1 =   PRESENT   * = PROBABLE DIFF. ANGLE FOR K-BETA RADIATION

DETAILED ANALYSIS OF PHASE(S) ACTUALLY PRESENT

S.N.	PHASE PRESENT	DIFF. ANGLE	PEAK INT	I/IO	D MEAS	D STD	DIFF PLANE	INT STD	CONF LIMIT
(1)	AUSTENITE	65.2	5	100	1.798	1.800	200	80	99.9
		126.6	5	100	1.084	1.083	311	80	99.7
(2)	FE3C(CEMENTITE)	55.2	100	100	2.091	2.100	121	60	99.8
		56.0	7	7	2.064	2.060	210	70	99.9
(3)	MN5C2	54.4	5	5	2.120	2.121	211	80	100.0
		55.2	100	100	2.091	2.084	120	80	99.8
		56.0	7	7	2.064	2.060	015	80	99.9
		56.8	7	7	2.037	2.034	204	60	99.9
		63.9	8	8	1.831	1.831	115	60	100.0
		64.5	28	28	1.816	1.818	213	60	99.9
(4)	FE7C3(2)	54.4	5	18	2.120	2.122	012	40	99.9
		64.5	28	100	1.816	1.820	301	10	99.8
		120.4	8	31	1.116	1.117	133	6	99.9
(5)	CR7C3	54.4	5	18	2.120	2.120	202	70	100.0
		56.8	7	25	2.037	2.040	421	100	99.9
		64.5	28	100	1.816	1.810	431	70	99.8
		98.5	10	37	1.279	1.280	---	60	99.9
(6)	(CR,FE)7C3	54.4	5	18	2.120	2.120	202	60	100.0
		56.8	7	25	2.037	2.040	122	100	99.9
		64.5	28	100	1.816	1.810	431	60	99.8
		67.8	12	43	1.737	1.740	322	60	99.9
(7)	COPPER	55.2	100	100	2.091	2.088	111	100	99.9
		98.5	10	10	1.279	1.278	220	20	99.9
		125.2	39	39	1.091	1.090	311	17	99.8
(8)	FE8SI2C	55.2	100	100	2.091	2.090	130	80	100.0
		56.0	7	7	2.064	2.070	210	80	99.8
		64.5	28	28	1.816	1.810	015	20	99.8
		65.2	5	5	1.798	1.794	312	20	99.8
		67.8	12	12	1.737	1.740	225	20	99.9
(9)	CRMN3	56.0	7	80	2.064	2.069	330	100	99.9
		56.8	7	80	2.037	2.036	202	70	100.0
		63.9	8	100	1.831	1.838	222	40	99.7
(10)	MN15C4	54.4	5	5	2.120	2.129	301	10	99.7
		55.2	100	100	2.091	2.094	213	100	99.9
		56.8	7	7	2.037	2.037	302	100	100.0

TABLE-5.11   SUMMARY TABLE OF DIFFRACTOGRAM INDEXING

ALLOY: P1;   H/T TEMPERATURE: 1000°C ;   SOAKING DURATION: 2 HOURS

DIFF. ANGLE	PHASE(S) 1 3 5 7 9 11 13 15 17 19 21 23 25 27 29	INT
47.1	0 0 0 0 0 0 1 0 0 1 0 0 0 0 0 0 0 0 1 0 0 0 0 0 0 0 0 0 0 1	4.0
48.0	0 0 0 1 1 1 0 1 0 0 0 0 0 0 1 0 0 1 0 0 0 0 0 0 0 0 0 0 0 0	3.0
51.6	0 0 0 0 0 0 0 0 0 0 0 0 1 0 0 1 1 0 0 0 0 0 0 0 0 1 0 0 0 0	4.0
54.7	0 0 0 0 0 0 1 0 0 1 0 0 0 0 0 1 1 0 1 0 0 0 0 0 0 0 0 0 0 1	6.0
55.2	0 0 0 0 0 1 0 0 1 0 0 1 0 0 0 0 0 0 0 0 0 0 0 1 1 0 0 1 0	10.0
57.0	1 0 0 0 0 0 0 0 1 1 1 0 0 1 1 1 0 0 0 0 1 0 0 0 0 0 0 1 1 0	4.0
58.5	0 0 0 0 0 0 0 1 0 1 1 1 0 0 0 0 1 0 0 0 0 1 0 0 1 0 0 0 0 0	4.0
58.8	0 0 0 0 0 1 0 0 0 1 0 0 0 0 0 0 0 0 0 0 0 0 1 0 1 0 0 0 0 0	5.0
64.5	0 0 0 0 0 0 1 0 1 1 1 1 1 1 0 0 1 0 0 0 1 0 0 1 0 0 0 0 0 0	6.0
66.4	0 0 0 0 0 0 0 0 0 0 0 0 0 0 0 0 1 0 0 0 0 0 0 0 0 0 0 1 1 0	4.0
75.0	0 0 0 0 0 0 0 0 0 0 1 0 0 0 0 0 0 1 0 0 1 0 0 0 0 0 0 0 1 0	4.0
98.8	0 0 0 0 0 0 0 0 0 0 0 0 0 0 0 0 0 0 0 0 0 0 0 0 1 0 0 0 0 0	3.0
124.9	0 0 0 0 0 0 0 0 0 0 0 0 0 0 0 0 0 0 0 0 0 0 0 0 0 0 0 0 0 0	15.0
	0 0 0 0 0 3 3 3 3 6 2 4 3 2 2 2 5 3 0 0 0 2 0 0 2 5 0 3 4 2	

0 =   ABSENT   1 =   PRESENT   * = PROBABLE DIFF. ANGLE FOR K-BETA RADIATION

DETAILED ANALYSIS OF PHASE(S) ACTUALLY PRESENT

S.N.	PHASE PRESENT	DIFF. ANGLE	PEAK INT	I/IO	D MEAS	D STD	DIFF PLANE	INT STD	CONF LIMIT
(1)	FE3C(CEMENTITE)	48.0	20	30	2.382	2.380	112	65	100.0
		55.2	66	100	2.091	2.100	121	60	99.8
		58.8	40	60	1.974	1.970	211	55	99.9
(2)	FE5C2	47.1	26	66	2.425	2.421	311	15	99.9
		54.7	40	100	2.109	2.112	112	25	99.9
		64.5	40	100	1.816	1.814	312	25	99.9
(3)	MN5C2	55.2	66	100	2.091	2.084	120	80	99.8
		57.0	26	40	2.031	2.034	204	60	99.9
		64.5	40	60	1.816	1.818	213	60	99.9
(4)	FE7C3(2)	58.5	33	83	1.983	1.989	300	16	99.8
		64.5	40	100	1.816	1.820	301	10	99.8
(5)	CR7C3	51.6	26	66	2.226	2.220	102	50	99.8
		57.0	26	66	2.031	2.040	421	100	99.7
		64.5	40	100	1.816	1.810	431	70	99.8
		98.2	20	50	1.282	1.280	---	60	99.8
(6)	(CR,FE)7C3	57.0	26	66	2.031	2.040	122	100	99.7
		64.5	40	100	1.816	1.810	431	60	99.8
(7)	(CR7C3+MN7C3)	48.0	20	75	2.382	2.380	333	80	100.0
		57.0	26	100	2.031	2.040	666	100	99.7
(8)	COPPER	55.2	66	100	2.091	2.088	111	100	99.9
		98.8	20	30	1.276	1.278	220	20	99.8
(9)	FE8SI2C	51.6	26	40	2.226	2.220	014	40	99.8
		55.2	66	100	2.091	2.090	130	80	100.0
		58.5	33	50	1.983	1.980	114	60	99.9
		58.8	40	60	1.974	1.970	212	60	99.9
		64.5	40	60	1.816	1.810	015	20	99.8
(10)	CRMN3	57.0	26	66	2.031	2.036	202	70	99.8
		58.8	40	100	1.974	1.970	420	100	99.9
		66.4	26	66	1.770	1.764	500	60	99.8
(11)	MN15C4	55.2	66	100	2.091	2.094	213	100	99.9
		57.0	26	40	2.031	2.037	302	100	99.8
		66.4	26	40	1.770	1.772	116	50	99.9
		75.0	26	40	1.592	1.591	224	50	100.0

TABLE-5.13   SUMMARY TABLE OF DIFFRACTOGRAM INDEXING

ALLOY: P1;   H/T   TEMPERATURE: 1000°C ;   SOAKING DURATION: 10 HOURS

```
.DIFF.                        PHASE(S)                                        INT
 ANGLE  1  3  5  7  9 11 13 15 17 19 21 23 25 27 29

  49.7  0 0 0 0 0 0 0 0 0 0 0 0 0 1 0 0 1 0 0 0 0 0 0 0 0 0 0 0 0 0    3.0
  54.1  0 0 0 0 0 0 0 1 0 1 0 1 1 1 0 0 1 0 1 0 1 0 0 0 0 1 1 1 1      4.0
* 55.2  0 0 0 0 0 1 0 0 1 0 0 1 0 0 0 0 0 0 0 0 0 0 0 0 1 1 0 0 1 0   74.0
  56.0  0 0 1 0 0 1 0 1 1 1 0 0 0 0 0 0 0 1 0 0 1 0 0 0 0 1 1 1 0 0   10.0
  64.6  0 0 0 0 0 0 1 0 1 1 1 1 1 1 0 0 1 0 0 0 0 1 0 0 1 1 0 0 0 0   26.0
  98.5  0 0 0 0 0 0 0 0 0 0 0 0 1 0 0 0 1 0 0 0 0 0 1 0 1 0 0 0 0 0   46.0
 124.0  0 0 0 0 0 0 0 0 0 0 0 0 0 0 0 0 0 0 0 0 0 0 0 0 0 0 0 0 0 0    6.0
 125.5  0 0 0 0 0 0 0 1 0 0 0 0 0 0 0 0 0 0 0 0 0 0 0 0 1 0 0 0 0 0   20.0

        0 0 0 0 0 2 0 2 4 2 2 2 3 3 0 0 3 2 0 0 0 0 0 0 4 3 2 2 2 0
```

0 = ABSENT   1 = PRESENT   * = PROBABLE DIFF. ANGLE FOR K-BETA RADIATION

DETAILED ANALYSIS OF PHASE(S) ACTUALLY PRESENT

S.N.	PHASE PRESENT	DIFF. ANGLE	PEAK INT	I/IO	D MEAS	D STD	DIFF PLANE	INT STD	CONF LIMIT
(1)	FE3C(CEMENTITE)	55.2	100	100	2.091	2.100	121	60	99.8
		56.0	13	13	2.064	2.060	210	70	99.9
(2)	FE5C2(HAGG)	56.0	13	50	2.064	2.060	510	100	99.9
		125.5	27	100	1.090	1.090	404	20	99.9
(3)	MN5C2	54.1	5	5	2.131	2.121	211	80	99.7
		55.2	100	100	2.091	2.084	120	80	99.8
		56.0	13	13	2.064	2.060	015	80	99.9
		64.6	35	35	1.813	1.818	213	60	99.8
(4)	MN5C2(PD5B2)	56.0	13	38	2.064	2.058	510	80	99.8
		64.6	35	100	1.813	1.820	312	70	99.7
(5)	FE7C3(2)	54.1	5	15	2.131	2.122	012	40	99.8
		64.6	35	100	1.813	1.807	022	20	99.7
(6)	CR7C3(2)	55.2	100	100	2.091	2.100	012	60	99.8
		64.6	35	35	1.813	1.820	301	30	99.7
(7)	CR7C3	54.1	5	8	2.131	2.120	202	70	99.7
		64.6	35	56	1.813	1.810	431	70	99.9
		98.5	62	100	1.279	1.280	---	60	99.9
(8)	(CR,FE)7C3	49.7	4	11	2.306	2.300	141	40	99.9
		54.1	5	15	2.131	2.120	202	60	99.7
		64.6	35	100	1.813	1.810	431	60	99.9
(9)	COPPER	55.2	100	100	2.091	2.088	111	100	99.9
		64.6	35	35	1.813	1.808	200	46	99.8
		98.5	62	62	1.279	1.278	220	20	99.9
		125.5	27	27	1.090	1.090	311	17	99.9
(10)	FE8SI2C	55.2	100	100	2.091	2.090	130	80	100.0
		56.0	13	13	2.064	2.070	210	80	99.8
		64.6	35	35	1.813	1.810	015	20	99.9
(11)	CRMN3	54.1	5	40	2.131	2.132	410	100	100.0
		56.0	13	100	2.064	2.069	330	100	99.9
(12)	MN15C4	54.1	5	5	2.131	2.129	301	10	100.0
		55.2	100	100	2.091	2.094	213	100	99.9

TABLE-5.14   SUMMARY TABLE OF DIFFRACTOGRAM INDEXING

ALLOY: P1;   H/T TEMPERATURE:1050°C ;   SOAKING DURATION: 2 HOURS

```
DIFF.                          PHASE(S)
ANGLE  1  3  5  7  9 11 13 15 17 19 21 23 25 27 29                INT

 45.8  0 0 0 0 0 0 1 0 0 0 0 0 0 0 0 0 1 0 0 0 0 1 0 0 0 0 0 0 0 0   7.0
 50.5  0 0 0 0 0 1 0 1 1 1 1 1 1 0 0 0 0 0 0 0 0 1 0 0 0 0 1 1 1 0   5.0
 54.4  0 0 0 0 0 0 1 0 1 1 1 0 1 1 1 1 1 1 0 1 0 1 0 0 0 0 0 1 0 1 1  5.0
 55.0  0 0 0 0 0 1 0 0 0 0 0 1 0 0 0 0 0 0 1 0 0 0 0 0 1 1 0 0 1 1  20.0
*57.0  1 0 0 0 0 0 0 1 1 1 0 0 1 1 1 0 0 0 0 1 0 0 0 0 0 0 0 1 1 0   6.0
 57.6  0 0 1 0 0 1 1 0 1 1 1 1 1 0 0 0 0 0 0 0 0 0 0 0 1 1 0 1 0     5.0
 64.4  0 0 0 0 0 1 0 1 1 1 1 0 0 0 0 0 1 0 0 1 0 0 1 0 0 0 1 0 0 0 0 18.0
 64.9  0 1 0 1 1 0 0 1 0 0 1 0 1 1 0 0 1 0 0 1 0 0 1 0 0 0 1 1 0 0 1 0  5.0
 69.4  0 0 0 0 0 0 0 0 1 0 0 0 0 0 0 0 0 0 0 0 0 0 1 0 0 1 0 0 0 0   5.0
 99.0  0 0 0 0 0 0 0 0 0 0 0 0 0 0 0 0 0 0 0 0 0 0 0 1 0 0 0 0 0 0   3.0
124.5  0 0 0 0 0 0 0 0 0 0 0 0 0 0 0 0 0 0 0 0 0 0 0 0 0 0 0 0 0 0  11.0
125.3  0 0 0 0 0 0 0 1 0 0 0 0 0 0 0 0 0 0 0 0 0 0 0 0 1 0 0 0 0 0   5.0

       0 0 0 0 0 2 2 5 5 4 4 3 4 3 2 0 3 0 2 3 0 2 3 0 3 2 0 3 4 2 2 5 2
```

O =   ABSENT   1 =   PRESENT   * = PROBABLE DIFF. ANGLE FOR K-BETA RADIATION

DETAILED ANALYSIS OF PHASE(S) ACTUALLY PRESENT

S.N.	PHASE PRESENT	DIFF. ANGLE	PEAK INT	I/IO	D MEAS	D STD	DIFF PLANE	INT STD	CONF LIMIT
(1)	FE3C(CEMENTITE)	50.5	25	25	2.272	2.260	200	25	99.7
		55.0	100	100	2.098	2.100	121	60	100.0
(2)	FE5C2	54.4	25	27	2.120	2.112	112	25	99.8
		57.6	25	27	2.011	2.010	312	40	100.0
		64.4	90	100	1.818	1.814	312	25	99.8
(3)	MN5C2	50.5	25	27	2.272	2.277	020	40	99.9
		54.4	25	27	2.120	2.121	211	80	100.0
		57.0	30	33	2.031	2.034	204	60	99.9
		64.4	90	100	1.818	1.818	213	60	100.0
		69.4	25	27	1.702	1.697	215	60	99.8
(4)	FE7C3(2)	50.5	25	27	2.272	2.270	002	8	100.0
		54.4	25	27	2.120	2.122	012	40	99.9
		64.4	90	100	1.818	1.820	301	10	99.9
		64.9	25	27	1.806	1.807	022	20	100.0
(5)	CR7C3	50.5	25	83	2.272	2.280	411	70	99.8
		54.4	25	83	2.120	2.120	202	70	100.0
		57.0	30	100	2.031	2.040	421	100	99.7
		64.9	25	83	1.806	1.810	431	70	99.8
(6)	(CR7C3+MN7C3)	54.4	25	83	2.120	2.120	555	100	100.0
		57.0	30	100	2.031	2.040	666	100	99.7
(7)	COPPER	55.0	100	100	2.098	2.088	111	100	99.7
		64.9	25	25	1.806	1.808	200	46	99.9
		125.3	25	25	1.091	1.090	311	17	99.9
(8)	FE8SI2C	55.0	100	100	2.098	2.090	130	80	99.8
		64.4	90	90	1.818	1.820	031	20	99.9
		64.9	25	25	1.806	1.810	015	20	99.8
		69.4	25	25	1.702	1.700	303	20	99.9
(9)	CRMN3	50.5	25	83	2.272	2.272	002	60	100.0
		57.0	30	100	2.031	2.036	202	70	99.8
(10)	MN15C4	50.5	25	25	2.272	2.262	105	50	99.8
		54.4	25	25	2.120	2.129	301	10	99.7
		55.0	100	100	2.098	2.094	213	100	99.9
		57.0	30	30	2.031	2.037	302	100	99.8
		64.9	25	25	1.806	1.800	310	20	99.8

TABLE-5.15 SUMMARY TABLE OF DIFFRACTOGRAM INDEXING

ALLOY: P1; H/T TEMPERATURE:1050°C ; SOAKING DURATION: 6 HOURS

DIFF. ANGLE	1		3		5		7		9		11		13		15		17		19		21		23		25		27		29		INT
53.6	0	0	0	0	0	0	0	0	0	0	0	1	0	1	0	0	1	0	0	0	0	0	0	0	0	0	0	0	0	0	6.0
54.5	0	0	0	0	0	0	1	0	1	1	1	0	1	1	1	1	1	1	1	0	0	0	0	0	0	0	0	0	0	1	5.0
55.1	0	0	0	0	0	1	0	0	0	0	0	1	0	0	0	0	0	0	0	0	0	0	0	0	1	1	0	0	1	1	13.0
57.3	1	0	1	0	0	1	0	1	1	1	1	1	1	0	0	0	0	0	0	1	0	0	0	0	0	0	1	0	1	0	5.0
64.4	0	0	0	0	0	0	1	0	1	1	1	0	1	0	0	0	0	0	1	0	0	1	0	0	0	1	0	0	0	0	48.0
68.2	0	0	0	0	0	0	0	0	0	1	0	1	0	0	0	0	0	0	0	0	0	0	0	0	0	0	0	0	1	0	5.0
97.4	0	0	0	0	1	0	0	0	0	0	0	0	1	0	0	0	0	0	0	0	0	0	0	0	0	0	0	0	0	0	8.0
98.0	0	0	0	0	0	0	0	0	0	0	0	0	0	0	0	0	0	0	0	0	0	1	0	0	0	0	0	0	0	0	24.0
100.3	0	0	0	0	0	0	0	0	0	0	0	0	1	0	1	0	1	0	0	0	0	0	0	0	0	0	0	0	0	0	4.0
114.5	0	0	0	0	0	0	0	0	0	0	1	0	0	0	0	0	1	1	0	0	0	0	0	0	0	0	0	0	0	0	10.0
115.4	0	0	0	0	0	0	0	0	0	0	1	0	0	0	0	0	0	0	0	0	0	0	0	0	0	0	0	0	0	0	5.0
116.3	0	0	0	0	0	0	0	1	0	0	0	0	0	0	0	0	0	0	0	0	0	1	0	0	0	0	0	0	0	0	6.0
	0	0	0	0	0	2	2	2	3	4	5	4	5	0	3	0	3	3	2	0	0	0	0	0	0	2	0	0	3	2	

0 = ABSENT   1 = PRESENT   * = PROBABLE DIFF. ANGLE FOR K-BETA RADIATION

DETAILED ANALYSIS OF PHASE(S) ACTUALLY PRESENT

S.N.	PHASE PRESENT	DIFF. ANGLE	PEAK INT	I/IO	D MEAS	D STD	DIFF PLANE	INT STD	CONF LIMIT
(1)	FE3C(CEMENTITE)	55.1	27	100	2.095	2.100	121	60	99.9
		57.3	10	38	2.021	2.020	022	60	100.0
(2)	FE5C2	54.5	10	10	2.116	2.112	112	25	99.9
		64.4	100	100	1.818	1.814	312	25	99.8
(3)	MN5C2	54.5	10	10	2.116	2.121	211	80	99.9
		57.3	10	10	2.021	2.019	213	100	99.9
		64.4	100	100	1.818	1.818	213	60	100.0
(4)	FE7C3(2)	54.5	10	10	2.116	2.122	012	40	99.8
		57.3	10	10	2.021	2.019	121	100	99.9
		64.4	100	100	1.818	1.820	301	10	99.9
		114.5	20	20	1.152	1.153	501	10	99.8
		115.4	10	10	1.146	1.146	330	16	100.0
(5)	CR7C3	53.6	12	75	2.149	2.140	112	50	99.8
		54.5	10	62	2.116	2.120	202	70	99.9
		57.3	10	62	2.021	2.020	---	50	100.0
		97.4	16	100	1.290	1.290	---	60	100.0
		100.3	8	50	1.262	1.260	---	70	99.8
(6)	(CR7C3+MN7C3)	53.6	12	100	2.149	2.150	444	40	100.0
		54.5	10	83	2.116	2.120	555	100	99.9
		100.3	8	66	1.262	1.260	555	60	99.8
(7)	FE8SI2C	55.1	27	27	2.095	2.090	130	80	99.9
		64.4	100	100	1.818	1.820	031	20	99.9
(8)	MN15C4	55.1	27	100	2.095	2.094	213	100	100.0
		57.3	10	38	2.021	2.012	006	50	99.7
		68.2	10	38	1.728	1.726	312	20	99.9

TABLE-5.16 SUMMARY TABLE OF DIFFRACTOGRAM INDEXING

ALLOY: P1;   H/T TEMPERATURE:1050°C ;   SOAKING DURATION: 6 HOURS

```
DIFF.                          PHASE(S)                                                INT
ANGLE  1  3  5  7  9 11 13 15 17 19 21 23 25 27 29

 49.7  0 0 0 0 0 0 0 0 0 0 0 1 0 0 1 0 0 0 0 0 0 0 0 0 0 0 0 0 0 0    3.0
 53.3  0 0 0 1 0 0 0 0 0 0 0 0 0 1 0 0 1 0 0 0 0 0 0 0 0 0 0 1 1 0    6.0
 54.5  0 0 0 0 0 0 1 0 1 1 1 0 1 1 1 1 1 1 1 0 0 0 0 0 0 0 0 0 0 1    8.0
 55.1  0 0 0 0 0 1 0 0 0 0 0 1 0 0 0 0 0 0 0 0 0 0 0 0 1 1 0 0 1 1  130.0
 55.8  0 1 0 0 0 0 1 0 0 1 0 0 0 0 0 0 0 0 0 1 0 0 0 0 1 0 1 0 0 0   10.0
 56.2  0 0 1 1 1 1 1 1 1 1 0 0 0 0 0 0 0 1 0 0 0 1 0 0 0 1 1 0 0 0   10.0
 64.4  0 0 0 0 0 0 1 0 1 1 1 1 0 0 0 0 0 0 1 0 0 1 0 0 1 0 0 0 0 0    5.0
 66.5  0 0 0 0 0 0 0 0 0 0 0 0 0 0 0 0 1 0 0 0 0 0 0 0 0 0 1 1 0 0    6.0
 98.1  0 0 0 0 0 0 0 0 0 0 0 0 0 0 0 0 0 0 0 0 0 1 0 0 0 0 0 0 0 0   20.0
 98.6  0 0 0 0 0 0 0 0 0 0 0 0 1 0 0 0 1 0 0 0 0 0 0 1 0 0 0 0 0 0    7.0
 99.2  0 1 0 0 0 0 1 0 0 0 0 1 0 0 0 0 0 0 0 0 0 0 1 0 0 0 0 0 0 0    5.0
114.9  0 0 0 0 0 0 0 0 0 0 0 0 0 0 0 0 1 1 0 0 0 1 0 0 0 0 0 0 0 0    5.0

       0 2 0 2 0 2 4 2 3 4 2 2 3 2 2 0 5 4 2 0 0 3 2 0 2 4 0 3 3 2
```

0 = ABSENT   1 = PRESENT   * = PROBABLE DIFF. ANGLE FOR K-BETA RADIATION

DETAILED ANALYSIS OF PHASE(S) ACTUALLY PRESENT

S.N.	PHASE PRESENT	DIFF. ANGLE	PEAK INT	I/IO	D MEAS	D STD	DIFF PLANE	INT STD	CONF LIMIT
(1)	AUSTENITE	55.8	7	100	2.071	2.080	111	100	99.7
		99.2	3	50	1.272	1.270	220	50	99.8
(2)	FE3C(CEMENTITE)	55.1	100	100	2.095	2.100	121	60	99.9
		56.2	7	7	2.057	2.060	210	70	99.9
(3)	FE5C2	54.5	6	80	2.116	2.112	112	25	99.9
		55.8	7	100	2.071	2.080	021	70	99.7
		56.2	7	100	2.057	2.049	510	100	99.8
		64.4	3	50	1.818	1.814	312	25	99.8
(4)	MN5C2	54.5	6	80	2.116	2.121	211	80	99.9
		56.2	7	100	2.057	2.060	015	80	99.9
		64.4	3	50	1.818	1.818	213	60	100.0
(5)	FE7C3(2)	54.5	6	100	2.116	2.122	012	40	99.8
		64.4	3	62	1.818	1.820	301	10	99.9
(6)	CR7C3	54.5	6	100	2.116	2.120	202	70	99.9
		98.6	5	87	1.278	1.280	---	60	99.8
		99.2	3	62	1.272	1.270	---	30	99.8
(7)	(CR,FE)7C3	49.7	2	37	2.306	2.300	141	40	99.9
		54.5	6	100	2.116	2.120	202	60	99.9
(8)	(CR7C3+MN7C3)	53.3	4	75	2.160	2.150	444	40	99.7
		54.5	6	100	2.116	2.120	555	100	99.9
(9)	COPPER	55.1	100	100	2.095	2.088	111	100	99.8
		98.6	5	5	1.278	1.278	220	20	100.0
(10)	FE8SI2C	55.1	100	100	2.095	2.090	130	80	99.9
		55.8	7	7	2.071	2.070	210	80	100.0
		56.2	7	7	2.057	2.050	121	80	99.8
		64.4	3	3	1.818	1.820	031	20	99.9
(11)	CRMN3	53.3	4	60	2.160	2.162	321	40	100.0
		55.8	7	100	2.071	2.069	330	100	99.9
		66.5	4	60	1.767	1.764	500	60	99.9
(12)	MN15C4	53.3	4	4	2.160	2.163	300	50	99.9
		55.1	100	100	2.095	2.094	213	100	100.0
		66.5	4	4	1.767	1.772	116	50	99.8

TABLE-5.17   SUMMARY TABLE OF DIFFRACTOGRAM INDEXING

ALLOY: P1;   H/T TEMPERATURE:1050°C ;   SOAKING DURATION: 10 HOURS

DIFF. ANGLE	PHASE(S) 1 3 5 7 9 11 13 15 17 19 21 23 25 27 29	INT
53.7	0 0 0 0 0 0 0 0 0 0 0 0 1 0 1 0 0 1 0 0 1 0 0 0 0 0 0 0 0 0	6.0
55.3	0 1 0 0 0 0 1 0 1 1 0 0 0 0 0 0 0 0 0 0 0 0 1 1 0 0 1 0 0 0	114.0
64.4	0 0 0 0 0 0 1 0 1 1 1 1 0 0 0 0 0 1 0 0 1 0 0 1 0 0 0 0 0 0	6.0
96.8	0 0 0 1 0 0 0 0 0 0 0 0 0 0 0 1 0 1 0 0 1 1 0 0 0 0 0 0 0 0	8.0
98.6	0 0 0 0 0 0 0 0 0 0 0 1 0 0 0 1 0 0 0 0 0 0 1 0 0 0 0 0 0 0	6.0
112.8	0 0 0 0 0 0 0 0 0 0 0 0 0 0 0 0 0 0 0 0 0 0 0 0 0 0 0 0 0 1	5.0
113.1	0 0 0 0 0 0 0 1 0 0 0 0 1 0 0 1 0 0 1 0 0 1 0 0 0 0 0 0 0 0	6.0
*113.5	0 0 0 0 0 0 0 0 0 0 1 0 0 0 0 1 0 0 1 0 0 0 0 0 0 0 0 0 0 0	6.0
115.0	0 0 0 0 0 0 0 0 0 0 0 0 0 0 0 0 1 0 0 0 1 0 0 0 0 0 0 0 0 0	7.0
124.6	0 0 0 0 0 0 0 0 0 0 0 0 0 0 0 0 0 0 0 0 0 0 0 0 0 0 0 0 0 0	5.0
125.1	0 0 0 0 0 0 0 0 0 0 0 0 0 0 0 0 0 0 0 0 0 0 0 0 0 0 0 0 0 0	5.0
	0 0 0 0 0 0 2 0 2 2 0 2 2 0 0 0 4 2 2 0 0 3 0 0 2 2 0 0 0 0	

0 = ABSENT   1 = PRESENT   * = PROBABLE DIFF. ANGLE FOR K-BETA RADIATION

DETAILED ANALYSIS OF PHASE(S) ACTUALLY PRESENT

S.N.	PHASE PRESENT	DIFF. ANGLE	PEAK INT	I/I0	D MEAS	D STD	DIFF PLANE	INT STD	CONF LIMIT
(1)	FE5C2	55.3	100	100	2.088	2.080	021	70	99.8
		64.4	5	5	1.818	1.814	312	25	99.8
(2)	MN5C2	55.3	100	100	2.088	2.084	120	80	99.9
		64.4	5	5	1.818	1.818	213	60	100.0
(3)	MN5C2(PD5B2)	55.3	100	100	2.088	2.078	021	100	99.7
		64.4	5	5	1.818	1.820	312	70	99.9
(4)	CR7C3(2)	64.4	5	100	1.818	1.820	301	30	99.9
		113.5	5	100	1.158	1.159	330	30	99.9
(5)	CR7C3	53.7	5	100	2.145	2.140	112	50	99.9
		98.6	5	100	1.278	1.280	---	60	99.8
(6)	CR3C2	96.8	7	100	1.296	1.298	340	5	99.8
		98.6	5	75	1.278	1.280	531	5	99.8
		113.1	5	75	1.161	1.161	901	40	100.0
		113.5	5	75	1.158	1.159	821	10	99.9
(7)	COPPER	55.3	100	100	2.088	2.088	111	100	100.0
		98.6	5	5	1.278	1.278	220	20	100.0
(8)	FE8SI2C	55.3	100	100	2.088	2.080	131	80	99.8
		64.4	5	5	1.818	1.820	031	20	99.9

TABLE-5.18   SUMMARY TABLE OF DIFFRACTOGRAM INDEXING

ALLOY: P2;   (AS-CAST)

```
DIFF.                        PHASE(S)
ANGLE  1  3  5  7  9  11 13 15 17 19 21 23 25 27 29          INT

 51.6  0 0 0 0 0 0 0 0 0 0 0 1 0 0 1 1 0 0 0 0 0 0 0 0 0 1 0 0 0 0   5.0
 54.2  0 0 0 0 0 0 0 0 1 1 1 0 1 1 1 1 0 0 1 0 1 0 0 0 0 0 0 1 1 1 1  5.0
 55.0  0 0 0 0 0 1 0 0 0 0 0 1 0 0 0 0 0 0 1 0 0 0 0 0 1 1 0 0 1 1  20.0
 55.6  0 1 0 0 0 0 1 0 1 1 0 0 0 0 0 0 0 0 0 1 0 0 0 0 1 0 1 0 0   8.0
 56.6  0 0 0 1 1 0 1 0 0 0 0 0 1 1 1 0 0 0 0 0 0 1 0 0 0 1 0 0 0 0   5.0
 57.0  1 0 0 0 0 0 0 1 1 1 0 0 0 0 0 0 0 0 0 1 0 0 0 0 0 0 0 1 1 0   7.0
 64.5  0 0 0 0 0 0 1 0 1 1 1 1 1 1 0 0 1 0 0 0 0 1 0 0 0·1 0 0 0 0   6.0
 66.3  0 0 0 0 0 0 0 0 1 0·0 0 0 0 0 1 0 0 0 0 0 0 0 0 0 0 0 0 1 0   5.0
 98.1  0 0 0 0 0 0 0 0 0 0 1 0 0 0 1 0 0 0 0 0 1 0 0 0 0 0 0 0 0   8.0
 98.8  0 0 0 0 0 0 0 0 0 0 0 0 0 0·0 0 0 0 0 0 0 0 0 1 0 0 0 0 0 0   5.0
113.6  0 0 0 0 0 0 0 0 0 1 0 0 0 0 1 0 0 1 0 0 0 0 0 0 0 0 0 0 1   5.0
114.2  0 0 0 0 0 0 0 0 0 1 1 0 0 0 1 0 0 0 0 0 0 0 0 0 0 0 0 0 0   4.0
124.8  0 0 0 0 0 0 0 0 0 0 0 0 0 0 0 0 0 0 0 0 0 0 0 0 0 0 0 0 0 0   5.0

       0 0 0 0 0 0 3 0 4 5 3 4 5 3 2 0 6 0 0 3 0 2 0 0 2 5 0 3 4 3
```

0 = ABSENT   1 = PRESENT   * = PROBABLE DIFF. ANGLE FOR K-BETA RADIATION

DETAILED ANALYSIS OF PHASE(S) ACTUALLY PRESENT

S.N.	PHASE PRESENT	DIFF. ANGLE	PEAK INT	I/IO	D MEAS	D STD	DIFF PLANE	INT STD	CONF LIMIT
(1)	FE5C2	55.6	40	100	2.078	2.080	021	70	99.9
		56.6	25	62	2.044	2.049	510	100	99.8
		64.5	30	75	1.816	1.814	312	25	99.9
(2)	MN5C2	54.2	25	62	2.127	2.121	211	80	99.8
		55.6	40	100	2.078	2.084	120	80	99.8
		57.0	35	87	2.031	2.034	204	60	99.9
		64.5	30	75	1.816	1.818	213	60	99.9
(3)	FE7C3(2)	54.2	25	83	2.127	2.122	012	40	99.9
		64.5	30	100	1.816	1.820	301	10	99.8
		114.2	20	66	1.154	1.153	501	10	99.9
(4)	CR7C3(2)	55.0	100	100	2.098	2.100	012	60	100.0
		64.5	30	30	1.816	1.820	301	30	99.8
		113.6	25	25	1.158	1.159	330	30	99.8
		114.2	20	20	1.154	1.154	999	30	100.0
(5)	(CR,FE)7C3	54.2	25	83	2.127	2.120	202	60	99.8
		56.6	25	83	2.044	2.040	122	100	99.9
		64.5	30	100	1.816	1.810	431	60	99.8
(6)	(CR7C3+MN7C3)	54.2	25	100	2.127	2.120	555	100	99.8
		56.6	25	100	2.044	2.040	666	100	99.9
(7)	COPPER	55.0	100	100	2.098	2.088	111	100	99.7
		98.8	25	25	1.276	1.278	220	20	·99.8
(8)	FE8SI2C	51.6	25	25	2.226	2.220	014	40	99.8
		55.0	100	100	2.098	2.090	130	80	99.8
		55.6	40	40	2.078	2.070	210	80	99.8
		56.6	25	25	2.044	2.050	121	80	99.8
		64.5	30	30	1.816	1.810	015	20	99.8
(9)	CRMN3	54.2	25	62	2.127	2.132	410	100	99.9
		55.6	40	100	2.078	2.069	330	100	99.7
		57.0	35	87	2.031	2.036	202	70	99.8
(10)	MN15C4	54.2	25	25	2.127	2.129	301	10	99.9
		55.0	100	100	2.098	2.094	213	100	99.9
		57.0	35	35	2.031	2.037	302	100	99.8
		66.3	25	25	1.772	1.772	116	50	100.0

TABLE-5.19   SUMMARY TABLE OF DIFFRACTOGRAM INDEXING

ALLOY: P2;   H/T TEMPERATURE: 800°C ;   SOAKING DURATION: 6 HOURS

```
DIFF.                       PHASE(S)                                          INT
ANGLE   1  3  5  7  9 11 13 15 17 19 21 23 25 27 29

 50.6   0 0 0 0 0 1 0 1 1 0 1 1 0 0 0 0 0 0 0 0 0 0 1 0 0 0 0 1 1 1 0      7.0
 55.4   0 1 0 0 0 0 1 0 1 1 0 0 0 0 0 0 0 0 0 0 0 0 0 1 1 0 0 1 0      5.0
 57.0   1 0 0 0 0 0 0 1 1 1 0 0 1 1 1 0 0 0 1 0 0 0 0 0 0 0 1 1 0      3.0
 63.7   0 0 0 0 0 0 0 0 1 1 0 0 1 0 0 0 0 0 0 1 0 0 0 0 1 1 1 0 0      6.0
 64.8   0 0 0 0 0 0 1 0 0 0 1 0 1 1 0 0 1 0 0 0 0 0 0 1 1 0 0 0 0     24.0
 72.0   0 0 0 0 0 0 0 0 0 0 0 0 0 0 0 0 0 0 0 0 0 0 0 0 0 1 0 0 1 0      7.0
 92.7   0 0 0 0 0 0 0 1 0 0 0 1 0 0 0 0 0 0 0 0 0 0 0 0 0 0 0 0 0      6.0
125.6   0 0 0 0 0 0 0 1 0 0 0 0 0 0 0 0 0 0 0 0 0 0 0 1 0 0 0 0 1      4.0

        0 0 0 0 0 0 2 4 4 3 2 2 3 2 0 0 0 0 0 0 0 0 0 3 4 2 3 4 0
```

O = ABSENT   1 = PRESENT   * = PROBABLE DIFF. ANGLE FOR K-BETA RADIATION

DETAILED ANALYSIS OF PHASE(S) ACTUALLY PRESENT

S.N.	PHASE PRESENT	DIFF. ANGLE	PEAK INT	I/IO	D MEAS	D STD	DIFF PLANE	INT STD	CONF LIMIT
(1)	FE5C2	55.4	20	20	2.084	2.080	021	70	99.9
		64.8	100	100	1.808	1.814	312	25	99.8
(2)	FE5C2(HAGG)	50.6	29	100	2.267	2.260	020	50	99.8
		57.0	12	42	2.031	2.030	312	100	100.0
		92.7	25	85	1.339	1.340	331	10	99.9
		125.6	16	57	1.089	1.090	404	20	99.8
(3)	MN5C2	50.6	29	100	2.267	2.277	020	40	99.8
		55.4	20	71	2.084	2.084	120	80	100.0
		57.0	12	42	2.031	2.034	204	60	99.9
		63.7	25	85	1.836	1.831	115	60	99.8
(4)	MN5C2(PD5B2)	55.4	20	83	2.084	2.078	021	100	99.8
		57.0	12	50	2.031	2.035	402	70	99.9
		63.7	25	100	1.836	1.829	511	70	99.7
(5)	FE7C3(2)	50.6	29	29	2.267	2.255	120	30	99.7
		64.8	100	100	1.808	1.807	022	20	99.9
(6)	CR7C3(2)	50.6	29	100	2.267	2.270	120	50	99.9
		92.7	25	85	1.339	1.340	321	30	99.9
(7)	CR7C3	57.0	12	12	2.031	2.040	421	100	99.7
		63.7	25	25	1.836	1.840	601	60	99.9
		64.8	100	100	1.808	1.810	431	70	99.9
(8)	(CR,FE)7C3	57.0	12	12	2.031	2.040	122	100	99.7
		64.8	100	100	1.808	1.810	431	60	99.9
(9)	COPPER	55.4	20	20	2.084	2.088	111	100	99.9
		64.8	100	100	1.808	1.808	200	46	100.0
		125.6	16	16	1.089	1.090	311	17	99.8
(10)	FE8SI2C	55.4	20	20	2.084	2.080	131	80	99.9
		63.7	25	25	1.836	1.840	015	60	99.9
		64.8	100	100	1.808	1.810	015	20	99.9
		72.0	29	29	1.648	1.650	302	10	99.9
(11)	CRMN3	50.6	29	100	2.267	2.272	002	60	99.9
		57.0	12	42	2.031	2.036	202	70	99.8
		63.7	25	85	1.836	1.838	222	40	99.9
(12)	MN15C4	50.6	29	100	2.267	2.262	105	50	99.9
		55.4	20	71	2.084	2.094	213	100	99.7
		57.0	12	42	2.031	2.037	302	100	99.8
		72.0	29	100	1.648	1.643	313	10	99.7

TABLE-5.20 SUMMARY TABLE OF DIFFRACTOGRAM INDEXING

ALLOY: P2;   H/T TEMPERATURE: 850°C ;   SOAKING DURATION: 6 HOURS

```
DIFF.                            PHASE(S)                                              INT
ANGLE  1  3  5  7  9 11 13 15 17 19 21 23 25 27 29

 54.4  0  0  0  0  0  0  1  0  1  1  1  0  1  1  1  1  1  1  0  1  0  0  0  0  0  0  1  0  1  1    4.0
 55.3  0  1  0  0  0  0  1  0  1  1  0  0  0  0  0  0  0  0  0  0  0  0  0  1  1  0  0  1  0       6.0
 57.0  1  0  0  0  0  0  0  1  1  1  0  0  1  1  1  0  0  0  0  1  0  0  0  0  0  0  1  1  0       4.0
 58.4  0  0  0  0  0  0  0  1  1  1  1  1  0  0  0  0  1  0  0  0  0  1  0  0  1  0  1  0  0  0    4.0
 62.9  0  0  0  0  0  1  0  0  0  0  0  0  0  0  1  0  1  0  0  0  0  0  0  0  0  0  0  0  0  0    3.0
 63.8  0  0  0  0  0  0  0  0  1  1  0  0  1  0  0  0  0  0  0  1  0  0  0  0  1  1  1  0  0       3.0
 64.5  0  0  0  0  0  0  1  0  1  1  1  1  1  1  1  0  0  1  0  0  0  0  1  0  0  0  1  0  0  0   12.0
 99.0  0  0  0  0  0  0  0  0  0  0  0  0  0  0  0  0  0  0  0  0  0  0  0  1  0  0  0  0  0  0    2.0
125.0  0  0  0  0  0  0  0  0  0  0  0  0  0  0  0  0  0  0  0  0  0  0  0  0  0  0  0  0  0  0    4.0

       0  0  0  0  0  0  3  2  6  6  3  2  4  3  3  0  4  0  0  2  0  0  2  0  0  4  2  2  3  0
```

O = ABSENT 1 = PRESENT * = PROBABLE DIFF. ANGLE FOR K-BETA RADIATION

DETAILED ANALYSIS OF PHASE(S) ACTUALLY PRESENT

S.N.	PHASE PRESENT	DIFF. ANGLE	PEAK INT	I/IO	D MEAS	D STD	DIFF PLANE	INT STD	CONF LIMIT
(1)	FE5C2	54.4	33	33	2.120	2.112	112	25	99.8
		55.3	50	50	2.088	2.080	021	70	99.8 ·
		64.5	100	100	1.816	1.814	312	25	99.9
(2)	FE5C2(HAGG)	57.0	33	100	2.031	2.030	312	100	100.0
		58.4	33	100	1.986	1.980	511	20	99.8
(3)	MN5C2	54.4	33	33	2.120	2.121	211	80	100.0
		55.3	50	50	2.088	2.084	120	80	99.9
		57.0	33	33	2.031	2.034	204	60	99.9
		58.4	33	33	1.986	1.994	115	80	99.7
		63.8	25	25	1.834	1.831	115	60	99.9
		64.5	100	100	1.816	1.818	213	60	99.9
(4)	FE7C3(2)	54.4	33	33	2.120	2.122	012	40	99.9
		58.4	33	33	1.986	1.989	300	16	99.9
		64.5	100	100	1.816	1.820	301	10	99.8
(5)	CR7C3(2)	58.4	33	33	1.986	1.990	300	20	99.9
		64.5	100	100	1.816	1.820	301	30	99.8
(6)	CR7C3	54.4	33	33	2.120	2.120	202	70	100.0
		57.0	33	33	2.031	2.040	421	100	99.7
		63.8	25	25	1.834	1.840	601	60	99.8
		64.5	100	100	1.816	1.810	431	70	99.8
(7)	(CR,FE)7C3	54.4	33	33	2.120	2.120	202	60	100.0
		57.0	33	33	2.031	2.040	122	100	99.7
		64.5	100	100	1.816	1.810	431	60	99.8
(8)	(CR7C3+MN7C3)	54.4	33	100	2.120	2.120	555	100	100.0
		57.0	33	100	2.031	2.040	666	100	99.7
		62.9	25	75	1.857	1.850	999	80	99.7
(9)	FE8SI2C	55.3	50	50	2.088	2.080	131	80	99.8
		58.4	33	33	1.986	1.980	114	60	99.8
		63.8	25	25	1.834	1.840	015	60	99.8
		64.5	100	100	1.816	1.810	015	20	99.8
(10)	CRMN3	57.0	33	100	2.031	2.036	202	70	99.8
		63.8	25	75	1.834	1.838	222	40	99.8
(11)	MN15C4	54.4	33	66	2.120	2.129	301	10	99.7
		55.3	50	100	2.088	2.094	213	100	99.8
		57.0	33	66	2.031	2.037	302	100	99.8

TABLE-5.21 SUMMARY TABLE OF DIFFRACTOGRAM INDEXING

ALLOY: P2; H/T TEMPERATURE: 900°C ; SOAKING DURATION: 2

DIFF. ANGLE	1		3		5		7		9		11		13		15		17		19		21		23		25		27		29	INT
54.5	0	0	0	0	0	0	1	0	1	1	1	0	1	1	1	1	1	1	1	0	0	0	0	0	0	0	0	0	1	9.0
55.2	0	0	0	0	0	1	0	0	1	0	0	1	0	0	0	0	0	0	0	0	0	0	0	1	1	0	0	1	0	8.0
57.1	1	0	1	0	0	1	0	1	1	1	1	1	1	1	0	0	0	0	0	0	1	0	0	0	0	0	0	1	1	8.0
61.8	0	0	0	1	1	0	0	0	0	0	1	0	0	0	0	0	1	0	0	0	0	0	0	0	1	0	1	0	0	10.0
64.2	0	0	0	0	0	0	1	0	1	1	1	1	0	0	0	0	0	1	0	0	0	0	0	1	1	0	0	0	0	12.0
64.6	0	0	0	0	0	0	1	0	1	0	1	0	1	1	0	0	1	0	0	0	1	0	0	1	1	0	0	0	0	60.0
118.0	0	0	0	0	0	0	0	1	0	0	1	0	0	0	0	0	0	0	0	0	0	0	0	0	0	0	0	0	0	8.0
121.2	0	0	0	0	0	0	0	0	0	0	0	0	0	0	0	0	0	0	0	0	0	0	0	0	0	0	0	0	0	10.0
124.0	0	0	0	0	0	0	0	0	0	0	0	0	0	0	0	0	0	0	0	0	0	0	0	0	0	0	0	0	0	8.0
125.2	0	0	0	0	0	0	0	1	0	0	0	0	0	0	0	0	0	0	0	0	0	0	0	1	0	0	0	0	0	8.0
127.4	0	0	0	0	0	0	0	0	0	0	0	0	0	0	0	0	0	0	0	0	0	0	0	0	0	0	0	0	0	10.0
	0	0	0	0	0	2	3	3	5	3	6	3	3	2	0	0	3	0	2	0	0	0	0	3	4	0	2	2	0	

0 = ABSENT 1 = PRESENT * = PROBABLE DIFF. ANGLE FOR K-BETA RADIATION

DETAILED ANALYSIS OF PHASE(S) ACTUALLY PRESENT

S.N.	PHASE PRESENT	DIFF. ANGLE	PEAK INT	I/IO	D MEAS	D STD	DIFF PLANE	INT STD	CONF LIMIT
(1)	FE3C(CEMENTITE)	55.2	13	100	2.091	2.100	121	60	99.8
		57.1	13	100	2.027	2.020	022	60	99.8
(2)	FE5C2	54.5	15	15	2.116	2.112	112	25	99.9
		64.2	20	20	1.823	1.821	511	20	99.9
		64.6	100	100	1.813	1.814	312	25	100.0
(3)	MN5C2	54.5	15	15	2.116	2.121	211	80	99.9
		55.2	13	13	2.091	2.084	120	80	99.8
		57.1	13	13	2.027	2.019	213	100	99.7
		64.2	20	20	1.823	1.831	115	60	99.7
		64.6	100	100	1.813	1.818	213	60	99.8
(4)	FE7C3(2)	54.5	15	15	2.116	2.122	012	40	99.8
		57.1	13	13	2.027	2.019	121	100	99.7
		61.8	16	16	1.887	1.895	112	6	99.7
		64.2	20	20	1.823	1.820	301	10	99.9
		64.6	100	100	1.813	1.807	022	20	99.7
		118.0	13	13	1.130	1.131	004	6	99.9
(5)	CR7C3	54.5	15	15	2.116	2.120	202	70	99.9
		57.1	13	13	2.027	2.020	---	50	99.8
		64.6	100	100	1.813	1.810	431	70	99.9
(6)	(CR,FE)7C3	54.5	15	15	2.116	2.120	202	60	99.9
		64.6	100	100	1.813	1.810	431	60	99.9
(7)	COPPER	55.2	13	13	2.091	2.088	111	100	99.9
		64.6	100	100	1.813	1.808	200	46	99.8
		125.2	13	13	1.091	1.090	311	17	99.8
(8)	FE8SI2C	55.2	13	13	2.091	2.090	130	80	100.0
		61.8	16	16	1.887	1.880	331	60	99.8
		64.2	20	20	1.823	1.820	031	20	99.9
		64.6	100	100	1.813	1.810	015	20	99.9
(9)	CRMN3	57.1	13	80	2.027	2.036	202	70	99.7
		61.8	16	100	1.887	1.888	777	90	100.0
(10)	MN15C4	55.2	13	100	2.091	2.094	213	100	99.9
		57.1	13	100	2.027	2.037	302	100	99.7

TABLE-5.22   SUMMARY TABLE OF DIFFRACTOGRAM INDEXING

ALLOY: P2;   H/T TEMPERATURE: 900°C ;   SOAKING DURATION: 10 HOURS

DIFF. ANGLE	1	3	5	7	9	11	13	15	17	19	21	23	25	27	29	INT
54.5	0 0	0 0	0 0	1 0	1 1	1 0	1 1	1 1	1 1	1 0	0 0	0 0	0 0	0 0	0 1	10.0
55.2	0 0	0 0	0 1	0 0	1 0	0 1	0 0	0 0	0 0	0 0	0 0	1 1	0 0	1 0	1 0	17.0
57.0	1 0	0 0	0 0	0 1	1 1	0 0	1 1	1 0	0 0	0 1	0 0	0 0	0 0	0 1	1 0	9.0
63.0	0 0	0 0	0 1	0 0	0 0	0 0	0 0	1 0	1 0	0 0	0 0	0 1	0 0	0 0	0 0	10.0
64.0	0 0	0 0	0 0	0 0	1 1	0 0	0 0	0 0	0 0	1 0	0 0	0 0	0 0	1 0	0 0	9.0
64.5	0 0	0 0	0 0	1 0	1 1	1 1	1 1	1 0	0 1	0 0	0 0	1 0	0 1	0 0	0 0	56.0
67.5	0 0	0 0	0 0	0 0	0 0	0 0	1 1	0 0	1 0	0 0	0 0	0 1	0 0	0 0	0 0	10.0
97.8	0 0	0 0	0 0	0 0	0 0	0 0	0 0	0 0	0 0	0 0	0 0	0 0	0 0	0 0	0 0	8.0
98.5	0 0	0 0	0 0	0 0	0 0	0 1	0 0	0 1	0 0	0 0	0 1	0 1	0 0	0 0	0 0	16.0
123.8	0 0	0 0	0 0	0 0	0 0	0 0	0 0	0 0	0 0	0 0	0 0	0 0	0 0	0 0	0 0	10.0
125.0	0 0	0 0	0 0	0 0	0 0	0 0	0 0	0 0	0 0	0 0	0 0	0 0	0 0	0 0	0 0	30.0
125.8	0 0	0 0	0 0	0 0	0 0	0 0	0 0	0 0	0 0	0 0	0 0	1 0	0 0	0 0	0 1	13.0
126.2	0 0	0 0	1 0	0 0	0 0	0 0	0 0	0 0	0 0	0 0	0 0	0 0	0 0	0 0	0 0	8.0
128.0	0 0	0 0	0 0	0 0	0 0	0 0	0 0	0 0	0 0	0 0	0 0	0 0	0 0	0 0	0 0	10.0
129.0	0 0	0 0	0 0	0 0	0 0	0 0	0 0	0 0	0 0	0 0	0 0	0 0	0 0	0 0	0 0	10.0

0 0 0 0 0 2 2 0 5 4 2 2 5 4 3 0 5 0 2 0 0 2 0 0 2 3 0 0 2 2

O = ABSENT   1 = PRESENT   * = PROBABLE DIFF. ANGLE FOR K-BETA RADIATION

DETAILED ANALYSIS OF PHASE(S) ACTUALLY PRESENT

S.N.	PHASE PRESENT	DIFF. ANGLE	PEAK INT	I/IO	D MEAS	D STD	DIFF PLANE	INT STD	CONF LIMIT
(1)	FE3C(CEMENTITE)	55.2	30	100	2.091	2.100	121	60	99.8
		63.0	17	58	1.854	1.850	122	40	99.8
(2)	FE5C2	54.5	17	17	2.116	2.112	112	25	99.9
		64.5	100	100	1.816	1.814	312	25	99.9
(3)	MN5C2	54.5	17	17	2.116	2.121	211	80	99.9
		55.2	30	30	2.091	2.084	120	80	99.8
		57.0	16	16	2.031	2.034	204	60	99.9
		64.0	16	16	1.828	1.831	115	60	99.9
		64.5	100	100	1.816	1.818	213	60	99.9
(4)	FE7C3(2)	54.5	17	17	2.116	2.122	012	40	99.8
		64.5	100	100	1.816	1.820	301	10	99.8
(5)	CR7C3	54.5	17	17	2.116	2.120	202	70	99.9
		57.0	16	16	2.031	2.040	421	100	99.7
		64.5	100	100	1.816	1.810	431	70	99.8
		67.5	17	17	1.744	1.750	412	70	99.7
		98.5	28	28	1.279	1.280	---	60	99.9
(6)	(CR,FE)7C3	54.5	17	17	2.116	2.120	202	60	99.9
		57.0	16	16	2.031	2.040	122	100	99.7
		64.5	100	100	1.816	1.810	431	60	99.8
		67.5	17	17	1.744	1.740	322	60	99.8
(7)	(CR7C3+MN7C3)	54.5	17	100	2.116	2.120	555	100	99.9
		57.0	16	90	2.031	2.040	666	100	99.7
		63.0	17	100	1.854	1.850	999	80	99.8
(8)	COPPER	55.2	30	100	2.091	2.088	111	100	99.9
		98.5	28	94	1.279	1.278	220	20	99.9
(9)	FE8SI2C	55.2	30	30	2.091	2.090	130	80	100.0
		64.5	100	100	1.816	1.810	015	20	99.8
		67.5	17	17	1.744	1.740	225	20	99.8
(10)	MN15C4	55.2	30	100	2.091	2.094	213	100	99.9
		57.0	16	52	2.031	2.037	302	100	99.8

TABLE-5.23   SUMMARY TABLE OF DIFFRACTOGRAM INDEXING

ALLOY: P2;   H/T TEMPERATURE: 900°C ;   SOAKING DURATION: 6 HOURS

```
DIFF.                              PHASE(S)                                            INT
ANGLE   1  3  5  7  9 11 13 15 17 19 21 23 25 27 29

 54.4   0 0 0 0 0 0 1 0 1 1 1 0 1 1 1 1 1 1 0 1 0 0 0 0 0 0 1 0 1 1    5.0
 55.3   0 1 0 0 0 0 1 0 1 1 0 0 0 0 0 0 0 0 0 0 0 0 0 0 1 1 0 0 1 0    5.0
 63.8   0 0 0 0 0 0 0 0 1 1 0 0 1 0 0 0 0 0 0 1 0 0 0 0 0 1 1 1 0 0    5.0
 64.6   0 0 0 0 0 0 1 0 1 1 1 1 1 1 1 0 0 1 0 0 0 0 1 0 0 1 1 0 0 0   11.0
 65.2   0 1 0 1 1 0 0 1 0 0 0 0 0 0 0 0 0 0 0 0 1 0 0 0 0 1 0 0 1 0    3.0
 98.0   0 0 0 0 0 0 0 0 0 0 0 0 0 0 0 0 0 0 0 0 0 0 0 1 0 0 0 0 0 0    8.0
104.5   0 0 0 0 0 0 0 0 0 0 0 0 1 0 0 0 1 0 0 0 1 0 0 0 0 0 1 0 0 0    6.0
116.5   0 0 0 0 0 0 0 1 0 0 0 0 0 0 0 0 0 0 0 0 1 1 0 0 0 0 1 0 0 0    7.0
118.7   0 0 0 0 0 0 0 0 0 0 0 0 0 0 0 0 0 0 0 0 0 0 0 0 0 0 0 0 0 0    4.0
121.7   0 0 0 0 0 0 0 1 0 0 0 0 0 0 0 0 0 0 0 0 0 0 0 0 0 0 0 0 0 0    5.0
125.2   0 0 0 0 0 0 0 1 0 0 0 0 0 0 0 0 0 0 0 0 0 0 0 0 0 1 0 0 0 0   13.0
126.1   0 0 0 0 1 0 0 0 0 0 0 0 0 0 0 0 0 0 0 0 0 0 0 0 1 0 0 0 0 1    5.0

        0 2 0 0 2 0 3 4 4 4 2 0 4 2 0 0 3 0 0 3 3 2 0 0 3 4 4 0 3 2
```

0 = ABSENT   1 = PRESENT   * = PROBABLE DIFF. ANGLE FOR K-BETA RADIATION

DETAILED ANALYSIS OF PHASE(S) ACTUALLY PRESENT

S.N.	PHASE PRESENT	DIFF. ANGLE	PEAK INT	I/IO	D MEAS	D STD	DIFF PLANE	INT STD	CONF LIMIT
(1)	AUSTENITE	55.3	38	100	2.088	2.080	111	100	99.8
		65.2	23	60	1.798	1.800	200	80	99.9
(2)	FE5C2	54.4	38	45	2.120	2.112	112	25	99.8
		55.3	38	45	2.088	2.080	021	70	99.8
		64.6	84	100	1.813	1.814	312	25	100.0
(3)	MN5C2	54.4	38	45	2.120	2.121	211	80	100.0
		55.3	38	45	2.088	2.084	120	80	99.9
		63.8	38	45	1.834	1.831	115	60	99.9
		64.6	84	100	1.813	1.818	213	60	99.8
(4)	FE7C3(2)	54.4	38	45	2.120	2.122	012	40	99.9
		64.6	84	100	1.813	1.807	022	20	99.7
(5)	CR7C3	54.4	38	45	2.120	2.120	202	70	100.0
		63.8	38	45	1.834	1.840	601	60	99.8
		64.6	84	100	1.813	1.810	431	70	99.9
		104.5	46	54	1.225	1.227	---	60	99.8
(6)	(CR,FE)7C3	54.4	38	45	2.120	2.120	202	60	100.0
		64.6	84	100	1.813	1.810	431	60	99.9
(7)	COPPER	55.3	38	38	2.088	2.088	111	100	100.0
		64.6	84	84	1.813	1.808	200	46	99.8
		125.2	100	100	1.091	1.090	311	17	99.8
(8)	FE8SI2C	55.3	38	45	2.088	2.080	131	80	99.8
		63.8	38	45	1.834	1.840	015	60	99.8
		64.6	84	100	1.813	1.810	015	20	99.9
		65.2	23	27	1.798	1.794	312	20	99.8
(9)	MN15C4	54.4	38	100	2.120	2.129	301	10	99.7
		55.3	38	100	2.088	2.094	213	100	99.8
		65.2	23	60	1.798	1.800	310	20	99.9

Table-5.58 %TG' data of 1000°C, 10 hours heat treated samples of the experimental alloys

Temperature °C	Alloy		
	P1	P2	P3
R.T	0	0	0
100	0	0	0
200	0	0	0
300	0	0	0
400	0	0	0
500	0	0	0
600	0	0	0
700	0.5	0.5	0.5
800	1.2	1.8	1.3
900	2.0	2.2	1.9
950	3.0	3.8	2.5

* Experiment discontinued at 950°C

Table 6.1 Effect of heat treatment on compressive behaviour

Alloy P1

H/T condition	Compressive Strength		% Strain
	TSI	MN/m²	
As-Cast	133.55	2064.67	25.20
850,2,AC	174.12	2691.87	29.60
850,10,AC	150.64	2328.95	26.22
900,2,AC	110.49	1708.15	20.77
900,6,AC	153.68	2375.90	25.78
900,10,AC	149.73	2314.89	27.65
950,2,AC	100.51	1553.91	22.16
950,6,AC	182.08	2814.91	32.00
1000,2,AC	154.42	2387.32	27.05
1000,10,AC	140.05	2165.15	30.74
1050,2,AC	141.49	2187.50	38.63
1050,6,AC	163.80	2532.31	34.95
1050,10,AC	171.90	2657.58	39.39

Table 6.2 Effect of heat treatment on compressive behaviour

Alloy P2

H/T condition	Compressive Strength		% Strain
	TSI	MN/m^2	
As-Cast	97.43	1506.20	24.45
850,2,AC	131.62	2034.84	22.64
900,2,AC	165.53	2559.09	27.12
900,6,AC	126.90	1961.81	22.06
900,10,AC	108.04	1670.23	20.89
950,2,AC	153.80	2377.69	25.88
950,10,AC	183.06	2830.13	32.85
1000,2,AC	119.58	1848.72	27.26
1000,10,AC	170.89	2642.00	35.96
1050,2,AC	116.56	1802.00	25.70
1050,6,AC	168.82	2609.96	35.10
1050,10,AC	202.47	3130.19	40.95

Table 6.3 Effect of heat treatment on compressive behaviour

Alloy P3

H/T condition	Compressive Strength		% Strain
	TSI	MN/m^2	
As-Cast	130.96	2024.65	23.11
850,2,AC	90.98	1406.55	18.96
850,10,AC	163.25	2523.91	27.27
900,2,AC	150.81	2331.62	27.24
900,6,AC	159.85	2471.26	27.12
900,10,AC	143.49	2218.34	27.26
950,2,AC	130.61	2019.29	23.18
950,6,AC	150.57	2327.80	29.50
950,10,AC	97.92	1543.72	26.75
1000,2,AC	122.49	1893.55	33.00
1050,2,AC	125.88	1945.91	32.59
1050,6,AC	151.93	2348.64	35.42
1050,10,AC	119.81	1852.01	28.61

Table-6.4 Summary table of the predicted and experimentally determined compressive strength values (based on Equations 6.2-6.4)

	Hardness	CSexp	Rexp	Rpred	CSpred	%error
P1,850,2	458	2691.87	5.88	5.05	2313.55	16.35
P1,850,10	450	2328.95	5.18	5.05	2273.17	-2.45
P1,900,2	456	1708.15	3.75	5.05	2302.26	25.81
P1,900,6	451	2375.90	5.27	5.05	2277.53	-4.32
P1,900,10	435	2314.89	5.32	5.13	2230.28	-3.79
P1,950,2	435	1553.91	3.57	5.13	2230.28	30.33
P1,950,6	432	2814.91	6.52	5.15	2226.53	-26.43
P1,1000,2	417	2387.32	5.72	5.35	2229.96	-7.08
P1,1000,10	398	2165.15	5.44	5.73	2282.18	5.13
P1,1050,2	390	2187.50	5.61	5.94	2318.18	5.64
P1,1050,6	363	2532.31	6.98	6.86	2489.89	-1.70
P1,1050,10	343	2657.58	7.75	7.74	2655.70	-.07
P2,850,2	459	2034.84	4.43	4.81	2206.64	7.79
P2,900,2	436	2559.09	5.87	4.84	2109.92	-21.29
P2,900,6	441	1961.81	4.45	4.80	2115.58	7.27
P2,900,10	430	1670.23	3.88	4.92	2113.66	20.98
P2,950,2	429	2377.69	5.54	4.93	2115.36	-12.40
P2,950,10	422	2830.13	6.71	5.06	2135.65	-32.52
P2,1000,2	413	1848.72	4.48	5.28	2182.29	15.29
P2,1000,10	389	2642.00	6.79	6.19	2407.25	-9.75
P2,1050,2	402	1802.00	4.48	5.64	2268.34	20.56
P2,1050,6	365	2609.96	7.15	7.54	2752.91	5.19
P2,1050,10	350	3130.19	8.94	8.62	3015.86	-3.79
P3,850,2	445	1406.55	3.16	4.84	2155.01	34.73
P3,850,10	449	2523.91	5.62	4.82	2165.38	-16.56
P3,900,2	433	2331.62	5.38	4.91	2125.02	-9.72
P3,900,6	436	2471.26	5.67	4.89	2132.37	-15.89
P3,900,10	408	2218.34	5.44	5.07	2067.02	-7.32
P3,950,2	417	2019.29	4.84	5.01	2087.31	3.26
P3,950,6	421	2327.80	5.53	4.98	2096.52	-11.03
P3,950,10	405	1543.72	3.81	5.09	2060.38	25.08
P3,1000,2	406	1893.55	4.66	5.08	2062.59	8.20
P3,1050,2	392	1945.91	4.96	5.18	2032.20	4.25
P3,1050,6	376	2348.64	6.25	5.31	1998.44	-17.52
P3,1050,10	330	1852.01	5.61	5.76	1901.68	2.61

Table-6.5 Summary table of the predicted and experimentally
determined % strain (based on Equations 6.5-6.7)

	Hardness	%strain exp	Rexp	Rpred	%strain pred	%error
P1,850,2	458	29.60	.065	.054	24.89	-18.92
P1,850,10	450	26.22	.058	.057	25.76	-1.77
P1,900,2	456	20.77	.046	.055	25.11	17.27
P1,900,6	451	25.78	.057	.057	25.65	-.50
P1,900,10	435	27.65	.064	.063	27.50	-.55
P1,950,2	435	22.16	.051	.063	27.50	19.42
P1,950,6	432	32.00	.074	.064	27.86	-14.86
P1,1000,2	417	27.05	.065	.071	29.72	8.98
P1,1000,10	398	30.74	.077	.081	32.16	4.43
P1,1050,2	390	38.63	.099	.085	33.21	-16.31
P1,1050,6	363	34.95	.096	.101	36.75	4.91
P1,1050,10	343	39.39	.115	.115	39.30	-.23
P2,850,2	459	22.64	.049	.048	22.23	-1.82
P2,900,2	436	27.12	.062	.057	24.72	-9.73
P2,900,6	441	22.06	.050	.055	24.09	8.44
P2,900,10	430	20.89	.049	.059	25.52	18.14
P2,950,2	429	25.88	.060	.060	25.66	-.87
P2,950,10	422	32.85	.078	.063	26.68	-23.15
P2,1000,2	413	27.26	.066	.068	28.09	2.94
P2,1000,10	389	35.96	.092	.083	32.32	-11.26
P2,1050,2	402	25.70	.064	.075	29.95	14.19
P2,1050,6	365	35.10	.096	.102	37.05	5.27
P2,1050,10	350	40.95	.117	.115	40.15	-1.99
P3,850,2	445	18.96	.043	.053	23.73	20.11
P3,850,10	449	27.27	.061	.051	22.78	-19.72
P3,900,2	433	27.24	.063	.061	26.24	-3.82
P3,900,6	436	27.12	.062	.059	25.66	-5.69
P3,900,10	408	27.26	.067	.073	29.85	8.69
P3,950,2	417	23.18	.056	.069	28.79	19.49
P3,950,6	421	29.50	.070	.067	28.23	-4.49
P3,950,10	405	26.75	.066	.074	30.15	11.28
P3,1000,2	406	33.00	.081	.074	30.05	-9.80
P3,1050,2	392	32.59	.083	.079	31.12	-4.71
P3,1050,6	376	35.42	.094	.084	31.66	-11.88
P3,1050,10	330	28.61	.087	.090	29.74	3.79

Table-6.6 Polarization data

H/T schedule	Ecorr(I=0) mV	Ecorr(mV) cathodic	anodic	Icorr μA/cm²	corrosion rate mils/y	MDD	IPY
P1,900,10	-510.82	329.39	75.51	21.998	10.27	55.75	0.0103
P1,950,2	-453.66	873.43	89.5	37.656	17.57	95.38	0.0176
P1,950,10	-536.11	409.98	45.63	14.674	6.84	37.13	0.0068
P1,1000,2	-598.86	173.22	101.15	8.933	4.17	22.64	0.0042
P1,1000,10	-553.85	344.49	94.59	9.024	4.21	22.85	0.0042
P1,1050,2	-495.44	179.25	33.88	5.587	2.61	14.17	0.0026
P1,1050,10	-417.72	579.23	51.12	23.268	10.86	58.96	0.0109
P2,900,2	-584.12	1017.8	156.59	63.041	29.42	159.7	0.0294
P2,1050,2	-603.94	3348.2	126.22	41.600	19.41	105.4	0.0194
P2,1050,10	-567.37	470.63	99.66	11.852	5.53	30.02	0.0055
P3,900,10	-632.58	673.83	84.49	16.552	7.72	41.91	0.0077
P3,1000,2	-530.71	727.56	104.48	18.090	8.44	47.99	0.0084
P3,1000,10	-513.57	701.16	110.26	19.952	9.31	50.54	0.0093
P3,1050,2	-650.55	340.32	79.99	13.049	6.09	30.06	0.0061
P3,1050,10	-785.39	53.54	118.87	13.235	6.18	33.55	0.0062

Table 6.7   Corrosion data in 5% NaCl solution

ALLOY DESIG- NATION	HEAT TREAT- MENT	AREA SQ.CM	WEIGHT LOSS (GMS)	CORROSION RATE	
				MDD	IPY
P1	AS-CAST	5.5134	.00810	20.98791	.00387
P1	900 2	4.9549	.00777	22.40224	.00413
P1	900 10	6.2309	.00800	18.34153	.00338
P1	950 2	5.7074	.00721	18.04635	.00333
P1	950 10	5.6575	.00668	16.86750	.00311
P1	1000 2	7.2783	.00765	15.01612	.00277*
P1	1000 10	4.6958	.00509	15.48568	.00285*
P1	1050 2	7.3963	.00684	13.21076	.00243*
P1	1050 10	5.1705	.00410	11.32900	.00209*
P2	AS-CAST	7.8112	.00983	17.97883	.00331
P2	900 2	5.7042	.00742	18.58279	.00342
P2	900 10	5.4363	.00800	21.02243	.00387
P2	950 2	6.0547	.00820	19.34670	.00357
P2	950 10	5.5973	.00659	16.81905	.00310
P2	1000 2	4.9207	.00535	15.53254	.00286*
P2	1000 10	4.5465	.00433	13.60504	.00251*
P2	1050 2	3.9400	.00370	13.41558	.00247*
P2	1050 10	4.3369	.00361	11.89097	.00219*
P3	AS-CAST	5.4441	.00715	18.76274	.00346
P3	900 2	7.4875	.00903	17.22743	.00317
P3	900 10	5.5140	.00750	19.43150	.00358
P3	950 2	5.7848	.00865	21.36097	.00394
P3	950 10	5.0983	.00650	18.21270	.00336
P3	1000 2	7.4700	.00751	14.36257	.00265*
P3	1000 10	5.6684	.00522	13.15559	.00242*
P3	1050 2	6.5597	.00561	12.21743	.00225*
P3	1050 10	4.7474	.00365	10.98247	.00202*

* values comparable to those attained in Ni-Resist compositions

Table 6.8 Comparative corrosion rates(in mdd) of the experimental alloys
          in the heat treated condition

ALLOY	900°C		950°C		1000°C		1050°C	
	2 h	10 h	2 h	10 h	2 h	10 h	2 h	10 h
P1	22.40	18.34	18.05	16.87	15.02	15.49	13.21	11.33
P2	18.58	21.02	19.35	16.82	15.53	13.61	13.42	11.89
P3	17.23	19.43	21.36	18.21	14.36	13.16	12.22	10.98

Table-6.9 Summary table of predicted vs experimentally determined CR values based on NOP (based on Equations 6.20-6.22)

H/T	CR$_{exp}$	I factor	II factor	CR$_{pre}$	% error
P1,900,2	22.402	28.940	.742	21.466	4.36
P1,900,10	18.341	24.376	.717	17.466	5.01
P1,950,2	18.046	23.856	.711	16.969	6.35
P1,950,10	16.867	21.623	.750	16.208	4.07
P1,1000,2	15.016	20.049	.722	14.478	3.72
P1,1000,10	15.485	19.237	.768	14.771	4.83
P2,900,2	18.583	16.722	1.124	18.796	1.13
P2,900,10	21.022	18.553	1.124	20.854	.80
P2,950,2	19.346	15.637	1.105	17.284	11.93
P2,950,2	16.819	15.346	1.093	16.770	.29
P2,1000,2	15.532	15.860	1.105	17.531	11.40
P2,1000,10	13.605	12.599	1.085	13.671	.48
P3,900,2	17.227	12.348	1.554	19.186	10.21
P3,900,10	19.431	11.642	1.673	19.473	.22
P3,950,2	21.361	12.084	1.554	18.776	13.77
P3,950,10	18.213	10.779	1.698	18.300	.48
P3,1000,2	14.362	10.047	1.517	15.247	5.80
P3,1000,10	13.160	8.417	1.517	12.772	3.04

Table 6.10   Summary table of predicted vs experimentally
             determined CR based on NOP (with constraints)
             (based on Equations 6.23-6.25)

H/T	CR$_{exp}$	I factor	II factor	CR$_{pre}$	% error
P1,900,2	22.402	28.938	.776	22.450	.21
P1,900,10	18.341	24.373	.753	18.360	.11
P1,950,2	18.046	23.853	.749	17.858	1.05
P1,950,10	16.867	21.621	.783	16.923	.33
P1,1000,2	15.016	20.046	.758	15.201	1.22
P1,1000,10	15.485	19.235	.799	15.367	.77
P2,900,2	18.583	19.510	.950	18.534	.26
P2,900,10	21.022	22.039	.950	20.937	.41
P2,950,2	19.346	18.039	.957	17.264	12.06
P2,950,10	16.819	17.651	.962	16.977	.93
P2,1000,2	15.532	18.340	.957	17.551	11.51
P2,1000,10	13.605	14.138	.965	13.640	.26
P3,900,2	17.227	20.181	.998	20.137	14.45
P3,900,10	19.431	18.364	.997	18.317	6.08
P3,950,2	21.361	19.435	.998	19.392	10.15
P3,950,10	18.213	16.707	.997	16.663	9.30
P3,1000,2	14.362	15.593	.998	15.561	7.70
P3,1000,10	13.160	13.706	.998	13.678	3.79

Table 6.11 Summary table of predicted vs experimentally
determined CR based on NOP (unified model)
(based on Equation 6.26)

H/T	CR$_{exp}$	I factor	II factor	CR$_{pre}$	% error
P1,900,2	22.402	20.116	1.128	22.692	1.28
P1,900,10	18.341	17.134	1.144	19.599	6.42
P1,950,2	18.046	16.759	1.147	19.226	6.14
P1,950,10	16.867	14.996	1.123	16.846	.13
P1,1000,2	15.016	13.473	1.140	15.363	2.26
P1,1000,10	15.485	12.435	1.112	13.833	11.94
P2,900,2	18.583	16.270	1.132	18.425	.86
P2,900,10	21.022	17.581	1.132	19.909	5.59
P2,950,2	19.346	15.448	1.112	17.185	12.58
P2,950,10	16.819	15.220	1.099	16.727	.55
P2,1000,2	15.532	15.621	1.112	17.377	10.62
P2,1000,10	13.605	12.801	1.091	13.963	2.56
P3,900,2	17.227	16.945	1.112	18.850	8.61
P3,900,10	19.431	16.031	1.132	18.154	7.03
P3,950,2	21.361	16.574	1.112	18.437	15.86
P3,950,10	18.213	15.164	1.137	17.234	5.68
P3,1000,2	14.362	14.559	1.106	16.103	10.81
P3,1000,10	13.160	13.473	1.106	14.902	11.69

Table 6.12 Summary table of predicted vs experimentally
determined CR based on DF
(based on Equations 6.27-6.29)

H/T	CR$_{exp}$	I factor	II factor	CR$_{pre}$	% error
P1,900,2	22.402	20.235	1.104	22.348	.24
P1,900,10	18.341	16.671	1.112	18.537	1.06
P1,950,2	18.046	16.292	1.106	18.013	.18
P1,950,10	16.867	14.779	1.132	16.732	.81
P1,1000,2	15.016	13.926	1.076	14.989	.18
P1,1000,10	15.485	13.678	1.136	15.535	.32
P2,900,2	18.583	8.484	2.174	18.445	.75
P2,900,10	21.022	8.824	2.381	21.015	.04
P2,950,2	19.346	8.148	2.394	19.505	.81
P2,950,10	16.819	8.036	2.033	16.339	2.94
P2,1000,2	15.532	8.227	1.943	15.984	2.83
P2,1000,10	13.605	6.181	2.204	13.620	.11
P3,900,2	17.227	33.905	.571	19.363	11.03
P3,900,10	19.431	32.308	.577	18.647	4.20
P3,950,2	21.361	33.362	.571	19.053	12.11
P3,950,10	18.213	29.915	.614	18.376	.89
P3,1000,2	14.362	27.655	.568	15.721	8.65
P3,1000,10	13.160	22.151	.568	12.593	4.51

Table 6.13   Summary table of predicted vs experimentally
determined CR based on DF (with constraints)
(based on Equations 6.30-6.32)

H/T	CR$_{exp}$	I factor	II factor	CR$_{pre}$	% error
P1,900,2	22.402	18.389	1.188	21.840	2.57
P1,900,10	18.341	15.765	1.202	18.944	3.18
P1,950,2	18.046	15.444	1.190	18.378	1.81
P1,950,10	16.867	13.973	1.240	17.324	2.64
P1,1000,2	15.016	12.763	1.136	14.497	3.58
P1,1000,10	15.485	11.983	1.247	14.940	3.65
P2,900,2	18.583	15.557	1.195	18.596	.07
P2,900,10	21.022	17.149	1.221	20.932	.43
P2,950,2	19.346	14.561	1.222	17.795	8.72
P2,950,10	16.819	14.286	1.177	16.816	.02
P2,1000,2	15.532	14.770	1.165	17.205	9.72
P2,1000,10	13.605	11.377	1.199	13.642	.27
P3,900,2	17.227	19.984	1.003	20.046	14.06
P3,900,10	19.431	18.374	1.003	18.429	5.43
P3,950,2	21.361	19.339	1.003	19.399	10.11
P3,950,10	18.213	16.770	1.003	16.815	8.31
P3,1000,2	14.362	15.599	1.003	15.647	8.21
P3,1000,10	13.160	13.373	1.003	13.415	1.90

Table 6.14 Summary table of predicted vs experimentally determined CR based on DF (unified model) (based on Equation 6.33)

H/T	CR_{exp}	I factor	II factor	CR_{pre}	% error
P1,900,2	22.402	20.730	1.093	22.654	1.11
P1,900,10	18.341	17.782	1.099	19.550	6.18
P1,950,2	18.046	17.395	1.094	19.029	5.16
P1,950,10	16.867	15.515	1.117	17.335	2.70
P1,1000,2	15.016	13.784	1.068	14.721	2.00
P1,1000,10	15.485	12.528	1.120	14.037	10.31
P2,900,2	18.583	16.885	1.095	18.485	.53
P2,900,10	21.022	18.238	1.106	20.179	4.18
P2,950,2	19.346	16.008	1.107	17.722	9.16
P2,950,10	16.819	15.761	1.086	17.120	1.76
P2,1000,2	15.532	16.194	1.080	17.498	11.23
P2,1000,10	13.605	12.979	1.096	14.231	4.40
P3,900,2	17.227	17.588	1.068	18.776	8.25
P3,900,10	19.431	16.632	1.066	17.734	9.57
P3,950,2	21.361	17.203	1.068	18.365	16.31
P3,950,10	18.213	15.699	1.059	16.618	9.60
P3,1000,2	14.362	15.029	1.068	16.053	10.54
P3,1000,10	13.160	13.784	1.068	14.724	10.62

Table 6.15 Experimentally determined and predicted compressive
strength values(based on Equations 6.35-6.37)

	CR	CS$_{exp}$	CS$_{pre}$	CS$_{exp}$-CS$_{pre}$
P1,900,2	22.40000	1708.15000	1657.18600	50.96423
P1,900,10	18.34000	2314.89000	1976.07000	338.82030
P1,950,2	18.05000	1553.91000	1998.84700	-444.93700
P1,1000,2	15.02000	2387.32000	2236.83200	150.48850
P1,1000,10	15.49000	2165.15000	2199.91700	-34.76660
P1,1050,2	13.21000	2187.50000	2378.99400	-191.49410
P1,1050,10	11.33000	2657.58000	2526.65500	130.92550
P2,900,2	18.58000	2559.09000	2209.80700	349.28300
P2,900,10	21.02000	1670.23000	2053.28800	-383.05760
P2,950,2˙	19.35000	2377.69000	2160.41400	217.27640
P2,950,10	16.82000	2830.13000	2322.70600	507.42360
P2,1000,2	15.53000	1848.72000	2405.45600	-556.73630
P2,1000,10	13.61000	2642.00000	2528.61900	113.38090
P2,1050,2	13.42000	1802.00000	2540.80700	-738.80710
P2,1050,10	11.89000	3130.19000	2638.95300	491.23730
P3,900,2	17.23000	2331.62000	1987.71700	343.90300
P3,900,10	19.43000	2218.34000	2023.06600	195.27430
P3,950,2	21.36000	2019.29000	2054.07600	-34.78613
P3,950,10	18.21000	1543.72000	2003.46300	-459.74340
P3,1000,2	14.36000	1893.55000	1941.60300	-48.05322
P3,1050,2	12.22000	1945.91000	1907.21900	38.69141
P3,1050,10	10.98000	1852.01000	1887.29500	-35.28479

Table 6.16 Experimentally determined and predicted %strain
values(based on Equations 6.38-6.40)

	CR	% strain$_{exp}$	%strain$_{pre}$	(% strain$_{exp}$ - %strain$_{pre}$)
P1,900,2	22.40000	20.77000	18.48539	2.28461
P1,900,10	18.34000	27.65000	25.76166	1.88834
P1,950,2	18.05000	22.16000	26.28140	-4.12140
P1,1000,2	15.02000	27.05000	31.71172	-4.66172
P1,1000,10	15.49000	30.74000	30.86939	-.12939
P1,1050,2	13.21000	38.63000	34.95557	3.67443
P1,1050,10	11.33000	39.39000	38.32488	1.06512
P2,900,2	18.58000	27.12000	26.07087	1.04913
P2,900,10	21.02000	20.89000	22.35616	-1.46616
P2,950,2	19.35000	25.88000	24.89861	.98139
P2,950,10	16.82000	32.85000	28.75033	4.09966
P2,1000,2	15.53000	27.26000	30.71426	-3.45426
P2,1000,10	13.61000	35.96000	33.63731	2.32269
P2,1050,2	13.42000	25.70000	33.92657	-8.22657
P2,1050,10	11.89000	40.95000	36.25587	4.69413
P3,900,2	17.23000	27.24000	27.70111	-.46111
P3,900,10	19.43000	27.26000	26.17783	1.08217
P3,950,2	21.36000	23.18000	24.84149	-1.66149
P3,950,10	18.21000	26.75000	27.02256	-.27256
P3,1000,2	14.36000	33.00000	29.68831	3.31169
P3,1050,2	12.22000	32.59000	31.17005	1.41995
P3,1050,10	10.98000	28.61000	32.02863	-3.41863
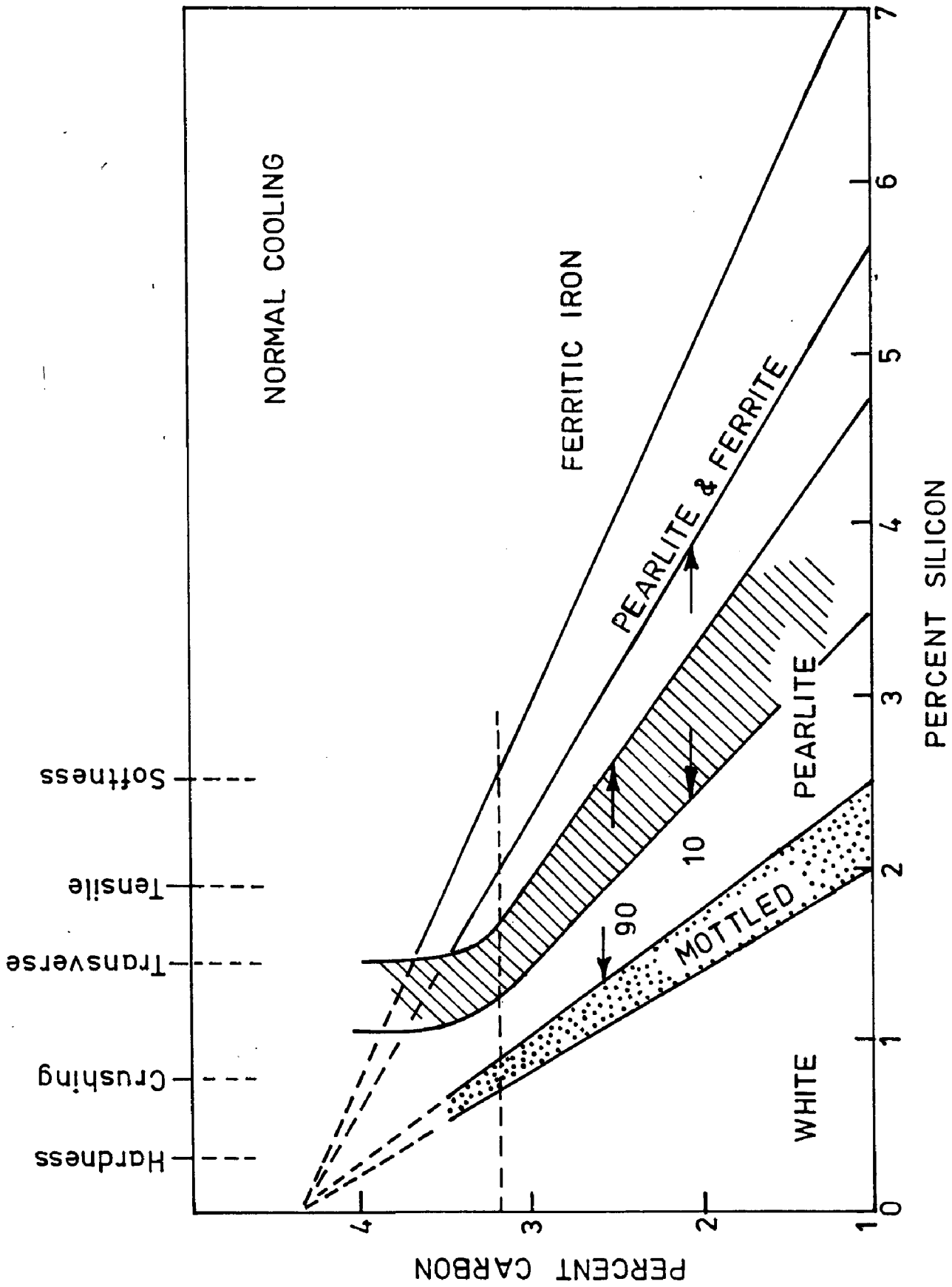
Fig.1.1 Maurer diagram (8) shaded area shows compositions common to 10 mm and 90 mm sections.
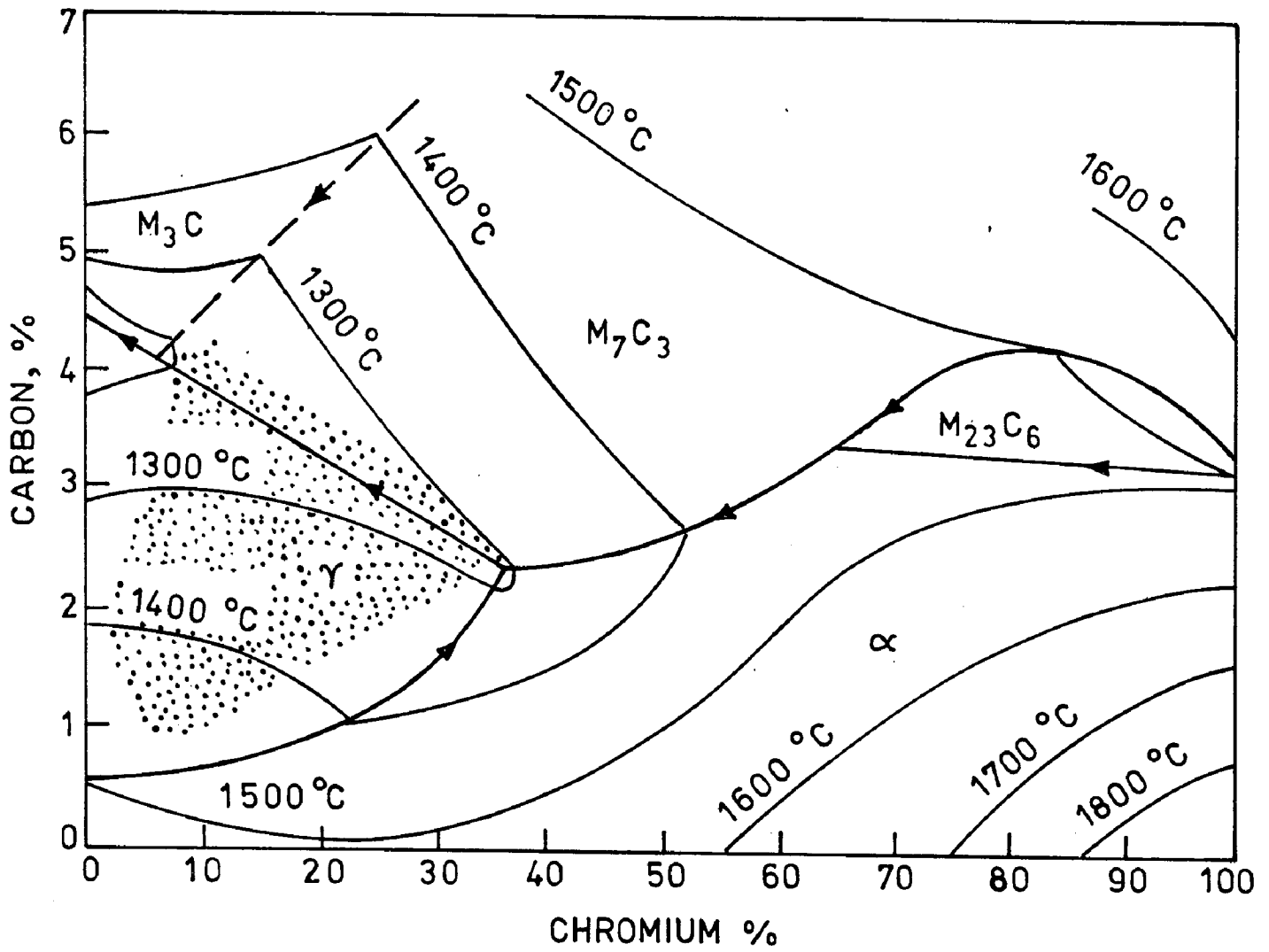
Fig.1.2 Liquidus surface of the Fe-Cr-C metastable system
showing different carbides (16,17).
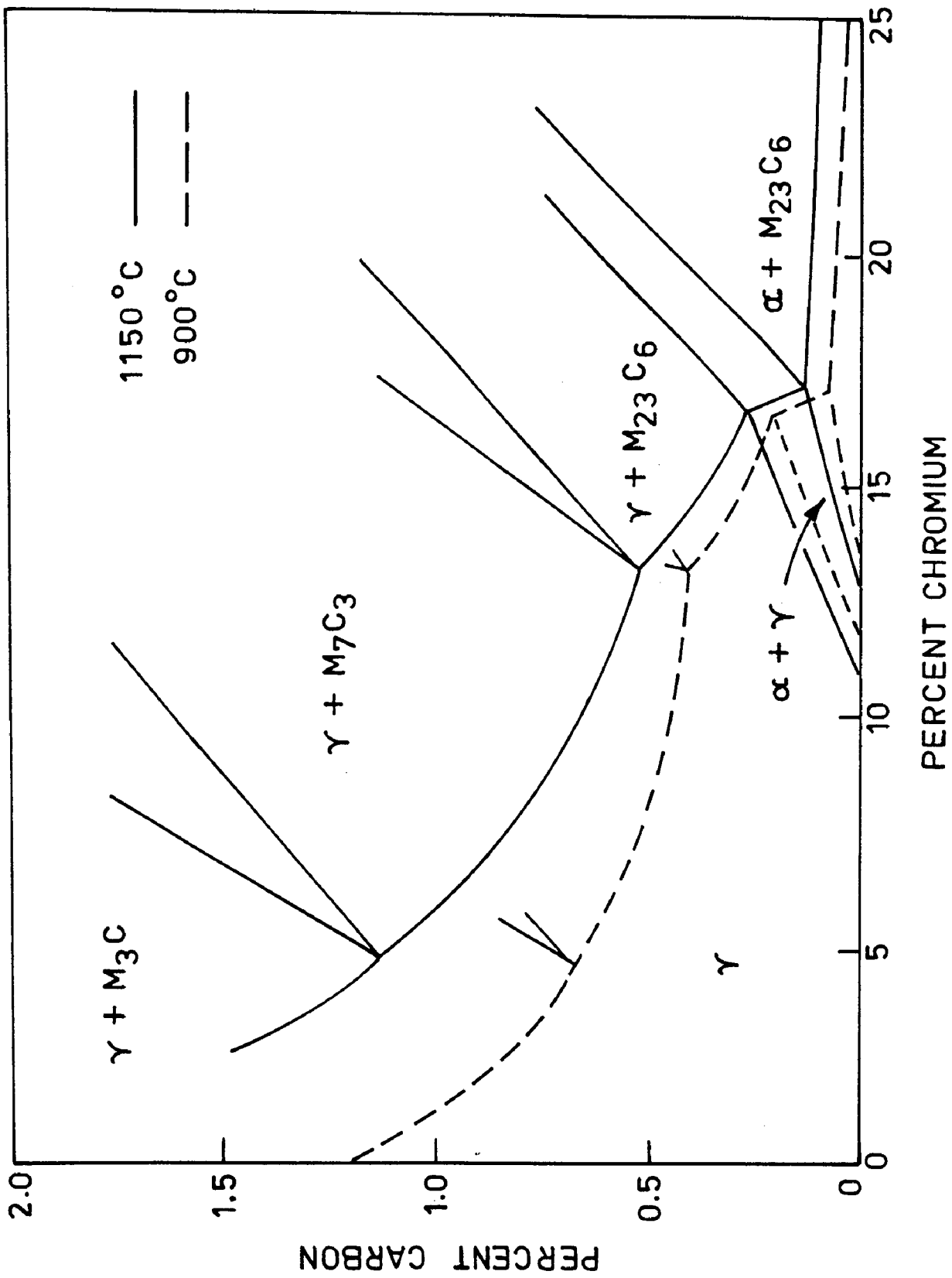
Fig. 1.3 900°C and 1150°C isothermal sections of the
Fe - Cr - C system (22, 23).
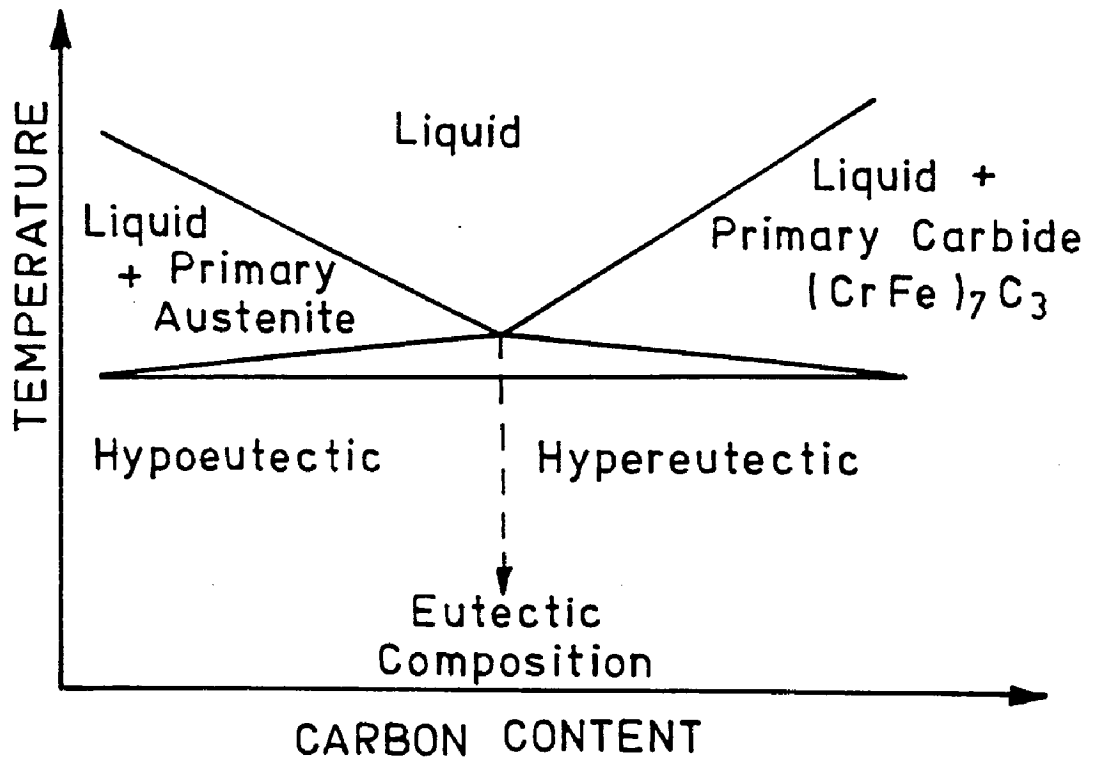
Fig. 1.4 Eutectic reaction in Fe-Cr-C system (37, 39).
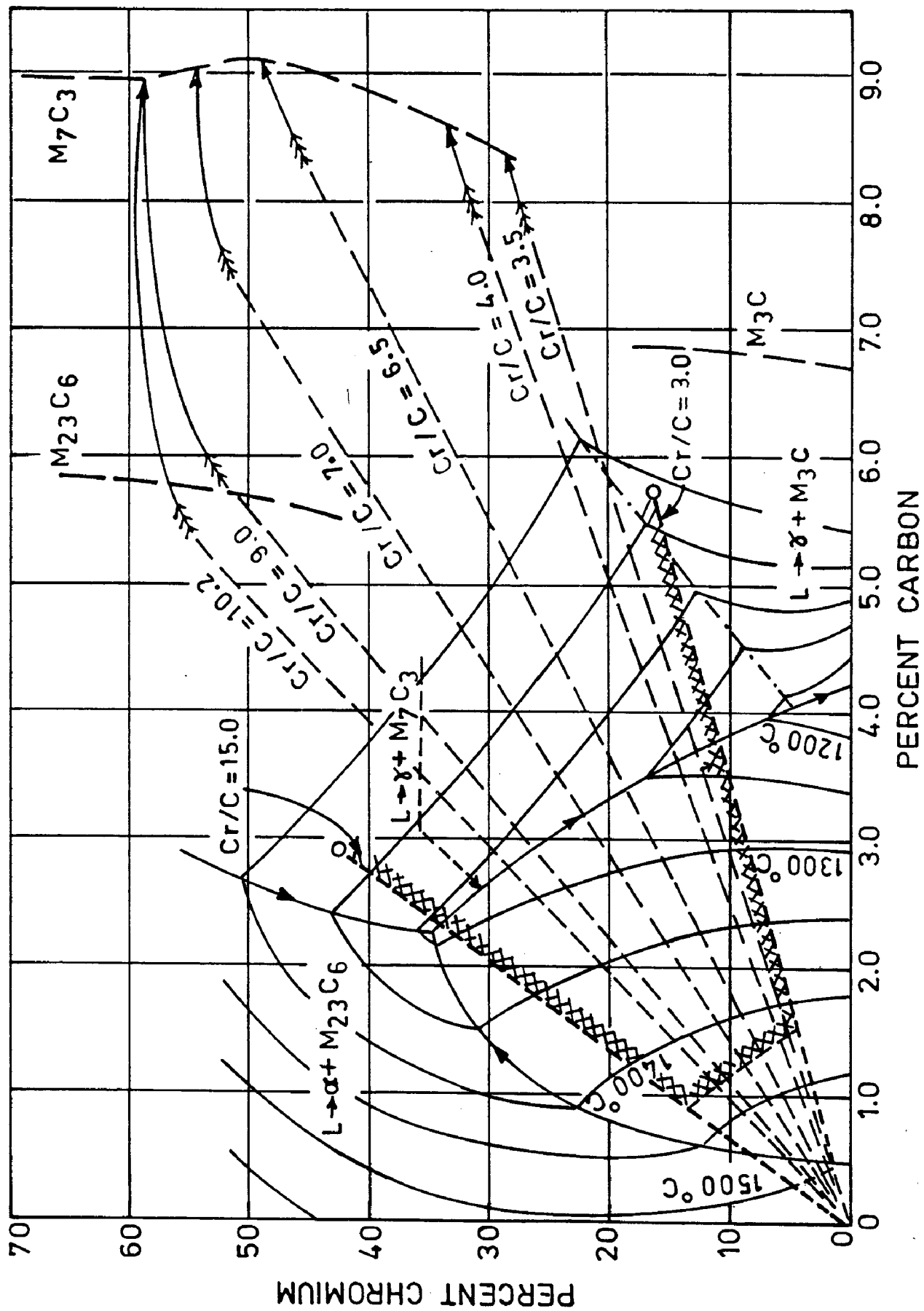
Fig.1.5 The liquid surface of Fe-Cr-C system (37, 38).
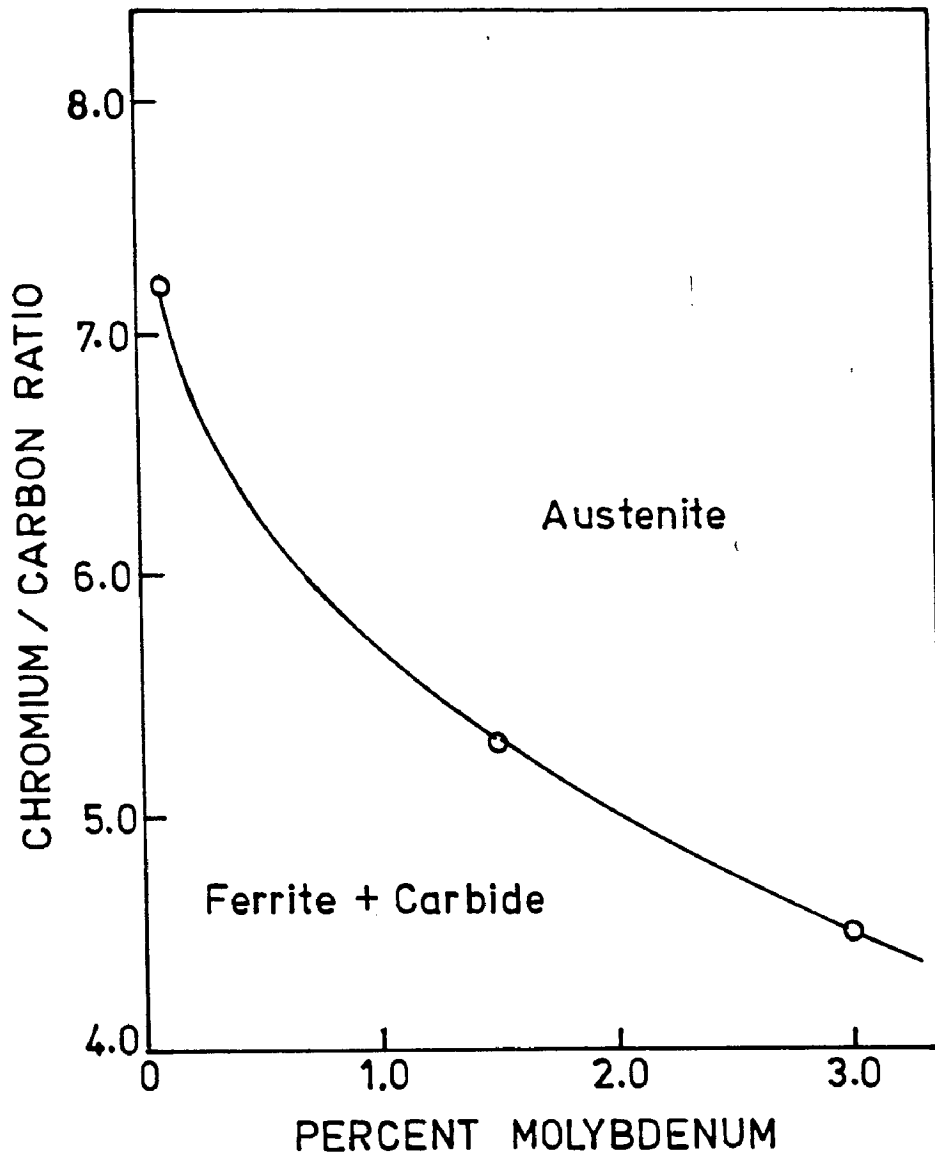
Fig. 1.6 The relationship between the Cr/C
ratio and molybdenum content for an
as-cast 25-mm diameter round (37,38)
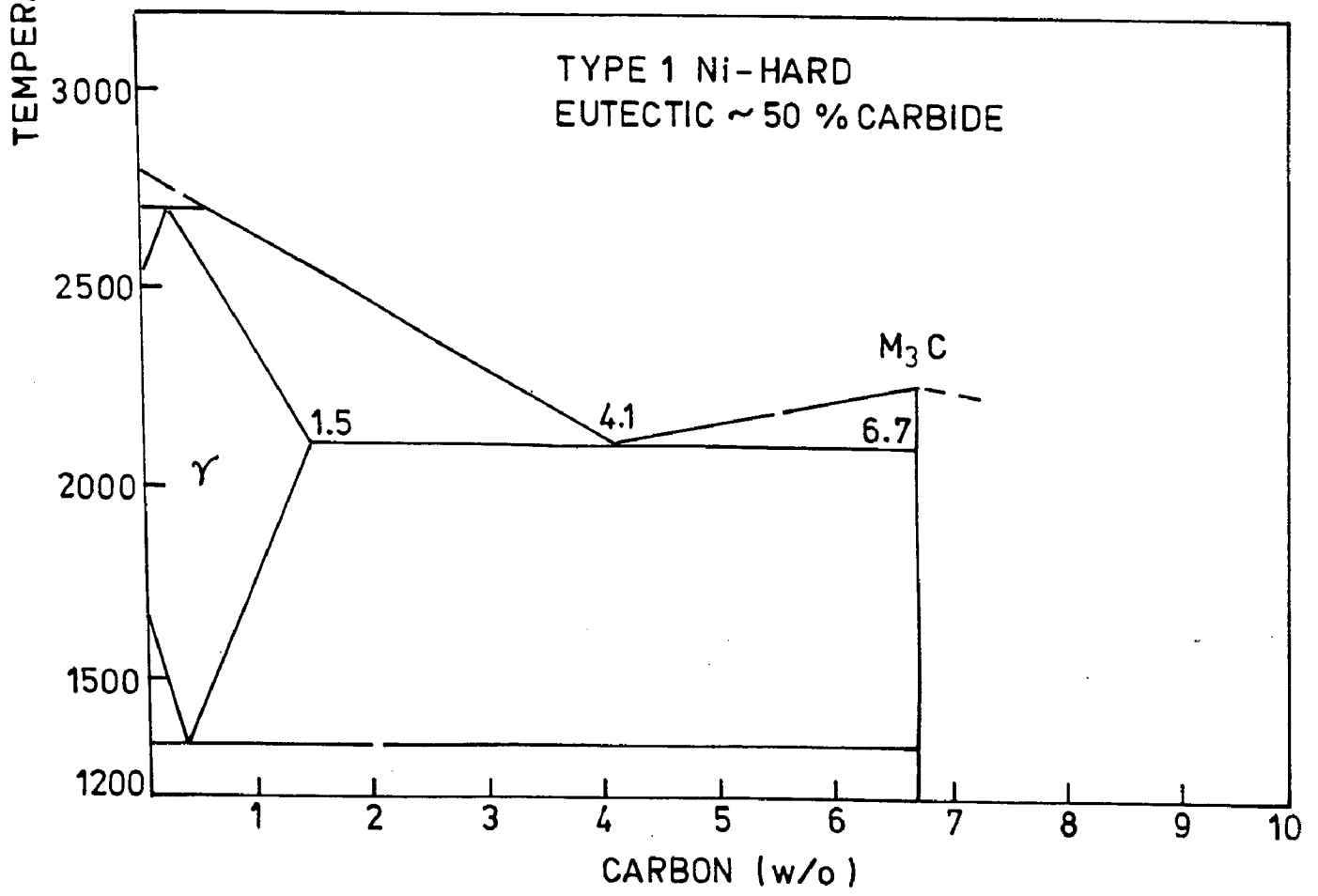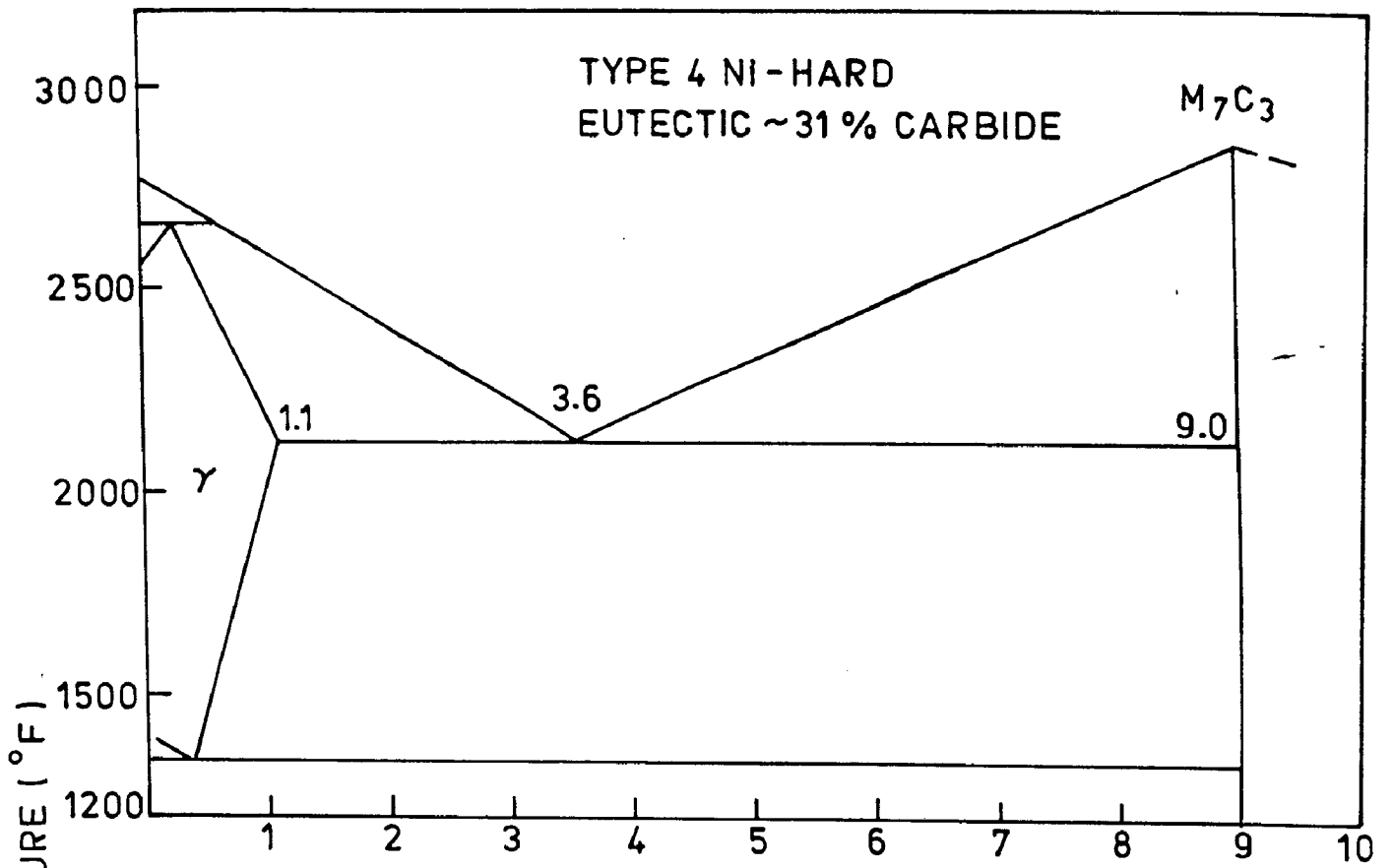
Fig. 1.7 Pseudo-binary phase diagrams of Ni-hard irons (44)

FIG. 4.1 Effect of h/t time on hardness
Alloy P1 (base curve)

As-cast hardness = 482 HV30

800 deg.C   850 deg.C   900 deg.C
950 deg.C   1000 deg.C   1050 deg.C

F-8
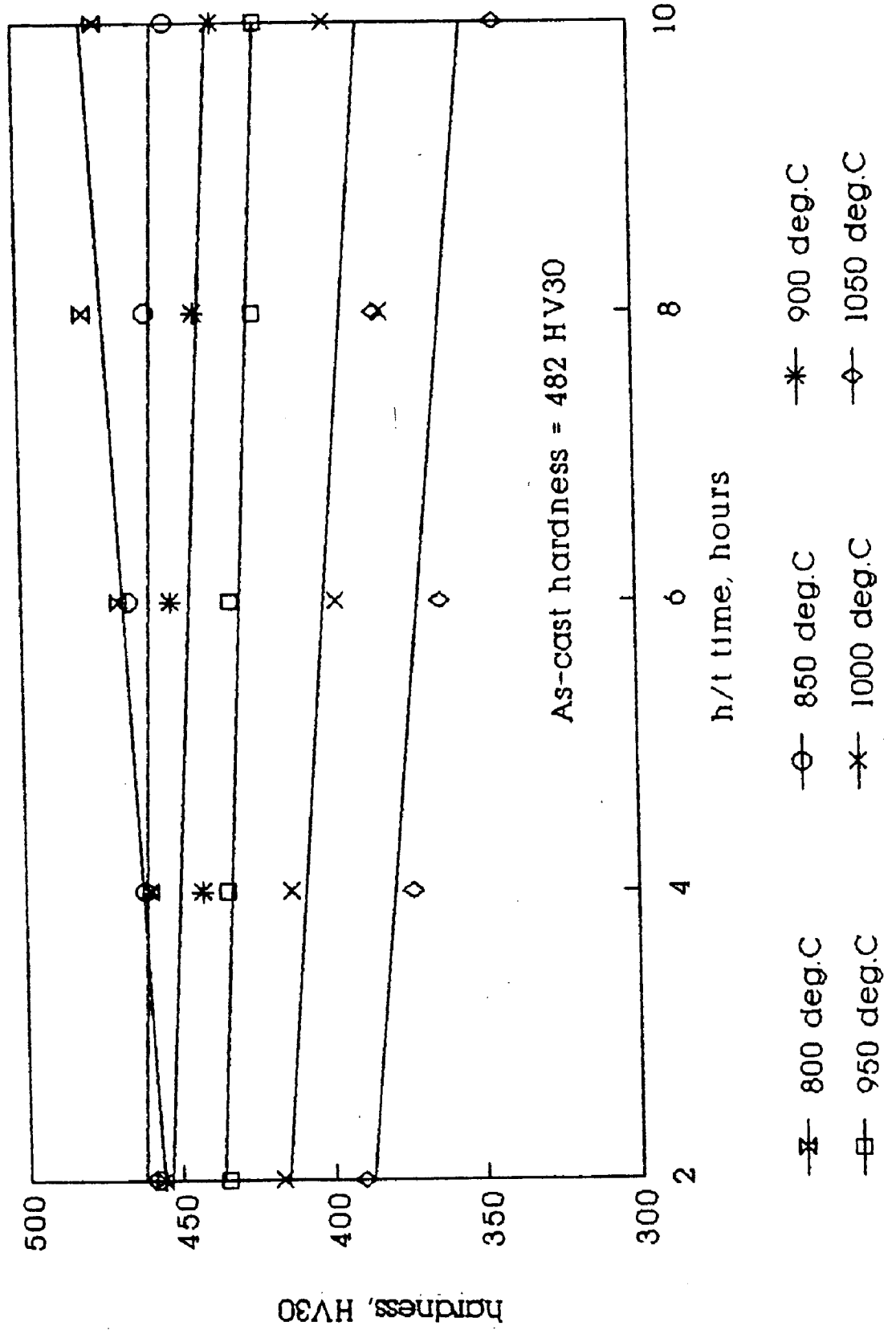
FIG. 4.2 Effect of h/t time on hardness
Alloy P2 (base curve)

As-cast hardness = 464 HV30

h/t time, hours

hardness, HV30

500 450 400 350 300

2   4   6   8   10

800 deg.C   900 deg.C
850 deg.C   1050 deg.C
950 deg.C   1000 deg.C
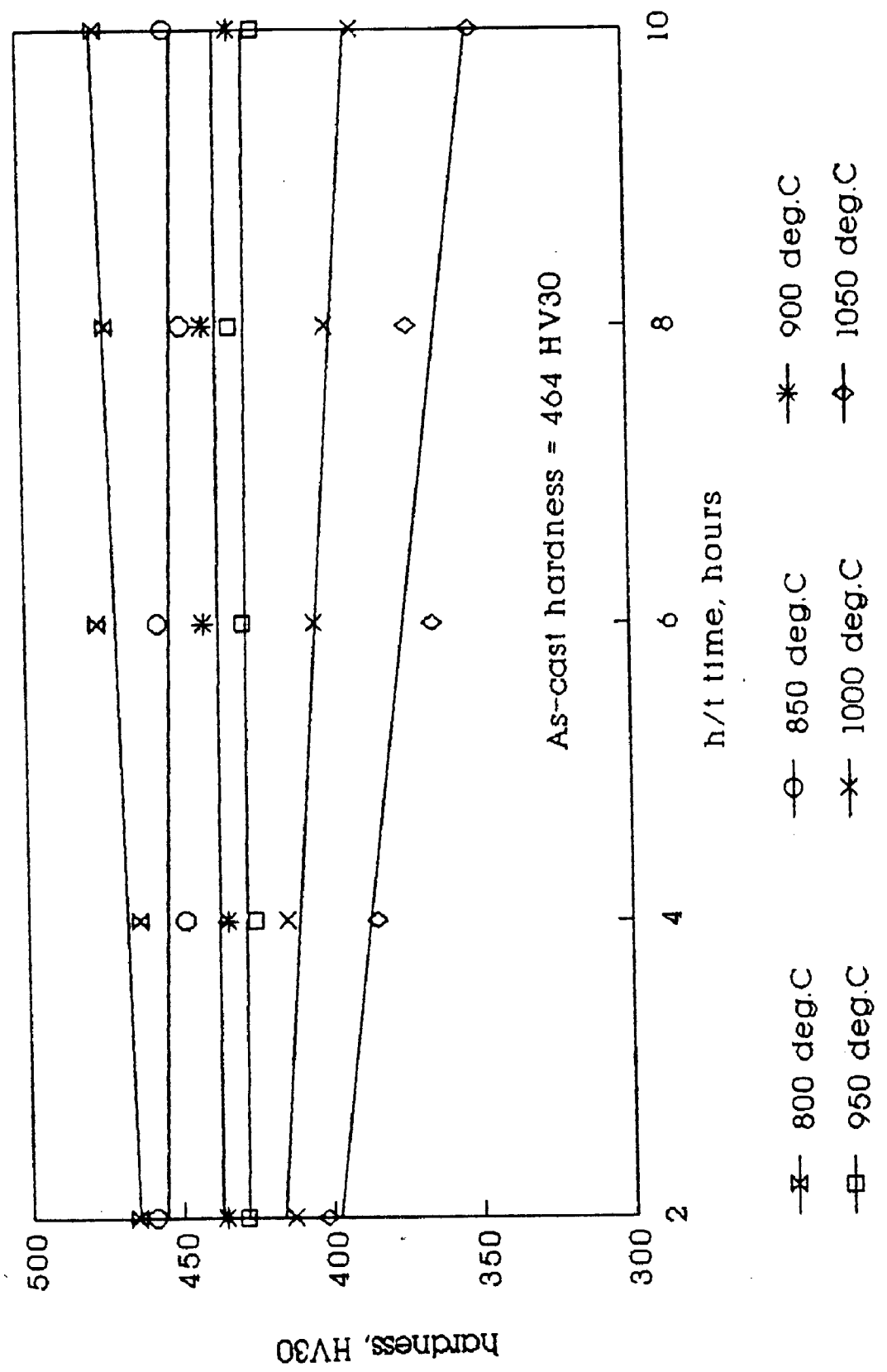
FIG. 4.3 Effect of h/t time on hardness
Alloy P3 (base curve)

As-cast hardness = 457 HV30

h/t time, hours

hardness, HV30

| 800 deg.C | 850 deg.C | 900 deg.C |
| 950 deg.C | 1000 deg.C | 1050 deg.C |
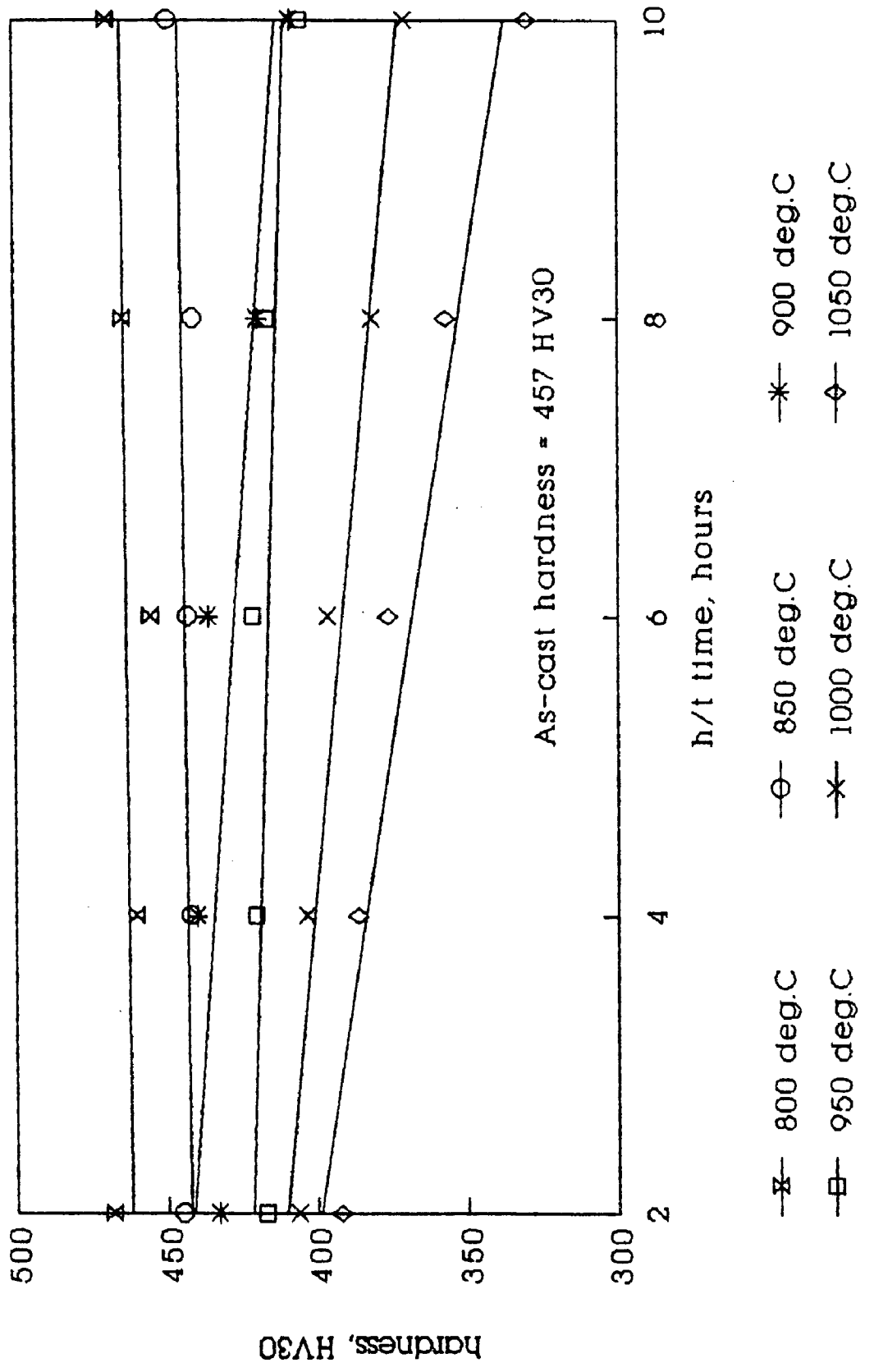
FIG. 4.4 Effect of heat treatment on hardness
Comparative plot (800 deg.C)

h/t time, hours

hardness, HV30

* — Alloy P1
□ — Alloy P2
◇ — Alloy P3
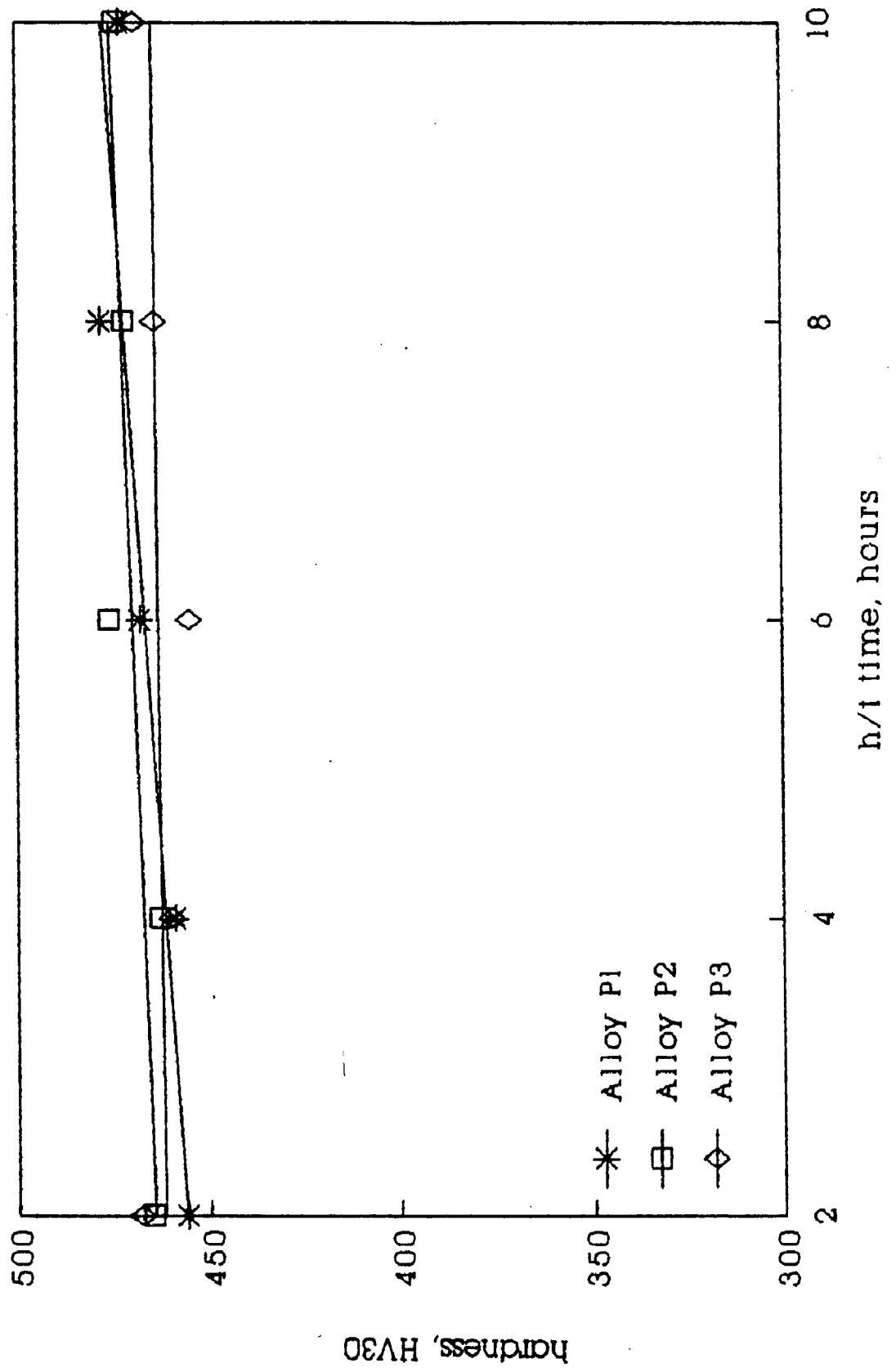
FIG. 4.5 Effect of heat treatment on hardness
Comparative plot (850 deg.C)

hardness, HV30

h/t time, hours

Alloy P1
Alloy P2
Alloy P3
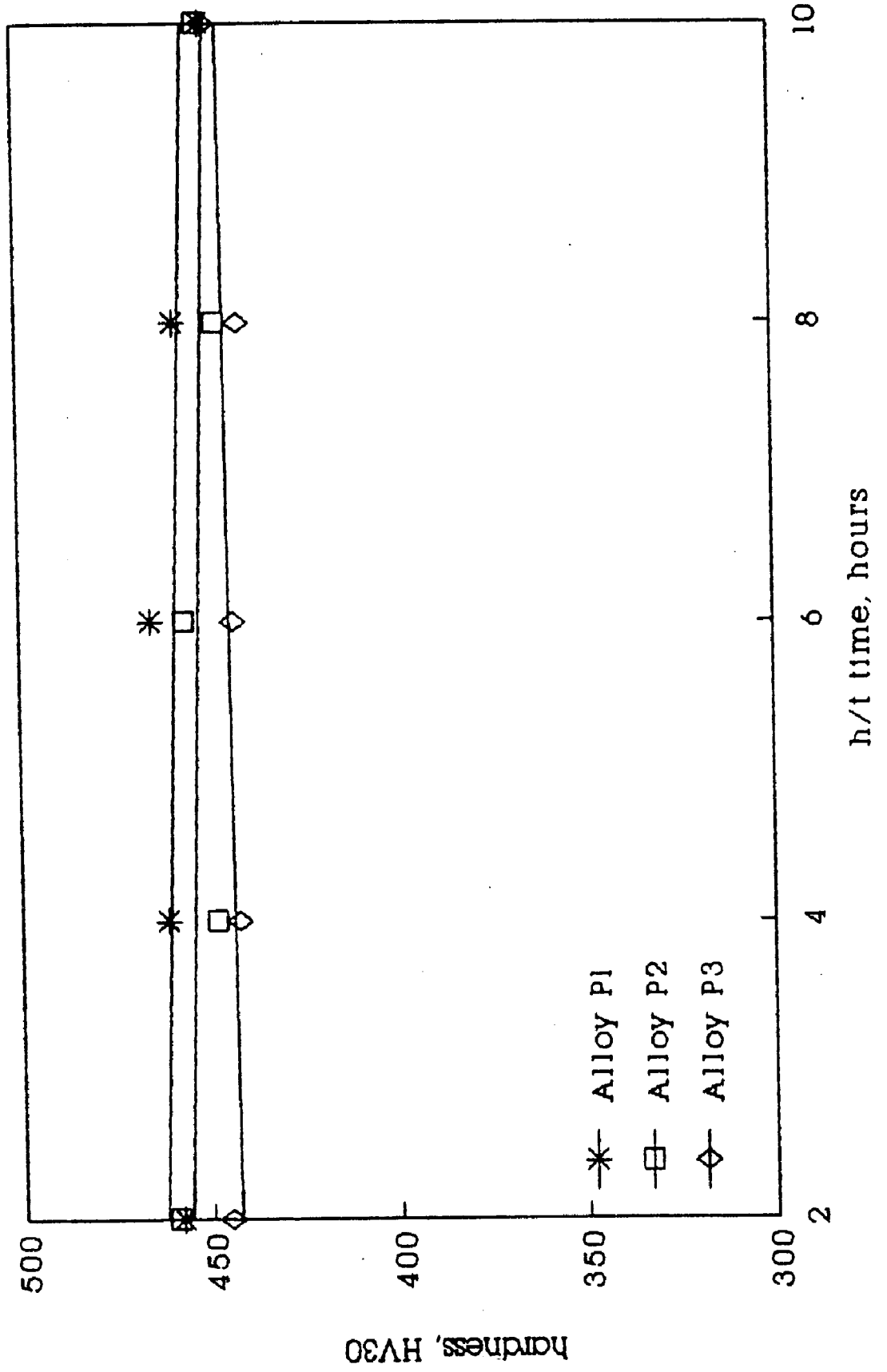
FIG. 4.6 Effect of heat treatment on hardness
Comparative plot (900 deg.C)

Alloy P1
Alloy P2
Alloy P3

h/t time, hours

hardness, HV30

F-13
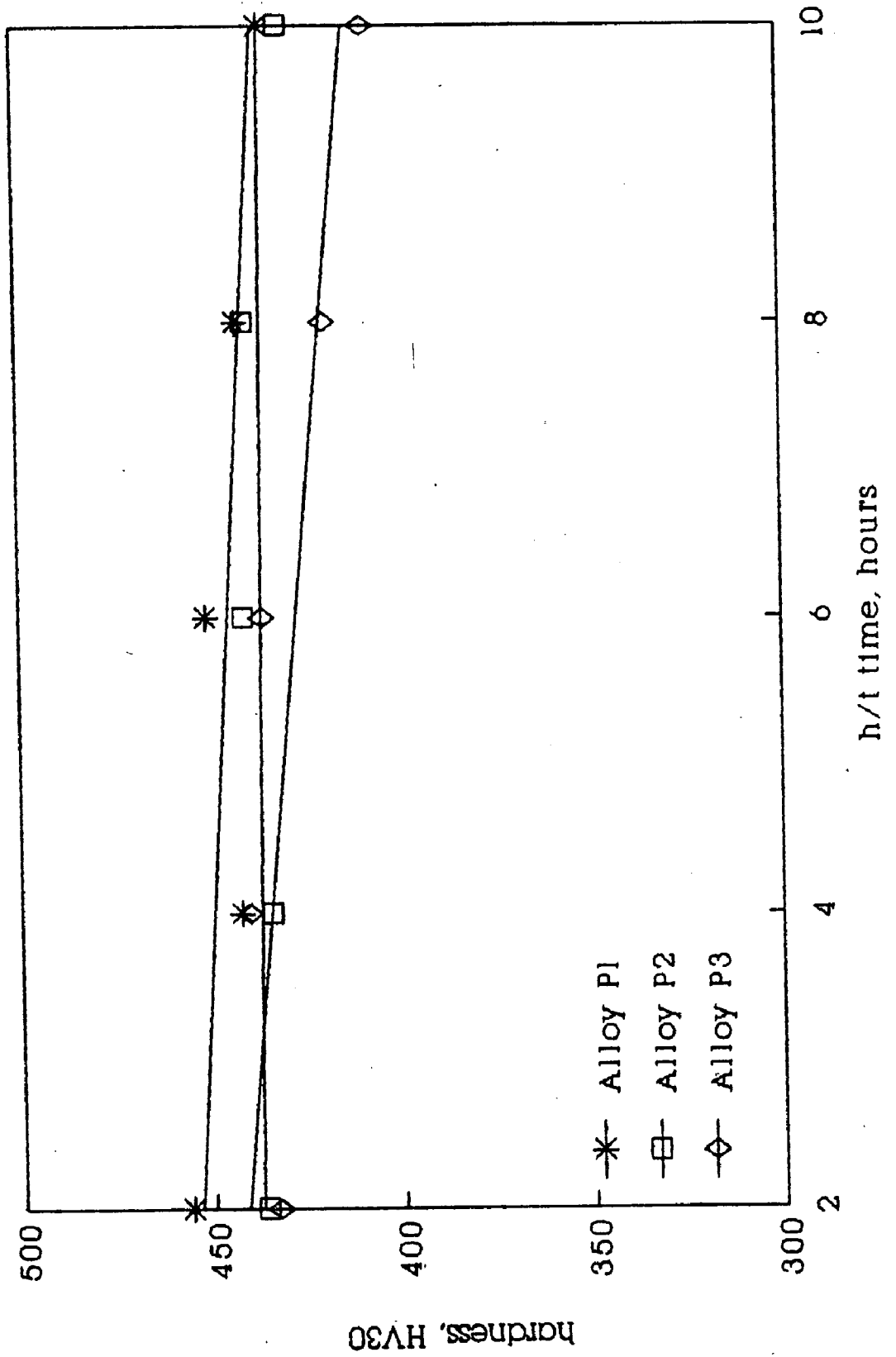
FIG. 4.7 Effect of heat treatment on hardness
Comparative plot (950 deg.C)
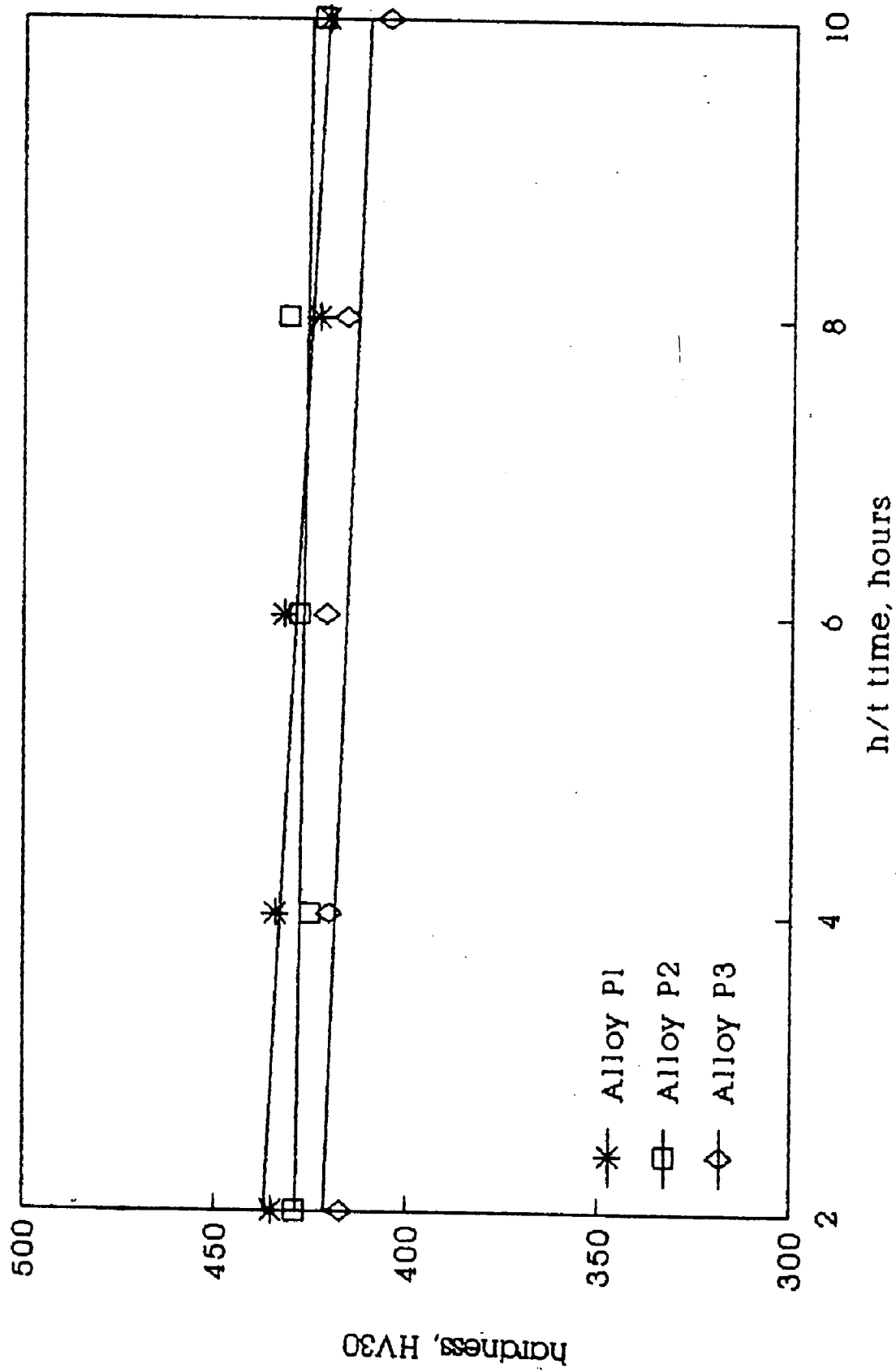
FIG. 4.8 Effect of heat treatment on hardness
Comparative plot (1000 deg.C)
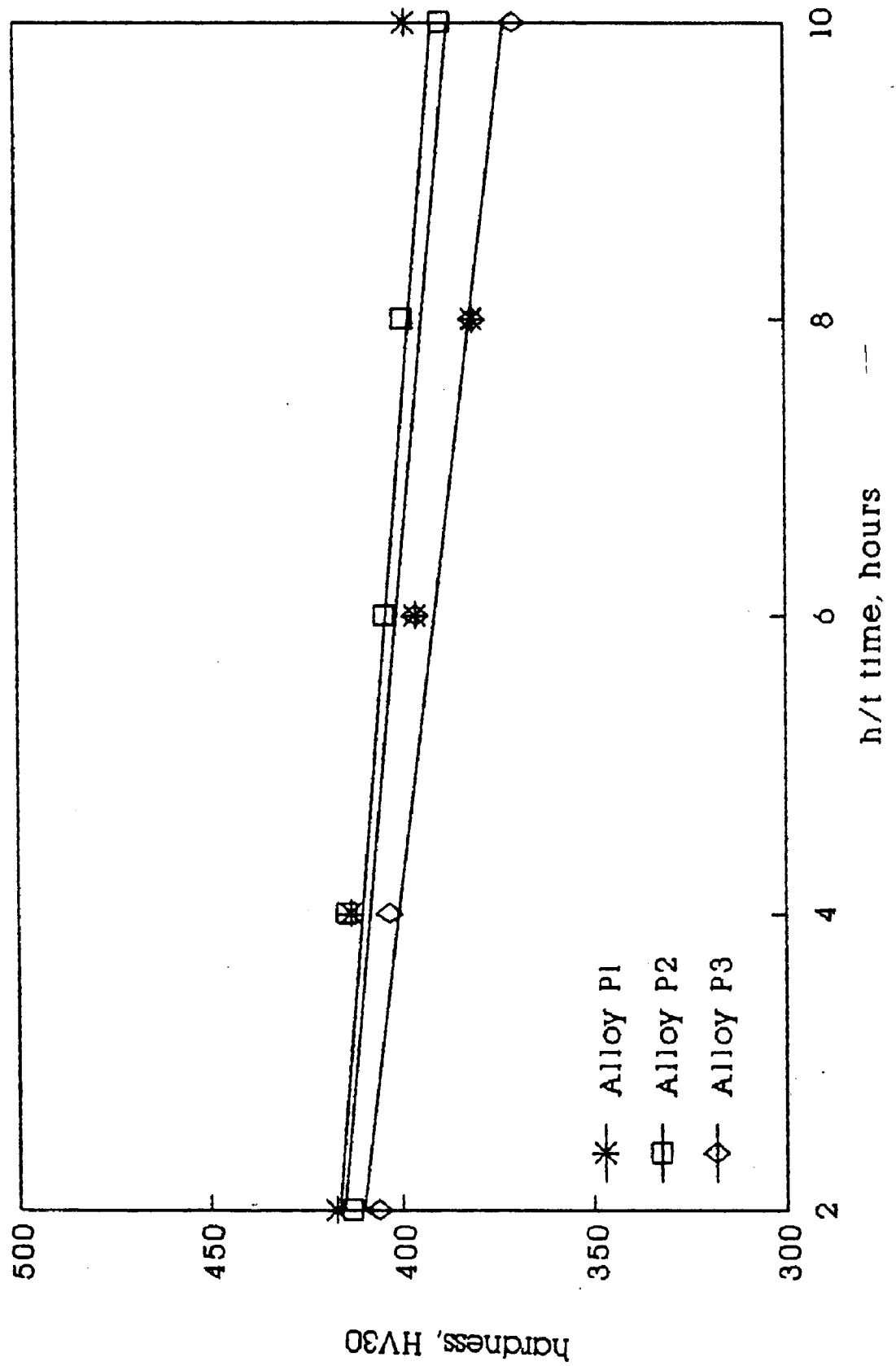
FIG. 4.9 Effect of heat treatment on hardness
Comparative plot (1050 deg.C)
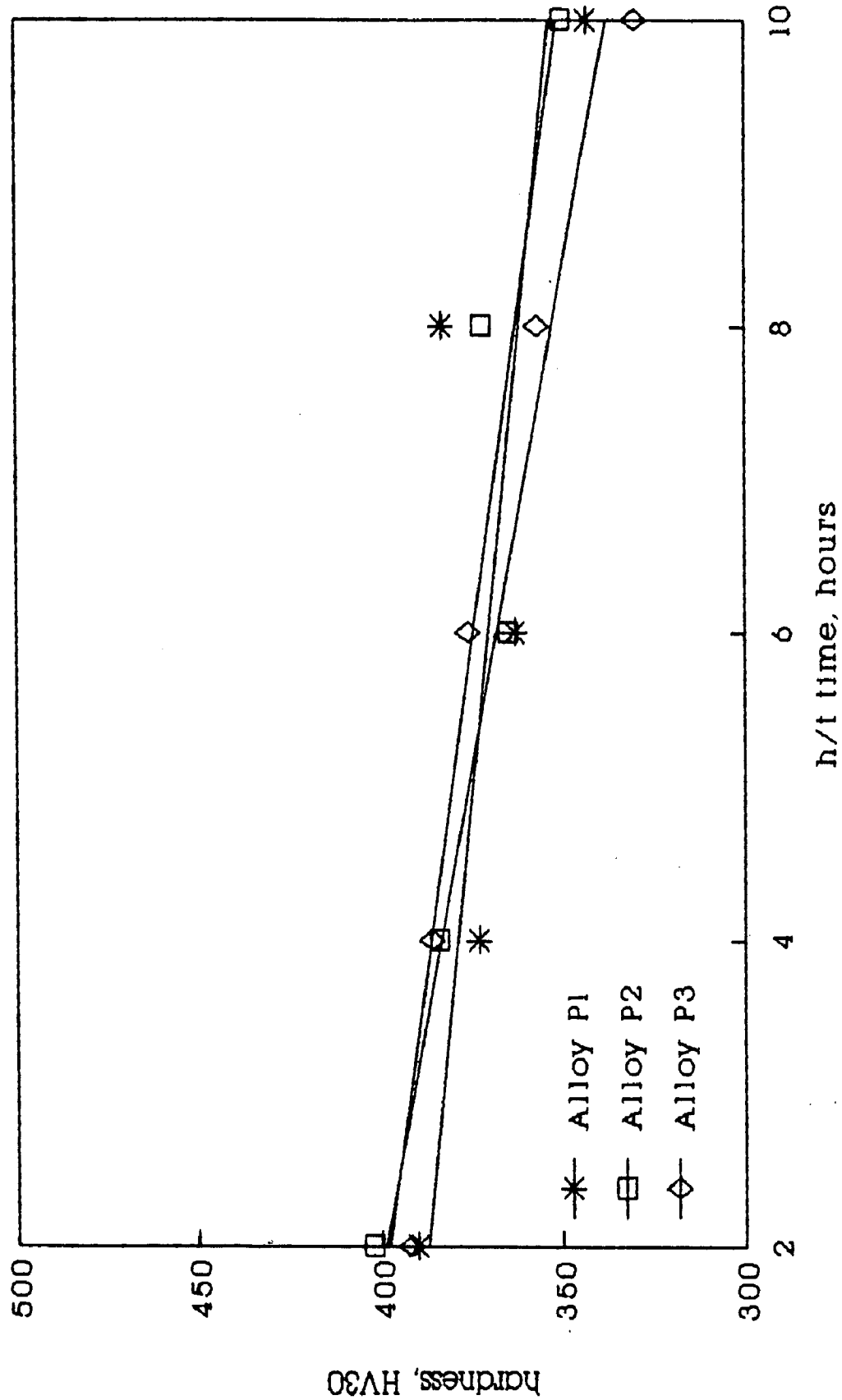
FIG. 4.10 Effect of h/t temperature on hardness as influenced by h/t time (Alloy P1)

(a) 2 hours

As-cast hardness = 482 HV30

(b) 4 hours

As-cast hardness = 482 HV30

(c) 6 hours

As-cast hardness = 482 HV30

(d) 8 hours

As-cast hardness = 482 HV30

(e) 10 hours

As-cast hardness = 482 HV30

FIG. 4.11 Effect of h/t temperature on hardness as influenced by h/t time (Alloy P2)
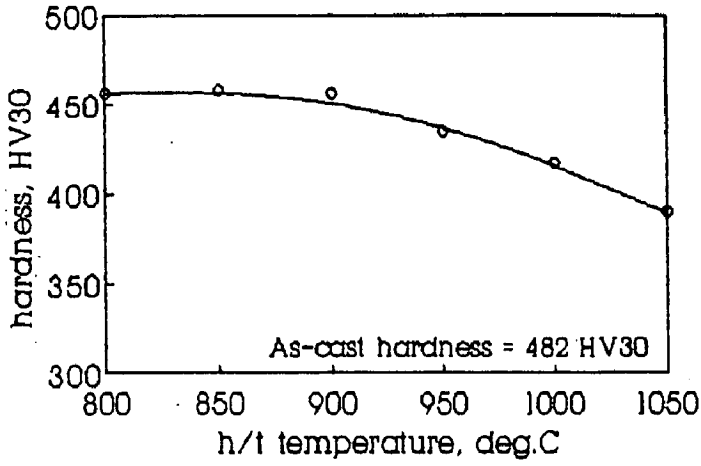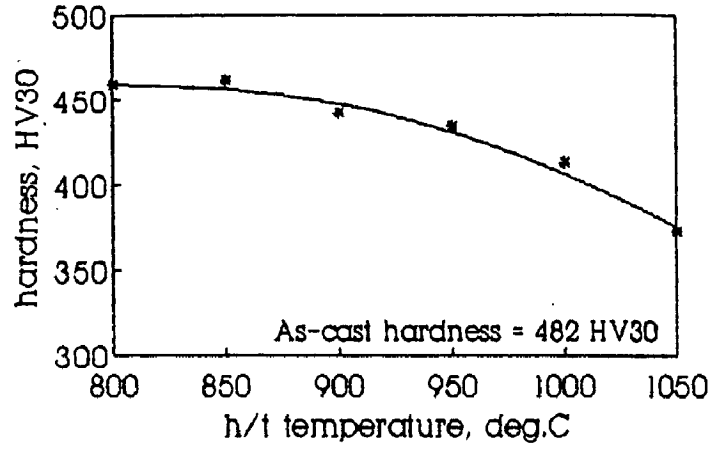
(a) 2 hours
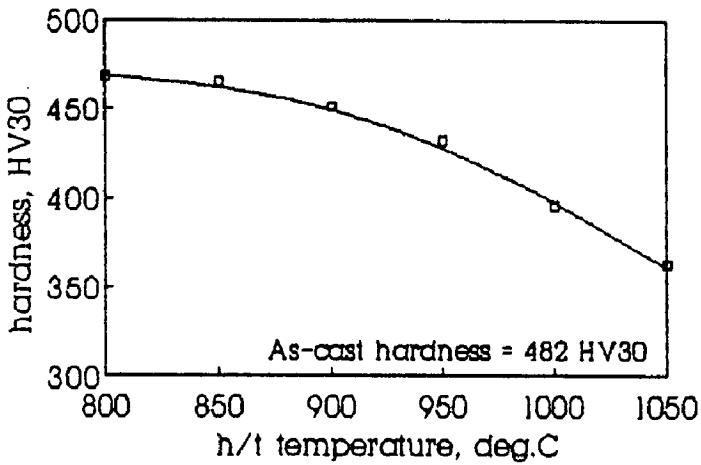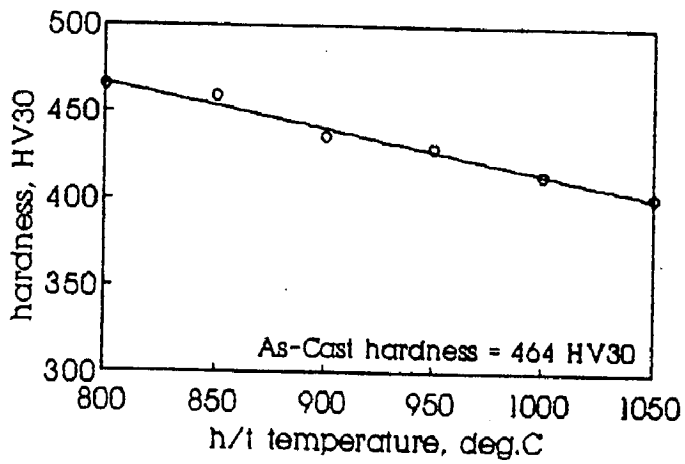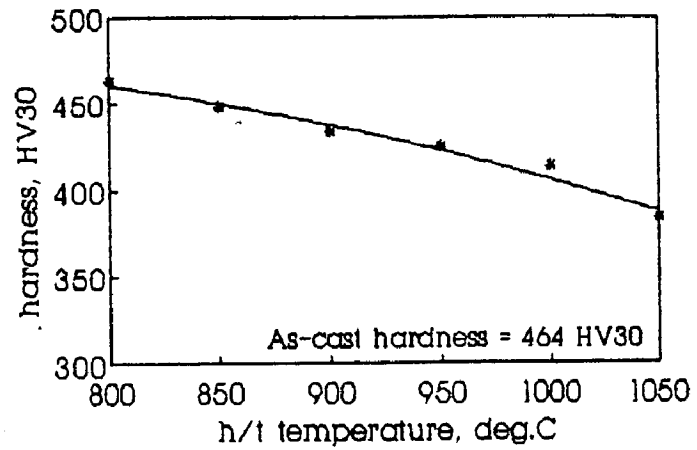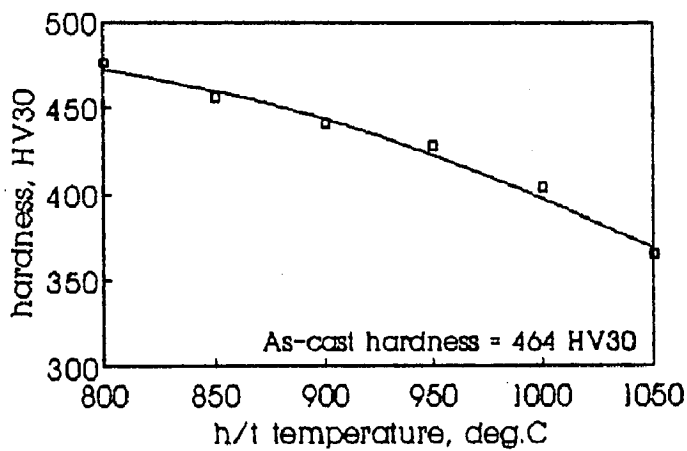
(b) 4 hours
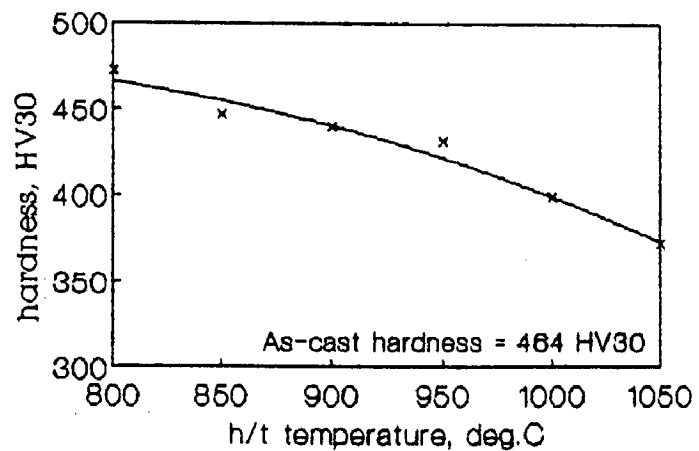
(c) 6 hours
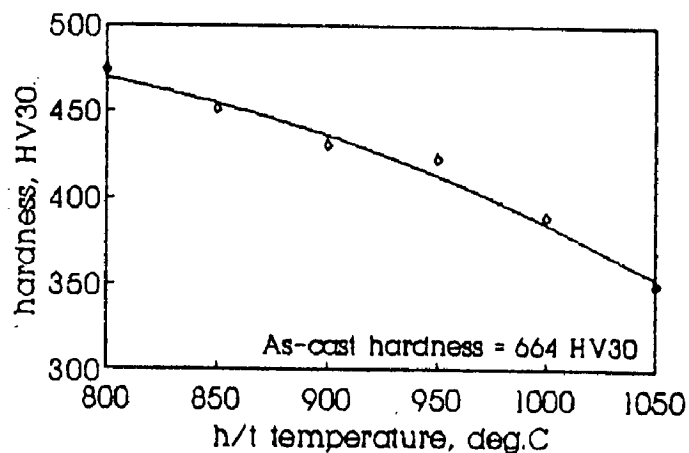
(d) 8 hours

(e) 10 hours

FIG. 4.12 Effect of h/t temperature on hardness as influenced by h/t time (Alloy P3)

(a) 2 hours

As-cast hardness = 467 HV30

(b) 4 hours

As-cast hardness = 467 HV30

(c) 6 hours

As-cast hardness = 467 HV30

(d) 8 hours

As-cast hardness = 467 HV30

(e) 10 hours

As-cast hardness = 467 HV30
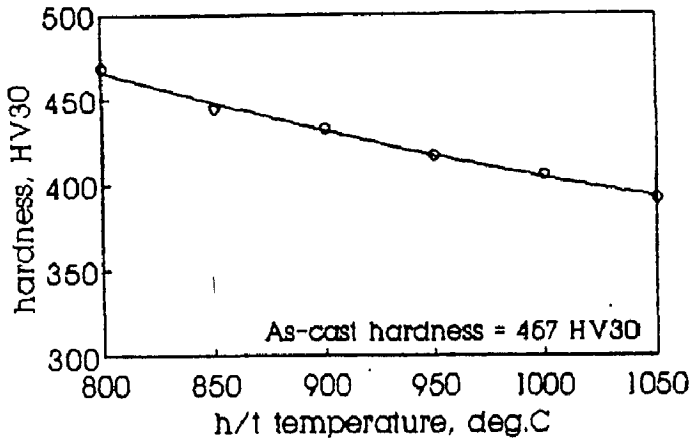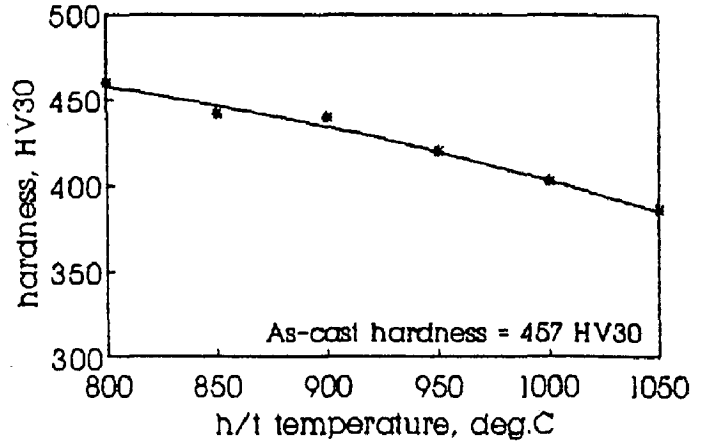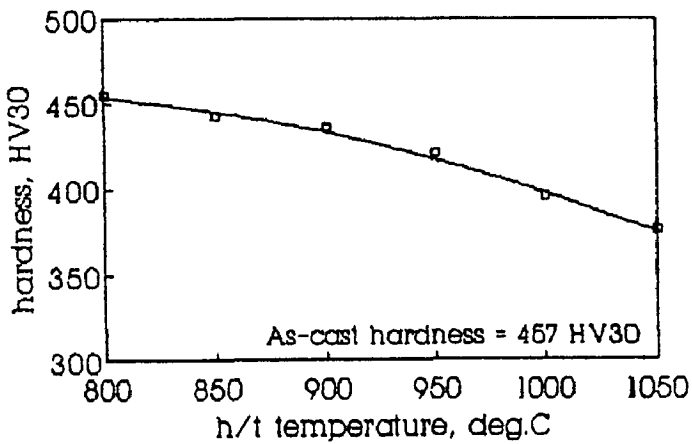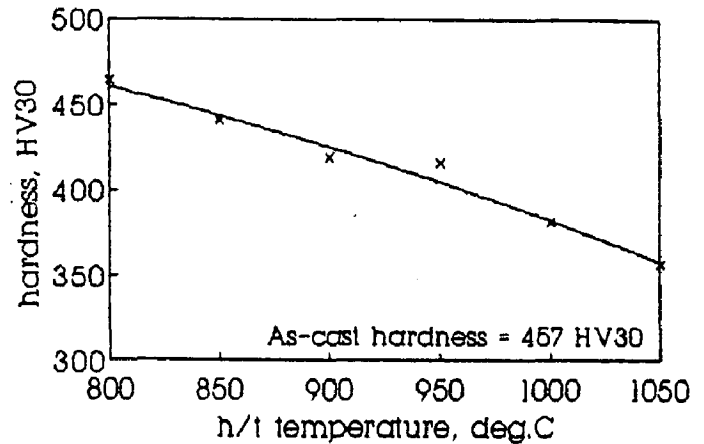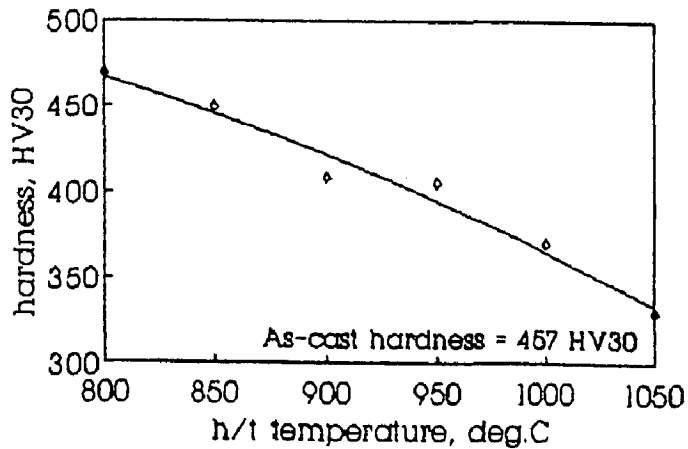
FIG. 4.13 Effect of h/t temperature on hardness
(2 hours)

Alloy P1
Alloy P2
Alloy P3

hardness, HV30

h/t temperature, deg.C
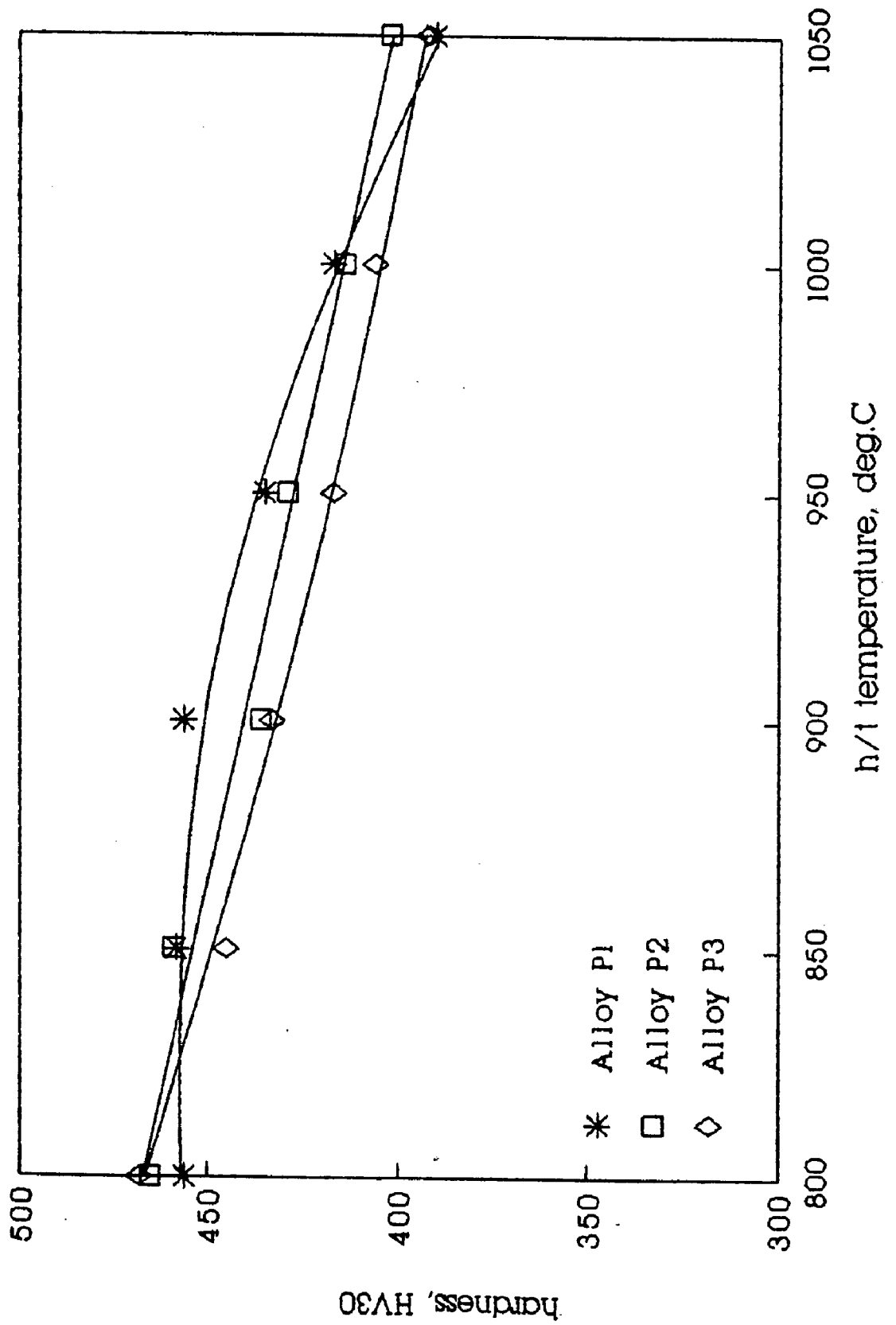
FIG. 4.14 Effect of h/t temperature on hardness
(4 hours)

hardness, HV30

h/t temperature, deg.C

* Alloy P1
□ Alloy P2
◇ Alloy P3
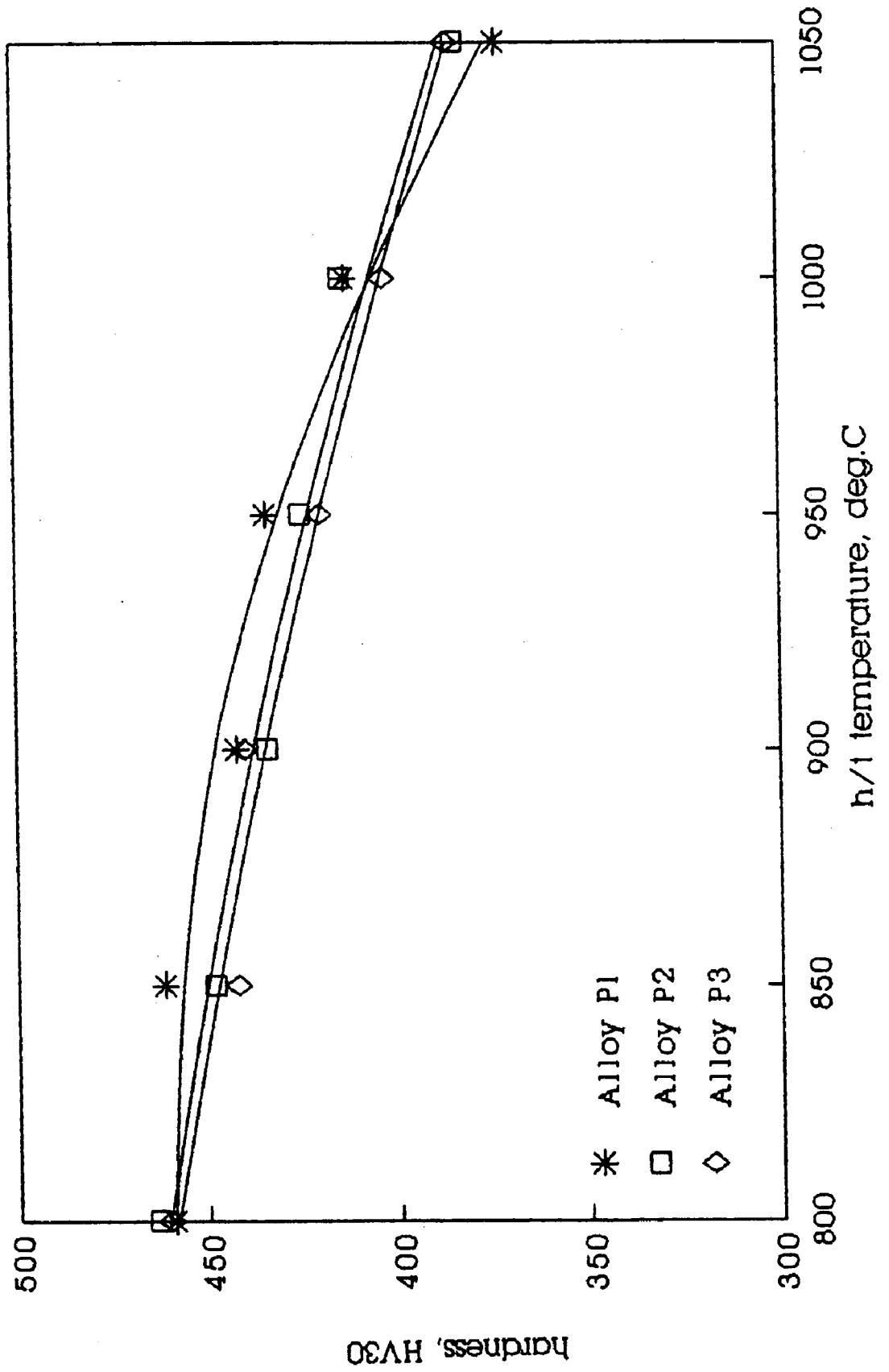
FIG. 4.15 Effect of h/t temperature on hardness
(6 hours)
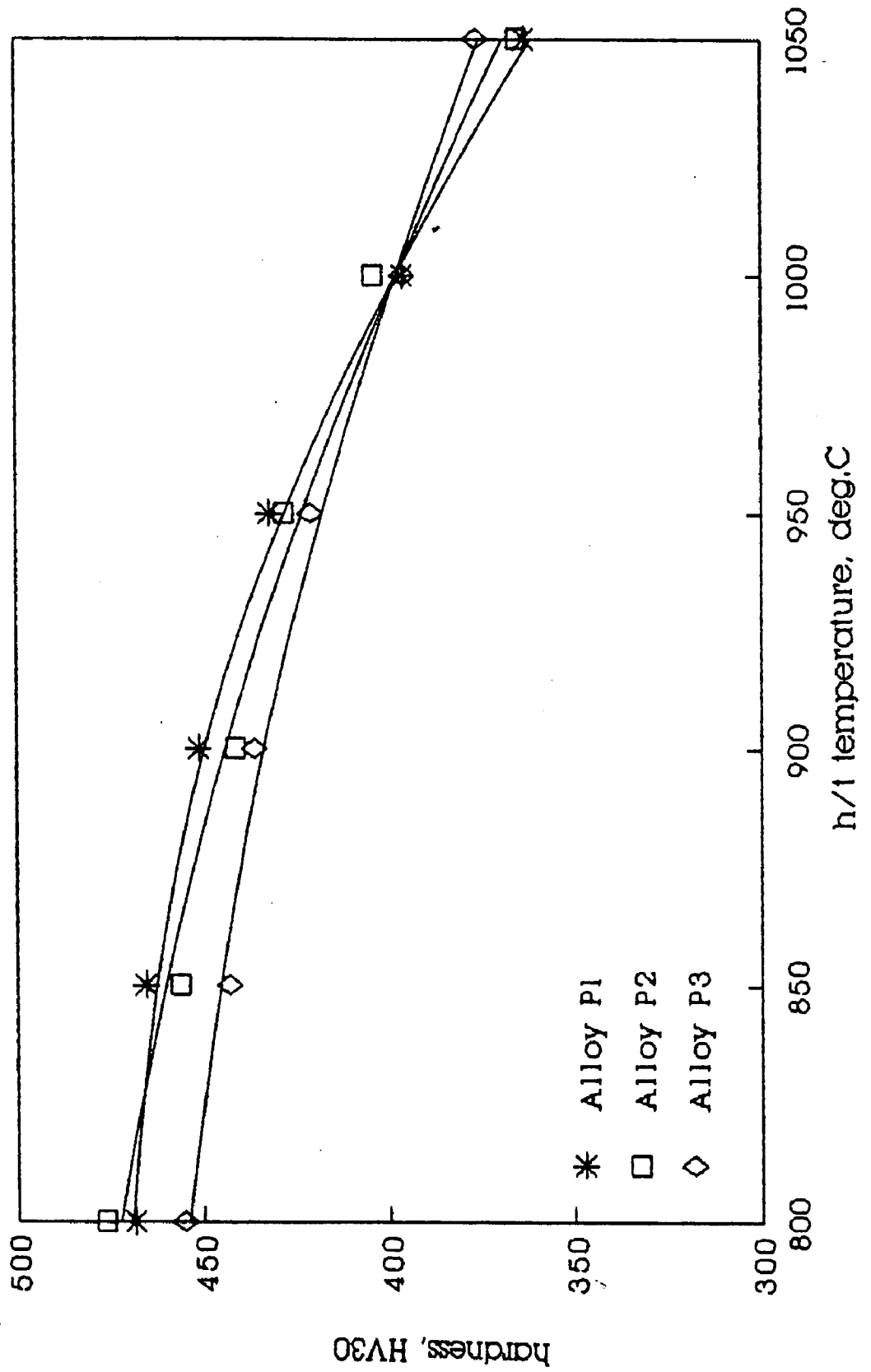
FIG. 4.16 Effect of h/t temperature on hardness
(8 hours)
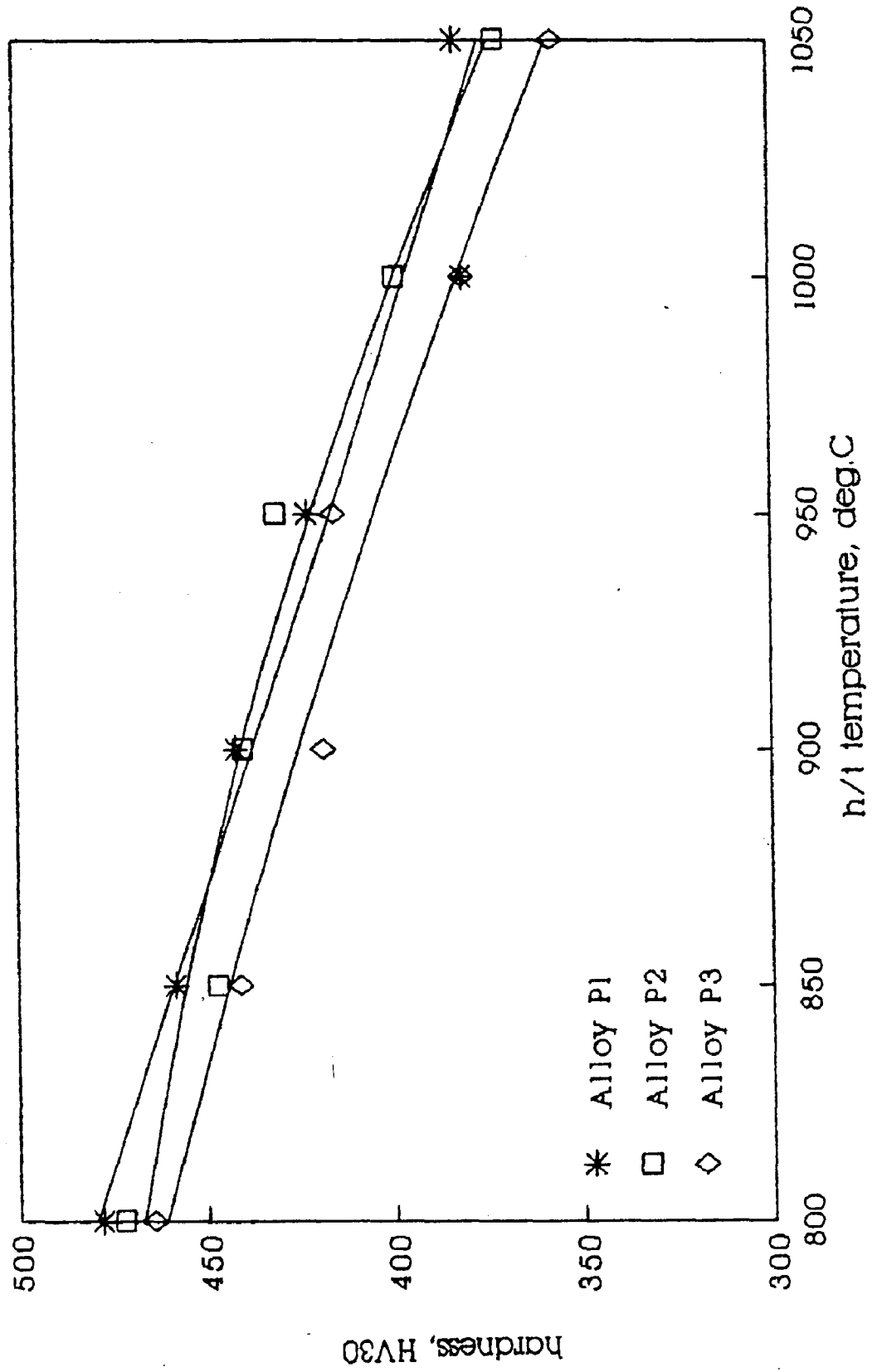
FIG. 4.17 Effect of h/t temperature on hardness
(10 hours)
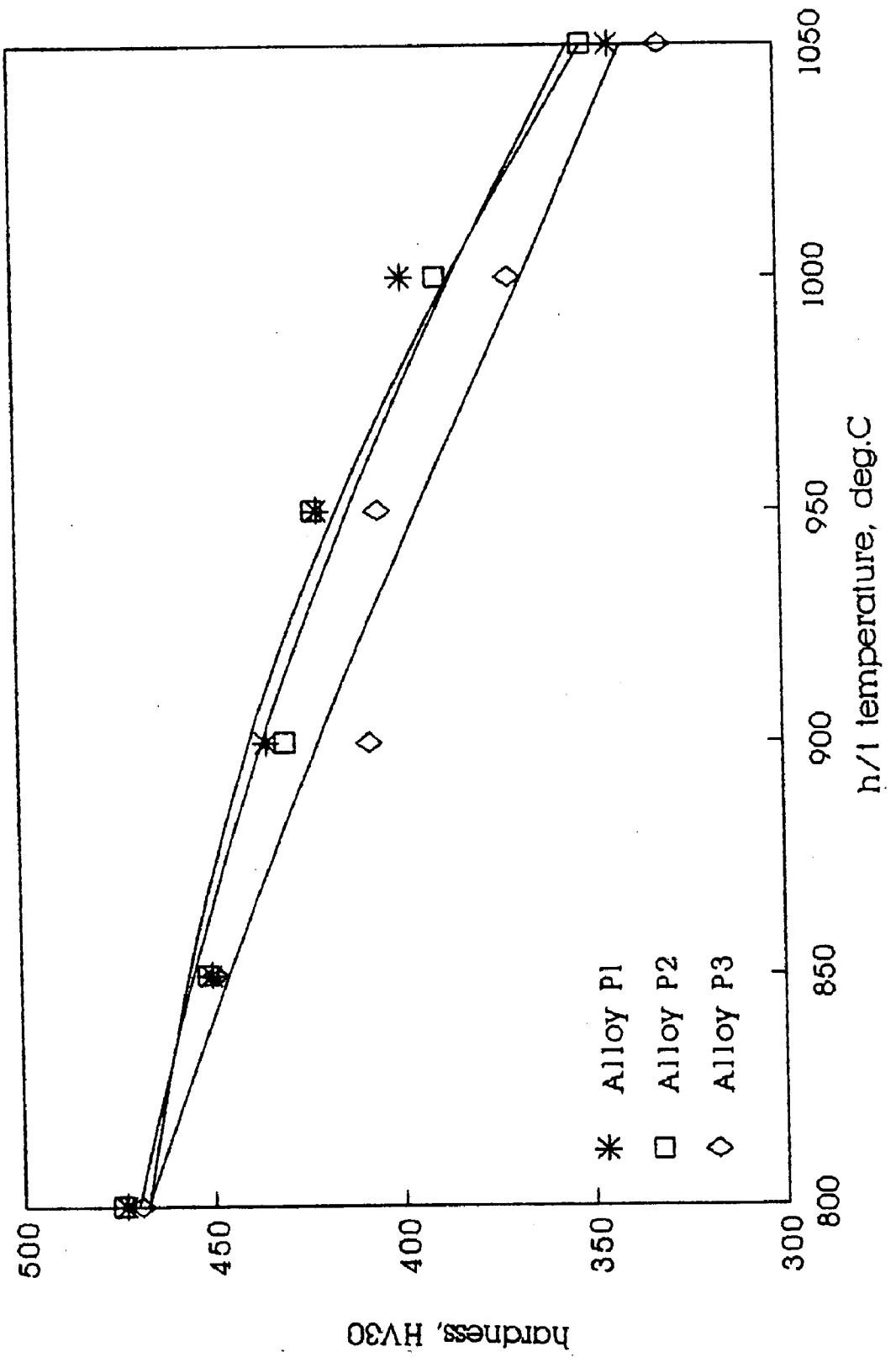
FIG. 4.18 Summary bar diagrams depicting the effect of alloy composition on hardness
(variable h/t temperature)
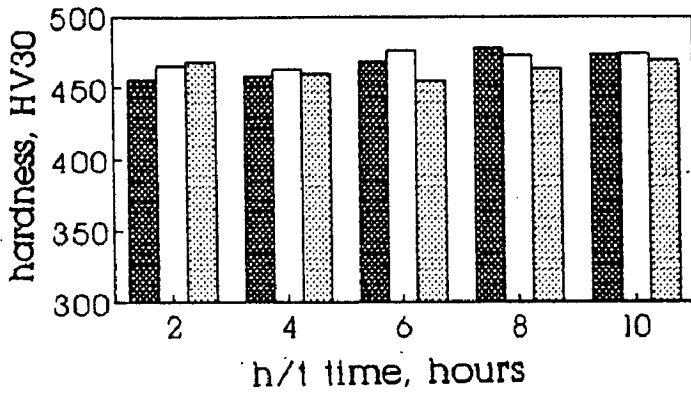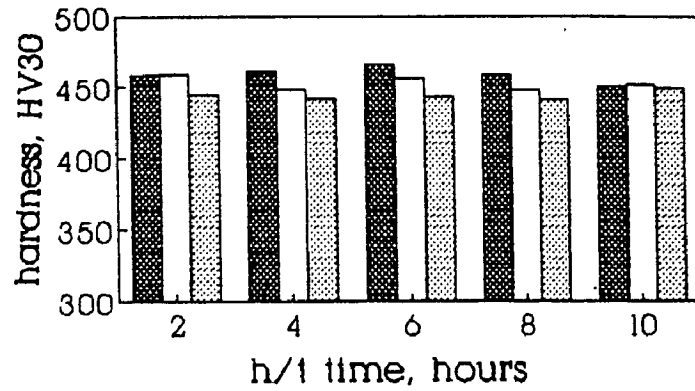
(a) 800 deg.C
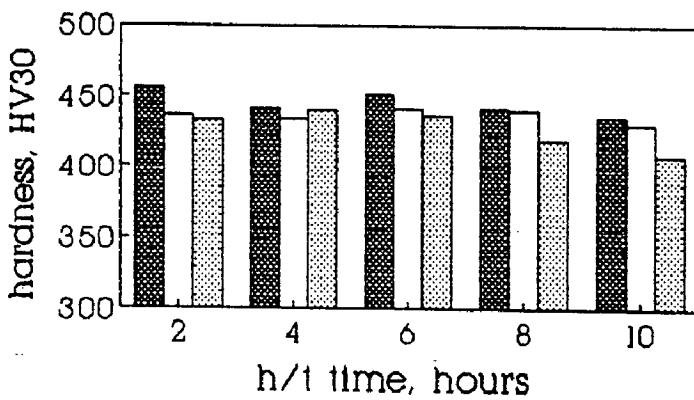
(b) 850 deg.C
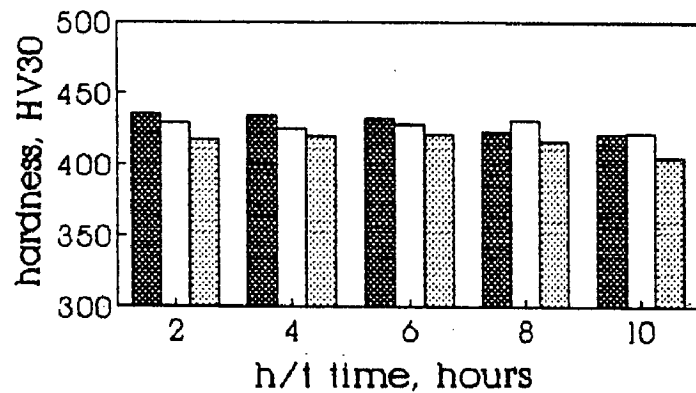
(c) 900 deg.C

(d) 950 deg.C

(e) 1000 deg.C
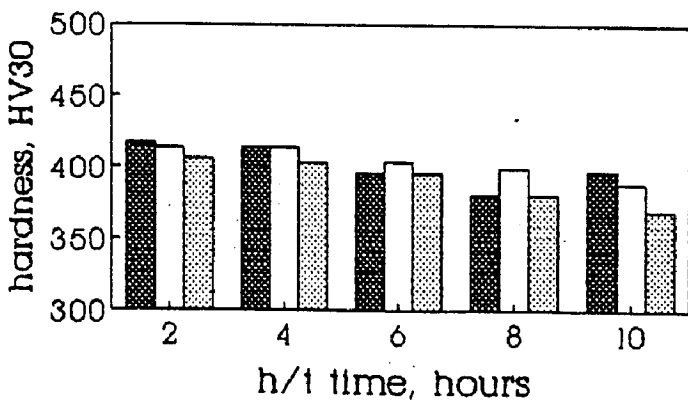
(f) 1050 deg.C
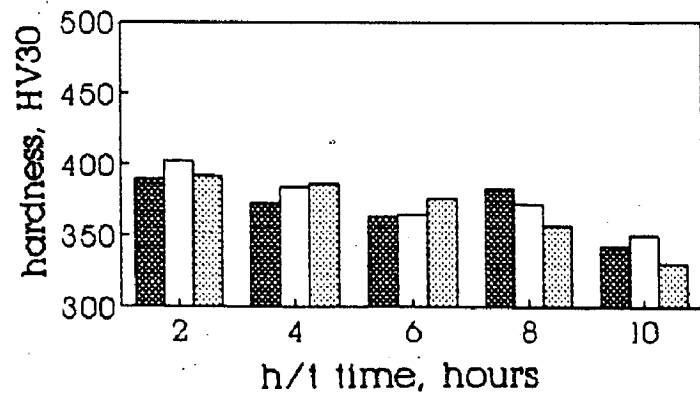
ALLOY P1   ALLOY P2
ALLOY P3

FIG. 4.19 Summary bar diagrams depicting the effect of alloy composition on hardness
(variable h/t time)
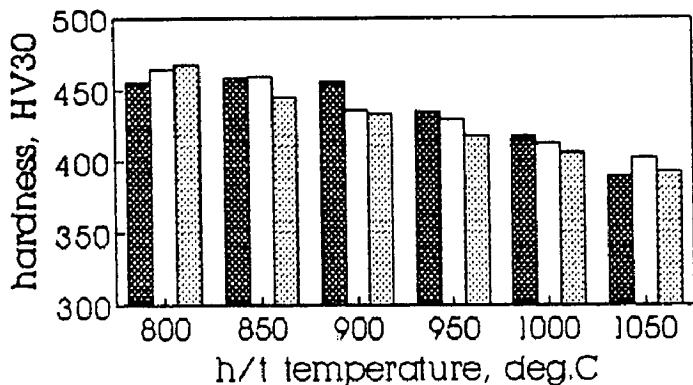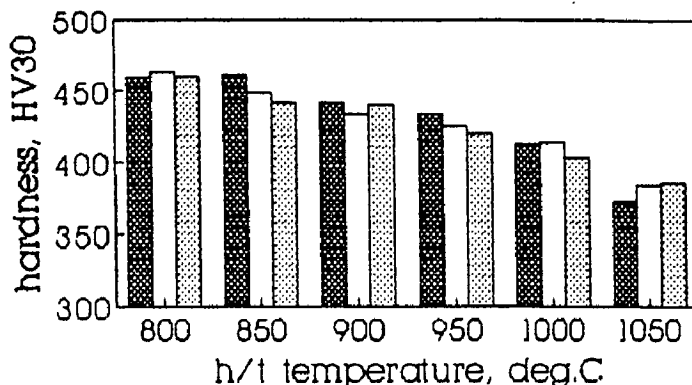
(a) 2 hours
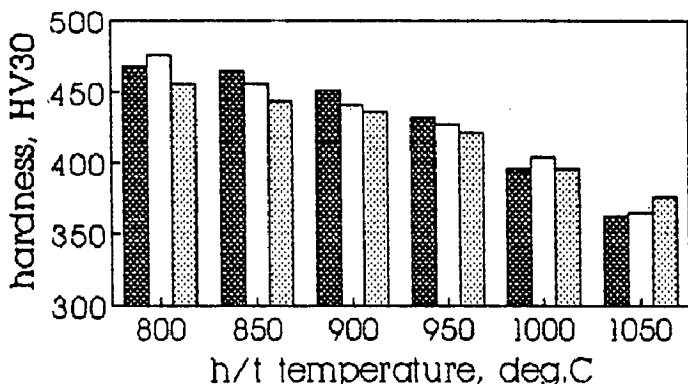
(b) 4 hours
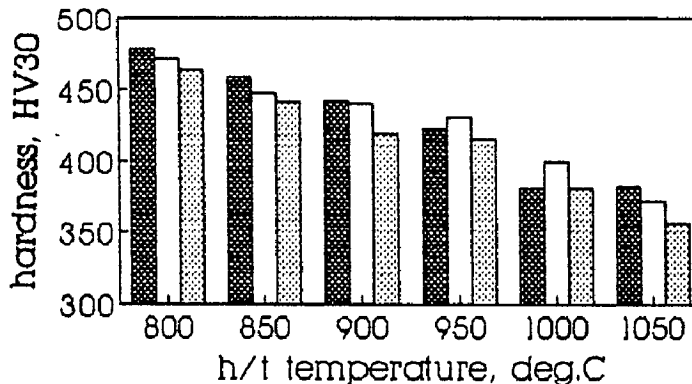
(c) 6 hours
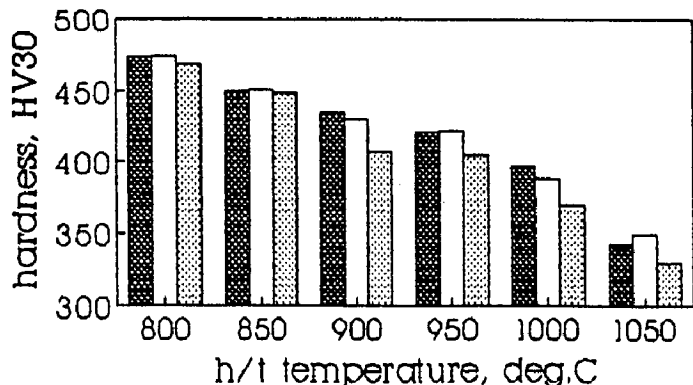
(d) 8 hours

(e) 10 hours

ALLOY P1   ALLOY P2
ALLOY P3

FIG. 4.20 Summary bar diagrams depicting the effect of h/t time on hardness
(variable h/t temperature)
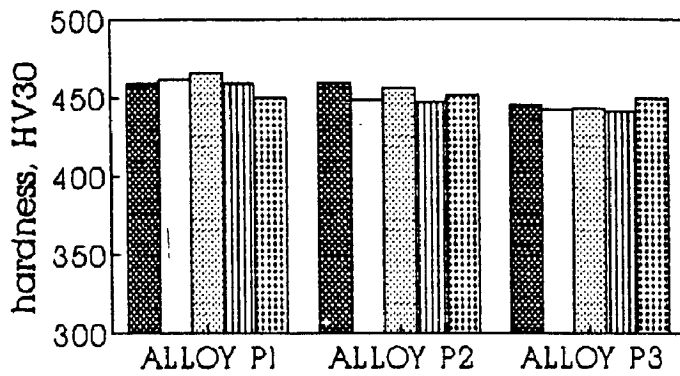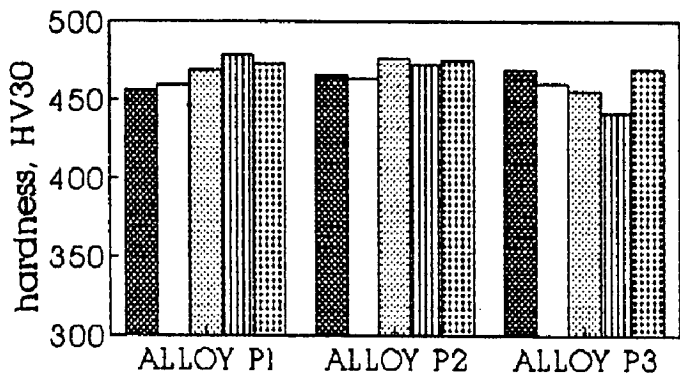
(a) 800 deg.C

(b) 850 deg.C
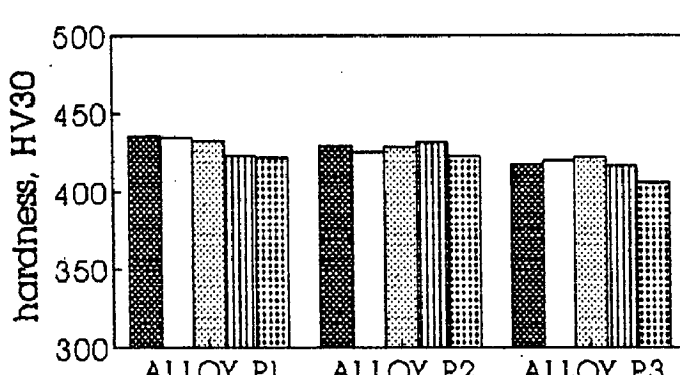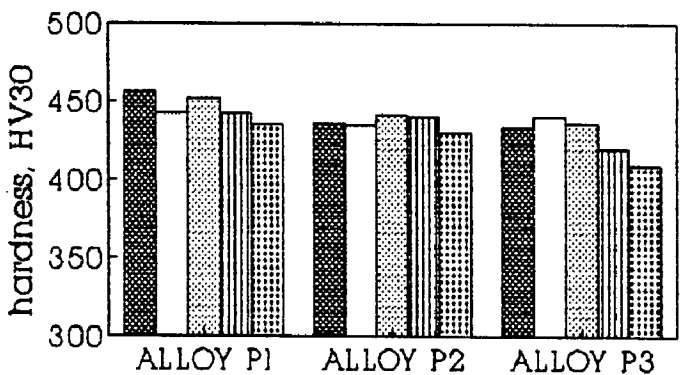
(c) 900 deg.C

(d) 950 deg.C

(e) 1000 deg.C

(f) 1050 deg.C
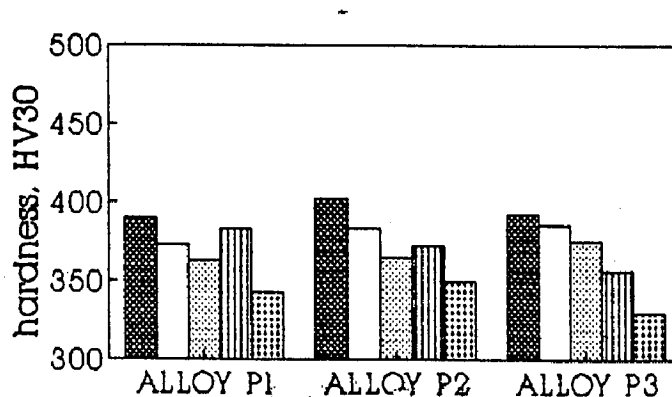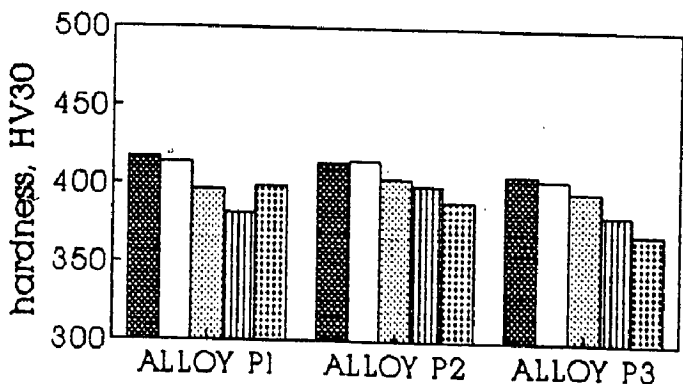
2 HOURS ☐ 4 HOURS ▨ 6 HOURS
▥ 8 HOURS ▦ 10 HOURS

FIG. 4.21 Summary bar diagrams depicting the effect of h/t temperature on hardness
(variable h/t time)

(a) 2 hours

(b) 4 hours

(c) 6 hours

(d) 8 hours

(e) 10 hours

σ
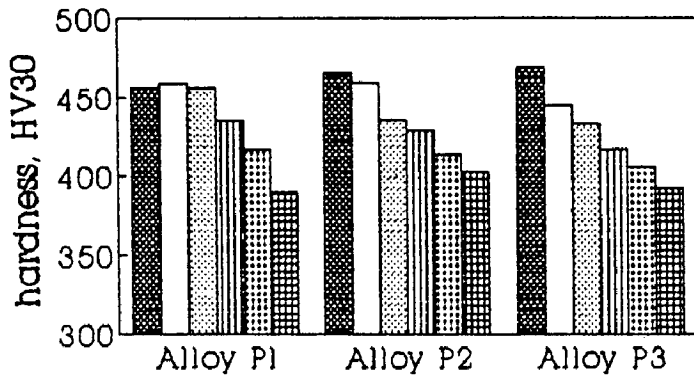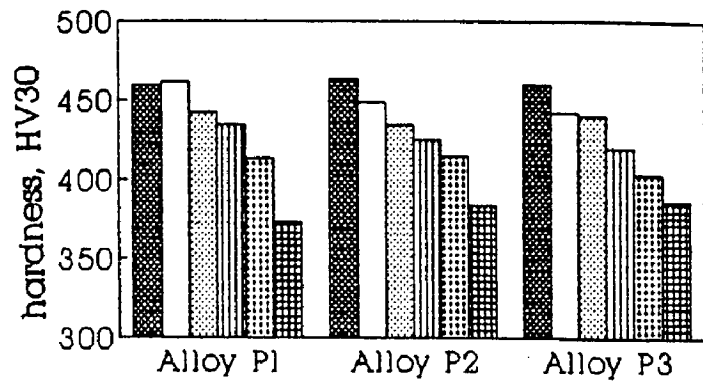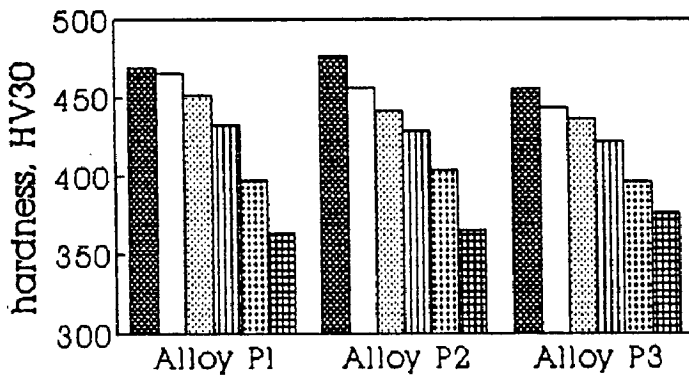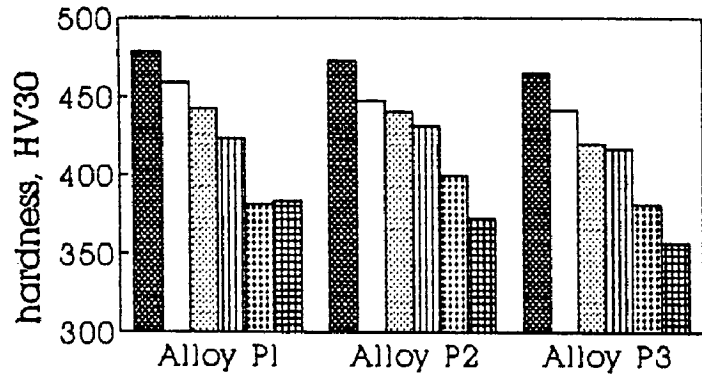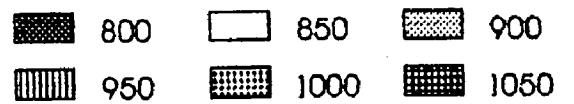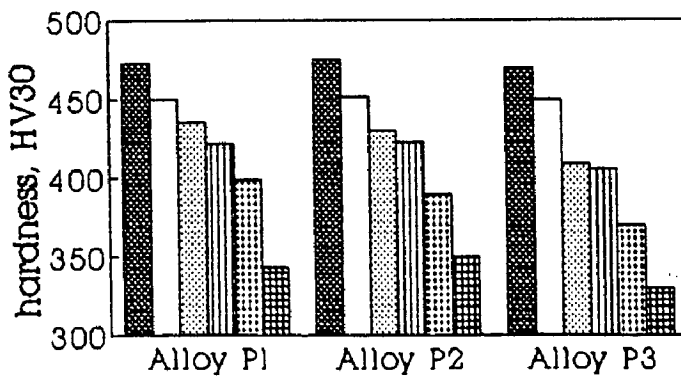
FIG. 4.22

(a) P1, As-cast   (b) P1, As-cast

X 200   X 1000

(c) P1, As-cast

X 1000

TABLE-5.24   SUMMARY TABLE OF DIFFRACTOGRAM INDEXING

ALLOY: P2;   H/T TEMPERATURE: 950°C ;   SOAKING DURATION: 2 HOURS

```
DIFF.                        PHASE(S)                                              INT
ANGLE  1  3  5  7  9 11 13 15 17 19 21 23 25 27 29

 50.4  0 0 0 0 0 0 1 0 1 1 1 1 1 0 0 0 0 0 0 0 0 1 1 0 0 0 0 0 1 1 0   3.0
 53.1  0 0 0 1 1 0 0 0 0 0 0 0 0 0 0 0 0 0 0 0 0 0 1 0 0 0 0 0 0 1 1 0   3.0
 54.1  0 0 0 0 0 0 0 0 1 0 1 0 1 1 1 0 0 1 0 1 0 1 0 0 0 0 0 0 1 1 1 1   3.0
 55.2  0 0 0 0 0 1 0 0 1 0 0 1 0 0 0 0 0 0 0 0 0 0 0 0 1 1 0 0 1 0   8.0
 57.0  1 0 0 0 0 0 0 1 1 1 0 0 1 1 1 0 0 0 1 0 0 0 0 0 0 0 1 1 0   7.0
 64.5  0 0 0 0 0 0 1 0 1 1 1 1 1 1 0 0 1 0 0 0 0 1 0 0 0 1 0 0 0 0  11.0
 75.2  0 0 0 0 0 0 0 0 0 0 0 0 1 0 0 0 0 0 1 0 0 0 0 0 0 0 0 0 0 1 0   3.0
 98.4  0 0 0 0 0 0 0 0 0 0 0 0 0 1 0 0 0 1 0 0 0 0 0 1 0 1 0 0 0 0 0   5.0
124.9  0 0 0 0 0 0 0 0 0 0 0 0 0 0 0 0 0 0 0 0 0 0 0 0 0 0 0 0 0 0 0   7.0

       0 0 0 0 0 0 2 0 5 3 3 4 5 3 2 0 2 2 0 2 1 3 0 0 2 3 0 4 6 0
```

O = ABSENT   1 = PRESENT   * = PROBABLE DIFF. ANGLE FOR K-BETA RADIATION

DETAILED ANALYSIS OF PHASE(S) ACTUALLY PRESENT

S.N.	PHASE PRESENT	DIFF. ANGLE	PEAK INT	I/IO	D MEAS	D STD	DIFF PLANE	INT STD	CONF LIMIT
(1)	FE5C2	50.4	27	27	2.276	2.287	020	20	99.7
		64.5	100	100	1.816	1.814	312	25	99.9
(2)	MN5C2	50.4	27	27	2.276	2.277	020	40	100.0
		54.1	27	27	2.131	2.121	211	80	99.7
		55.2	72	72	2.091	2.084	120	80	99.8
		57.0	63	63	2.031	2.034	204	60	99.9
		64.5	100	100	1.816	1.818	213	60	99.9
(3)	FE7C3(2)	50.4	27	27	2.276	2.270	002	8	99.9
		54.1	27	27	2.131	2.122	012	40	99.8
		64.5	100	100	1.816	1.820	301	10	99.8
(4)	CR7C3	50.4	27	27	2.276	2.280	411	70	99.9
		54.1	27	27	2.131	2.120	202	70	99.7
		57.0	63	63	2.031	2.040	421	100	99.7
		64.5	100	100	1.816	1.810	431	70	99.8
		98.4	45	45	1.280	1.280	---	60	100.0
(5)	(CR,FE)7C3 .	54.1	27	27	2.131	2.120	202	60	99.7
		57.0	63	63	2.031	2.040	122	100	99.7
		64.5	100	100	1.816	1.810	431	60	99.8
(6)	(CR7C3+MN7C3)	54.1	27	42	2.131	2.120	555	100	99.7
		57.0	63	100	2.031	2.040	666	100	99.7
(7)	COPPER	55.2	72	100	2.091	2.088	111	100	99.9
		98.4	45	62	1.280	1.278	220	20	99.8
(8)	FE8SI2C	55.2	72	72	2.091	2.090	130	80	100.0
		64.5	100	100	1.816	1.810	015	20	99.8
(9)	CRMN3	50.4	27	42	2.276	2.272	002	60	99.9
		53.1	27	42	2.168	2.162	321	40	99.8
		54.1	27	42	2.131	2.132	410	100	100.0
		57.0	63	100	2.031	2.036	202	70	99.8
(10)	MN15C4	50.4	27	37	2.276	2.273	212	50	99.9
		53.1	27	37	2.168	2.163	300	50	99.9
		54.1	27	37	2.131	2.129	301	10	100.0
		55.2	72	100	2.091	2.094	213	100	99.9
		57.0	63	87	2.031	2.037	302	100	99.8
		75.2	27	37	1.588	1.591	224	50	99.8

TABLE-5.25   SUMMARY TABLE OF DIFFRACTOGRAM INDEXING

ALLOY: P2;   H/T TEMPERATURE: 950°C ;   SOAKING DURATION: 6 HOURS

```
DIFF.                        PHASE(S)                                              INT
ANGLE  1  3  5  7  9  11 13 15 17 19 21 23 25 27 29
  54.6  0 0 0 0 0 0 1 0 1 1 1 0 1 1 1 1 1 1 1 0 0 0 0 0 0 0 0 0 0 1    7.0
  55.2  0 0 0 0 0 1 0 0 1 0 0 1 0 0 0 0 0 0 0 0 0 0 0 1 1 0 0 1 0      5.0
  59.2  0 0 0 0 0 1 0 0 0 0 0 0 1 0 0 0 0 0 0 0 0 0 0 0 1 1 1 0 0 0    5.0
  62.5  0 0 0 0 0 1 0 0 0 0 0 0 0 1 0 1 0 0 0 0 0 0 0 0 0 0 0 0 1 0    6.0
  64.0  0 0 0 0 0 0 0 0 1 1 0 0 0 0 0 0 0 0 0 1 0 0 0 0 0 0 1 0 0 0    7.0
  64.4  0 0 0 0 0 0 1 0 1 1 1 1 0 0 0 0 0 0 0 0 0 1 0 0 0 1 0 0 0 0   27.0
* 66.0  0 0 0 1 0 0 0 0 1 0 0 1 0 1 0 1 0 1 0 0 0 0 0 0 0 1 0 0 1 0    5.0
  68.8  0 0 0 0 0 0 0 1 0 0 1 0 1 0 1 0 1 0 0 0 0 0 0 0 0 0 0 0 1 0    6.0
  98.3  0 0 0 0 0 0 0 0 0 0 0 0 1 0 0 0 1 0 0 0 0 0 1 0 1 0 0 0 0 0   16.0
 116.2  0 0 0 0 0 0 0 1 0 0 0 0 0 0 0 0 0 0 0 0 0 1 0 0 0 0 0 0 0 0    6.0
 124.9  0 0 0 0 0 0 0 0 0 0 0 0 0 0 0 0 0 0 0 0 0 0 0 0 0 0 0 0 0 0   18.0

        0 0 0 0 0 3 2 2 4 4 3 2 5 0 4 0 4 0 2 0 0 0 0 0 2 4 2 0 4 0
```

0 = ABSENT   1 = PRESENT   * = PROBABLE DIFF. ANGLE FOR K-BETA RADIATION

DETAILED ANALYSIS OF PHASE(S) ACTUALLY PRESENT

S.N.	PHASE PRESENT	DIFF. ANGLE	PEAK INT	I/IO	D MEAS	D STD	DIFF PLANE	INT STD	CONF LIMIT
(1)	FE3C(CEMENTITE)	55.2	18	83	2.091	2.100	121	60	99.8
		59.2	18	83	1.962	1.970	211	55	99.7
		62.5	22	100	1.868	1.870	113	30	99.9
(2)	FE5C2(HAGG)	68.8	22	100	1.715	1.720	421	10	99.8
		116.2	22	100	1.141	1.140	821	20	99.8
(3)	MN5C2	54.6	25	25	2.113	2.121	211	80	99.8
		55.2	18	18	2.091	2.084	120	80	99.8
		64.0	25	25	1.828	1.831	115	60	99.9
		64.4	100	100	1.818	1.818	213	60	100.0
(4)	FE7C3(2)	54.6	25	25	2.113	2.122	012	40	99.7
		64.4	100	100	1.818	1.820	301	10	99.9
		68.8	22	22	1.715	1.720	220	16	99.8
(5)	CR7C3	54.6	25	43	2.113	2.120	202	70	99.8
		59.2	18	31	1.962	1.960	511	70	99.9
		66.0	18	31	1.779	1.780	521	50	100.0
		68.8	22	37	1.715	1.710	611	60	99.8
		98.3	59	100	1.281	1.280	---	60	99.9
(6)	(CR7C3+MN7C3)	54.6	25	100	2.113	2.120	555	100	99.8
		62.5	22	85	1.868	1.860	888	100	99.7
		66.0	18	71	1.779	1.780	980	60	100.0
		68.8	22	85	1.715	1.710	111	60	99.8
(7)	COPPER	55.2	18	31	2.091	2.088	111	100	99.9
		98.3	59	100	1.281	1.278	220	20	99.7
(8)	FE8SI2C	55.2	18	18	2.091	2.090	130	80	100.0
		59.2	18	18	1.962	1.960	224	60	99.9
		64.4	100	100	1.818	1.820	031	20	99.9
		66.0	18	18	1.779	1.780	301	20	100.0
(9)	MN15C4	55.2	18	83	2.091	2.094	213	100	99.9
		62.5	22	100	1.868	1.873	220	20	99.8
		66.0	18	83	1.779	1.772	116	50	99.7
		68.8	22	100	1.715	1.710	206	20	99.8

TABLE-5.26   SUMMARY TABLE OF DIFFRACTOGRAM INDEXING

ALLOY: P2;   H/T TEMPERATURE: 950°C ;   SOAKING DURATION: 10 HOURS

DIFF. ANGLE	1		3		5		7		9		11		13		15		17		19		21		23		25		27		29		INT
50.8	0	0	0	0	0	1	0	1	0	0	1	1	0	0	0	0	0	0	0	0	0	1	0	0	0	0	1	0	1	0	4.0
55.2	0	0	0	0	0	1	0	0	1	0	0	1	0	0	0	0	0	0	0	0	0	0	0	1	1	0	0	1	0	0	4.0
57.0	1	0	0	0	0	0	0	1	1	1	0	0	1	1	1	0	0	0	0	1	0	0	0	0	0	0	1	1	0		4.0
* 61.4	0	0	0	0	0	0	0	0	0	0	1	1	1	0	1	0	1	0	1	0	0	0	0	0	0	0	1	0	0	1	5.0
62.2	0	0	0	1	1	1	0	0	0	0	0	0	0	0	0	0	0	0	0	0	0	1	0	0	1	1	0	1	0		5.0
64.5	0	0	0	0	0	0	1	0	1	1	1	1	1	1	0	0	1	0	0	0	1	0	0	1	0	0	1	0	0	0	35.0
70.7	0	0	0	0	0	1	0	1	0	0	0	0	0	0	0	0	1	0	1	0	1	1	0	0	1	0	0	0	0		6.0
93.8	0	0	0	0	1	0	0	0	0	0	0	0	1	0	0	0	1	0	0	0	0	0	0	0	0	0	1	0	0	0	3.0
95.0	0	0	0	0	0	0	0	0	0	0	0	1	0	0	0	0	0	0	0	0	0	0	0	0	0	0	0	0	0	0	5.0
95.8	0	0	0	0	0	0	0	0	0	0	0	0	0	0	0	0	0	0	0	0	0	0	0	1	0	0	0	0	0	0	5.0
98.4	0	0	0	0	0	0	0	0	0	0	0	1	0	0	0	1	0	0	0	0	0	1	0	1	0	0	0	0	0		20.0
99.4	0	1	0	0	0	0	0	1	0	0	0	1	0	0	0	0	0	0	0	0	0	1	0	0	0	0	0	0	0	0	4.0
119.9	0	0	0	0	0	0	0	0	0	0	0	0	0	0	0	0	0	0	0	1	0	0	1	0	0	0	0	0	0	0	4.0
124.9	0	0	0	0	0	0	0	0	0	0	0	0	0	0	0	0	0	0	0	0	0	0	0	0	0	0	0	0	0	0	5.0
	0	0	0	0	2	4	0	4	3	2	3	5	6	2	2	0	4	0	0	3	0	3	5	0	2	5	3	0	5	0	

0 =   ABSENT   1 =   PRESENT   * = PROBABLE DIFF. ANGLE FOR K-BETA RADIATION

DETAILED ANALYSIS OF PHASE(S) ACTUALLY PRESENT

S.N.	PHASE PRESENT	DIFF. ANGLE	PEAK INT	I/IO	D MEAS	D STD	DIFF PLANE	INT STD	CONF LIMIT
(1)	FE3C(CEMENTITE)	50.8	11	66	2.259	2.260	200	25	100.0
		55.2	11	66	2.091	2.100	121	60	99.8
		62.2	14	83	1.876	1.870	113	30	99.8
		70.7	17	100	1.675	1.680	023	16	99.7
(2)	FE5C2(HAGG)	50.8	11	66	2.259	2.260	020	50	100.0
		57.0	11	66	2.031	2.030	312	100	100.0
		70.7	17	100	1.675	1.670	512	10	99.8
		99.4	11	66	1.270	1.270	531	20	100.0
(3)	MN5C2	55.2	11	11	2.091	2.084	120	80	99.8
		57.0	11	11	2.031	2.034	204	60	99.9
		64.5	100	100	1.816	1.818	213	60	99.9
(4)	FE7C3(2)	50.8	11	11	2.259	2.255	120	30	99.9
		61.4	14	14	1.898	1.895	112	6	99.9
		64.5	100	100	1.816	1.820	301	10	99.8
(5)	CR7C3	57.0	11	11	2.031	2.040	421	100	99.7
		61.4	14	14	1.898	1.900	222	50	99.9
		64.5	100	100	1.816	1.810	431	70	99.8
		93.8	8	8	1.327	1.330	---	50	99.7
		98.4	57	57	1.280	1.280	---	60	100.0
		99.4	11	11	1.270	1.270	---	30	100.0
(6)	(CR,FE)7C3	57.0	11	11	2.031	2.040	122	100	99.7
		64.5	100	100	1.816	1.810	431	60	99.8
(7)	(CR7C3+MN7C3)	57.0	11	80	2.031	2.040	666	100	99.7
		61.4	14	100	1.898	1.900	777	60	99.9
(8)	COPPER	55.2	11	20	2.091	2.088	111	100	99.9
		98.4	57	100	1.280	1.278	220	20	99.8
(9)	MN15C4	50.8	11	80	2.259	2.262	105	50	99.9
		55.2	11	80	2.091	2.094	213	100	99.9
		57.0	11	80	2.031	2.037	302	100	99.8
		61.4	14	100	1.898	1.903	214	100	99.8
		62.2	14	100	1.876	1.873	220	20	99.9

TABLE-5.27   SUMMARY TABLE OF DIFFRACTOGRAM INDEXING

ALLOY: P2;   H/T TEMPERATURE: 1000°C ;   SOAKING DURATION: 2 HOURS

DIFF. ANGLE	1		3		5		7		9		11		13		15		17		19		21		23		25		27		29		INT
54.4	0	0	0	0	0	0	1	0	1	1	1	0	1	1	1	1	1	1	0	1	0	0	0	0	0	0	1	0	1	1	5.0
55.8	0	1	1	0	0	0	1	0	0	1	0	0	0	0	0	0	0	0	0	0	1	0	0	0	0	1	1	1	0	0	4.0
64.3	0	0	0	0	0	0	1	0	1	1	1	1	0	0	0	0	0	0	1	0	0	1	0	0	0	1	0	0	0	0	30.0
65.2	0	1	0	1	1	0	0	1	0	0	0	0	0	0	0	0	0	0	1	0	0	0	0	0	0	1	0	0	1	0	4.0
66.4	0	0	0	0	0	0	0	0	0	0	0	0	0	0	0	0	1	0	0	0	0	0	0	0	0	0	0	1	1	0	6.0
115.6	0	0	0	0	0	0	0	0	0	0	1	0	0	0	0	0	0	0	0	0	0	0	0	0	1	0	0	0	0	0	6.0
122.0	0	0	0	0	0	0	0	0	0	0	0	0	0	0	0	0	0	0	0	0	0	0	0	0	0	0	0	0	0	0	4.0
123.5	0	0	0	0	0	0	0	0	0	0	0	0	0	0	0	0	0	0	0	0	0	0	0	0	0	0	0	0	0	0	9.0
124.3	0	0	0	0	0	0	0	0	0	0	0	0	0	0	0	0	0	0	0	0	0	0	0	0	0	0	0	0	0	0	19.0
124.5	0	0	0	0	0	0	0	0	0	0	0	0	0	0	0	0	0	0	0	0	0	0	0	0	0	0	0	0	0	0	20.0
124.8	0	0	0	0	0	0	0	0	0	0	0	0	0	0	0	0	0	0	0	0	0	0	0	0	0	0	0	0	0	0	13.0
127.6	0	0	0	0	0	0	0	0	0	0	0	0	0	0	0	0	0	0	0	0	0	0	0	0	0	0	0	0	0	0	6.0
	0	2	0	0	0	0	3	0	2	3	3	0	0	0	0	0	2	0	0	2	0	0	0	0	0	3	2	2	3	0	

0 = ABSENT   1 = PRESENT   * = PROBABLE DIFF. ANGLE FOR K-BETA RADIATION

DETAILED ANALYSIS OF PHASE(S) ACTUALLY PRESENT

S.N.	PHASE PRESENT	DIFF. ANGLE	PEAK INT	I/I0	D MEAS	D STD	DIFF PLANE	INT STD	CONF LIMIT
(1)	AUSTENITE	55.8	13	100	2.071	2.080	111	100	99.7
		65.2	13	100	1.798	1.800	200	80	99.9
(2)	FE5C2	54.4	16	16	2.120	2.112	112	25	99.8
		55.8	13	13	2.071	2.080	021	70	99.7
		64.3	100	100	1.821	1.814	312	25	99.7
(3)	MN5C2(PD5B2)	54.4	16	16	2.120	2.117	112	70	99.9
		55.8	13	13	2.071	2.078	021	100	99.8
		64.3	100	100	1.821	1.820	312	70	100.0
(4)	FE7C3(2)	54.4	16	16	2.120	2.122	012	40	99.9
		64.3	100	100	1.821	1.820	301	10	100.0
		115.6	20	20	1.145	1.146	330	16	99.8
(5)	FE8SI2C	55.8	13	13	2.071	2.070	210	80	100.0
		64.3	100	100	1.821	1.820	031	20	100.0
		65.2	13	13	1.798	1.794	312	20	99.8
(6)	CRMN3	55.8	13	66	2.071	2.069	330	100	99.9
		66.4	20	100	1.770	1.764	500	60	99.8
(7)	MN15C4	54.4	16	83	2.120	2.129	301	10	99.7
		65.2	13	66	1.798	1.800	310	20	99.9
		66.4	20	100	1.770	1.772	116	50	99.9

TABLE-5.28   SUMMARY TABLE OF DIFFRACTOGRAM INDEXING

ALLOY: P2;   H/T TEMPERATURE: 1000°C ;   SOAKING DURATION: 6 HOURS

DIFF. ANGLE	PHASE(S) 1 3 5 7 9 11 13 15 17 19 21 23 25 27 29	INT
49.0	0 0 0 0 0 0 0 0 0 0 0 0 1 0 0 0 0 1 0 0 0 0 0 0 0 0 0 1 1 0	3.0
53.3	0 0 0 1 0 0 0 0 0 0 0 0 0 1 0 0 1 0 0 0 0 0 0 0 0 0 0 1 1 0	5.0
55.3	0 1 0 0 0 0 1 0 1 1 0 0 0 0 0 0 0 0 0 0 0 0 0 1 1 0 0 1 0	6.0
64.5	0 0 0 0 0 0 1 0 1 1 1 1 1 1 0 0 1 0 0 0 0 1 0 0 1 0 0 0 0	42.0
124.8	0 0 0 0 0 0 0 0 0 0 0 0 0 0 0 0 0 0 0 0 0 0 0 0 0 0 0 0 0 0	8.0
125.4	0 0 0 0 0 0 0 1 0 0 0 0 0 0 0 0 0 0 0 0 0 0 0 0 1 0 0 0 0 0	10.0
	0 0 0 0 0 0 2 0 2 2 0 0 2 0 0 0 0 2 0 0 0 0 0 0 2 2 0 2 3 0	

0 = ABSENT   1 = PRESENT   * = PROBABLE DIFF. ANGLE FOR K-BETA RADIATION

DETAILED ANALYSIS OF PHASE(S) ACTUALLY PRESENT

S.N.	PHASE PRESENT	DIFF. ANGLE	PEAK INT	I/IO	D MEAS	D STD	DIFF PLANE	INT STD	CONF LIMIT
(1)	FE5C2	55.3	14	14	2.088	2.080	021	70	99.8
		64.5	100	100	1.816	1.814	312	25	99.9
(2)	MN5C2	55.3	14	14	2.088	2.084	120	80	99.9
		64.5	100	100	1.816	1.818	213	60	99.9
(3)	MN5C2(PD5B2)	55.3	14	14	2.088	2.078	021	100	99.7
		64.5	100	100	1.816	1.820	312	70	99.8
(4)	CR7C3	49.0	7	7	2.337	2.350	321	20	99.7
		64.5	100	100	1.816	1.810	431	70	99.8
(5)	COPPER	55.3	14	60	2.088	2.088	111	100	100.0
		125.4	23	100	1.090	1.090	311	17	100.0
(6)	FE8SI2C	55.3	14	14	2.088	2.080	131	80	99.8
		64.5	100	100	1.816	1.810	015	20	99.8
(7)	CRMN3	49.0	7	60	2.337	2.340	311	40	99.9
		53.3	11	100	2.160	2.162	321	40	100.0
(8)	MN15C4	49.0	7	50	2.337	2.350	114	50	99.7
		53.3	11	83	2.160	2.163	300	50	99.9
		55.3	14	100	2.088	2.094	213	100	99.8

TABLE-5.29 SUMMARY TABLE OF DIFFRACTOGRAM INDEXING

ALLOY: P2;   H/T TEMPERATURE: 1000°C ;   SOAKING DURATION: 10 HOURS

DIFF. ANGLE	PHASE(S) 1 3 5 7 9 11 13 15 17 19 21 23 25 27 29	INT
54.6	0 0 0 0 0 0 1 0 1 1 1 0 1 1 1 1 1 1 1 1 0 0 0 0 0 0 0 0 0 1	10.0
56.9	1 0 0 0 0 0 0 1 1 1 0 0 1 1 1 1 0 0 0 0 1 0 0 0 0 0 0 1 1 0	5.0
64.4	0 0 0 0 0 0 1 0 1 1 1 1 0 0 0 0 0 1 0 0 1 0 0 0 1 0 0 0 0 0	17.0
65.2	0 1 0 1 1 0 0·1 0 0 0 0 0 0 0 0 0 0 1 0 0 0 0 0 1 0 0 1 0 0	8.0
97.5	0 0 0 0 1 0 0 0 0 0 0 0 1 0 0 0 0 0 0 0 0 0 0 0 0 0 0 0 0 0	10.0
98.1	0 0 0 0 0 0 0 0 0 0 0 0 0 0 0 0 0 0 0 0 0 0 0 0 0 0 0 0 0 0	52.0
98.3	0 0 0 0 0 0 0 0 0 0 0 0 1 0 0 0 1 0 0 0 0 0 1 0 1 0 0 0 0 0	41.0
	0 0 0 0 2 0 2 2 3 3 2 0 4 2 2 0 2 0 2 2 0 0 0 0 2 0 0 2 0	

0 = ABSENT   1 = PRESENT   * = PROBABLE DIFF. ANGLE FOR K-BETA RADIATION

DETAILED ANALYSIS OF PHASE(S) ACTUALLY PRESENT

S.N.	PHASE PRESENT	DIFF. ANGLE	PEAK INT	I/IO	D MEAS	D STD	DIFF PLANE	INT STD	CONF LIMIT
(1)	FE5C2	54.6	19	58	2.113	2.112	112	25	100.0
		64.4	32	100	1.818	1.814	312	25	99.8
(2)	FE5C2(HAGG)	56.9	9	62	2.034	2.030	312	100	99.9
		65.2	15	100	1.798	1.800	312	70	99.9
(3)	MN5C2	54.6	19	58	2.113	2.121	211	80	99.8
		56.9	9	29	2.034	2.034	204	60	100.0
		64.4	32	100	1.818	1.818	213	60	100.0
(4)	MN5C2(PD5B2)	54.6	19	58	2.113	2.117	112	70	99.9
		56.9	9	29	2.034	2.035	402	70	100.0
		64.4	32	100	1.818	1.820	312	70	99.9
(5)	FE7C3(2)	54.6	19	58	2.113	2.122	012	40	99.7
		64.4	32	100	1.818	1.820	301	10	99.9
(6)	CR7C3	54.6	19	24	2.113	2.120	202	70	99.8
		56.9	9	12	2.034	2.040	421	100	99.8
		97.5	19	24	1.289	1.290	---	60	99.9
		98.3	78	100	1.281	1.280	---	60	99.9
(7)	(CR,FE)7C3	54.6	19	100	2.113	2.120	202	60	99.8
		56.9	9	50	2.034	2.040	122	100	99.8
(8)	(CR7C3+MN7C3)	54.6	19	100	2.113	2.120	555	100	99.8
		56.9	9	50	2.034	2.040	666	100	99.8
(9)	FE8SI2C	64.4	32	100	1.818	1.820	031	20	99.9
		65.2	15	47	1.798	1.794	312	20	99.8
(10)	MN15C4	56.9	9	62	2.034	2.037	302	100	99.9
		65.2	15	100	1.798	1.800	310	20	99.9

TABLE-5.30 SUMMARY TABLE OF DIFFRACTOGRAM INDEXING

ALLOY: P2; H/T TEMPERATURE:1050°C ; SOAKING DURATION: 2 HOURS

DIFF. ANGLE	1		3		5		7		9		11		13		15		17		19		21		23		25		27		29		INT
54.4	0	0	0	0	0	0	1	0	1	1	1	0	1	1	1	1	1	1	0	1	0	0	0	0	0	0	1	0	1	1	5.0
55.1	0	0	0	0	0	1	0	0	0	0	0	1	0	0	0	0	0	0	0	0	0	0	0	0	1	1	0	0	1	1	5.0
59.4	0	0	0	0	0	0	1	0	0	0	0	0	1	0	0	0	0	0	0	0	0	0	0	0	1	1	0	0	0	0	4.0
60.0	0	0	0	0	0	0	0	0	0	0	0	0	0	0	0	0	1	0	0	0	0	0	0	0	0	0	0	0	1	0	4.0
63.6	0	0	0	0	0	0	0	0	0	0	0	0	1	0	0	0	0	0	0	0	1	0	0	0	1	0	1	0	0	0	4.0
64.4	0	0	0	0	0	0	1	0	1	1	1	1	0	0	0	0	0	0	1	0	0	1	0	0	1	0	0	0	0	0	27.0
68.4	0	0	0	0	0	0	0	1	0	0	1	1	0	0	0	0	0	0	0	0	0	0	0	0	0	0	0	0	1	0	5.0
72.3	0	0	0	0	0	1	0	0	0	0	0	0	0	0	0	0	0	0	0	0	0	0	0	0	0	0	1	0	1	0	5.0
96.0	0	0	0	0	0	0	0	0	0	0	0	0	0	0	0	0	0	0	0	0	0	0	0	1	0	0	0	0	0	0	4.0
97.2	0	0	0	1	1	0	0	0	0	0	0	0	1	0	0	0	0	0	1	0	0	0	0	0	0	0	0	0	0	0	4.0
98.0	0	0	0	0	0	0	0	0	0	0	0	0	0	0	0	0	0	0	0	0	0	1	0	0	0	0	0	0	0	0	4.0
99.0	0	0	0	0	0	0	0	0	0	0	0	0	0	0	0	0	0	0	0	0	0	1	0	0	0	0	0	0	0	0	2.0
118.4	0	0	0	0	0	0	0	0	0	0	0	0	0	0	0	0	0	0	0	0	0	0	0	0	0	0	0	0	0	0	4.0
124.6	0	0	0	0	0	0	0	0	0	0	0	0	0	0	0	0	0	0	0	0	0	0	0	0	0	0	0	0	0	0	3.0
125.0	0	0	0	0	0	0	0	0	0	0	0	0	0	0	0	0	0	0	0	0	0	0	0	0	0	0	0	0	0	0	3.0
127.0	0	1	0	0	0	0	0	0	0	0	0	0	0	0	0	0	0	0	0	0	0	0	1	0	0	0	0	0	0	0	4.0
	0	0	0	0	0	2	3	0	2	2	3	3	4	0	0	0	2	0	2	0	0	0	3	0	0	4	3	0	5	2	

0 = ABSENT   1 = PRESENT   * = PROBABLE DIFF. ANGLE FOR K-BETA RADIATION

DETAILED ANALYSIS OF PHASE(S) ACTUALLY PRESENT

S.N.	PHASE PRESENT	DIFF. ANGLE	PEAK INT	I/IO	D MEAS	D STD	DIFF PLANE	INT STD	CONF LIMIT
(1)	FE3C(CEMENTITE)	55.1	18	100	2.095	2.100	121	60	99.9
		72.3	18	100	1.643	1.640	221	8	99.9
(2)	FE5C2	54.4	18	18	2.120	2.112	112	25	99.8
		59.4	14	14	1.956	1.950	221	45	99.8
		64.4	100	100	1.818	1.814	312	25	99.8
(3)	MN5C2	54.4	18	18	2.120	2.121	211	80	100.0
		64.4	100	100	1.818	1.818	213	60	100.0
(4)	MN5C2(PD5B2)	54.4	18	18	2.120	2.117	112	70	99.9
		64.4	100	100	1.818	1.820	312	70	99.9
(5)	FE7C3(2)	54.4	18	18	2.120	2.122	012	40	99.9
		64.4	100	100	1.818	1.820	301	10	99.9
		68.4	18	18	1.724	1.720	220	16	99.8
(6)	CR7C3	54.4	18	100	2.120	2.120	202	70	100.0
		59.4	14	80	1.956	1.960	511	70	99.9
		63.6	14	80	1.839	1.840	601	60	100.0
		97.2	14	80	1.292	1.290	---	60	99.8
(7)	FE8SI2C	55.1	18	18	2.095	2.090	130	80	99.9
		59.4	14	14	1.956	1.960	224	60	99.9
		63.6	14	14	1.839	1.840	015	60	100.0
		64.4	100	100	1.818	1.820	031	20	99.9
(8)	MN15C4	54.4	18	100	2.120	2.129	301	10	99.7
		55.1	18	100	2.095	2.094	213	100	100.0
		60.0	14	80	1.938	1.937	205	50	100.0
		68.4	18	100	1.724	1.720	215	20	99.8
		72.3	18	100	1.643	1.643	313	10	100.0

TABLE-5.31   SUMMARY TABLE OF DIFFRACTOGRAM INDEXING

ALLOY: P2;   H/T TEMPERATURE:1050°C ;   SOAKING DURATION: 10 HOURS

DIFF. ANGLE	1		3		5		7		9		11		13		15		17		19		21		23		25		27		29		INT
50.0	0	0	0	0	0	0	1	0	0	0	0	0	0	1	0	0	1	0	0	0	1	0	0	0	0	0	0	0	0	0	3.0
50.5	0	0	0	0	0	1	0	1	1	1	1	1	1	0	0	0	0	0	0	0	0	1	0	0	0	0	1	1	1	0	3.0
54.4	0	0	0	0	0	0	0	0	1	1	1	0	1	1	1	0	0	1	0	1	0	0	0	0	0	0	1	0	1	1	5.0
54.8	0	0	0	0	0	1	1	0	0	0	0	1	0	0	0	1	1	0	1	0	0	0	0	0	0	0	0	0	0	1	7.0
56.4	0	0	0	1	1	1	1	1	1	1	0	0	0	0	0	0	0	1	0	0	0	1	0	0	0	1	0	0	0	0	3.0
64.2	0	0	0	0	0	0	1	0	1	1	1	1	0	0	0	0	0	0	1	0	0	1	0	0	0	1	1	0	0	0	110.0
97.8	0	0	0	0	0	0	0	0	0	0	0	0	0	0	0	0	0	0	0	0	0	0	0	0	0	0	0	0	0	0	6.0
124.3	0	0	0	0	0	0	0	0	0	0	0	0	0	0	0	0	0	0	0	0	0	0	0	0	0	0	0	0	0	0	39.0
125.4	0	0	0	0	0	0	0	1	0	0	0	0	0	0	0	0	0	0	0	0	0	0	0	0	1	0	0	0	0	0	6.0
	0	0	0	0	0	3	4	3	4	4	3	3	2	2	0	0	2	2	2	0	0	3	0	0	0	2	3	0	2	2	

0 = ABSENT   1 = PRESENT   * = PROBABLE DIFF. ANGLE FOR K-BETA RADIATION

DETAILED ANALYSIS OF PHASE(S) ACTUALLY PRESENT

S.N.	PHASE PRESENT	DIFF. ANGLE	PEAK INT	I/IO	D MEAS	D STD	DIFF PLANE	INT STD	CONF LIMIT
(1)	FE3C(CEMENTITE)	50.5	2	42	2.272	2.260	200	25	99.7
		54.8	6	100	2.106	2.100	121	60	99.8
		56.4	2	42	2.050	2.060	210	70	99.7
(2)	FE5C2	50.0	2	2	2.293	2.287	020	20	99.9
		54.8	6	6	2.106	2.112	112	25	99.8
		56.4	2	2	2.050	2.049	510	100	100.0
		64.2	100	100	1.823	1.821	511	20	99.9
(3)	FE5C2(HAGG)	50.5	2	50	2.272	2.260	020	50	99.7
		56.4	2	50	2.050	2.060	510	100	99.7
		125.4	5	100	1.090	1.090	404	20	100.0
(4)	MN5C2	50.5	2	2	2.272	2.277	020	40	99.9
		54.4	4	4	2.120	2.121	211	80	100.0
		56.4	2	2	2.050	2.060	015	80	99.7
		64.2	100	100	1.823	1.818	213	60	99.8
(5)	MN5C2(PD5B2)	50.5	2	2	2.272	2.282	020	70	99.8
		54.4	4	4	2.120	2.117	112	70	99.9
		56.4	2	2	2.050	2.058	510	80	99.8
		64.2	100	100	1.823	1.820	312	70	99.9
(6)	FE7C3(2)	50.5	2	2	2.272	2.270	002	8	100.0
		54.4	4	4	2.120	2.122	012	40	99.9
		64.2	100	100	1.823	1.820	301	10	99.9
(7)	CR7C3(2)	50.5	2	2	2.272	2.270	120	50	100.0
		54.8	6	6	2.106	2.100	012	60	99.8
		64.2	100	100	1.823	1.820	301	30	99.9
(8)	(CR,FE)7C3	50.0	2	60	2.293	2.300	141	40	99.8
		54.4	4	100	2.120	2.120	202	60	100.0
(9)	FE8SI2C	56.4	2	2	2.050	2.050	121	80	100.0
		64.2	100	100	1.823	1.820	031	20	99.9
(10)	MN15C4	50.5	2	60	2.272	2.262	105	50	99.8
		54.4	4	100	2.120	2.129	301	10	99.7

TABLE-5.32 SUMMARY TABLE OF DIFFRACTOGRAM INDEXING

ALLOY: P3;   (AS-CAST)

DIFF. ANGLE	PHASE(S) 1 3 5 7 9 11 13 15 17 19 21 23 25 27 29	INT
46.6	0 0 0 0 0 0 0 0 0 0 0 0 0 0 0 0 0 0 0 0 0 0 0 0 0 0 0 0 1 0	4.0
49.0	0 0 0 0 0 0 0 0 0 0 0 0 1 0 0 0 0 1 0 0 0 0 0 0 0 0 0 1 1 0	4.0
50.2	0 0 0 0 0 0 1 0 1 1 0 0 1 0 0 0 0 0 0 0 1 0 0 0 0 0 0 1 1 0	5.0
54.0	0 0 0 0 0 0 0 0 0 0 0 0 1 0 0 0 0 0 0 1 0 0 0 0 0 0 1 1 1 1	4.0
54.8	0 0 0 0 0 1 1 0 0 0 0 1 0 0 0 1 1 0 1 0 0 0 0 0 0 0 0 0 0 1	9.0
55.2	0 0 0 0 0 0 0 0 1 0 0 0 0 0 0 0 0 0 0 0 0 0 1 1 0 0 1 0	3.0
57.0	1 0 0 0 0 0 0 1 1 1 0 0 1 1 1 0 0 0 0 1 0 0 0 0 0 0 0 1 1 0	7.0
57.6	0 0 1 0 0 1 1 0 1 1 1 1 1 0 0 0 0 0 0 0 0 0 0 0 1 1 0 1 0	7.0
64.5	0 0 0 0 0 0 1 0 1 1 1 1 1 1 0 0 1 0 0 0 0 1 0 0 0 1 0 0 0 0	73.0
99.8	0 0 0 0 0 0 0 0 0 0 0 0 0 0 0 1 0 0 1 0 0 0 0 0 0 0 0 1 0 0	4.0
124.2	0 0 0 0 0 0 0 0 0 0 0 0 0 0 0 0 0 0 0 0 0 0 0 0 0 0 0 0 0 0	7.0
124.8	0 0 0 0 0 0 0 0 0 0 0 0 0 0 0 0 0 0 0 0 0 0 0 0 0 0 0 0 0 0	7.0
125.2	0 0 0 0 0 0 1 0 0 0 0 0 0 0 0 0 0 0 0 0 0 0 0 0 1 0 0 0 0 0	5.0
125.8	0 0 0 0 1 0 0 0 0 0 0 0 0 0 0 0 0 0 0 0 0 0 0 1 0 0 0 0 0 1	5.0
	0 0 0 0 0 2 4 2 5 4 2 3 6 2 0 2 2 0 2 2 0 2 0 2 0 0 2 3 2 5 7 3	

0 = ABSENT 1 = PRESENT * = PROBABLE DIFF. ANGLE FOR K-BETA RADIATION

DETAILED ANALYSIS OF PHASE(S) ACTUALLY PRESENT

S.N.	PHASE PRESENT	DIFF. ANGLE	PEAK INT	I/IO	D MEAS	D STD	DIFF PLANE	INT STD	CONF LIMIT
(1)	FE3C(CEMENTITE)	54.8	12	100	2.106	2.100	121	60	99.8
		57.6	9	77	2.011	2.010	103	100	100.0
(2)	FE5C2	50.2	6	6	2.284	2.287	020	20	99.9
		54.8	12	12	2.106	2.112	112	25	99.8
		57.6	9	9	2.011	2.010	312	40	100.0
		64.5	100	100	1.816	1.814	312	25	99.9
(3)	MN5C2	50.2	6	6	2.284	2.277	020	40	99.8
		55.2	4	4	2.091	2.084	120	80	99.8
		57.0	9	9	2.031	2.034	204	60	99.9
		57.6	9	9	2.011	2.019	213	100	99.8
		64.5	100	100	1.816	1.818	213	60	99.9
(4)	FE7C3(2)	57.6	9	9	2.011	2.019	121	100	99.8
		64.5	100	100	1.816	1.820	301	10	99.8
		91.9	5	5	1.348	1.349	023	8	99.9
(5)	CR7C3	49.0	5	5	2.337	2.350	321	20	99.7
		50.2	6	6	2.284	2.280	411	70	99.9
		54.0	5	5	2.134	2.140	112	50	99.8
		57.0	9	9	2.031	2.040	421	100	99.7
		57.6	9	9	2.011	2.020	---	50	99.7
		64.5	100	100	1.816	1.810	431	70	99.8
(6)	(CR,FE)7C3	57.0	9	9	2.031	2.040	122	100	99.7
		64.5	100	100	1.816	1.810	431	60	99.8
(7)	COPPER	55.2	4	60	2.091	2.088	111	100	99.9
		125.2	6	100	1.091	1.090	311	17	99.8
(8)	FE8SI2C	55.2	4	4	2.091	2.090	130	80	100.0
		57.6	9	9	2.011	2.010	322	100	100.0
		64.5	100	100	1.816	1.810	015	20	99.8
		75.8	4	4	1.577	1.580	021	10	99.8
(9)	CRMN3	50.2	6	71	2.284	2.272	002	60	99.7
		54.0	5	57	2.134	2.132	410	100	99.9
		57.0	9	100	2.031	2.036	202	70	99.8
		99.8	5	57	1.267	1.265	710	90	99.8

TABLE-5.33   SUMMARY TABLE OF DIFFRACTOGRAM INDEXING

ALLOY: P3;   H/T   TEMPERATURE: 900°C ;   SOAKING DURATION: 2 HOURS

```
DIFF.                          PHASE(S)                                          INT
ANGLE  1  3  5  7  9 11 13 15 17 19 21 23 25 27 29

47.0   0 0 0 0 0 1 0 0 1 0 0 0 0 0 0 0 1 0 0 0 0 0 0 0 0 0 0 0 1      6.0
48.0   0 0 0 1 1 1 0 1 0 0 0 0 0 0 1 0 0 1 0 0 0 0 0 0 0 0 0 0 0      4.0
50.5   0 0 0 0 0 1 0 1 1 1 1 1 1 0 0 0 0 0 0 0 0 1 0 0 0 1 1 1 0      6.0
54.3   0 0 0 0 0 0 0 0 0 0 1 0 0 0 0 0 0 0 0 1 0 0 0 0 0 1 1 1 1      5.0
54.4   0 0 0 0 0 0 1 0 1 1 0 0 1 1 1 1 1 1 1 0 0 0 0 0 0 0 0 0 0     82.0
57.0   1 0 0 0 0 0 0 1 1 1 0 0 1 1 1 0 0 0 1 0 0 0 0 0 0 0 1 1 0      7.0
59.0   0 0 0 0 0 1 0 0 0 1 0 0 1 0 0 0 0 0 0 0 0 0 0 0 1 1 1 0 0      5.0
62.8   0 0 0 0 0 0 0 0 0 0 0 0 0 0 0 1 0 1 0 0 0 0 0 0 0 0 0 0 0      5.0
64.0   0 0 0 0 0 0 0 0 1 1 0 0 0 0 0 0 0 0 1 0 0 0 0 0 0 1 0 0 0      7.0
64.4   0 0 0 0 0 0 1 0 1 1 1 1 0 0 0 0 0 0 0 0 0 1 0 0 1 0 0 0 0     10.0
96.4   0 0 0 0 0 0 0 0 0 0 0 0 0 0 0 0 1 1 0 0 0 0 0 0 0 0 0 0 0      6.0
97.4   0 0 0 0 1 0 0 0 0 0 0 0 0 1 0 0 0 0 0 0 0 0 0 0 0 0 0 0 0      6.0
98.1   0 0 0 0 0 0 0 0 0 0 0 0 1 0 0 0 1 0 0 0 0 1 0 0 0 0 0 0 0      7.0
125.2  0 0 0 0 0 0 0 1 0 0 0 0 0 0 0 0 0 0 0 0 0 0 0 1 0 0 0 0 0     13.0
126.2  0 0 0 0 1 0 0 0 0 0 0 0 0 0 0 0 0 0 0 0 0 0 0 0 0 0 0 0 0      7.0


       0 0 0 0 3 3 3 4 5 7 3 2 6 2 4 0 4 4 0 2 0 2 0 0 2 4 4 3 2
```

0 = ABSENT   1 = PRESENT   * = PROBABLE DIFF. ANGLE FOR K-BETA RADIATION

DETAILED ANALYSIS OF PHASE(S) ACTUALLY PRESENT

S.N.	PHASE PRESENT	DIFF. ANGLE	PEAK INT	I/IO	D MEAS	D STD	DIFF PLANE	INT STD	CONF LIMIT
(1)	FE3C(CEMENTITE)	48.0	4	66	2.382	2.380	112	65	100.0
		50.5	7	100	2.272	2.260	200	25	99.7
		59.0	6	83	1.968	1.970	211	55	99.9
(2)	FE5C2	47.0	7	7	2.430	2.421	311	15	99.8
		54.4	100	100	2.120	2.112	112	25	99.8
		64.4	12	12	1.818	1.814	312	25	99.8
(3)	MN5C2	50.5	7	7	2.272	2.277	020	40	99.9
		54.4	100	100	2.120	2.121	211	80	100.0
		57.0	8	8	2.031	2.034	204	60	99.9
		64.0	8	8	1.828	1.831	115	60	99.9
		64.4	12	12	1.818	1.818	213	60	100.0
(4)	FE7C3(2)	50.5	7	60	2.272	2.270	002	8	100.0
		54.3	6	50	2.123	2.122	012	40	100.0
		64.4	12	100	1.818	1.820	301	10	99.9
(5)	CR7C3	50.5	7	7	2.272	2.280	411	70	99.8
		54.4	100	100	2.120	2.120	202	70	100.0
		57.0	8	8	2.031	2.040	421	100	99.7
		59.0	6	6	1.968	1.960	511	70	99.7
		97.4	7	7	1.290	1.290	---	60	100.0
		98.1	8	8	1.283	1.280	---	60	99.7
(6)	(CR7C3+MN7C3)	48.0	4	4	2.382	2.380	333	80	100.0
		54.4	100	100	2.120	2.120	555	100	100.0
		57.0	8	8	2.031	2.040	666	100	99.7
		62.8	6	6	1.860	1.860	888	100	100.0
(7)	CRMN3	50.5	7	85	2.272	2.272	002	60	100.0
		54.3	6	71	2.123	2.132	410	100	99.8
		57.0	8	100	2.031	2.036	202	70	99.8
		59.0	6	71	1.968	1.970	420	100	99.9
(8)	MN15C4	50.5	7	85	2.272	2.262	105	50	99.8
		54.3	6	71	2.123	2.129	301	10	99.8
		57.0	8	100	2.031	2.037	302	100	99.8

TABLE-5.34 SUMMARY TABLE OF DIFFRACTOGRAM INDEXING

ALLOY: P3;   H/T TEMPERATURE: 900°C ;   SOAKING DURATION: 10 HOURS

```
DIFF.                          PHASE(S)                                              INT
ANGLE  1  3  5  7  9  11 13 15 17 19 21 23 25 27 29

 49.6  0 0 0 0 0 0 0 0 0 0 0 0 0 1 0 0 1 0 1 0 1 0 0 0 0 0 0 1 0 0     5.0
 54.5  0 0 0 0 0 0 1 0 1 1 1 0 1 1 1 1 1 1 1 0 0 0 0 0 0 0 0 0 0 1     6.0
 55.0  0 0 0 0 0 1 0 0 0 0 0 1 0 0 0 0 0 0 0 1 0 0 0 0 1 1 0 0 1 1   100.0
 56.2  0 0 1 1 1 1 1 1 1 1 0 0 0 0 0 0 0 1 0 0 0 1 0 0 0 1 1 0 0 0     3.0
 56.9  1 0 0 0 0 0 0 1 1 1 0 0 1 1 1 0 0 0 0 1 0 0 0 0 0 0 0 1 1 0     6.0
 58.9  0 0 0 0 0 1 0 0 0 1 0 0 0 0 0 0 0 0 0 0 0 0 0 0 0 1 1 1 0 0     5.0
 64.1  0 0 0 0 0 0 1 0 1 1 0 0 0 0 0 0 0 0 0 1 0 0 0 0 0 0 1 0 0 0     6.0
 64.5  0 0 0 0 0 0 1 0 1 1 1 1 0 0 0 0 0 0 0 0 1 0 0 0 1 0 0 0 0 0    11.0
*71.6  0 0 0 0 0 0 0 0 0 0 0 0 0 0 0 0 0 0 0 0 0 0 0 1 0 0 0 0 0 0     4.0
 77.8  0 0 0 0 0 0 0 0 0 0 0 0 0 0 0 0 0 0 1 0 0 0 0 0 0 0 0 0 0 0     4.0
 89.5  0 0 0 0 0 0 0 0 0 0 0 0 0 0 0 0 0 0 0 0 0 0 0 0 0 0 0 0 0 1     5.0
 98.4  0 0 0 0 0 0 0 0 0 0 0 0 1 0 0 0 1 0 0 0 0 0 1 0 1 0 0 0 0 0    11.0
 99.1  0 0 0 0 0 0 0 0 0 0 0 0 0 0 0 0 0 0 0 0 0 1 0 0 0 0 0 0 0 0     4.0
118.2  0 0 0 0 0 0 0 1 0 0 0 0 0 0 0 0 0 0 0 0 0 0 0 0 0 0 0 0 0 0     5.0
119.3  0 0 0 0 0 0 0 0 0 0 0 0 0 0 0 0 0 0 0 0 0 1 1 0 0 0 0 0 0 0     4.0
125.1  0 0 0 0 0 0 0 0 0 0 0 0 0 0 0 0 0 0 0 0 0 0 0 0 0 0 0 0 0 0    12.0
126.0  0 0 0 0 1 0 0 0 0 0 0 0 0 0 0 0 0 0 0 0 0 0 0 0 1 0 0 0 0 1     4.0

       0 0 0 0 2 3 4 3 5 6 2 2 3 3 2 0 3 2 3 2 0 4 4 0 2 5 3 2 2 4
```

0 = ABSENT   1 = PRESENT   * = PROBABLE DIFF. ANGLE FOR K-BETA RADIATION

DETAILED ANALYSIS OF PHASE(S) ACTUALLY PRESENT

S.N.	PHASE PRESENT	DIFF. ANGLE	PEAK INT	I/IO	D MEAS	D STD	DIFF PLANE	INT STD	CONF LIMIT
(1)	FE3C(CEMENTITE)	55.0	100	100	2.098	2.100	121	60	100.0
		56.2	3	3	2.057	2.060	210	70	99.9
		58.9	5	5	1.971	1.970	211	55	100.0
(2)	FE5C2(HAGG)	56.2	3	50	2.057	2.060	510	100	99.9
		56.9	6	100	2.034	2.030	312	100	99.9
		118.2	5	83	1.129	1.130	133	50	99.8
(3)	MN5C2	54.5	6	54	2.116	2.121	211	80	99.9
		56.2	3	27	2.057	2.060	015	80	99.9
		56.9	6	54	2.034	2.034	204	60	100.0
		64.1	6	54	1.826	1.831	115	60	99.8
		64.5	11	100	1.816	1.818	213	60	99.9
(4)	FE7C3(2)	54.5	6	54	2.116	2.122	012	40	99.8
		64.5	11	100	1.816	1.820	301	10	99.8
(5)	CR7C3(2)	55.0	100	100	2.098	2.100	012	60	100.0
		64.5	11	11	1.816	1.820	301	30	99.8
(6)	(CR,FE)7C3	49.6	5	83	2.310	2.300	141	40	99.8
		54.5	6	100	2.116	2.120	202	60	99.9
		56.9	6	100	2.034	2.040	122	100	99.8
(7)	COPPER	55.0	100	100	2.098	2.088	111	100	99.7
		98.4	11	11	1.280	1.278	220	20	99.8
(8)	FE8SI2C	49.6	5	5	2.310	2.320	104	40	99.8
		55.0	100	100	2.098	2.090	130	80	99.8
		56.2	3	3	2.057	2.050	121	80	99.8
		58.9	5	5	1.971	1.970	212	60	100.0
		64.5	11	11	1.816	1.820	031	20	99.8
(9)	CRMN3	56.9	6	100	2.034	2.036	202	70	99.9
		58.9	5	83	1.971	1.970	420	100	100.0
(10)	MN15C4	55.0	100	100	2.098	2.094	213	100	99.9
		56.9	6	6	2.034	2.037	302	100	99.9

TABLE-5.35   SUMMARY TABLE OF DIFFRACTOGRAM INDEXING

ALLOY: P3;   H/T TEMPERATURE: 950°C ;   SOAKING DURATION: 2 HOURS

```
DIFF.                          PHASE(S)                                          INT
ANGLE   1  3  5  7  9 11 13 15 17 19 21 23 25 27 29

 50.3   0 0 0 0 0 0 1 0 1 1 1 1 1 0 0 0 0 0 0 0 1 0 0 0 0 0 0 1 1 0    6.0
 52.4   0 0 0 0 0 1 1 0 0 1 0 0 0 0 0 0 0 0 0-0 0 1 0 0 0 0 0 0 1 0 1  6.0
 54.5   0 0 0 0 0 0 1 0 1 1 1 0 1 1 1 1 1 0 0 0 0 0 0 0 0 0 0 0 0 1    4.0
 55.0   0 0 0 0 0 1 0 0 0 0 0 1 0 0 0 0 0 1 0 0 0 0 0 1 0 0 1 1       15.0
 55.5   0 1 0 0 0 0 1 0 1 1 0 0 0 0 0 0 0 0 0 0 0 0 0 1 1 0 0 0 0     4.0
 57.0   1 0 0 0 0 0 0 1 1 1 0 0 1 1 1 0 0 0 0 1 0 0 0 0 0 0 1 1 0     4.0
 64.4   0 0 0 0 0 0 1 0 1 1 1 1 0 0 0 0 0 1 0 0 1 0 0 0 1 0 0 0 0     8.0
 65.0   0 1 0 1 1 0 0 1 0 0 1 0 1 1 0 0 1 0 0 1 0 0 0 1 1 0 0 1 0     2.0
 98.5   0 0 0 0 0 0 0 0 0 0 0 0 1 0 0 0 1 0 0 0 0 0 1 0 1 0 0 0 0     4.0
125.0   0 0 0 0 0 0 0 0 0 0 0 0 0 0 0 0 0 0 0 0 0 0 0 0 0 0 0 0 0    60.0
128.0   0 0 0 0 0 0 0 0 0 0 0 0 0 0 0 0 0 0 0 0 0 0 0 0 0 0 0 0 0     4.0

        0 2 0 0 0 2 5 2 5 6 4 3 5 3 2 0 3 0 2 2 2 0 0 0 3 4 0 3 4 3
```

0 = ABSENT   1 = PRESENT   * = PROBABLE DIFF. ANGLE FOR K-BETA RADIATION

DETAILED ANALYSIS OF PHASE(S) ACTUALLY PRESENT

S.N.	PHASE PRESENT	DIFF. ANGLE	PEAK INT	I/IO	D MEAS	D STD	DIFF PLANE	INT STD	CONF LIMIT
(1)	AUSTENITE	55.5	6	100	2.081	2.080	111	100	100.0
		65.0	3	50	1.803	1.800	200	80	99.9
(2)	FE3C(CEMENTITE)	52.4	10	40	2.195	2.200	120	25	99.9
		55.0	25	100	2.098	2.100	121	60	100.0
(3)	FE5C2	50.3	10	75	2.280	2.287	020	20	99.8
		52.4	10	75	2.195	2.190	202	30	99.9
		54.5	6	50	2.116	2.112	112	25	99.9
		55.5	6	50	2.081	2.080	021	70	100.0
		64.4	13	100	1.818	1.814	312	25	99.8
(4)	MN5C2	50.3	10	75	2.280	2.277	020	40	99.9
		54.5	6	50	2.116	2.121	211	80	99.9
		55.5	6	50	2.081	2.084	120	80	99.9
		57.0	6	50	2.031	2.034	204	60	99.9
		64.4	13	100	1.818	1.818	213	60	100.0
(5)	FE7C3(2)	50.3	10	75	2.280	2.270	002	8	99.8
		54.5	6	50	2.116	2.122	012	40	99.8
		64.4	13	100	1.818	1.820	301	10	99.9
		65.0	3	25	1.803	1.807	022	20	99.9
(6)	CR7C3	50.3	10	100	2.280	2.280	411	70	100.0
		54.5	6	66	2.116	2.120	202	70	99.9
		57.0	6	66	2.031	2.040	421	100	99.7
		65.0	3	33	1.803	1.810	431	70	99.7
		98.5	6	66	1.279	1.280	---	60	99.9
(7)	(CR,FE)7C3	54.5	6	100	2.116	2.120	202	60	99.9
		57.0	6	100	2.031	2.040	122	100	99.7
		65.0	3	50	1.803	1.810	431	60	99.7
(8)	COPPER	55.5	6	100	2.081	2.088	111	100	99.8
		65.0	3	50	1.803	1.808	200	46	99.8
		98.5	6	100	1.279	1.278	220	20	99.9
(9)	CRMN3	50.3	10	100	2.280	2.272	002	60	99.8
		52.4	10	100	2.195	2.200	400	40	99.9
		57.0	6	66	2.031	2.036	202	70	99.8
(10)	MN15C4	50.3	10	40	2.280	2.273	212	50	99.8
		55.0	25	100	2.098	2.094	213	100	99.9
		57.0	6	26	2.031	2.037	302	100	99.8

TABLE-5.36 SUMMARY TABLE OF DIFFRACTOGRAM INDEXING

ALLOY: P3;   H/T TEMPERATURE: 950°C ;   SOAKING DURATION: 10 HOURS

DIFF. ANGLE	PHASE(S) 1 3 5 7 9 11 13 15 17 19 21 23 25 27 29	INT
* 54.4	0 0 0 0 0 0 1 0 1 1 1 0 1 1 1 1 1 1 0 1 0 0 0 0 0 0 1 0 1 1	6.0
55.2	0 0 0 0 0 1 0 0 1 0 0 1 0 0 0 0 0 0 0 0 0 0 0 1 1 0 0 1 0	43.0
56.8	0 0 0 0 0 0 0 1 1 1 0 0 1 1 1 0 0 0 0 1 0 0 0 0 0 0 1 1 0	5.0
* 60.5	0 0 0 0 0 0 0 0 1 0 0 0 0 0 0 0 0 0 0 0 0 0 0 0 1 1 1 0 0	7.0
64.5	0 0 0 0 0 0 1 0 1 1 1 1 0 0 0 0 0 0 0 1 0 0 0 1 0 0 0 0	9.0
64.8	0 0 0 0 0 0 0 0 0 0 1 0 1 1 0 0 1 0 0 0 0 0 0 1 1 0 0 0 0	5.0
68.6	0 0 0 0 0 0 0 1 0 0 1 0 0 0 0 0 0 0 0 0 0 0 0 0 0 0 1 0	5.0
99.2	0 0 0 0 0 0 0 0 0 0 0 0 0 0 0 0 0 0 0 0 0 1 0 0 0 0 0 0	6.0
99.5	0 1 0 0 0 0 0 1 0 0 0 0 1 0 0 0 0 1 0 0 0 0 0 0 0 0 0 0	5.0
125.2	0 0 0 0 0 0 0 1 0 0 0 0 0 0 0 0 0 0 0 0 0 0 1 0 0 0 0 0	9.0

0 0 0 0 0 0 2 4 5 3 4 2 4 3 2 0 2 0 0 2 0 0 0 0 3 4 2 2 4 0

0 = ABSENT 1 = PRESENT * = PROBABLE DIFF. ANGLE FOR K-BETA RADIATION

DETAILED ANALYSIS OF PHASE(S) ACTUALLY PRESENT

S.N. PHASE PRESENT	DIFF. ANGLE	PEAK INT	I/IO	D MEAS	D STD	DIFF PLANE	INT STD	CONF LIMIT
(1) FE5C2(HAGG)	56.8	11	55	2.037	2.030	312	100	99.8
	68.6	11	55	1.719	1.720	421	10	100.0
	99.5	11	55	1.269	1.270	531	20	99.9
	125.2	20	100	1.091	1.090	404	20	99.8
(2) MN5C2	54.4	13	13	2.120	2.121	211	80	100.0
	55.2	100	100	2.091	2.084	120	80	99.8
	56.8	11	11	2.037	2.034	204	60	99.9
	60.5	16	16	1.923	1.920	006	60	99.9
	64.5	20	20	1.816	1.818	213	60	99.9
(3) FE7C3(2)	54.4	13	66	2.120	2.122	012	40	99.9
	64.5	20	100	1.816	1.820	301	10	99.8
	64.8	11	55	1.808	1.807	022	20	99.9
	68.6	11	55	1.719	1.720	220	16	100.0
(4) CR7C3	49.0	6	50	2.337	2.350	321	20	99.7
	54.4	13	100	2.120	2.120	202	70	100.0
	56.8	11	83	2.037	2.040	421	100	99.9
	64.8	11	83	1.808	1.810	431	70	99.9
	99.5	11	83	1.269	1.270	---	30	99.9
(5) (CR,FE)7C3	54.4	13	100	2.120	2.120	202	60	100.0
	56.8	11	83	2.037	2.040	122	100	99.9
	64.8	11	83	1.808	1.810	431	60	99.9
(6) COPPER	55.2	100	100	2.091	2.088	111	100	99.9
	64.8	11	11	1.808	1.808	200	46	100.0
	125.2	20	20	1.091	1.090	311	17	99.8
(7) FE8SI2C	55.2	100	100	2.091	2.090	130	80	100.0
	60.5	16	16	1.923	1.920	122	20	99.9
	64.5	20	20	1.816	1.820	031	20	99.8
	64.8	11	11	1.808	1.810	015	20	99.9
(8) CRMN3	49.0	6	42	2.337	2.340	311	40	99.9
	56.8	11	71	2.037	2.036	202	70	100.0
	60.5	16	100	1.923	1.918	331	90	99.8
(9) MN15C4	49.0	6	6	2.337	2.350	114	50	99.7
	54.4	13	13	2.120	2.129	301	10	99.7
	55.2	100	100	2.091	2.094	213	100	99.9
	56.8	11	11	2.037	2.037	302	100	100.0
	68.6	11	11	1.719	1.720	215	20	100.0

TABLE-5.37   SUMMARY TABLE OF DIFFRACTOGRAM INDEXING

ALLOY: P3;   H/T TEMPERATURE: 1000°C ;   SOAKING DURATION: 2 HOURS

DIFF. ANGLE	1		3		5		7		9		11		13		15		17		19		21		23		25		27		29		INT
50.4	0	0	0	0	0	0	1	0	1	1	1	1	1	0	0	0	0	0	0	0	0	1	1	0	0	0	0	0	1	1	6.0
53.2	0	0	0	1	0	0	0	0	0	0	0	0	0	0	0	0	0	0	0	0	0	0	0	0	0	0	0	0	1	1	5.0
54.5	0	0	0	0	0	0	1	0	1	1	1	0	1	1	1	1	1	1	1	0	0	0	0	0	0	0	0	0	0	1	7.0
55.2	0	0	0	0	0	1	0	0	1	0	0	1	0	0	0	0	0	0	0	0	0	0	0	1	1	0	0	1	0	0	80.0
56.9	1	0	0	0	0	0	0	1	1	1	0	0	1	1	1	0	0	0	0	1	0	0	0	0	0	0	0	1	1	0	6.0
* 63.3	0	0	0	0	0	1	0	0	0	0	0	0	1	0	1	0	0	0	0	0	0	0	0	1	0	1	0	0	0	0	3.0
64.4	0	0	0	0	0	0	1	0	1	1	1	1	0	0	0	0	0	1	0	0	1	0	0	1	0	0	1	0	0	0	35.0
98.0	0	0	0	0	0	0	0	0	0	0	0	0	0	0	0	0	0	0	0	0	0	1	0	0	0	0	0	0	0	0	18.0
113.2	0	0	0	0	0	0	0	1	0	0	0	1	0	1	0	0	1	0	0	0	1	0	0	0	0	0	0	0	0	0	4.0
120.6	0	0	0	0	0	0	0	0	0	0	0	0	0	0	0	0	0	0	0	0	0	0	0	0	0	0	0	0	0	0	3.0
123.6	0	0	0	0	0	0	0	0	0	0	0	0	0	0	0	0	0	0	0	0	0	0	0	0	0	0	0	0	0	0	5.0
124.5	0	0	0	0	0	0	0	0	0	0	0	0	0	0	0	0	0	0	0	0	0	0	0	0	0	0	0	0	0	0	14.0
125.4	0	0	0	0	0	0	0	1	0	0	0	0	0	0	0	0	0	0	0	0	0	0	0	0	1	0	0	0	0	0	4.0
	0	0	0	0	0	2	3	3	5	4	3	4	4	3	3	0	2	0	2	2	2	2	0	0	2	3	0	3	4	0	

0 = ABSENT 1 = PRESENT * = PROBABLE DIFF. ANGLE FOR K-BETA RADIATION

DETAILED ANALYSIS OF PHASE(S) ACTUALLY PRESENT

S.N.	PHASE PRESENT	DIFF. ANGLE	PEAK INT	I/IO	D MEAS	D STD	DIFF PLANE	INT STD	CONF LIMIT
(1)	FE3C(CEMENTITE)	55.2	100	100	2.091	2.100	121	60	99.8
		63.3	3	3	1.847	1.850	122	40	99.9
(2)	FE5C2(HAGG)	56.9	7	100	2.034	2.030	312	100	99.9
		113.2	5	66	1.160	1.160	423	20	99.9
		125.4	5	66	1.090	1.090	404	20	100.0
(3)	MN5C2	50.4	7	7	2.276	2.277	020	40	100.0
		54.5	8	8	2.116	2.121	211	80	99.9
		55.2	100	100	2.091	2.084	120	80	99.8
		56.9	7	7	2.034	2.034	204	60	100.0
		64.4	43	43	1.818	1.818	213	60	100.0
(4)	FE7C3(2)	50.4	7	17	2.276	2.270	002	8	99.9
		54.5	8	20	2.116	2.122	012	40	99.8
		64.4	43	100	1.818	1.820	301	10	99.9
(5)	CR7C3	50.4	7	85	2.276	2.280	411	70	99.9
		54.5	8	100	2.116	2.120	202	70	99.9
		56.9	7	85	2.034	2.040	421	100	99.8
		63.3	3	42	1.847	1.840	601	60	99.7
(6)	(CR,FE)7C3	54.5	8	100	2.116	2.120	202	60	99.9
		56.9	7	85	2.034	2.040	122	100	99.8
		113.2	5	57	1.160	1.160	750	60	99.9
(7)	COPPER	55.2	100	100	2.091	2.088	111	100	99.9
		125.4	5	5	1.090	1.090	311	17	100.0
(8)	FE8SI2C	55.2	100	100	2.091	2.090	130	80	100.0
		63.3	3	3	1.847	1.840	015	60	99.7
		64.4	43	43	1.818	1.820	031	20	99.9
(9)	CRMN3	50.4	7	100	2.276	2.272	002	60	99.9
		53.2	6	83	2.164	2.162	321	40	99.9
		56.9	7	100	2.034	2.036	202	70	99.9
(10)	MN15C4	50.4	7	7	2.276	2.273	212	50	99.9
		53.2	6	6	2.164	2.163	300	50	100.0
		55.2	100	100	2.091	2.094	213	100	99.9
		56.9	7	7	2.034	2.037	302	100	99.9

TABLE-5.38 SUMMARY TABLE OF DIFFRACTOGRAM INDEXING

ALLOY: P3;   H/T TEMPERATURE: 1000°C ;   SOAKING DURATION: 6 HOURS

DIFF. ANGLE	1		3		5		7		9		11		13		15		17		19		21		23		25		27		29	INT
54.1	0	0	0	0	0	0	0	0	0	0	0	1	0	0	0	0	0	0	1	0	0	0	0	0	0	1	1	1	0	6.0
54.4	0	0	0	0	0	0	0	0	1	1	1	0	1	1	1	0	0	1	0	0	0	0	0	0	0	0	0	0	1	8.0
54.8	0	0	0	0	0	1	1	0	0	0	0	1	0	0	0	1	1	0	1	0	0	0	0	0	0	0	0	0	1	8.0
55.2	0	0	0	0	0	0	0	0	0	0	0	0	0	0	0	0	0	0	0	0	0	0	0	1	1	0	0	1	0	22.0
55.4	0	0	0	0	0	0	0	0	1	0	0	0	0	0	0	0	0	0	0	0	0	0	0	0	0	0	0	0	0	10.0
55.6	0	1	0	0	0	0	1	0	0	1	0	0	0	0	0	0	0	0	0	1	0	0	0	0	1	0	1	0	0	4.0
64.4	0	0	0	0	0	0	1	0	1	1	1	1	0	0	0	0	0	0	1	0	0	1	0	0	1	0	0	0	0	29.0
98.3	0	0	0	0	0	0	0	0	0	0	0	1	0	0	0	1	0	0	0	0	0	1	0	1	0	0	0	0	0	4.0
124.6	0	0	0	0	0	0	0	0	0	0	0	0	0	0	0	0	0	0	0	0	0	0	0	0	0	0	0	0	0	6.0
125.1	0	0	0	0	0	0	0	0	0	0	0	0	0	0	0	0	0	0	0	0	0	0	0	0	0	0	0	0	0	8.0
	0	0	0	0	0	0	3	0	3	3	2	2	3	0	0	0	2	0	2	0	0	0	0	0	2	3	0	2	2	2

O = ABSENT 1 = PRESENT * = PROBABLE DIFF. ANGLE FOR K-BETA RADIATION

DETAILED ANALYSIS OF PHASE(S) ACTUALLY PRESENT

S.N.	PHASE PRESENT	DIFF. ANGLE	PEAK INT	I/IO	D MEAS	D STD	DIFF PLANE	INT STD	CONF LIMIT
(1)	FE5C2	54.8	27	27	2.106	2.112	112	25	99.8
		55.6	13	13	2.078	2.080	021	70	99.9
		64.4	100	100	1.818	1.814	312	25	99.8
(2)	MN5C2	54.4	27	27	2.120	2.121	211	80	100.0
		55.4	34	34	2.084	2.084	120	80	100.0
		64.4	100	100	1.818	1.818	213	60	100.0
(3)	FE7C3(2)	54.4	27	27	2.120	2.122	012	40	99.9
		64.4	100	100	1.818	1.820	301	10	99.9
(4)	CR7C3(2)	54.8	27	27	2.106	2.100	012	60	99.8
		64.4	100	100	1.818	1.820	301	30	99.9
(5)	CR7C3	54.1	20	75	2.131	2.140	112	50	99.7
		54.4	27	100	2.120	2.120	202	70	100.0
		98.3	13	50	1.281	1.280	---	60	99.9
(6)	COPPER	55.2	75	100	2.091	2.088	111	100	99.9
		98.3	13	18	1.281	1.278	220	20	99.7
(7)	FE8SI2C	55.2	75	75	2.091	2.090	130	80	100.0
		55.6	13	13	2.078	2.070	210	80	99.8
		64.4	100	100	1.818	1.820	031	20	99.9
(8)	CRMN3	54.1	20	100	2.131	2.132	410	100	100.0
		55.6	13	66	2.078	2.069	330	100	99.7
(9)	MN15C4	54.1	20	27	2.131	2.129	301	10	100.0
		55.2	75	100	2.091	2.094	213	100	99.9
(10)	FE2C	54.4	27	100	2.120	2.125	111	100	99.9
		54.8	27	100	2.106	2.103	101	100	99.9

TABLE-5.39 SUMMARY TABLE OF DIFFRACTOGRAM INDEXING

ALLOY: P3;   H/T TEMPERATURE: 1000°C ;   SOAKING DURATION: 10 HOURS

DIFF. ANGLE	PHASE(S) 1 3 5 7 9 11 13 15 17 19 21 23 25 27 29	INT
51.9	0 0 0 0 0 0 1 0 1 1 0 0 1 0 0 1 0 0 1 0 0 1 0 0 0 0 0 1 0 0 1 0	5.0
55.1	0 0 0 0 0 1 0 0 0 0 0 1 0 0 0 0 0 0 0 0 0 0 0 0 1 1 0 0 1 1	34.0
55.8	0 1 1 0 0 0 1 0 0 1 0 0 0 0 0 0 0 0 0 0 1 0 0 0 0 1 1 1 0 0	4.0
64.5	0 0 0 0 0 0 1 0 1 1 1 1 1 1 0 0 1 0 0 0 0 1 0 0 1 0 0 0 0 0	62.0
65.2	0 1 0 1 1 0 0 1 0 0 0 0 0 0 0 0 0 1 0 0 0 0 0 1 0 0 1 0 1 0	3.0
67.4	0 0 0 0 0 0 0 0 0 0 0 0 1 1 0 0 1 0 0 0 0 0 0 0 1 0 0 0 0 0	5.0
98.4	0 0 0 0 0 0 0 0 0 0 0 0 1 0 0 0 1 0 0 0 0 0 1 0 0 0 0 0 0 0	4.0
98.7	0 0 0 0 0 0 0 0 0 0 0 0 0 0 0 0 0 0 0 0 0 0 0 1 0 0 0 0 0 0	5.0
111.3	0 0 1 0 0 0 0 0 0 0 1 1 0 0 0 0 0 0 0 1 0 0 0 0 0 0 0 0 0 0	6.0
124.6	0 0 0 0 0 0 0 0 0 0 0 0 0 0 0 0 0 0 0 0 0 0 0 0 0 0 0 0 0 0	6.0
125.6	0 0 0 0 0 0 1 0 0 0 0 0 0 0 0 0 0 0 0 0 0 0 0 1 0 0 0 0 0 1	4.0
	0 2 2 0 0 3 2 2 3 0 3 5 2 0 0 3 0 0 0 0 2 0 0 3 6 0 0 3 2	

0 = ABSENT   1 = PRESENT   * = PROBABLE DIFF. ANGLE FOR K-BETA RADIATION

DETAILED ANALYSIS OF PHASE(S) ACTUALLY PRESENT

S.N.	PHASE PRESENT	DIFF. ANGLE	PEAK INT	I/IO	D MEAS	D STD	DIFF PLANE	INT STD	CONF LIMIT
(1)	AUSTENITE	55.8	6	100	2.071	2.080	111	100	99.7
		65.2	4	75	1.798	1.800	200	80	99.9
(2)	FE5C2	51.9	8	8	2.214	2.206	112	45	99.8
		55.8	6	6	2.071	2.080	021	70	99.7
		64.5	100	100	1.816	1.814	312	25	99.9
(3)	FE5C2(HAGG)	65.2	4	75	1.798	1.800	312	70	99.9
		125.6	6	100	1.089	1.090	404	20	99.8
(4)	MN5C2(PD5B2)	51.9	8	8	2.214	2.212	112	80	99.9
		55.8	6	6	2.071	2.078	021	100	99.8
		64.5	100	100	1.816	1.820	312	70	99.8
(5)	CR7C3(2)	55.1	54	54	2.095	2.100	012	60	99.9
		64.5	100	100	1.816	1.820	301	30	99.8
		111.3	9	9	1.173	1.172	501	50	99.8
(6)	CR7C3	51.9	8	8	2.214	2.220	102	50	99.9
		64.5	100	100	1.816	1.810	431	70	99.8
		67.4	8	8	1.746	1.750	412	70	99.8
		98.4	6	6	1.280	1.280	---	60	100.0
		111.3	9	9	1.173	1.174	---	70	99.9
(7)	(CR,FE)7C3	64.5	100	100	1.816	1.810	431	60	99.8
		67.4	8	8	1.746	1.740	322	60	99.7
(8)	COPPER	55.1	54	100	2.095	2.088	111	100	99.8
		98.7	8	14	1.277	1.278	220	20	99.9
		125.6	6	11	1.089	1.090	311	17	99.8
(9)	FE8SI2C	51.9	8	8	2.214	2.220	014	40	99.9
		55.1	54	54	2.095	2.090	130	80	99.9
		55.8	6	6	2.071	2.070	210	80	100.0
		64.5	100	100	1.816	1.810	015	20	99.8
		65.2	4	4	1.798	1.794	312	20	99.8
		67.4	8	8	1.746	1.740	225	20	99.7
(10)	MN15C4	51.9	8	14	2.214	2.209	204	50	99.9
		55.1	54	100	2.095	2.094	213	100	100.0
		65.2	4	8	1.798	1.800	310	20	99.9

TABLE-5.40   SUMMARY TABLE OF DIFFRACTOGRAM INDEXING

ALLOY: P3;   H/T TEMPERATURE:1050°C ;   SOAKING DURATION: 2 HOURS

DIFF. ANGLE	PHASE(S) 1 3 5 7 9 11 13 15 17 19 21 23 25 27 29	INT
54.4	0 0 0 0 0 0 1 0 1 1 1 0 1 1 1 1 1 1 0 1 0 0 0 0 0 0 1 0 1 1	8.0
55.1	0 0 0 0 0 1 0 0 0 0 0 1 0 0 0 0 0 0 0 0 0 0 0 0 1 1 0 0 1 1	43.0
55.6	0 1 0 0 0 0 1 0 1 1 0 0 0 0 0 0 0 0 0 1 0 0 0 0 1 0 1 0 0 0	4.0
57.0	1 0 0 0 0 0 0 1 1 1 0 0 1 1 1 0 0 0 1 0 0 0 0 0 0 0 0 1 1 0	5.0
63.8	0 0 0 0 0 0 0 0 1 1 0 0 1 0 0 0 0 0 0 1 0 0 0 0 1 1 1 0 0 0	8.0
64.3	0 0 0 0 0 0 1 0 1 1 1 1 0 0 0 0 0 1 0 0 1 0 0 0 1 0 0 0 0 0	9.0
64.8	0 0 0 0 0 0 1 0 0 0 1 0 1 1 0 0 1 0 0 0 0 0 0 0 1 1 0 0 0 0	5.0
98.0	0 0 0 0 0 0 0 0 0 0 0 0 0 0 0 0 0 0 0 0 0 0 1 0 0 0 0 0 0 0	13.0
98.8	0 0 0 0 0 0 0 0 0 0 0 0 0 0 0 0 0 0 0 0 0 0 0 0 1 0 0 0 0 0	4.0
124.3	0 0 0 0 0 0 0 0 0 0 0 0 0 0 0 0 0 0 0 0 0 0 0 0 0 0 0 0 0 0	7.0
124.8	0 0 0 0 0 0 0 0 0 0 0 0 0 0 0 0 0 0 0 0 0 0 0 0 0 0 0 0 0 0	7.0
125.4	0 0 0 0 0 0 0 1 0 0 0 0 0 0 0 0 0 0 0 0 0 0 0 0 0 1 0 0 0 0	4.0
	0 0 0 0 0 0 4 2 5 5 3 2 4 3 2 0 2 0 0 2 2 0 0 4 5 2 3 3 2	

0 = ABSENT   1 = PRESENT   * = PROBABLE DIFF. ANGLE FOR K-BETA RADIATION

DETAILED ANALYSIS OF PHASE(S) ACTUALLY PRESENT

S.N.	PHASE PRESENT	DIFF. ANGLE	PEAK INT	I/IO	D MEAS	D STD	DIFF PLANE	INT STD	CONF LIMIT
(1)	FE5C2	54.4	18	88	2.120	2.112	112	25	99.8
		55.6	9	44	2.078	2.080	021	70	99.9
		64.3	20	100	1.821	1.821	511	20	100.0
		64.8	11	55	1.808	1.814	312	25	99.8
(2)	MN5C2	54.4	18	88	2.120	2.121	211	80	100.0
		55.6	9	44	2.078	2.084	120	80	99.8
		57.0	11	55	2.031	2.034	204	60	99.9
		63.8	18	88	1.834	1.831	115	60	99.9
		64.3	20	100	1.821	1.818	213	60	99.9
(3)	FE7C3(2)	54.4	18	88	2.120	2.122	012	40	99.9
		64.3	20	100	1.821	1.820	301	10	100.0
		64.8	11	55	1.808	1.807	022	20	99.9
(4)	CR7C3	54.4	18	100	2.120	2.120	202	70	100.0
		57.0	11	62	2.031	2.040	421	100	99.7
		63.8	18	100	1.834	1.840	601	60	99.8
		64.8	11	62	1.808	1.810	431	70	99.9
(5)	(CR,FE)7C3	54.4	18	100	2.120	2.120	202	60	100.0
		57.0	11	62	2.031	2.040	122	100	99.7
		64.8	11	62	1.808	1.810	431	60	99.9
(6)	COPPER	55.1	100	100	2.095	2.088	111	100	99.8
		64.8	11	11	1.808	1.808	200	46	100.0
		98.8	9	9	1.276	1.278	220	20	99.8
		125.4	9	9	1.090	1.090	311	17	100.0
(7)	FE8SI2C	55.1	100	100	2.095	2.090	130	80	99.9
		55.6	9	9	2.078	2.070	210	80	99.8
		63.8	18	18	1.834	1.840	015	60	99.8
		64.3	20	20	1.821	1.820	031	20	100.0
		64.8	11	11	1.808	1.810	015	20	99.9
(8)	CRMN3	55.6	9	50	2.078	2.069	330	100	99.7
		57.0	11	62	2.031	2.036	202	70	99.8
		63.8	18	100	1.834	1.838	222	40	99.8
(9)	MN15C4	54.4	18	18	2.120	2.129	301	10	99.7
		55.1	100	100	2.095	2.094	213	100	100.0
		57.0	11	11	2.031	2.037	302	100	99.8

TABLE-5.41   SUMMARY TABLE OF DIFFRACTOGRAM INDEXING

ALLOY: P3;   H/T TEMPERATURE:1050°C ;   SOAKING DURATION: 6 HOURS

DIFF. ANGLE	1		3		5		7		9		11		13		15		17		19		21		23		25		27		29		INT
52.7	0	0	0	0	1	0	1	1	0	0	0	0	0	0	0	0	0	0	0	0	0	1	0	0	0	1	0	0	0	1	4.0
55.2	0	0	0	0	0	1	0	0	1	0	0	1	0	0	0	0	0	0	0	0	0	0	0	0	1	1	0	0	1	0	42.0
56.1	0	0	1	0	1	1	0	1	1	1	0	0	0	0	0	0	0	1	0	0	1	0	0	0	0	1	1	1	0	0	12.0
63.9	0	0	0	0	0	0	0	0	1	1	0	0	0	0	0	0	0	0	1	0	1	0	0	0	0	0	1	1	0	0	12.0
64.5	0	0	0	0	0	0	1	0	1	1	1	1	1	1	0	0	1	0	0	0	0	1	0	0	1	0	0	0	0	0	32.0
65.6	0	0	0	0	0	0	0	0	0	0	0	1	0	0	0	0	0	0	0	0	0	0	0	0	0	1	0	0	1	0	6.0
83.7	0	0	0	0	0	0	0	0	0	0	0	0	0	0	0	0	0	0	0	0	1	0	0	0	0	0	0	0	0	0	7.0
98.4	0	0	0	0	0	0	0	0	0	0	0	0	0	1	0	0	0	1	0	0	0	0	0	1	0	1	0	0	0	0	12.0
124.6	0	0	0	0	0	0	0	0	0	0	0	0	0	0	0	0	0	0	0	0	0	0	0	0	0	0	0	0	0	0	10.0
	0	0	0	0	2	2	2	4	3	0	3	2	0	0	0	2	0	0	0	2	0	0	0	3	2	0	0	2	5	2	2 2 2 0

0 =   ABSENT   1 = PRESENT   * = PROBABLE DIFF. ANGLE FOR K-BETA RADIATION

DETAILED ANALYSIS OF PHASE(S) ACTUALLY PRESENT

S.N.	PHASE PRESENT	DIFF. ANGLE	PEAK INT	I/IO	D MEAS	D STD	DIFF PLANE	INT STD	CONF LIMIT
(1)	FE3C(CEMENTITE)	55.2	100	100	2.091	2.100	121	60	99.8
		56.1	28	28	2.061	2.060	210	70	100.0
(2)	FE5C2	52.7	9	12	2.183	2.190	202	30	99.8
		64.5	76	100	1.816	1.814	312	25	99.9
(3)	FE5C2(HAGG)	52.7	9	33	2.183	2.180	112	50	99.9
		56.1	28	100	2.061	2.060	510	100	100.0
(4)	MN5C2	55.2	100	100	2.091	2.084	120	80	99.8
		56.1	28	28	2.061	2.060	015	80	100.0
		63.9	28	28	1.831	1.831	115	60	100.0
		64.5	76	76	1.816	1.818	213	60	99.9
(5)	MN5C2(PD5B2)	56.1	28	37	2.061	2.058	510	80	99.9
		63.9	28	37	1.831	1.829	511	70	99.9
		64.5	76	100	1.816	1.820	312	70	99.8
(6)	CR7C3(2)	55.2	100	100	2.091	2.100	012	60	99.8
		64.5	76	76	1.816	1.820	301	30	99.8
		65.6	14	14	1.789	1.790	022	50	99.9
(7)	CR7C3	64.5	76	100	1.816	1.810	431	70	99.8
		98.4	28	37	1.280	1.280	---	60	100.0
(8)	COPPER	55.2	100	100	2.091	2.088	111	100	99.9
		98.4	28	28	1.280	1.278	220	20	99.8
(9)	FE8SI2C	52.7	9	9	2.183	2.180	113	40	99.9
		55.2	100	100	2.091	2.090	130	80	100.0
		56.1	28	28	2.061	2.070	210	80	99.7
		64.5	76	76	1.816	1.810	015	20	99.8
		65.6	14	14	1.789	1.794	312	20	99.8
(10)	CRMN3	56.1	28	100	2.061	2.069	330	100	99.8
		63.9	28	100	1.831	1.838	222	40	99.7
(11)	MN15C4	55.2	100	100	2.091	2.094	213	100	99.9
		65.6	14	14	1.789	1.789	222	50	100.0

TABLE-5.42 SUMMARY TABLE OF DIFFRACTOGRAM INDEXING

ALLOY: P3;   H/T TEMPERATURE:1050°C ;   SOAKING DURATION: 10 HOURS

Phase columns are labelled (left to right): 1, 3, 5, 7, 9, 11, 13, 15, 17, 19, 21, 23, 25, 27, 29 (each label heads two adjacent columns).

DIFF. ANGLE	PHASE(S)	INT
50.1	0 0 0 0 0 0 1 0 1 1 0 0 1 1 0 0 1 0 0 0 1 0 0 0 0 0 0 0 0 0	7.0
52.8	0 0 0 1 1 0 1 1 0 0 0 0 0 0 0 0 0 0 0 0 1 0 0 0 1 0 0 0 0 1	4.0
54.4	0 0 0 0 0 0 1 0 1 1 1 0 1 1 1 1 1 1 0 1 0 1 0 0 0 0 1 0 1 1	4.0
55.2	0 0 0 0 0 1 0 0 1 0 0 1 0 0 0 0 0 0 0 0 0 0 0 0 1 1 0 0 1 0	58.0
56.0	0 0 1 0 0 0 0 0 0 0 0 0 0 0 0 0 0 0 0 1 0 0 0 0 1 1 1 0 0 0	3.0
56.2	0 0 0 1 1 1 1 1 1 1 0 0 0 0 0 0 0 1 0 0 0 1 0 0 1 0 0 0 0 0	5.0
60.1	0 0 0 0 0 0 0 0 0 0 0 0 0 0 0 0 1 0 0 0 0 0 0 0 1 0 1 0 0 0	4.0
63.2	0 0 0 0 0 1 0 0 0 0 0 0 0 0 1 0 0 0 0 0 0 0 1 0 0 0 0 0 0 0	4.0
64.3	0 0 0 0 0 0 1 0 1 1 1 1 0 0 0 0 0 0 1 0 0 1 0 0 1 0 0 0 0 0	29.0
95.8	0 0 0 0 0 0 0 0 0 0 0 0 0 0 0 0 0 0 0 0 0 0 0 1 0 0 0 0 0 0	5.0
98.2	0 0 0 0 0 0 0 0 0 0 0 1 0 0 0 1 0 0 0 0 0 1 0 0 0 0 0 0 0 0	5.0
113.3	0 0 0 0 0 0 0 1 0 0 0 1 0 1 0 0 1 0 0 1 0 0 1 0 0 0 0 0 0 0	5.0
115.6	0 0 0 0 0 0 0 0 0 1 0 0 0 0 0 0 0 0 0 0 0 0 1 0 0 0 0 0 0 0	4.0
126.8	0 1 0 0 0 0 0 0 0 0 0 0 0 0 0 0 0 0 0 0 0 0 1 0 0 0 0 0 0 0	6.0
	0 0 0 2 2 3 5 3 5 4 3 3 3 3 2 0 5 2 0 2 2 3 4 2 0 5 3 0 3 2	

0 = ABSENT   1 = PRESENT   * = PROBABLE DIFF. ANGLE FOR K-BETA RADIATION

DETAILED ANALYSIS OF PHASE(S) ACTUALLY PRESENT

S.N.	PHASE PRESENT	DIFF. ANGLE	PEAK INT	I/IO	D MEAS	D STD	DIFF PLANE	INT STD	CONF LIMIT
(1)	FE3C(CEMENTITE)	55.2	100	100	2.091	2.100	121	60	99.8
		56.2	8	8	2.057	2.060	210	70	99.9
		63.2	6	6	1.849	1.850	122	40	100.0
(2)	FE5C2	50.1	12	24	2.288	2.287	020	20	100.0
		52.8	6	13	2.179	2.190	202	30	99.7
		54.4	6	13	2.120	2.112	112	25	99.8
		56.2	8	17	2.057	2.049	510	100	99.8
		64.3	50	100	1.821	1.814	312	25	99.7
(3)	MN5C2	50.1	12	12	2.288	2.277	020	40	99.7
		54.4	6	6	2.120	2.121	211	80	100.0
		55.2	100	100	2.091	2.084	120	80	99.8
		56.2	8	8	2.057	2.060	015	80	99.9
		64.3	50	50	1.821	1.818	213	60	99.9
(4)	FE7C3(2)	54.4	6	13	2.120	2.122	012	40	99.9
		64.3	50	100	1.821	1.820	301	10	100.0
		115.6	6	13	1.145	1.146	330	16	99.8
(5)	CR7C3(2)	55.2	100	100	2.091	2.100	012	60	99.8
		64.3	50	50	1.821	1.820	301	30	100.0
		113.3	8	8	1.160	1.159	330	30	99.9
(6)	(CR,FE)7C3	50.1	12	100	2.288	2.300	141	40	99.7
		54.4	6	57	2.120	2.120	202	60	100.0
		113.3	8	71	1.160	1.160	750	60	100.0
(7)	(CR7C3+MN7C3)	54.4	6	100	2.120	2.120	555	100	100.0
		63.2	6	100	1.849	1.850	999	80	100.0
(8)	FE8SI2C	52.8	6	6	2.179	2.180	113	40	100.0
		55.2	100	100	2.091	2.090	130	80	100.0
		56.0	5	5	2.064	2.070	210	80	99.8
		56.2	8	8	2.057	2.050	121	80	99.8
		64.3	50	50	1.821	1.820	031	20	100.0
(9)	MN15C4	54.4	6	6	2.120	2.129	301	10	99.7
		55.2	100	100	2.091	2.094	213	100	99.9
		60.1	6	6	1.935	1.937	205	50	99.9

Table-5.43 Summary of the x-ray diffractometric data (Alloy P1)

	Matrix	M_3C	M_7C_3	M_5C_2	Fe_8Si_2C	$CrMn_3$	Cu	$Mn_{15}C_4$
As-cast	A+M	P	P	P	S/T	S		P
800,6	A	P	P	P	P		P	S
850,6	A	P	P	P	P		P	
900,2	A	P	P	P	P/S	P	S	P
900,6	A		S	P	P	P	P	P
900,10	A	S	P	P	P	S	P	P
1000,2	A	T	P	P	P	P	S	P
1000,6	A		S	S	P	S/T	S/T	S/T
1000,10	A	T	S	T	S	S	P	S
1050,2	A	S	P	P	S	S	P	P
1050,6		S/T	P	P	T			P
1050,10	A	P/S	P/S	T	T		S	

Table-5.44 Summary of x-ray diffractometric data (Alloy P2)

	Matrix	M_3C	M_7C_3	M_5C_2	Fe_8Si_2C	$CrMn_3$	Cu	$Mn_{15}C_4$
As-Cast	A+M		P	P	S	P	T	P
800,6	A		S	S	S	S	S	S
850,6	A		P	P	S	S		P/S
900,2		S/T	P	S	S	S	T	S
900,6	A		P	P	S	S	S	P
900,10	A	T	P	P	T		T	P/S
950,2	A		P	P	S	S	S	P
950,6	A	T	P	P	S	P	S	P/S
950,10	A	T	P	S	S/T		T	P
1000,2	A		S	S	T	T	T	P/S
1000,6	A		P/S	S	T	T	T	P/S
1000,10	A		P	P/S				S/T
1050,2		S	P	S	S			P
1050,10		S	P/S	P/S	T			T

Table-5.45 Summary of x-ray diffractometric data (Alloy P3)

	Matrix	M_3C	M_7C_3	M_5C_2	Fe_8Si_2C	$CrMn_3$	Cu	$Mn_{15}C_4$
As-Cast	A+M	S	P	P/S	S	P/S	S	P
900,2		S	P	P	T	P/S		P
900,10		P/S	P	P	S	S	P	P
950,2	A	P/S	P	P	P/S	P/S	P	P
950,10	A	P/S	P	P	P/S	P	P	P
1000,2	A	P/S	P	P	P/S	P/S	P	P
1000,6	A		P/S	P/S	S	P	P	P
1050,2	A		P	P	S/P	S	P	P
1050,8	A	S	S/P	S/P	P/S	P/S	P	P/S
1050,10	A	S	P	S/P	S			P

T-113

Table-5.46a   Element distribution into the matrix (weight %)
as influenced by heat treatment

H/T		Fe	C	Mn	Cr	Cu	Si
P1	AS-CAST	83.191	.710	8.187	4.179	1.668	2.065
P1	900 2	83.944	1.017	8.219	2.218	1.727	2.909
P1	900 10	83.238	1.389	8.377	2.066	1.800	3.138
P1	950 2	83.593	.884	8.978	1.860	1.884	2.801
P1	950 10	83.549	.719	8.229	2.087	1.706	2.965
P1	1000 2	83.713	.696	8.930	2.375	1.777	2.509
P1	1000 10	83.554	.359	9.044	3.243	1.604	2.197
P1	1050 2	81.303	1.076	9.886	3.768	1.927	2.428
P1	1050 10	82.038	1.315	9.241	3.704	1.841	2.279
P2	AS-CAST	82.903	1.526	7.171	3.648	2.907	1.844
P2	900 2	82.556	.682	8.618	2.231	3.470	2.441
P2	900 10	83.410	.316	8.380	2.149	3.381	2.314
P2	950 2	82.296	.683	8.744	2.203	3.609	2.466
P2	950 10	82.324	.835	8.816	2.219	3.491	2.268
P2	1000 2	82.180	.851	8.959	2.419	3.315	2.275
P2	1000 10	82.107	.800	2.175	8.952	2.736	3.229
P2	1050 2	82.744	1.061	8.263	2.491	3.168	2.272
P2	1050 10	81.165	.998	9.161	3.394	3.205	2.080
P3	AS-CAST	79.689	1.693	7.837	3.899	4.980	1.900
P3	900 2	80.224	2.066	7.664	2.076	5.591	2.379
P3	900 10	80.975	.990	8.201	2.204	5.164	2.467
P3	950 2	80.631	1.348	7.744	2.153	5.282	1.917
P3	950 10	80.000	.715	8.674	2.986	5.366	2.318
P3	1000 2	80.891	1.193	7.970	2.396	5.245	2.707
P3	1000 10	81.070	.624	7.891	2.991	5.140	2.448
P3	1050 2	81.126	.634	8.664	2.383	4.887	2.305
P3	1050 10	80.030	1.216	8.532	2.674	5.347	2.201

Table-5.46b Element distribution into matrix (atom %) as influenced by heat treatment

H/T			Fe	C	Mn	Cr	Cu	Si
P1	AS-CAST		79.326	3.146	7.936	4.279	1.398	3.916
P1	900	2	78.664	4.431	7.830	2.232	1.422	5.421
P1	900	10	76.892	5.966	7.867	2.050	1.461	5.765
P1	950	2	78.822	3.876	8.606	1.883	1.561	5.252
P1	950	10	79.651	3.187	7.975	2.137	1.429	5.621
P1	1000	2	79.629	3.078	8.635	2.426	1.485	4.746
P1	1000	10	80.590	1.610	8.868	3.359	1.360	4.214
P1	1050	2	76.038	4.679	9.399	3.785	1.584	4.516
P1	1050	10	76.191	5.678	8.725	3.694	1.503	4.209
P2	AS-CAST		77.171	6.605	6.786	3.647	2.378	3.413
P2	900	2	78.785	3.026	8.361	2.286	2.911	4.631
P2	900	10	80.762	1.423	8.248	2.235	2.877	4.456
P2	950	2	78.525	3.030	8.482	2.257	3.026	4.679
P2	950	10	78.307	3.693	8.525	2.267	2.919	4.290
P2	1000	2	78.059	3.758	8.651	2.468	2.767	4.297
P2	1000	10	77.112	3.493	2.077	9.029	2.258	6.031
P2	1050	2	78.020	4.651	7.920	2.522	2.625	4.260
P2	1050	10	76.778	4.387	8.810	3.448	2.664	3.913
P3	AS-CAST		73.875	7.297	7.386	3.882	4.057	3.503
P3	900	2	73.268	8.773	7.115	2.036	4.487	4.321
P3	900	10	76.590	4.354	7.885	2.239	4.292	4.640
P3	950	2	76.401	5.939	7.459	2.191	4.398	3.612
P3	950	10	76.428	3.176	8.424	3.064	4.505	4.404
P3	1000	2	75.525	5.179	7.565	2.402	4.304	5.026
P3	1000	10	77.512	2.774	7.670	3.071	4.319	4.654
P3	1050	2	77.767	2.826	8.443	2.453	4.117	4.394
P3	1050	10	75.284	5.318	8.159	2.701	4.420	4.117

Table 5.47a Element distribution into the massive carbide (weight %) as influenced by heat treatment

H/T			Fe	C	Mn	Cr	Cu	Si
P1	AS-CAST		55.003	7.875	14.005	23.071	.015	.031
P1	900	2	55.772	7.680	14.460	21.836	.020	.078
P1	900	10	55.099	8.155	14.377	22.271	.105	.000
P1	950	2	54.426	10.122	14.194	21.203	.030	.025
P1	950	10	54.620	8.437	15.275	21.732	.016	.000
P1	1000	2	59.278	7.254	13.645	19.387	.145	.291
P1	1000	10	54.373	9.752	15.168	20.638	.046	.023
P1	1050	2	55.200	9.227	14.245	21.424	.000	.000
P1	1050	10	55.470	7.088	13.184	24.333	.009	.016
P2	AS-CAST		55.726	8.253	14.219	21.739	.060	.003
P2	900	2	54.974	8.246	14.800	21.926	.038	.015
P2	900	10	54.907	7.829	14.511	22.641	.094	.018
P2	950	2	55.030	8.435	14.136	22.305	.065	.028
P2	950	10	56.120	8.577	13.805	21.430	.068	.000
P2	1000	2	56.741	8.427	15.595	19.141	.073	.022
P2	1000	10	55.237	8.559	14.854	21.302	.016	.031
P2	1050	2	55.679	8.998	14.086	20.807	.118	.316
P2	1050	10	55.128	6.973	14.163	23.644	.081	.010
P3	AS-CAST		54.124	8.299	13.669	23.756	.124	.030
P3	900	2	56.222	8.933	16.544	18.243	.053	.005
P3	900	10	52.919	10.396	14.580	21.931	.170	.004
P3	950	2	52.883	10.376	14.876	21.127	.067	.713
P3	950	10	53.569	9.452	16.129	21.537	.199	.000
P3	1000	2	52.399	10.883	14.333	21.920	.223	.049
P3	1000	10	53.735	9.526	13.467	23.070	.226	.000
P3	1050	2	56.025	8.358	14.462	20.991	.134	.028
P3	1050	10	53.776	7.590	14.281	24.278	.039	.037

Table-5.47b Element distribution in the massive carbide (weight %) as influenced by heat treatment

H/T		Fe	C	Mn	Cr	Cu	Si
P1	AS-CAST	42.081	28.013	10.892	18.956	.010	.047
P1	900 2	42.967	27.509	11.325	18.066	.014	.119
P1	900 10	41.856	28.803	11.102	18.169	.070	.000
P1	950 2	39.222	33.915	10.398	16.410	.019	.036
P1	950 10	41.152	29.555	11.699	17.584	.011	.000
P1	1000 2	46.166	26.267	10.803	16.215	.099	.451
P1	1000 10	39.577	33.004	11.224	16.133	.029	.033
P1	1050 2	40.711	31.640	10.680	16.969	.000	.000
P1	1050 10	43.336	25.746	10.471	20.416	.006	.025
P2	AS-CAST	42.230	29.079	10.954	17.692	.040	.005
P2	900 2	41.657	29.052	11.401	17.843	.025	.023
P2	900 10	42.077	27.895	11.305	18.633	.063	.027
P2	950 2	41.474	29.557	10.830	18.053	.043	.042
P2	950 10	42.162	29.960	10.543	17.290	.045	.000
P2	1000 2	42.843	29.584	11.970	15.521	.048	.033
P2	1000 10	41.505	29.902	11.346	17.190	.011	.046
P2	1050 2	41.271	31.010	10.614	16.563	.077	.466
P2	1050 10	43.262	25.442	11.299	19.926	.056	.016
P3	AS-CAST	40.914	29.168	10.504	19.286	.082	.045
P3	900 2	41.887	30.944	12.530	14.596	.035	.007
P3	900 10	37.857	34.578	10.603	16.849	.107	.006
P3	950 2	37.662	34.358	10.770	16.159	.042	1.010
P3	950 10	39.040	32.027	11.949	16.856	.127	.000
P3	1000 2	37.056	35.784	10.304	16.648	.139	.069
P3	1000 10	39.312	32.402	10.015	18.125	.145	.000
P3	1050 2	42.346	29.372	11.112	17.039	.089	.042
P3	1050 10	41.441	27.195	11.188	20.093	.026	.057

Table-5.48a Element distribution in massive carbide (grey) (weight %) as influenced by heat treatment

H/T		Fe	C	Mn	Cr	Cu	Si
P1	AS-CAST	69.330	5.835	15.622	9.117	.078	.018
P1	900 2	52.797	9.887	14.609	21.749	.035	.008
P1	900 10	52.649	9.601	15.288	22.547	.075	.015
P1	1000 10	52.915	9.564	14.568	22.913	.022	.017
P2	900 2	68.243	6.901	15.823	8.940	.073	.019
P2	900 10	68.134	6.318	15.174	10.256	.095	.020
P2	950 2	70.668	6.055	16.159	7.003	.098	.016
P2	1000 2	65.878	7.044	12.317	12.910	1.240	.611
P3	AS-CAST	76.796	4.338	8.270	3.479	0.079	.036
P3	900 2	67.968	7.224	17.490	7.261	.037	.020
P3	900 10	65.409	7.309	16.154	11.104	.016	.007

Table-5.48b Element distribution in the massive carbide(grey)
(atom %) as influenced by heat treatment

H/T			Fe	C	Mn	Cr	Cu	Si
P1	AS-CAST		56.718	22.194	12.992	8.010	.056	.029
P1	900	2	38.532	33.549	10.839	17.046	.022	.012
P1	900	10	38.391	32.550	11.332	17.656	.048	.022
P1	1000	10	38.666	32.493	10.821	17.981	.014	.025
P2	900	2	54.111	25.441	12.754	7.613	.051	.030
P2	900	10	54.915	23.676	12.433	8.877	.067	.032
P2	950	2	57.507	22.909	13.367	6.120	.070	.026
P2	1000	2	51.742	25.723	9.834	10.890	.856	.954
P3	AS-CAST		65.930	17.316	11.581	5.052	.060	.061
P3	900	2	53.432	26.404	13.977	6.130	.026	.031
P3	900	10	51.194	26.598	12.853	9.333	.011	.011

Table-5.49a Element distribution within flower type carbide
(weight %)

H/T			Fe	C	Mn	Cr	Cu	Si
P1	900	8	47.369	11.333	15.017	24.169	2.032	.081
P1	950	2	67.289	8.299	15.607	8.773	.027	.005
P1	1000	2	67.537	6.724	14.896	10.766	.057	.021
P1	1000	10	63.614	6.558	12.927	15.598	.557	.746

Table-5.50a Element distribution within new grey phase
(weight %)

H/T			Fe	C	Mn	Cr	Cu	Si
P2	1050	10	71.543	8.279	14.724	2.074	2.184	1.195
P3	1050	10	69.484	10.229	15.067	2.194	1.891	1.135

Table-5.51a Element distribution within 'needle' (weight %)

H/T			Fe	C	Mn	Cr	Cu	Si
P1	900	8	52.422	13.224	12.396	12.928	8.440	.590
P2	900	2	71.039	5.886	10.581	10.619	1.170	.705

Table-5.52a Element distribution within DC (weight %)

H/T			Fe	C	Mn	Cr	Cu	Si
P1	900	8	62.847	8.470	11.457	9.361	7.006	.859

Table-5.49b Element distribution within flower type carbide (atom %)

H/T			Fe	C	Mn	Cr	Cu	Si
P1	900	8	33.072	36.789	10.658	18.122	1.247	.112
P1	950	2	51.289	29.411	12.093	7.181	.018	.008
P1	1000	2	53.773	24.892	12.057	9.206	.040	.033
P1	1000	10	50.499	24.205	10.432	13.298	.389	1.178

Table-5.50b Element distribution within grey new phase (atom %)

H/T			Fe	C	Mn	Cr	Cu	Si
P2	1050	10	54.394	29.266	11.380	1.693	1.459	1.807
P3	1050	10	50.120	34.305	11.048	1.700	1.199	1.628

Table-5.51b Element distribution within 'needle' (atom %)

H/T			Fe	C	Mn	Cr	Cu	Si
P1	900	8	35.187	41.270	8.458	9.319	4.979	.788
P2	900	2	57.757	22.250	8.745	9.272	.836	1.140

Table-5.52b Element distribution within DC (atom %)

H/T			Fe	C	Mn	Cr	Cu	Si
P1	900	8	47.686	29.881	8.837	7.628	4.672	1.296

Table-5.53 Partitioning ratios of Mn and Cr between carbide and matrix

H/T	Mn$_{carbide}$/Mn$_{matrix}$			Cr$_{carbide}$/Cr$_{matrix}$		
	P1	P2	P3	P1	P2	P3
As-cast	1.71	1.98	1.74	5.52	5.96	6.09
900,2	1.76	1.72	2.16	9.84	9.83	8.79
900,10	1.72	1.73	1.78	10.77	10.54	9.95
950,2	1.58	1.62	1.92	11.39	10.12	9.81
950,10	1.86	1.57	1.86	10.41	9.66	7.21
1000,2	1.53	1.74	1.80	8.16	7.91	9.15
1000,10	1.68	1.66	1.71	6.36	9.79	7.71
1050,2	1.44	1.70	1.67	5.69	8.35	8.81
1050,10	1.43	1.55	1.67	6.57	6.97	9.08

Table-5.54 Transformation temperatures, °C

Alloy designation	Transformation temperature, °C		
	I	II	III
P1	560	995	1020
P2	540	945	---
P3	545	960	---

Table-5.55 DTA, mV

Alloy designation	DTA, mV		
	I	II	III
P1	-0.51	1.83	1.52
P2	-0.37	2.28	---
P3	-0.25	2.12	---

Table-5.56 Effect of heat treating on the %TG

Alloy						Temperature, °C						
	RT	100	200	300	400	500	600	700	800	900	1000	1080
P1	0.0	0.82	1.25	1.54	1.75	2.05	2.46	2.87	3.69	5.13	10.27	18.78
P2	0.0	0.31	0.93	1.24	1.38	1.45	2.06	2.62	3.93	6.19	14.77	22.31
P3	0.0	1.75	2.47	2.68	3.09	3.51	3.92	4.33	5.26	7.01	15.67	24.64

Table-5.57 Percent increase in %TG on heat treating in the different temperature ranges

Alloy						Temperature range					
	I	II	III	IV	V	VI	VII	VIII	IX	X	XI
P1	...	52.43	23.20	13.31	17.65	20.02	16.63	28.60	143.70	100.00	83.01
P2	...	200.65	33.37	11.70	4.48	42.87	26.82	49.81	57.91	138.30	51.05
P3	...	41.14	8.50	15.29	13.43	11.75	10.54	21.41	33.35	123.53	57.24
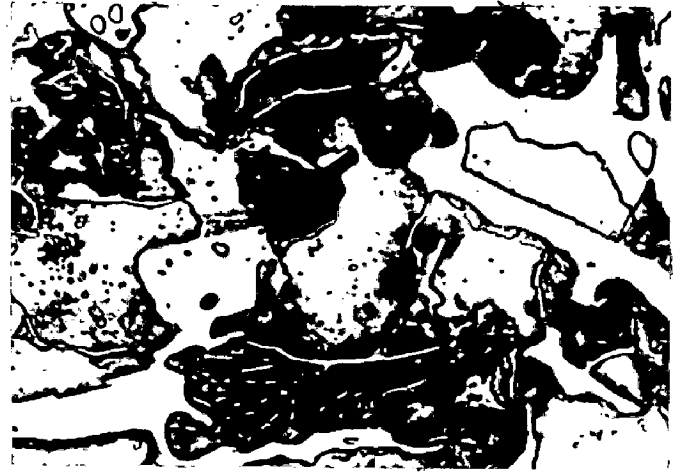
FIG. 4.23

(a) P1,800,2

    X 1000

(b) P1,800,2

    X 200

(c) P1,800,6

    X 1000

(d) P1,800,10

    X 1000

(e) P1,800,10

    X 200

(f) P1,800,10

    X 1000
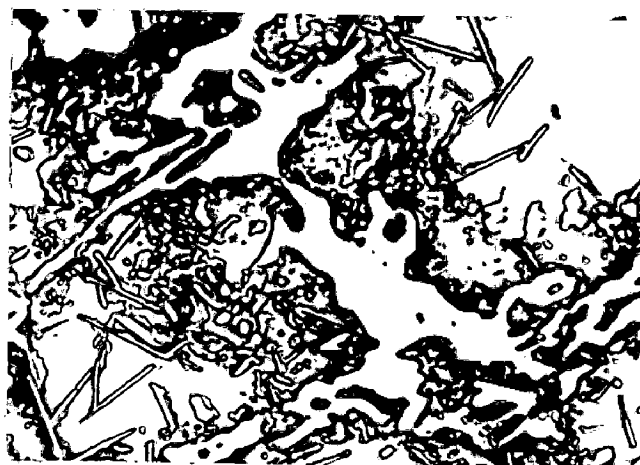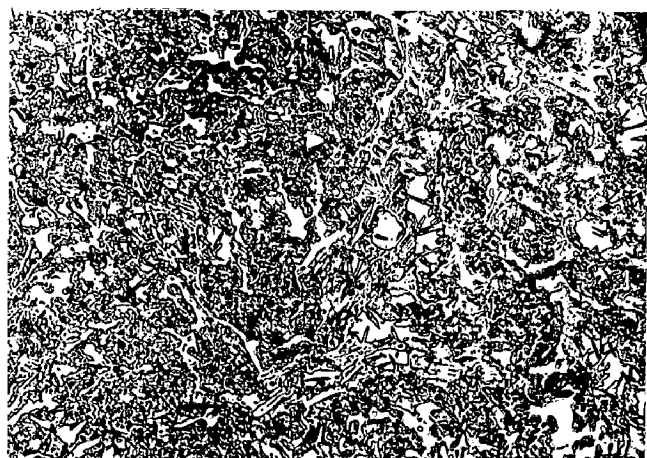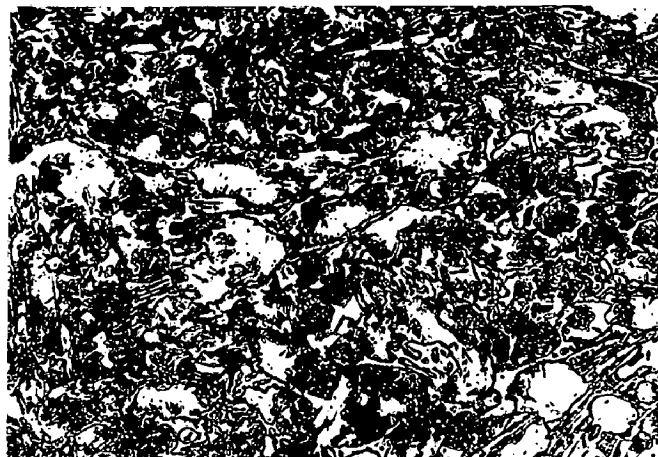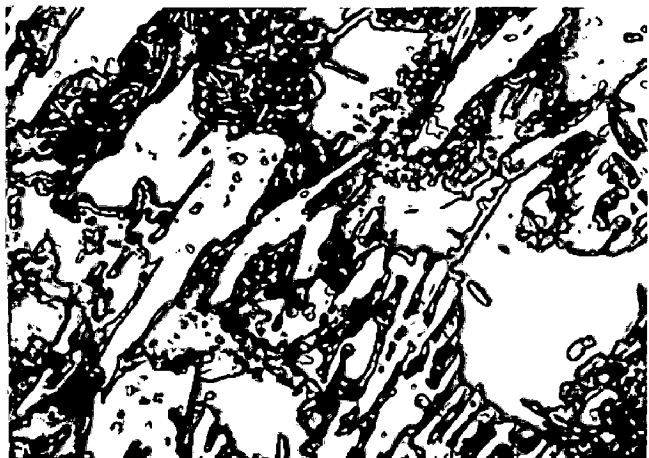
FIG. 4.24

(a) P1,850,2

X 1000

(b) P1,850,2

X 1000

(c) P1,850,2

X 200

(d) P1,850,6

X 1000

(e) P1,850,10

X 1000

(f) P1,850,10

X 1000

(g) P1,850,10

X 200
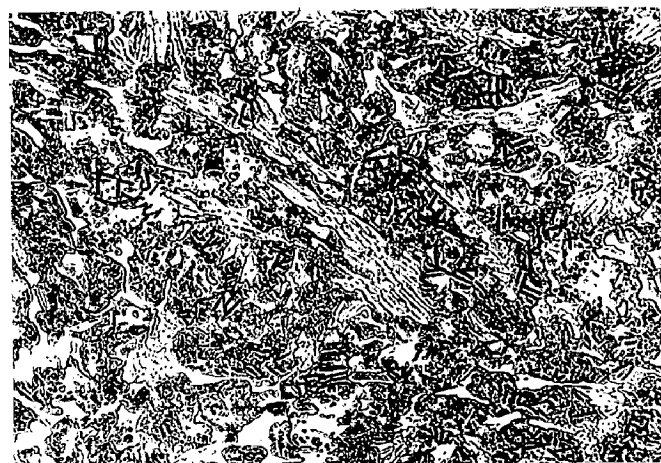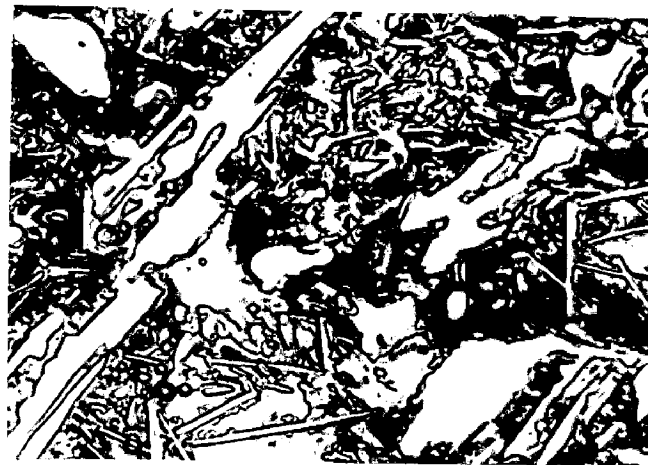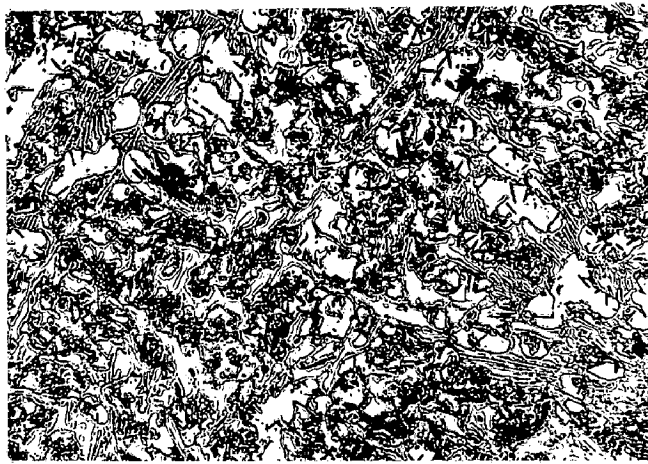
FIG. 4.25

(a) P1,900,2

   X 200

(b) P1,900,2

   X 1000

(c) P1,900,2

   X 1000

(d) P1,900,2

   X 1000

F-32
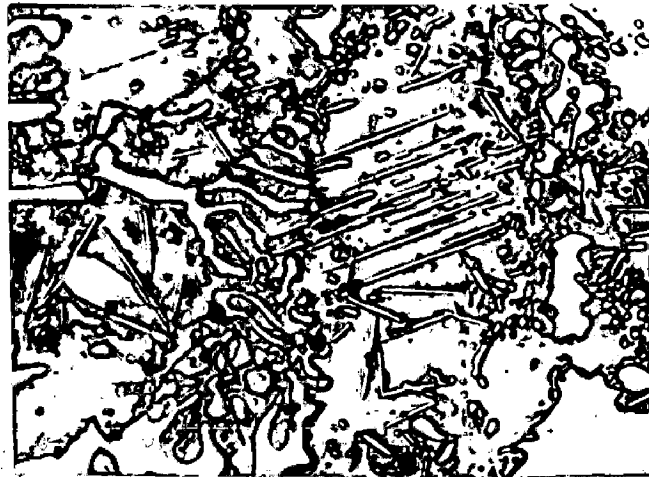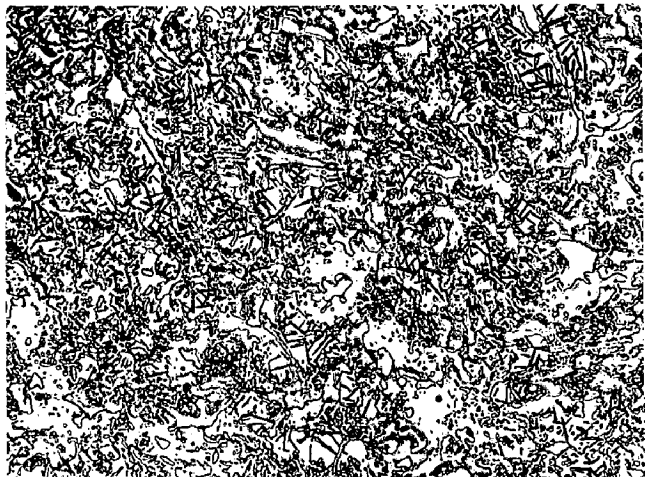
(e) P1,900,6

    X 1000

                                        (f) P1,900,6

                                            X 1000

(g) P1,900,10

    X 1000

                                        (h) P1,900,10

                                          X 200

(i) P1,900,10

    X 1000

F-33

FIG. 4.26

(a) P1,950,2

   X 1000

(b) P1,950,2

   X 200

(c) P1,950,2

   X 1000

(d) P1,950,10

   X 1000

(e) P1,950,10

   X 200

(f) P1,950,10

   X 1000
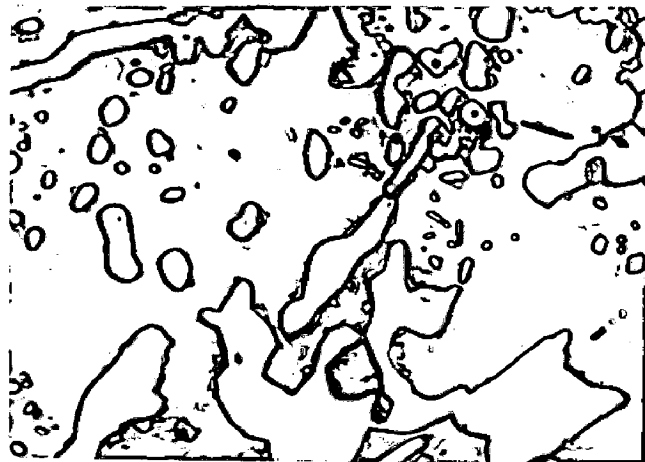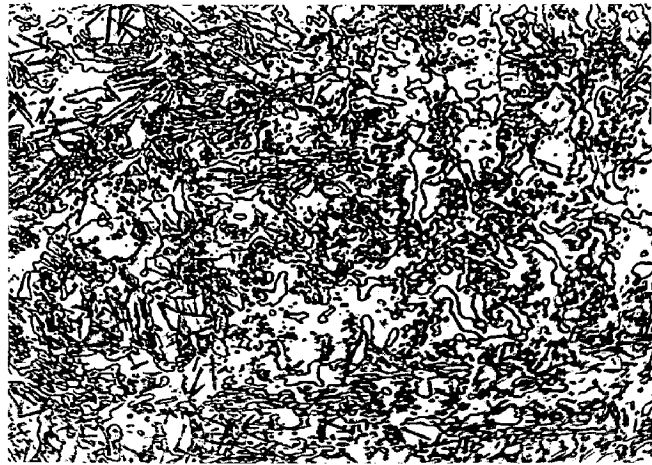
FIG. 4.27

(a) P1,1000,2

X 200

(b) P1,1000,2

X 1000

(c) P1,1000,6

X 1000

(d) P1,1000,6

X 200

(e) P1,1000,6

X 1000
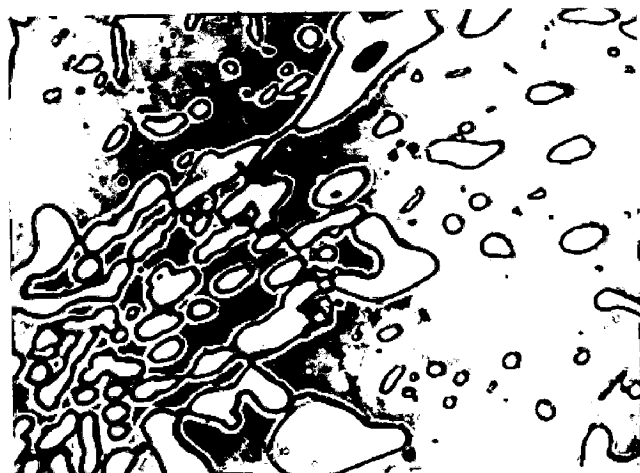
(f) P1,1000,10

    X 1000

(g) P1,1000,10

    X 1000

(h) P1,1000,10

    X 200

(i) P1,1000,10

    X 1000

FIG. 4.28

(a) P1,1050,2

X 1000

(b) P1,1050,2

X 200

(c) P1,1050,2

X 1000
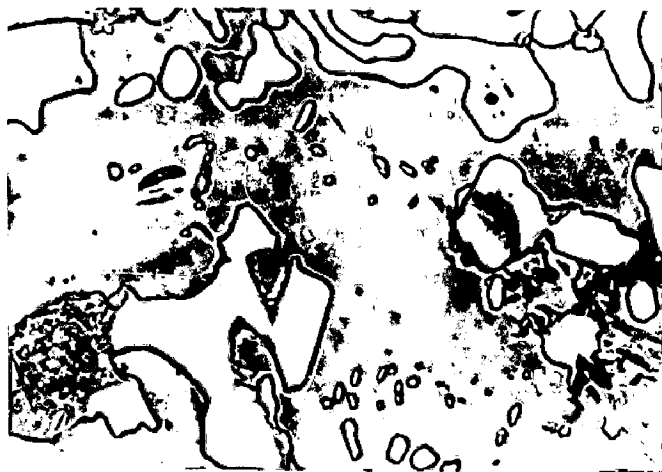
(d) P1,1050,6

    X 200

(e) P1,1050,6

    X 1000

(f) P1,1050,6
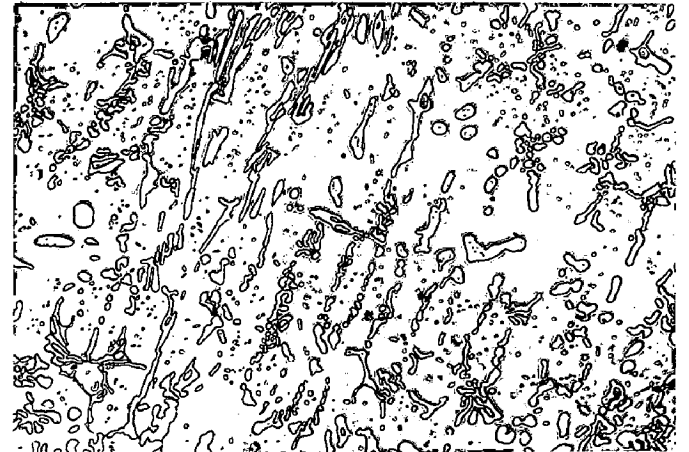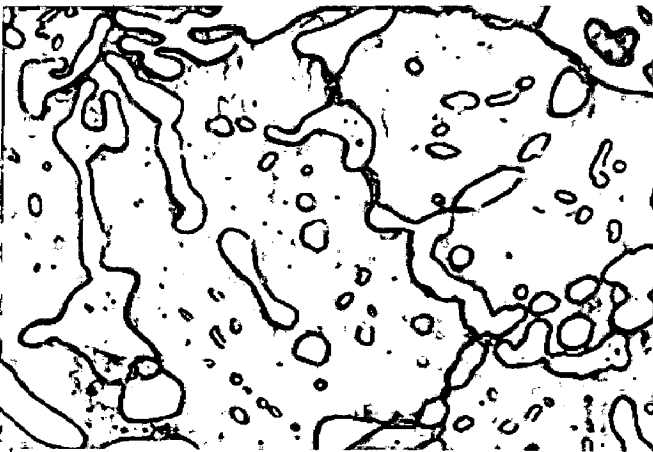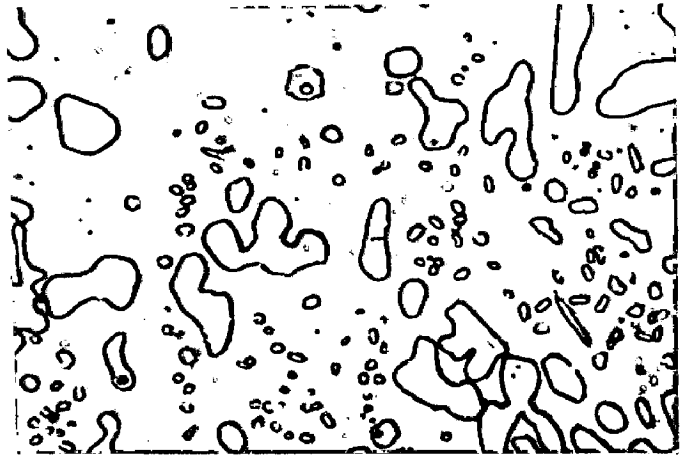
    X 1000

(g) P1,1050,6

    X 1000

(h) P1,1050,10

    X 1000

(i) P1,1050,10

    X 200

(j) P1,1050,10

    X 1000
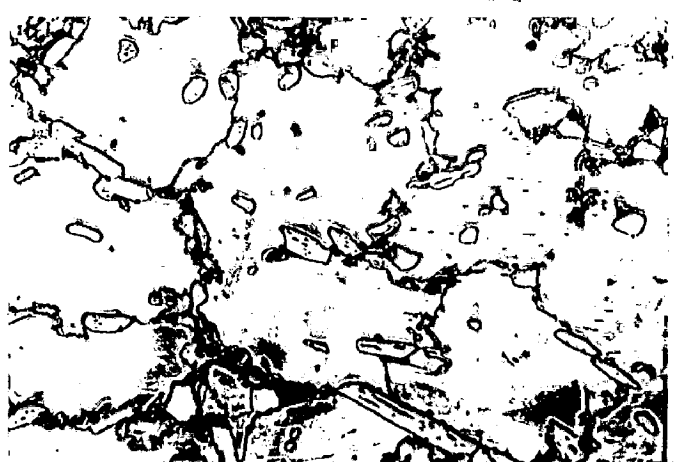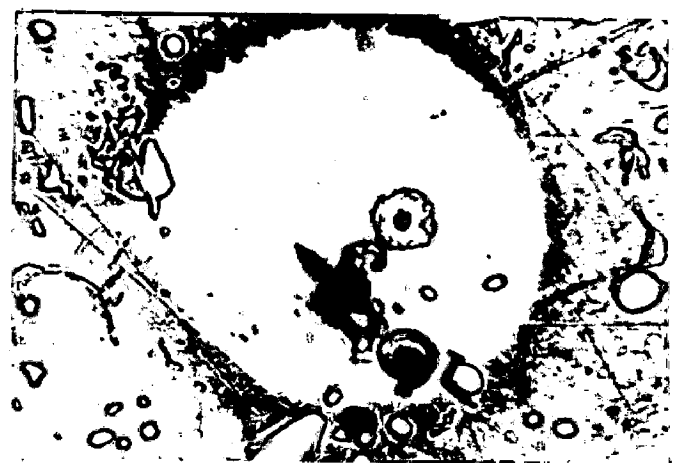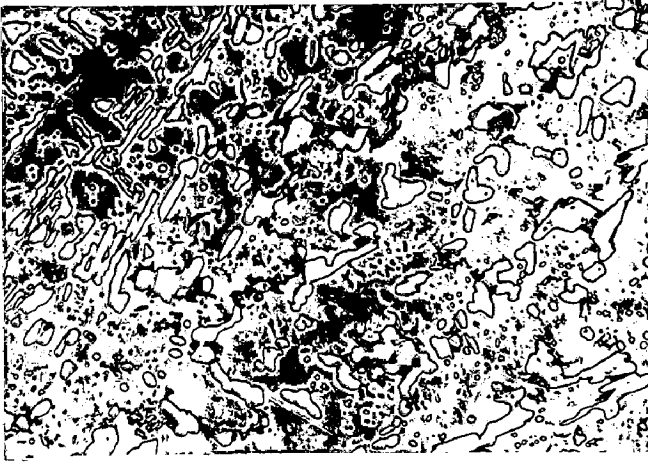
FIG. 4.29

F-39

(a) P2,As-cast

X 1000

(b) P2,As-cast

X 200

(c) P2,As-cast

X 1000
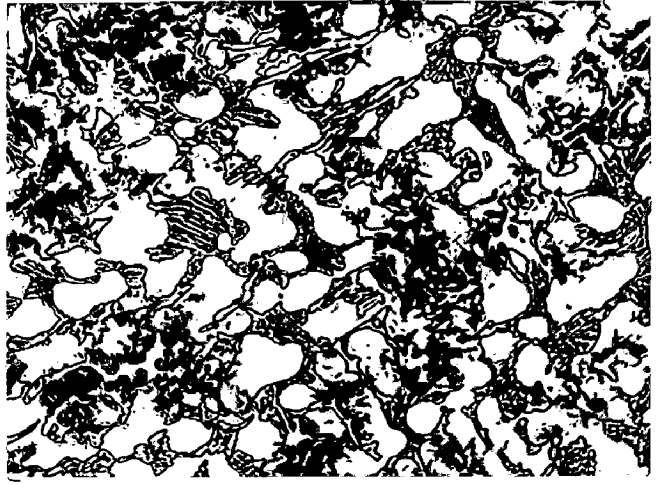
FIG. 4.30

(a) P2,800,2

    X 1000

(b) P2,800,2

    X 200

(c) P2,800,2

    X 1000

(d) P2,800,6

    X 1000

(e) P2,800,6

    X 1000

(f) P2,800,10

    X 1000

(g) P2,800,10

    X 1000

(h) P2,800,10

    X 200
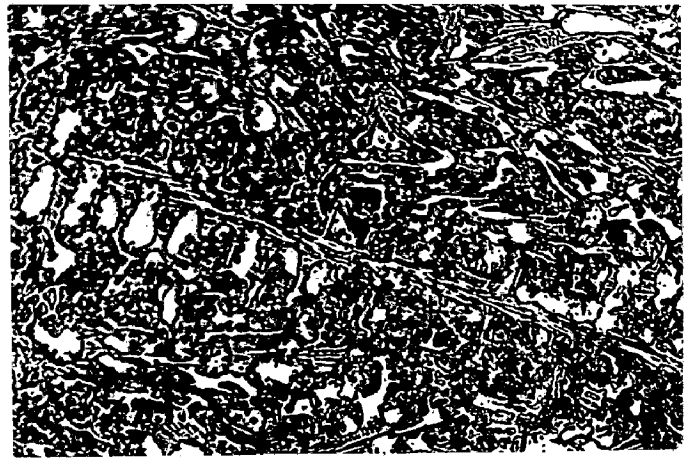
FIG. 4.31

(a) P2,850,2

X 1000

(b) P2,850,2

X 200

(c) P2,850,2

X 1000

(d) P2,850,6

X 200

(e) P2, 850,6

X 1000

(f) P2,850,10

X 200

(g) P2,850,10

X 1000

(h) P2,850,10

X 1000
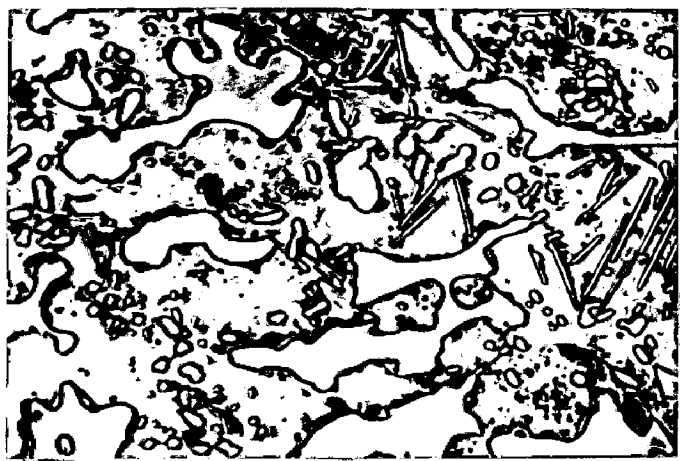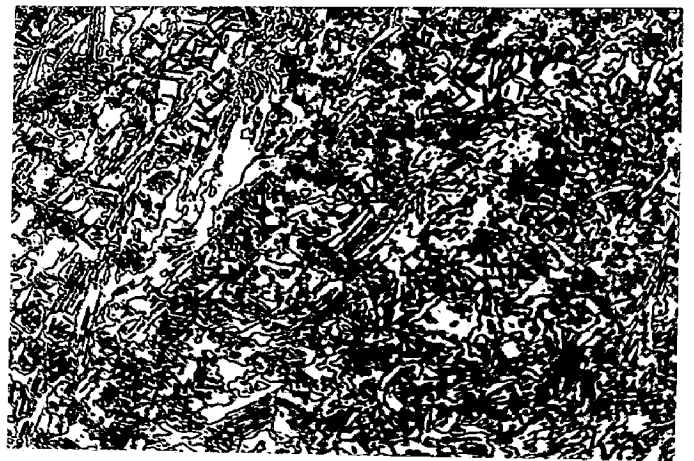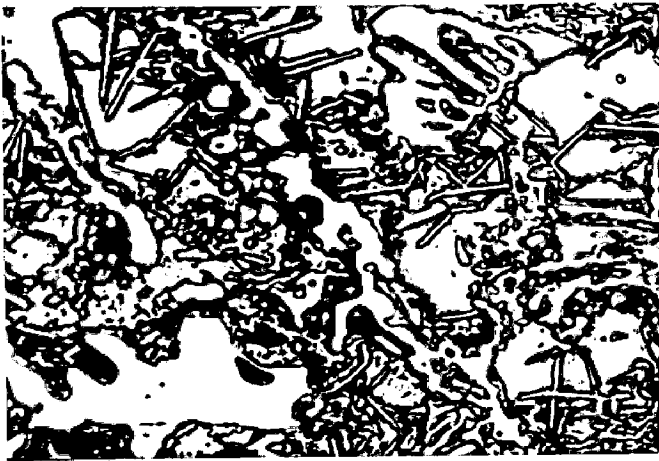
FIG. 4.32

(a) P2,900,2

    X 1000

(b) P2,900,2

    X 200

(c) P2,900,2

    X 1000

(d) P2,900,10

    X 650

(e) P2,900,10
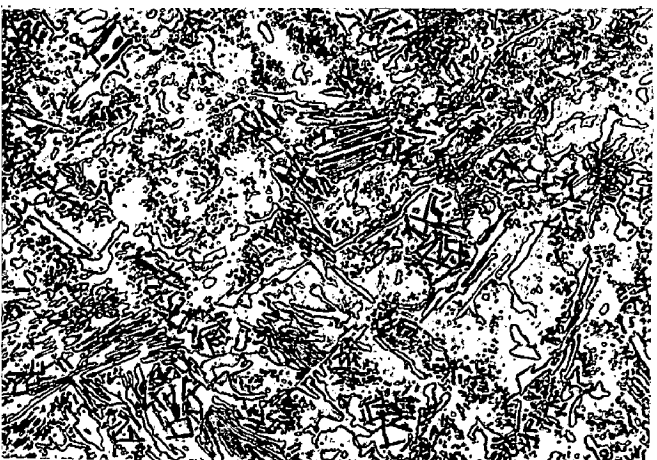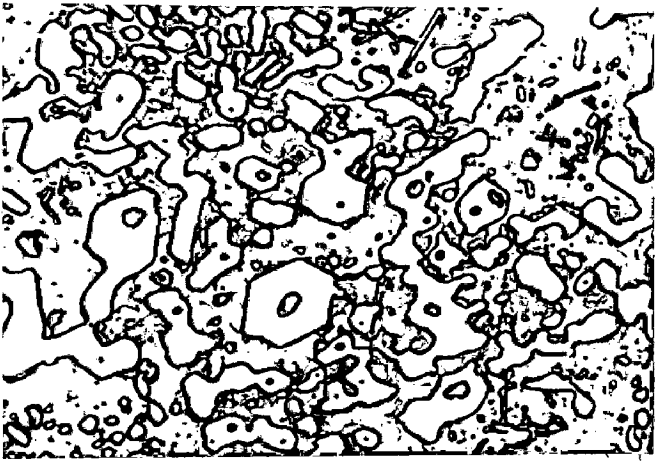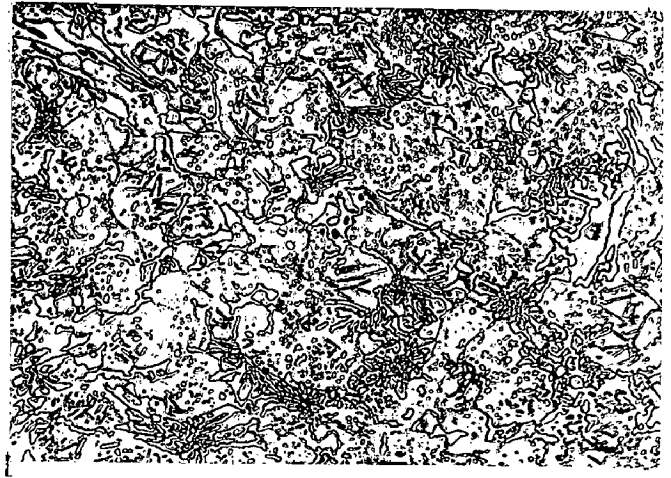
    X 1000

(f) P2,900,10

    X 1000
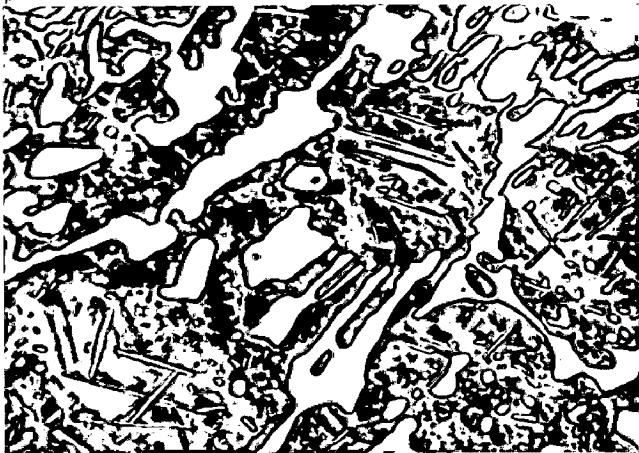
FIG. 4.33

(a) P2,950,2

X 1000

(b) P2,950,2

X 200

(c) P2,950,2

X 1000

(d) P2,950,6

X 1000

(e) P2,950,6

X 1000

(f) P2,950,10

X 200

(g) P2,950,10

X 1000
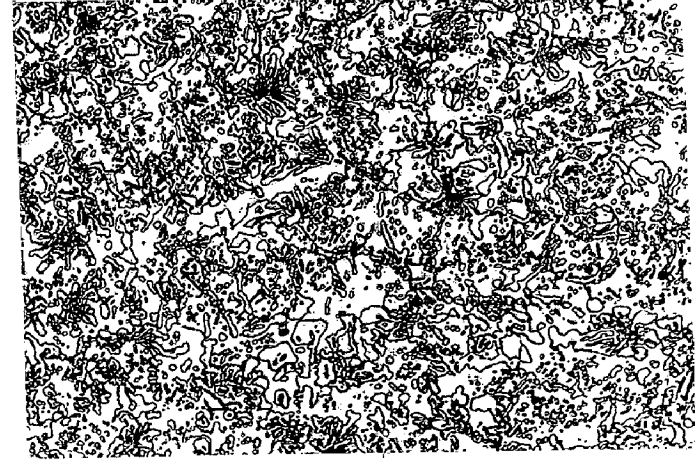
FIG. 6.15 SEM photographs of the corroded samples (Alloy P3)

(a) P3,As-cast

    X (1250 x 1.0)

(b) P3,As-cast

    X (640 x 1.0)

(c) P3,900,10

    X (160 x 1.0)

(d) P3,900,10

    X (320 x 1.0)

(e) P3,950,10

    X (320 x 1.0)

(f) P3,1000,2

    X (640 x 1.1)

(g) P3,1050,10

    X (640 x 1.0)

(h) P3,1050,10

    X (1250 x 1.0)
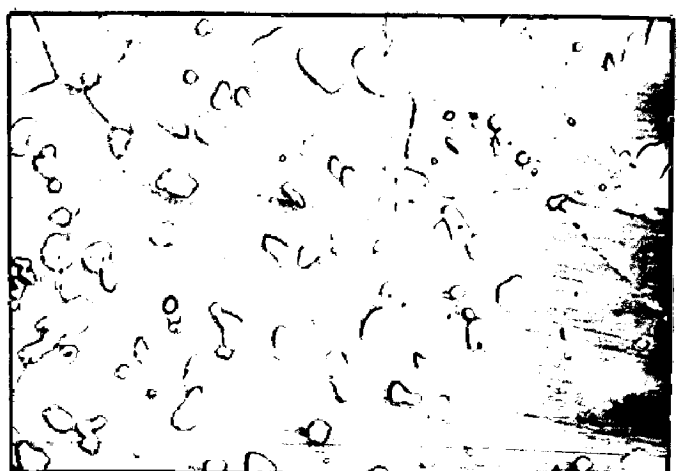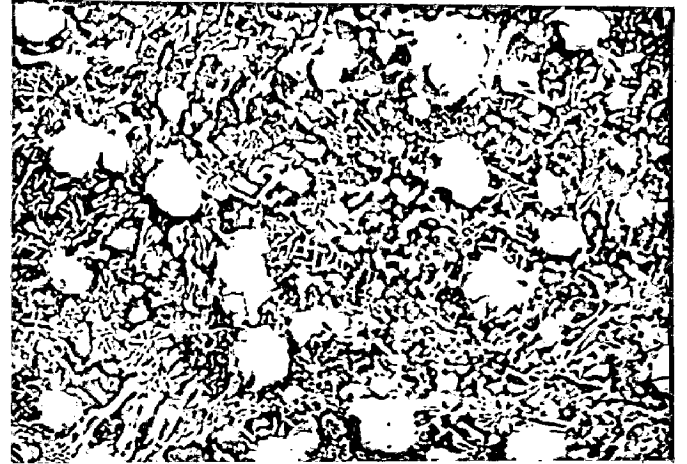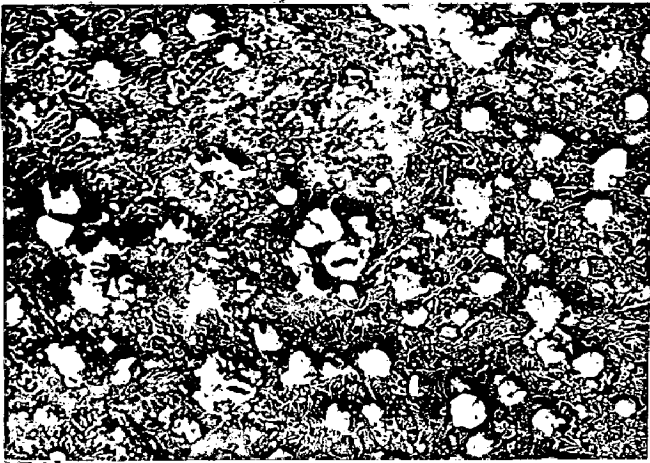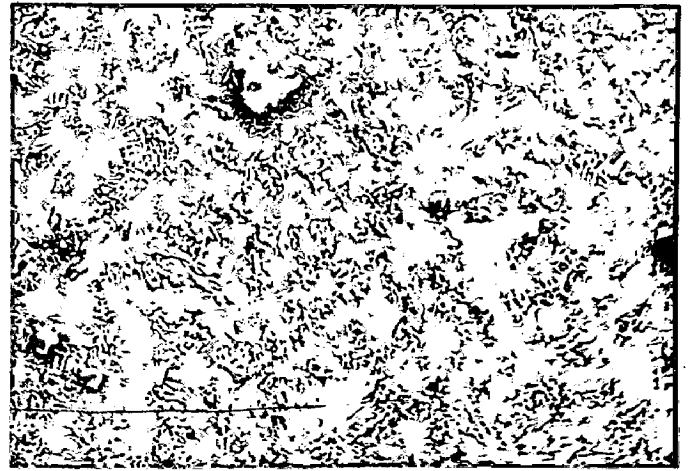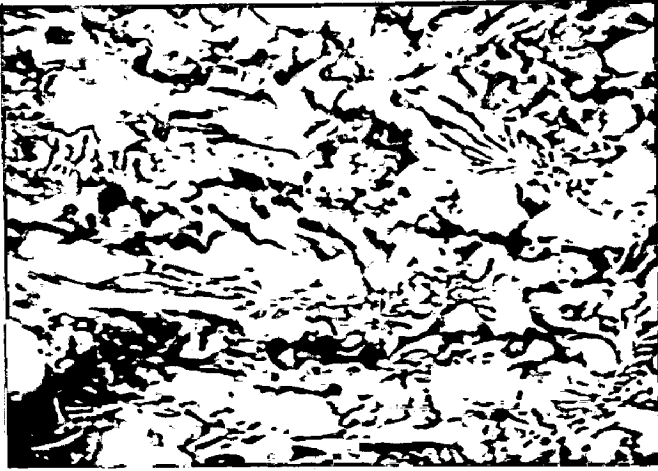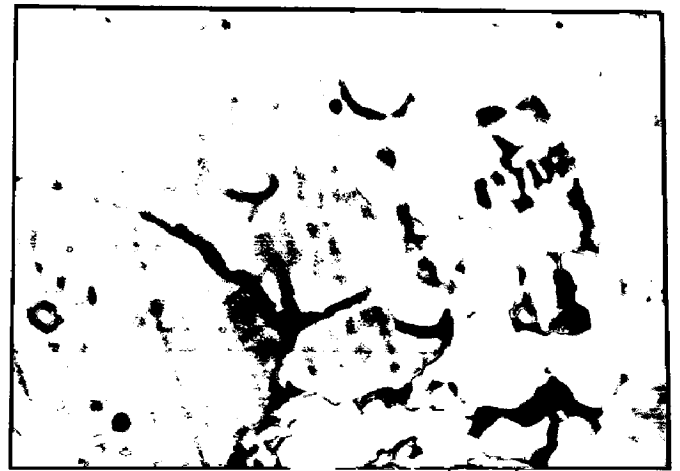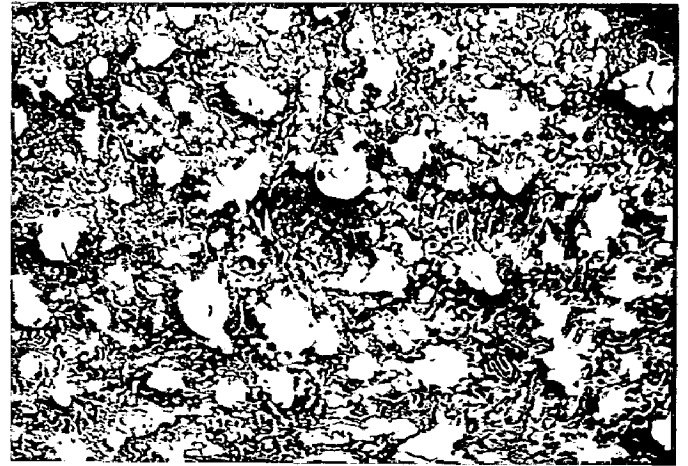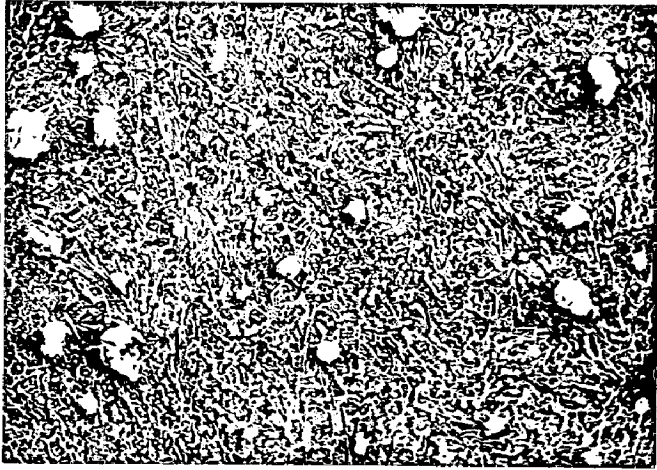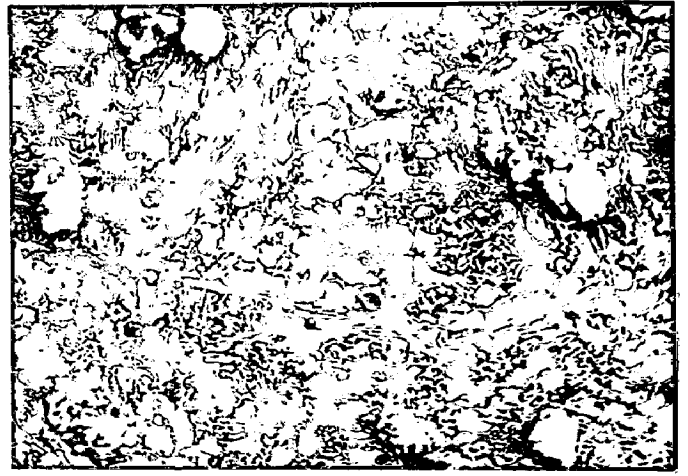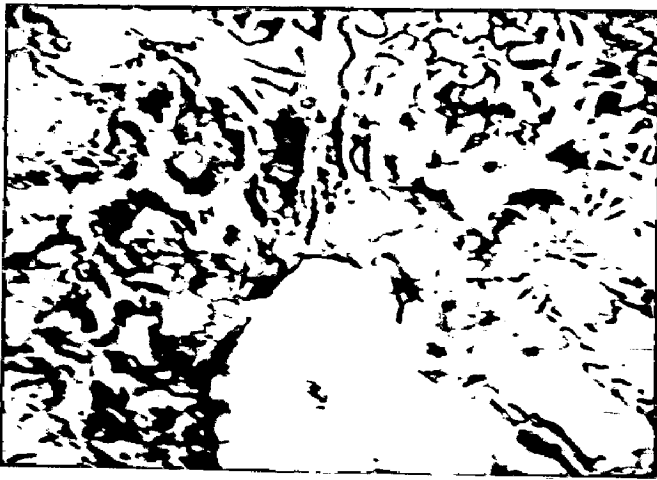
FIG. 6.14 SEM photographs of the corroded samples (Alloy P2)

(a) P2,As-cast

    X (1250 x 1.1)

(b) P2,As-cast

    X (640 x 1.1)

(c) P2,950,2

    X (640 x 1.0)

(d) P2,950,10

    X (640 x 1.0)

(e) P2,1000,2

    X (640 x 1.0)

(f) P2,1050,10

    X (1250 x 1.0)

(g) P2,950,2

    X (1250 x 1.0)
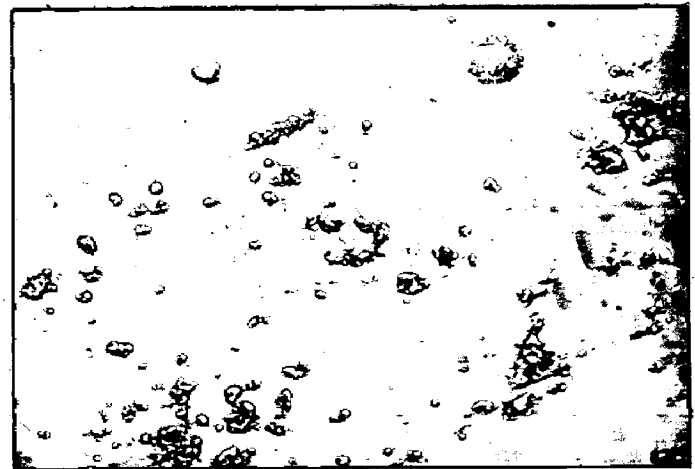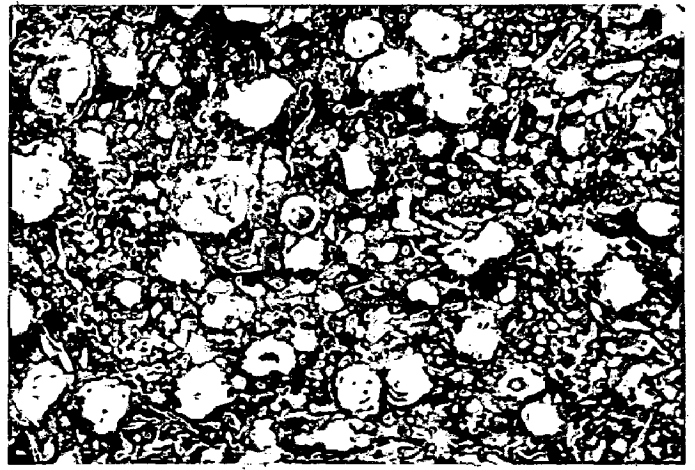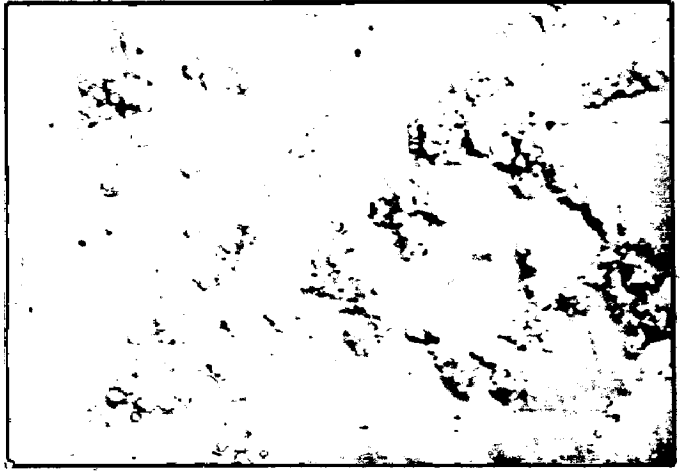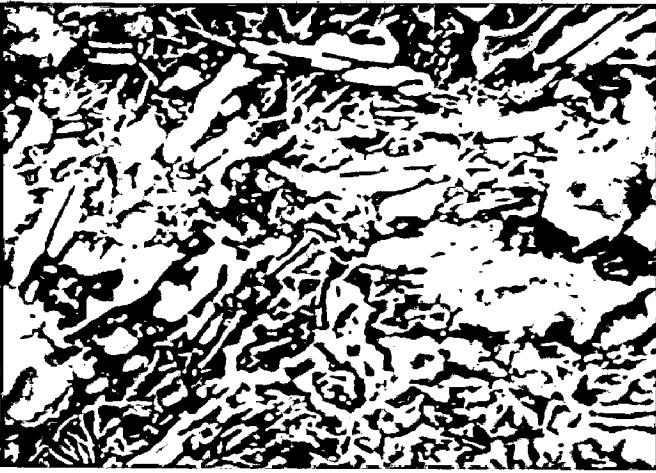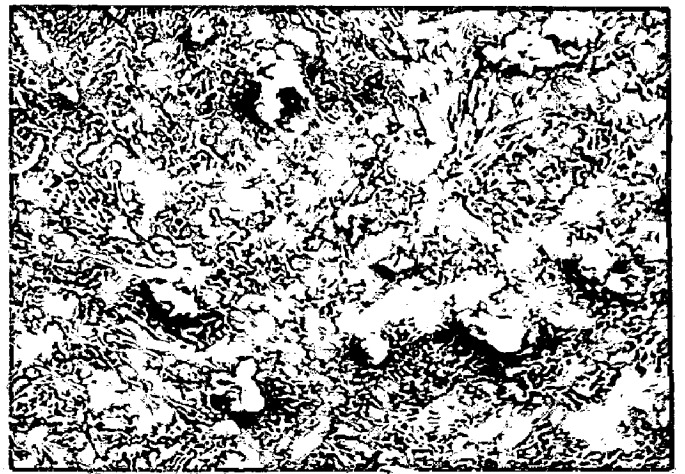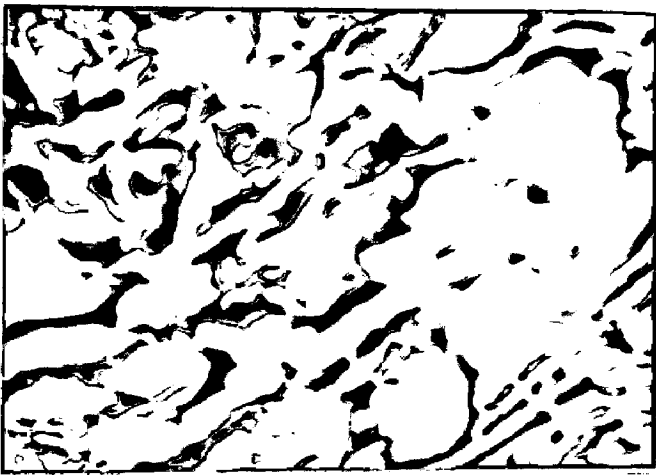
FIG. 6.3 Effect of heat treatment on deformation behaviour under compression

(a) P3 As-Cast
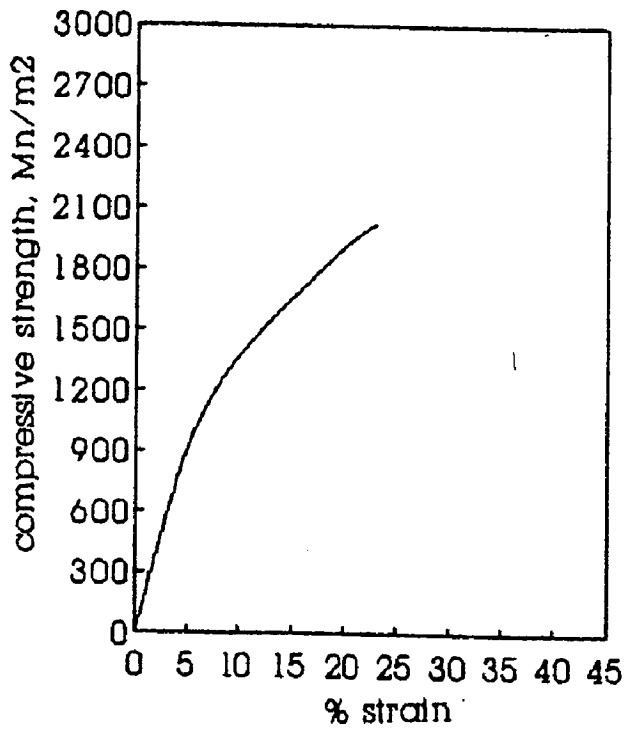
(b) P3 850,10,AC
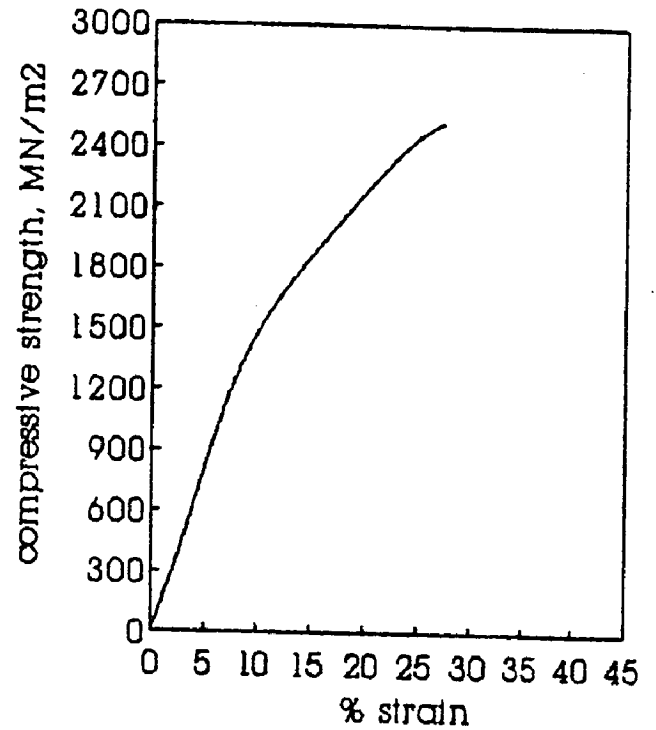
(c) P3 900,2,AC
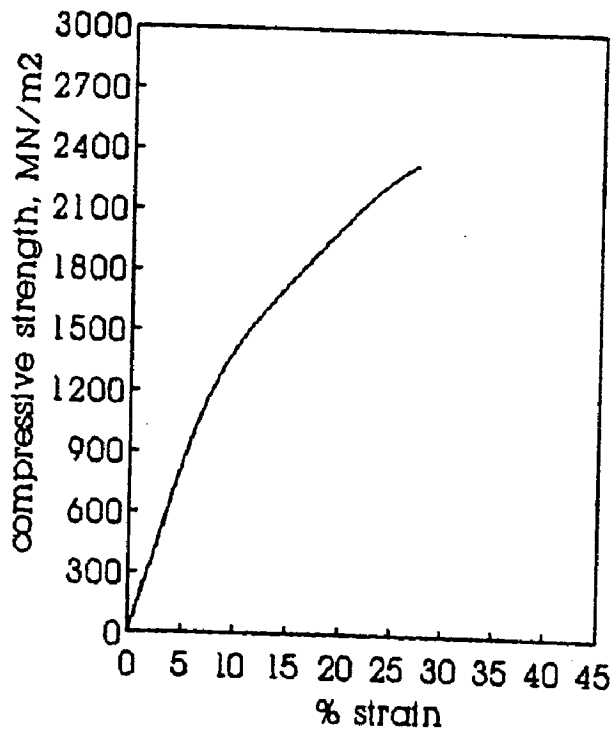
(d) P3 900,10,AC
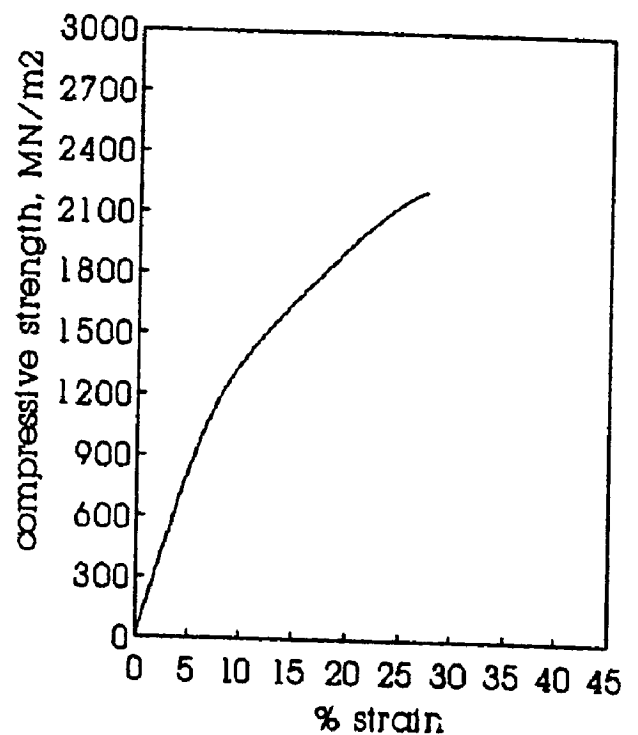
(e) P3 950,2,AC
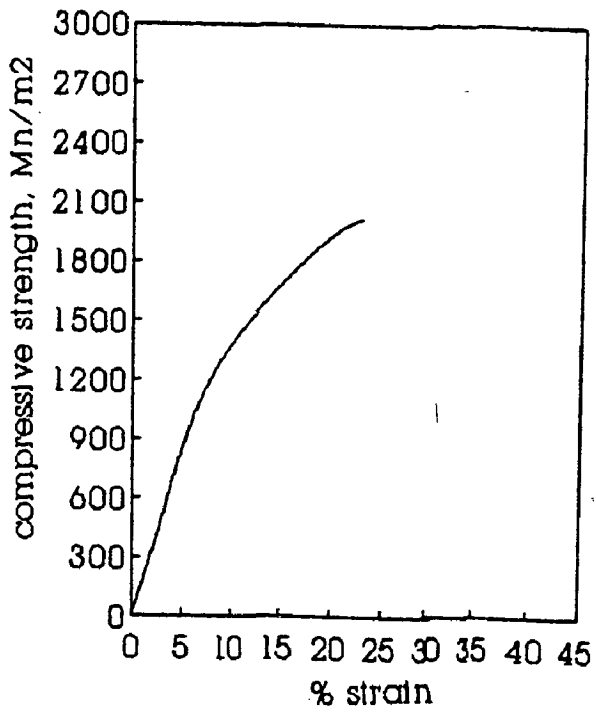
(f) P3 950,10,AC
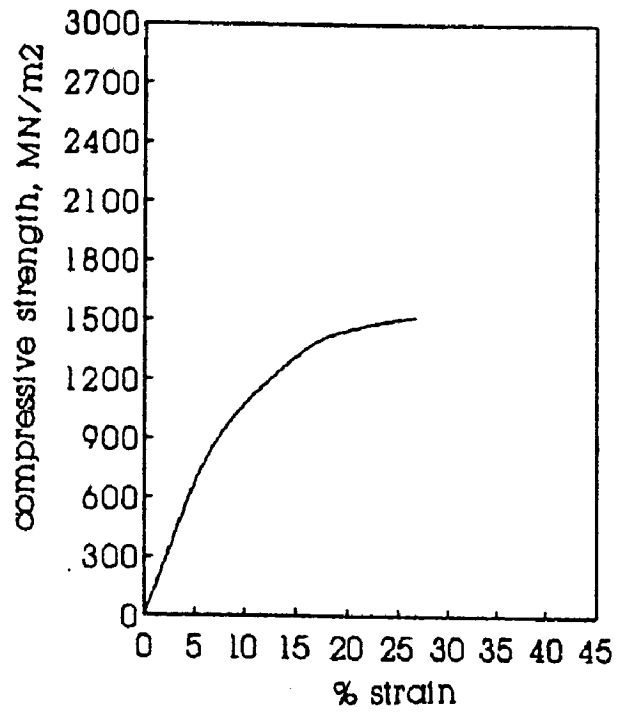
(g) P3 1000,2,AC
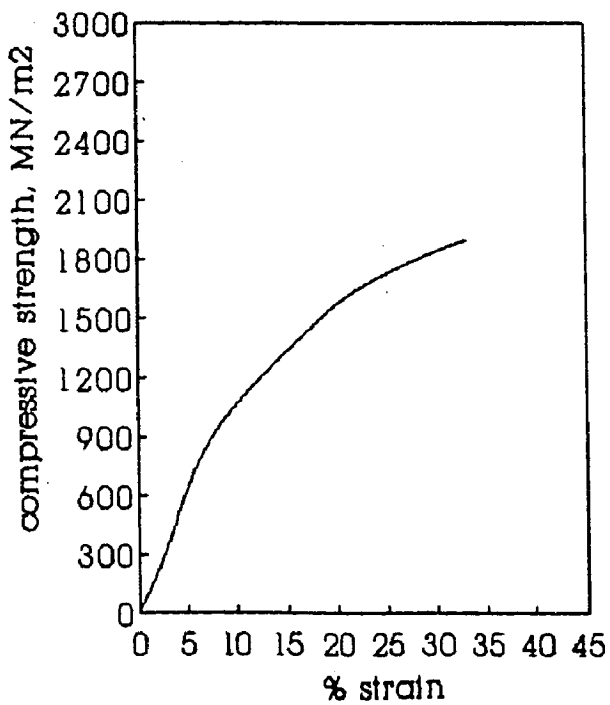
(h) P3 1050,2,AC

FIG. 6.4 Variation in C.S. with temperature as influenced by soaking period
(Alloy Pl)

(a) 2 hours

* exp   —✕— pre   ○ +15%   ✕ -15%
(of the predicted value)

(b) 10 hours

* exp   —✕— pred   ○ +15%   ✕ -15%
(of the predicted value)
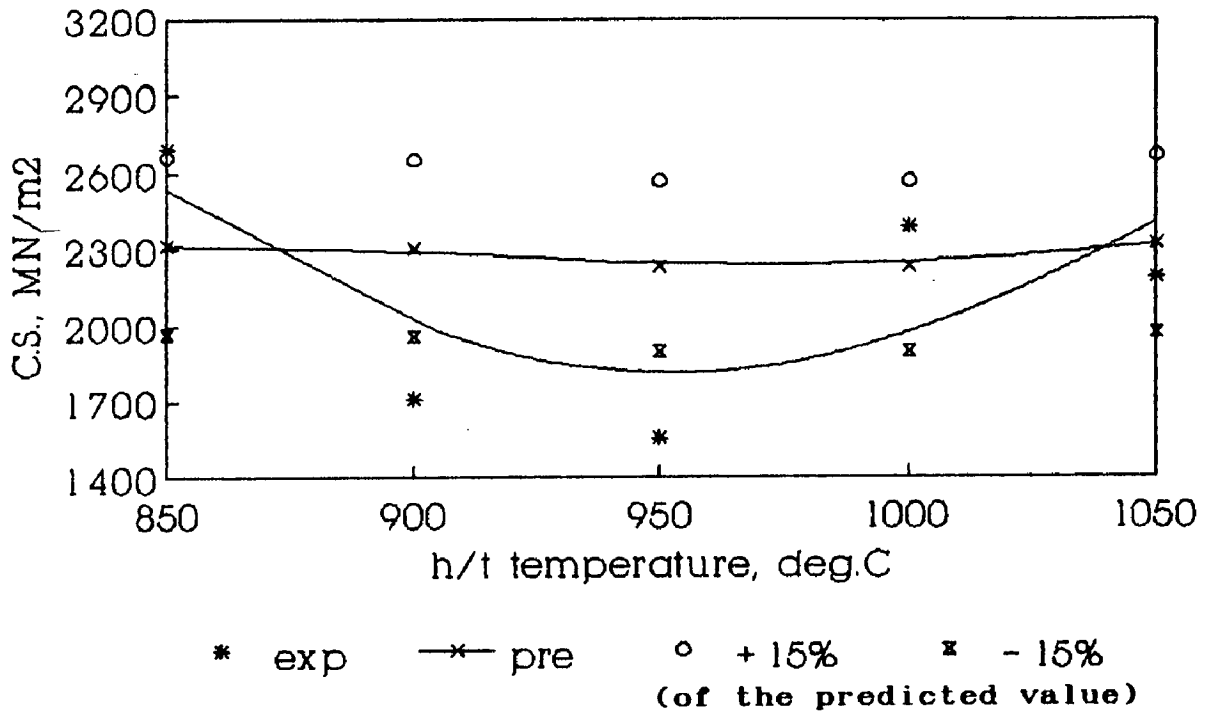
FIG. 6.5 Variation in C.S. with temperature as influenced by soaking period
(Alloy P2)

(a) 2 hours

C.S., MN/m2 vs h/t temperature, deg.C

□ exp —✻— pred ○ +15% ✕ -15%
(of the predicted value)

(b) 10 hours

C.S., MN/m2 vs h/t temperature, deg.C

□ exp —✻— pred ○ +15% ✕ -15%
(of the predicted value)
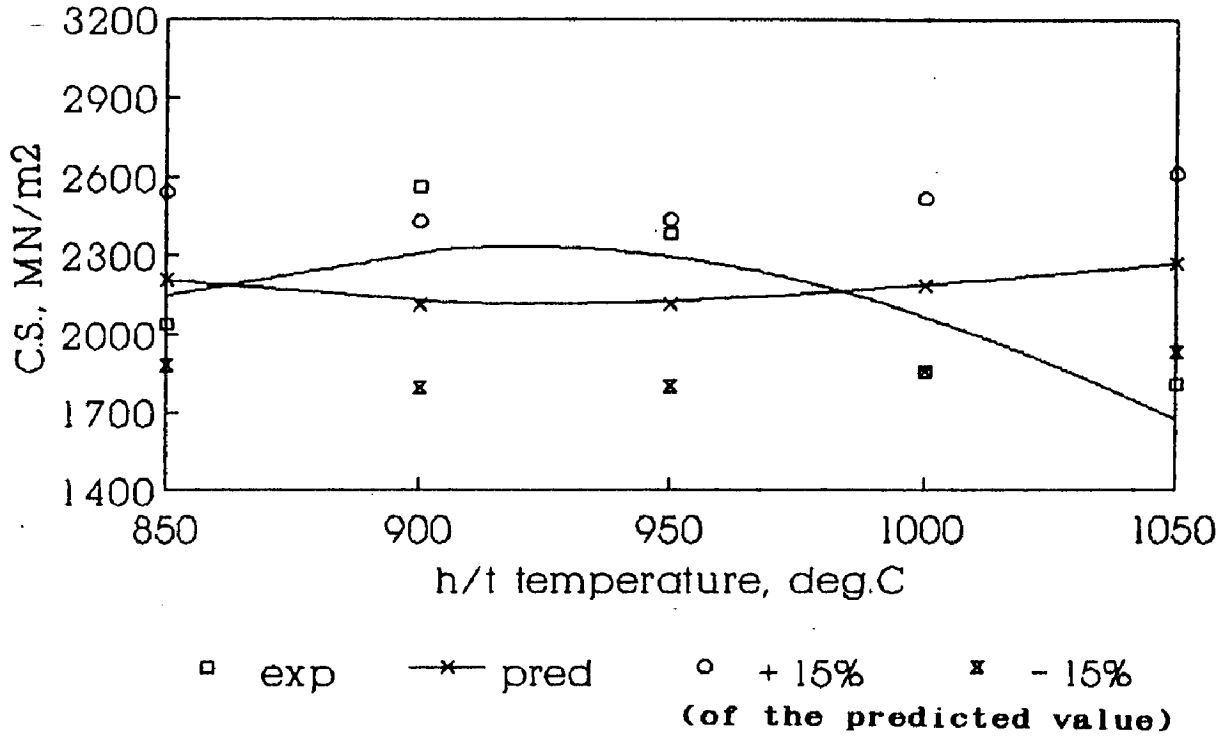
FIG. 6.6 Variation in C.S. with temperature as influenced by soaking period
(Alloy P3)

(a) 2 hours

◊ exp   —✕— pred   ○ + 15%   ✕ - 15%
(of the predicted value)

(b) 10 hours

◊ exp   —✕— pred   ○ + 15%   ✕ - 15%
(of the predicted value)
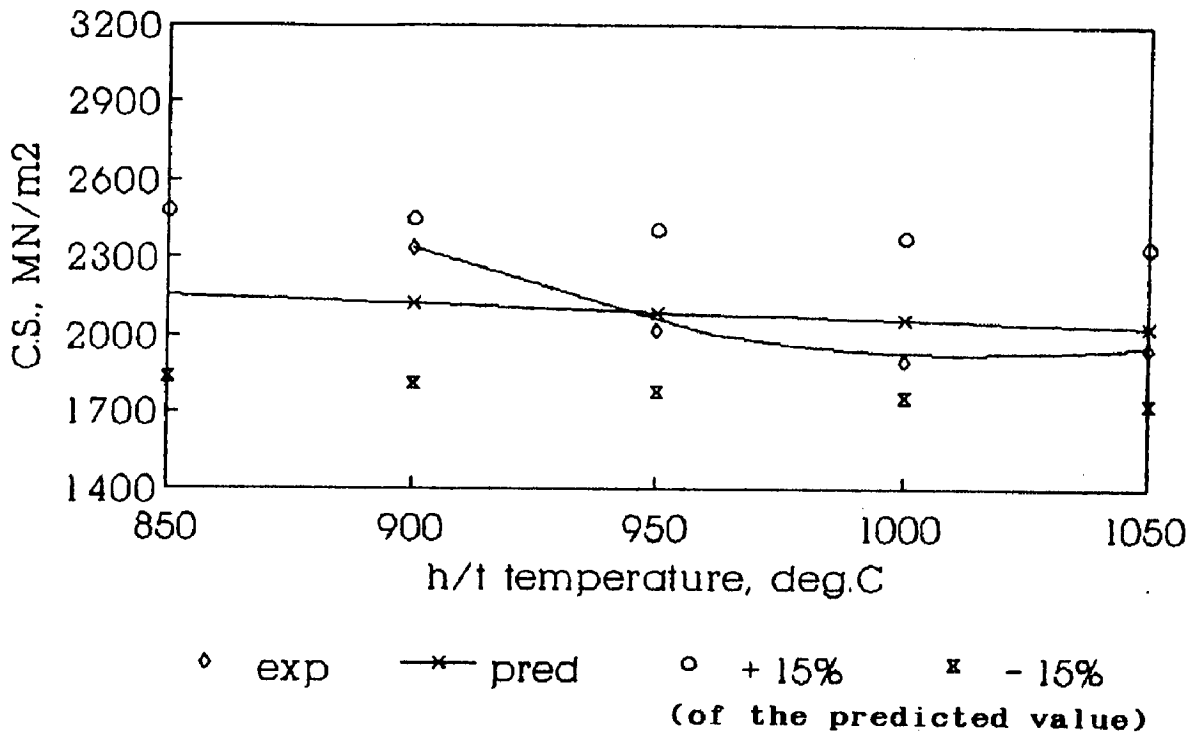
FIG. 6.7 Tafel plots of Alloy Pl

(a) Pl,1000,2

(b) P1,1050,10

FIG. 6.8 Tafel plots of Alloy P2

(a) P2,900,2

(b) P2,1050,10

F-89
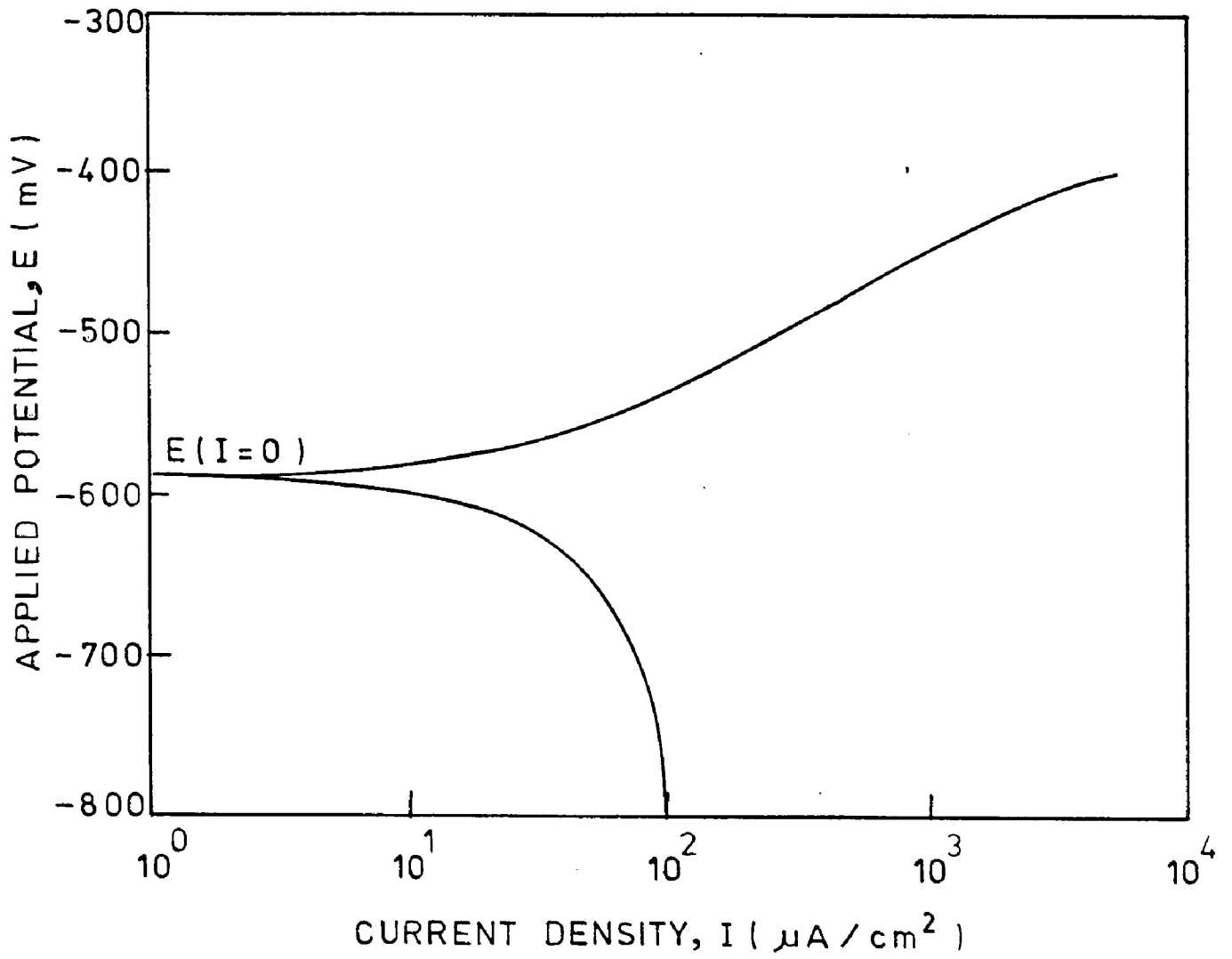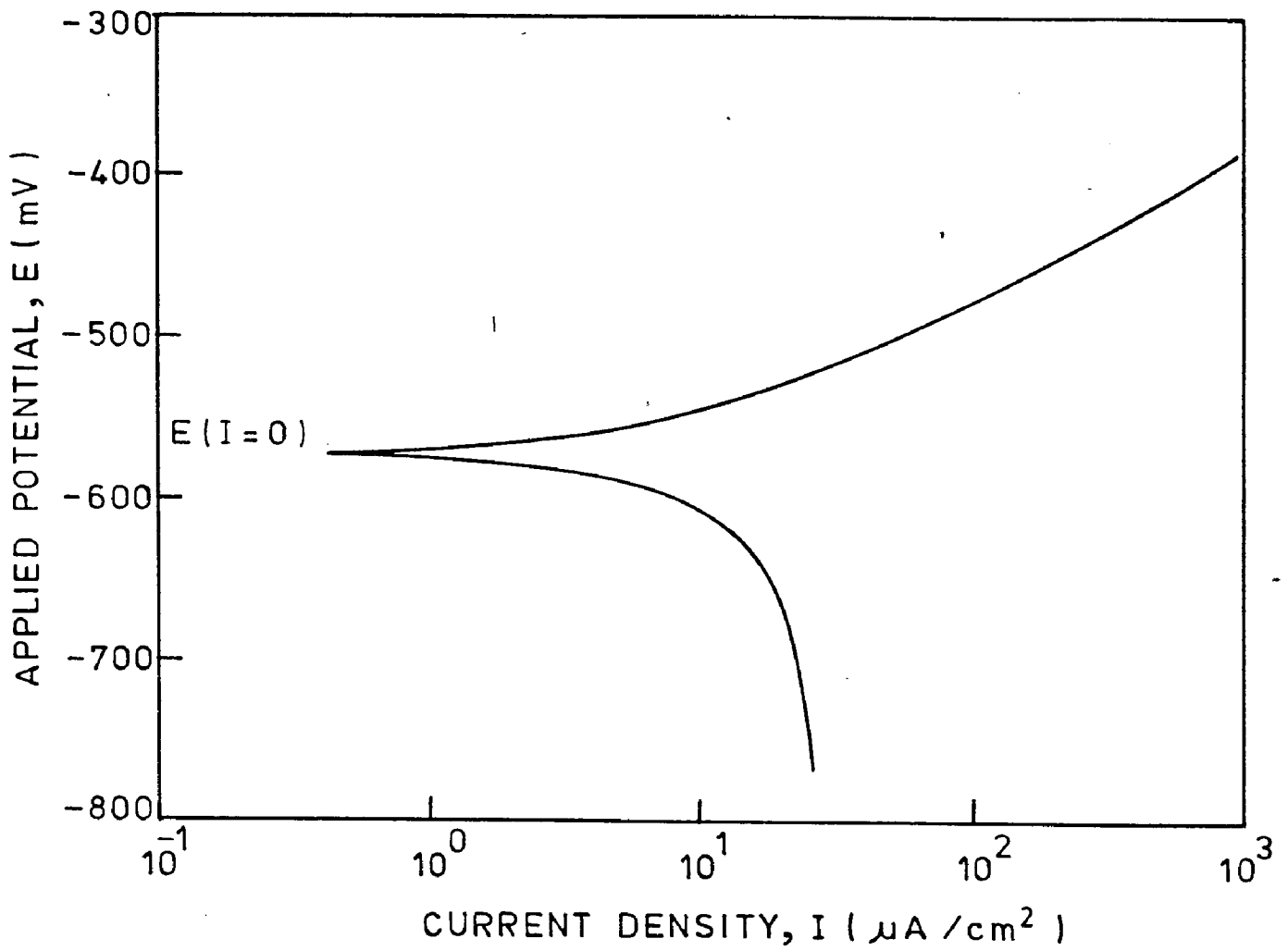
FIG. 6.9 Tafel plots of Alloy P3

(a) P3,900,10

(b) P3,1000,10

F-91
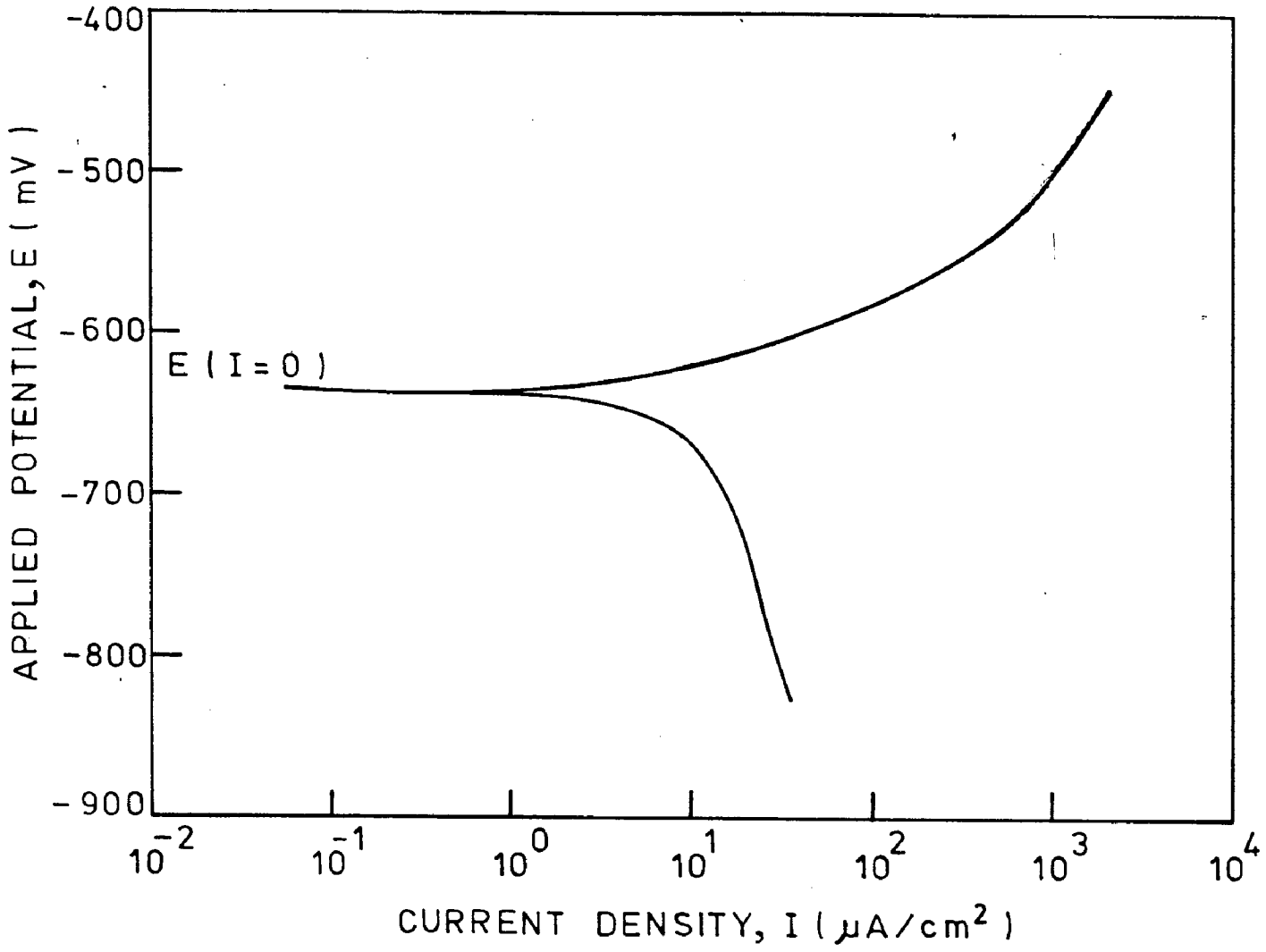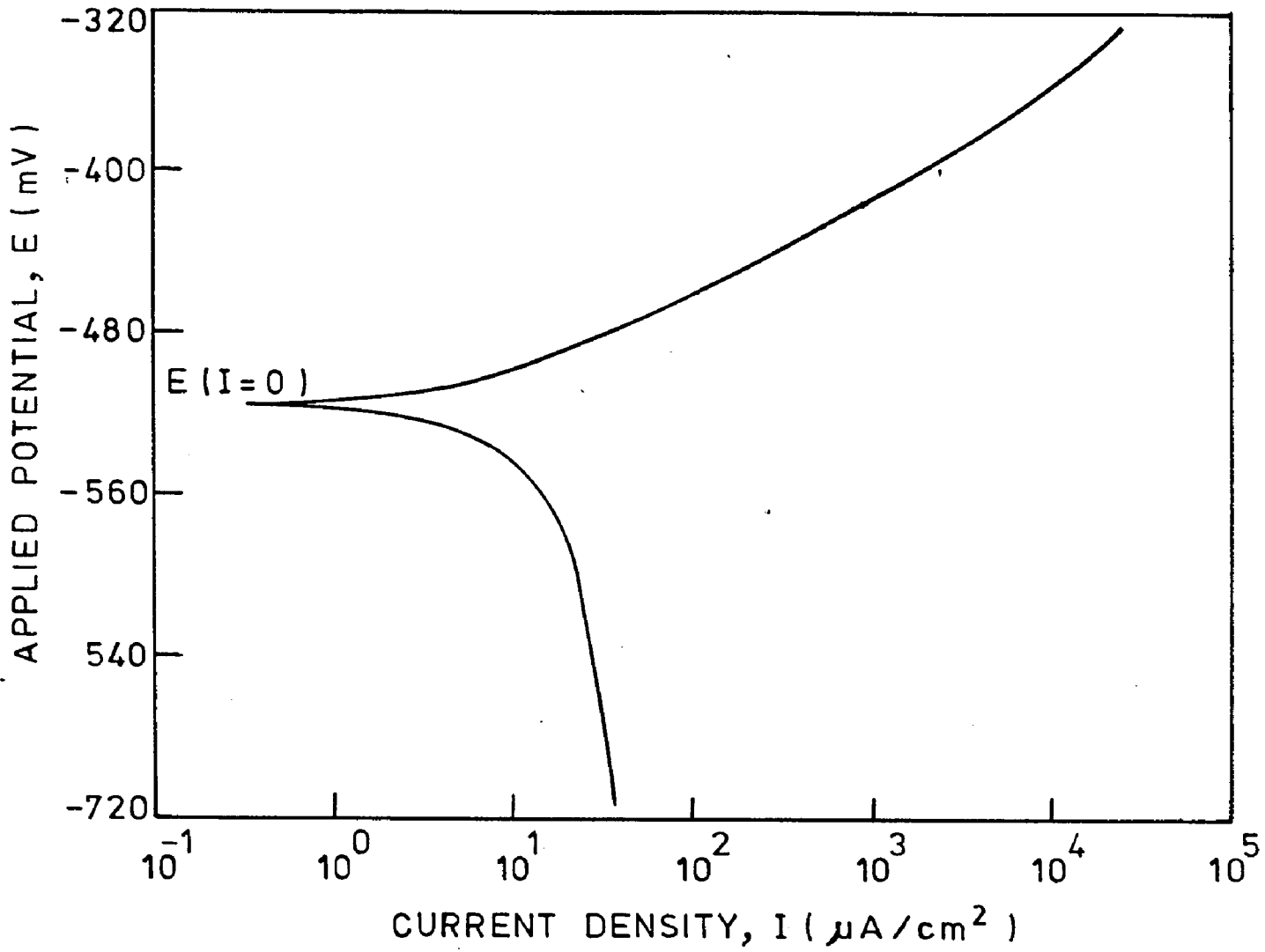
FIG. 6.10 Effect of heat treatment on corrosion behaviour (Alloy PI)

(a) 2 hours
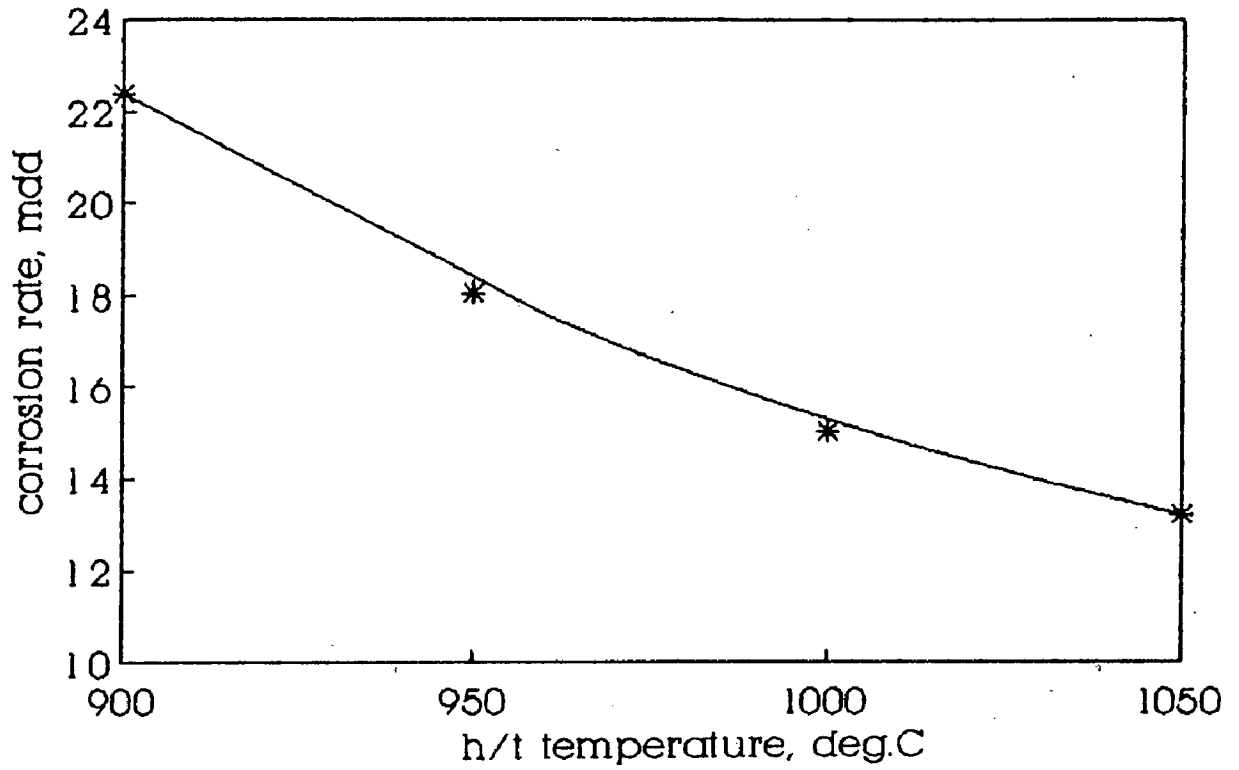
(b) 10 hours
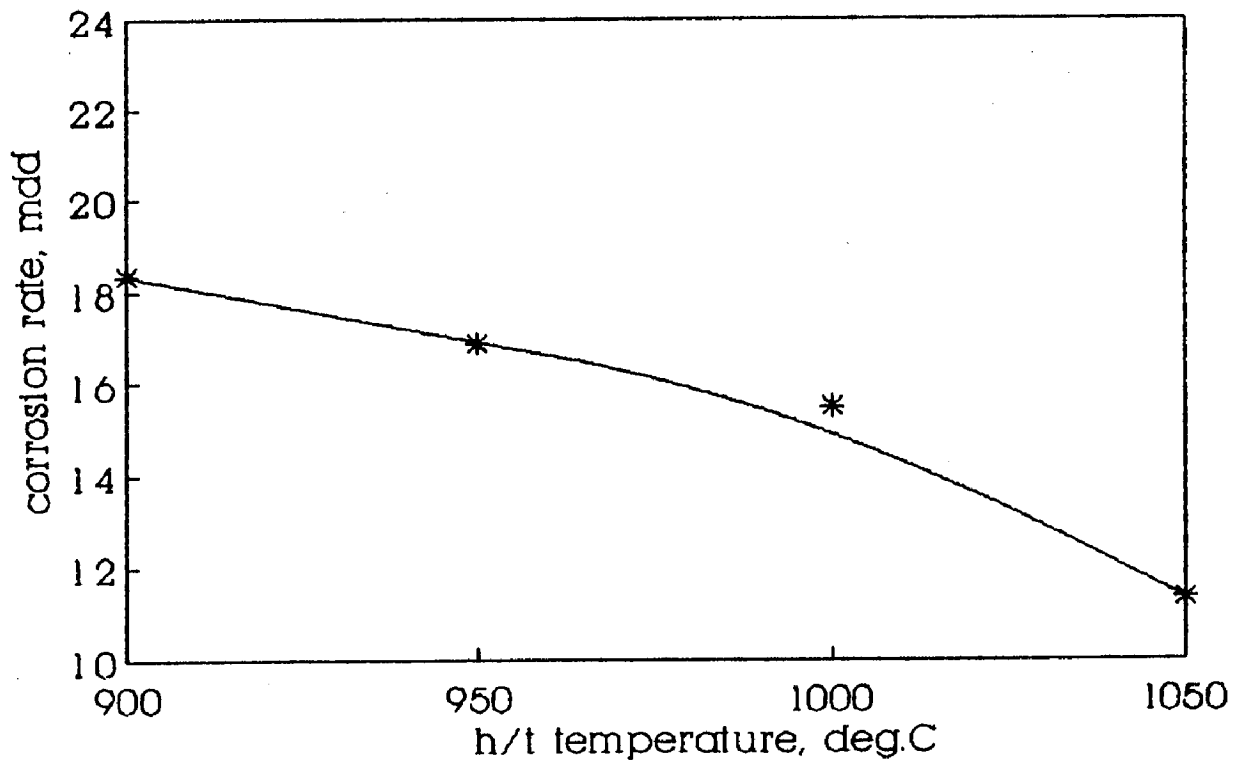
FIG. 6.11 Effect of heat treatment on corrosion behaviour (Alloy P2)

(a) 2 hours
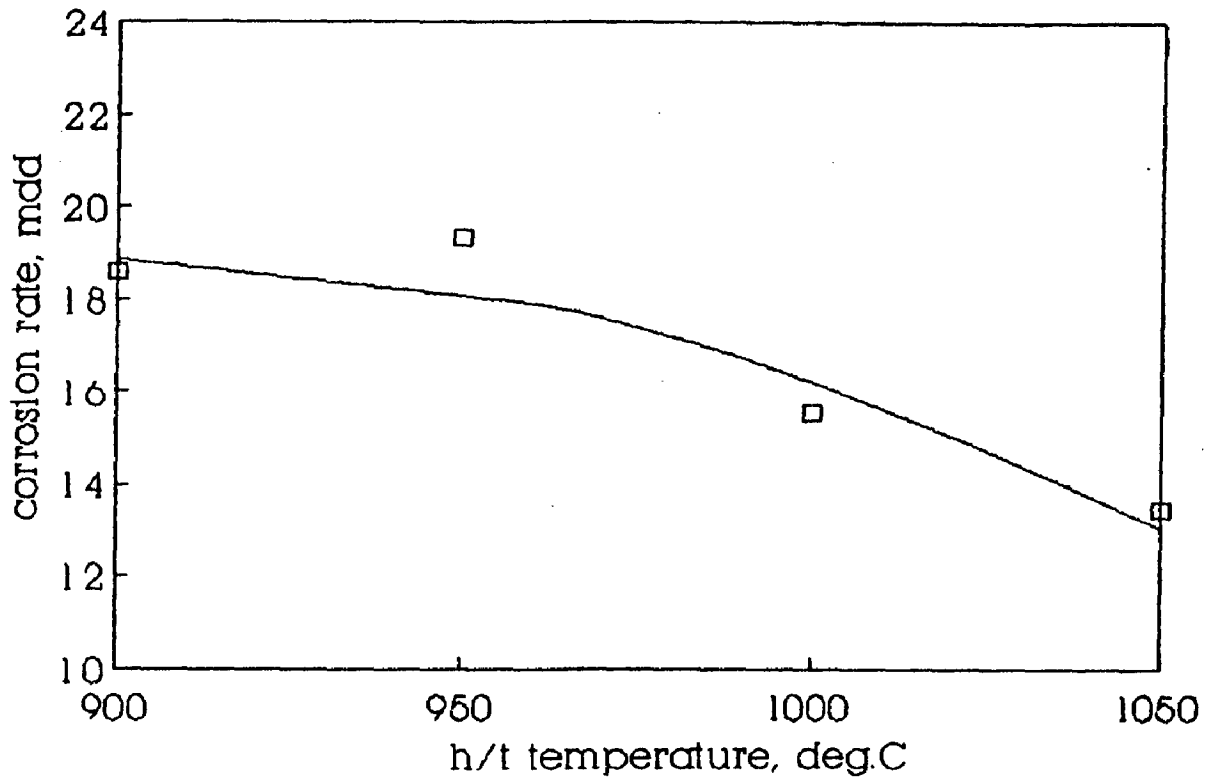
(b) 10 hours
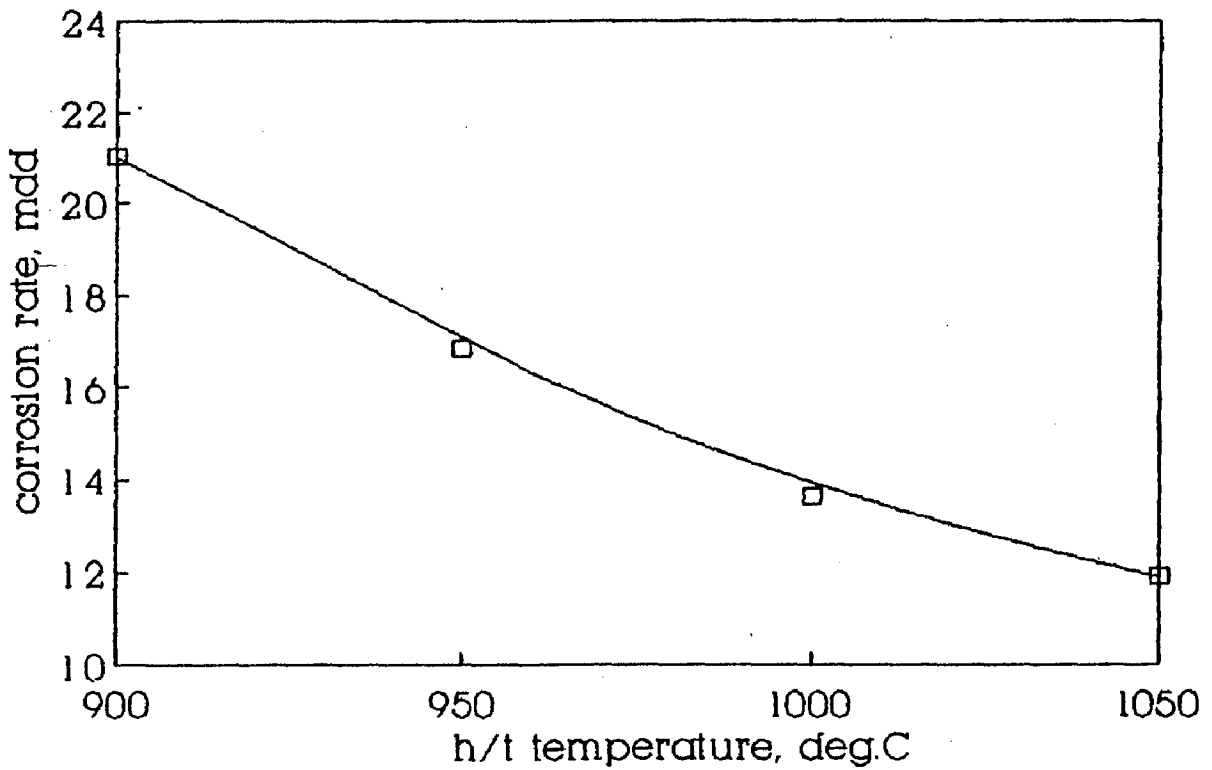
FIG. 6.12 Effect of heat treatment on corrosion behaviour (Alloy P3)

(a) 2 hours
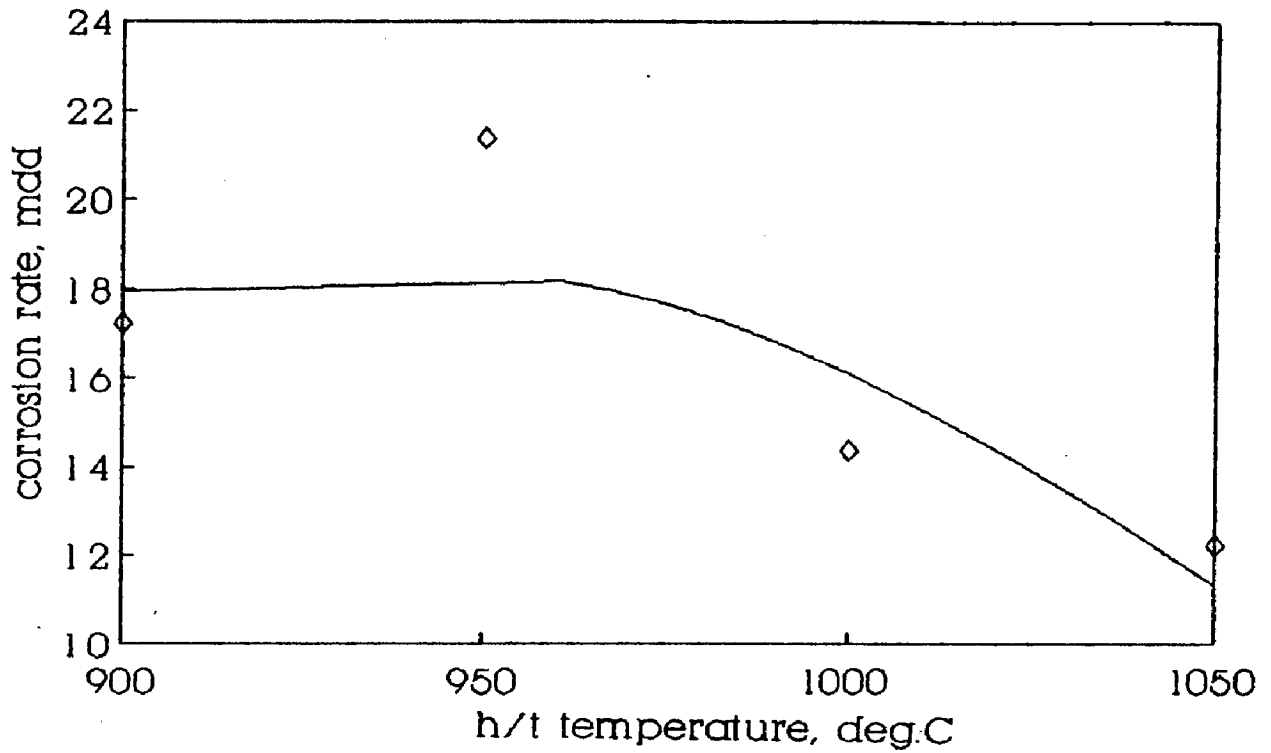
(b) 10 hours
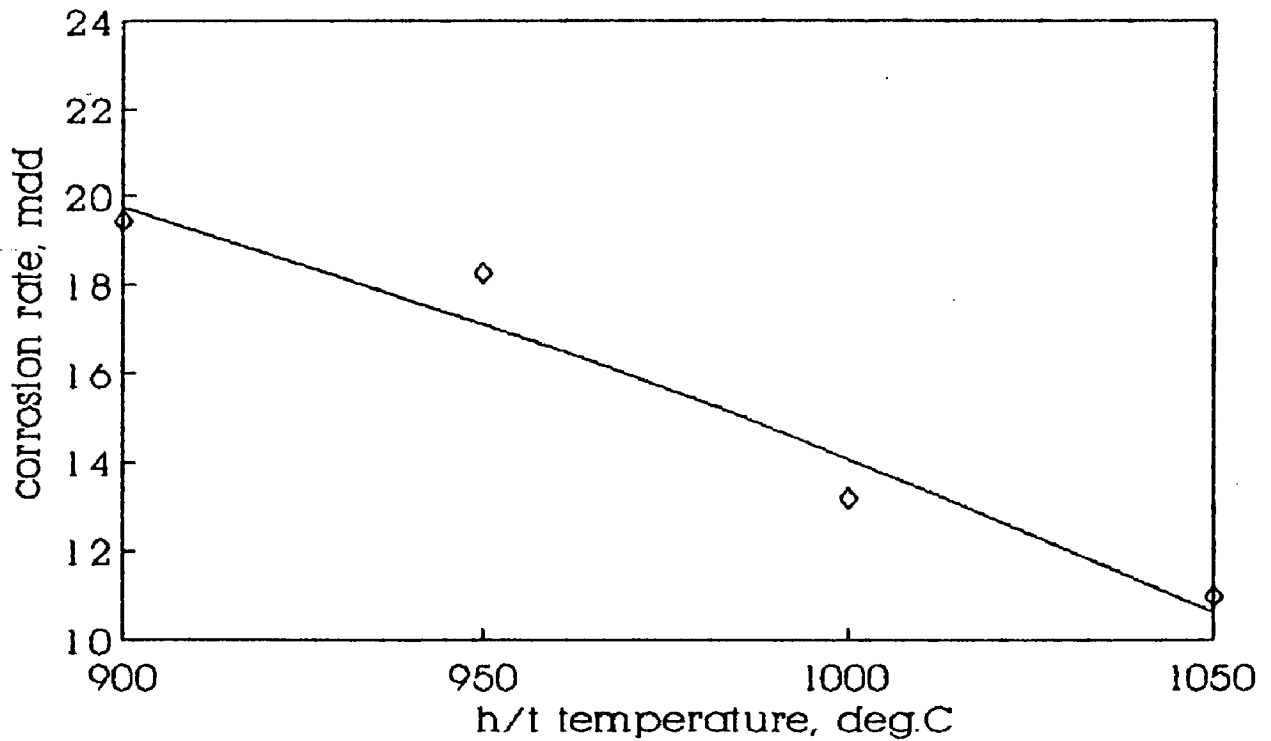
FIG. 6.13 SEM photographs of the corroded samples (Alloy P1)

(a) P1,As-cast

   X (1250 x 1.0)

(b) P1,As-cast

   X (160 x 1.0)

(c) P1,900,2

   X (640 x 1.0)

(d) P1,1000,2

   X (640 x 1.0)

(e) P1,1050,2

   X (1250 x 1.0)

(f) P1,1050,2

   X (160 x 1.0)

(g) P1,1050,10

   X (640 x 1.0)

(h) P1,1050,10

   X (160 x 1.0)

(e) P2 1000,2,AC
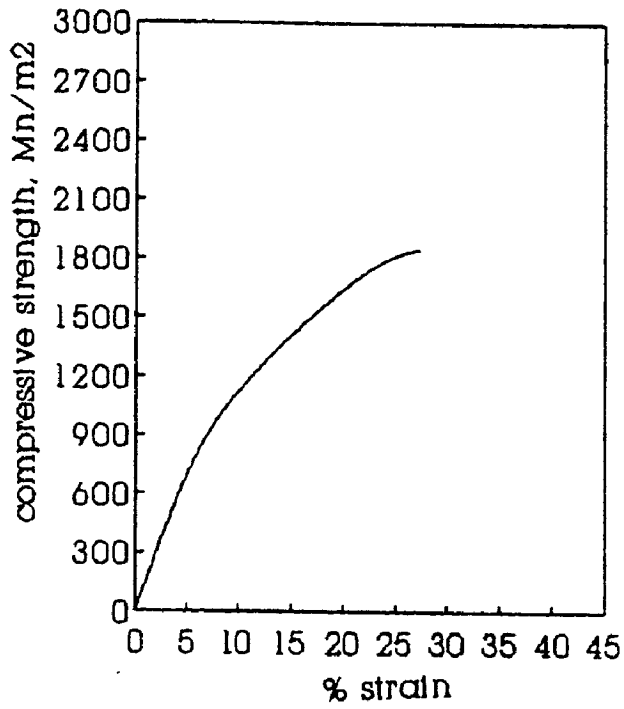
(f) P2 1000,10,AC
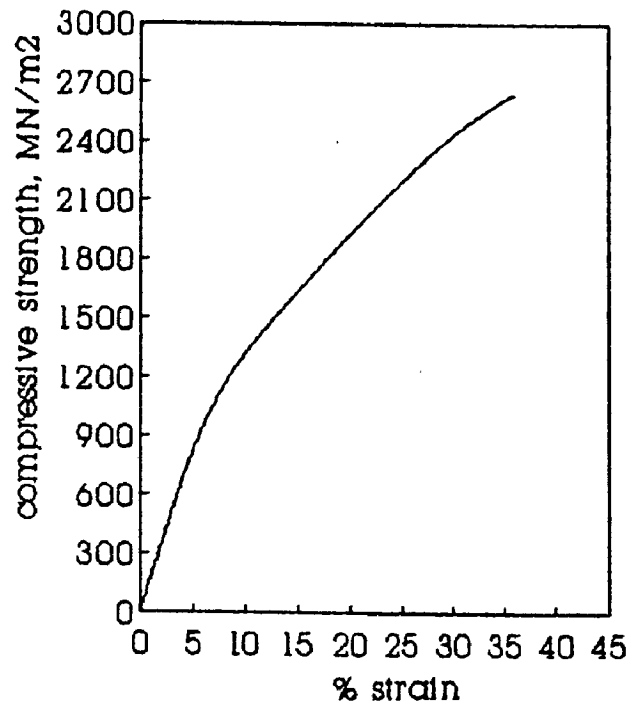
(g) P2 1050,2,AC

(h) P2 1050,10,AC

F-80
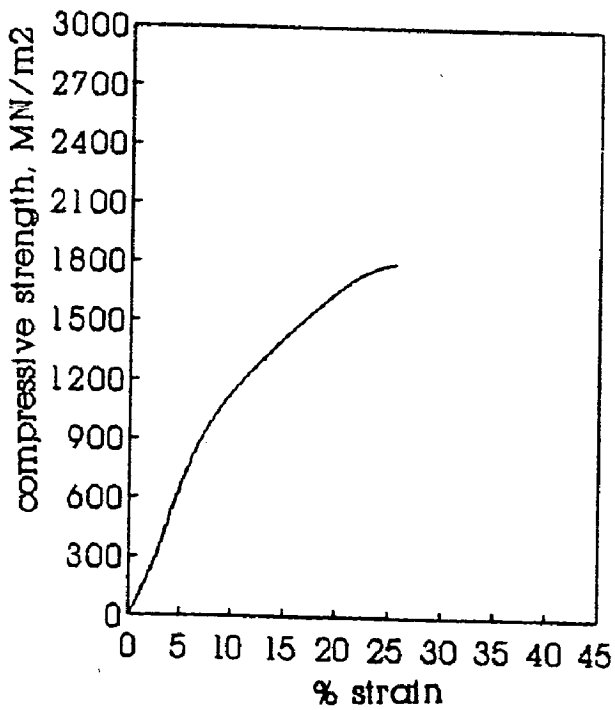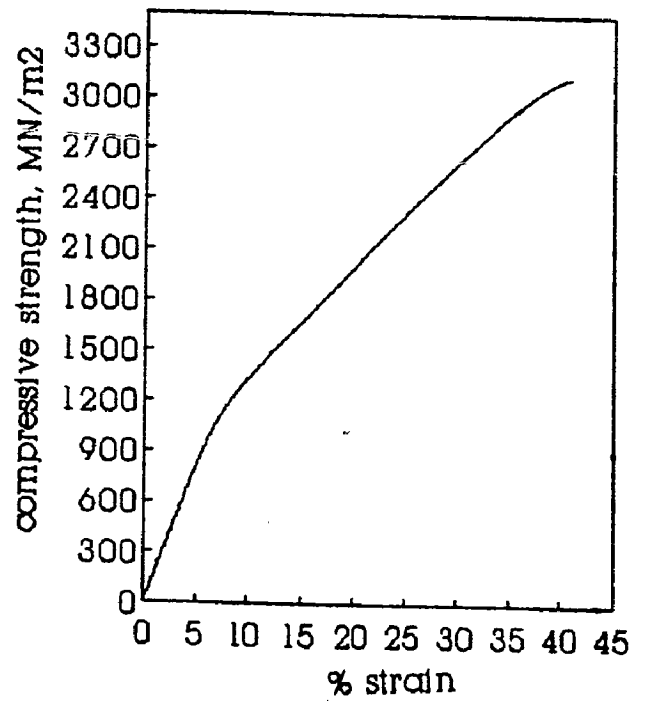
FIG. 6.2 Effect of heat treatment on deformation behaviour under compression (Alloy P2)

(a) P2 As-Cast
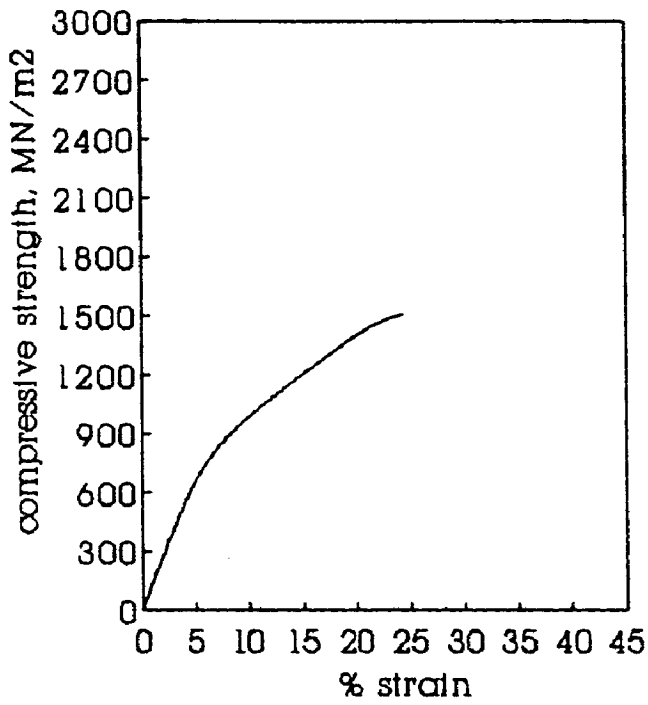
(b) P2 850,2,AC
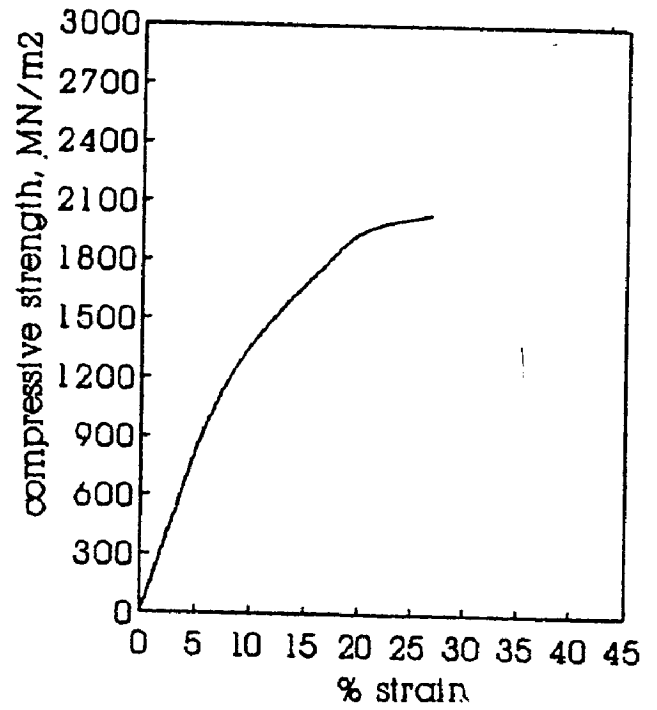
(c) P2,900,2,AC

(d) P2,950,2,AC

(e) Pl 950,2,AC

(f) Pl 1000,10,AC

(g) Pl 1050,2,AC
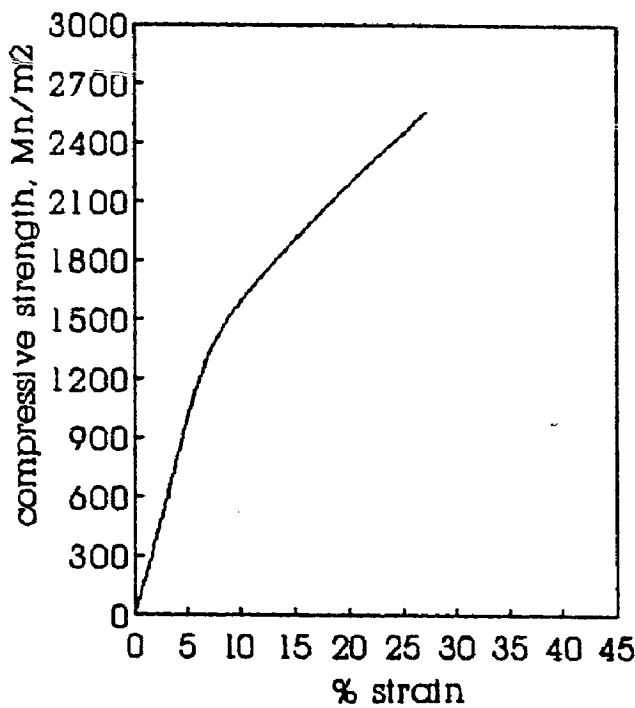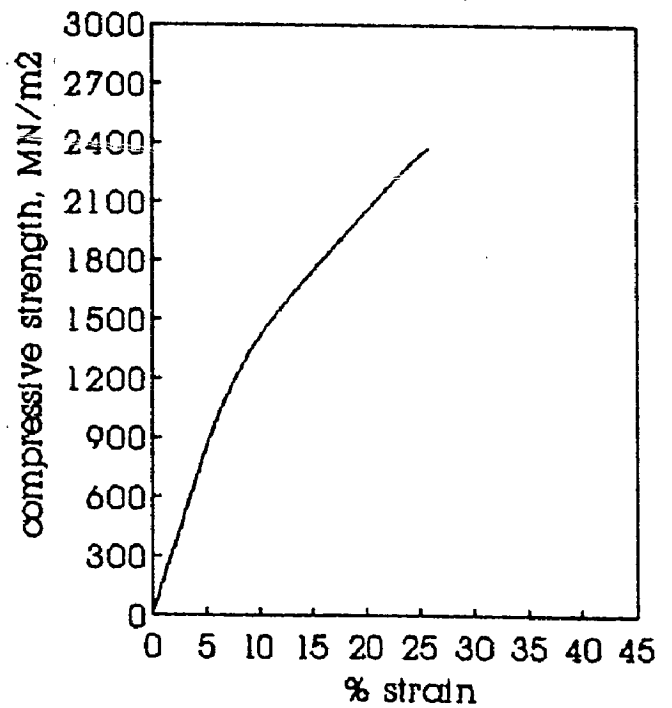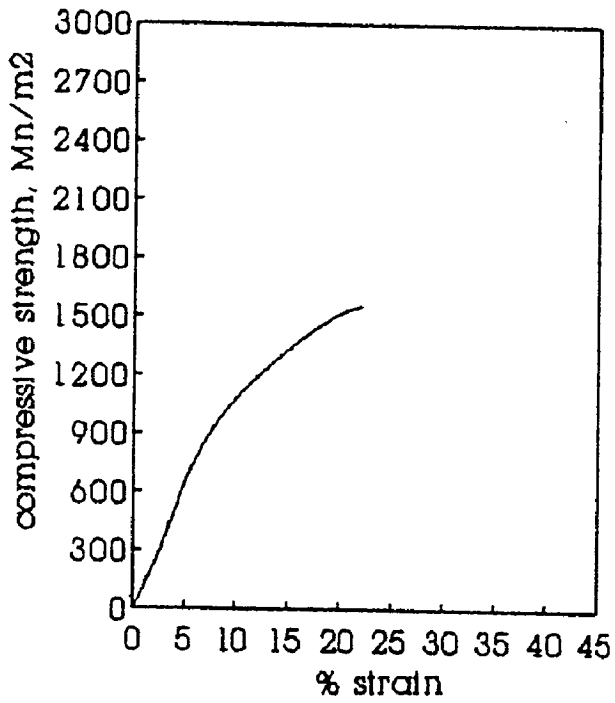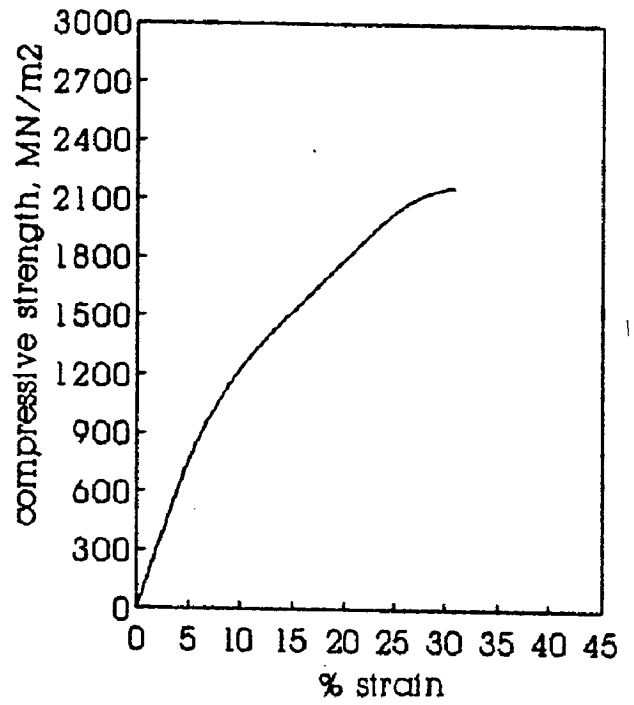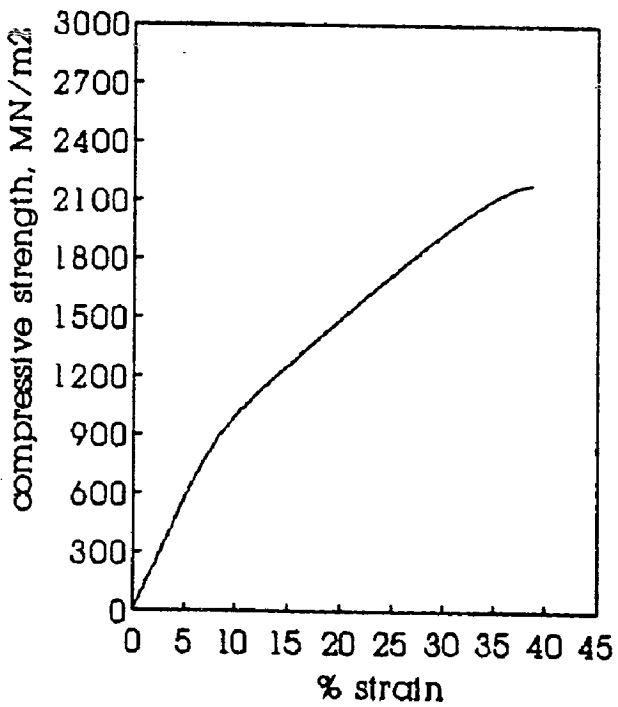
(h) Pl 1050,10,AC
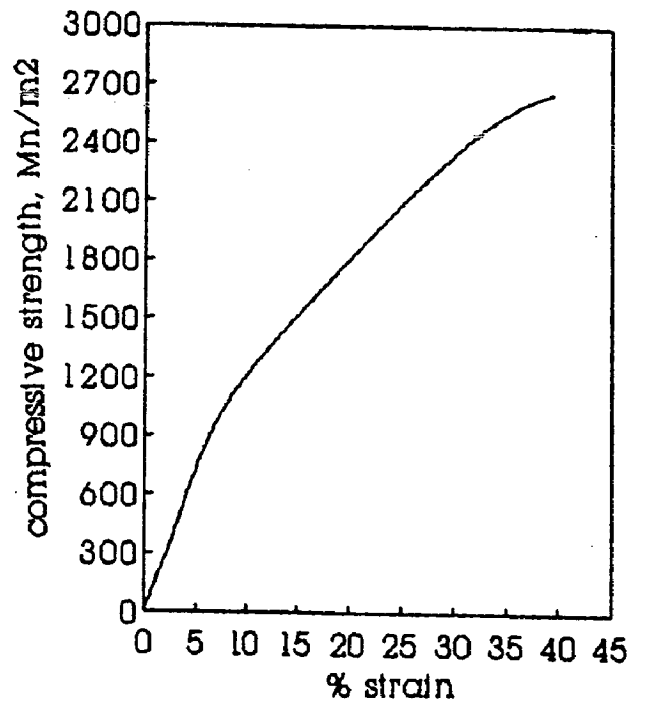
FIG. 6.1 Effect of heat treatment on deformation behaviour under compression (Alloy P1)

(a) P1 As-Cast

(b) P1 850,10,AC

(c) P1 900,2,AC
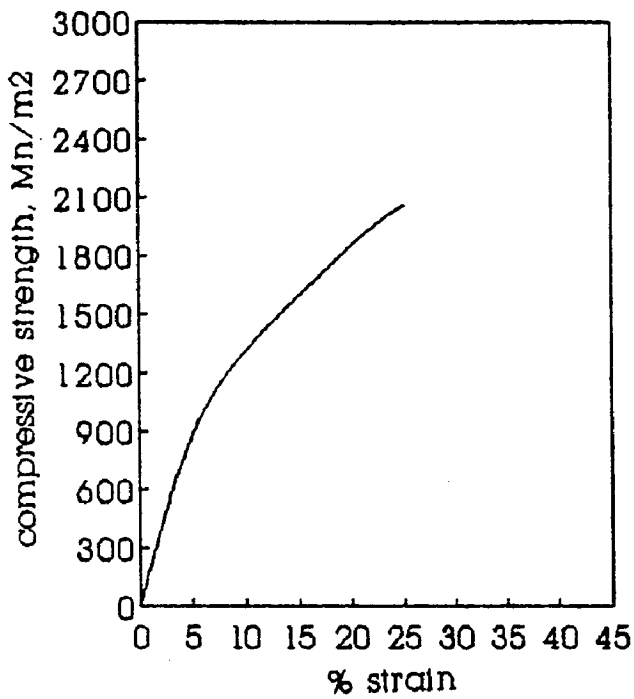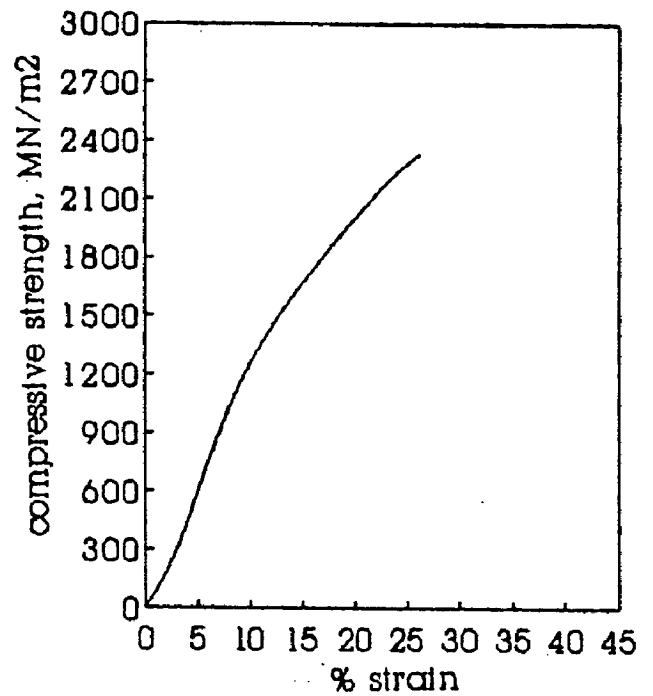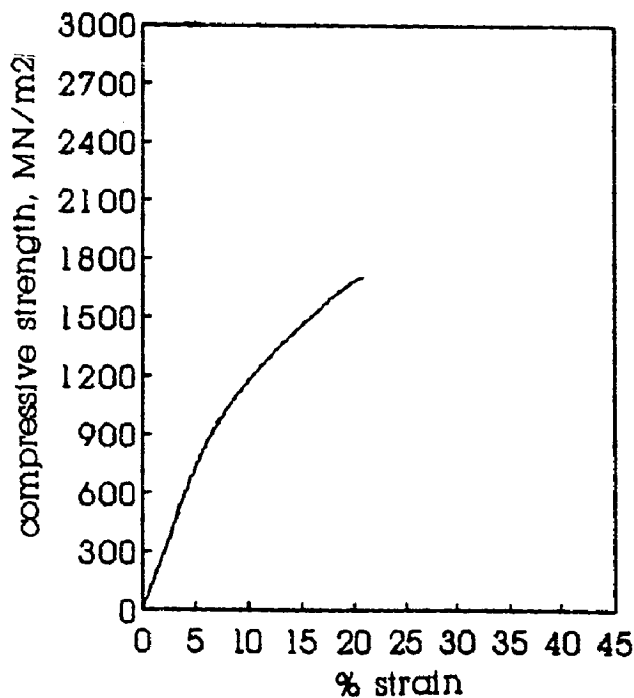
(d) P1 900,10,AC
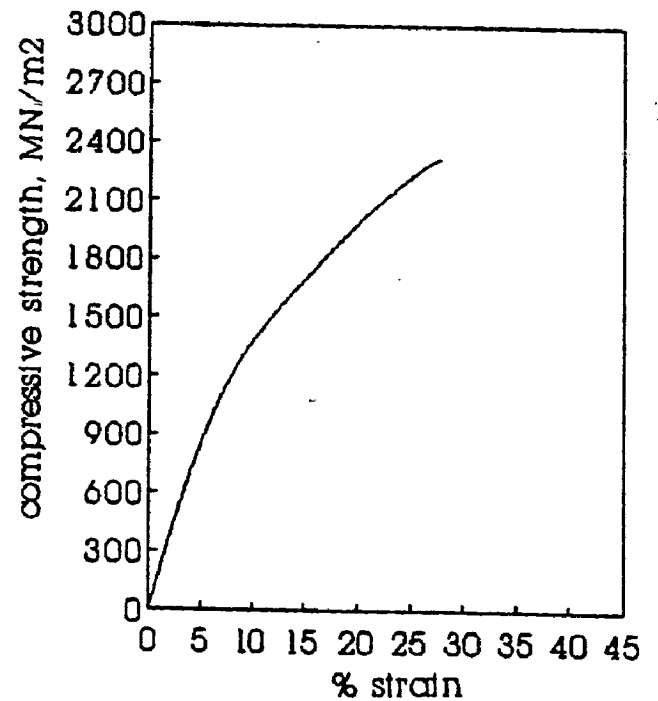
FIG. 5.6 Experimental vs predicted %TG plots of experimental alloys
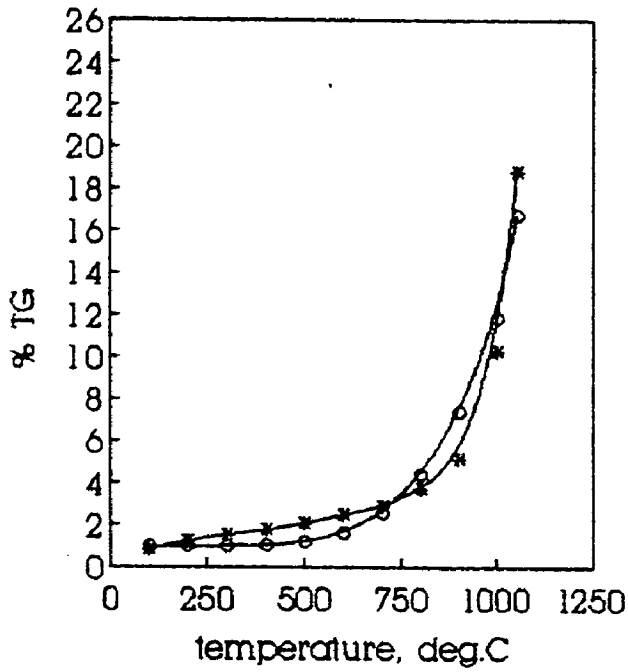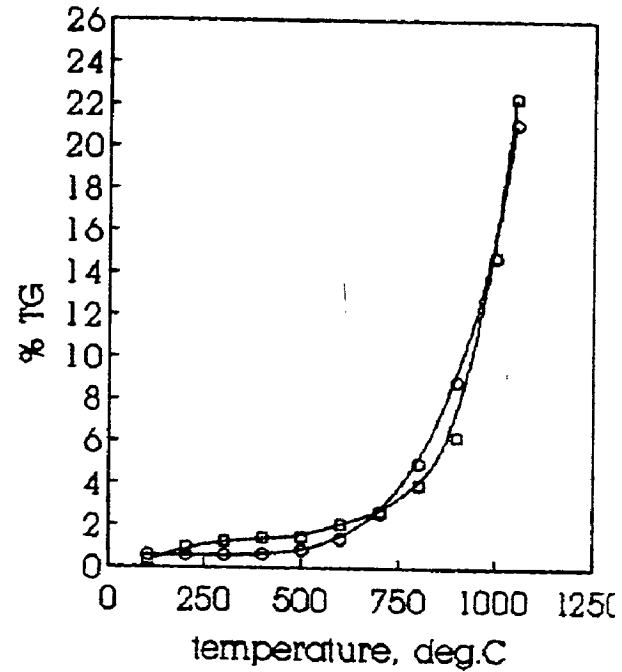
(a) Alloy P1
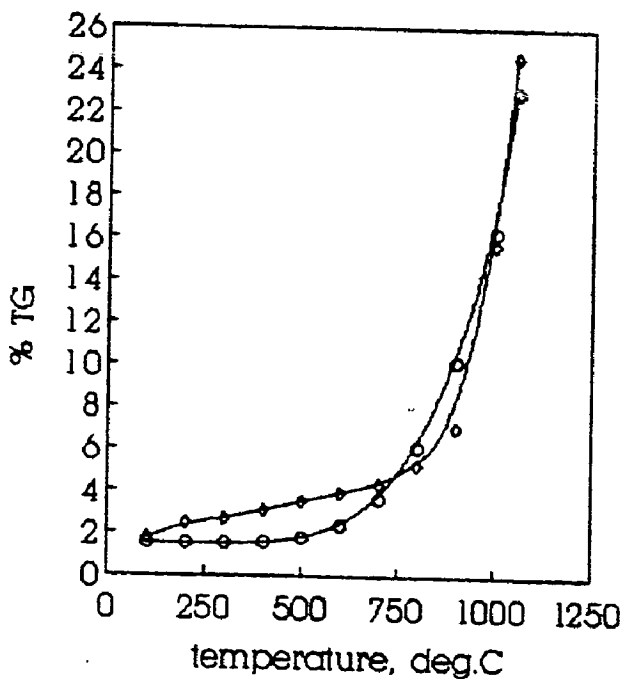
(b) Alloy P2

(c) Alloy P3

*   experimental

□   experimental

◇   experimental

○   predicted

FIG. 5.5 A summary plot of differential thermal analysis
of experimental alloys
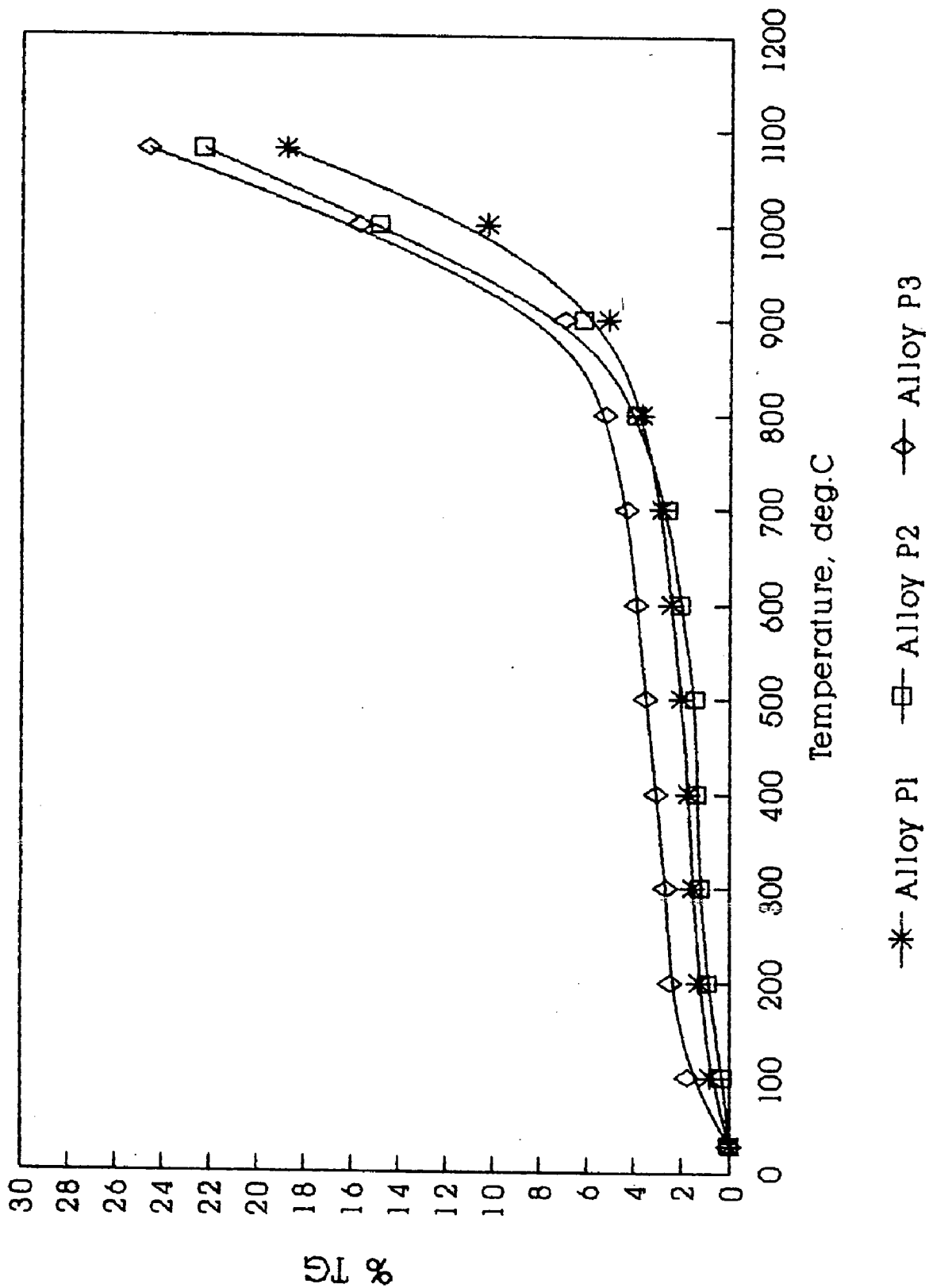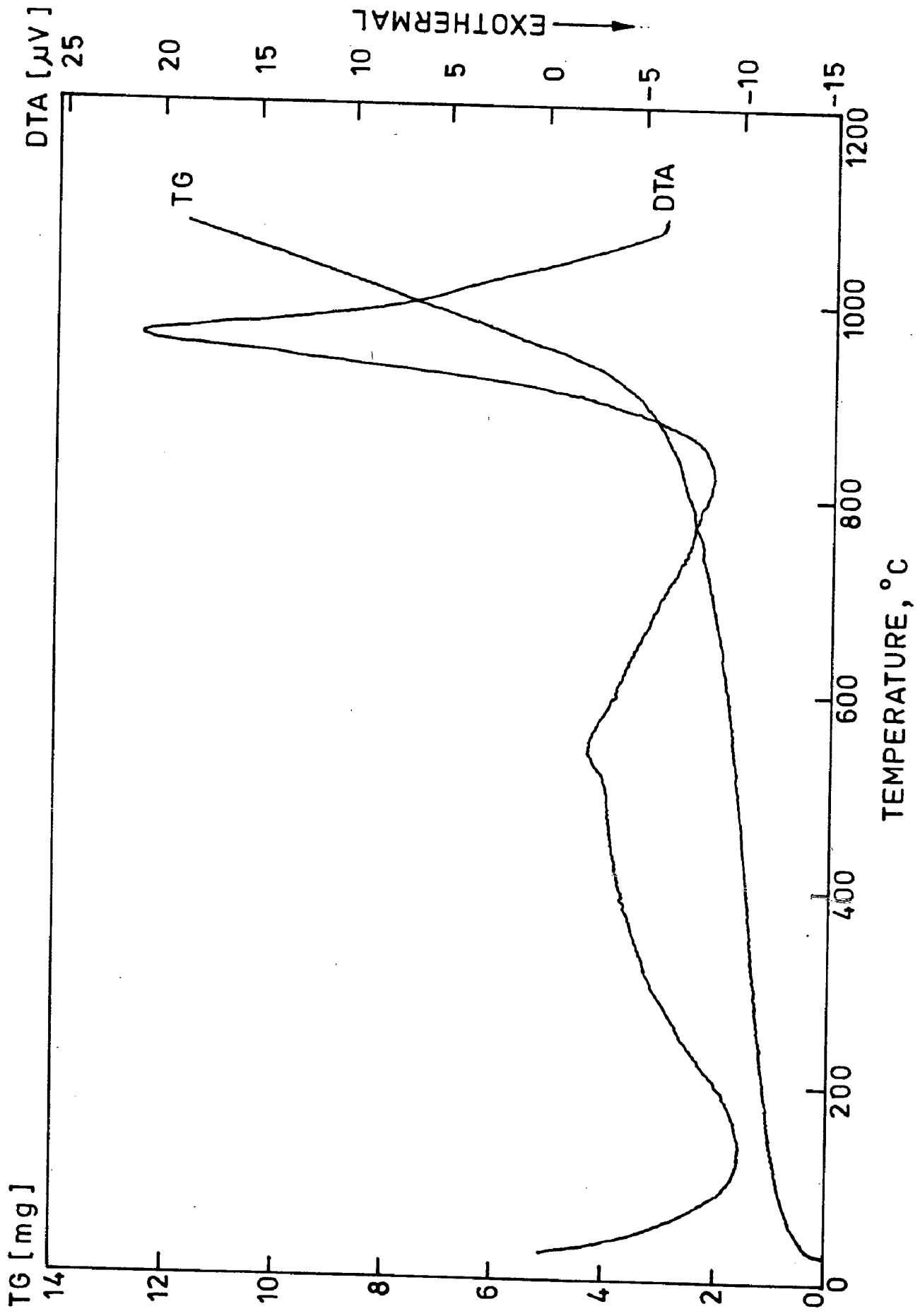
Fig. 5.4 Differential thermal analysis plot of alloy P3.
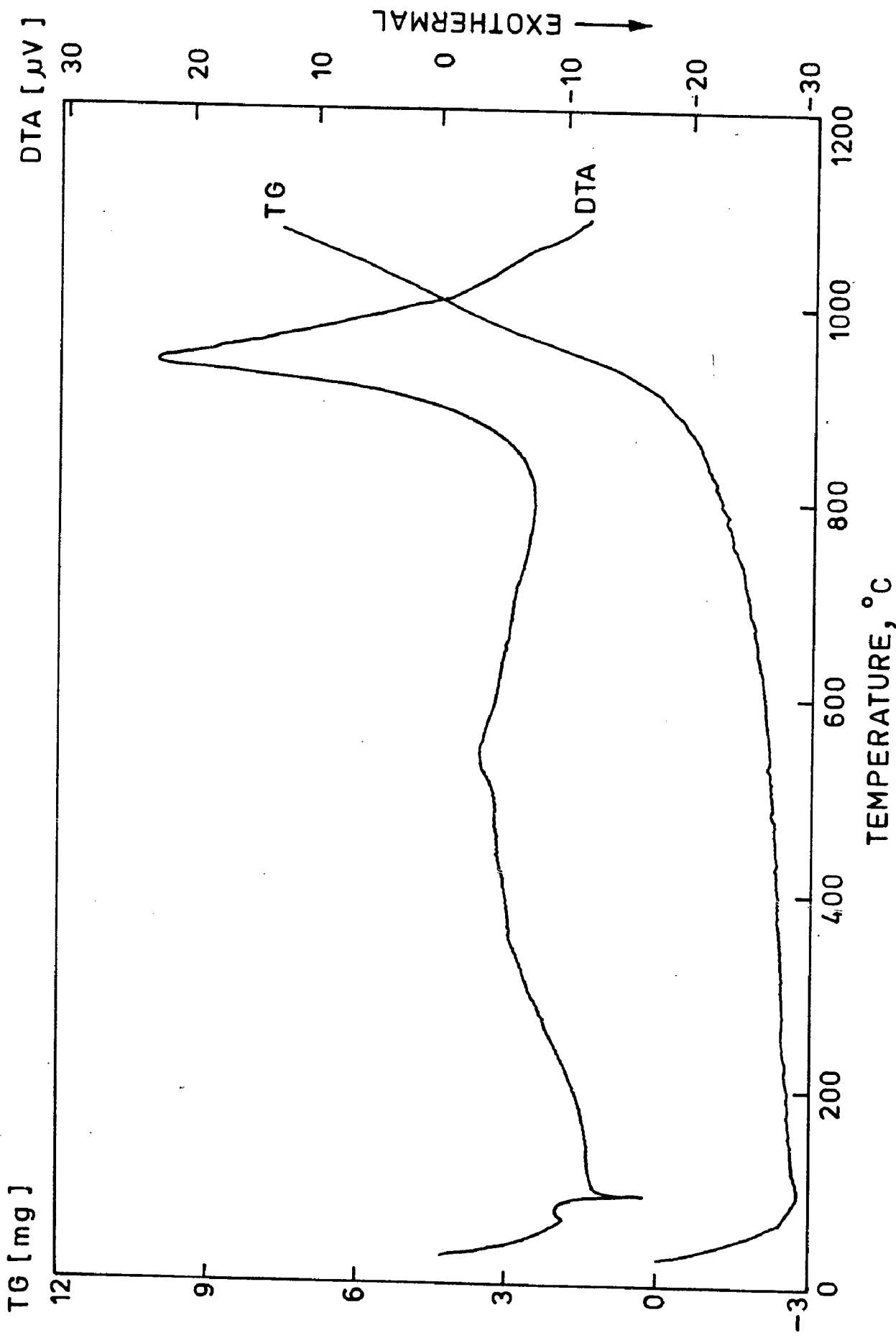
Fig.5.3 Differential thermal analysis plot of alloy P2.
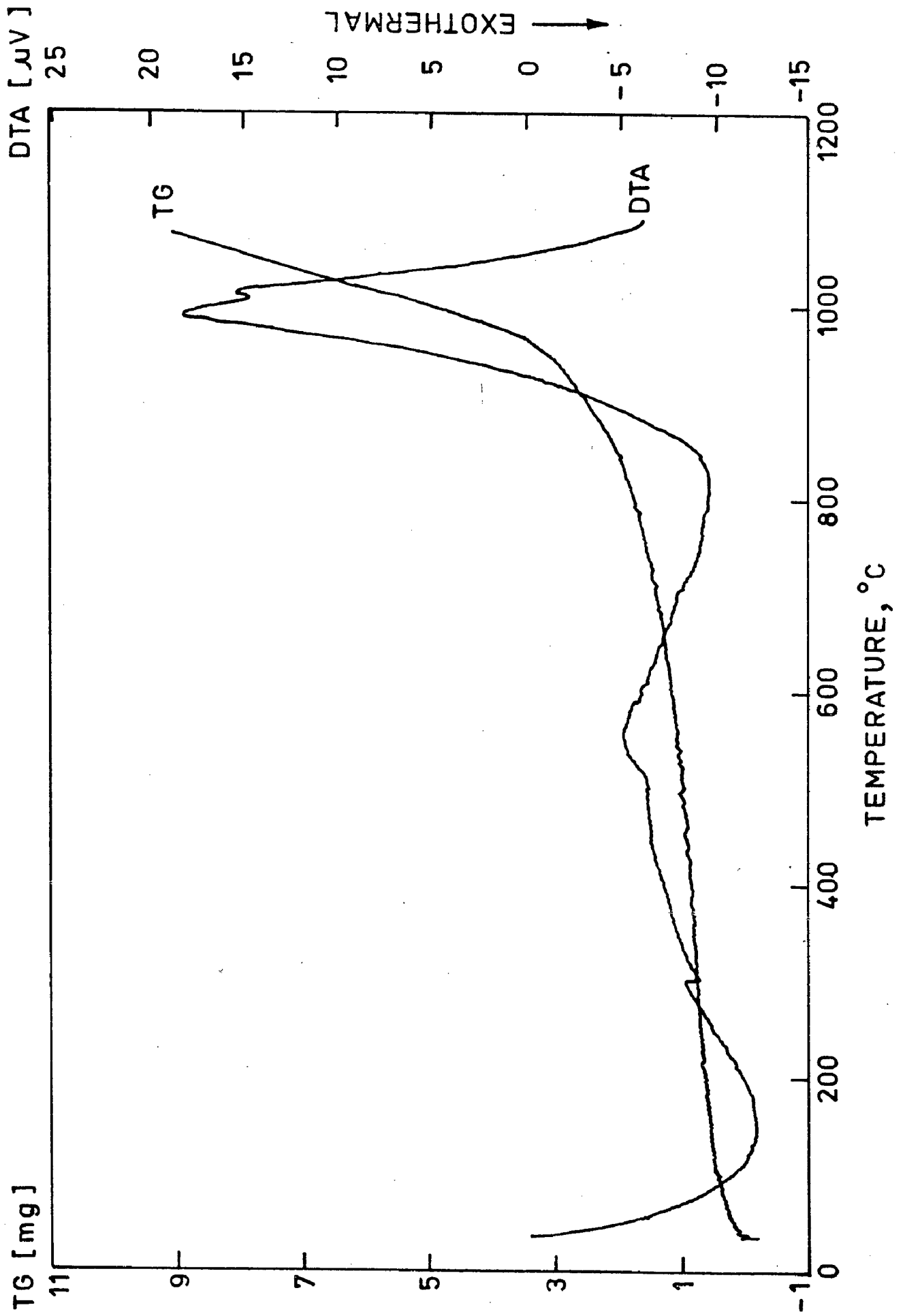
Fig.5.2 Differential thermal analysis plot of alloy P1.
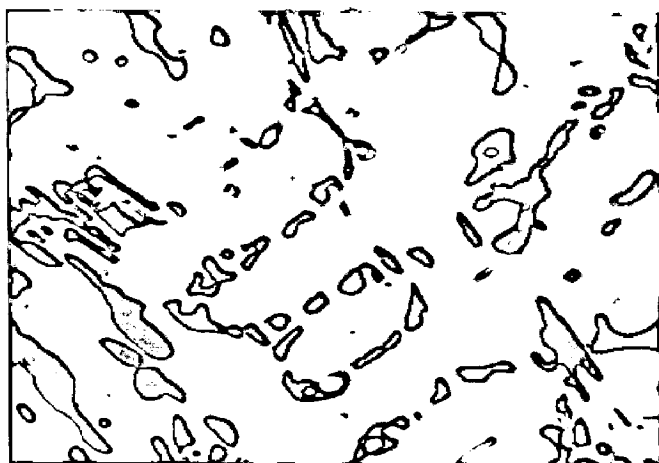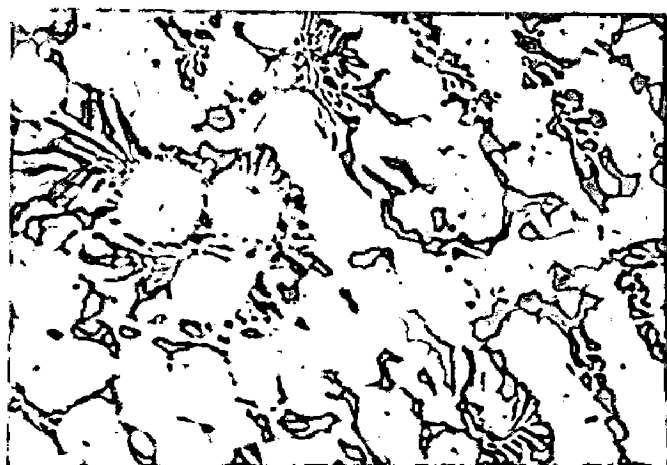
(g) P2,950,2

    X 400

(h) P2,1000,2

    X 800

(i) P2,1000,10

    X 800

(j) P2,1050,10

    X 400

(k) P3,900,2

    X 800

(l) P3,900,10

    X 800

(m) P3,1050,2

    X 400
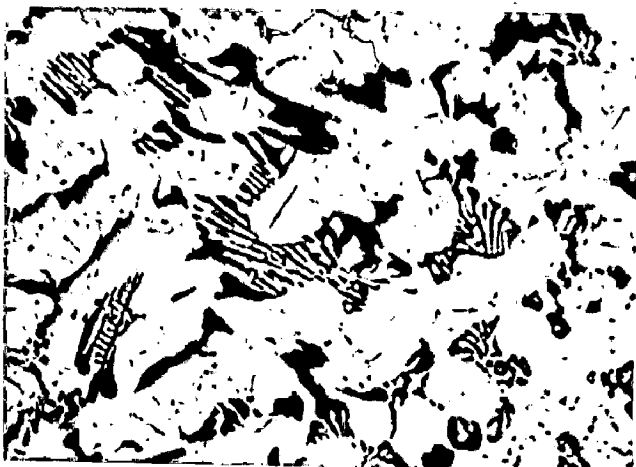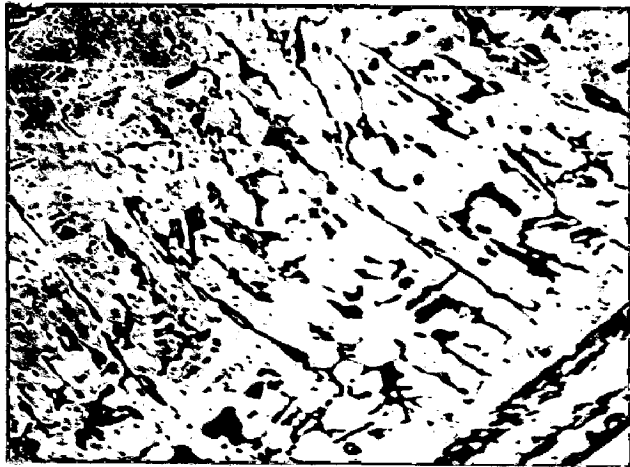
FIG. 4.53 3D plot depicting the effect of heat treating
parameters on hardness (Alloy P2)
Based on Equation 4.26
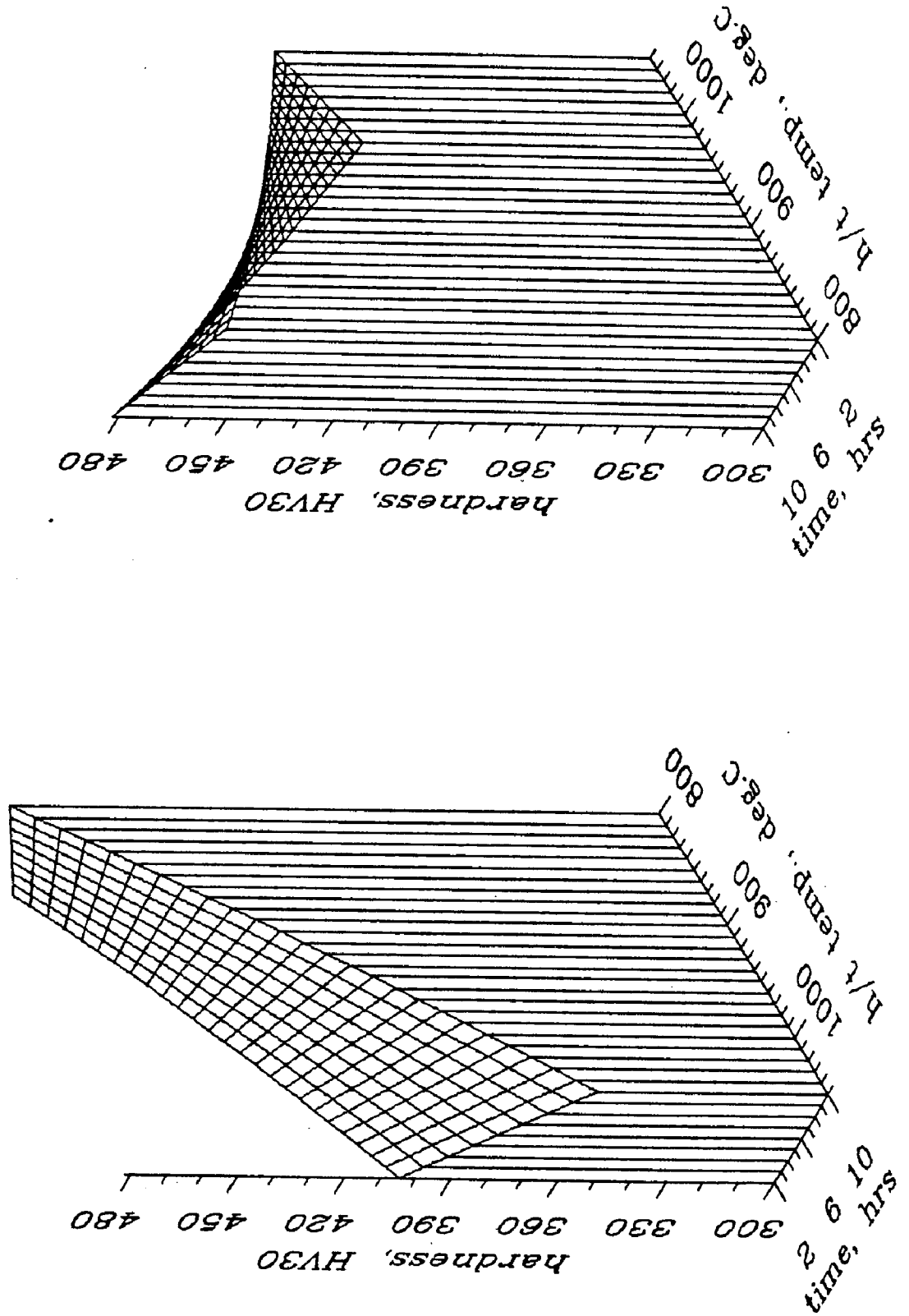
FIG. 5.54 3D plot depicting the effect of heat treating parameters on hardness (Alloy P3)

Based on Equation 4.27
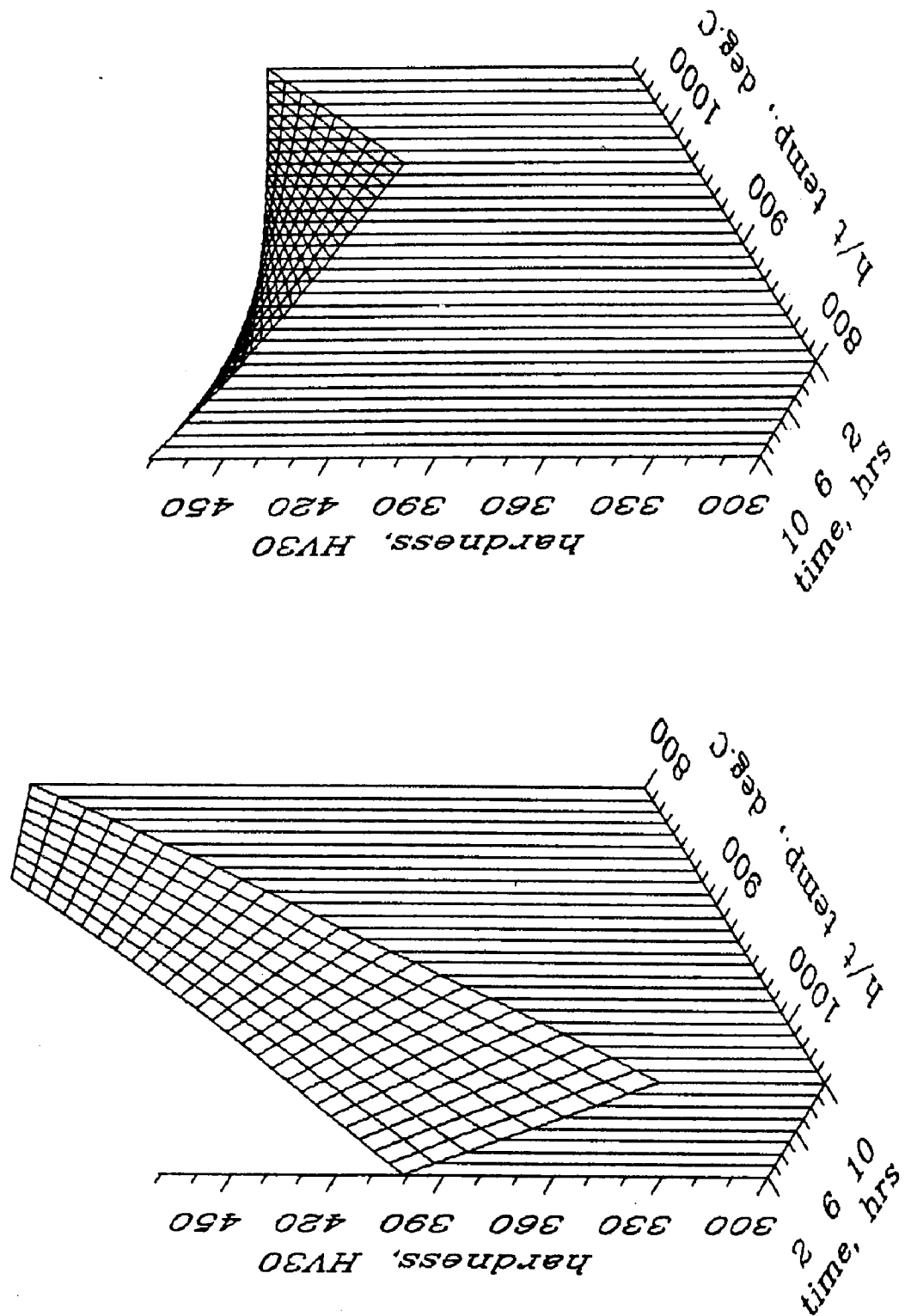
FIG. 4.55 Iso-hardness plot of Alloy P1
Based on Equation 4.25
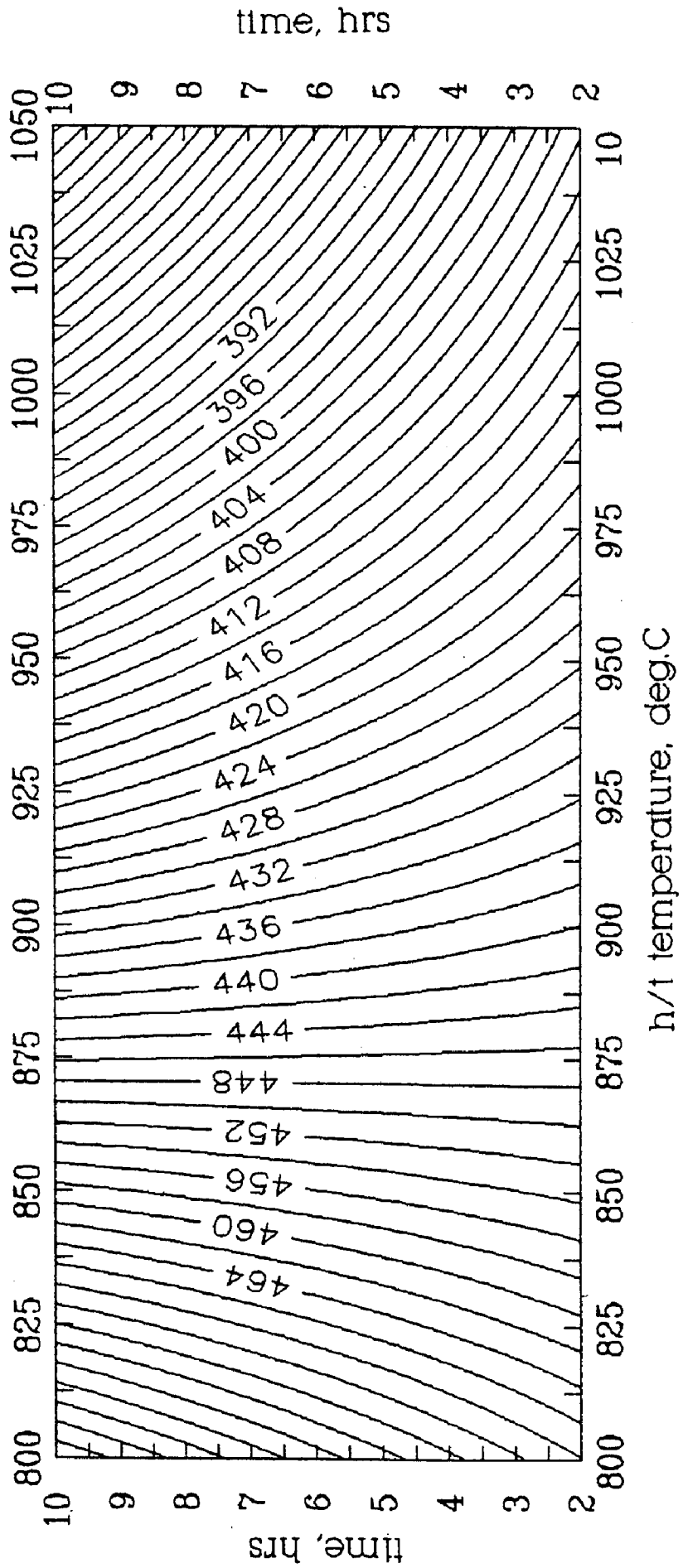
FIG. 4.56 Iso-hardness plot of Alloy P2

Based on Equation 4.26

F-68
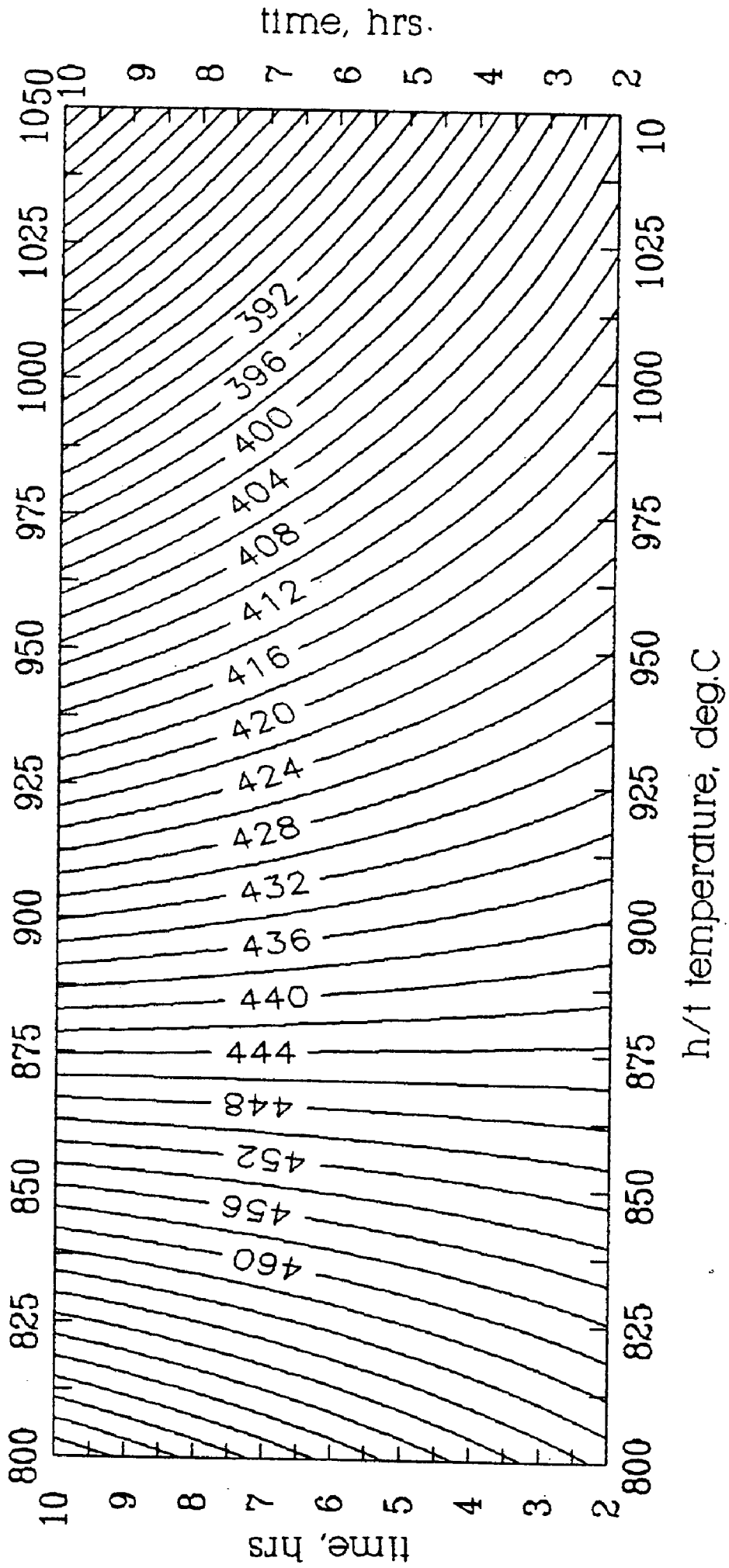
FIG. 4.57 Iso-hardness plot of Alloy P3

Based on Equation 4.27
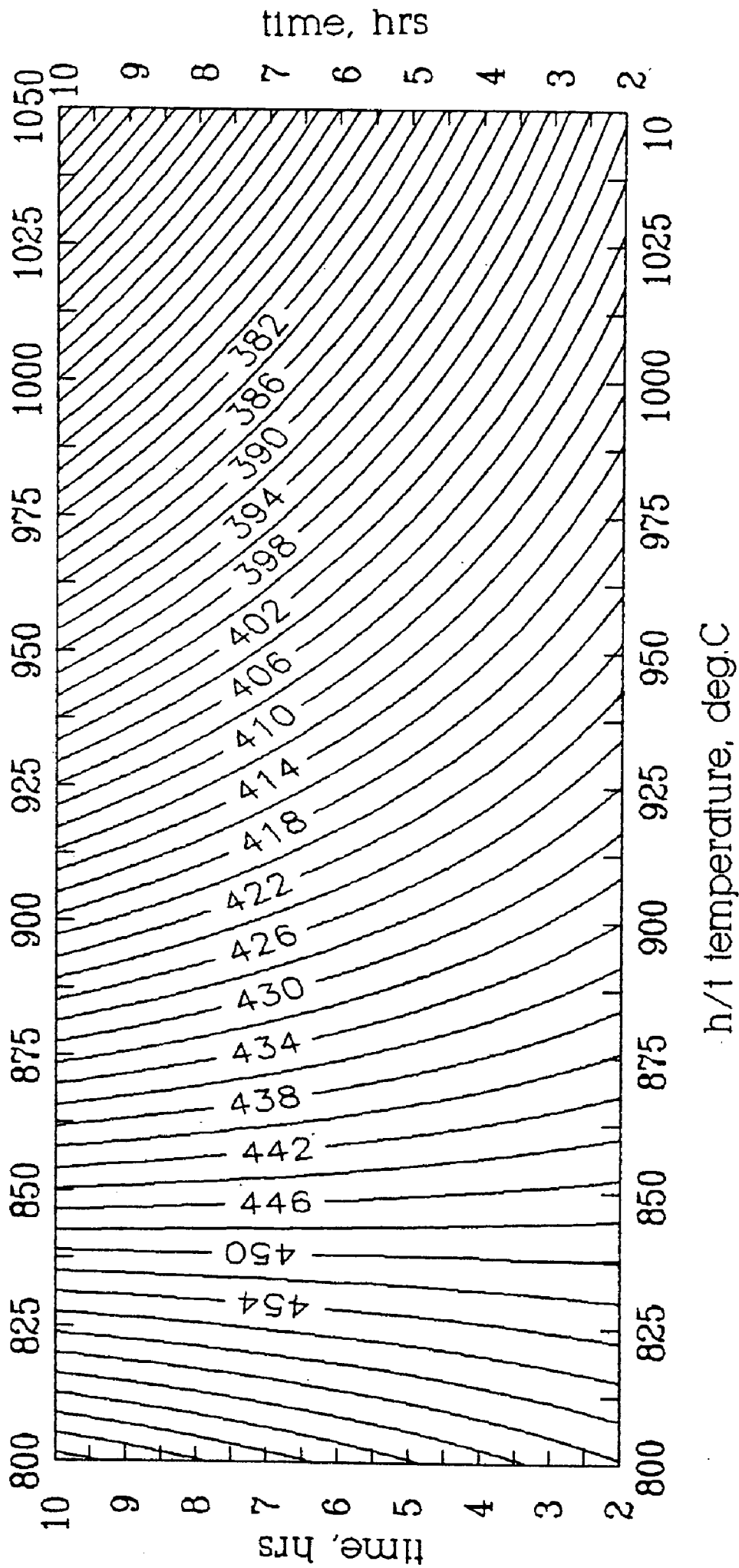
FIG. 5.1 Back scattered Electron images of the alloys

(a) P1,As-cast

    X 800

(b) P1,1000,2

    X 400

(c) P1,1000,2

    X 200

(d) P2,As-Cast

    X 800

(e) P2,900,2

    X 400

(f) P2,900,10

    X 400

FIG. 4.44 Effect of heat treatment on volume fraction of massive carbide (Alloy P2)

(a) 2 hours
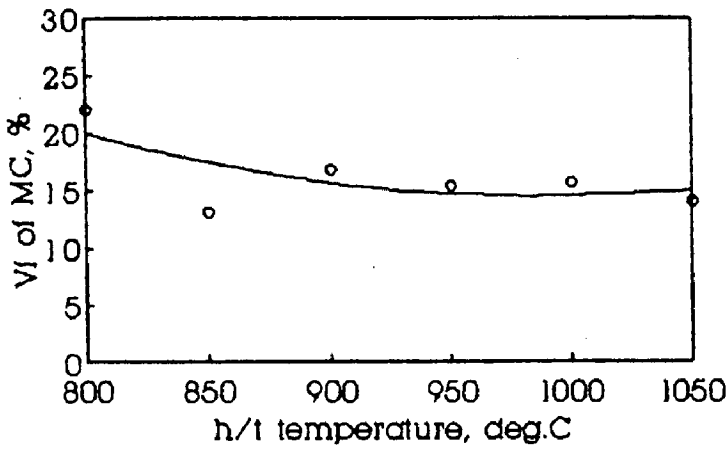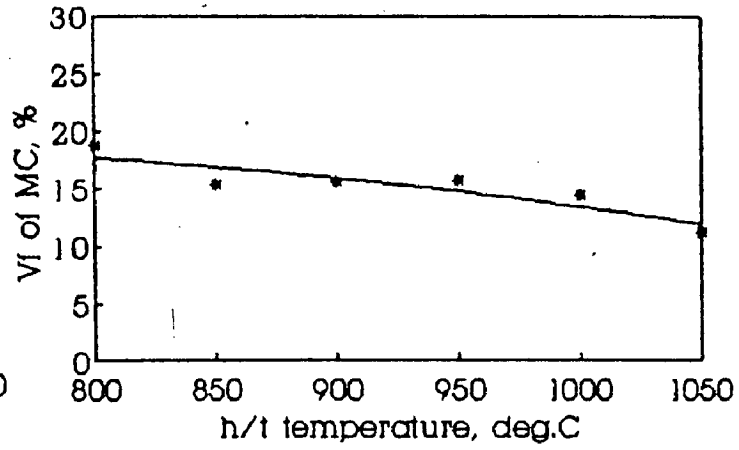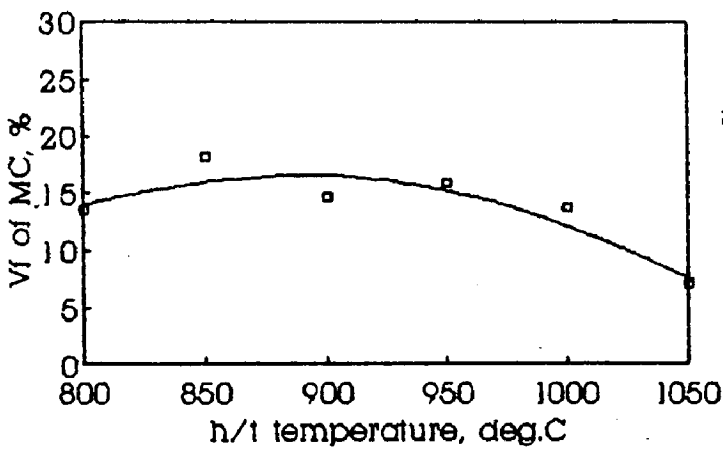
(b) 4 hours
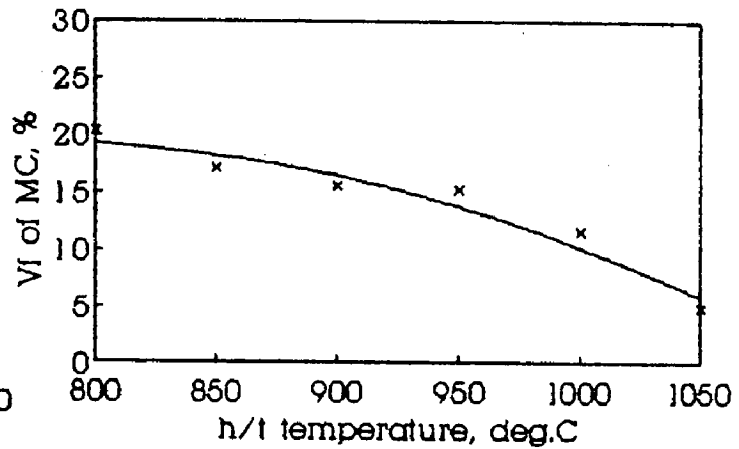
(c) 6 hours
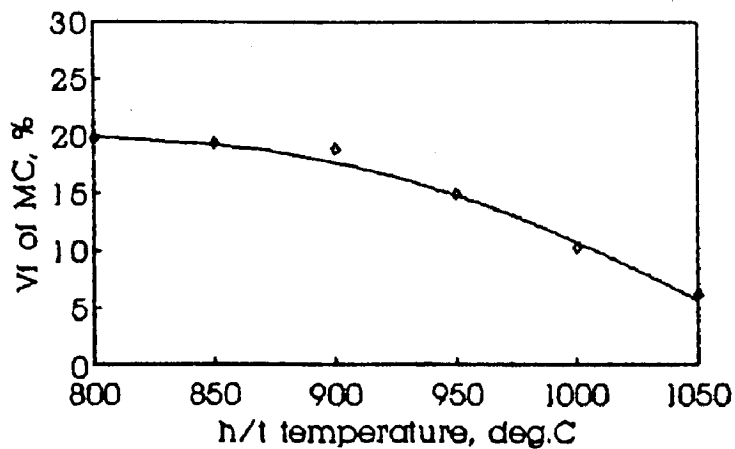
(d) 8 hours

(e) 10 hours

FIG. 4.45 Effect of heat treatment on volume fraction of massive carbide (Alloy P3)

(a) 2 hours
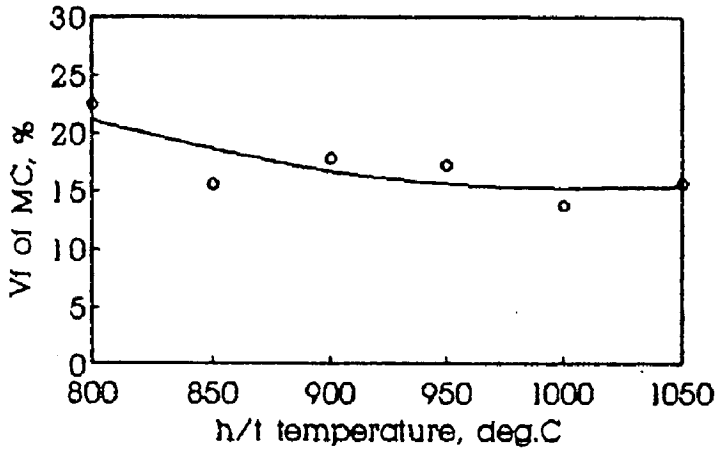
(b) 4 hours
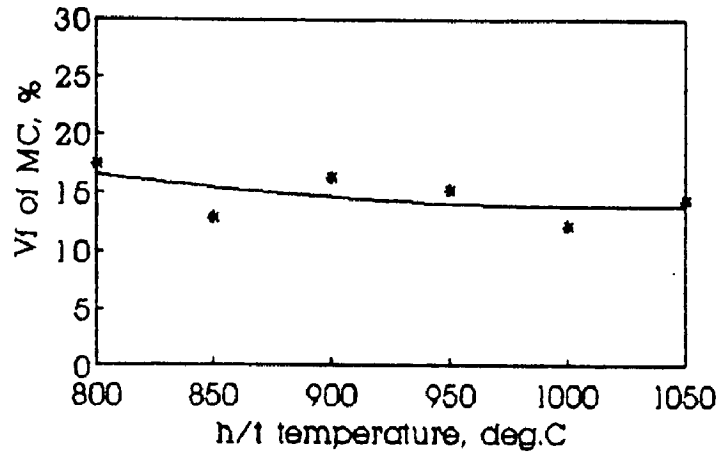
(c) 6 hours
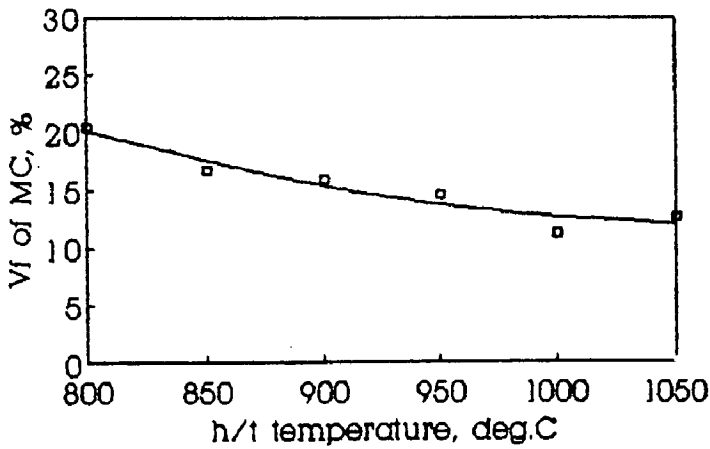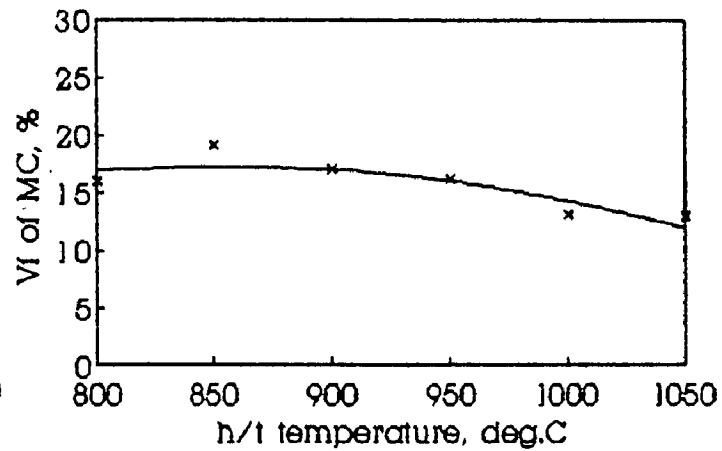
(d) 8 hours

(e) 10 hours
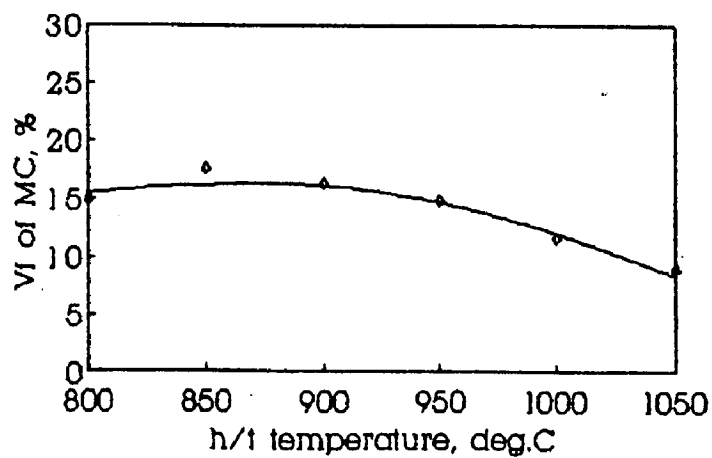
FIG. 4.46 % area of DCs in different classes at different locations
(850 deg.C, 2 hours heat treatment)

(a) Alloy P1

(b) Alloy P2

(c) Alloy P3

I class

II class

III class

F-58
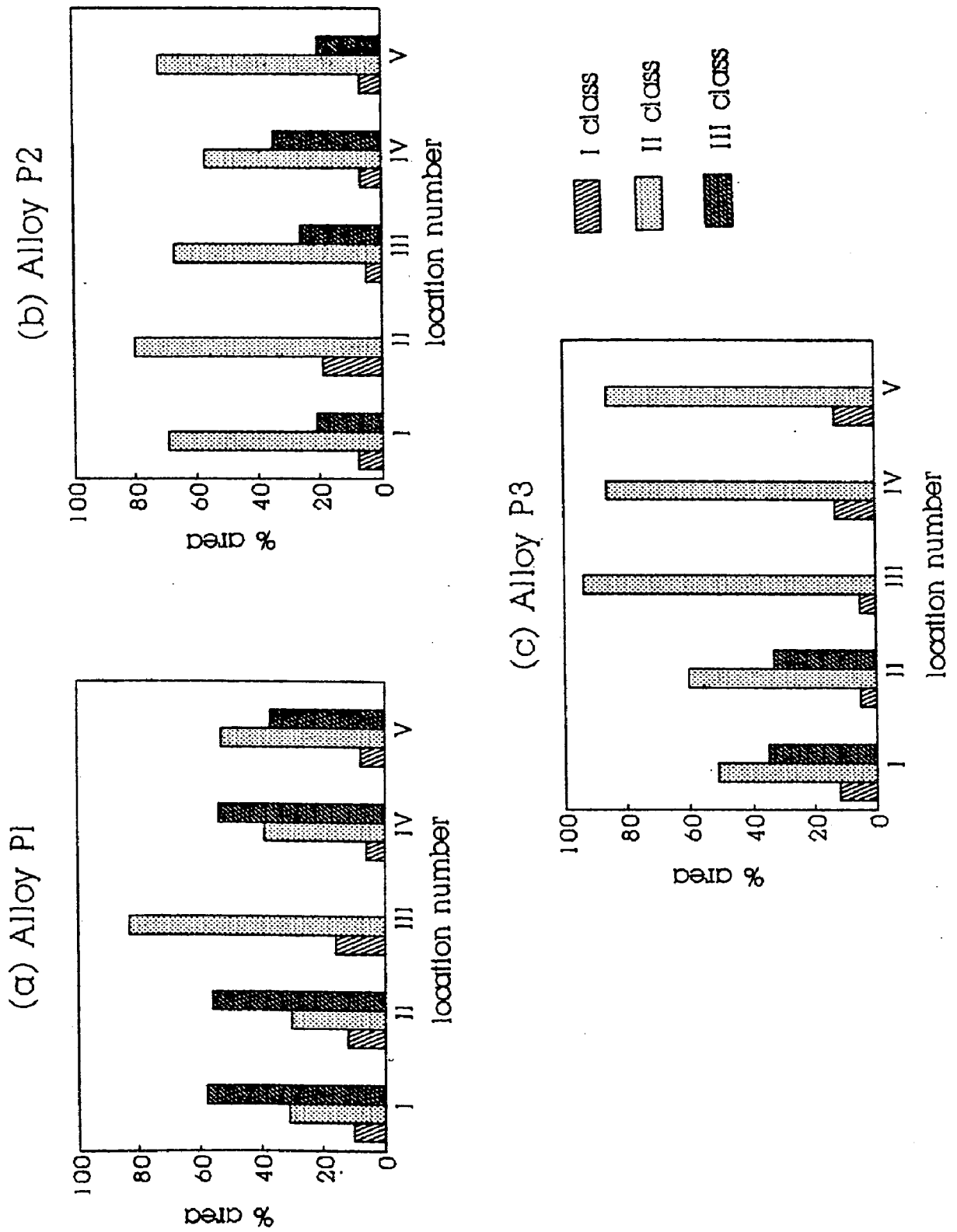
FIG. 4.47 % area of DCs in different classes at different locations
(1000 deg.C, 8 hours heat treatment)

(a) Alloy P1

(b) Alloy P2

(c) Alloy P3

I class
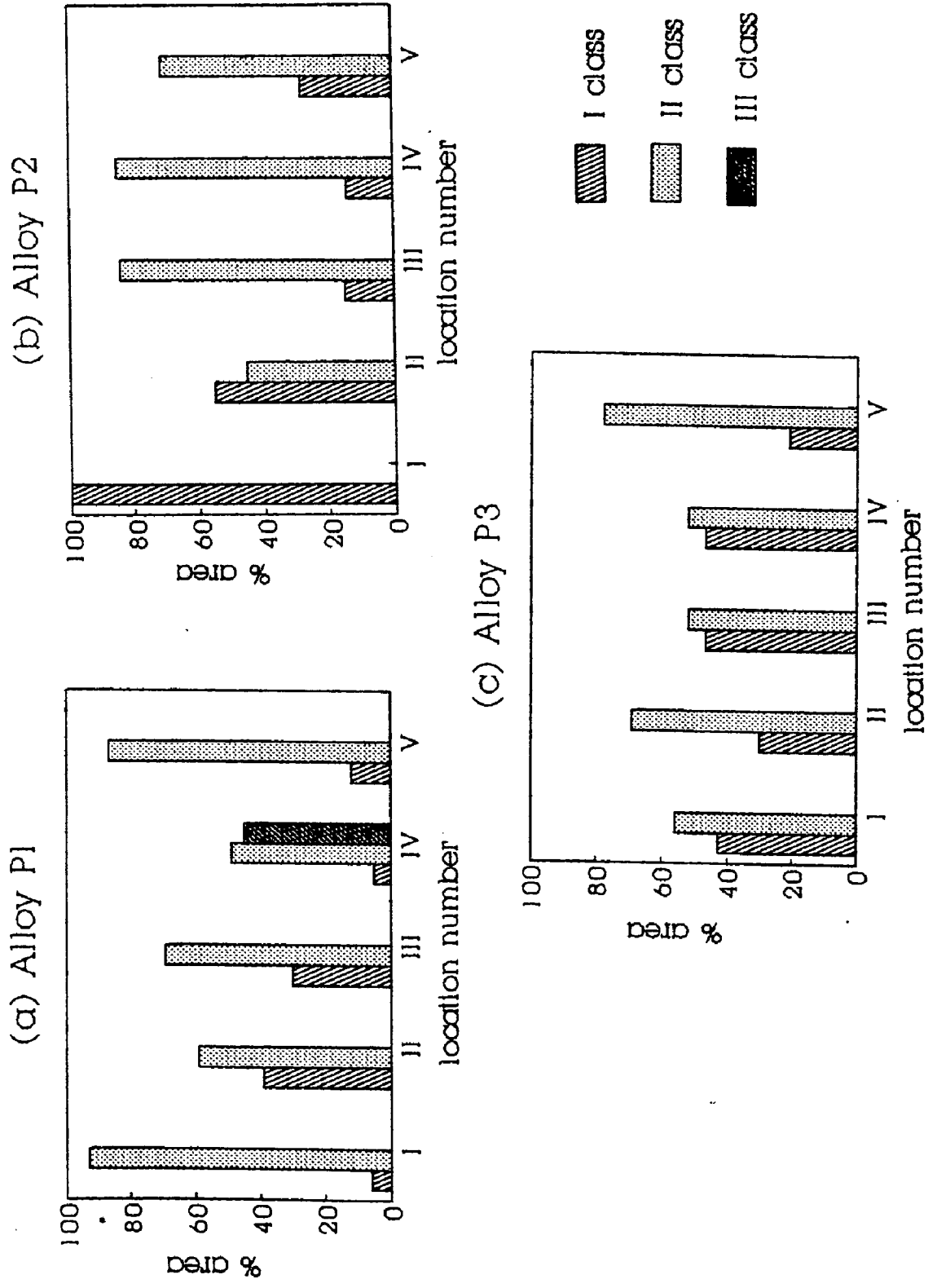
II class

III class

FIG. 4.48 Effect of heat treatment on DF of DCs
(Alloy P1)
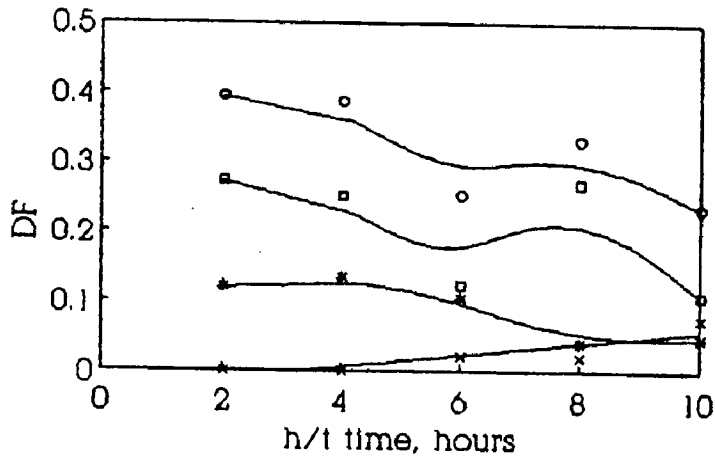
(a) 800 deg.C
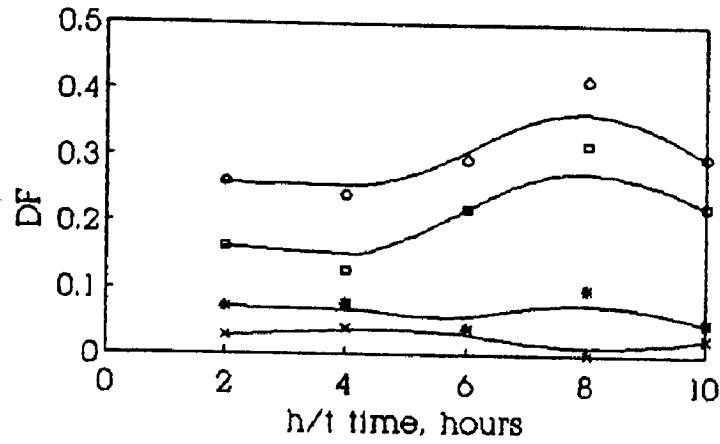
(b) 850 deg.C
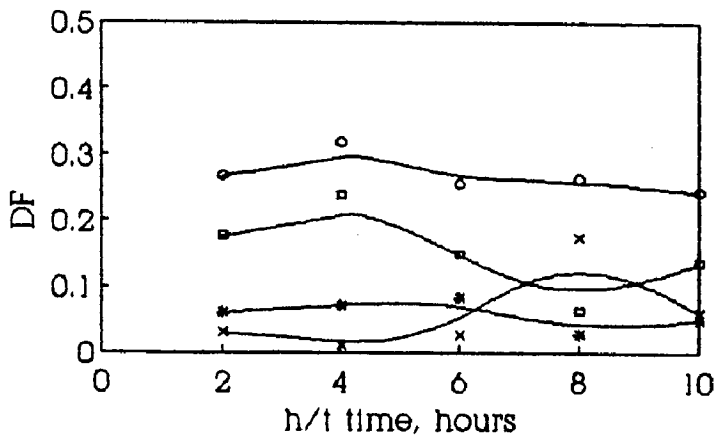
(c) 900 deg.C
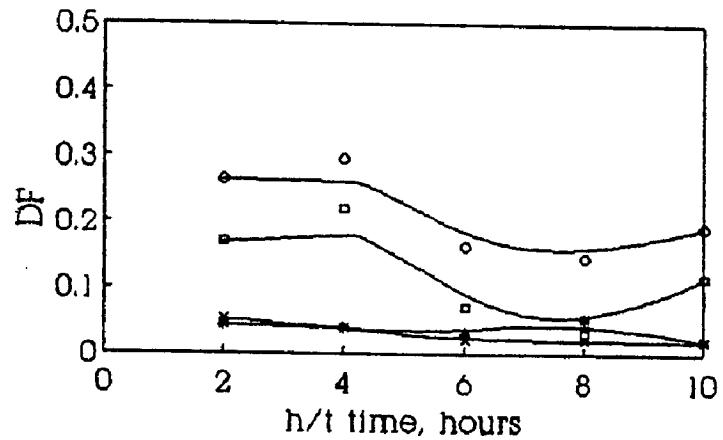
(d) 950 deg.C
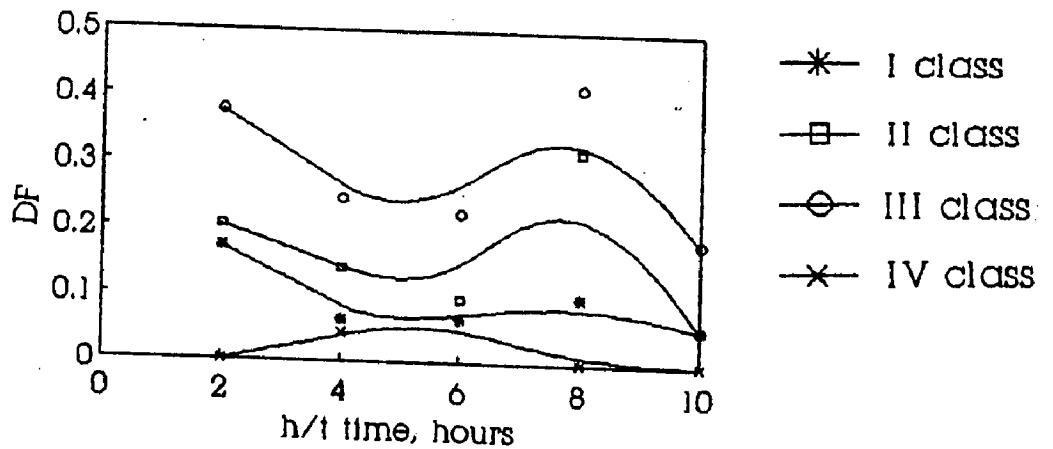
(e) 1000 Deg.C

Legend:
- I class
- II class
- III class
- IV class

FIG. 4.49 Effect of heat treatment on DF of DCs
(Alloy P2)

(a) 800 deg.C

(b) 850 deg.C

(c) 900 deg.C

(d) 950 deg.C

(e) 1000 deg.C

—*— I class
—□— II class
—○— III class
—×— IV class
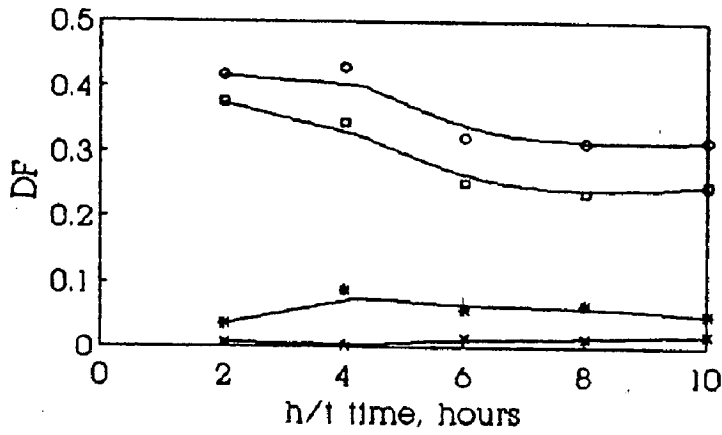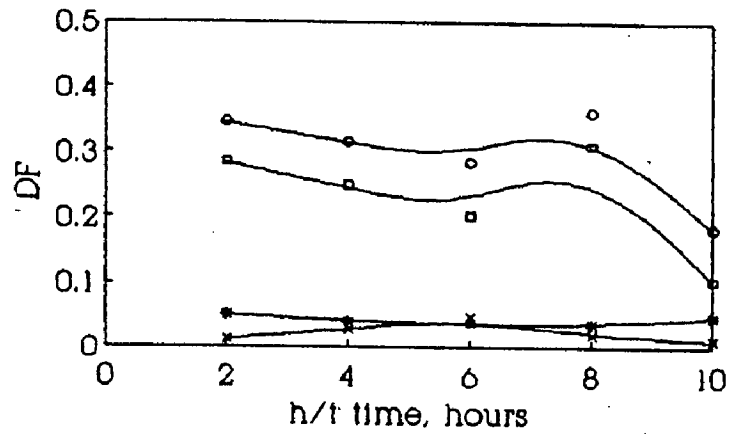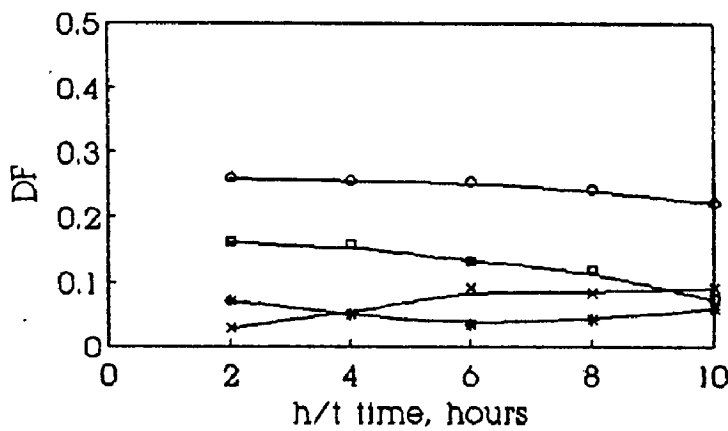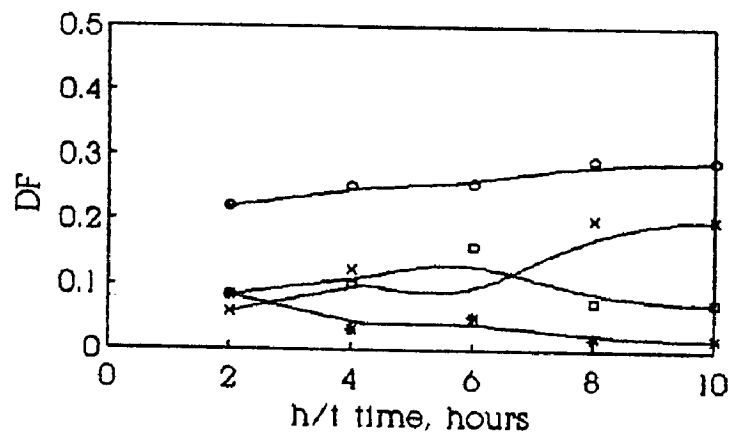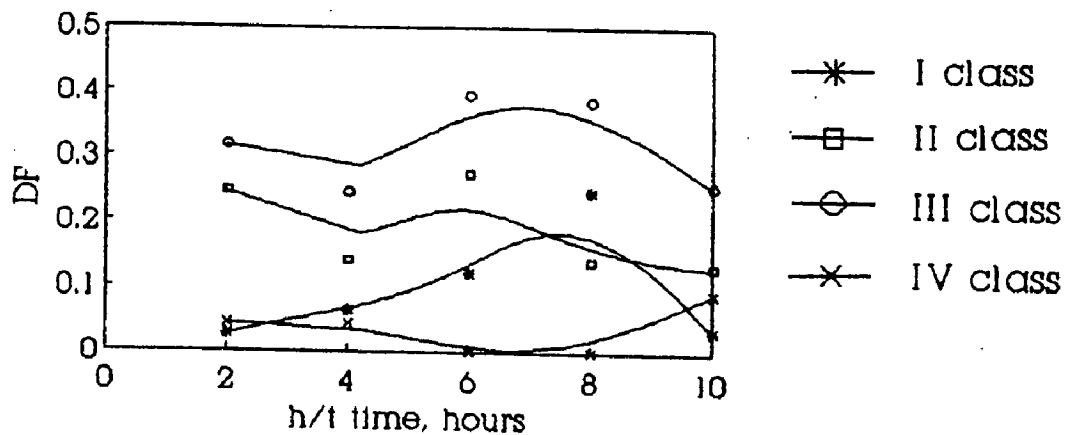
FIG. 4.50 Effect of heat treatment on DF of DCs
(Alloy P3)

(a) 800 deg.C

(b) 850 deg.C

(c) 900 deg.C

(d) 950 deg.C

(e) 1000 deg.C

—✱— I class
—□— II class
—○— III class
—✕— IV class
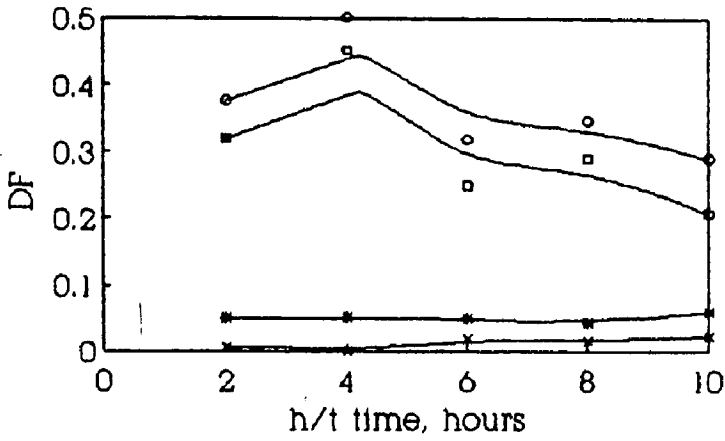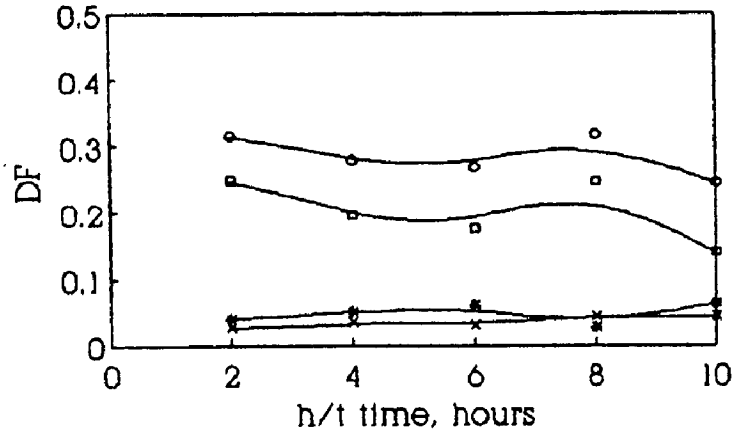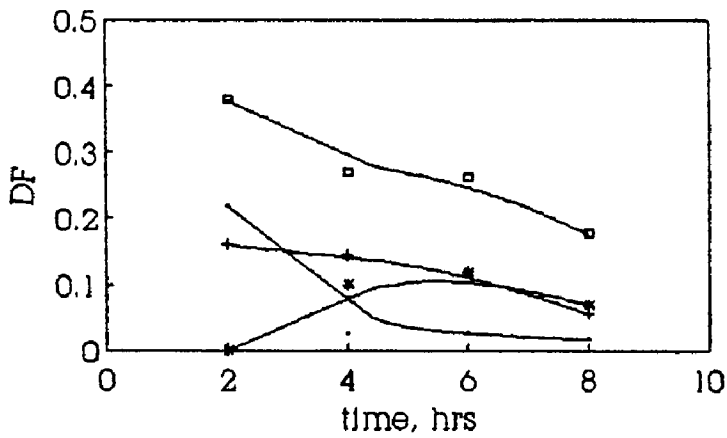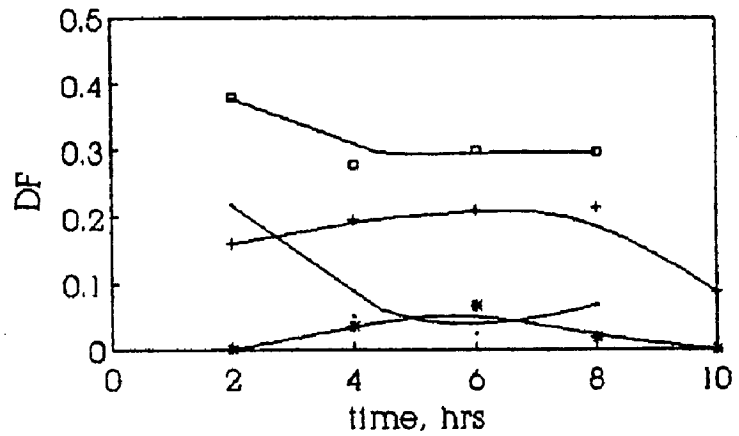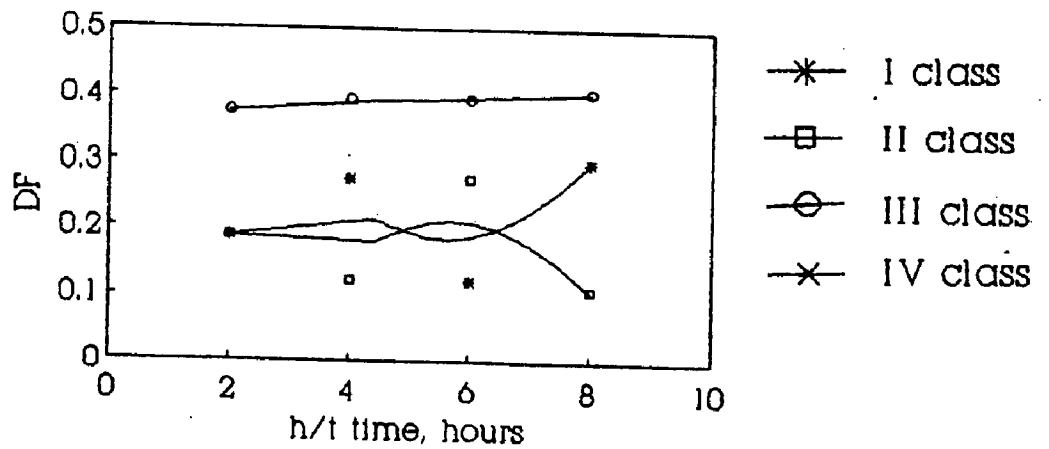
FIG. 4.51 Experimental vs predicted hardness values of the experimental alloys

(a) Alloy P1
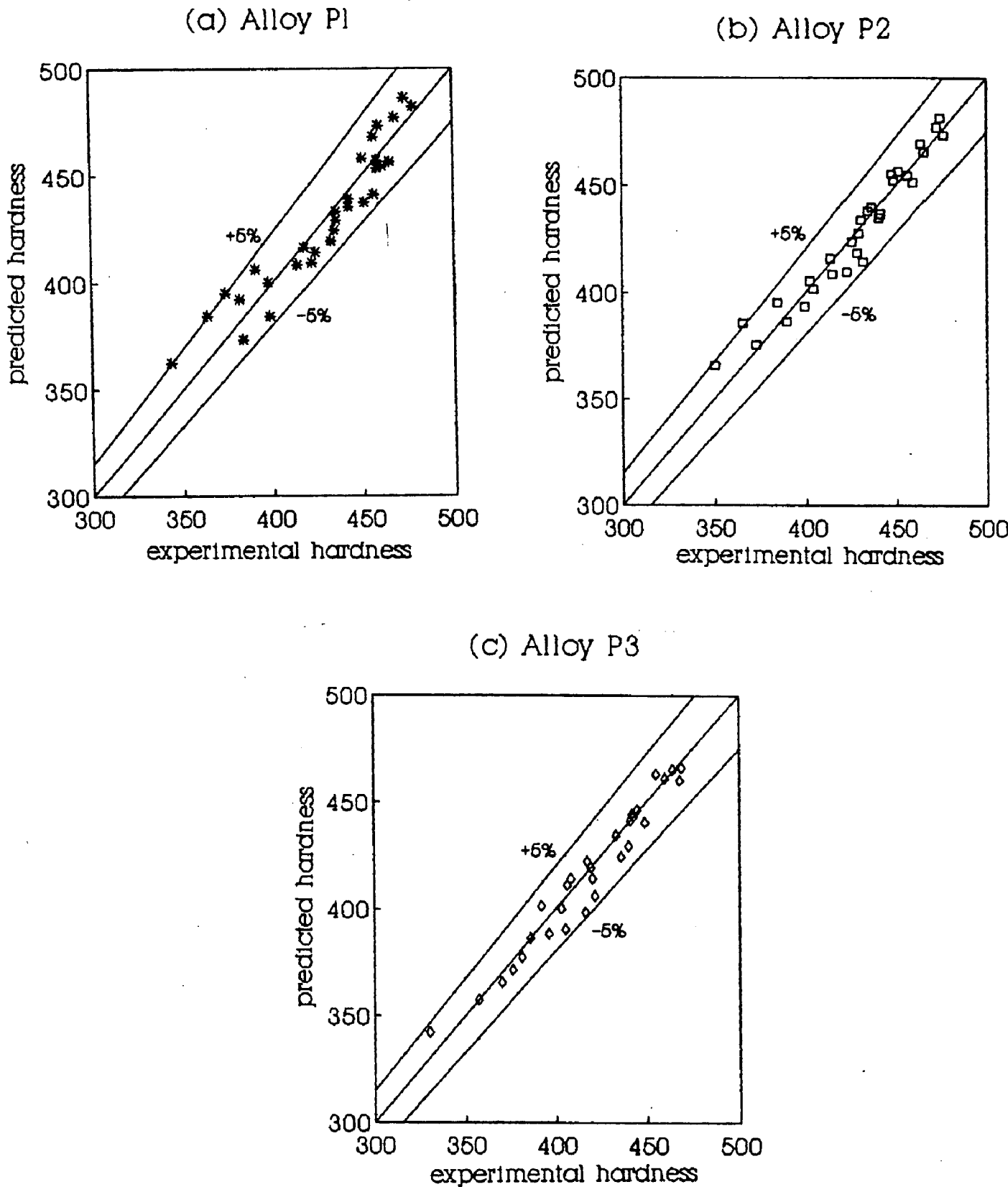
(b) Alloy P2

(c) Alloy P3

FIG. 4.52 3D plot depicting the effect of heat treating
parameters on hardness (Alloy Pl)
Based on Equation 4.25
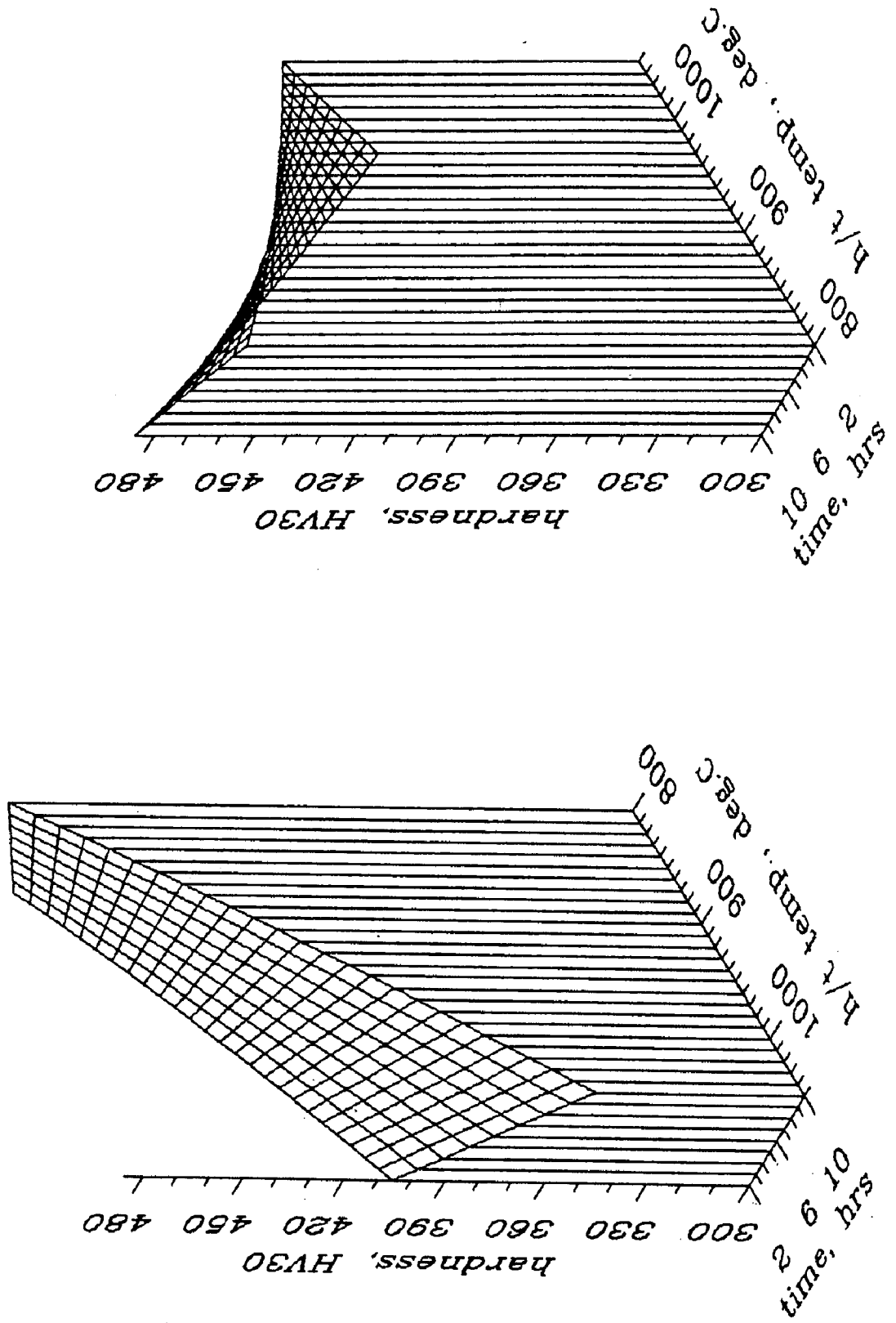
FIG. 4.43 Effect of heat treatment on volume fraction of massive carbide (Alloy P1)

(a) 2 hours
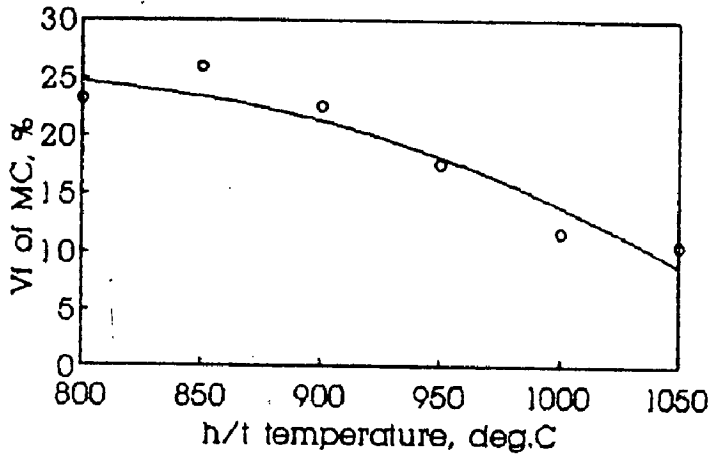
(b) 4 hours
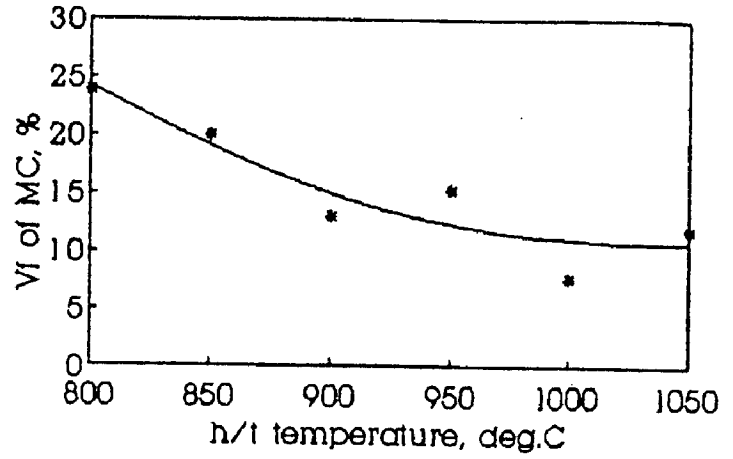
(c) 6 hours
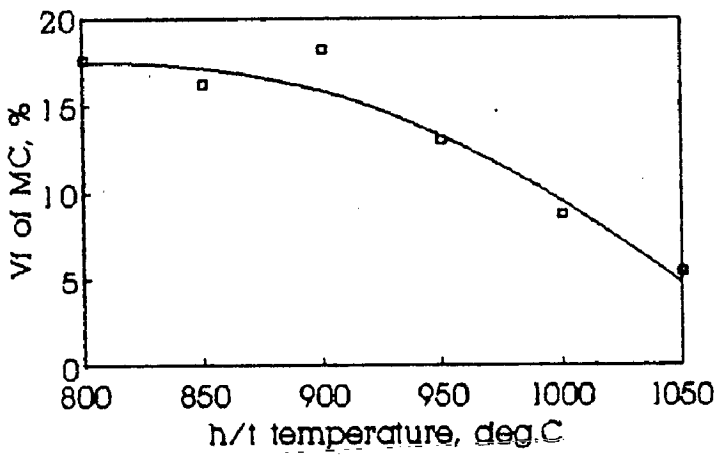
(d) 8 hours
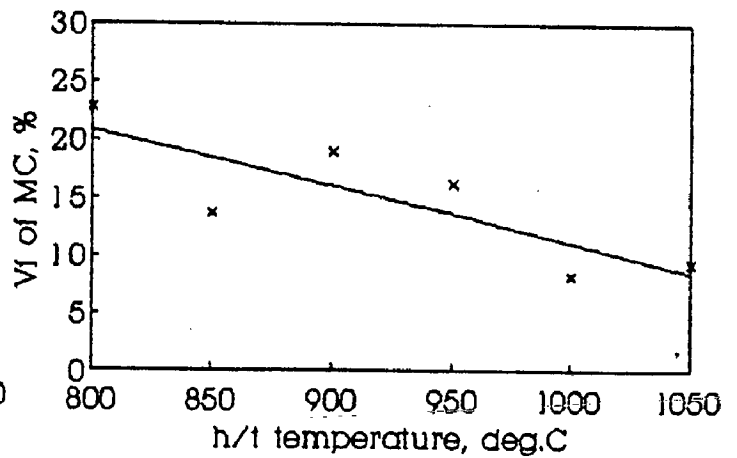
(e) 10 hours
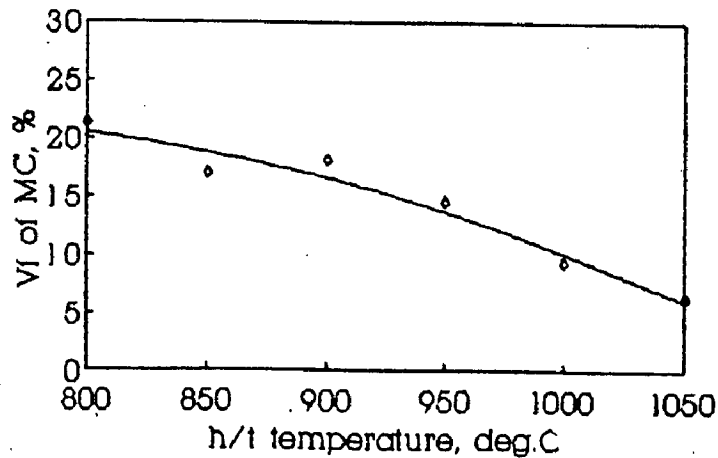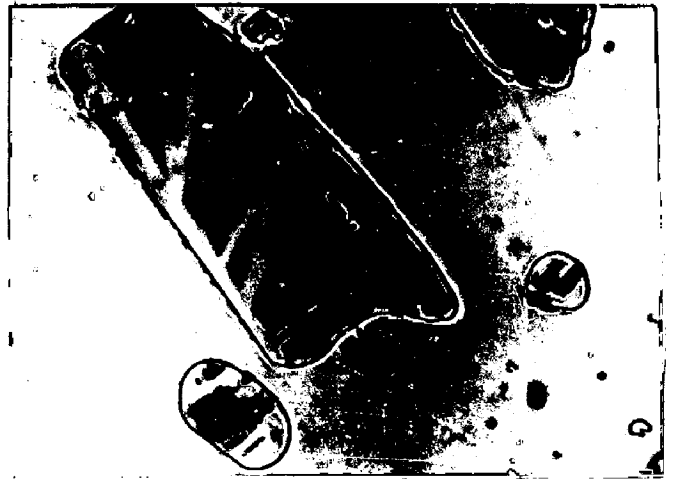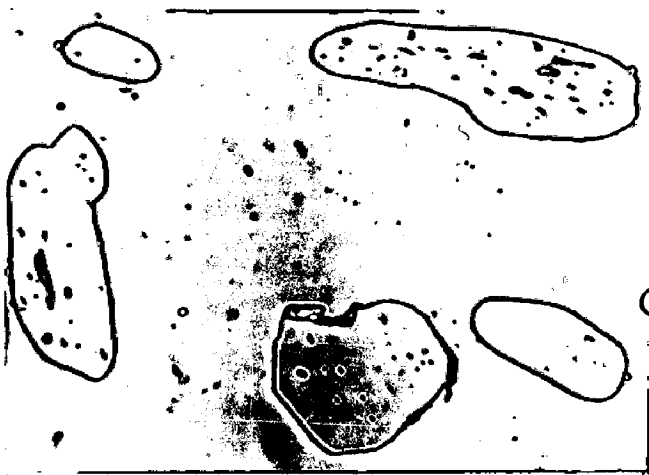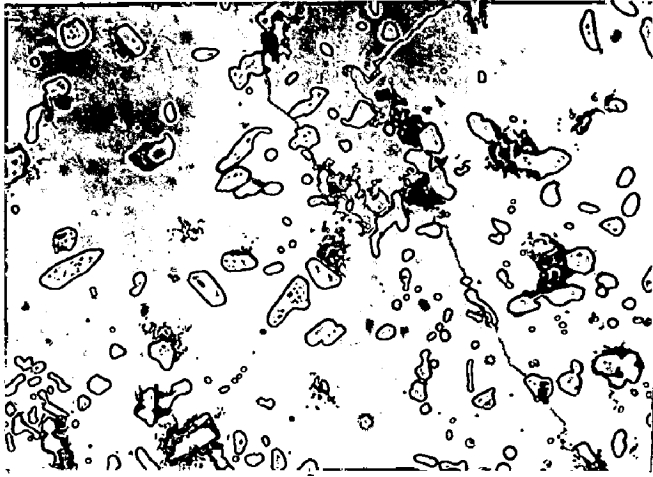
(h) P3,1050,10

X 200

(i) P3,1050,10

X 1000

(j) P3,1050,10

X 1000

(k) P3,1050,10

X 1000
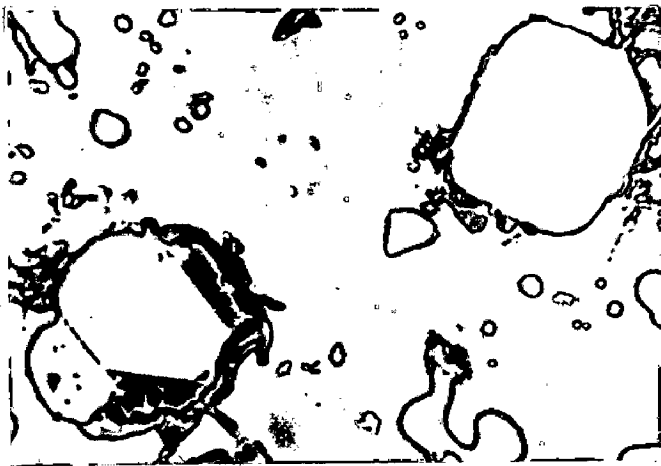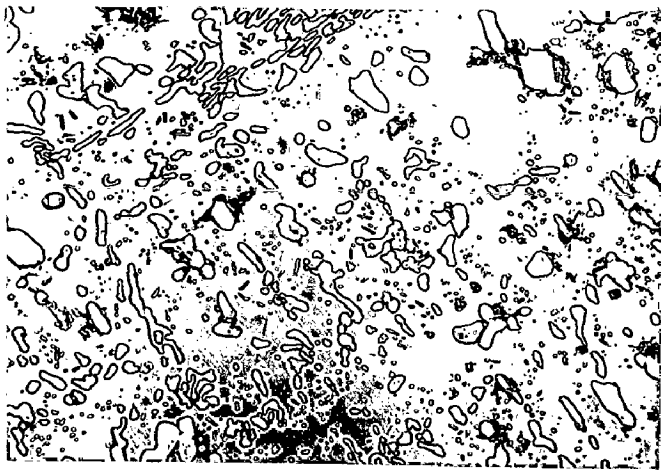
FIG. 4.42

(a) P3,1050,2

X 1000

(b) P3,1050,2

X 200

(c) P3,1050,2

X 1000

(d) P3,1050,6

X 1000

(e) P3,1050,6

X 1000

(f) P3,1050,6

X 200

(g) P3,1050,6

X 1000
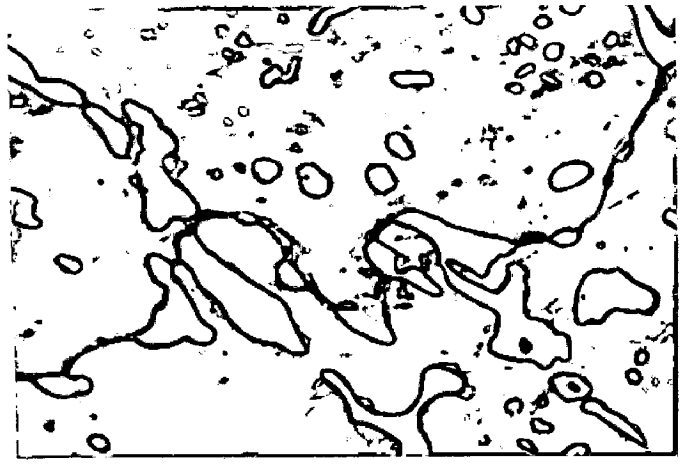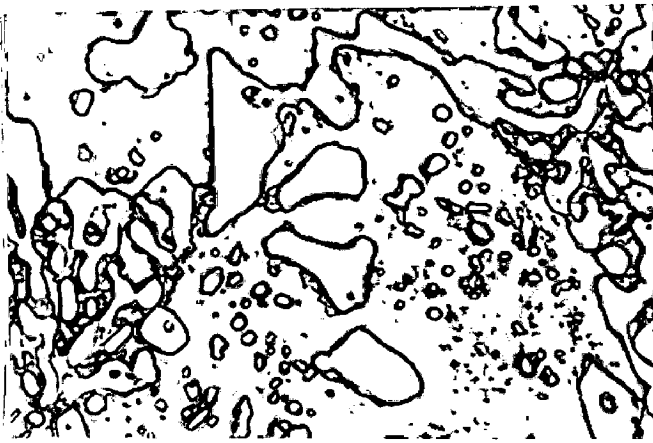
FIG. 4.41

(a) P3,1000,2

    X 200

(b) P3,1000,2

    X 1000

(c) P3,1000,2

    X 1000

(d) P3,1000,6

    X 1000

(e) P3,1000,6

    X 1000

(f) P3,1000,10

    X 200

(g) P3,1000,10

    X 1000

(h) P3,1000,10

    X 1000
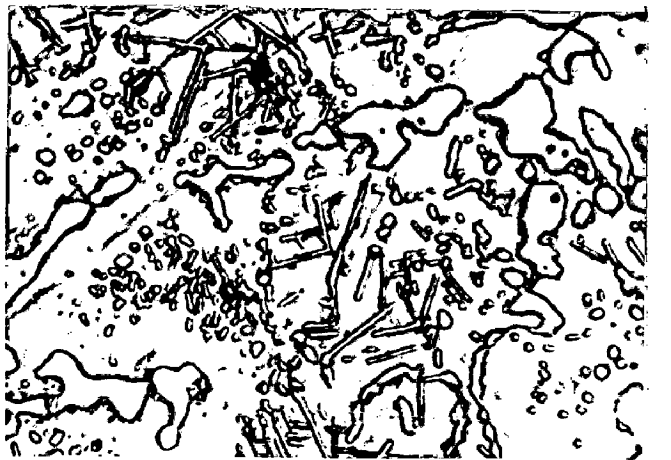
FIG. 4.40

(a) P3,950,2

X 1000

(b) P3,950,2

X 200

(c) P3,950,2

X 1000

(d) P3,950,6

X 1000

(e) P3,950,6

X 1000

(f) P3,950,10

X 1000

(g) P3,950,10

X 200

(h) P3,950,10

X 1000
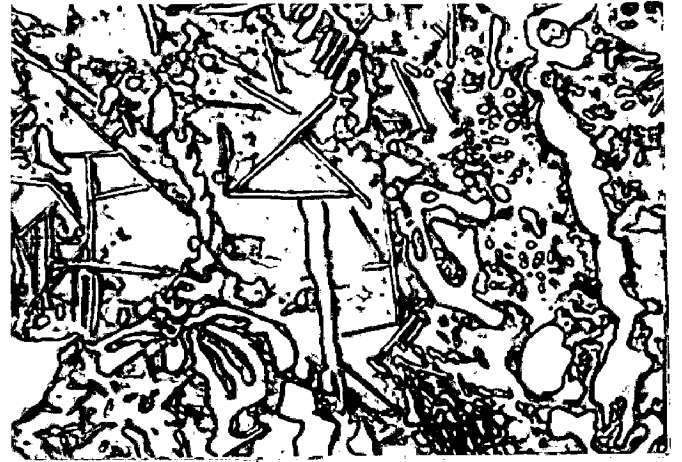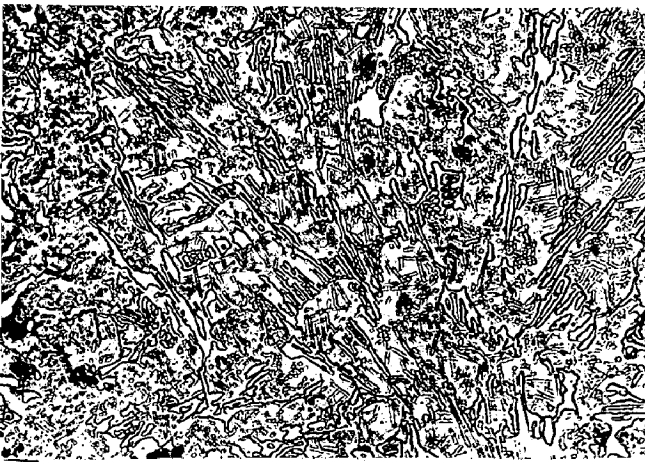
FIG. 4.39

(a) P3,900,2

X 200

(b) P3,900,2

X 1000

(c) P3,900,6

X 1000

(d) P3,900,6

X 1000

(e) P3,900,10

X 200

(f) P3,900,10

X 1000

(g) P3,900,10

X 1000
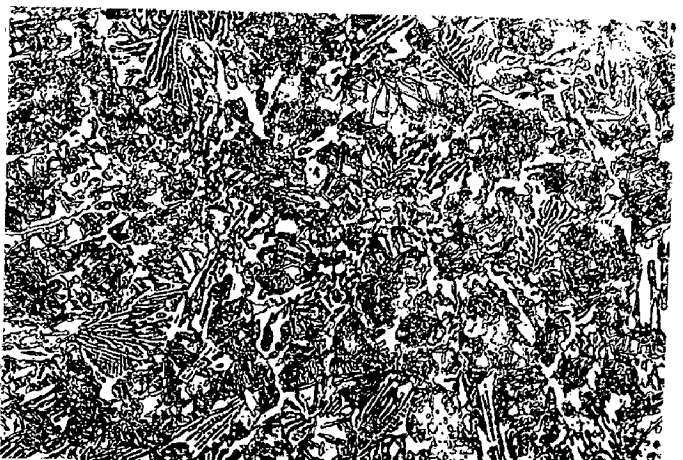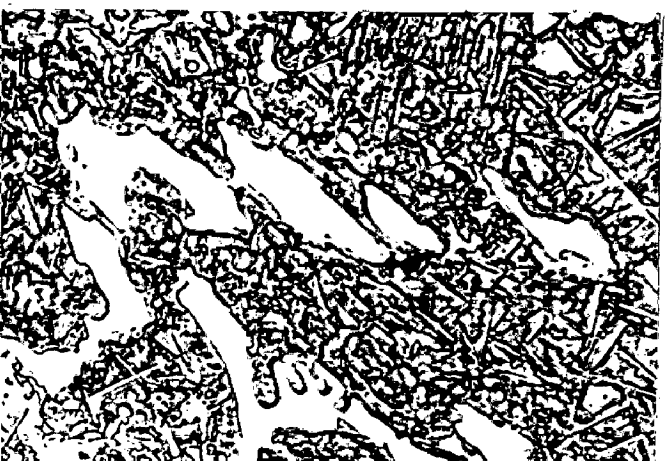
FIG. 4.38

(a) P3,850,2

X 1000

(b) P3,850,2

X 200

(c) P3,850,2

X 1000

(d) P3,850,6

X 1000

(e) P3,850,6

X 1000

(f) P3,850,10

X 1000

(g) P3,850,10

X 200

(h) P3,850,10

X 1000

FIG. 4.37

(a) P3,800,2

    X 200

(b) P3,800,2

    X 1000

(c) P3,800,2

    X 1000

(d) P3,800,6

    X 1000

(e) P3,800,6

    X 1000

(f) P3,800,10

    X 1000

(g) P3,800,10

    X 200

(h) P3,800,10

    X 1000
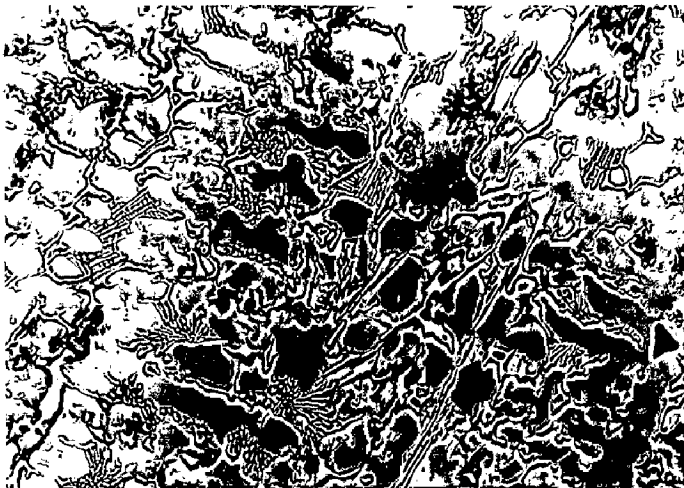
FIG. 4.36

(a) P3, As-cast

X 200

(b) P3, As-cast

X 1000
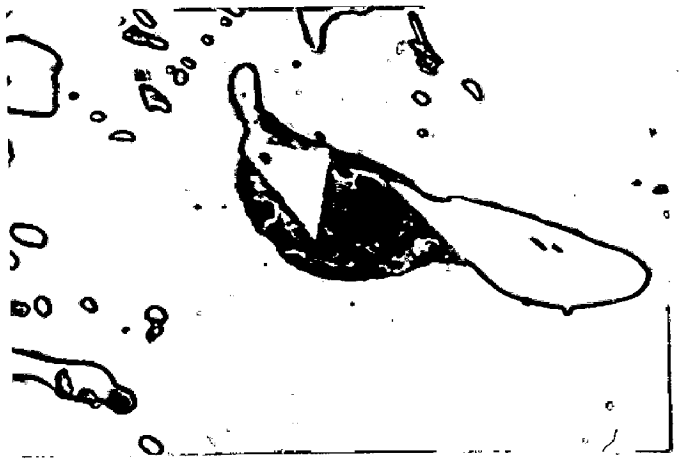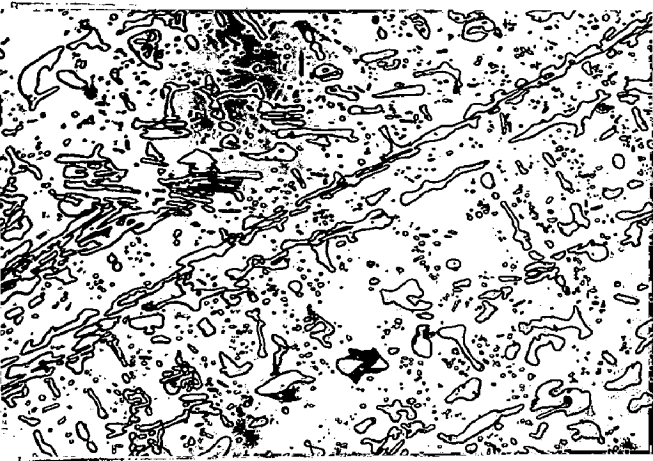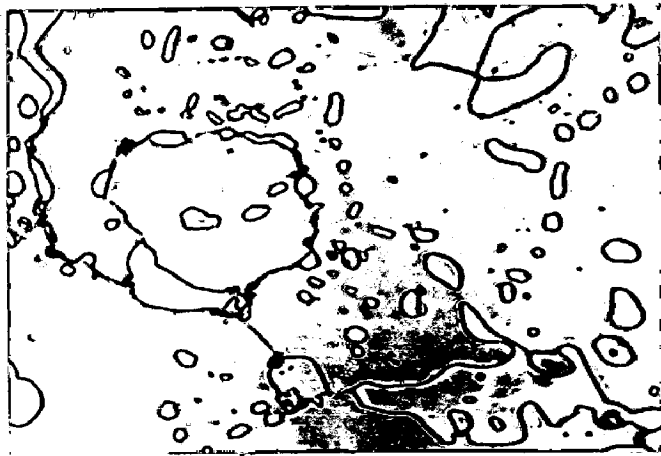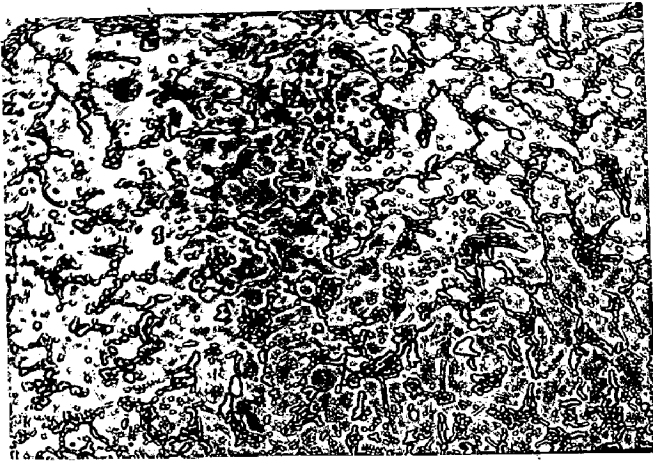
FIG. 4.35

(a) P2,1050,2

X 1000

(b) P2,1050,2

X 1000

(c) P2,1050,2

X 200

(d) P2,1050,6

X 1000

(e) P2,1050,6

X 200

(f) P2,1050,6

X 1000
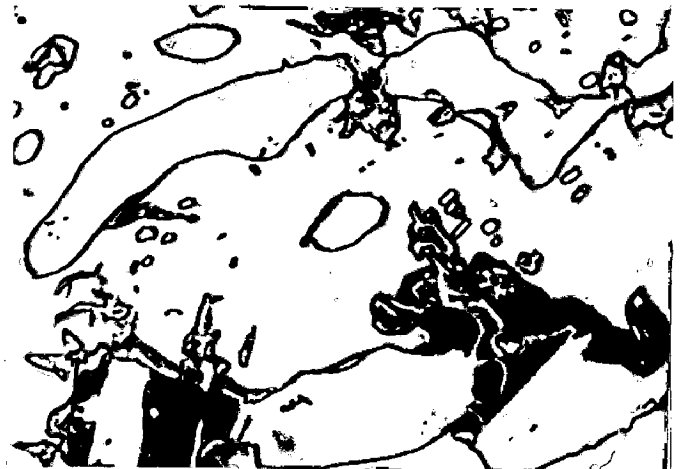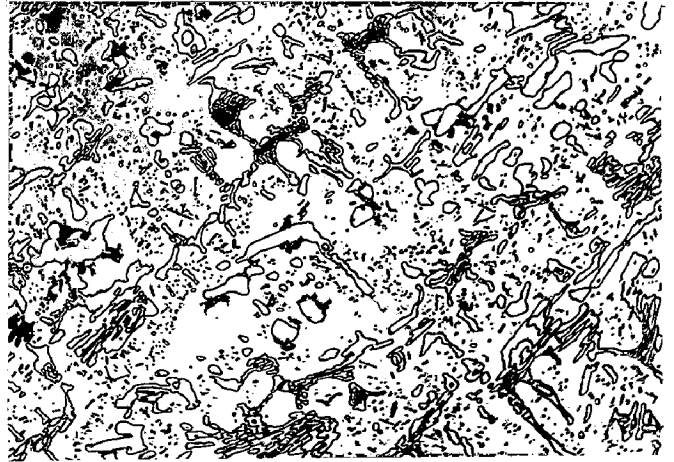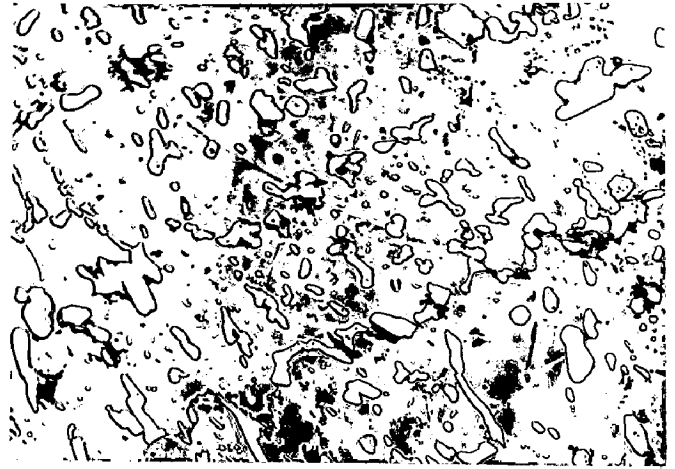
(g) P2,1050,10

    X 1000

(h) P2,1050,10

    X 1000

(i) P2,1050,10

    X 1000

(j) P2,1050,10

    X 200

(k) P2,1050,10

    X 200

F-46
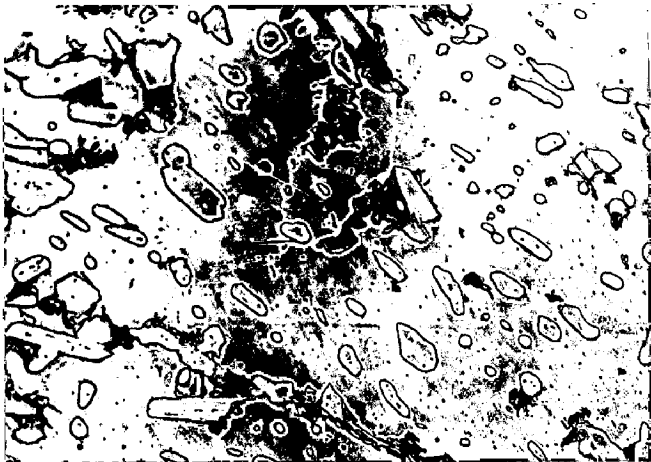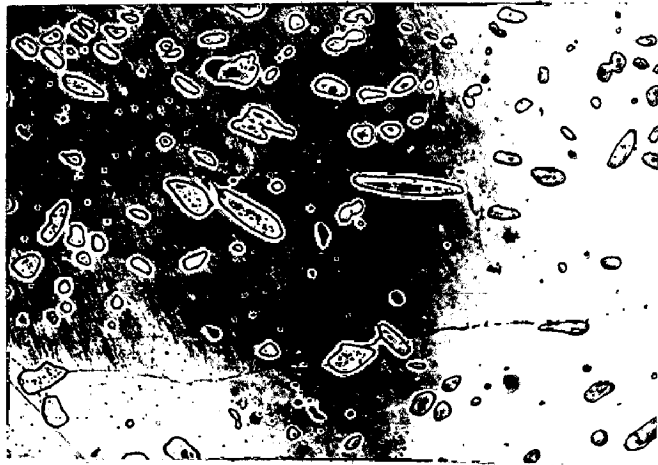
FIG. 4.34

(a) P2,1000,2
    X 200

(b) P2,1000,2
    X1000

(c) P2,1000,6
    X 1000

(d) P2,1000,10
    X 200

(e) P2,1000,10
    X 1000

(f) P2,1000,10
    X 1000

(g) P2,1000,10
    X 1000

F-44

FIG. 6.16a 3D plot depicting the effect of VMC & NOP
on corrosion rate

(Alloy P1)

Based on Equation 6.23
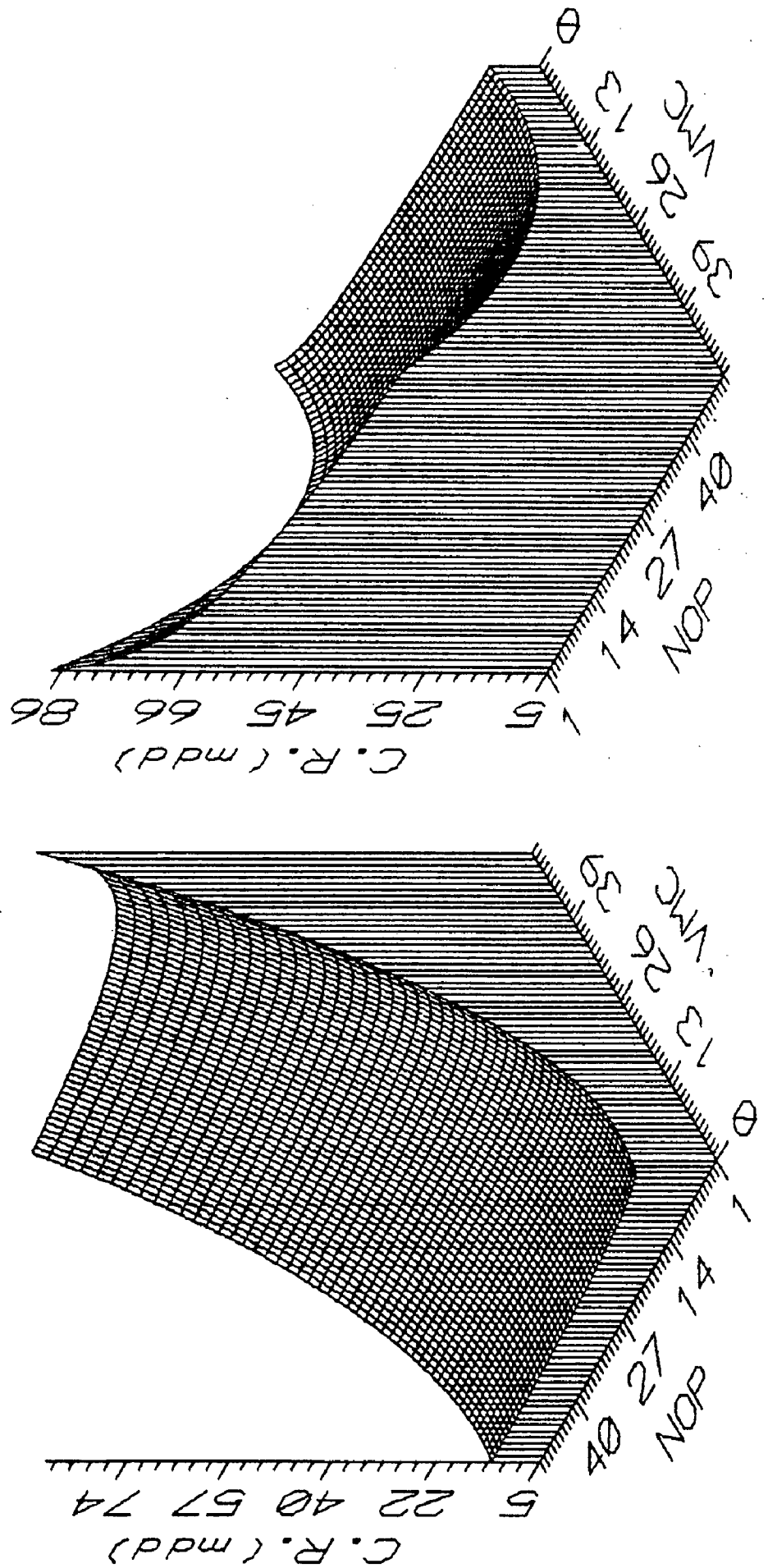
FIG. 6.16b 3D plot depicting the effect of VMC & NOP
on corrosion rate

(Alloy P2)

Based on Equation 6.24
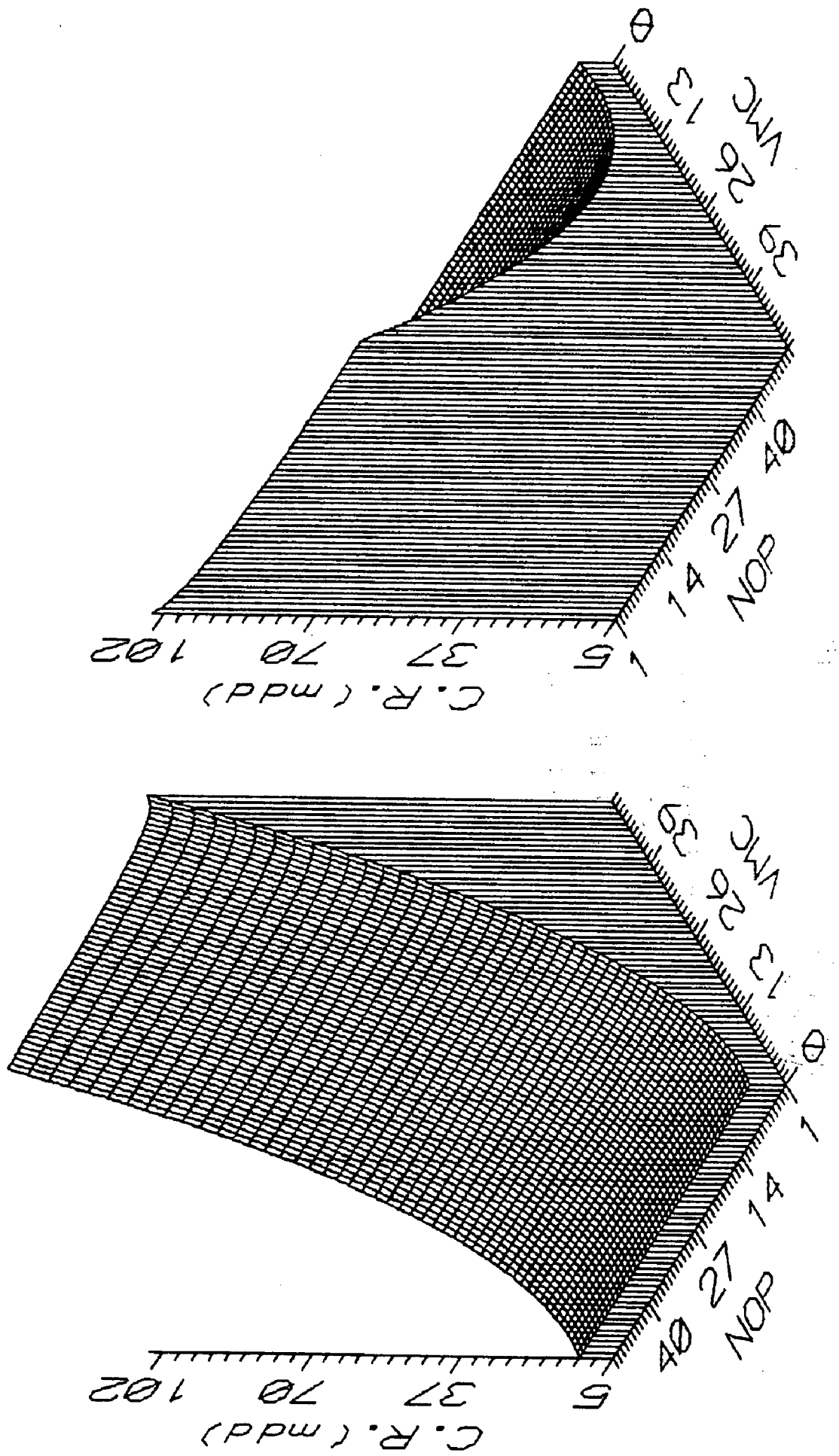
FIG. 6.16c 3D plot depicting the effect of VMC & NOP
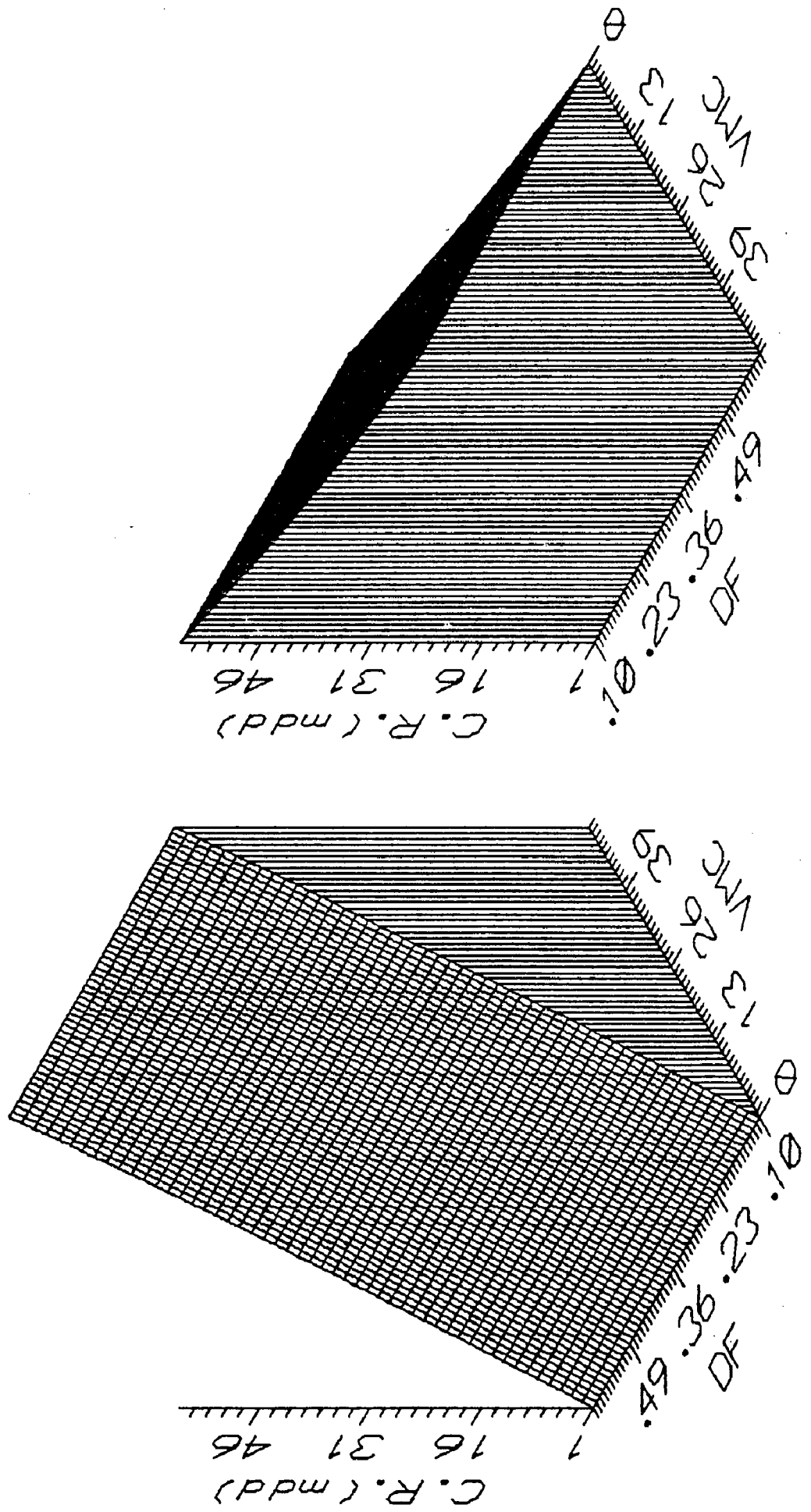on corrosion rate

(Alloy P3)

Based on Equation 6.25
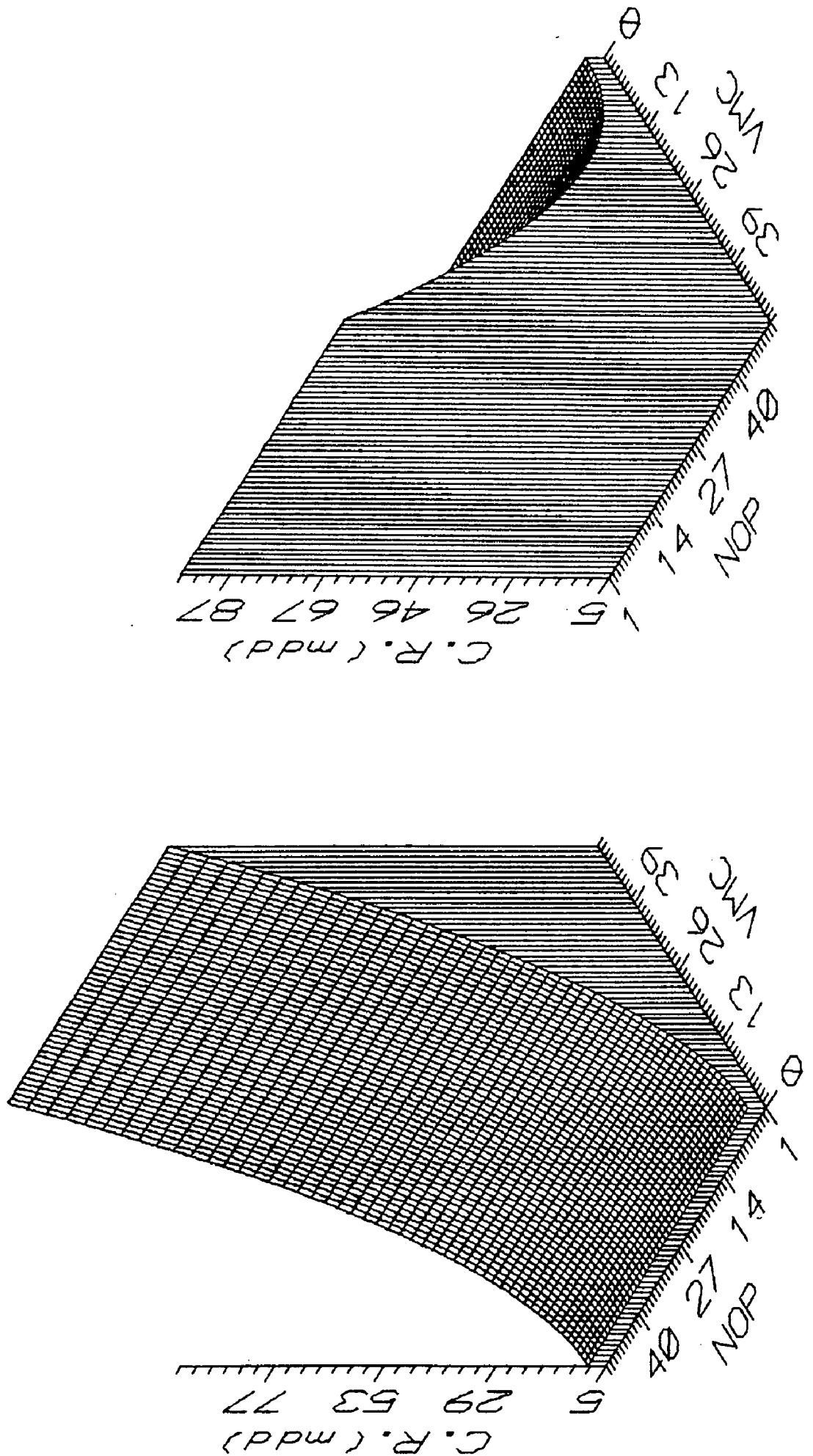
FIG. 6.17   3D plot depicting the effect of VMC & NOP
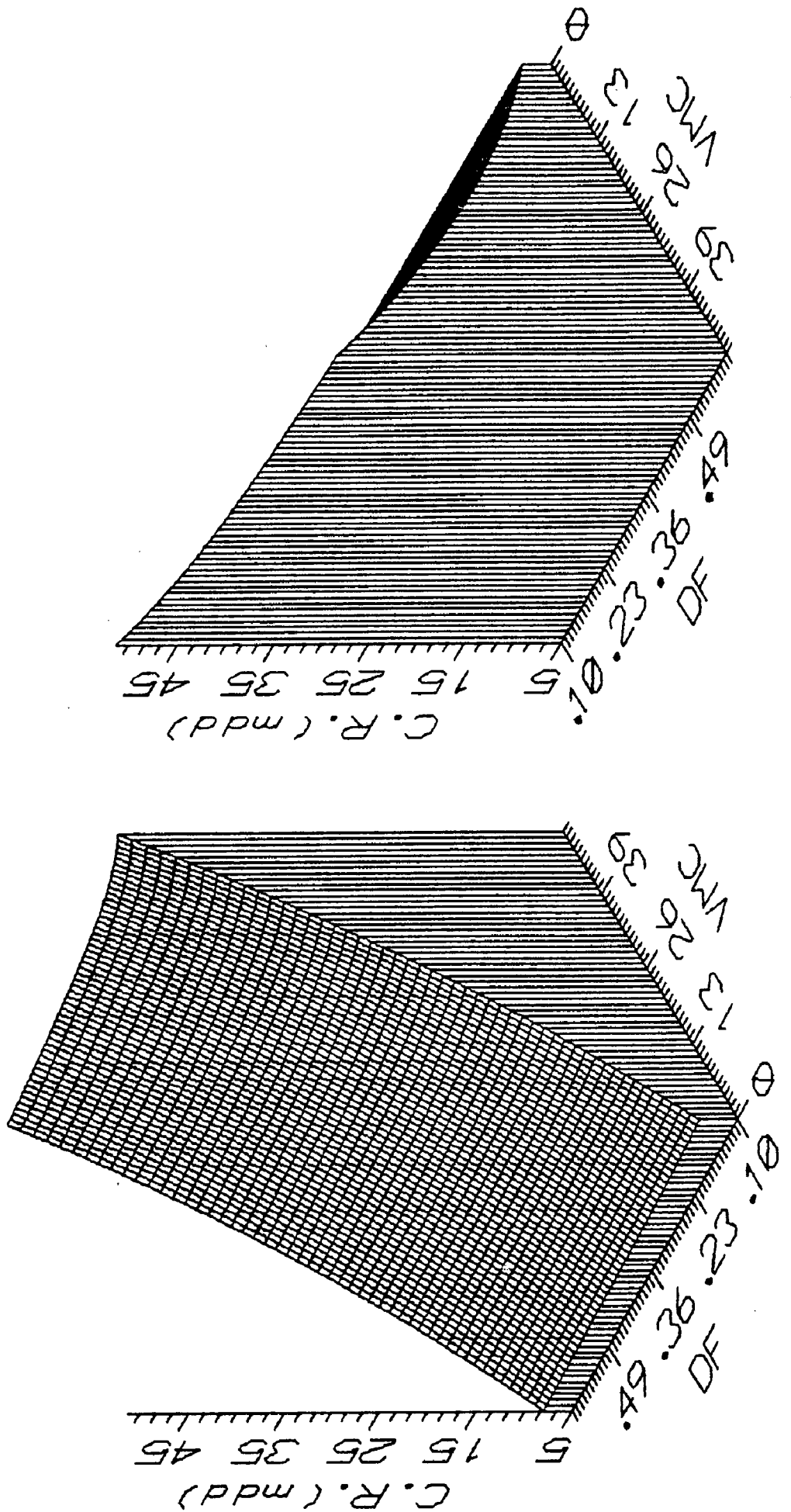on corrosion rate(based on unifled model)

Based on Equation 6.26
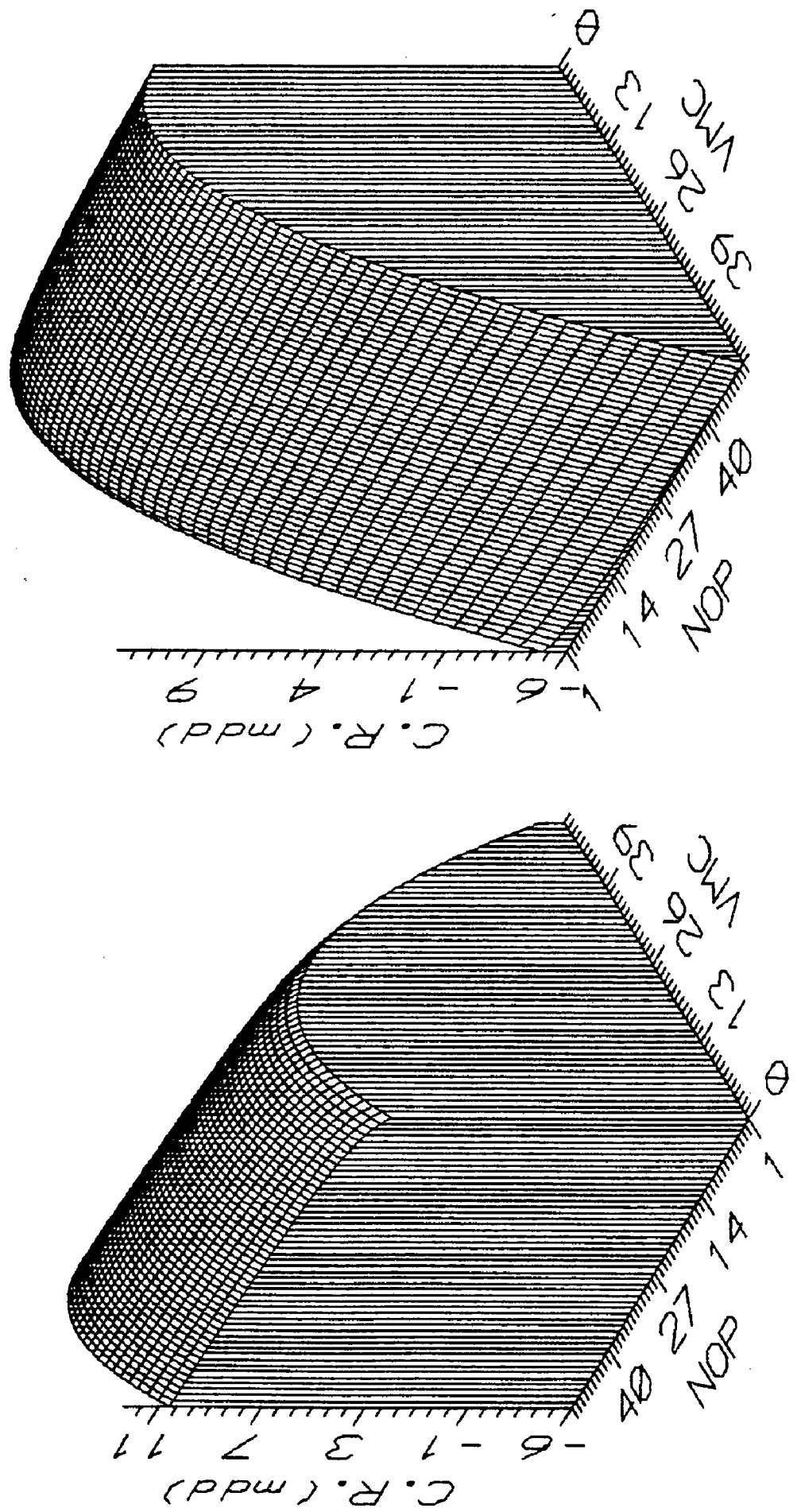
FIG. 6.18a Contour plot depicting the combined effect of VMC & NOP on corrosion rate
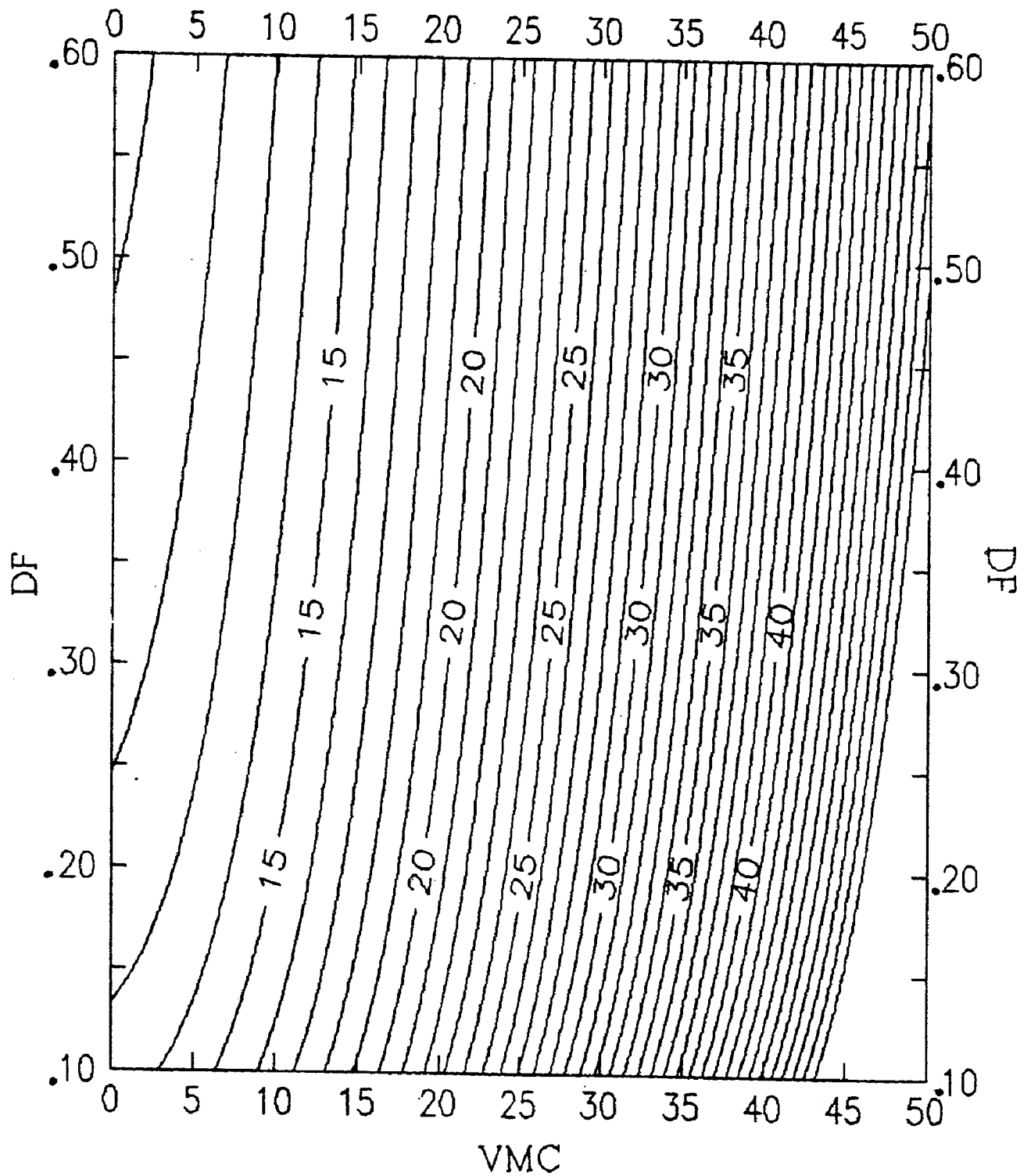## (Alloy P1)
Based on Equation 6.23
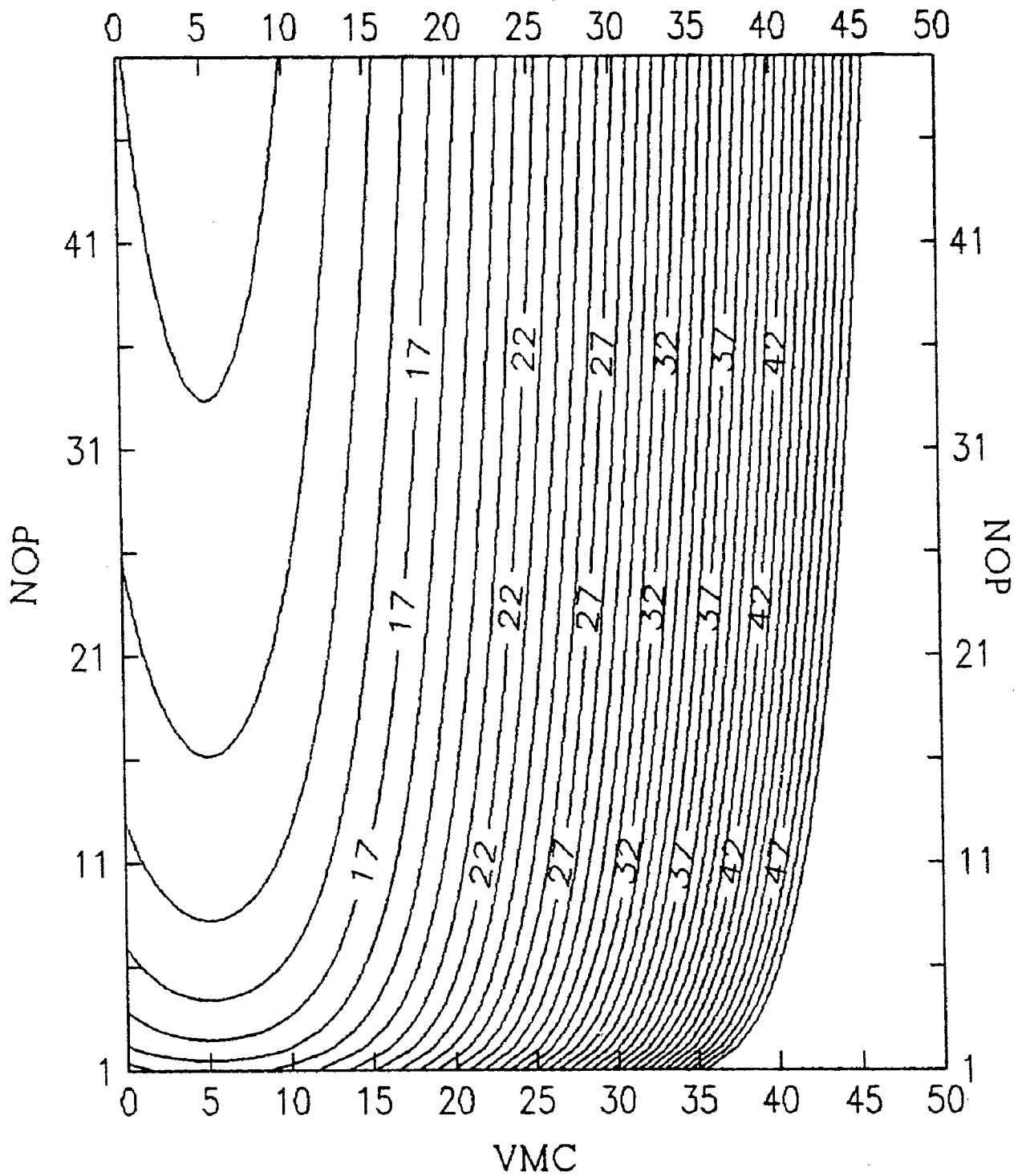
FIG. 6.18b Contour plot depicting the combined effect of
VMC & NOP on corrosion rate
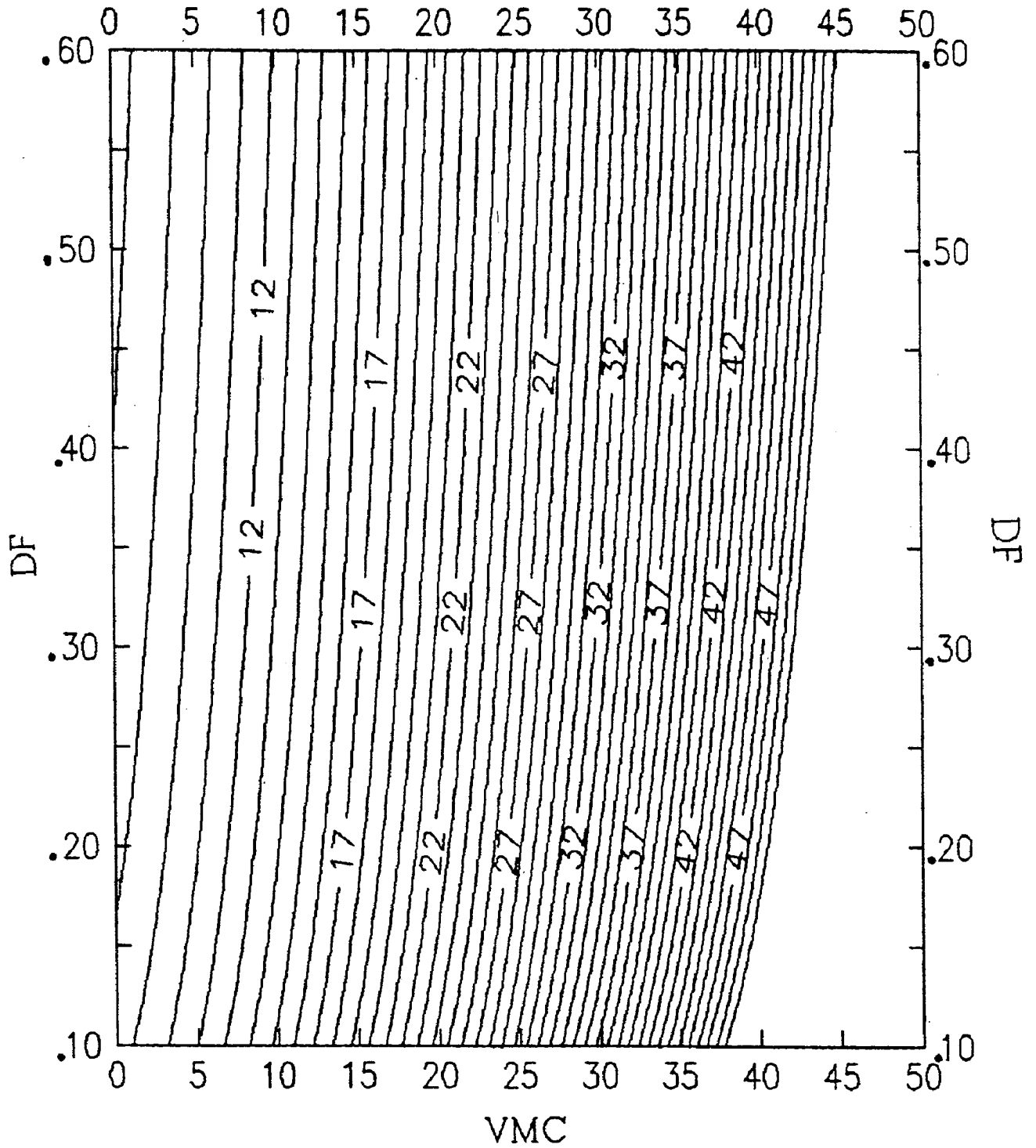(Alloy P2)
Based on Equation 6.24
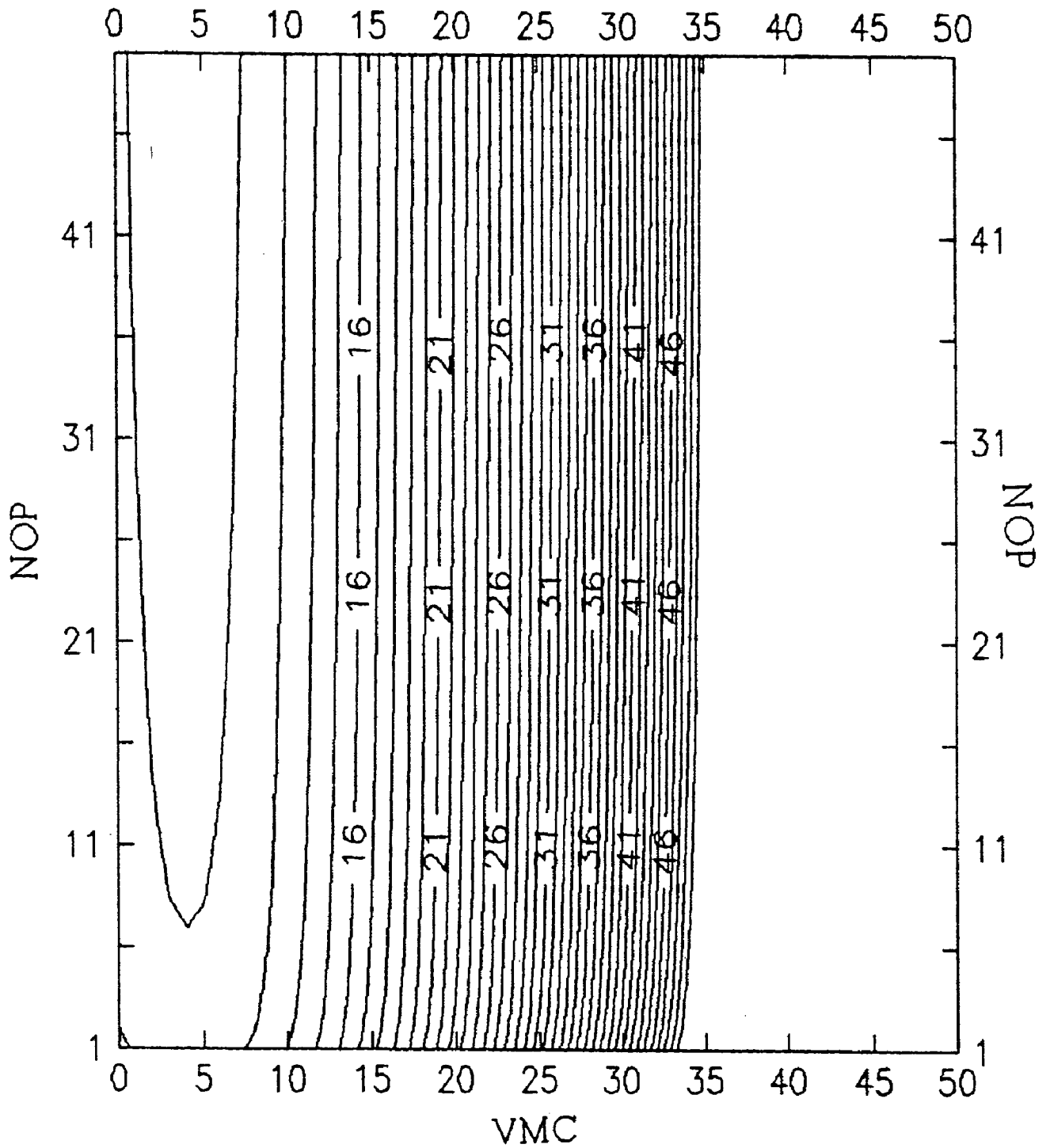
FIG. 6.18c Contour plot depicting the combined effect of VMC & NOP on corrosion rate (Alloy P3)

Based on Equation 6.25
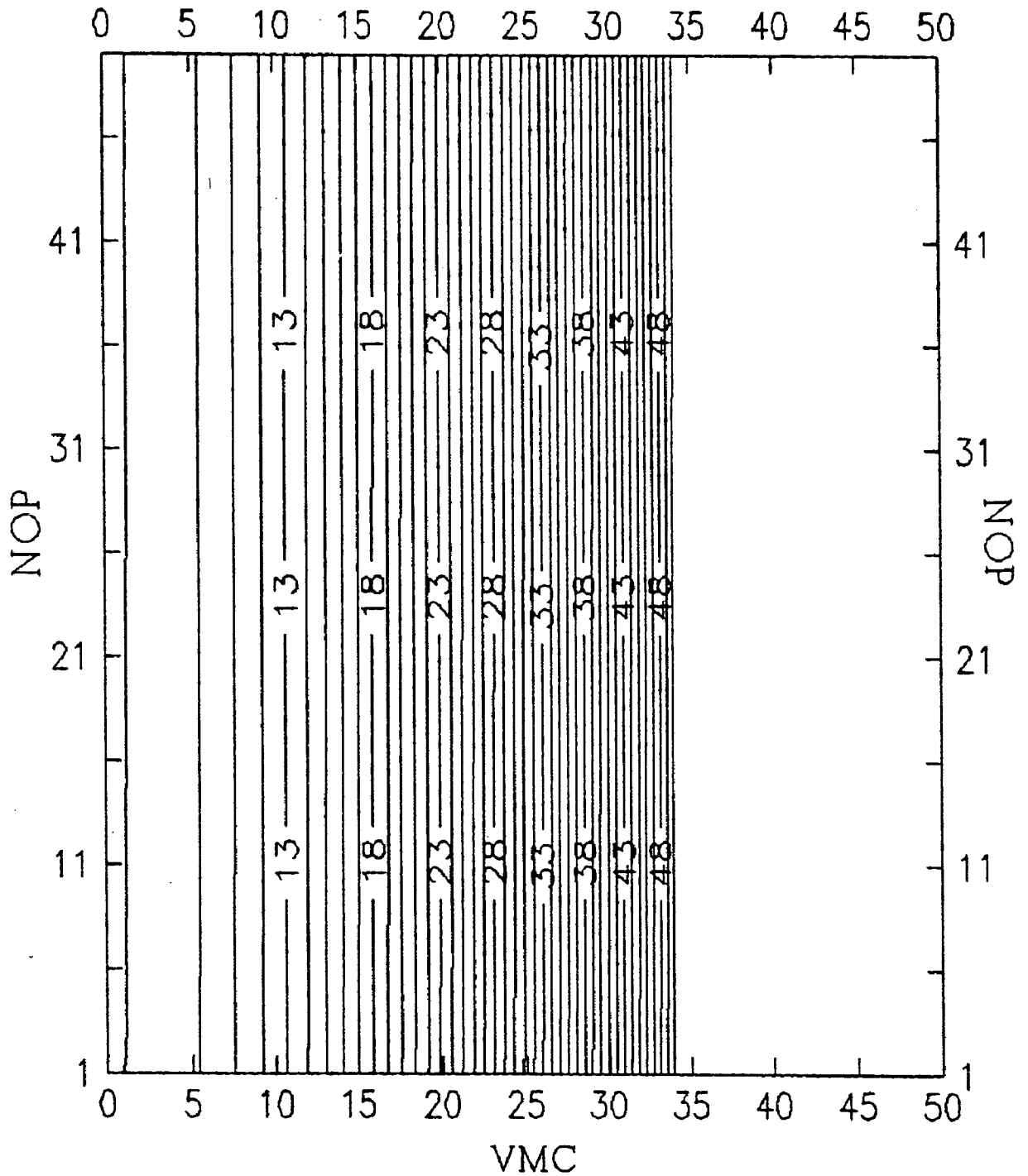
FIG. 6.19 Contour plot depicting the combined effect of VMC & NOP on corrosion rate(based on unified model) Based on Equation 6.26
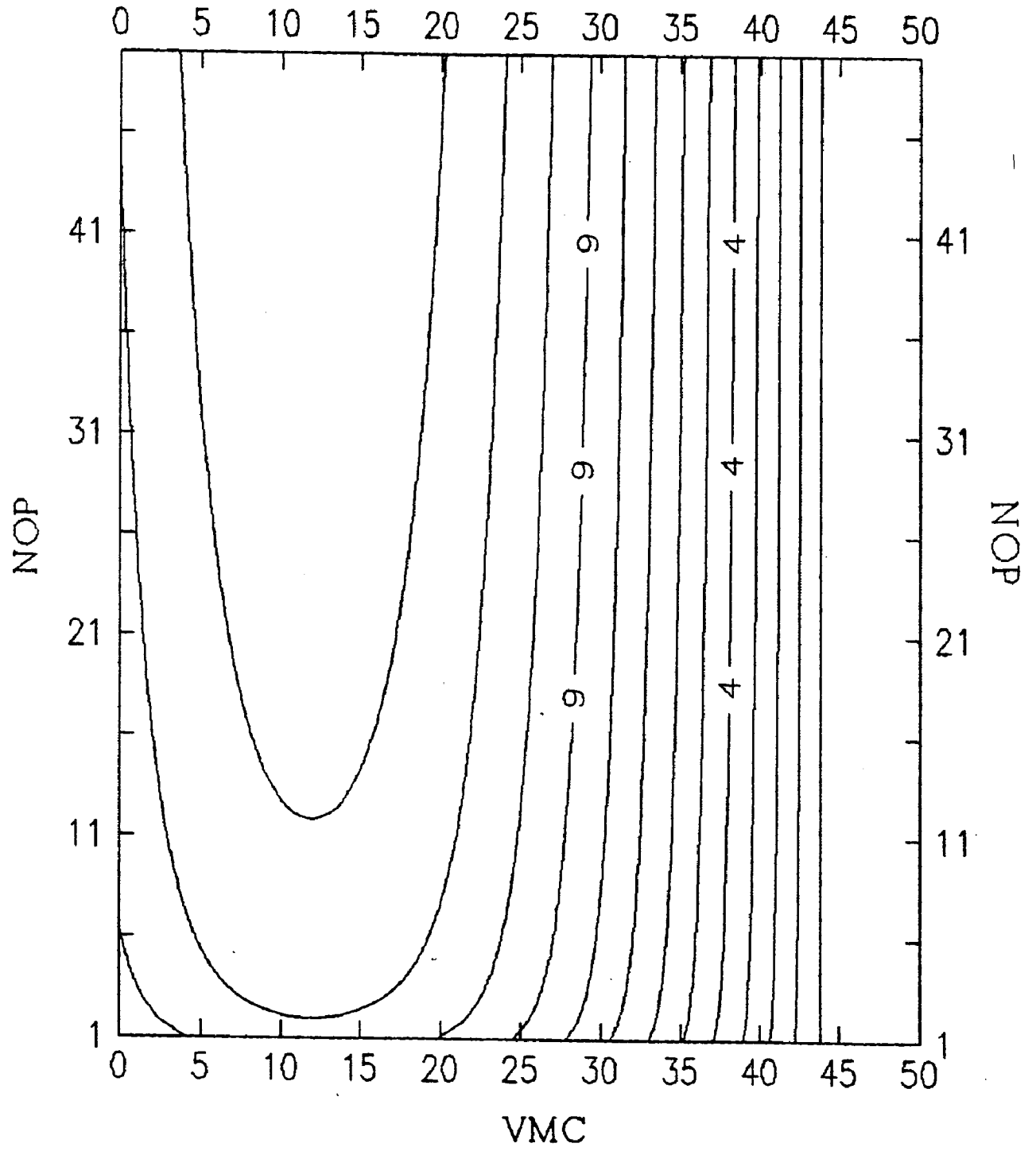
FIG. 6.20a 3D plot depicting the effect of VMC & DF
on corrosion rate

(Alloy Pl)

Based on Equation 6.30
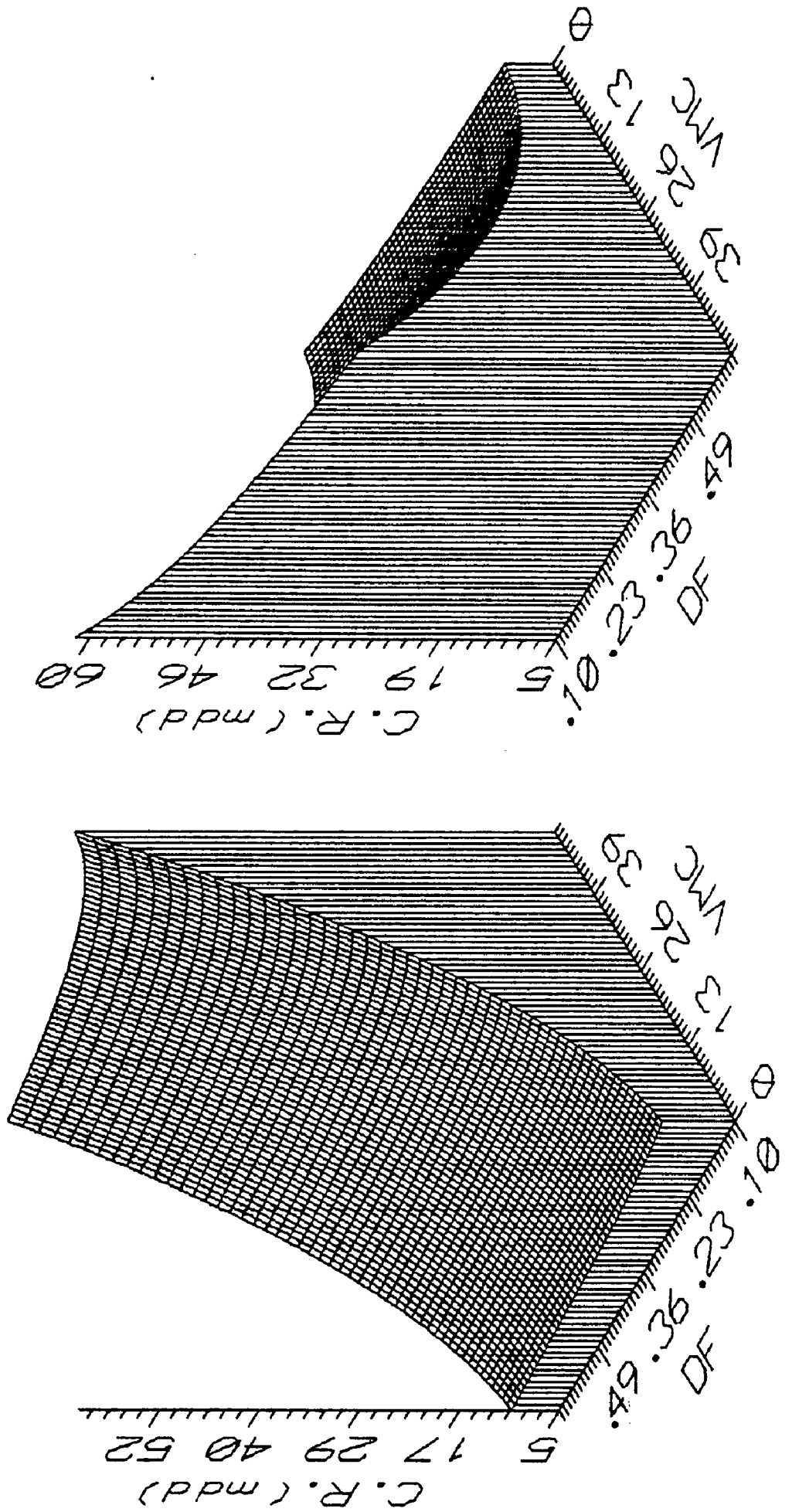
FIG. 6.20b 3D plot depicting the effect of VMC & DF
on corrosion rate
(Alloy P2)
Based on Equation 6.31
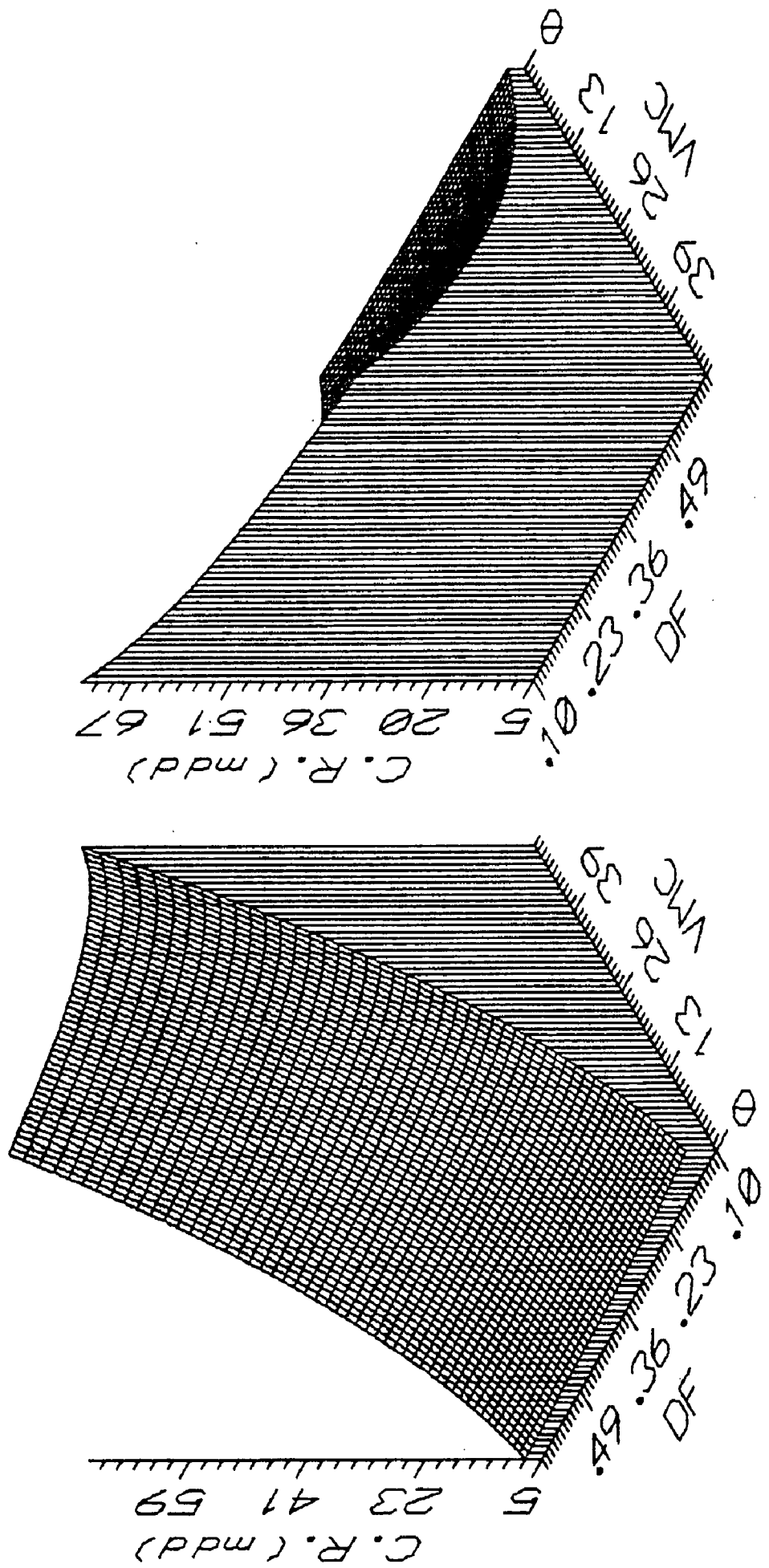
FIG. 6.20c 3D plot depicting the effect of VMC & DF
on corrosion rate

(Alloy P3)

Based on Equation 6.32

FIG. 6.2I   3D plot depicting the effect of VMC & DF
on corrosion rate(based on unified model)

Based on Equation 6.33

FIG. 6.22a Contour plot depicting the combined effect
of VMC & DF on corrosion rate
Based on Equation 6.30

(Alloy Pl)

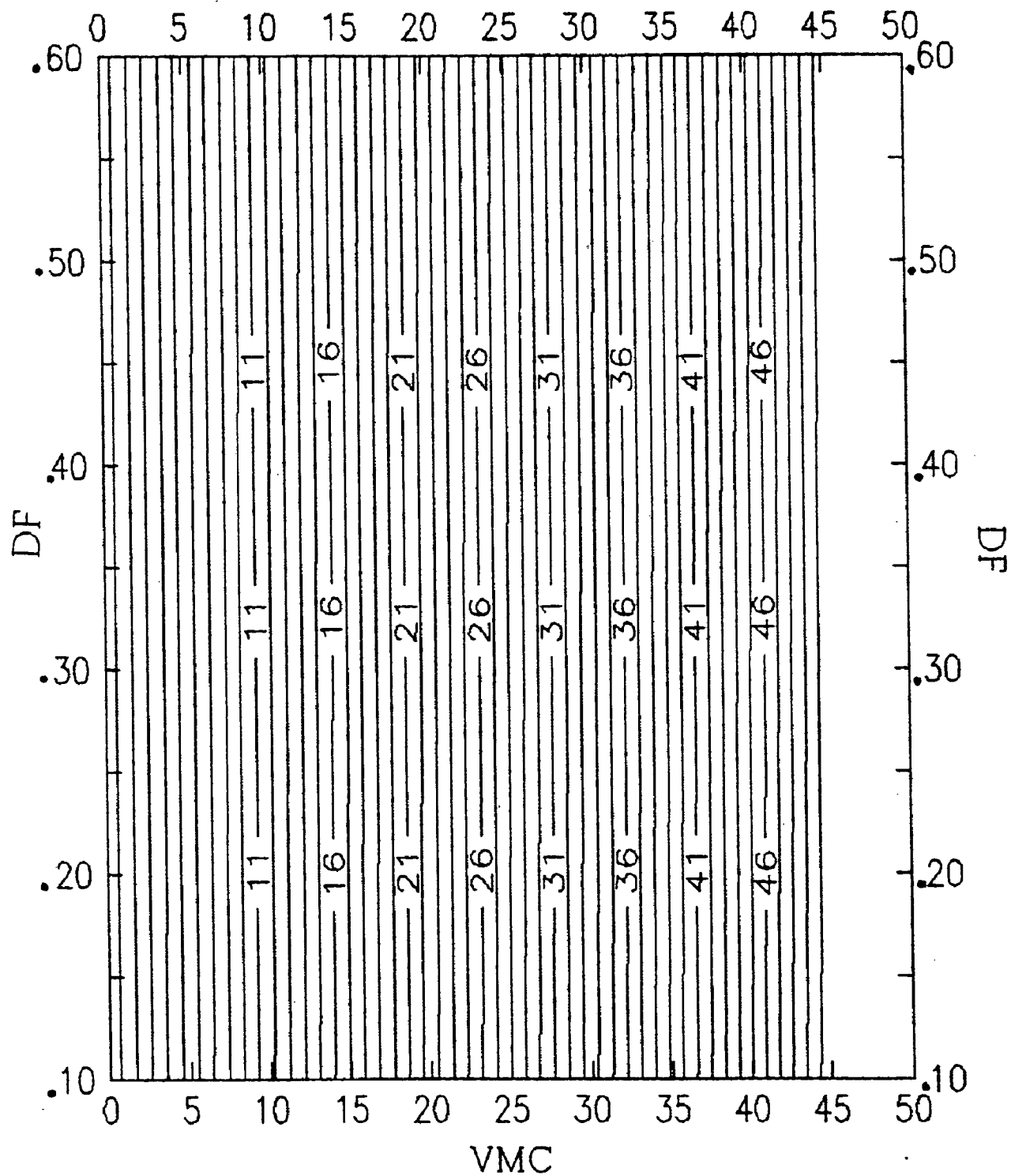## FIG. 6.22b Contour plot depicting the combined effect of VMC & DF on corrosion rate (Alloy P2)

Based on Equation 6.31

FIG. 6.22c Contour plot depicting the combined effect of VMC & DF on corrosion rate
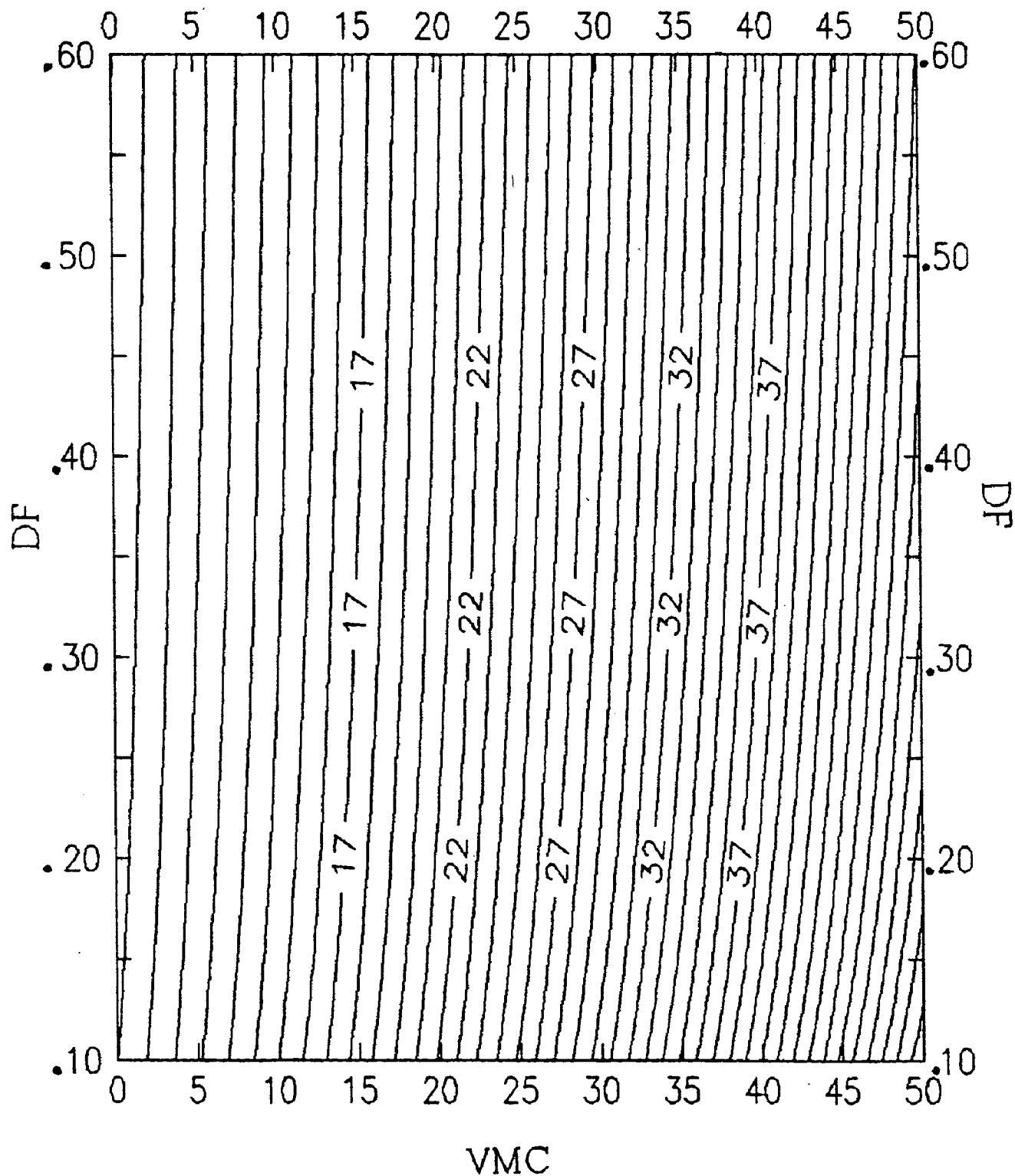(Alloy P3)
Based on Equation 6.32

FIG. 6.23 Contour plot depicting the combined effect of VMC & DF on corrosion rate(based on unified model) Based on Equation 6.33

F-113

Appendix- A1 Percent area of particles in different classes at different locations as influenced by heat treating parameters (Alloy P1)

h/t		location I	location II	location III	location IV	location V	location VI	location VII
800	2	30 69 0	10 64 25 0	13 86 0 0	20 80 0 0	34 65 0 0	11 88	0
800	4	28 71 0	16 83 0 0	12 62 24 0	100 0 0 0	18 55 25 0	88	0
800	6	28 71 0	10 29 60 0	52 47 0 0	9 62 28 0	13 86 0 0		
800	8	14 85 0	5 60 33 0	7 59 32 0	5 39 54 0	8 50 40 0		
800	10	10 13 75 0	12 51 35 0	18 81 0 0	6 25 34 34	11 88 0 0	7 38 53	0
850	2	10 31 58 0	12 30 56 0	16 83 0 0	6 39 54 0	8 53 37 0	7 44	
850	4	6 32 60 0	3 33 62 0	12 87 0 0	8 53 37 0	28 71 0 0	44 0	48
850	6	7 54 37 0	2 62 34 0	10 52 36 0	3 96 0 0	12 23 64 0		
850	8	12 87 0 0	9 64 25 0	12 87 0 0	26 73 0 0	19 80 0 0		
850	10	8 62 29 0	6 32 60 0	11 56 31 0	4 72 22 0	57 42 0 0	4 56 39	0
900	2	10 90 0 0	27 72 0 0	11 45 42 0	3 17 47 31	6 24 68 0	8 62 28	0
900	4	47 52 0 0	11 67 20 0	17 82 0 0	6 46 16 31	10 68 21 0	12 36 51	0
900	6	18 81 0 0	12 87 0 0	2 34 63 0	14 50 35 0	9 62 28 0		
900	8	8 24 67 0	5 25 69 0	3 20 38 37	6 44 49 0	4 31 64 0		
900	10	9 67 23 0	7 63 29 0	11 37 51 0	8 17 25 48	6 42 50 0	12 56 31	0
950	2	11 88 0 0	6 30 63 0	5 30 63 0	8 51 40 0	8 50 40 0	5 39 54	0
950	4	4 33 61 0	4 25 23 46	5 40 0 54	4 61 34 0	9 31 58 0		
950	6	30 69 0 0	4 6 18 71	6 55 38 0	11 56 31 0	6 60 33 0		
950	8	2 6 54 35	15 22 62 0	13 86 0 0	8 14 0 77	9 0 90 0		
950	10	3 20 0 75	11 52 36 0	5 31 21 42	2 18 52 25	16 83 0 0	14 85 0	3 57 39 0
1000	2	18 81 0 0	35 64 0 0	15 57 26 0	20 79 0 0	16 43 40 0	5 25 69	
1000	4	10 37 52 0	13 44 41 0	16 83 0 0	30 69 0 0	10 90 0 0		
1000	6	13 44 41 0	15 84 0 0	14 85 0 0	7 14 78 0	15 22 62 0		
1000	8	6 93 0 0	39 59 0 0	30 69 0 0	5 49 45 0	12 87 0 0		
1000	10	12 36 51 0	43 56 0 0	18 81 0 0				

Frame area = 207.81 μm²

A-1

Appendix- A2 Percent area of particles in different classes at different locations as influenced by heat treating parameters (Alloy P2)

h/t		location I	location II	location III	location IV	location V	location VI	location VII
800	2	8 50 40	5 94 0	8 74 16	13 86 0	6 77 15		
800	4	8 53 37	7 92 0	21 78 0	18 81 0			
800	6	18 48 33	11 88 0	12 60 27	12 36 51	12 87 0	4 61 34	
800	8	12 60 27	4 61 34	14 58 27	11 45 42	10 61 28		
800	10	14 85 0	10 90 0	9 69 21	9 62 28	5 49 45	4 7 44 43	
850	2	8 69 21	19 80 0	5 67 26	7 57 35	7 72 20		
850	4	4 65 30	4 44 50	14 44 40	7 63 29	4 49 45		
850	6	8 65 26	6 24 69	4 40 55	8 69 21	13 86 0		
850	8	4 65 30	3 33 62	5 94 0	12 87 0	10 52 36	4 76 19	
850	10	10 29 60	10 50 39	3 21 15 59	20 79 0	10 46 43	4 47 16 32	
900	2	30 69 0	10 89 0	11 45 42	10 31 58	10 46 43		
900	4	4 40 55	11 52 36	7 92 0	10 37 52	14 85 0		
900	6	14 85 0	4 44 50	4 10 85	6 33 0 60	14 85 0	3 25 70	
900	8	6 32 60	5 6 53 34	4 44 50	7 43 48	4 33 31 30		
900	10	17 48 33	5 25 69	3 40 0 55	13 0 86 0	10 42 47	5 12 50 32	
950	2	39 59 0	15 84 0	5 25 69	12 36 51	8 24 67	13 44 41	
950	4	5 49 45	6 55 38	30 69 0	4 25 70	6 24 68		
950	6	28 71 0	30 69 0	4 18 26 51	10 90 0	10 90 0	2 34 63	
950	8	1 10 29 58	5 25 69	6 39 54 0	2 12 51 33	3 10 86	1 34 64	1 26 24 47
950	10	6 14 79	4 18 26 51	0 35 64 0	4 40 55 0	12 87 0		
1000	2	2 62 34	6 55 38	10 90 0	7 92 0	10 90 0	28 71 0	
1000	4	27 72 0	21 78 0	12 36 51	16 83 0	3 10 86	7 54 37	
1000	6	14 85 0	20 80 0	43 56 0	12 87 0	11 45 42		
1000	8	100 0 0	55 45 0	15 84 0	14 85 0	28 71 0	34 65 0	
1000	10	5 25 69	7 0 92	2 26 71	6 60 33 0	6 39 54		

Frame area = 207.81 μm^2

Appendix- A3 Percent area of particles in different classes at different locations as influenced by heat treating parameters (Alloy P3)

Values shown are the class percentages within each location (reading: class 1 · class 2 · class 3 · class 4). Frame area = 207.81 µm².

| h/t		location I	location II	location III	location IV	location V	location VI	location VII
800	2	3 25 70	9 90 0	10 89 0	10 89 0	13 86 0	17 82 0	
800	4	17 82 0	10 90 0	9 90 0	9 90 0	8 71 19	11 88 0	
800	6	18 81 0	20 80 0	15 84 0	15 84 0	5 51 42		
800	8	8 43 48	7 66 26	14 54 30	14 54 30	3 71 24	3 50 46	
800	10	18 81 0	21 78 0	11 56 31	11 56 31	4 68 27		
850	2	12 51 35	5 60 33	13 86 0	13 86 0	5 94 0		
850	4	8 65 26	11 60 28	8 38 53	8 38 53	20 79 0	7 92 0	
850	6	6 24 68	5 60 33	11 88 0	11 88 0	8 91 0	25 74 0	
850	8	2 25 71	5 49 45	1 41 57	1 41 57	2 41 56	10 37 52	
850	10	7 32 60	4 68 27	6 32 60	18 56 31	18 33 47		
900	2	21 78 0	27 72 0	6 30 63	43 56 0	8 91 0		
900	4	4 10 85	3 20 38 37	10 42 47	7 92 0	2 37 59		
900	6	14 44 40	3 25 42 27	3 20 75		2 37 59		
900	8	7 48 44	2 15 41 40	4 12 17 66	5 64 29	3 21 45 29	3 36 60	6 10 83
900	10	30 69 0	28 71 0	14 85 0	14 85 0			
950	2	6 55 38	6 39 54	33 66 0	33 66 0	16 83 0		
950	4	10 46 43	4 56 39	3 33 62	49 45 0	15 84 0		
950	6	2 40 28 27	3 7 88	6 67 26	78 18 0	10 57 32		
950	8	9 67 23	10 90 0	11 88 0	14 44 40	30 69 0	6 39 54	
950	10	57 42 0	65 34 0	37 62 0	20 79 0	37 62 0		
1000	2	21 78 0	33 66 0	30 69 0	20 79 0	14 85 0		
1000	4	55 45 0	50 50 0	55 45 0				
1000	6	14 85 0	39 59 0					
1000	8	43 56 0	30 69 0	47 52 0	47 52 0	21 78 0		

Frame area = 207.81 µm²

FIG. A-4 Variation in the Vf of MC as influenced by h/t temperature (Alloy P1) (2 hours soaking period)
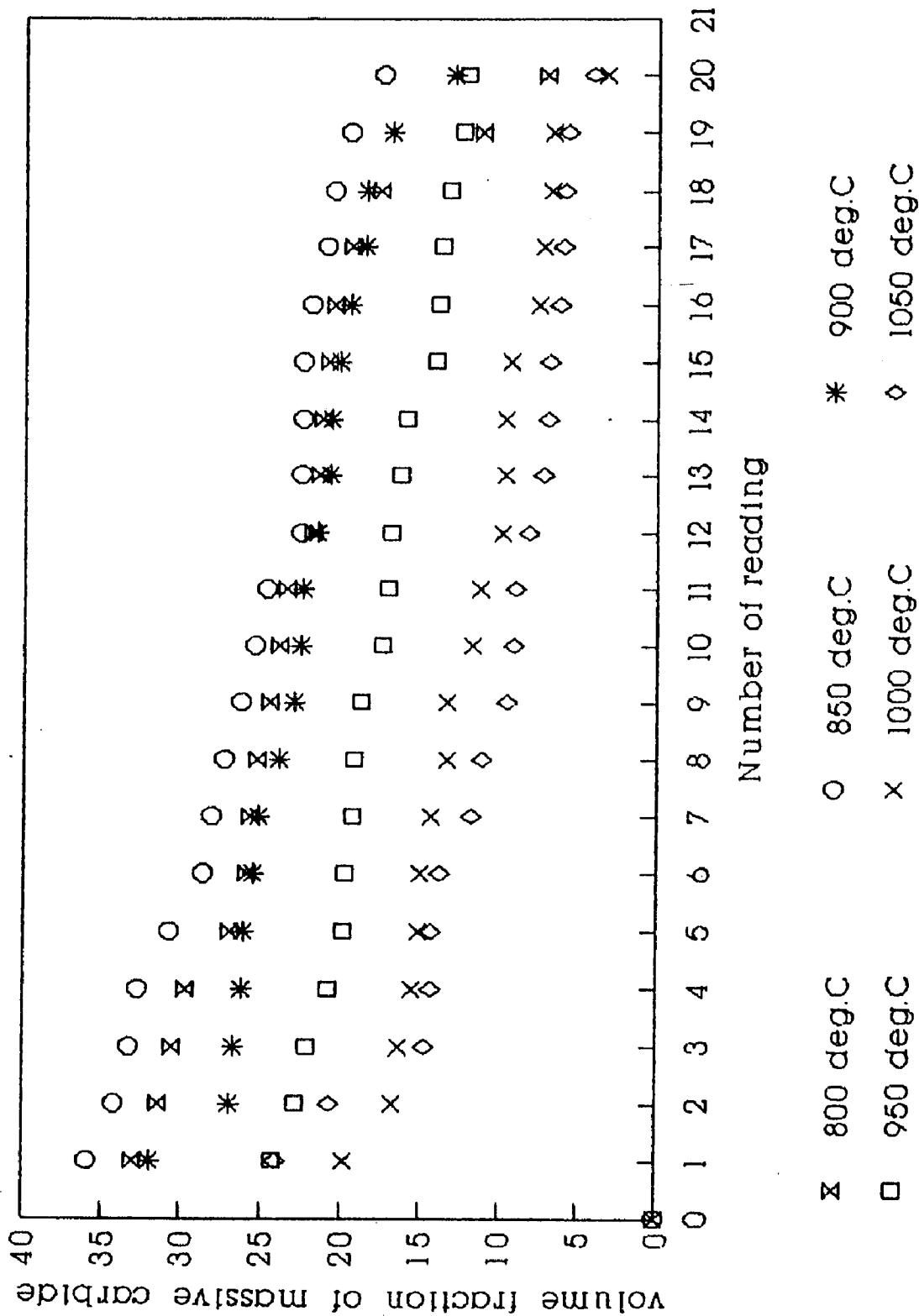
FIG. A-5 Variation in the Vf of MC as influenced by h/t temperature (Alloy P2) (2 hours soaking period)
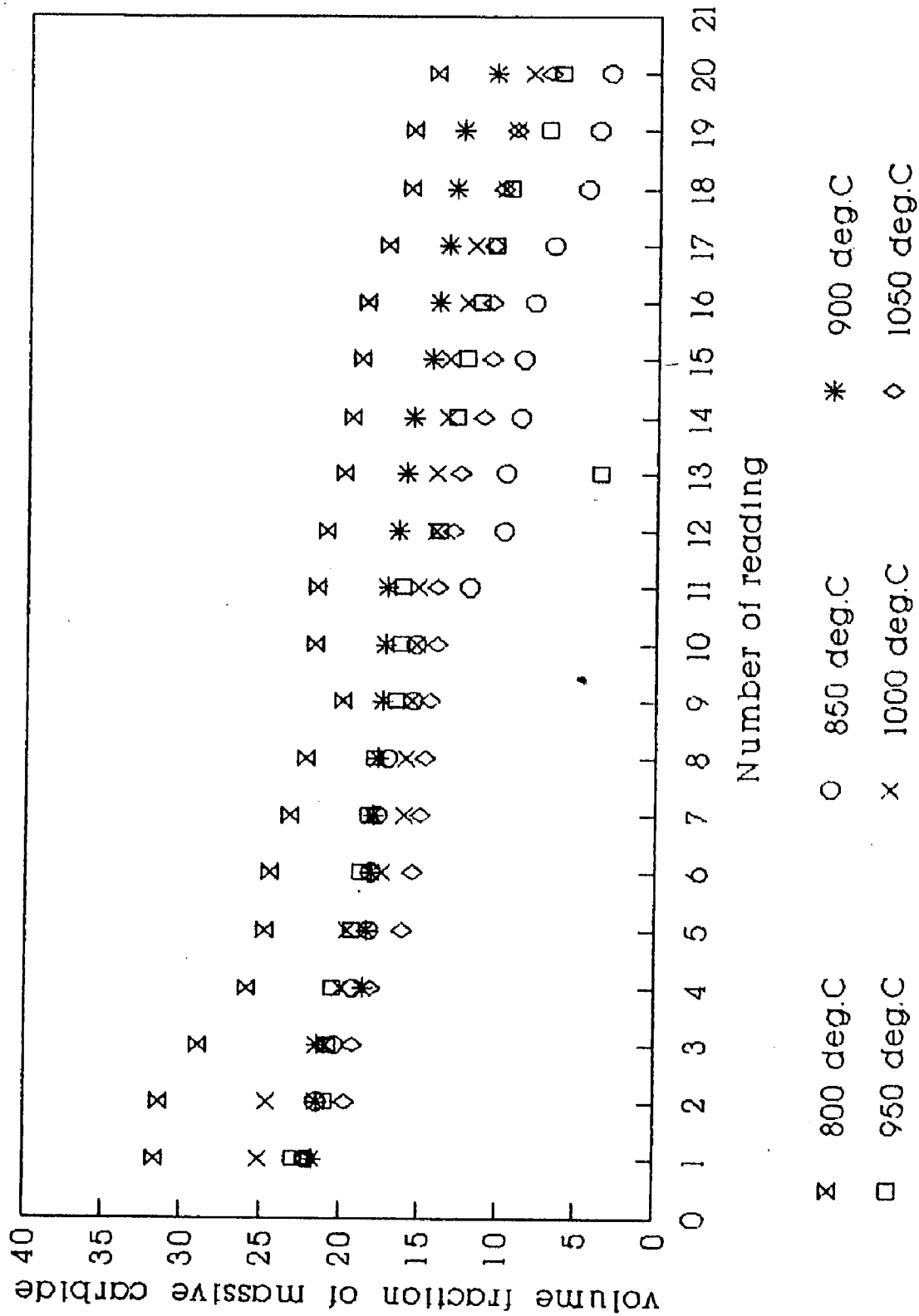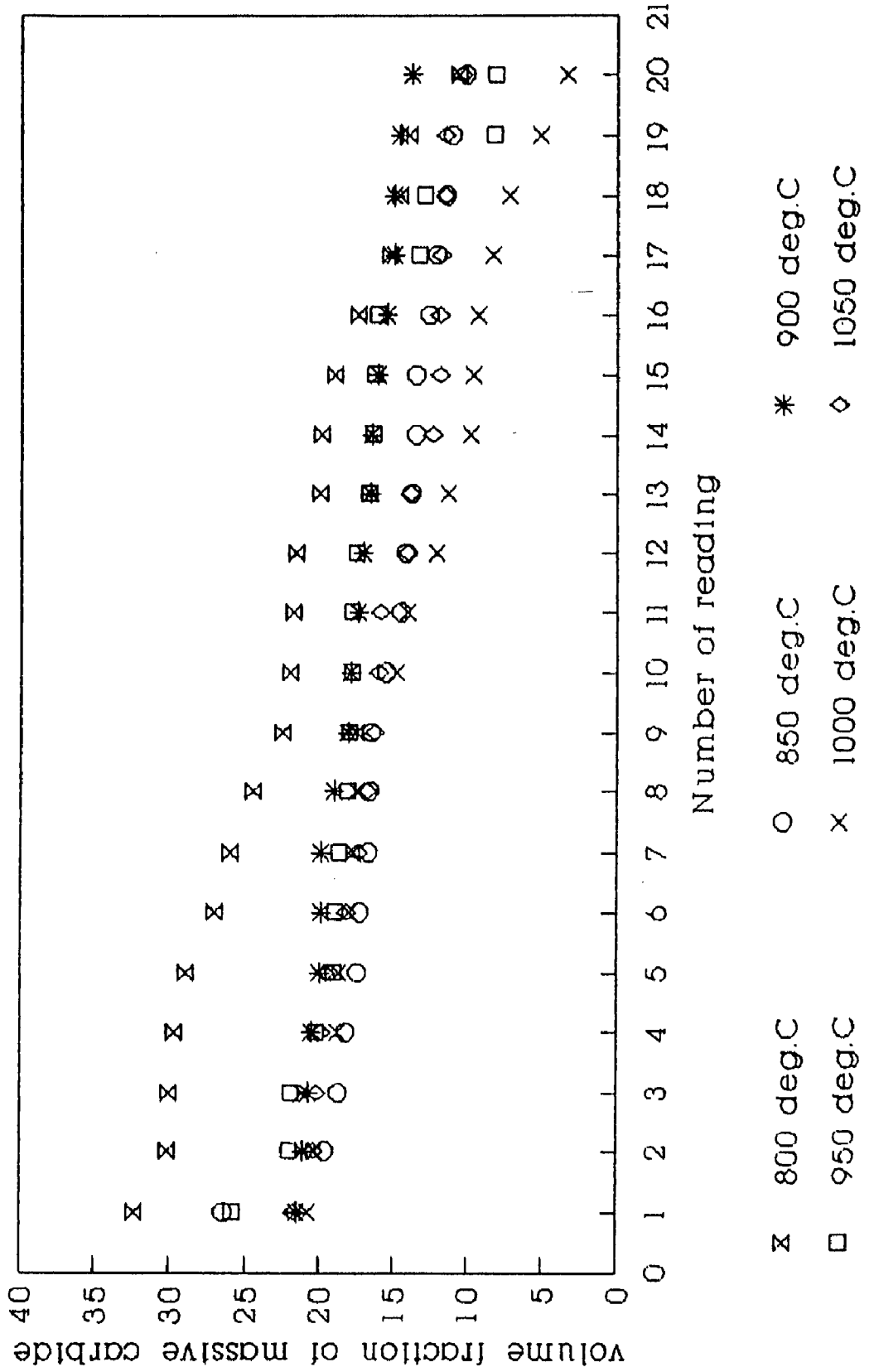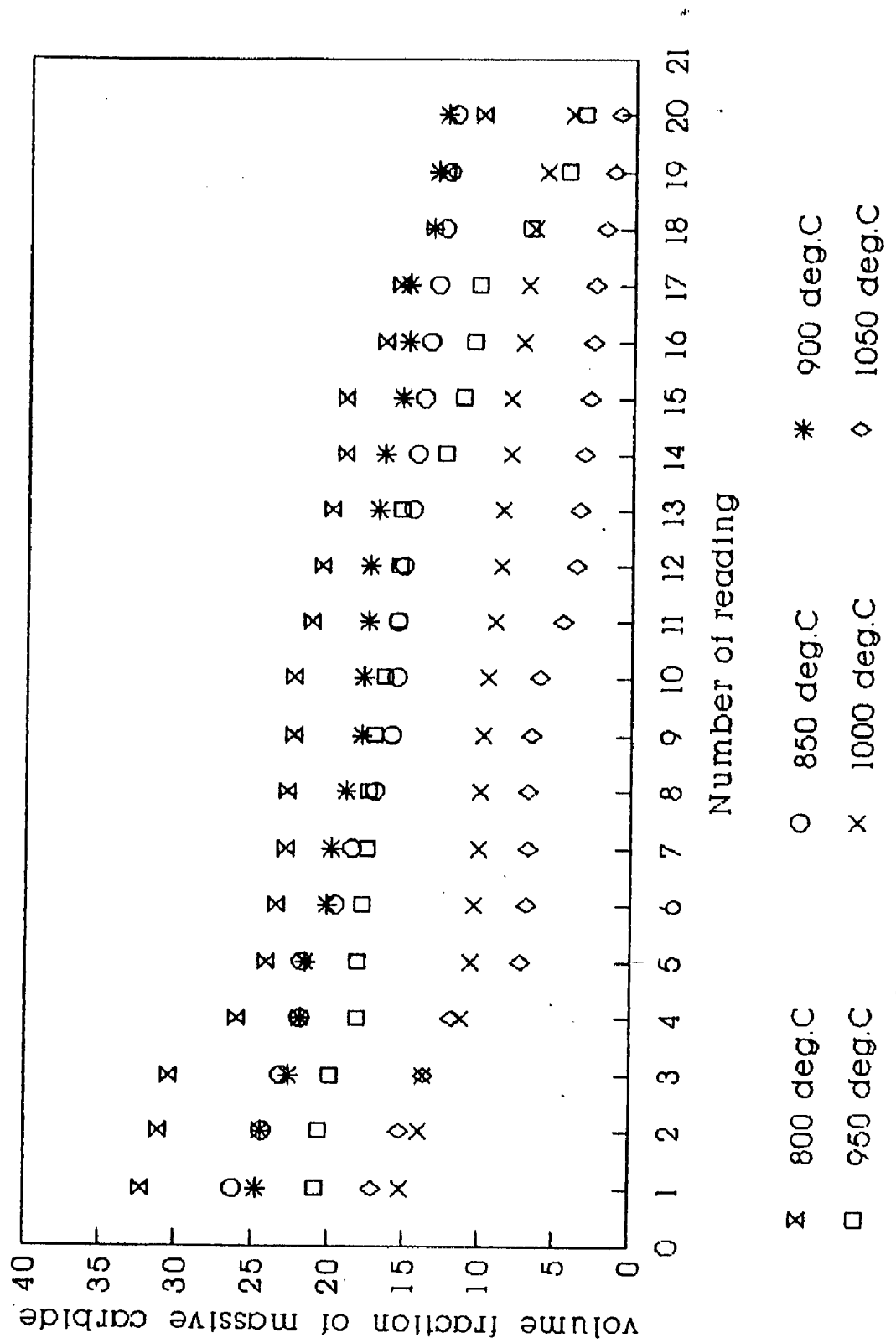
800 deg.C   ◇ 850 deg.C   * 900 deg.C

950 deg.C   × 1000 deg.C   ◇ 1050 deg.C

Number of reading

volume fraction of massive carbide

FIG. A-6 Variation in the Vf of MC as influenced by h/t temperature (Alloy P3) (2 hours soaking period)

A-6

FIG. A-7 Variation in the Vf of MC as influenced by
h/t temperature (Alloy P1)
(10 hours soaking period)

FIG. A-8 Variation in the Vf of MC as influenced by h/t temperature (Alloy P2) (10 hours soaking period)
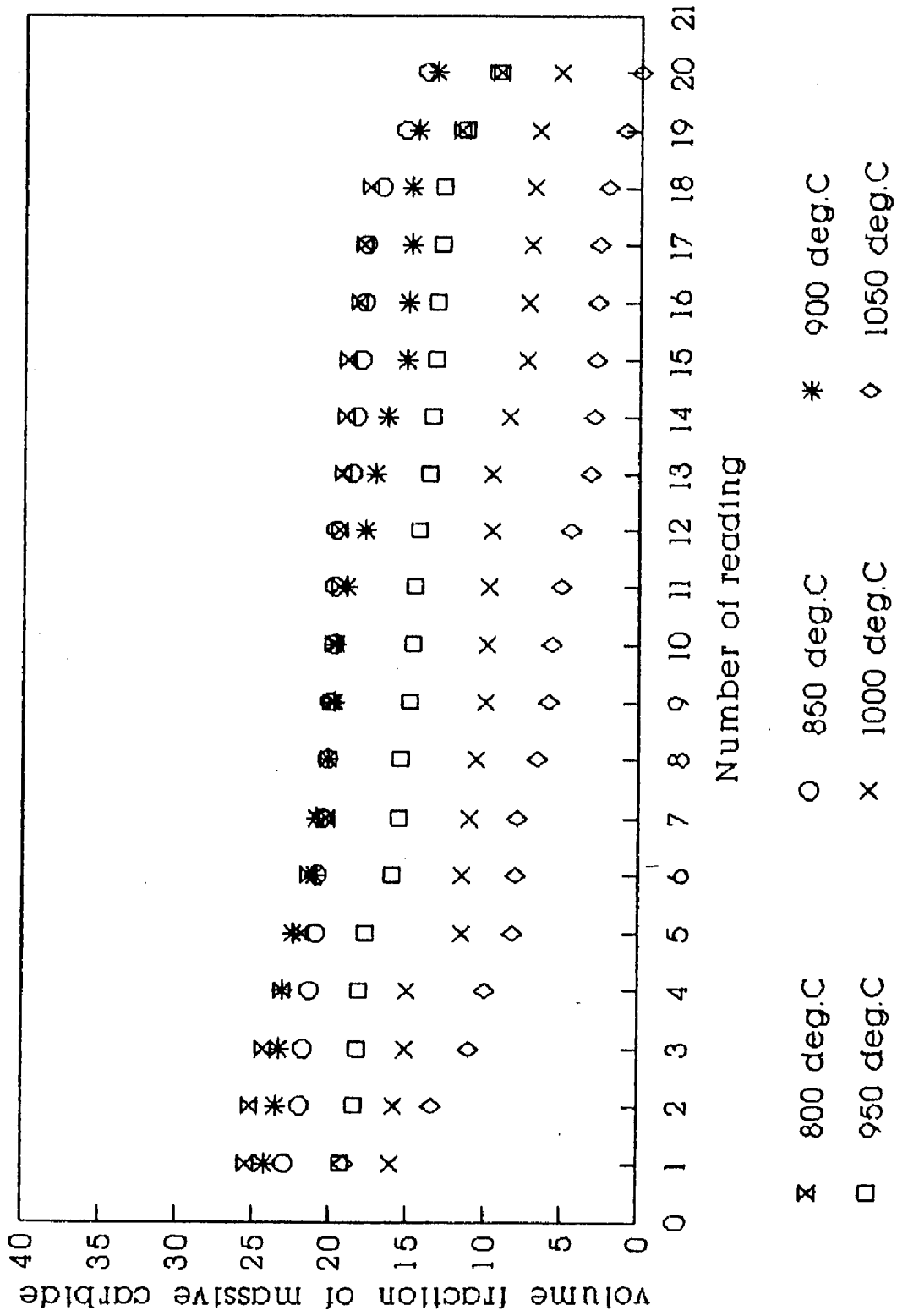
FIG. A-9 Variation in the Vf of MC as influenced by h/t temperature (Alloy P3)
(10 hours soaking period)